SELECTIVE METAL COORDINATION IN ANTIFOULING COATINGS

BY

HANNAH ROBINSON

A thesis

submitted to the Victoria University of Wellington

in fulfilment of the requirements for the degree of

Doctor of Philosophy in Chemistry

Victoria University of Wellington

2020

ABSTRACT

Marine biofouling is the accumulation of biological material (*e.g.* microorganisms, soft- and hard-fouling organisms) on the surface of an object submerged in seawater, and it remains a worldwide problem for shipping industries. The fouling of ship hulls results in a reduction of speed and manoeuvrability due to frictional drag, as well as increased fuel consumption and accelerated corrosion, and the exorbitant expenses and losses of efficiency attributed to biofouling have prompted the development of antifouling coatings. Current antifouling paints use copper as a biocidal agent, but copper-based paints are increasingly being banned due to environmental concerns about the non-target effects of leached copper. This project aims to circumvent these concerns and tightening regulations *via* a revolutionary concept: the development of marine antifouling paints that incorporate Cu(II)-selective ligands to draw the biocidal ingredient (*i.e.* Cu(II)) from seawater. A multistage strategy emerged for the development of this technology. First, criteria were established for the project's ideal ligand, and ligands were synthesised or selected based on these criteria. Second, the ligands were incorporated in coatings through covalent modification of the paint binder or additives. Third, methodology was developed and implemented to test each coating's ability to coordinate and retain Cu(II), as well as its subsequent ability to prevent microfouling by marine bacteria.

The suitability of two ligand classes was assessed: acylhydrazones and tetraaza macrocycles, specifically cyclen. Unlike the acylhydrazones, cyclen met the established criteria and was initially evaluated as a curing agent and/or surface-modifier in a two-pack epoxy system with resin Epikote™ 235. However, the Cu(II)-loading by these coatings was relatively low, being at most ~0.05% w/w, and the modification of silica, a common paint additive, with cyclen was explored as an alternative formulation route. The method for the functionalisation of silica with cyclen was optimised, and the maximum Cu(II)-loading achieved by the product was 2.60% w/w. The cyclen-functionalised silica was incorporated on the surface of an epoxy coating, and a bacterial adherence assay was developed to assess the cellular attachment of marine bacterium *Vibrio harveyi* to this coating, which was found to be undeterred. Yet, the development of the strategy and testing methodology by which the project's goals may be achieved provides a solid foundation for future work.

ACKNOWLEDGMENTS

DECLARATION AND COPYRIGHT

The work in this thesis was completed by the author at the Victoria University of Wellington, New Zealand. It has not been submitted before, in part or in whole, for a higher degree at this university or any other.

Some of the work described in this thesis has been reported in the following poster and publication:

1. **Robinson, H.**, Burr, D., Daines, A. M., Glenny, M., Hinkley, S. F. R., & Williams, D. B. G. Assessing the antimicrobial activity of copper-coordinating coatings. in *ASM Microbe Conference* (2018), *SCANZ Convention* (2018), & *Microbes & Molecules NZMS Annual Conference* (2018).

2. Daines, A. M., **Robinson, H.**, Glenny, M., Williams, D. B. G. & Hinkley, S. F. R. Linear and macrocyclic water soluble polyacylhydrazones and their utilisation in coatings. *Prog. Org. Coatings* **121**, 38–44 (2018).

The author wrote **Sections 2.4** (paragraphs 1–2, 4) and **3.2** (paragraphs 1–2, 4) in the research article above, and these sections are included in Chapters 2 (**Section 2.3.2**) and 6 (**Section 6.2.2.2**) of this thesis, as permitted by Elsevier and the Victoria University of Wellington Faculty of Graduate Research.

TABLE OF CONTENTS

LIST OF FIGURES

LIST OF TABLES

LIST OF SCHEMES

LIST OF ABBREVIATIONS

Ac	acetyl group
AcOH	acetic acid
ADH	adipic acid dihydrazide
AHEW	amine hydrogen equivalent weight
AHL	*N*-acyl-homoserine lactone
Al(OTf)$_3$	aluminium triflate (trifluoromethanesulfonate)
ANOVA	analysis of variance
aq	aqueous
ATR	attenuated total reflectance
AU	absorbance units
BET	Brunauer, Emmett, and Teller
BPA	bisphenol A
BPF	bisphenol F
br	broad (IR, NMR), biological replicate (statistics)
BSED	backscattered electron detector
CDCl$_3$	chloroform-*d*
CD$_3$OD	methanol-*d$_4$*
CFSE	crystal field stabilisation energy
CFT	crystal field theory
CFU	colony forming unit
CHX	chlorhexidine
Cn(Gm)$_n$	cyclen-(GLYMO)$_n$
CnGmSiO$_2$	cyclen-GLYMO-silica
COSY	correlation spectroscopy
CP-MAS	cross-polarisation magic angle spinning
Cu(II)-CnGm	copper(II)-cyclen-GLYMO
Cu(II)-CnGmSiO$_2$	copper(II)-cyclen-GLYMO-silica
DAp/acr	DiLevDEG/ADH polyacylhydrazone/acrylic
DCM	dichloromethane
dd	doublet of doublets
ddH$_2$O	double-distilled water
DEG	diethylene glycol

DETA	diethylenetriamine
DGEBA	bisphenol A diglycidyl ether
DiLevDEG	dilevulinoyl diethylene glycol
DLVO	Derjaguin-Landau-Verwey-Overbeek
DMF	dimethylformamide
DMSO	dimethylsulfoxide
DTPA	diethylene triamine pentaacetic acid
e^-	electron
ec-GmSiO$_2$	end-capped GLYMO-silica
EDTA	ethylene diamine tetraacetic acid
en	ethylenediamine
EPA	Environmental Protection Agency
EPS	extracellular polymeric substances
eq	equivalents
ESI	electrospray ionisation
Et	ethyl
EtAc	ethyl acetate
EtOH	ethanol
FT-IR	Fourier-transform infrared spectroscopy
GA	glutaraldehyde
GLYMO	(3-glycidyloxypropyl)trimethoxysilane
GmSiO$_2$	GLYMO-silica
h	hour
HBH	*o*-hydroxyacetophenone benzoylhydrazone
H$_2$L^1	2-thiophenecarbonyl hydrazone of 3-isatin
HMBC	heteronuclear multi-bond correlation
HRMS	high-resolution mass spectrometry
HSAB	Hard Soft Acid Base
HSQC	heteronuclear single quantum correlation
HV	accelerating voltage
I	ionic strength
ICP-MS	inductively coupled plasma mass spectrometry
ICP-OES	inductively coupled plasma optical emission spectroscopy
IR	infrared

ISO	International Organisation for Standardisation
JIS	Japanese Industry Standard
k	constant
K_d	dissociation constant
kDa	kilodalton
K_f	formation constant
kph	kilometres *per* hour
L	ligand
LA	laser ablation
LC-MS	liquid chromatography mass spectrometry
LFD	low vacuum secondary electron detector
LMB	Luria marine broth
LOD	limit of detection
Log_{10}	logarithm (base 10)
LPS	lipopolysaccharide
M	metal
m	medium (IR), multiplet (NMR)
Me	methyl
MeOH	methanol
min	minute
MIR	mid infrared
MPG	monopropylene glycol
MRI	magnetic resonance imaging
MS	mass spectrometry
MSN	mesoporous silica nanoparticle
m/z	mass-to-charge
NIR	near infrared
NMR	nuclear magnetic resonance
NO	nitric oxide
ns	not significant
NZRM	New Zealand Reference Culture Collection: Medical Section
OD_{600}	optical density (measured at 600 nm)
p	pentet
PDA	polydopamine

PDMSe	poly(dimethylsiloxane) elastomer
PEG	polyethylene glycol
PEI	polyethyleneimine
PET	positron emission tomography
phr	*per* hundred resin
ppb	parts *per* billion
ppm	parts *per* million
ppt	parts *per* trillion
Pr	propyl
PTSA	*p*-toluenesulfonic acid
QAS	quaternary ammonium salt
RCF	relative centrifugal force
ROS	reactive oxygen species
RSD	relative standard deviation
RT	room temperature
S	sonicate
s	strong (IR), singlet (NMR)
SD	standard deviation
SE	secondary electrons
SEM-EDS	scanning electron microscopy/energy dispersive X-ray spectroscopy
SFE	surface free energy
SiO_2	silica
SiO_2/epx	silica/epoxy
sp.	species
sxt	sextet
t	triplet
TBT	tributyltin
*t*Bu	*tert*-butyl
TEG	triethylene glycol
TETA	triethylenetetramine
TLC	thin-layer chromatography
TMCS	trimethylchlorosilane
TMS	tetramethylsilane
tr	technical replicate

T20	Tween 20
UV-Vis	ultraviolet-visible
V	vortex
vbr	very broad
vs	very strong
vw	very weak
w	weak
WD	working distance
WPE	weight *per* epoxide
XRC	X-ray crystallography
XRF	X-ray fluorescence

1 INTRODUCTION

1.1 BIOFOULING

1.1.1 Stages of Biofouling

Following submersion in seawater in the marine environment, an object, artificial or natural, will accumulate biological material on its surface through a process known as biofouling, beginning with the formation of a conditioning layer of adsorbed proteins, polypeptides, and polysaccharides within one minute of immersion (**Figure 1.1**, **Table 1.1**).[1–4] This molecular conditioning film, the first stage of biofouling, is the result of physical forces, such as Brownian motion, electrostatic interactions, and Van der Waals forces.[3] The succeeding biofouling stages involve colonisation by fouling organisms, which are divided into three groups: microorganisms (*e.g.* fungi, diatoms, marine bacteria, cyanobacteria, protozoans, microalgae), soft-fouling organisms (*e.g.* bryozoans, sponges, brown and multicellular algae, soft corals, anemones, tunicates, hydroids), and hard-fouling organisms (*e.g.* polychaete worms, mussels, barnacles).[2–4] In common parlance, the resultant fouling from the organisms in these three categories is referred to as slime, weed, and shell, respectively.[5,6]
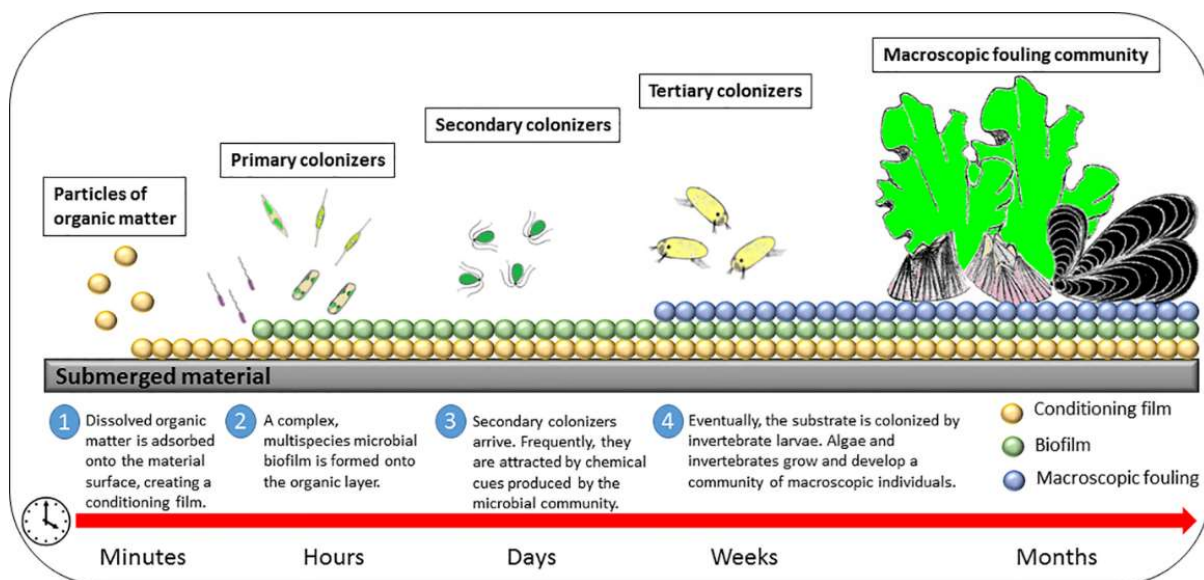
Figure 1.1. Stages of marine biofouling.[7]

Table 1.1. Stages of marine biofouling (adapted from Almeida *et al.*[3]).

Processes Involved	Attached Organisms	Nature of Film Formed	Approximate Initiation Time
STAGE 1: Physical forces (*e.g.* electrostatic interactions, Brownian motion, Van der Waals forces)	Adhesion of organic molecules (*e.g.* proteins, polysaccharides, polypeptides, proteoglycans, some inorganic molecules)	Conditioning	1 min
STAGE 2: Reversible adsorption of organisms by, usually, physical forces, and their subsequent adhesion interacting together with protozoans and rotifers	Bacteria (*e.g. Pseudomonas putrefaciens, Vibrio alginofyticos*); Fungi; Diatoms – unicellular algae (*e.g. Achnantes brevipes, Amphora coffeaeformis, Amphiprora paludosa, Nifzschia pusilla, Licmophora abbreviata*)	Microbial biofilm	1–24 h
STAGE 3: Arrangement of microorganisms with greater protection from predators, toxicants, and environmental alterations, making it easier to obtain the nutrients necessary for the attachment of other microorganisms	Spores of microalgae (*e.g. Ulothrix zonata, Enteromorpha intestinalis*); Protozoans (*e.g. Vaginicola* sp., *Zoolhamnium* sp., *Vorticella* sp.)	Biofilm	1 week
STAGE 4: Increase in the capture of more particles and organisms (*e.g.* larvae of marine macroorganisms) as a consequence of the pre-existence of the biofilm and the roughness created by the irregular microbial colonies that comprise it	Larvae of macroorganisms (*e.g. Balanus amphitrite* (*Crustacea*), *Laomedia flexuosa* (*Coelenterata*), *Electra crustulenta* (*Bryozoa*), *Spirorbis borealis* (*Polychaeta*), *Mytilus edulis* (*Mollusca*), *Styela coriacea* (*Tunicata*))	Film consisting of the attachment and development of marine invertebrates and growth of macroalgae (seaweed)	2–3 weeks

In the second stage of biofouling, the conditioning layer promotes adhesion by serving as a source of nutrients and site of interaction with organic molecules, and microorganisms, such as bacteria, fungi, and diatoms (*i.e.* unicellular algae), colonise the conditioned surface within hours of submersion.[3,8] Among these primary colonisers, bacteria are dominant due to their high concentration in seawater (10^5–10^6 cells/mL).[9] Microorganisms are transported to the surface by fluid dynamics, diffusion, gravity, Brownian motion, cell mobility, and electrostatic interactions. Their initial adhesion to the surface is reversible, resulting from weak interactions (*e.g.* Van der Waals forces, hydrophobic and electrostatic interactions). But, following the production of extracellular polymeric substances (EPS), adhesion becomes irreversible, and a microbial biofilm develops.[8] This biofilm, sometimes called microfouling, is an aggregation of attached cells embedded in the matrix of self-produced EPS, which are highly hydrated biopolymers (*e.g.* polysaccharides, lipids, nucleic acids, proteins).[4,10,11] The matrix keeps the cells in close proximity, allowing for synergistic interactions. Microbial life in a biofilm has numerous advantages compared to planktonic cells living individually: biofilm cells form microconsortia, experience enhanced nutrient acquisition from the environment, retain extracellular enzymes, communicate and cooperate intercellularly, have a large gene pool available for genetic exchanges, recycle nutrients, and display enhanced tolerance to antibiotics and biocides.[10,11] As antimicrobial substances diffuse through the biofilm, they can bind to or be degraded by EPS in the matrix, rendering them inactive.[11] These advantages allow microbial communities to thrive in the challenging marine environment in which conditions are changeable and sometimes detrimental and nutrients are often growth-limiting.[12]

The microbial biofilm may promote or deter successive stages of biofouling. Further colonisation is determined by the surface chemistry, micro-topography, and presence of microbial products.[9,13] In the case of promotion, the biofilm provides food and may contain chemical attractants, encouraging the settlement of secondary colonisers: protozoans (*i.e.* unicellular eukaryotes) and microalgal spores. These microorganisms, characteristic of the third biofouling stage, attach with polysaccharide and protein glues and add to the biofilm within one week of immersion of the substrate in seawater. This leads to the increased capture of more organisms. The fourth and final stage of biofouling occurs within a few weeks of submersion and involves colonisation by the larvae of soft- and hard-fouling macroorganisms (tertiary colonisers).[3,7,8] These larvae become fixed to the surface and grow, developing into a community of macroalgae and marine invertebrates.[4] Previous reports suggest that the inhibition of biofilm development may result in a surface unsuitable for the attachment of macrofouler larvae, and, therefore, disruption of biofilm formation may reduce biofouling.[14] However, the biofouling process is dynamic rather than successive, and a causal relationship between fouling stages should not necessarily be assumed. For instance, blocking biofilm formation will not prevent all

macrofouling; experiments have shown positive, negative, and neutral effects of bacterial biofilms on algal spore and invertebrate larvae attachment.[15] As over 4000 species of marine fouling organisms exist, the final biofouling community is highly complex and diverse.[3]

The composition of the biofouling community is dependent upon parameters related to the submerged object, as well as the seawater, geographical location, season, competition, and predation.[3,15,16] For example, the biofouling of ship hulls is influenced by the hull geometry, depth of submersion, cruising speed at sea, length of time in port, and the intensity of sunlight at the hull's surface. It is well-known that the majority of organisms responsible for the fouling of ship hulls cannot adhere to ships traveling above 4–5 knots (7–9 kph). Therefore, slow, idle ships that spend a long time in port are more vulnerable to biofouling than high-speed ships that are rarely in port. The temperature, dissolved salts, density, pH, oxygen concentration, and salinity of seawater also affect biofouling.[3,16] In particular, the temperature, salinity, and density vary with latitude, providing an explanation for the diversity of biofouling in different geographical locations. For instance, the fouling species in tropical and equatorial regions differ from those in cold and temperate regions. Although, certain species have adapted to a wide range of environmental conditions and are ubiquitous.[3] Biofouling communities are difficult to remove once established, and biofouling remains a worldwide problem for shipping industries.[17]

1.1.2 Negative Consequences of Biofouling

The fouling of ship hulls (**Figure 1.2**) results in a reduction of speed and manoeuvrability, as well as increased fuel consumption and accelerated corrosion.[17] As a ship moves through the water, the drag resulting from water moving over the hull (*i.e.* skin friction) opposes the forward motion of the ship. To maximise performance, the drag must be minimised, meaning that biofouling on the wetted hull area must be limited.[16] A study by Schultz[18] calculated power penalties caused by different fouling types and coverage on the hull of a mid-sized naval surface combatant operating at cruising or near maximum speed, and it was determined that even a light slime layer on the ship's hull would require an approximately 11% increase in shaft power relative to a clean hull. Heavy calcareous fouling was predicted to necessitate an 86% increase in shaft power. A separate study by Schultz *et al.*[19] analysed the overall cost of hull fouling of a mid-sized naval surface ship (Arleigh Burke-class destroyer DDG-51). Expenditures included hull cleaning, fuel, hull coatings, and hull coating application and removal. These expenses totalled an estimated US$56 million *per* year for the entire DDG-51 class (56 ships as of 2011), the primary cost being increased fuel consumption due to frictional drag. Fuel expenses for a fouled ship can be 30–40% greater than for an unfouled ship, and, in total, increased fuel

consumption due to biofouling is estimated to cost the US Navy greater than US$1 billion *per* year.[20] A study for International Paint by Tobias Boren[21] reported that an unprotected very large crude carrier with 40,000 m[2] underwater area can, in less than six months, gather 150 kg of fouling *per* m[2]. By using an antifouling coating on the vessel, the study reported fuel savings of 39,429 tonnes over 15 years and, consequently, cost savings of US$28.5 million.[22] The performance and economic penalties from biofouling are staggering, but they are not the only negative consequences of fouling on ship hulls.

Figure 1.2. Biofouling on ship hulls.[23]

Reprinted from *Marine Pollution Bulletin*, 62(3), Dafforn, K. A., Lewis, J. A. & Johnston E. L., "Antifouling strategies: History and regulation, ecological impacts and mitigation", 453–465, Copyright © 2011, with permission from Elsevier.

Another negative consequence of fouled ship hulls is that they have been directly responsible for the introduction of invasive species and, thus, are a threat to biosecurity.[5] For example, ship traffic is the main route by which non-indigenous marine species are introduced to New Zealand, and hull fouling is a significant mechanism for these introductions. Merchant vessels constitute 75% of international ship traffic to New Zealand but typically have little biofouling. In contrast, slower-moving commercial vessels, such as tugs and barges, constitute less than 1% of New Zealand's international ship traffic but can be heavily fouled and, consequently, a biosecurity risk.[24,25] For instance, an invasive colonial ascidian, *Didemnum vexillum* (*i.e.* carpet sea squirt), was carried on the hull of a heavily fouled barge and introduced to Shakespeare Bay, New Zealand, which is an international shipping port adjacent to an important mussel aquaculture region.[24,26] In a study by Hopkins and Forrest[24], the hull fouling on seven slow-moving commercial vessels (five barges, two tugs) in New Zealand ports was sampled over one year, and, out of the 29 identified taxa, 24% were indigenous to New Zealand, 17% were non-indigenous, and 59% were classified as unknown. Such biosecurity threats, as well as losses of efficiency and exorbitant expenses, attributed to biofouling have prompted the continuous development of antifouling technology for ship hulls.

1.2 ANTIFOULING COATINGS

1.2.1 History of Antifouling Technology

Written records of the methods employed to mitigate the adverse effects of hull fouling date back as early as the 7th century B.C., and antifouling technology has been in development since that time (**Table 1.2**).[3] The Greek philosopher Plutarch (45–125 A.D.) was the first to document the negative impact of biofouling on ship performance and that, by scraping away the slime, algae, and filth from a ship's sides, the ship could move more easily through the water.[20,27] Ancient civilisations used wax, tar, and asphalt on wooden hulls to prevent biofouling. The Carthaginians and Phoenicians (700 B.C.) were said to have used pitch and, possibly, copper sheathing, and they are credited by some sources as being the first to use copper for antifouling purposes, although this is contentious. Similarly, the Greeks and Romans (200 B.C.–45 A.D.) used lead sheathing secured with copper nails. Metallic sheathing remained a popular antifouling technique, and a British patent granted to William Beale in 1625 is the first official acknowledgement of copper's efficacy as an antifoulant. The first authenticated use of copper sheathing is by the British 32-gun frigate HMS *Alarm* (**Figure 1.3**) in 1758, for which the sheathing provided protection against shipworms and fouling during its deployment to the West Indies. However, the corrosion of iron when in contact with copper was noted. Copper was widely used by the British Navy in the 1780s, but, following the introduction of iron ships in the late-18th century, copper sheathing was nearly abandoned due to its dangerously corrosive effects on iron. In the early-19th century while studying the corrosion process, Sir Humphrey Davy discovered that the mechanism of action by which copper prevents biofouling is dependent upon copper's dissolution in seawater. This further complicated the use of copper sheathing, since strategies proposed to prevent corrosion did not allow for the dissolution of copper. Thus, alternative antifouling methods were explored; specifically, antifouling paints were developed in the mid-19th century (**Table 1.3**).[3,4,27,28]

Figure 1.3. British 32-gun frigate HMS *Alarm.*

Image: https://commons.wikimedia.org/wiki/File:HMS_Alarm_(1758).jpg.

Table 1.2. Antifouling products used prior to the mid-19th century (adapted from Almeida *et al*.[3]).

Approximate Time Period	Civilisation/Navigator	Antifouling Product
Oldest	Oldest	Wax, tar, asphalt
700 B.C.	Phoenicians, Carthaginians	Pitch, possibly copper sheathing
700 B.C.	Phoenicians	Lead sheathing, tallow
500 B.C.	Phoenicians	Coatings of sulfur and arsenic mixed with oil
300 B.C.	Greeks	Wax, tar, lead sheathing
200 B.C.–45 A.D.	Romans, Greeks	Lead sheathing with copper nails
10 A.D.	Vikings	Seal tar
45–125 A.D.	Plutarch	Scraping slime, algae, and filth from the ship's sides
13th–15th centuries	Several	Pitch and mixtures with resin, oils, or tallow
	Columbus	Pitch and tallow
1618–1625	Various	Copper, possibly with a mixture of powdered iron, cement, and a copper compound (copper sulfide or copper arsenic ore)
18th century	Various	Sacrificial wooden sheathing on a layer of animal hair and pitch
		Wooden sheathing covered with mixtures of tar, fat, sulfur, and pitch, with numerous metallic nails arranged with their heads forming a type of metallic sheathing
1758	English (Frigate HMS *Alarm*)	Copper sheathing (abandoned for causing galvanic corrosion of iron nails)
1786	English	Copper sheathing, using copper and zinc alloy nails
Early-19th century	English	Sir Humphrey Davy demonstrated that copper dissolution in seawater prevented fouling
1758–1816	Various	Sheathing of lead, zinc, arsenic, nickel, and galvanised steel and alloys of tin, zinc, and antimony followed by copper-plated wood sheathing
		Non-metallic sheathing (ebonite, rubber, enamel, cork, *etc.*)
1862	Various	Wood sheathing covered with copper sheathing (abandoned due to cost)
Mid-19th century	Various	Paints containing a toxicant (copper, arsenic, or mercury oxides) dispersed in a polymeric binder (shellac, linseed oil, colophony)

Table 1.3. Antifouling paints used on steel hulls after the mid-19th century (adapted from Almeida *et al.*[3]).

Product Type	First Used	Main Components	
		Binder	**Pigment/Biocide**
First paints	Mid-19th century	Linseed oil, shellac varnish, tar, resins	Copper, arsenic, or mercury oxides
Application of insulating primer under antifouling paint	1847	Linseed oil, shellac varnish, tar, and resins; preliminary insulating varnish coating	Copper, arsenic, or mercury oxides
"Hot plastic paints"	1860	Metallic soap composition, colophony	Copper sulfate, other copper compounds
Antifouling paint	1863	Tar	Copper oxide
Rust preventer	Late-19th century	Shellac primer and shellac antifouling paint	Different toxicants
Spirit varnish paints	1908–1926	Grade A "Gum Shellac"	Red mercury oxide or zinc oxide, zinc dust and India red
"Cold plastic paints"	1926	Coal tar or coal tar + colophony, shellac varnish, synthetic resins	Copper or mercury oxides
First organo-metallic paints	1950–1960	Acrylic esters or others	Copper compounds ± co-biocides
Soluble matrix	1950	Colophony and others	Copper, arsenic, zinc, mercury, or iron oxides
Insoluble matrix or contact paint	1955	Acrylic resins, vinyl resins, chlorinated rubber polymers	Copper and zinc oxides ± organo-metallic compounds
Self-polishing paints containing tin	1974–1985	Acrylic polymer with TBT groups bonded to main chain by ester binders (copolymer)	Zinc oxide and insoluble pigments or copper oxide, tri-organo-tin, and co-biocides

Antifouling paints on ship hulls minimise biofouling and, therefore, frictional drag leading to increased fuel costs. In general, a paint is composed of a varnish and pigment (**Figure 1.4**). The varnish includes additives, the film-former (*i.e.* binder), and the solvent/diluent. Additives are substances that are added to the paint to perform special jobs, such as additives functioning as antifoulants (*i.e.* toxicants, biocides). When the paint is in its liquid form, it may contain chemical ingredients of the binder that will polymerise during the process of curing. When the paint is dry and cured, the binder is the resultant polymer (*e.g.* acrylic, polyurethane, epoxy) or the resin (*e.g.* rosin or colophony, shellac) that binds together all of the other paint components. The mixture of the binder and liquid is referred to as the vehicle for the pigment. The primary, coloured pigment, which is made up of fine organic (*e.g.* phthalocyanin blue) or inorganic (*e.g.* titanium dioxide) particles, has protective and decorative functions, providing colour, opacity, and other visual effects. An inexpensive extender (*i.e.* filler) consisting of coarse inorganic particles is often used in conjunction with the primary pigment to achieve a desired effect at a lower cost (*e.g.* calcium carbonate as a matting agent with titanium dioxide).[29,30] The first antifouling paints were based on the dispersal of a toxicant in a polymeric binder.[3]

PAINT

PIGMENT

- **COLOURED PIGMENT**
- **EXTENDER**

VARNISH

- **FILM-FORMER**
  - Polymer (or reactive components)
  - Plasticiser
- **LIQUID**
  - Solvent
  - Diluent
- **ADDITIVES**
  - Thickener
  - Flow agent
  - Matting agent
  - Catalyst
  - Accelerator
  - Inhibitor
  - Wetting agent
  - Dyestuffs
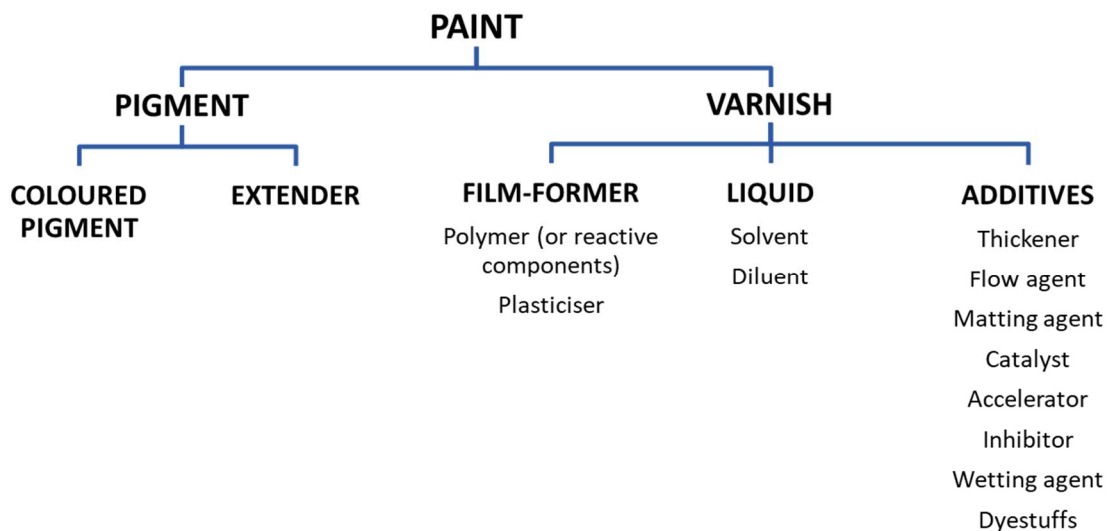
Figure 1.4. Paint components (adapted from *Introduction to Paint Chemistry*).[29]

Following renewed interest in antifouling coatings in the mid-19th century, the number of such products increased rapidly. Popular compositions utilised copper, arsenic, or mercury oxides as pigments or antifouling additives dispersed in the linseed oil, shellac varnish, tar, or other resins serving as coating binders (**Table 1.3**). However, since the toxicants were in direct contact with the

ship hull, corrosion was still a problem for the first steel hulls, and, consequently, primers (*i.e.* undercoats) emerged to protect the hulls. The first organometallic paints containing tin, mercury, arsenic, and other metals appeared in the mid-20th century.[3,27,28]

1.2.2 Biocide-Based Antifouling Coatings

The new biocide-based antifouling coatings began to be classified according to their toxicant release-mechanism, and the three main classifications still in use are soluble matrix (*i.e.* ablative, erodible, controlled depletion), insoluble matrix (*i.e.* contact), and self-polishing paints (**Table 1.3**, **Figure 1.5**). Soluble matrix paints incorporate seawater-soluble binders based on rosins (*i.e.* colophony) and their derivatives and toxic pigments, such as copper, iron, or zinc oxides. Because of their solubility in seawater, they have poor mechanical strength and erode constantly, assuring protection against antifouling for only 12–15 months. Insoluble matrix paints contain binders that are insoluble in seawater (*e.g.* vinyl, acrylic, epoxy, or chlorinated rubber polymers) and contain high concentrations of antifoulants (*e.g.* copper and zinc oxides ± organometallic compounds). As successive toxicant layers are dissolved or eroded by seawater penetrating the film, toxicants deeper in the coating have farther to diffuse, leading to a gradual decrease in the toxicant release rate and antifouling efficacy over time. Therefore, although these paints are mechanically strong, they have a short antifouling lifetime (12–24 months).[3,28]
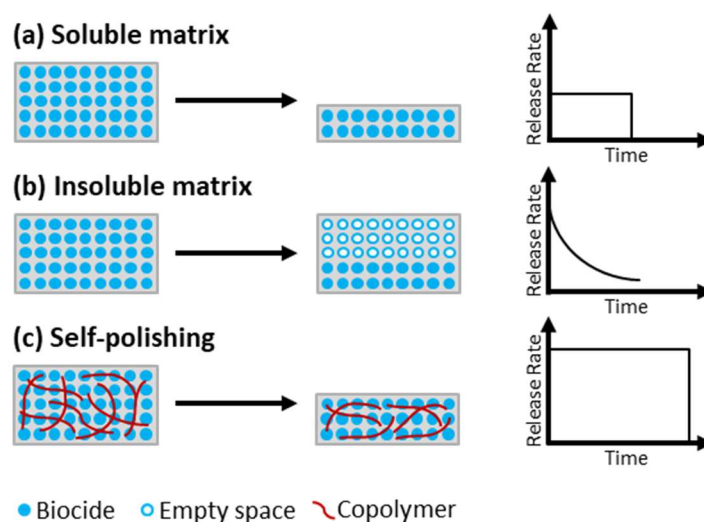
Figure 1.5. Classifications of biocide-based antifouling paints: (a) soluble matrix, **(b)** insoluble matrix, and **(c)** self-polishing paints (adapted from Yang *et al.*[31]).

Self-polishing paints have a hydrophobic matrix composed of a biocide linked to a polymer, and hydrolysis in the coating results in release of the biocide. A widely used organometallic paint of this type, introduced in 1974, contained tributyltin (TBT) groups bonded to the acrylic polymer chain (derived from methyl methacrylate) by hydrolytically unstable ester bonds, resulting in the slow, controlled release of TBT in seawater over time (**Scheme 1.1**). With the dissolution of pigment particles and consequent release of TBT from increased exposure to seawater, the surface of the film would become brittle and erode to expose a fresh layer of the active coating (self-polishing effect). The TBT self-polishing paint had a much longer lifetime, being up to five years, and was hugely successful in preventing biofouling.[2–4,23,28]
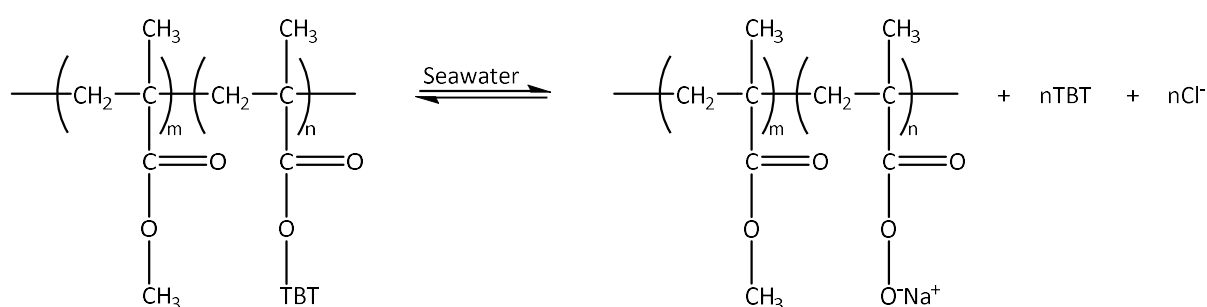
Scheme 1.1. Hydrolysis of TBT from the acrylic polymer (methyl methacrylate) in a TBT self-polishing paint.[3]

Following their introduction in 1974, TBT self-polishing paints became enormously popular, and their use was widespread – so much so that, in 1999, it was estimated that 70% of all commercial ships were coated with them, saving US$2.4 billion *per* year in fuel and other costs.[3] TBT is the most effective broad-spectrum antifoulant ever developed, having toxicity to molluscs, crustaceans, algae, and fish.[2,23] For years, it seemed like hull fouling would be a problem of the past, but, as soon as the early 1980s, the profoundly negative effects of TBT on non-target organisms were noted.[23] TBT leaching from coated ship hulls was environmentally damaging, for example, inducing sex changes in sea snails and dogwhelks.[2,22,32] Consequently, the use of TBT was restricted further and further until it was finally banned from use in coatings on all vessels after 1 January 2008 by the International Maritime Organization. Copper has replaced TBT as the biocide in many antifouling paints, and, with over 90% of US Navy ships coated with a copper ablative (*i.e.* soluble matrix) paint, copper-based antifouling coatings are the current standard in antifouling technology.[2,23,33]

Copper was viewed as a safe alternative to TBT because historical precedents exist for its use as an antifoulant, it is an essential trace element for all plants and animals, and it is naturally present in

seawater.[3] Antifouling coatings usually incorporate copper as metallic copper, cuprous oxide (Cu_2O), or copper thiocyanate (CuSCN), and such copper-impregnated coatings designed to slowly release copper vary in their copper content from 20% to 76%.[8,34] Since seawater is oxygenated, the released copper is rapidly oxidised to Cu(II), the primary biocidal form. Yet, Cu(II) is not an efficacious antifoulant for all marine foulers, and, from most to least, the order of Cu(II)-sensitivity among fouling organisms is as follows: microorganisms, invertebrates, algae, and macrophytes (*i.e.* aquatic plants). Additionally, the copper ions released from the paint often become bound to natural ligands in seawater, further reducing their toxicity.[3]

In copper-based antifouling coatings, formulations for the inert matrix and delivery are variable (*e.g.* copolymers, self-polishing, epoxy-based, ablative), differing in the passive flux of copper according to the matrix. However, all formulations require periodic (monthly) cleaning of the ship hull.[2,8,34] Due to the copper tolerance of some algal species (*e.g. Enteromorpha* sp.), the majority of copper antifouling paints also contain a booster biocide, often an herbicide detrimental to the growth of photosynthetic organisms, to target these algae. The most common commercially available booster biocides include Irgarol 1051, Diuron, Zineb, Sea-Nine 211, Chlorothalonil, and metallic compounds zinc pyrithione and copper pyrithione, and these biocides are meant to be less harmful to the environment than copper.[3,8,23,28] A toxicity study by Amara *et al*.[8] reported that, out of the common booster biocides, Diuron and Irgarol 1051 seem to be the least environmentally harmful, while Chlorothalonil and Sea-Nine 211 seem to be the most. Conversely, a study by Voulvoulis *et al.*[35] identified Zineb and zinc pyrithione as being less environmentally harmful than Diuron and Irgarol 1051, so the toxicity effects of the booster biocides have yet to be fully elucidated.[3] Although copper coatings are an effective method to mitigate fouling, the leaching of copper from these antifouling paints has become an environmental concern because of the toxic effects of elevated copper concentrations on non-target organisms.[36]

Widespread prohibition of copper-based paints has not yet occurred, but they are increasingly being banned due to concerns about copper leaching, especially in sensitive ecosystems.[22,37] For instance, antifouling paints leaching excessive amounts of copper have been restricted by the Swedish Chemicals Agency, which regards all copper-based paints as unacceptable for use on leisure boats (< 12 m) in the vulnerable Baltic Sea.[37] Despite copper being an essential trace element, copper concentrations higher than physiologically necessary are toxic to many marine organisms, including those not targeted by antifouling measures.[2] For instance, Andersson and Kautsky[38] found that even low concentrations of copper (*e.g.* 2.5 ppb) in brackish water could have detrimental effects on the reproduction of *Fucus vesiculosus* (*i.e.* bladderwrack), a key species in the Baltic Sea. This is particularly concerning because the release of *F. vesiculosus* gametes coincides with the launching of newly

painted leisure boats, which are major contributors (~30%) to the total copper burden in Swedish inland and coastal waters.[38,39] Additionally, Ytreberg, Karlsson, and Eklund[40] reported that, in semi-enclosed areas with high boat traffic, copper leached from antifouling paints may attain toxic concentrations for the non-target macroalga *Ceramium tenuicorne*. In places with little water exchange, such as marinas and harbours, therefore, elevated copper levels are a concern.[23] The average concentration of copper in seawater is approximately 2 ppb, but concentrations up to 22 ppb in a marina in San Diego Bay and 114 ppb in the coastal waters of India have been recorded, for instance.[41,42] Furthermore, antifouling paint particles shed during periodic hull maintenance (*e.g.* scraping, sandpapering, water blasting) and winter storage pollute the soil with copper at concentrations often exceeding national guidelines, possibly leaching into ground water.[1,36] Given the substantial diversity of fouling organisms (> 4000 species), a major challenge for biocide-based antifouling paints is finding an antifoulant that reduces target species but spares non-target species. Due to this challenge and the uncertain future of copper-impregnated coatings, the marine coatings industry desires alternatives to biocide-based antifouling paints.[15]

1.2.3 Biocide-Free Coatings

Biocide-free coatings utilise the surface physico-chemical and bulk materials properties (*e.g.* elastic modulus, frictional coefficient) of the film to either deter adherence of fouling organisms or reduce the strength with which they do attach, allowing for removal by shear forces as the ship moves through the water or is mechanically cleaned. This approach is dependent upon the molecular interactions between the surface of the film and the adhesive polymers (*e.g.* EPS) secreted by the fouling organisms. Thus, biocide-free coatings employ two different strategies, resulting in them being classified as antifouling or fouling-release coatings. Biocide-free antifouling coatings are unconducive to colonisation by fouling organisms and, therefore, prevent initial attachment, while fouling-release coatings weaken the interaction between the foulers' secreted adhesive polymers and the film surface after initial attachment. However, it should be noted that these two strategies are not mutually exclusive.[15]

1.2.3.1 Hydrophilic Antifouling Coatings

Hydrophilic coatings are a common type of biocide-free antifouling coating, containing hydrophilic polymer brushes that prevent or reduce the initial attachment of proteins, bacteria, and marine

foulers. Their preparation usually involves the application of a monolayer of polyethylene glycol (PEG) brushes to a surface by grafting with a, typically, siloxane linker (**Figure 1.6**).[22] PEG is the most commonly used polymer to stop protein adsorption to surfaces, and it is thought that the flexibility and large steric repulsion forces of the PEG chains discourage the approach of foulers.[43,44] A study by Roosjen *et al.*[45] reported a reduction in the attachment of bacteria (*Staphylococcus epidermidis*, *Pseudomonas aeruginosa*) and yeast (*Candida albicans*, *Candida tropicalis*) to a PEG brush-coated surface, with the initial attachment rate and number of adherent bacteria decreasing with increasing brush-length. Despite their success in reducing bacterial colonisation and preventing protein adsorption, these PEG coatings are of limited use, as they are quite fragile and even minor surface defects drastically reduce their efficacy. Additional drawbacks are that they are sensitive towards hydrolysis and oxidation.[22]
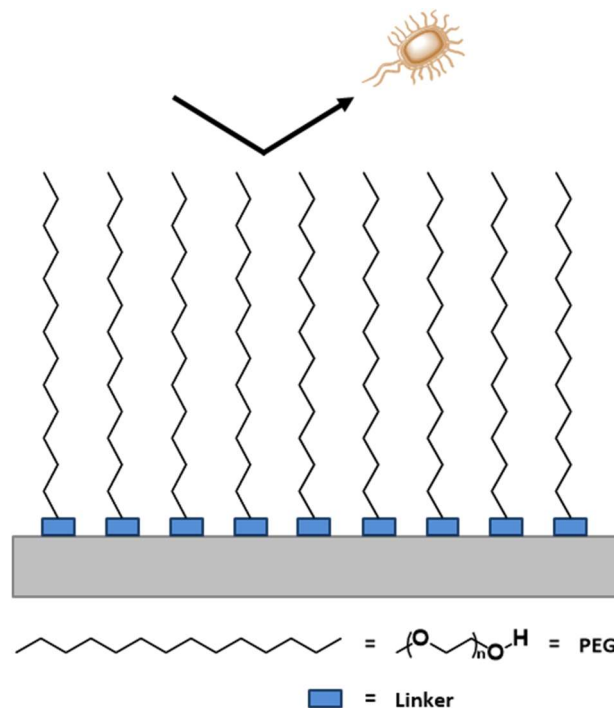
Figure 1.6. Hydrophilic antifouling coating with PEG brushes attached to the surface by a linker.[22]

1.2.3.2 Fouling-Release Coatings

Fouling-release coatings have an ultra-smooth, low-friction, hydrophobic surface that results in weak interactions between the surface and the foulers' adhesive polymers, enabling biofouling removal by shear forces (**Figure 1.7**). The smooth, glossy surface results in a decrease in frictional drag, allowing

for ships to achieve maximal speeds with minimal fuel consumption, and the hydrophobicity of the surface discourages the adhesion of polar molecules (*e.g.* adhesive proteins). Fouling-release coatings also have a low surface energy and low elastic modulus, providing little resistance to the removal of fouling organisms. Surface energy, determined by contact angle measurements, is the excess energy of surface molecules compared to those in the coating interior,[3,15,22,28,46] and the elastic modulus is the resistance of the film to elastic (*i.e.* "springy") deformation.[47] Other coating requirements to prevent adhesion are as follows:

1) A flexible, linear backbone,

2) A surface that is smooth at the molecular level, which precludes infiltration by biological adhesives,

3) A large number of active groups capable of moving freely over the surface, imparting the desired surface energy,

4) A thickness capable of controlling fracture mechanics (*e.g.* crack propagation) at the surface/adhesive interface,

5) High molecular mobility in the surface-active sidechains and backbone, and,

6) In addition to the requirements above, molecules that are stable in seawater for long periods of time.[48]
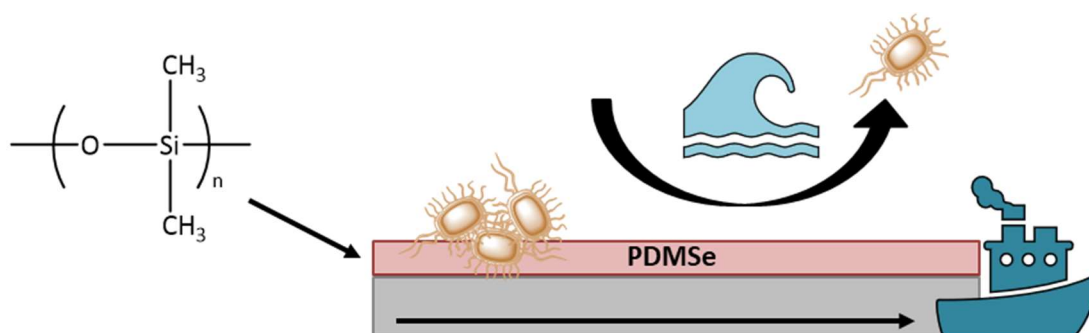
Figure 1.7. Detachment of marine foulers from a PDMSe-based fouling-release coating by shear forces as the vessel moves through the water.[28]

The only two types of materials that satisfy all of these requirements are fluoropolymers and silicones. Currently, the majority of commercial fouling-release coatings incorporate poly(dimethylsiloxane) elastomers (PDMSe; *i.e.* elastic polymers; **Figure 1.7**), which are hydrophobic and nonpolar and have a low surface energy and low microroughness. Due to the conformational mobility of their surfaces,

they appear as "moving targets" to functional groups of the adhesive polymers, deterring adhesion, and their lifetime is approximately two years. Fouling-release coatings are regarded as the best of the biocide-free coatings, yet they have several disadvantages. They need the ship to be moving through the water at a minimum speed of 22 knots (41 kph) to detach fouling organisms, and, accordingly, they are most effective for high-speed vessels and may be inappropriate for slower vessels that spend a long time in port. They are also expensive, demonstrate poor substrate-adhesion, and are soft and easily damaged.[3,15,22,28,46] As a result, the search continues for other environmentally friendly alternatives to biocide-based antifouling coatings.

1.2.4 Recent Developments

Numerous antifouling strategies have been inspired by natural phenomena, since many plants and animals are resistant to fouling. Some of the recent developments in environmentally friendly antifouling technology, many of them bioinspired, are discussed below.

1.2.4.1 Biomimetic Topographies

Multiple studies over the past 50 years have demonstrated that surface topography in the micrometre range influences cellular attachment.[49–54] For example, in a study by Carman *et al.*[55], the microscale topography (*e.g.* diamondlike riblets) of the naturally antifouling skin of fast-moving sharks was replicated on the surface of a PDMSe coating. This biomimetic coating, Sharklet AF™, was tested for the settlement of zoospores of the soft-fouling, green alga *Ulva linza*, which is a model system for biofouling experiments. It was found that zoospore settlement on Sharklet AF™ was reduced by approximately 85%. Other biomimetic surfaces have duplicated the topographies of the skin of pilot whale *Globicephala melas* and surfaces of fouling-resistant plants.[56] For instance, Fu *et al*.[57] duplicated the ridge-like surface morphology of the leaves of mangrove tree *Sonneratia apetala*, as these leaves are practically immune to biofouling. Following settlement tests with tubeworm larvae, it was confirmed that the replica could prevent biofouling.

1.2.4.2 Superhydrophobic Surfaces

Bioinspired superhydrophobic surfaces have been developed for antifouling purposes. Superhydrophobic surfaces have high contact angles (> 150°) and, therefore, are very difficult to wet.

They rely on the trapping of air and resist fouling by dramatically reducing contact between the surface and the fouler. The most famous example of this surface type in nature is the lotus leaf, on which water moves freely to collect contaminants and then roll off the surface. This self-cleaning mechanism (*i.e.* lotus leaf effect) is a result of the superhydrophobicity of the surface. The leaf's surface is coated in low surface energy waxes and has two structural levels: microscale mounds decorated with nanoscale hair-like structures (hydrophobic hydrocarbon tubules). Due to the entrapment of a stable air cushion by the hierarchical micro/nanostructures, interactions between the surface and water are substantially reduced, precluding the attachment of fouling organisms.[15,44,49,58] The multilevel structure of the lotus leaf has been replicated, for instance, by Zorba *et al.*[59] through ultrafast (femtosecond) irradiation of a silicon surface, producing an artificial surface equal to the lotus leaf in its ability to repel water.

1.2.4.3 Zwitterionic Polymers

Zwitterionic polymers, containing both cationic and anionic groups, are well-known for deterring protein adsorption and have been used extensively in antifouling materials. The deterrence of protein adsorption is attributed to the electrostatically induced hydration layer serving as a barrier to proteins; the superhydrophilic surface prefers to bind water molecules, rather than biological material. Zwitterionic polymers are classified as polybetaines, which have positive and negative charges in the same monomer unit, or polyampholytes, which have positive and negative charges in a 1:1 ratio on separate monomer units.[2,15,31,44,60,61] In a study by Zhang *et al.*[62], poly(sulfobetaine methacrylate) brushes were grafted onto glass surfaces, and these grafted surfaces inhibited the attachment of zoospores of the green alga *Ulva* and cells of the diatom *Navicula*. It was also demonstrated that the attachment strength of *Ulva* sporelings was low.

1.2.4.4 Amphiphilic Polymers

In an effort to combine the antifouling properties of hydrophobic and hydrophilic coatings, amphiphilic polymer coatings possessing both hydrophobic and hydrophilic blocks have been prepared. Fouling organisms are known to have diverse preferences regarding the hydrophobicity of a surface, and such an ambiguous surface is expected to "confuse" foulers during attachment and settlement, leading to a reduction in biofouling.[2,15,31,43,61] Gudipati *et al.*[63] published the first example of an amphiphilic marine antifouling coating, which was prepared by crosslinking diamino-terminated PEG (hydrophilic) and hyperbranched fluoropolymers (hydrophobic). The same lab group later

demonstrated reduced adsorption of proteins and lipopolysaccharides and reduced settlement of *Ulva* zoospores in compositions with high concentrations of PEG (45–55% w/w).[15,64]

1.2.4.5 Enzyme-Based Coatings

In recent years, enzyme-based antifouling coatings have gained attention, as they are thought to be harmless to the environment. The enzymes interfere with biofilm formation by two mechanisms: 1) quenching bacterial quorum sensing signals and 2) degrading the EPS matrix of the biofilm.[44,65] Intercellular communication between bacterial cells in a biofilm occurs *via* quorum sensing, during which the concentration of signalling molecules (*i.e.* autoinducers) secreted by bacteria in the biofilm increases with increasing cell density. Once the autoinducer concentration reaches a certain threshold, the quorum sensing bacteria respond as a group by altering their gene expression.[44,66] Most autoinducers (*e.g. N*-acyl-homoserine lactones, AHLs) are involved in biofilm formation and maturation and the regulation of bacterial virulence factors. Therefore, enzymes capable of quenching these signals (*e.g.* AHL lactonases, AHL acylases) have been incorporated in coatings to prevent bacterial colonisation.[44]

Coatings have also been prepared by incorporating enzymes with the ability to degrade the biofilm matrix. The EPS matrix, composed of polysaccharides, proteins, nucleic acids, and lipids, is secreted by microorganisms in the biofilm and plays a vital role in adhesion to the substrate. Consequently, enzymes, such as proteases (to degrade the proteins) and glycosylases (to degrade the polysaccharides), have been included in coatings to hinder bacterial attachment.[44,67] For instance, Tasso *et al.*[68] surface-functionalised maleic anhydride copolymer thin films with protease Subtilisin A and discovered that the coating reduced the adhesion strength of diatom *Navicula perminuta* cells and the settlement and adhesion strength of green alga *Ulva linza* zoospores. Unfortunately, enzyme-based coatings have limitations to their use because they are less stable in warm marine environments (*e.g.* the tropics).[67]

1.2.4.6 Quorum Sensing Inhibitors

The use of quorum sensing inhibitors in antifouling materials has been studied as another method for interfering with bacterial quorum sensing and, subsequently, reducing microfouling. Numerous marine organisms have evolved mechanisms to block bacterial quorum sensing, and these mechanisms include the inhibition of autoinducer production, enzymatic degradation of autoinducers

(as previously discussed), inhibition of DNA transcription, and competition with or suppression of autoinducer receptors.[69,70] For example, red alga *Delisea pulchra* produces halogenated furanones with similar structures to AHL autoinducers produced by marine bacteria. Accordingly, these AHL mimics displace AHL from its receptor, reducing bacterial adhesion and swarming.[69–72] Such quorum sensing inhibitors could serve as additives in antifouling coatings. In fact, Ozcelik *et al.*[73] incorporated a synthetic quorum sensing inhibitor (5-methylene-1-(prop-2-enoyl)-4-(2-fluorophenyl)-dihydropyrrol-2-one) in a PEG-based coating, and biofilm formation by *Staphylococcus aureus* and *Pseudomonas aeruginosa* was reduced on the prepared coating. It should be emphasised that, even though such inhibitors reduce colonisation by microorganisms, they would not necessarily prevent all biofouling.

1.2.4.7 Bacteria

Marine bacteria colonising a surface secrete many different bioactive compounds to inhibit fouling by other marine organisms (micro- and macro-foulers), securing them a competitive advantage. For example, marine bacterium *Pseudoalteromonas tunicata* (strain D2) produces at least four bioactive, extracellular molecules with activity against a variety of marine foulers.[2] Egan *et al.*[74] identified one of these molecules, which is heat-sensitive, polar, and 3–10 kDa in size, and this compound inhibited the germination of spores from the red alga *Polysiphonia* sp. and the common green alga *Ulva lactuca*. Therefore, research has been conducted regarding the incorporation of such bioactive natural products – or the bacteria that produce them – in antifouling coatings. Although, since these compounds often rapidly degrade in the marine environment, work needs to be done to extend their lifetimes when formulated in antifouling coatings.[2,75]

1.3 THESIS OBJECTIVE: COORDINATION OF CU(II) IN SEAWATER TO CREATE A RECHARGEABLE ANTIFOULING COATING

Despite the extensive research concerning "green" antifouling technology, copper-based antifouling coatings remain the current standard. Many of the mechanisms recently in consideration to combat biofouling have yet to overcome challenges associated with their commercialisation, such as high cost, instability, and a lack of broad-spectrum activity. Therefore, at this time, a comparable product has not achieved widespread commercial success, and the field is open to new possibilities. The project herein proposes a novel antifouling strategy that utilises copper as a biocide but circumvents the environmental concerns about copper leaching.

1.3.1 Concept

For this work, it has been proposed that antifouling technology can be developed to create marine paints that draw their biocidal ingredient, metals such as copper, zinc, cadmium, and chromium, from the sea. This is a revolutionary concept: no currently used antifouling paints draw their active component from seawater. Although the biocidal mode of action of these paints would be the same as existing paints pre-charged with metals, the environmental concerns and tightening regulations regarding metal-leaching would no longer be applicable; such paints would self-prime and self-regenerate from pre-existing metals in seawater. No new metals would be introduced to the marine environment. The technology would work by covalently binding ligands capable of selective metal ion complexation to components (*e.g.* binder, additives) in paint systems (**Figure 1.8**). High ligand concentrations in the paint would be required, and, at these high concentrations, the ligands would, in principle, capture enough of the metal to reach concentrations toxic to fouling organisms, thus preventing biofouling when applied to ship hulls. The project will initially focus on Cu(II) as the biocidal agent since it is currently the primary active form in copper-based antifouling paints and its efficacy has been well-documented. The specific aim of this project is to create a rechargeable, Cu(II)-based antifouling coating for use in the marine environment, but it has been acknowledged that such a coating would also have applications in the medical field, as nosocomial (*i.e.* hospital-acquired) infections and biofilm formation on implanted devices (*e.g.* artificial prostheses, catheters, dental implants, *etc.*) remain serious problems that could be mitigated by effective antimicrobial coatings.[76]
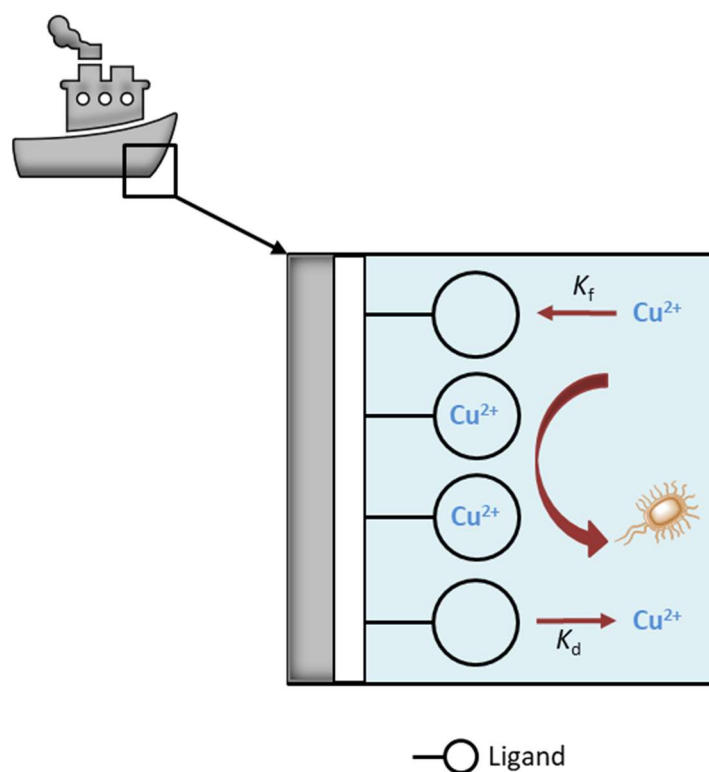
Figure 1.8. The goal of this project is to create a rechargeable Cu(II) coating by incorporating Cu(II)-selective ligands to bind Cu(II), making the coating antimicrobial and antifouling. This depends on the Cu(II) flux at the surface, which is related to the complex's formation (K_f) and dissociation (K_d) constants.

Previous research supports the viability of this route of inquiry. For instance, Lindén et al.[77] were the first to report on the use of polyethyleneimine (PEI)-based materials to scavenge Cu(II) from seawater for antifouling purposes. These glutaraldehyde (GA) crosslinked PEI, nano-thin coatings have demonstrated the efficient and preferential accumulation of Cu(II) from seawater, achieving a maximum Cu(II)-loading of 2% w/w.[77] Further work by this group has concerned the effect of the conditioning layer between the GA-PEI coating and seawater and of competing ligands in seawater on Cu(II)-binding.[78] They recognised that the flux of Cu(II) at the seawater/coating interface is necessary for antimicrobial activity (**Figure 1.8**) and could be impeded by the presence of the conditioning layer. This flux is dependent on the strength of the Cu(II) complex, which is described by its formation (K_f) and dissociation (K_d) constants (**Equation 1.1**), but the group acknowledged that the release of Cu(II) may require an artificial intervention, such as an electrochemical stimulus.[77,79] Furthermore, considering that > 99% of the Cu(II) dissolved in seawater is already strongly complexed by unidentified organic ligands with formation constants in the range of 10^9–10^{14}, the ligand in the coating would have to be a stronger Cu(II)-chelator than the natural ligands in seawater

(*i.e.* $K_f > 10^{14}$).[80] To model the conditioning layer and competing ligands, the GA-PEI film was coated with polysaccharides alginate and/or carrageenan, and the uptake of Cu(II) at the concentrations of contaminated harbours in artificial seawater was tested in the presence of competing-ligand ethylene diamine tetraacetic acid (EDTA). It was discovered that, in seawater, the polysaccharide layer swelled, allowing Cu(II) to diffuse readily, and GA-PEI outcompeted strong Cu(II)-chelator EDTA for Cu(II).[78] In regard to this work, the research group has applied for a patent.[81] Building on these studies, Elmas *et al.*[82] explored the controlled, electrochemical release of Cu(II) from crosslinked, porous PEI coated on conducting carbon cloth electrodes, and they reported that the coating could store and release Cu(II) in multiple cycles *via* the application of only 1 mA/cm^2 of current density through the electrode in artificial seawater. These results are encouraging and provide evidence for the feasibility of this project.

$$M + L \rightleftharpoons ML \qquad\qquad K_f = \frac{[ML]}{[M][L]} \qquad\qquad K_d = \frac{[M][L]}{[ML]}$$
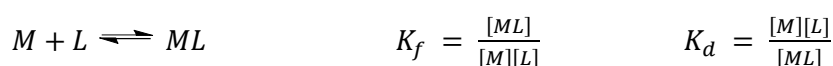
Equation 1.1. The formation (K_f) and dissociation (K_d) constants of a metal-ligand complex (M = metal, L = ligand).

1.3.2 Practical Considerations

In a preliminary approach to this project, there are questions that must be answered before proceeding:

1) How is a Cu(II) ligand designed?
2) What factors influence the stability of the Cu(II) complex, and how is the Cu(II) complex characterised?
3) What are the options for formulating the Cu(II) ligand in a coating?
4) What are the surface toxicity mechanisms of Cu(II)?

1.3.2.1 Design of Cu(II) Ligands

Since many other transition metal ions exist in seawater, the ligand chosen or designed and synthesised for this project must be selective for Cu(II). Selectivity depends on matching the "hardness" or "softness" of the Lewis acids (*i.e.* metal ions, *e.g.* Cu(II)) and Lewis bases (*i.e.* donor atoms of ligands), according to the Hard Soft Acid Base (HSAB) theory proposed by Ralph G. Pearson in 1963. In a coordination compound, the coordinate bond between the metal ion and the donor atom

of the ligand displays a certain polarity, dictating the ionic character of the bond. Small, highly charged Lewis acids have a high surface charge density, which results in their electron clouds being drawn inward and, thus, less efficient at the orbital overlap necessary for covalent bonding. Such ions are classified as "hard acids" and have a preference for ionic bonding. "Hard bases" are weakly polarisable and highly electronegative. In contrast, large, low-charged Lewis acids with a low surface charge density are classified as "soft"; their more diffuse and expanded electron clouds are better-suited for orbital overlap, so they have a preference for covalent bonding. "Soft bases" are highly polarisable and weakly electronegative. According to the "like prefers like" principle of the HSAB theory, hard ligands prefer hard metals, and soft ligands prefer soft metals. Cu(II) is classified as "borderline" (**Table 1.4**), meaning that it is between hard and soft, and it usually forms 4–6 coordinate bonds with hard bases (*e.g.* carbonyl and carboxylate oxygens, amines), borderline bases (*e.g.* azoles, pyridine), and/or sulfur.[83–87]

Table 1.4. Examples of hard, soft, and intermediate ligands and metal ions (adapted from *Introduction to Coordination Chemistry*[84] and Hancock and Martell[85]).

Hard	Borderline	Soft
Ligands		
F^-, O^{2-}, HO^-, H_2O, HOR, RO^-, R_2O, $CH_3CO_2^-$, RCO_2^-, NH_3, NR_3, RNH_2, RCN, Cl^-, NO_3^-, CO_3^{2-}, SO_4^{2-}, PO_4^{3-}, ClO_4^-	Br^-, RS^-, SO_3^{2-}, NO_2^-, N_3^-, N_2, SCN^-, $C_6H_5NH_2$, C_5H_5N, $C_3N_2H_4$	PR_3, RSH, R_2S, RS^-, SeR_2, AsR_3, CNR, CN^-, SCN^-, CO, I^-, H^-, R^-, C_2H_4, $S_2O_3^{2-}$
Metal Ions		
Mo^{5+}, Ti^{4+}, V^{4+}, Sc^{3+}, Cr^{3+}, Fe^{3+}, Co^{3+}, Al^{3+}, Eu^{3+}, Ga^{3+}, Cr^{2+}, Mn^{2+}, Ca^{2+}, Mg^{2+}, Be^{2+}, Sr^{2+}, Ba^{2+}, K^+, Na^+, Li^+, H^+	Sb^{3+}, Bi^{3+}, Rh^{3+}, Fe^{2+}, Co^{2+}, Ni^{2+}, **Cu^{2+}**, Zn^{2+}, Pb^{2+}, Sn^{2+}	Pt^{4+}, Te^{4+}, Pd^{2+}, Pt^{2+}, Hg^{2+}, Cd^{2+}, Cu^+, Hg^+, Rh^+, Ag^+, Au^+, Br^+, I^+, Tl^+

Well-documented Cu(II) ligands include polyamines, D-penicillamine, and EDTA. Macrocyclic (*e.g.* cyclen, cyclam) and linear (*e.g.* triethylenetetramine, TETA) polyamines (**Figure 1.9**) are known to be highly selective chelators of Cu(II) over other transition metals.[88,89] In fact, TETA has been used for more than two decades as an orphan drug in the treatment of Wilson's disease.[88,90] Wilson's disease is caused by a genetic mutation that leads to impaired copper detoxification in the liver and an accumulation of copper, primarily Cu(II), to toxic levels in the body.[86] D-Penicillamine is also used to treat Wilson's disease, but it is a less specific transition metal chelator.[88] It was introduced as a treatment in 1956 before TETA, and it is used worldwide, whereas TETA is mainly used in the US.[86]

Both drugs bind excess copper and promote its urinary excretion.[91] EDTA is relatively non-specific in its binding, yet Fe(III), Al(III), and Cu(II) form the most stable chelates.[92]
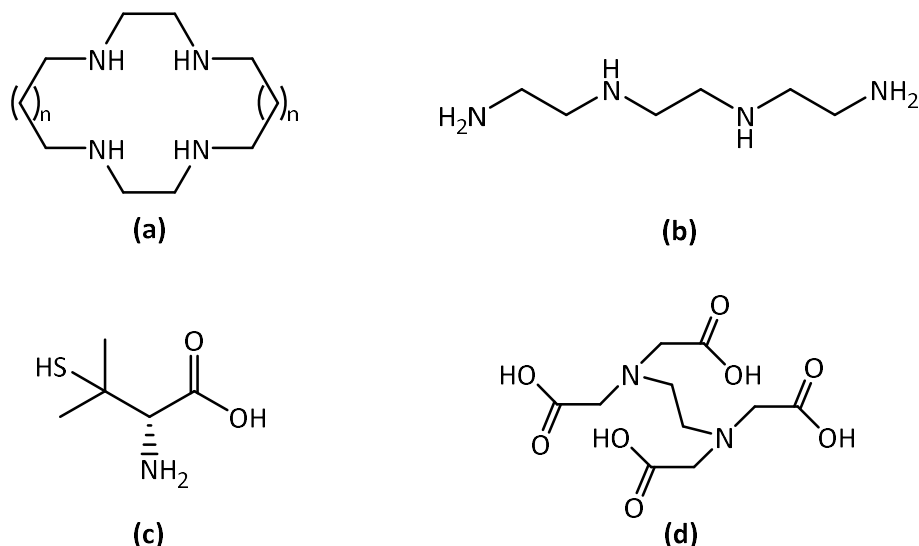
Figure 1.9. Examples of well-documented Cu(II) ligands: (a) cyclen (n = 0) or cyclam (n = 1), **(b)** TETA, **(c)** D-penicillamine, and **(d)** EDTA.

1.3.2.2 Cu(II) Complexes: Stability and Characterisation

In addition to the match in "hardness" between the metal ion and ligand's donor atoms, the stability of the metal complex is influenced by other factors dependent on the metal ion and the ligand. Regarding the metal ion, these factors include size, charge, and crystal field effects. A high formation (*i.e.* stability) constant is favoured by a high surface charge density, or, in other words, small, highly charged ions produce more stable metal complexes. For a series of transition metal ions (octahedral) with a 2+ charge, a general trend in the value of K_f exists, regardless of the ligand:

$$Mn^{2+} < Fe^{2+} < Co^{2+} < Ni^{2+} < Cu^{2+} > Zn^{2+}.$$
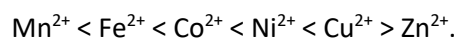
According to this trend, called the natural order of stabilities (*i.e.* Irving-Williams series), Cu(II) forms the most stable complexes, irrespective of the ligand. The position of Zn(II) within the series is variable. The stability of Cu(II) complexes may be explained, in part, by the trend of ionic radii:

$$Mn^{2+} > Fe^{2+} > Co^{2+} > Ni^{2+} < Cu^{2+} < Zn^{2+}.$$
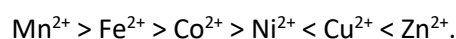
However, Cu(II) (electron configuration [Ar]3d^9), like other metals with an incomplete set of d electrons, receives a contribution to its stability from the crystal field stabilisation energy (CFSE).[84]

Crystal field theory (CFT) is a model that describes, upon formation of the metal ion-ligand complex, the effect of the ligands' electronic charges on the energies of the electrons in the d-orbitals of the metal ion. The CFSE is the additional stability that arises from placement of the metal ion in the crystal field produced by a set of ligands, and it is due to splitting of the d-orbitals in the ligand field.[93] For example, most d-block metals, including Cu(II), form six-coordinated complexes with an octahedral coordination geometry (**Figure 1.10**). Because of this geometry, the $d_{x^2-y^2}$ and d_{z^2} orbitals of Cu(II) experience repulsive forces due to their alignment with the ligands and, consequently, are higher in energy than the d_{xy}, d_{xz}, and d_{yz} orbitals. The octahedral geometry of Cu(II) experiences Jahn-Teller distortions in which either the equatorial bonds are longer than the axial (*i.e.* compression) or the axial bonds are longer than the equatorial (*i.e.* elongation; more common), and these deformations are more stable than the regular octahedral geometry.[94,95] This enhancement of the CFSE explains the exceptional stability of Cu(II) complexes.[84]
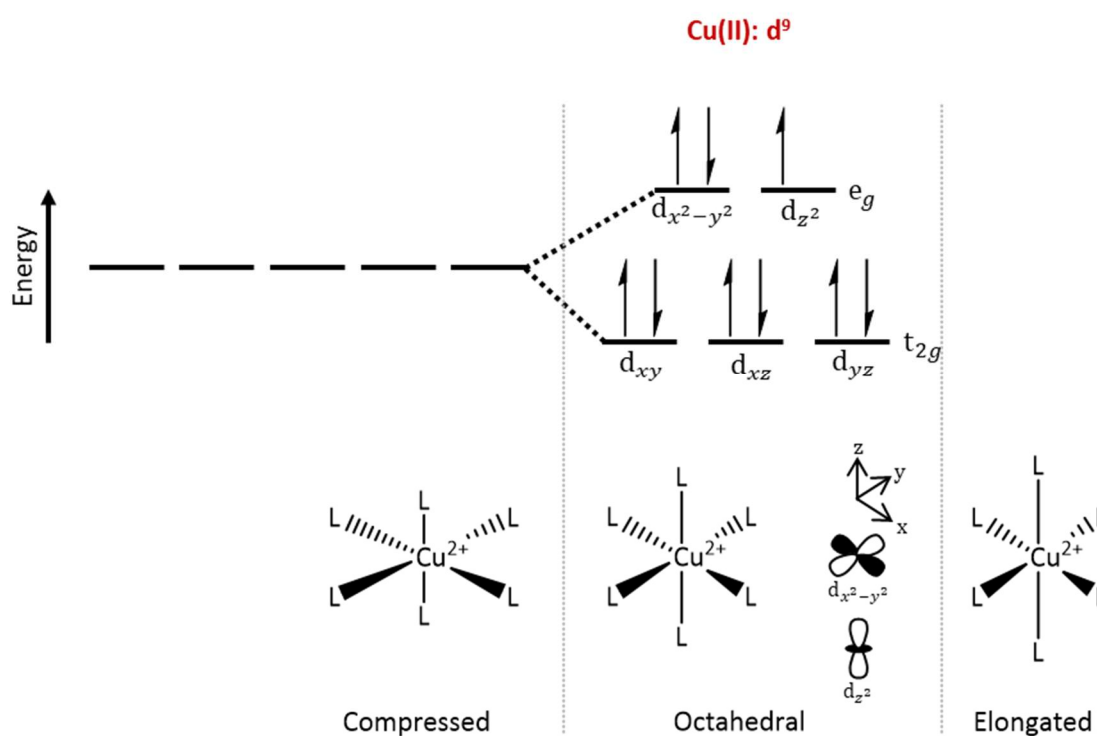
Figure 1.10. Crystal field splitting and structure of Cu(II) when complexed by ligands (L) in a six-coordinate, octahedral geometry, which may be elongated or compressed due to Jahn-Teller distortions.[96]

The factors influencing metal complex stability that are related to the ligand include base strength, the chelate effect, chelate ring size, and steric strain. First, as the base strength (*i.e.* affinity for H$^+$) of a ligand increases, its affinity for hard metal ions increases, and, therefore, the stability of the resultant

metal complex increases.[84] Second, the chelate effect is the observation that a metal complex formed with a bidentate or polydentate ligand has a higher K_f than a metal complex formed with an equal number of monodentate ligands containing the same donor atom (**Figure 1.11**).[97,98] A monodentate ligand binds a metal ion through one donor atom. When one ligand contains two donor atoms that bind the metal ion, it is called bidentate, and, when three or more donor atoms bind, the ligand is called polydentate. Complexes formed from bidentate and polydentate ligands are referred to as chelate complexes.[99] Third, the size of the chelate ring also influences stability, and saturated, five-membered rings form the most stable complexes with first-row d-block metals (**Figure 1.12**). Finally, when coordinating a metal ion, ligands containing large, bulky groups that interact sterically yield less stable complexes.[84]

$$K_f \, [\text{Cd(en)}_2]^{2+} \quad > \quad K_f \, [\text{Cd(NH}_2\text{Me)}_4]^{2+}$$
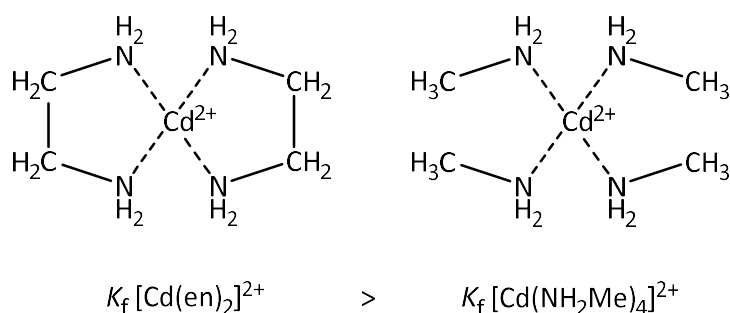
Figure 1.11. Example of the chelate effect. Ethylenediamine (en) is bidentate, and methylamine (NH$_2$Me; Me = methyl) is monodentate.[97]

3-membered < 4-membered < 5-membered > 6-membered > 7-membered
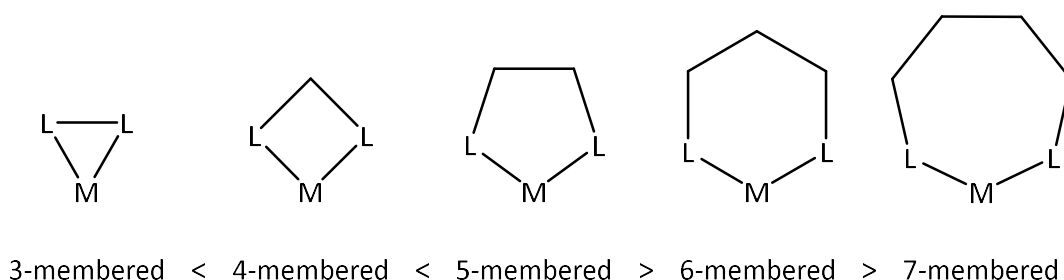
Figure 1.12. Trend of stability depending on chelate ring size for first-row d-block metals (M = metal, L = ligand).[84]

An understanding of the factors that influence the stability of a coordination compound is essential for designing and tuning the ligand in this project, as the ligand must be a stronger Cu(II)-chelator than the natural ligands in seawater (*i.e.* $K_f > 10^{14}$).[80] The formation constant of a metal complex can be

26

measured *via* numerous methods, including spectrophotometry, potentiometry, pH metric equilibrium studies, competitive equilibria, cation exchange resins, liquid-liquid partitioning, and nuclear magnetic resonance (NMR) spectroscopy. To determine K_f by spectrophotometric methods, the ultraviolet-visible (UV-Vis) spectra of a series of solutions of the ligand (L) and metal (M), for which the mole ratio $\left(\frac{[L]}{[M]+[L]}\right)$ varies from zero to one, are measured.[100] Nowadays, the data are analysed by computer programs, such as the HYPERQUAD suite of programs by Gans *et al.*[101], that calculate K_f.

Spectrophotometric methods are also used to construct Job plots to determine the stoichiometry of metal complexes (*i.e.* 1:1 M:L, 1:2 M:L, *etc.*). This is done by mixing aliquots of two equimolar solutions in such a manner that the mole ratio $\left(\frac{[L]}{[M]+[L]}\right)$ varies from zero to one but the total analytical concentration of metal plus ligand remains constant ([M] + [L] = k, k = constant). The absorbance of each solution is measured at a selected wavelength and plotted as a function of the mole ratio. The resultant curve is called a Job plot, and the peak absorbance of the curve reveals the metal:ligand ratio of the complex in solution. For example, as in **Figure 1.13**, a maximum at 0.5 for the mole ratio indicates that the stoichiometry of the complex is 1:1 metal:ligand. The requirements that must be met for a Job plot to be valid are as follows: conformance to Beer's law, one predominant complex, constant total analytical concentration of metal plus ligand, and constant pH and ionic strength.[102,103] For the current project, knowledge of the stoichiometry of the complex in solution is important for planning the formulation of the ligand in a coating, recognising that this stoichiometry might change once the ligand is immobilised in a film.
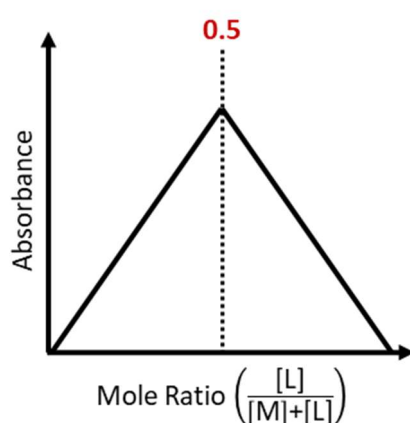
Figure 1.13. Example Job plot of a metal complex with 1:1 metal:ligand stoichiometry.

Various analytical techniques are employed to further characterise Cu(II) complexes. For instance, infrared (IR) spectroscopy is used to identify functional groups in a complex, and mass spectrometry (MS) measures a coordination compound's mass-to-charge ratio (*m/z*). Electronic transitions are observed using UV-Vis spectroscopy. CHNS elemental analysis gives the elemental concentrations of carbon, hydrogen, nitrogen and sulfur, while the Cu(II) concentration is determined *via* inductively coupled plasma mass spectrometry (ICP-MS), inductively coupled plasma optical emission spectroscopy (ICP-OES), or scanning electron microscopy/energy dispersive X-ray spectroscopy (SEM-EDS). Other common techniques include molar conductivity, magnetic susceptibility, and thermal analyses (*e.g.* thermogravimetric analysis, differential thermal analysis). X-ray crystallography (XRC) is one of the most useful techniques, as it reveals the structure and geometry of the complex.[104–108] Accordingly, these are all techniques that can be considered for the characterisation of Cu(II) complexes in this project. However, the use of NMR spectroscopy is limited due to the paramagnetic nature of Cu(II). Paramagnetic ions, atoms, or molecules have unpaired electrons (*e.g.* d^9 Cu(II)) and, thus, permanent magnetic moments, causing the broadening of NMR signals.[108,109]

1.3.2.3 Formulation of Cu(II) Ligands in Coatings

Several routes exist for incorporating the Cu(II) ligand in a coating. As seen in **Figure 1.4**, a paint is composed of a binder, additives, and pigments carried in a solvent,[29] and all of these components present an opportunity for functionalisation with the ligand. Although, in the literature, the more popular route seems to be the incorporation of the ligand in the polymeric binder.[41,79,87,110,111] For example, Trojer *et al.*[87] reported methods for affixing pendant azole ligands, which are strong Cu(II)-chelators, to polymers for protection against fouling organisms. El-Wahab *et al.*[112] simply add-mixed arylhydrazone ligand *o*-methoxybenzaldehyde benzoylhydrazone and its metal complexes in a polyurethane coating, and the film containing the Cu(II) complex had antimicrobial activity against Gram-positive and -negative bacteria and fungi. Evidence also exists that pigments can be functionalised with small molecules. For instance, González-Rodríguez *et al.*[113] modified the surface of titanium dioxide with glutaric acid to improve the dispersion of these pigments in waterborne paints. Therefore, these are all routes that can be explored in this project for formulating the Cu(II) ligand in a coating, but the initial focus should be on the binder.

1.3.2.4 Mechanisms of Cu(II) Surface Toxicity

In this work, an understanding of the mechanisms of Cu(II) surface toxicity to marine foulers is vital because it guides the coating design towards more effective antifouling formulations. After centuries of use as a disinfectant, copper and its alloys, being able to kill 99.9% of pathogenic bacteria in 2 h, were officially recognised in 2008 by the Environmental Protection Agency (EPA) as the first effective metallic antimicrobial agents.[114] Although copper is an essential trace element in the majority of living organisms, it is toxic at high concentrations.[1,115] Cu(II) is considerably less cytotoxic than Cu(I), but oxidising conditions (*e.g.* aerobic, aqueous) favour the formation of Cu(II).[116,117] Copper compounds and elemental copper have a broad spectrum of antimicrobial activity against fungi, viruses, and bacteria by several mechanisms, such as enzyme inhibition (*e.g.* through iron displacement in iron-sulfur clusters), disrupting plasma membrane integrity, degrading DNA, and causing oxidative damage to DNA and proteins by reactive oxygen species (ROS).[117,118] Upon exposure to copper ions, the likely sequence of events is membrane damage followed by the rapid influx of copper ions and, subsequently, oxidative damage, cell death, and DNA degradation (**Figure 1.14**). Therefore, the antimicrobial effect of copper surfaces has been linked to their ability to release copper ions,[114,115,117,119–121] and designing a system that allows the flux of Cu(II) at the surface is crucial for the success of this project.
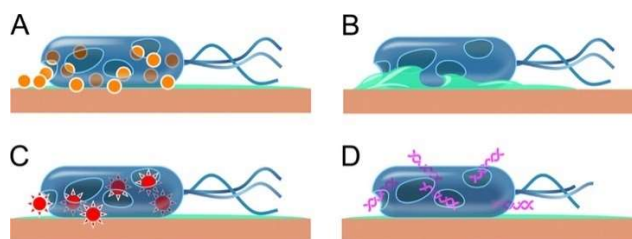
Figure 1.14. Sequence of events upon copper contact: (a) ionic copper causes cell damage, **(b)** the cell membrane ruptures, leading to the expulsion of cytoplasmic content, **(c)** ROS are generated and cause further cell damage, and **(d)** plasmid and genomic DNA are degraded (reproduced with permission: copyright © 2011, American Society for Microbiology).[115]

The exposure of microfoulers to copper results in a reduction of biofilm biomass, but the effect on macrofoulers is indirect and less understood. In a biofilm, copper is sequestered by components of the EPS, and the copper concentration in the biofilm rises until reaching a plateau. This copper can be retained by the biofilm for up to four weeks and is referred to as the "copper legacy". Macrofoulers seem to be more affected by this copper legacy than by direct exposure to copper: the presence of

copper changes the structure and composition of the microfouler biofilm and, consequently, macrofouler settlement, as it is mediated by chemical and biological characteristics of the biofilm. Due to differences in copper tolerance, the copper legacy selects for surface colonisation by more copper-tolerant species, but this mechanism is not well-understood.[122] For the current project, knowledge of these toxicity and antifouling mechanisms of Cu(II) directs the focus of attention on the microfouling stage.

1.3.3 Strategy

In light of all of these practical considerations, a multistage strategy emerges for meeting the goals of this project (**Table 1.5**). In the first stage, a ligand must be chosen based on selectivity and stability. Since Cu(II) is classified as borderline, the donor atoms should be hard bases, borderline bases, and/or sulfur to ensure the ligand is selective for Cu(II). The ligand must also be a stronger Cu(II)-chelator than the natural ligands in seawater (*i.e.* $K_f > 10^{14}$), and stability may be tuned by altering the ligand's base strength, denticity, chelate ring size, or steric strain. The Cu(II) complex will be characterised *via* the discussed methods and analytical techniques (*e.g.* Job plot, IR, MS, *etc.*). The second stage of the project will involve formulation of the ligand into a coating by modifying the polymeric binder, additives, or pigments, focusing first on the binder. The third stage will require the development and implementation of methodology to test the ability of the coating to coordinate and retain Cu(II) and to test the coating's subsequent antimicrobial activity. The results of the antimicrobial assay are intended to be reflective of the Cu(II) surface toxicity in the microfouling phase of biofouling. These relatively quick tests are important because they serve as the first filters for identifying a lead product. In the fourth and final stage of the project, time-permitting, the antifouling ability of this lead product will be tested in the marine environment.

Table 1.5. Stages of this project.

Stage	Description
1	Ligand chosen based on selectivity and stability
2	Incorporation of the ligand in a coating (binder, additives, pigments)
3	Development and implementation of the methodology to test the coating's Cu(II)-loading and antimicrobial activity
4	Test the antifouling ability of the lead product in the marine environment

2 SELECTION AND SYNTHESIS OF CU(II) LIGANDS

2.1 BACKGROUND

Chapter 1 (**Section 1.3.2**) discussed general considerations in the design of Cu(II) ligands (*e.g.* donor atom selection, chelate ring size, *etc.*), but, in the present work, the selection or design and synthesis of Cu(II) ligands must also be guided by the intended application. The application is to imbue a coating with antifouling properties through incorporation of the ligand and subsequent Cu(II)-loading from seawater to the requisite concentration. Therefore, it is essential that the ligand maintain its selectivity, stability, and performance both when it is formulated in a coating and when it is exposed to the marine environment. Furthermore, selection of the ligand should also be considered from the perspective of financial viability. Large quantities of the ligand should be cheaply accessible, meaning that it is synthesised in only a few high-yield steps, ideally, from non-hazardous reagents and solvents (*e.g.* water). Once synthesised, the product should be able to be easily manipulated for incorporation in a paint. This requires the ligand to have a functionalisable handle, such as an amine or hydroxyl functional group, for possible covalent modification of paint components. For instance, formulation of the ligand in the paint may involve covalent alteration of the paint binder or additives with the ligand, which is a route that could be chosen for numerous reasons, including increased ligand-retention in the paint. A ligand with a solubility profile compatible with such manipulations would also be beneficial, since highly insoluble compounds can be more difficult to characterise and modify. Following retention in a coating, the immobilised ligand should perform similarly to its unbound state,[123] remaining in the proper orientation to chelate Cu(II), and interaction of the immobilised ligand with the metal ions in seawater is essential.

To be successful in the marine environment, an ideal Cu(II)-chelator must meet certain criteria. First, the ligand's Cu(II)-selectivity should be retained in the presence of the significantly higher concentrations of alkali and alkaline earth metals in seawater.[123] As seen in **Figure 2.1**, the composition of seawater is complex, consisting of solids, gases, colloids, and dissolved solutes. The dissolved solutes are organic and inorganic, and the inorganic solutes consist of major (> 1 ppm) and minor (< 1 ppm) metals. The major metals in seawater, in order from most to least prevalent, are alkali and alkaline earth metals Na, Mg, Ca, K, and Sr, ranging from 10.76 g/kg (= parts *per* thousand) for Na to 0.0078 g/kg (7.8 ppm) for Sr (**Table 2.1**). In contrast, Cu (2 μg/L ≈ 2 ppb), present as Cu(II), and other transition metals are minor components in seawater (**Table 2.2**).[42] So, for this project, the ligand is required to still be selective for Cu(II) in the presence of all the major and minor metal ions in seawater. As previously discussed (Chapter 1, **Section 1.3.2.1**), a factor influencing the selectivity and stability of

metal complexes is the match between the metal ion and donor atom(s) of the ligand, according to the "like prefers like" principle of the HSAB theory. This theory classifies Cu(II) as borderline, preferring nitrogen donors. Other transition metal ions in seawater classified as borderline include Co(II), Ni(II), Zn(II), and Pb(II). Conversely, alkali and alkaline earth metal ions, such as the major metal ions in seawater (*i.e.* Na(I), Mg(II), Ca(II), K(I), and Sr(II)), are classified as hard and prefer oxygen donors. The disparity in donor preference between Cu(II) and the alkali and alkaline earth, as well as some of the transition, metal ions can, thus, be exploited in the design and selection of a Cu(II)-chelator, while additional factors will need to be considered for the other borderline transition metal ions.[42,83–85]

SEAWATER

- SOLIDS[a]
  - Particulate organic material (plant detritus)
  - Particulate inorganic material (minerals)
- GASES
  - Unreactive (N_2, Ar, Xe)
  - Reactive (O_2, CO_2)
- COLLOIDS[b]
  - Organic
  - Inorganic
- DISSOLVED SOLUTES
  - Inorganic solutes
    - Major (> 1 ppm)
    - Minor (< 1 ppm)
  - Organic solutes
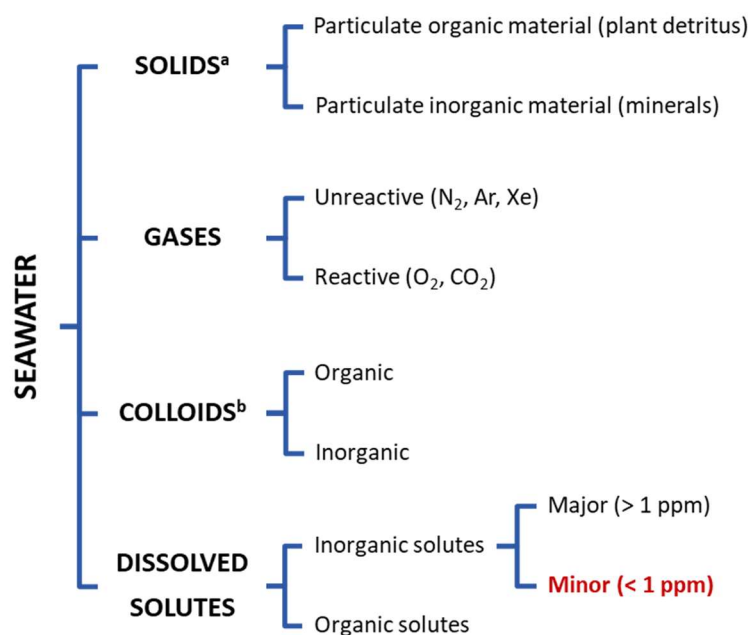
Figure 2.1. Major components of seawater (adapted from *Practical Handbook of Marine Science*).[42] [a] Material that does not pass through a 0.45 μm filter. [b] Passes through a 0.45 μm filter but is not dissolved.

Table 2.1. Major metals in seawater (alkali and alkaline earth metals).[a]

Metal	Probable Species	Concentration (g/kg)[b]	
		Average	**Range**
Ca	Ca^{2+}	0.4119	0.4098–0.4134
K	K^+	0.399	0.393–0.405
Mg	Mg^{2+}	1.297	1.292–1.301
Na	Na^+	10.76	10.72–10.80
Sr	Sr^{2+}	0.0078	0.0074–0.0079

[a] Adapted from *Practical Handbook of Marine Science*.[42]
[b] Normalised to 3.5% salinity.

Table 2.2. Minor metals in seawater (> 0.01 µg/L; transition metals).[a]

Metal	Probable Species	Concentration (µg/L, ≈ ppb)[b]	
		Average	**Range**
Ag	$AgCl_2^-$	0.29	0.055–1.5
Au	$AuCl_2^-$	0.068	-
Cd	$CdCl_2^-$	0.113	0.02–0.25
Co	Co^{2+}, $CoCO_3$	0.27	0.035–4.1
Cr	CrO_4^{2-}	0.3	0.23–0.43
Cu	**$CuCO_3$**	**2**	**0.2–4.0**
Fe	$Fe(OH)_3$	6.6	0.1–62
Hg	$HgCl_4^{2-}$	0.03	-
Mn	Mn^{2+}	1.5	0.2–8.6
Mo	MoO_4^{2-}	1	0.24–12.2
Nb	$NbCO_3^+$	0.01	0.01–0.02
Ni	$NiCO_3$	5.4	0.43–43
Pb	$PbCO_3$	0.06	0.02–0.4
Sc	$Sc(OH)_3$	0.04	-
Ti	$Ti(OH)_4$	1	-
V	HVO_4^{2-}, $H_2VO_4^-$	2.5	2.0–3.0
W	WO_4^{2-}	0.1	-
Y	YCO_3^+	0.0133	0.0112–0.0163
Zn	Zn^{2+}, $ZnOH^+$	6.5	2–18
Zr	$Zr(OH)_4$	0.026	-

[a] Adapted from *Practical Handbook of Marine Science*.[42]
[b] The concentration in µg/L is approximately equal to the concentration in ppb, since the density of seawater is 1.025 g/mL.[42]

The second requirement to be a successful Cu(II)-chelator in the marine environment is that the ligands and Cu(II) complexes must be stable in seawater's typical pH range. The pH of seawater is dependent on the cycle of dissolved carbon dioxide in seawater: 1) gaseous carbon dioxide in the atmosphere becomes dissolved in seawater, 2) the aqueous carbon dioxide is utilised for photosynthesis by marine plants but also equilibrates with water to produce carbonic acid, dissociating sequentially to form bicarbonate and carbonate ions, 3) solid calcium carbonate is generated and used by marine plants and animals to make shells, and 4) aqueous carbon dioxide is regenerated at greater depths from the oxidative destruction of organic matter. Carbonic acid, a weak acid, and its associated anions, bicarbonate and carbonate ions, act as a pH buffer system and stabilise the ocean pH at approximately 8.1. Although, the pH of deep waters can be as low as 7.5 due to the regeneration of carbon dioxide from the breakdown of organic matter.[124,125] The state of protonation of donor atoms in the Cu(II) ligand should be considered, since, for instance, neutral amine groups coordinate Cu(II) more readily than ammonium salts. But, as seawater is slightly alkaline, this is not as much of a concern. For example, Chouyyok *et al.*[126] prepared three nanoporous sorbents with diamine functionalities to chelate the Cu(II) in natural waters and found that, in seawater, Cu(II)-binding increased with increasing pH until it was at peak absorption at the pH of seawater (*i.e.* 8.1). However, in the present work, the stability of the ligand alone, as well as the stability of its Cu(II) complex, should also be appraised; in particular, the ligand should be hydrolytically stable at the pH of seawater and non-toxic. After all, a hydrolytically unstable ligand introducing new, toxic components into seawater from an antifouling paint would unequivocally fail to meet the specifications of the project.

To summarise, in the context of the application for this work, the ideal ligand should:

1) Be cheaply prepared in large quantities,
2) Be easily manipulated for incorporation in a coating,
3) Perform similarly to its unbound state when immobilised in a coating,
4) Retain its Cu(II)-selectivity in the presence of the major and minor metal ions in seawater, and
5) Be hydrolytically stable at pH 7.5–8.1, the pH range of seawater, and form stable complexes.[123]

2.2 Polyacylhydrazone: Dilevulinoyl Diethylene Glycol (DiLevDEG)/Adipic Acid Dihydrazide (ADH)

The present study was inspired by previous, foundational work by our research group in which a water-soluble polyacylhydrazone synthesised from dilevulinoyl diethylene glycol (DiLevDEG) and adipic acid dihydrazide (ADH) was successfully incorporated as part of the resin in a commercial acrylic paint (**Figure 2.2**). This DiLevDEG/ADH polyacylhydrazone was of interest due to its suitability for formulation in waterborne coatings and its derivation from renewable components, making it a "greener" film-forming additive than its petrochemical-derived counterparts. Evaporation of water from a concentrated (50% w/v), aqueous (aq) solution of DiLevDEG/ADH yielded a film that was glassy and hard, yet flexible. Consequently, the aqueous DiLevDEG/ADH polymer solution was used to substitute 30–50% w/w of the crosslinking resin in an acrylic paint, and the resultant coating performed well in standard industry tests for gloss, adherence, and hardness and displayed moderate water resistance.[127] The group noted that the acylhydrazone functionality (–C(=O)–NH–N=CR–) of DiLevDEG/ADH had the potential to coordinate Cu(II) (**Figure 2.3**) in a five-membered chelate ring by bidentate coordination through the carbonyl oxygen and azomethinic nitrogen atom, inspiring the idea that ligands could be incorporated in paint systems to impart antimicrobial activity following Cu(II)-chelation.
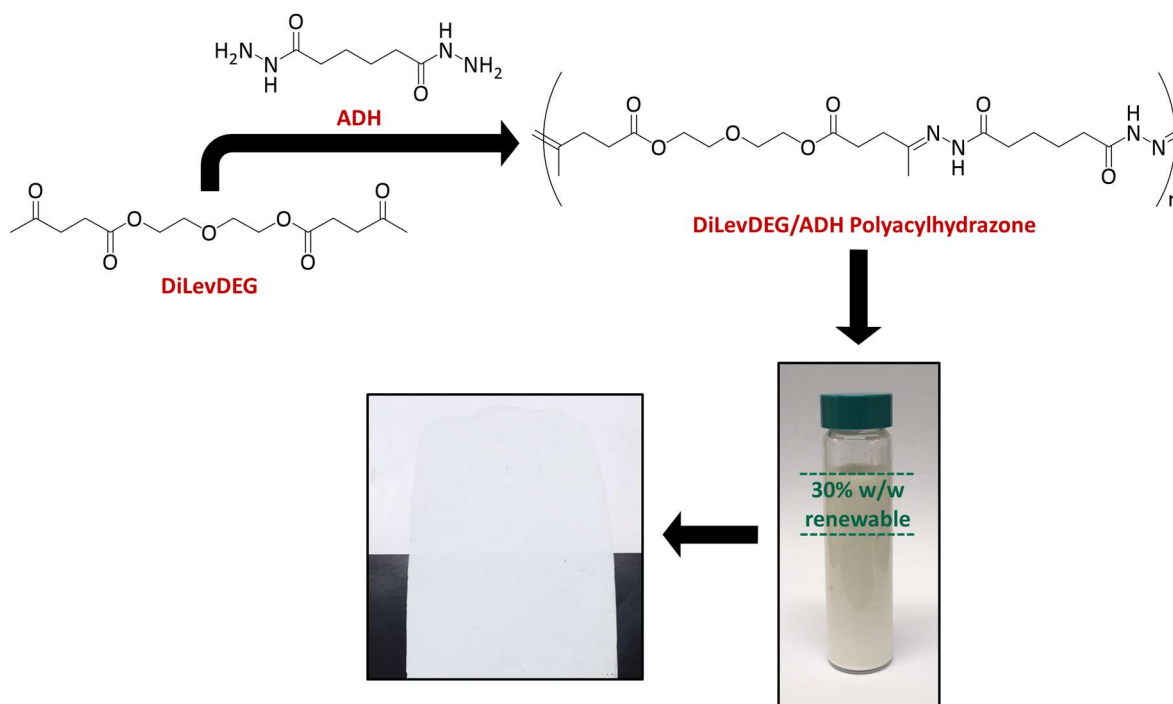
Figure 2.2. The DiLevDEG/ADH polyacylhydrazone, synthesised from DiLevDEG and ADH, substituted 30% w/w of the resin in a commercial acrylic paint with renewable components.[127]
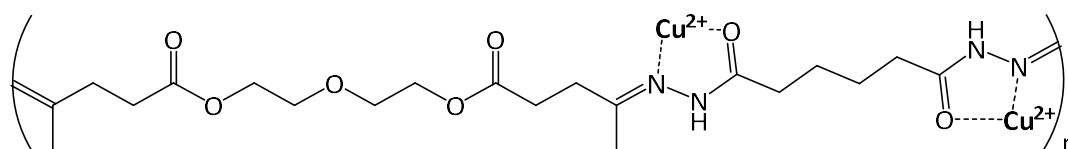
Figure 2.3. Proposed Cu(II)-chelation by the acylhydrazone functionality in DiLevDEG/ADH.

Since DiLevDEG/ADH had already been successfully formulated into a paint, it seemed reasonable to begin the present work by using this polyacylhydrazone as a proof-of-concept, even though, being a novel polymer, its affinity and selectivity for Cu(II) were unknown. The first stage of work required the synthesis of DiLevDEG/ADH and confirmation of its ability to chelate Cu(II). The second stage involved formulation of DiLevDEG/ADH into the commercial acrylic paint and evaluation of the coating's Cu(II)-loading when exposed to a Cu(II) salt solution and its subsequent antimicrobial activity. The first stage will be discussed below, and the second stage will be discussed in Chapter 3 (**Section 3.2**).

The DiLevDEG/ADH polyacylhydrazone was synthesised in two steps, following the procedures of Daines *et al.*[127] (**Scheme 2.1**). DiLevDEG was produced in the first step in a Fischer esterification reaction by heating diethylene glycol (DEG), *p*-toluenesulfonic acid (PTSA) monohydrate, and levulinic acid under reduced pressure and collecting the generated water by distillation. Cessation of water production signalled completion of the reaction, and DiLevDEG was isolated as an orange, viscous oil. In the second step, formation of the polyacylhydrazone proceeded by adding ADH to a solution of DiLevDEG in water, giving a clear, viscous solution of ~50% w/v solids.
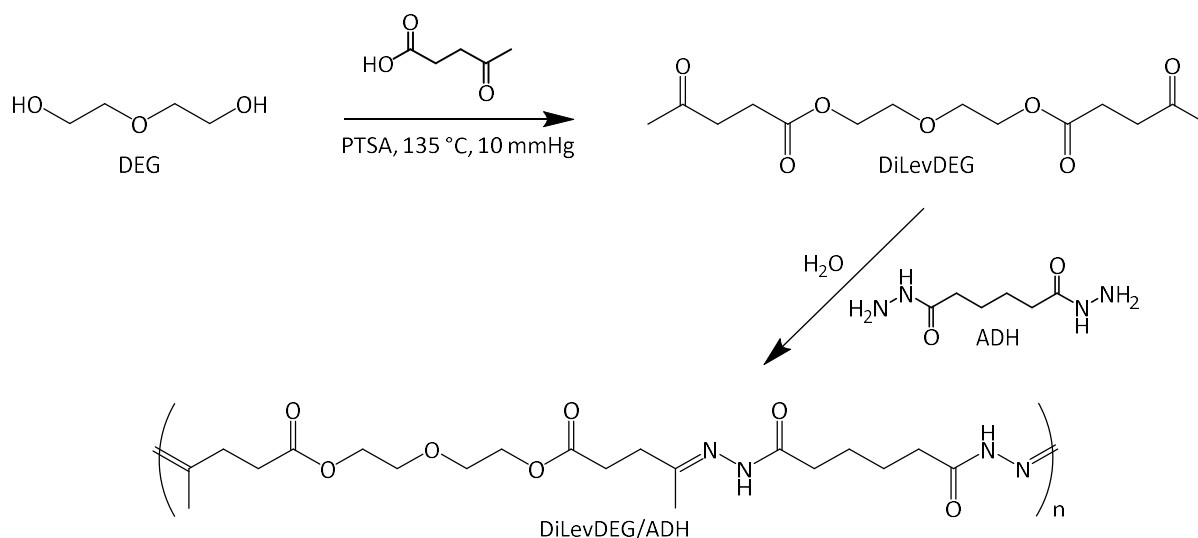
Scheme 2.1. Synthesis of the DiLevDEG/ADH polyacylhydrazone.

NMR spectral data provided evidence for the synthesis of DiLevDEG/ADH, being in good agreement with the reference spectra supplied by Daines.[127] In particular, the carbonyl and methyl regions of the ^{13}C NMR spectrum contained useful signals to confirm generation of the product (**Figure 2.4**). Upon formation of the polyacylhydrazone, methyl **C7** shifted upfield from δ_C 30.0 ppm to δ_C 16.2/15.8 ppm (**C3**). Doubled signals were thought to be due to rotamers caused by hindered rotation around the C–N amide bond. The signal at δ_C 163.1 ppm was assigned as **C2**, the carbon in the C=N bond, and the signal for DiLevDEG ketone **C6**, either as the unreacted monomer or end-group, was observed at δ_C 213.5 ppm. MS studies previously conducted in our group revealed that the polymeric structure never terminated with the free hydrazide, and the signal for **C1** was never observed in the ^{13}C NMR spectrum of DiLevDEG/ADH.[128] Likewise, **C1** was absent from the ^{13}C NMR spectrum of DiLevDEG/ADH prepared in the current study. The large signal for **C4** at δ_C 175.3 ppm was due to overlap with a signal attributed to a **C5** rotamer.[128] The ^{13}C NMR data supported the formation of the acylhydrazone functionality, which was then tested for its ability to chelate Cu(II).
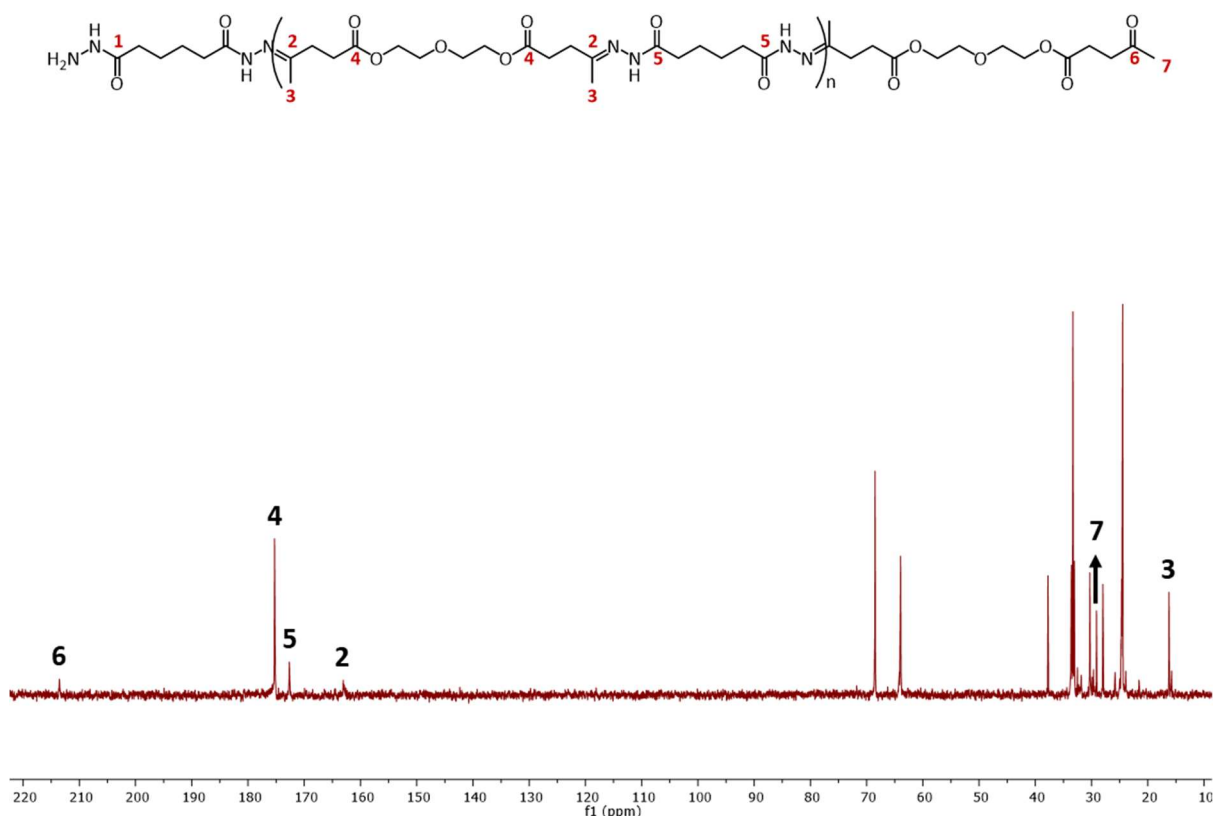
Figure 2.4. ^{13}C NMR spectrum (crude; D_2O) of the DiLevDEG/ADH polyacylhydrazone with select carbon assignments.

Following the addition of the Cu(II) salt, the vibrant colour change of the DiLevDEG/ADH solution was indicative of Cu(II)-coordination by the polyacylhydrazone. Once copper(II) nitrate was added, the pale-yellow, aqueous solution of DiLevDEG/ADH changed to a teal colour (**Figure 2.5**). The striking, characteristic colours of transition metal complexes are due to d-d transitions, which involve the excitation of an electron from a lower-energy to a higher-energy d-orbital (*i.e.* $t_{2g} \rightarrow e_g$) by a photon containing energy equal to the difference between the two d-orbitals (Δ_0). This difference often falls in the visible region of the electromagnetic spectrum. For example, Cu(II) has a total of nine electrons in its d-orbitals (Chapter 1, **Figure 1.10**), and, when one of the electrons in a lower-energy d-orbital absorbs energy in the visible region from a photon and is promoted, the observed colour of the Cu(II) complex is from the transmitted wavelengths.[93,129] UV-Vis spectroscopy is used to record this absorption for d-d transitions in transition metal complexes. Accordingly, the UV-Vis spectra of aqueous solutions of DiLevDEG/ADH, copper(II) nitrate, and DiLevDEG/ADH post-Cu(II)-addition (Cu(II)-DiLevDEG/ADH) were measured.
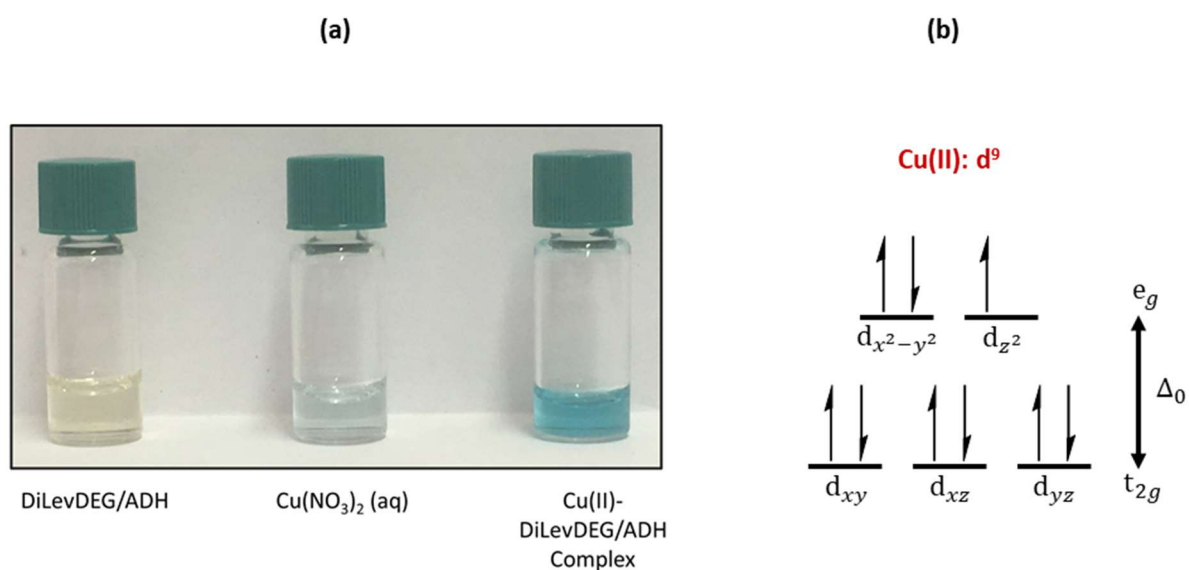
Figure 2.5. Relationship between the colour of Cu(II) complexes and the electron configuration of Cu(II): (a) colour change of the aq DiLevDEG/ADH solution upon the addition of $Cu(NO_3)_2$, which is caused by **(b)** d-d transitions ($t_{2g} \rightarrow e_g$; Δ_0 = crystal field splitting).[93]

The UV-Vis spectra provided evidence of Cu(II)-chelation by the DiLevDEG/ADH polyacylhydrazone (**Figure 2.6**). An aqueous solution of DiLevDEG/ADH absorbed at lower wavelengths, beginning around 420 nm (*i.e.* violet light), in its spectrum, which accounted for the pale-yellow colour of the solution. Copper(II) nitrate (aq) absorbed red light with $\lambda_{max} \geq 800$ nm, appearing pale-blue. Upon the addition of copper(II) nitrate, the aqueous DiLevDEG/ADH solution absorbed at both higher (λ_{max} = 782 nm) and lower (shoulder starting below ~470 nm) wavelengths; the absorption of red/orange light with λ_{max} = 782 nm was due to d-d transitions in the complex.[130] Blue/green light (~500 nm) was transmitted, and, thus, Cu(II)-DiLevDEG/ADH appeared to be a teal colour. Therefore, the UV-Vis data and observations of a colour change after Cu(II)-addition substantiated the hypothesised Cu(II)-coordination by DiLevDEG/ADH and completed the first stage of work for evaluating this polyacylhydrazone as a proof-of-concept. The second stage, involving formulation into a paint and subsequent performance testing, is addressed in the next chapter (Chapter 3, **Section 3.2**).
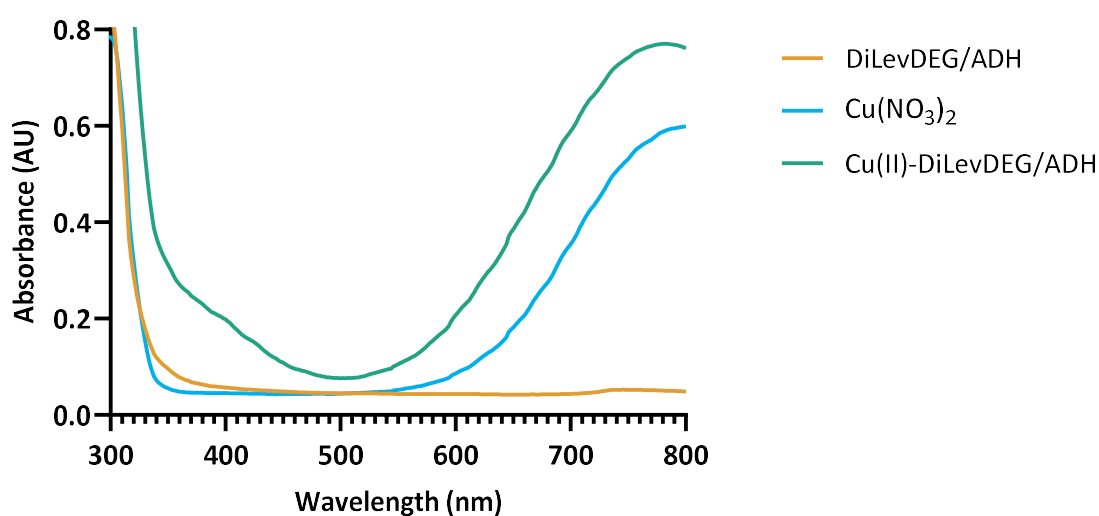
Figure 2.6. UV-Vis spectra of DiLevDEG/ADH, Cu(NO$_3$)$_2$, and Cu(II)-DiLevDEG/ADH.

2.3 SIMPLE ACYLHYDRAZONES

In light of the demonstrated ability of a polyacylhydrazone to coordinate Cu(II) and its successful formulation into a paint, acylhydrazones were proposed as a candidate ligand class to be evaluated for suitability in antifouling coatings. There is evidence in the literature of transition metal-acylhydrazone complexes possessing antimicrobial activity, even when incorporated in a coating. For instance, in a study by El-Wahab[131], acylhydrazone ligand *o*-hydroxyacetophenone benzoylhydrazone (HBH; **Figure 2.7a**) and its complexes with Co(II), Cr(III), and Fe(III) were added (1–2% w/w) to an epoxy resin. These coatings were antifouling and displayed antimicrobial activity against Gram-positive and Gram-negative bacteria and fungi, with the metal complexes having higher activities than uncoordinated HBH. The coating additives had no effect on the flexibility, hardness, or adhesion of the epoxy resin. Furthermore, there is also evidence in the literature of Cu(II)-acylhydrazone complexes, specifically, having comparable antimicrobial activities to complexes with other transition metals. For example, Rodríguez-Argüelles *et al.*[132] synthesised and characterised complexes of an acylhydrazone ligand, 2-thiophenecarbonyl hydrazone of 3-isatin (H_2L^1; **Figure 2.7b**), bound to Zn(II), Cu(II), Ni(II), and Co(II), and $[Cu(HL^1)_2]$ had antibacterial activity comparable to $[Zn(HL^1)_2]$, $[Ni(HL^1)_2]$, and $[Co(HL^1)_2]$ against both Gram-positive and Gram-negative bacteria. Therefore, considering the work with DiLevDEG/ADH in the present study and the literature evidence of Cu(II)-coordinated acylhydrazones having antimicrobial activity, a series of monoacylhydrazones and acyldihydrazones, as well as copper complexes of particular ligands of interest, were synthesised and characterised to better understand the chemical and physical properties of acylhydrazones.
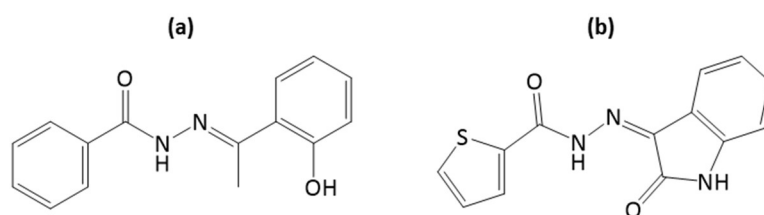
Figure 2.7. Structures of acylhydrazone ligands **(a)** HBH and **(b)** H_2L^1.

2.3.1 Synthesis

The acylhydrazones in **Scheme 2.2** were synthesised in carbonyl addition reactions, following the facile, general procedure by Zha and You[133] in which the hydrazide was added to a methanol or ethanol

solution containing the aldehyde or ketone. A catalytic amount of glacial acetic acid was then added dropwise to adjust to pH 4–5, and the reaction mixture was heated to reflux temperature. Hydrazone formation progressed *via* protonation of the carbonyl oxygen of the aldehyde or ketone (−RC=$\underline{O}$) and subsequent nucleophilic attack at its electrophilic carbonyl carbon (−R$\underline{C}$=O) by the primary amine of the hydrazide (−C(=O)−NH−$\underline{N}$H$_2$).[134] Loss of water and formation of the C=N double bond yielded the acylhydrazone product as a white or yellow precipitate, which was isolated by vacuum filtration and washed.
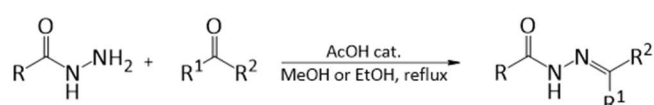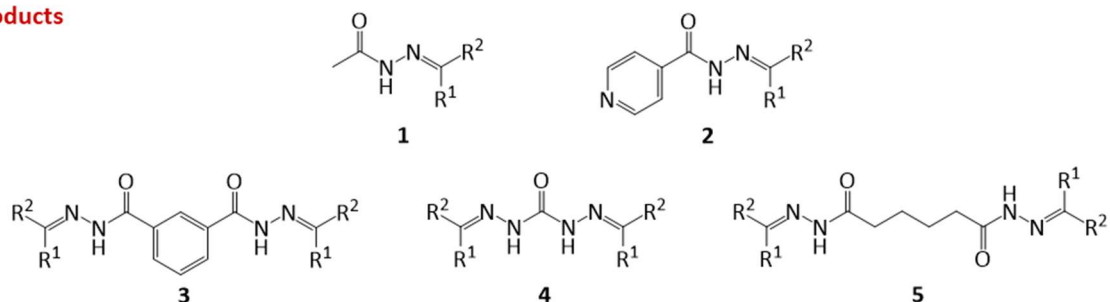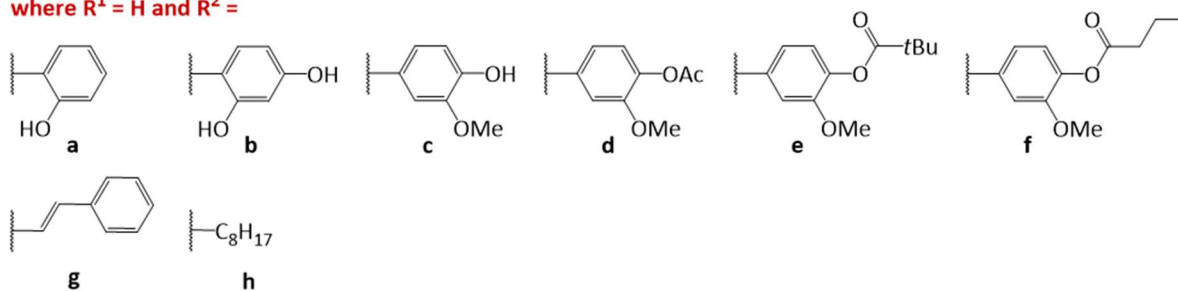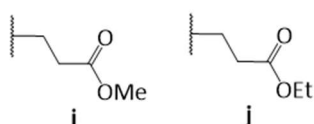
Scheme 2.2. General scheme for the synthesis of acylhydrazones (top; R, R^1, R^2: same or different). The synthesised acylhydrazones are as follows: **1a–b**, **1i–j**, **2a–b**, **3c–f**, **3h**, **4c**, **4g**, **5c**, and **5h–j**.

Successful preparation of acylhydrazones **1a–b**, **1i–j**, **2a–b**, **3c–f**, **3h**, **4c**, **4g**, **5c**, and **5h–j** was confirmed by high-resolution mass spectrometry (HRMS) and NMR spectroscopy, and these data, as well as

reaction yields, are reported in the Experimental (**Section 6.2.2.2**). The NMR spectra are included in the Appendix (**Section 8.1**). In general, synthesis was evidenced by distinct acylhydrazone resonance (–C(=O)–NH–N=$\underline{C}$R–) in the ^{13}C NMR spectrum around δ_C 140–155 ppm and resonance in the ^{1}H NMR spectrum consistent with the amide proton (–C(=O)–N$\underline{H}$–N=CR–) around δ_H 10–12 ppm and δ_H 9–10 ppm for aldehyde- and ketone-derived acylhydrazones, respectively. Typically, exchange of the amide proton in the ^{1}H NMR spectra of the acylhydrazones was not observed, since the majority were measured in an aprotic solvent. Acylhydrazones **1j**, **3d–f**, **3h**, and **5h** were novel compounds.

2.3.2 Isomers

It is known that acylhydrazones can exist in several geometric and conformational forms. The possible geometric (*E/Z*)-isomerism with respect to the C=N double bond and conformational (*E'/Z'*)-isomerism from hindered rotation around the C–N amide bond can result in four different configurations (*EE'*, *EZ'*, *ZE'*, ZZ'; **Figure 2.8**), which have been previously reported.[135–139] Rotamers (*i.e.* (*E'/Z'*)-isomers) are observed as doubled ^{1}H and ^{13}C NMR signals at a probe temperature of 30 °C that, subsequently, coalesce at 90 °C (**Figure 2.9**). In the present study, peak assignment in the NMR spectra of both aldehyde- and ketone-derived acylhydrazones, specifically of **1a–b**, **2a–b**, **5c**, and **5h–j** (Appendix, **Tables 8.1–2, 8.5–6, 8.14–17**), was often complicated by the presence of rotamers. Although, not every possible conformational or geometric isomer was seen in the NMR spectra of every acylhydrazone: isomers are favoured for multiple reasons, including intramolecular and intermolecular hydrogen bonds and experimental conditions (*e.g.* temperature, solvent). For example, the (*E*)-isomer of **1a–b** and **2a–b** could theoretically be stabilised by an intramolecular N···H–O hydrogen bond, making it favoured over the (*Z*)-isomer (**Figure 2.10**).[140–142]
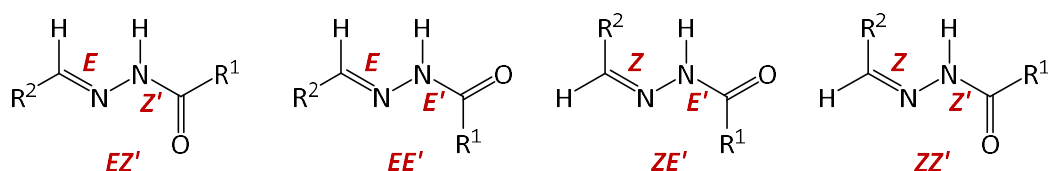
Figure 2.8. Possible geometric (*E/Z*)-isomers and (*E'/Z'*)-rotamers of acylhydrazones (adapted from Daines *et al.*[127]).
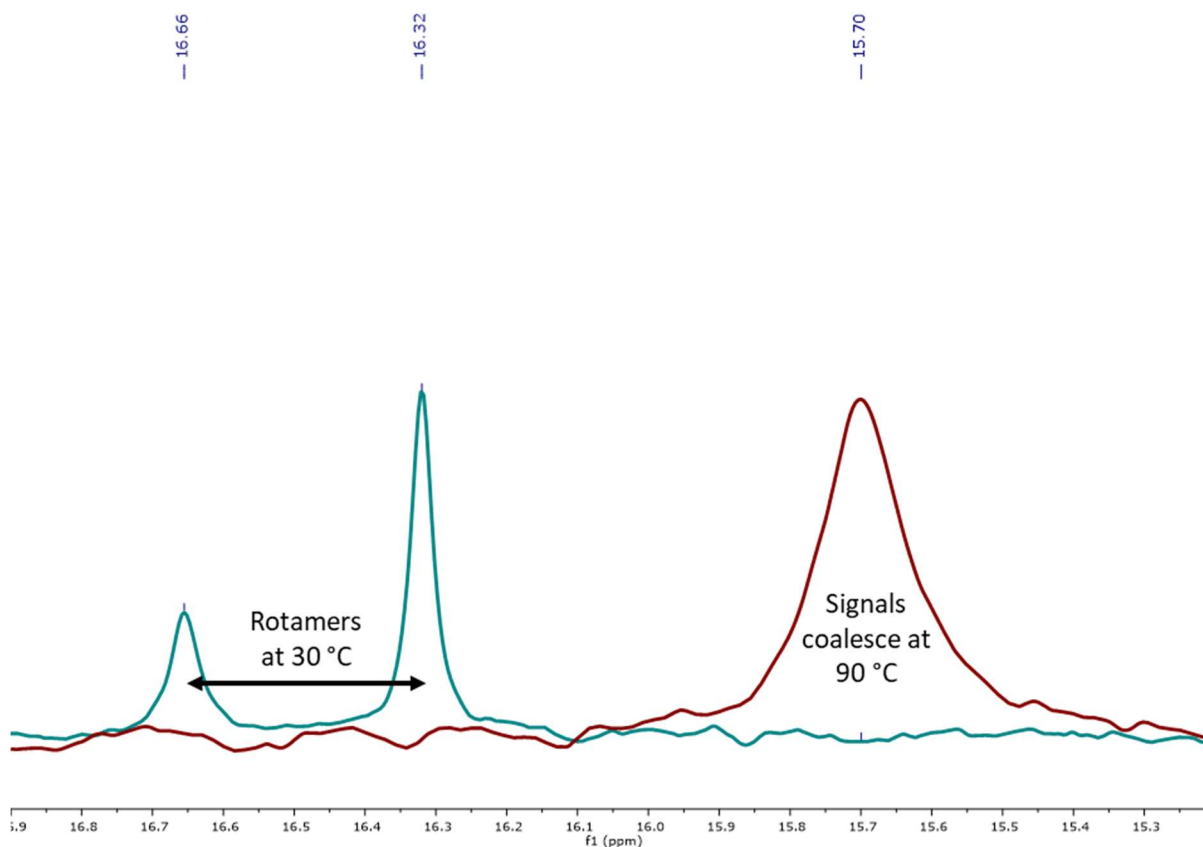
Figure 2.9. Signals attributed to rotamers in a ^{13}C NMR spectrum (**5i**: **C1**).
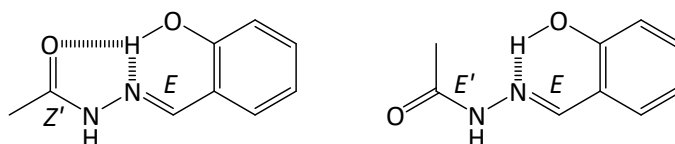
Figure 2.10. Examples of intramolecular hydrogen bonding in monoacylhydrazone **1a** (one geometric isomer (*E*) and (*E'*/*Z'*)-rotamers).[141,142]

(*E'*/*Z'*)-Rotamers, but only one geometric isomer, were observed in the ^{1}H and ^{13}C NMR spectra of both aldehyde- and ketone-derived acylhydrazones. For instance, regarding ADH- and aromatic aldehyde-derived acyldihydrazone **5c** (**Figure 2.11**), two signals in the ^{13}C NMR spectrum in a ratio of approximately 1:1 that were assigned as the hydrazone carbonyl resonances, **C1'**, appeared at δ_C 173.9 and 168.1 ppm (probe temperature 30 °C; Appendix, **Figure 8.16**); these merged to a single resonance observed at δ_C 173.4 ppm when spectra were obtained at a probe temperature of 90 °C. Likewise, the two ^{1}H NMR signals at δ_H 11.14 and 11.02 ppm for the amide N–H proton coalesced at δ_H 10.69 ppm at 90 °C. These signals were, therefore, attributed to the (*E'*/*Z'*)-rotameric forms of **5c**.

43

Only one geometric isomer was observed, and it was assigned as being in the (E)-configuration with respect to the C=N moiety, since it is noted in the literature that, generally, acylhydrazones derived from aldehydes adopt the (E)-configuration.[136,139,143] Furthermore, acylhydrazones, like **5c**, synthesised from aromatic aldehydes are known to prevailingly exist as the (E)-isomer due to steric hindrance.[136,137,139]
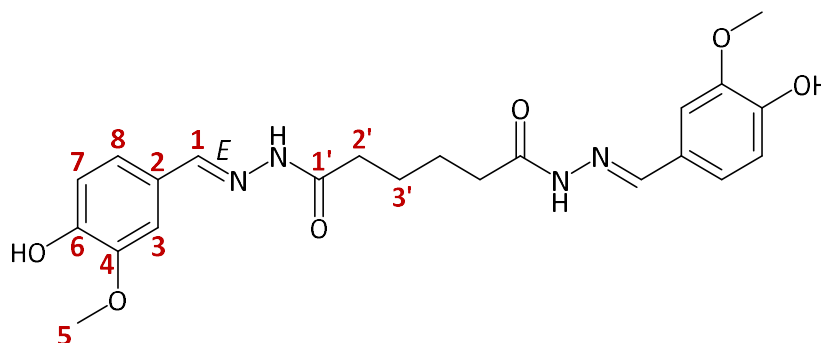
Figure 2.11. Aldehyde-derived acyldihydrazone **5c**.

Similar results to those obtained for ADH- and aldehyde-derived acyldihydrazone **5c** were observed for an ADH- and ketone-derived acyldihydrazone: **5i** (**Figure 2.12**). Rotamers were observed as a doubling of ^{13}C NMR signals in a 2:1 ratio at 30 °C, and coalescence of the doubled signals was observed when spectra were recorded at 90 °C. For example, the doubled ^{13}C NMR signals at δ_C 16.7 (minor) and 16.3 (major) ppm for the hydrazone methyl groups (**C1**; **Figure 2.9**; Appendix, **Figure 8.18**) and δ_C 51.2 (minor) and 51.1 (major) ppm for the methoxy groups (**C6**) collapsed into single signals at δ_C 15.7 ppm and δ_C 50.6 ppm, respectively. Evidence for the location of the bonds involved in generating rotamers was provided by the chemical shift difference (Δδ) between the major and minor resonances attributed to rotameric forms of each carbon in the ^{13}C NMR spectrum, as shown in **Figure 2.12** and **Table 2.3**. The difference in the chemical shift between rotamer signals was greater closer to the C–N amide bond, which is the bond of hindered rotation generating rotamers (e.g. $\Delta\delta_C$ 6.2 ppm for **C1'**). Again, only one predominant geometric isomer was observed, and the chemical shift data were consistent with the (E)-configuration. For instance, in a study by Palla et al.[139], the chemical shift of a methyl carbon analogous to **C1** was approximately δ_C ~17 ppm in the (E)-configuration but δ_C ~25 ppm in the (Z)-configuration. In the present study, the chemical shift of **C1** was δ_C 16.3 ppm, suggesting the likely presence of the (E)-isomer. Additionally, it is reported that, for acylhydrazones, the (Z)-isomer is thermodynamically less-favoured without stabilisation, such as through intramolecular hydrogen bonding.[144,145]
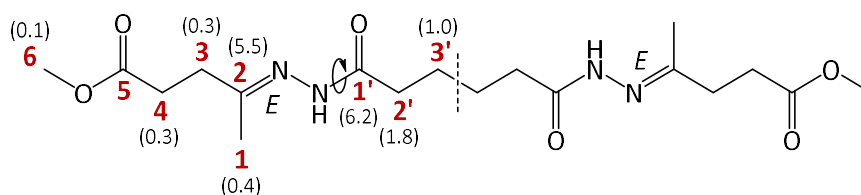
Figure 2.12. Ketone-derived acyldihydrazone **5i** (Δδ$_C$ between major and minor species at 30 °C in parentheses; adapted from Daines *et al.*[127]).

Table 2.3. ^{13}C NMR data for **5i** (refer to **Figure 2.12** above; adapted from Daines *et al.*[127]).

Carbon	δ$_C$ Major (ppm)	δ$_C$ Minor (ppm)	Δδ$_C$ │Major - Minor│ (ppm)
1'	174.5	168.3	6.2
2'	32.0	33.8	1.8
3'	24.1	25.1	1.0
1	16.3	16.7	0.4
2	149.9	155.4	5.5
3	32.7	33.0	0.3
4	29.4	29.7	0.3
5	172.8	-	-
6	51.1	51.2	0.1

2.3.3 Solubility

In general, the acylhydrazone products were only soluble in dipolar aprotic solvents, such as dimethylformamide (DMF) and dimethylsulfoxide (DMSO). However, this solubility profile was undesirable due to the ability of these solvents to form complexes with Cu(II) and the complications to further analysis, manipulation, and development. As previously discussed, an ideal ligand should be easily manipulated for formulation in a coating, and highly insoluble compounds do not meet this requirement. The derivatisation of vanillin by acylation with acetic, trimethylacetic, and butyric anhydride (**d**, **e**, and **f**, respectively) was explored as a method of altering the solubility profile of acylhydrazone **3c**. Yet, the solubility profiles of products **3d**, **3e**, and **3f** did not differ from underivatised **3c** (**Scheme 2.2**): they were all only soluble in DMF and DMSO. The acylhydrazones with more desirable solubility profiles were monoacylhydrazone **1a** and acyldihydrazone **3h** (both soluble in chloroform containing 10% v/v methanol; **Figure 2.13a,b**) and monoacylhydrazones **1i–j** (soluble in chloroform; **Figure 2.13c,d**). Efforts were focused on **1a**, which is better-known in the literature than

3h, **1i**, and **1j**. It was thought that, since **1a** and its Cu(II) complex are already well-characterised, the methodology used in this study for characterisation of Cu(II) complexes could be validated by comparing results to those reported in the literature before progressing to lesser-known or novel ligands. Therefore, **1a** served as a representative acylhydrazone ligand, and experiments were performed to characterise its Cu(II) complex.
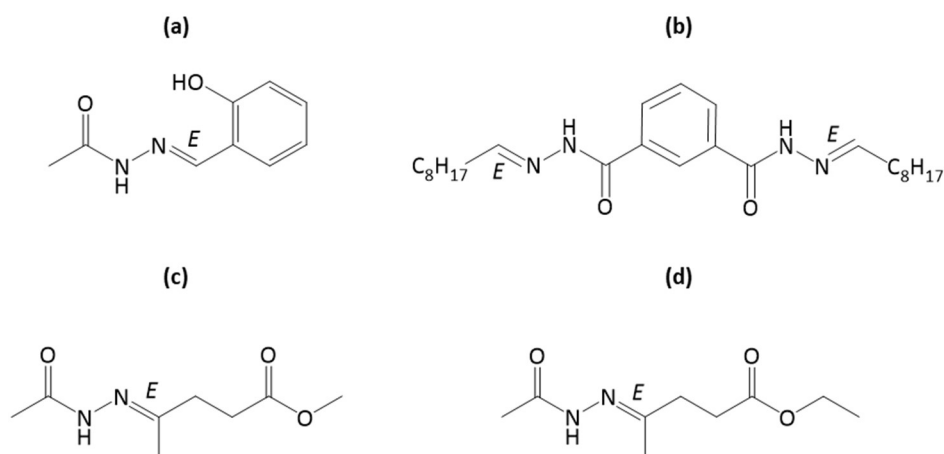
Figure 2.13. Ligands **(a) 1a**, **(b) 3h**, **(c) 1i**, and **(d) 1j**.

2.3.4 Cu(II)-Ligand Complexes

Previous research has assessed the Cu(II)-chelating ability of monoacylhydrazone **1a** and the characteristics and antimicrobial activity of its Cu(II) complex. For instance, the geometry, stoichiometry, and formation constant (K_f; **Equation 2.1**) of the Cu(II)-**1a** complex have been reported.[146,147] Furthermore, Yousef Ebrahimipour *et al.*[148] demonstrated that **1a** and the mixed-ligand Cu(II) complex with **1a** and phenanthroline have antimicrobial activity against *Escherichia coli*, *Staphylococcus aureus*, *Pseudomonas aeruginosa*, and *Candida albicans*, with the Cu(II) complex being more active. In the present work, the Cu(II)-**1a** complex was characterised by employing the techniques described in Chapter 1 (**Section 1.3.2.2**; *e.g.* MS, UV-Vis, Job plot, K_f). Unfortunately, the paramagnetic nature of Cu(II) precluded the use of NMR spectroscopy as a convenient analytical tool for characterisation. Method validation involved the generation of a Job plot to determine the metal:ligand stoichiometry and involved the attempted calculation of the K_f of the Cu(II) complex. Since these are both known for **1a**, agreement between reported values in the literature and measured values in this study would allow for confidence when employing the same processes for novel ligands.

$$M + L \rightleftharpoons ML \qquad\qquad K_f = \frac{[ML]}{[M][L]}$$
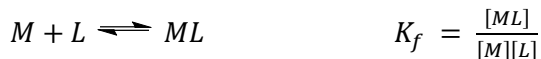
Equation 2.1. The formation constant (K_f) of a metal-ligand complex (M = metal, L = ligand).

For MS analysis, the Cu(II)-**1a** complex was prepared by adding one equivalent of copper(II) chloride to ligand **1a**, a light yellow solid, in methanol. The green, precipitated complex was isolated and analysed by electrospray ionisation (ESI)-HRMS. ESI-HRMS showed the formation of a complex with a molecular formula consistent with a 1:1 Cu(II):ligand complex minus a proton, giving the complex a +1 charge (calcd for $C_9H_9CuN_2O_2$ [M - H]$^+$ 239.9960; found 239.9963).

As shown in **Figure 2.14**, a Job plot was constructed for the Cu(II)-**1a** complex. This was done by combining aliquots of equimolar solutions of **1a** and copper(II) nitrate in 9:1 v/v chloroform:methanol in a manner that kept the total number of moles constant (moles **1a** + moles $Cu(NO_3)_2$ = k) while varying the metal:ligand molar ratio. The addition of tetrabutylammonium nitrate (0.1 M) ensured a constant ionic strength, and the absorbance of the complex was measured at λ_{max} = 388 nm.
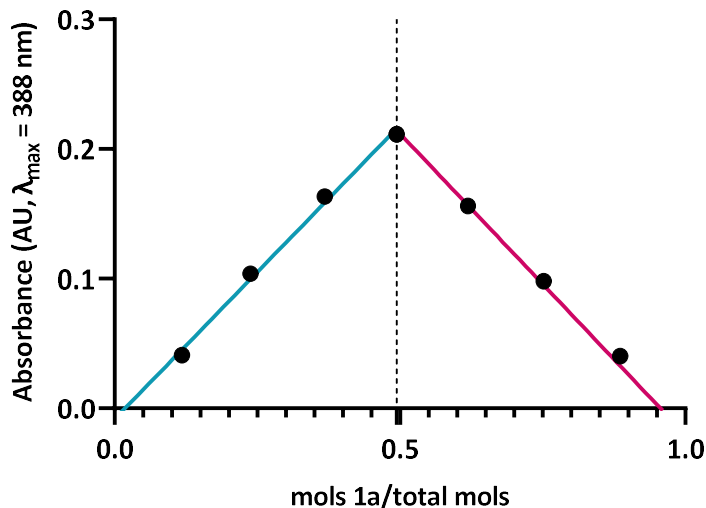
Figure 2.14. Job plot obtained by varying the molar ratio of ligand **1a** to copper(II) nitrate in 9:1 v/v chloroform:methanol (0.1 M tetrabutylammonium nitrate). The absorbance of the complex was measured at λ_{max} = 388 nm.

The Job plot revealed that the molar ratio of **1a** to the total number of moles was 0.494, suggesting that the metal:ligand ratio of Cu(II):**1a** was 1:1, which is consistent with reports in the literature.[146,147]

However, it has also been reported that **1a** is capable of forming dimeric complexes with Cu(II) (*i.e.* 1:2 Cu(II):**1a**). The experiment should be repeated with a different value for *k* and verified at a different wavelength: these are important crosschecks for evaluating the reliability of the data.[102] Knowledge of the Cu(II) complex's stoichiometry is essential for understanding its performance (*e.g.* Cu(II)-loading) when incorporated in a coating and for evaluating the strength of the interaction between the metal and the ligand, which is reported as the K_f of the complex and is another quantity of interest.

Since the formation constant of the Cu(II)-**1a** complex has been reported in the literature (3.76×10^4),[146,147,149] **1a** was used in an attempt to develop and verify a method for measuring the K_f of the Cu(II)-ligand complexes spectrophotometrically, which could then be applied to the synthesised ligands with unknown K_f values. It was thought that these values would provide a system for establishing lead compounds for further development: it was hypothesised that a relatively lower K_f, within certain parameters (*e.g.* still higher than for the natural ligands in seawater), would be desirable, resulting in Cu(II) being more readily released and, therefore, able to exert its antimicrobial effect maximally. Comparison of relative K_f values of the same ligand complexed with different metal ions would reveal metal ion-ligand selectivity as well. To measure the K_f of **1a**, the absorption spectra of 0.100 mM solutions of **1a** in 9:1 v/v chloroform:methanol containing concentrations of copper(II) nitrate ranging from 0–0.500 mM were measured .

The two absorbing chemical species in the UV-Vis spectra were ligand **1a** at ~323 nm and coordination complex Cu(II)-**1a** at ~388 nm, and, as the Cu(II) concentration increased, the absorbance at ~388 nm increased and the absorbance at ~323 nm decreased. Isosbestic points were observed at ~308 nm and ~346 nm (**Figure 2.15**). Isosbestic points are the points in an absorption spectrum at which the curves of absorbance *vs* wavelength for the two principle absorbing components, such as the ligand and transition metal complex, intersect, meaning that they have identical molar absorption coefficients. They are used in the determination of formation constants, and consistent isosbestic points indicate that the reaction proceeds without the formation of an intermediate or multiple products.[150,151] In the present study, an expanded view of the regions in the absorption spectra containing the supposed isosbestic points revealed that the curves do not all intersect precisely at these points (**Figure 2.16**). Through correspondence with Dr Peter Gans, co-author of Hyperquad, it was surmised that multiple complexes, likely CuL and CuL_2 and possibly a third species, were contributing to the spectra, resulting in the absence of consistent isosbestic points at ~308 nm and ~346 nm.[152] Multiple species in solution complicate the calculation of K_f, making the use of software, such as HypSpec, necessary to process the data efficiently. Due to the lack of access to this software, among other reasons, it was concluded that a different approach to ligand-selection was required.

— 9:1 v/v CHCl₃:MeOH Baseline
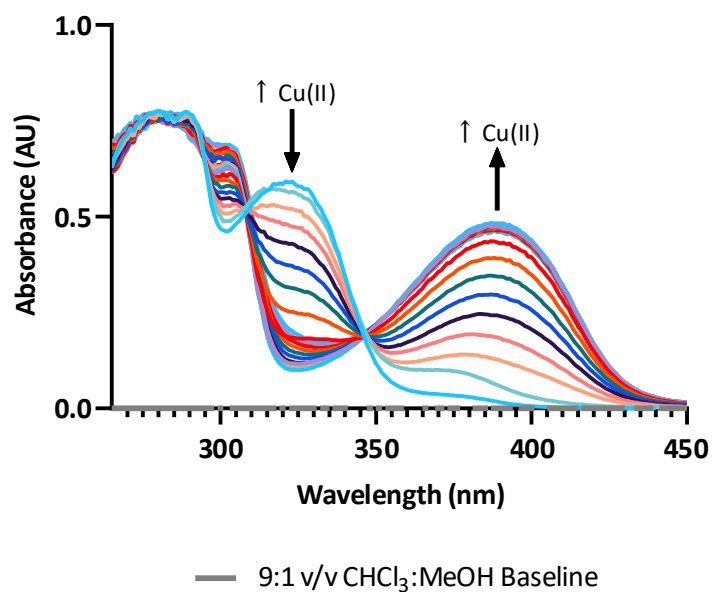
Figure 2.15. Absorption spectra of 0.100 mM solutions of **1a** and increasing concentrations of copper(II) nitrate in 9:1 v/v chloroform:methanol.
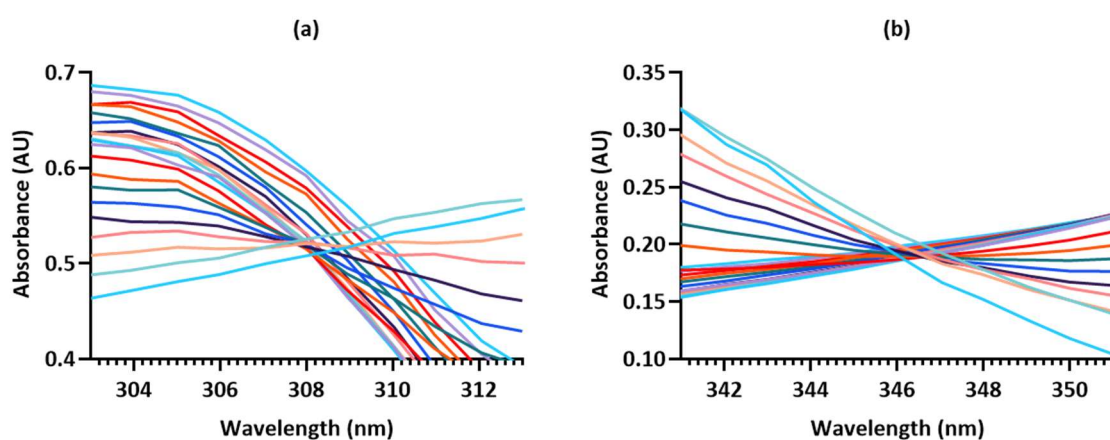
Figure 2.16. Expanded views of the regions in Figure 2.15 containing isosbestic points: (a) ~308 nm and **(b)** ~346 nm.

2.3.5 Conclusions

For multiple reasons, it was decided that a different ligand class should be pursued. First, the insolubility of the acylhydrazones was problematic. Most of them were only soluble in dipolar aprotic solvents, such as DMF and DMSO, which made characterisation of the ligand and its Cu(II) complex

difficult. Many of the techniques and experiments (*e.g.* UV-Vis for Job plot, *etc.*) require dissolution of the Cu(II) complex in a solvent for characterisation. Since both DMF and DMSO can coordinate Cu(II), experiments could be affected by ligand-competition for Cu(II). Also, when planning future stages of the project in which the acylhydrazone would be formulated into a coating, it was clear that the solubility limitations would restrict options, thus failing the requirement that the ligand be easily manipulated for incorporation in a coating. For instance, it would be difficult to incorporate an insoluble acylhydrazone into a paint binder. A few of the acylhydrazones were also soluble in chloroform or solutions of chloroform and methanol (*e.g.* **1a**, **3h**, **1i–j**), but this was not ideal either, as these solvents would be impossible to incorporate in a modern coating due to solvent restrictions.[153]

Second, the acylhydrazones have complex solution chemistry with multiple possible forms and isomers – not all of which are properly configured for Cu(II)-coordination (*e.g.* (*E'*)-rotamer of **1a**, **Figure 2.10**). Once affixed in a coating, there would be challenges in ensuring the correct ligand-orientation, especially given the dynamicity of acylhydrazones. This dynamicity includes different constitutional states (**Figure 2.17**), which are a result of the reversibility of acylhydrazone formation under acid-catalysed, mild conditions. Hydrolysis of an acylhydrazone in the presence of other hydrazides or aldehydes/ketones can generate a new acylhydrazone *via* recombination,[144,145,154–157] and this has been observed by our research group when working with aqueous solutions of the DiLevDEG/ADH polyacylhydrazone.[128] Such dynamicity complicates the ligand design, formulation, and product characterisation, making the ligand class less attractive for a proof-of-concept. It is unknown if the acylhydrazones would be stable or properly orientated for Cu(II)-chelation in the film, and this potentially violates the condition that the ligand perform similarly to its unbound state when immobilised in a coating.
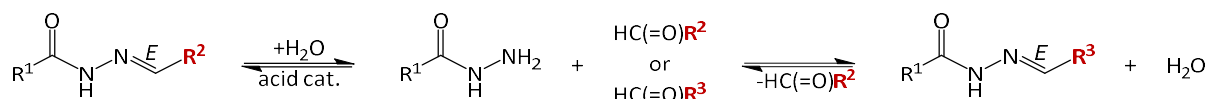
Figure 2.17. Example of different constitutional states in an acylhydrazone.[145]

Finally, it was acknowledged that simpler, better-characterised ligand systems were available and that, to meet the project goals, it was wise to begin with as few unknowns as possible, bearing in mind that the complexity increases upon formulation into a paint. Pursuing the acylhydrazones would necessitate complicated measurements already addressed in the literature for other ligand classes.

For instance, most of the acylhydrazones would require calculation of the K_f of their Cu(II) complexes ($K_{Cu(II)L}$) and experiments to determine if they are selective for Cu(II). The $K_{Cu(II)L}$ is important for confirming that the selected ligand is a stronger Cu(II)-chelator than the natural ligands in seawater, and Cu(II)-selectivity is important because there are many transition metal ions in seawater at concentrations comparable to Cu(II) with which acylhydrazones are able to form stable complexes.[132,158,159] An ideal ligand should retain its Cu(II)-selectivity and form stable Cu(II) complexes in seawater, so it seemed wiser to select a ligand class for which there was already evidence that it could fulfil such requirements. In light of all of these considerations, it was decided a new ligand class should be explored, and tetraaza/oxatriaza macrocycles were selected. Although, since it was already successfully formulated into a coating, it was still sensible to progress the DiLevDEG/ADH polyacylhydrazone to the second stage of testing in which the Cu(II)-loading and antimicrobial activity of the paint would be evaluated.

2.4 TETRAAZA/OXATRIAZA MACROCYCLES: CYCLEN

Tetraaza/oxatriaza macrocycles **6–15**, as in **Figure 2.18**, were selected as a new ligand class due to their Cu(II)-selectivity, antimicrobial activity, favourable $K_{Cu(II)L}$ values, and more convenient solubility profiles. It has been demonstrated that **6–15** are selective for Cu(II) over multiple other transition metal ions, including Mn(II), Co(II), Ni(II), Zn(II), Cd(II), and Pb(II).[89] They form very stable 1:1 complexes and display inertness to demetallation due to the macrocyclic effect.[76,89,160–164] The macrocyclic effect is the increased stability of complexes between metal ions and macrocyclic ligands, compared to their open-chain counterparts. For instance, the Log($K_{Cu(II)L}$) values for cyclen (**11**) and its open-chain counterpart, triethylenetetramine, are 23.3 and 20.0, respectively.[165–168] There are also examples in the literature of tetraaza macrocyclic compounds displaying antimicrobial activity when complexed with Cu(II).[169–171] This antimicrobial activity has even been retained after fixation of the Cu(II) complex to a surface. For example, a study by Pallavicini *et al.*[76] reported the grafting of the [13]aneN$_4$ (**13**) Cu(II) complex to glass and quartz surfaces and the significant antimicrobial effect of these surfaces, despite their inertness to demetallation.

R=H, [12]aneN$_3$O, **6**   R=H, [13]aneN$_3$O, **8**   R=H, [14]aneN$_3$O, **9**
R=CH$_3$, Me$_3$[12]aneN$_3$O, **7**   R=CH$_3$, Me$_3$[14]aneN$_3$O, **10**

R=H, cyclen, [12]aneN$_4$, **11**   R=H, [13]aneN$_4$, **13**   R=H, cyclam, [14]aneN$_4$, **14**
R=CH$_3$, Me$_4$[12]aneN$_4$, **12**   R=CH$_3$, Me$_4$[14]aneN$_4$, **15**
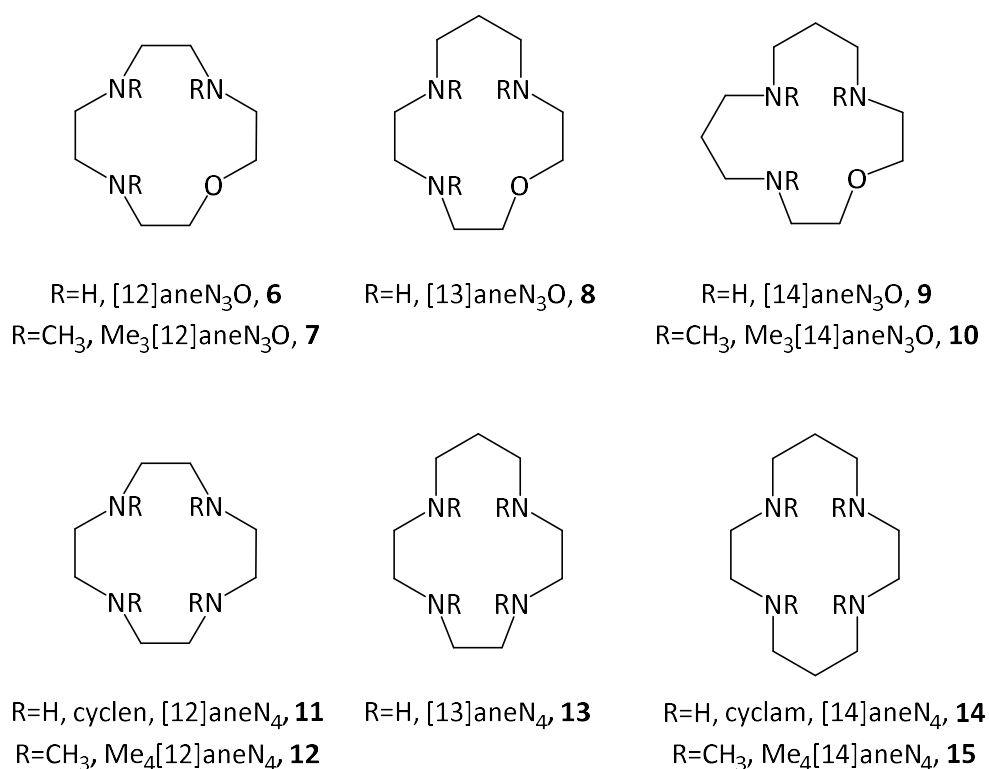
Figure 2.18. Tetraaza/oxatriaza macrocycles (**6–15**).[89]

Ligands **6–15**, as well as their Cu(II) complexes, are well-known in the literature: as seen in **Table 2.4**, all of the Log(K_f) values for the Cu(II)-ligand complexes have been previously reported and range from 13.60 (**10**) to 26.5 (**14**).[89] This range of Log(K_f) values is particularly desirable because it indicates that all but one of the macrocyclic ligands are stronger Cu(II)-chelators than the organic Cu(II) complexes in seawater (*i.e.* Log(K_f) > 13.8 for diethylene triamine pentaacetic acid (DTPA)-type ligand, **Table 2.4** "Seawater Complex").[80,172,173] Since the majority of dissolved copper in seawater is complexed with organic ligands (*e.g.* DTPA- or EDTA-type), macrocyclic ligands **6–15** may, therefore, be strong enough Cu(II)-chelators to displace these organic ligands in seawater.[80] Also, crystal structures of the Cu(II)-macrocyclic ligand complexes have been published, providing further valuable information, and the ligands and complexes are known to have convenient solubility profiles.[89,174] For example, cyclen (**11**) is water-soluble. To begin, cyclen was chosen specifically out of the series to serve as a model compound for a proof-of-concept and development of methodology.

Table 2.4. Stability constants ($K_{ML} = [ML]/[M][L]$; M = metal, L = ligand) of metal complexes of the macrocyclic compounds in **Figure 2.18** at I = 0.10 mol/dm^3 (KNO$_3$) and 25.0 ± 0.1 °C.[89]

Metal ion	Mn^{2+}	Co^{2+}	Ni^{2+}	Cu^{2+}	Zn^{2+}	Cd^{2+}	Pb^{2+}
Ligand	Log ($K_{Mn(II)L}$)	Log ($K_{Co(II)L}$)	Log ($K_{Ni(II)L}$)	Log ($K_{Cu(II)L}$)	Log ($K_{Zn(II)L}$)	Log ($K_{Cd(II)L}$)	Log ($K_{Pb(II)L}$)
6	5.85(1)	10.541(7)	12.36(3)	**15.63(1)**	10.43(7)	10.69(1)	11.54(1)
7	-	10.30(3)	11.42(4)	**14.98(4)**	10.006(8)	10.23(1)	10.53(1)
8	3.96(9)	9.29(1)	11.37(6)	**16.61(4)**	9.80(1)	9.32(3)	8.84(3)
9	-	8.87(4)	9.7(1)	**15.4(2)**	8.9(2)	7.13(1)	7.30(1)
10	-	5.8(1)	6.41(7)	**13.60(3)**	6.36(2)	4.7(3)	6.61(2)
11	-	13.8[175]	16.4[176]	**23.3[165]**	16.2[177]	14.3[177]	15.9[177]
12	-	-	-	**18.37[178]**	14.04[178]	13.06[178]	13.91[178]
13	-	14.28[175]	17.98[176]	**24.36[165]**	15.6[177]	12.71[165]	13.48[165]
14	-	12.71[175]	22.2[179]	**26.5[165]**	15.5[177]	11.23[165]	10.83[165]
15	-	7.58[180]	8.65[180]	**18.3[180]**	10.35[180]	9.0[180]	-
Seawater Complex[80,172,173]	-	-	-	**13.8^a, 11.7^b**	10.7^a, 9.4^b	-	-

[175]I = 0.2 mol/dm^3, 35 °C; [176] I = 0.1 mol/dm^3; [165] I = 0.1 mol/dm^3; [177] I = 0.2 mol/dm^3; [178] I = 0.1 mol/dm^3; [179] I = 0.1 mol/dm^3; [180] I = 0.1 mol/dm^3; [80,172,173] Dominant species in seawater at pH 8.1; ^{a} DTPA-type ligand; ^{b} EDTA-type ligand.

Cyclen (**11**) was chosen to be a model compound for several reasons. First, cyclen is commercially available and relatively inexpensive, saving time that would have been spent on synthesis to focus on its formulation and antifouling performance. One goal of the present work is to establish parameters for ligand-selection (*e.g.* Log($K_{Cu(II)L}$)) and the Cu(II)-loading and presentation of the complex in a coating, helping to create a framework for future work. A well-known, readily available ligand increases the likelihood of meeting this goal but also of having a more commercially viable product down the track, since it is fully characterised and less expensive than a specialised ligand with a lengthy synthesis. This meets the requirement that the ligand be cheaply prepared in large quantities. Second, being water-soluble, cyclen is more easily manipulated for characterisation and incorporation in a coating. Third, cyclen is selective for Cu(II) over other transition metal ions (*e.g.* Co(II), Ni(II), Zn(II), Cd(II), Pb(II)) and has a high Log($K_{Cu(II)L}$) (23.3), meaning that the Cu(II)-cyclen complex is stable and resistant to demetallation.[89] This fulfils the selectivity and stability criteria for the project's ideal ligand. Because the flux of bioavailable metal ions from the surface is necessary for antimicrobial activity,[115] it was hypothesised that a relationship may exist between the stability of the complex and surface toxicity. In the particular case of antifouling paints, the ligands would still need to outcompete the natural ligands in seawater, establishing the Log($K_{Cu(II)L}$) minimum value at 13.8.[80,172,173] Within the series of tetraaza/oxatriaza macrocycles (**Figure 2.18**), cyclen has one of the highest Log($K_{Cu(II)L}$) values (**Table 2.4**). Consequently, determining if such a strong ligand could still exert an antimicrobial effect when affixed in a coating was of interest. Finally, the literature concerning cyclen and its derivatives, as well as their transition metal complexes, is vast, and precedents exist for numerous applications, including their use as radiopharmaceuticals (*e.g.* imaging probes for positron emission tomography (PET)), antimicrobial agents, and generators of nitric oxide when affixed in polymeric coatings.[110,164,170,181] This is evidence that cyclen immobilised in a coating could retain its ability to chelate Cu(II). Therefore, cyclen meets all of the requirements listed in **Section 2.1** for an ideal ligand, and a solid base of work exists to support the current project. In the present study, initial experiments were completed to observe the coordination of Cu(II) by cyclen.

Formation of the Cu(II)-cyclen complex was confirmed by both HRMS and UV-Vis spectroscopy. It is known that cyclen chelates Cu(II) in the *trans*-I conformation, with Cu(II) rising above the plane of the donor atoms (**Figure 2.19**).[89,167,182] Cyclen (white solid) and copper(II) chloride (green solid, 2.2 eq) were added to methanol and stirred for 2 h. Then, the dark blue, precipitated Cu(II)-cyclen complex was isolated and analysed by ESI-HRMS. ESI-HRMS data were consistent with a 1:1 Cu(II):cyclen complex minus a proton, imparting a +1 charge (calcd for $C_8H_{19}CuN_4$ [M - H]$^+$ 234.0906; found 234.0916). An aqueous, equimolar solution of cyclen and copper(II) nitrate was prepared, and the UV-Vis spectrum of the resultant, dark blue complex was measured (**Figure 2.20**). Due to

d-d transitions, the complex absorbed from approximately 430 nm to 800 nm (λ_{max} = 590 nm), only transmitting blue light and, thus, accounting for the complex's dark blue colour. An aqueous solution of only copper(II) nitrate absorbed red light with $\lambda_{max} \geq$ 800 nm and appeared pale-blue. Both of these experiments demonstrated Cu(II)-chelation by the cyclen ligand.
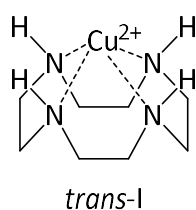
trans-I

Figure 2.19. Cu(II)-chelation by cyclen in the *trans*-I conformation.[167]
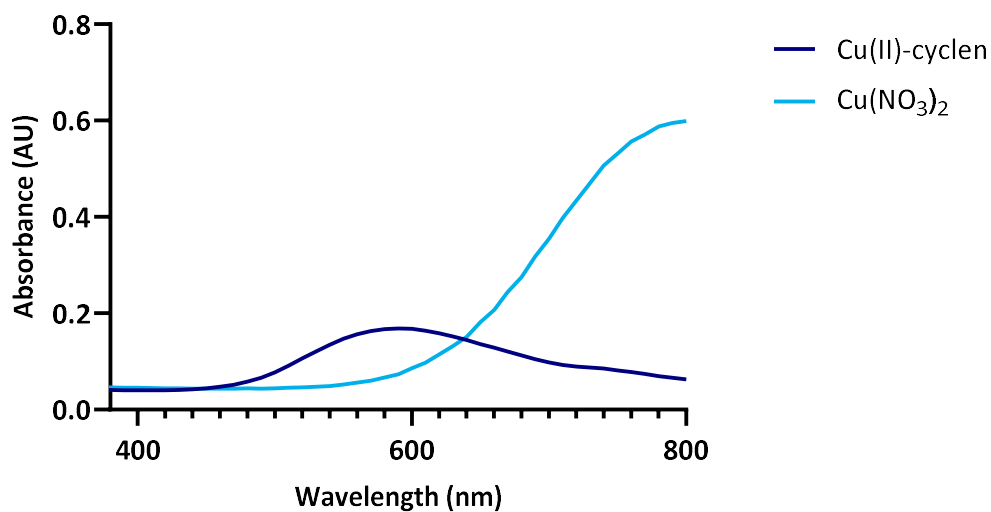
Figure 2.20. UV-Vis spectra of Cu(II)-cyclen and Cu(NO$_3$)$_2$.

2.5 Summary and Future Work

In the present study, the suitability of two ligand classes, acylhydrazones (*e.g.* DiLevDEG/ADH, **1a**) and tetraaza macrocycles (*e.g.* cyclen), was considered for the proposed antifouling application. The project developed out of the work by our research group in which the DiLevDEG/ADH polyacylhydrazone replaced 30–50% w/w of the acrylic resin in a commercial coating, producing a more environmentally friendly paint with functionality capable of Cu(II)-chelation (**Figure 2.2**).[127] Continuing from this research, it was hypothesised that the DiLevDEG/ADH-substituted paint could charge itself with Cu(II) from an aqueous solution and, thus, become antifouling. In the current work, testing of this hypothesis was designed to be completed in two stages: 1) DiLevDEG/ADH would be synthesised and its Cu(II)-coordination demonstrated, and 2) DiLevDEG/ADH would be formulated into the commercial acrylic paint and evaluated for Cu(II)-loading and antimicrobial activity after exposure to an aqueous solution of Cu(II). The first stage was completed in this chapter; DiLevDEG/ADH was successfully synthesised (**Figure 2.4**), and the ability of this polyacylhydrazone to chelate Cu(II) was confirmed *via* UV-Vis spectroscopy (**Figure 2.6**) and the observation of a colour change upon the addition of Cu(II) (**Figure 2.5**). The second stage of testing will be addressed in Chapter 3 (**Section 3.2**), and, based on the results, this coating may serve as the project's proof-of-concept. To search for other ligand candidates, simple acylhydrazones were synthesised.

A series of monoacylhydrazones and acyldihydrazones was successfully synthesised (**Scheme 2.2**) and characterised, including select Cu(II) complexes. (*E'/Z'*)-Rotamers, but only one geometric isomer (*E*), were observed in the NMR spectra of both aldehyde- and ketone-derived acylhydrazones. In general, the acylhydrazones were only soluble in DMF and DMSO, but one ligand with a more favourable solubility profile (**1a**) was progressed to complexation with Cu(II). A Job plot was constructed and an experiment was conducted to determine the $K_{Cu(II)L}$ of the Cu(II)-**1a** complex, which is known in the literature. This was done in an attempt to verify the methodology for later use on lesser-known acylhydrazones, and future experiments may pursue such $K_{Cu(II)L}$ measurements. However, due to the insolubility and complex solution chemistry of the acylhydrazones, as well as the acknowledgement of the existence of more suitable candidates, a different ligand class was pursued.

The new ligand class proposed for the project was tetraaza/oxatriaza macrocycles (**Figure 2.18**). Specifically, cyclen was selected out of the series to serve as a model ligand because it meets all of the project's requirements: it is commercially available, relatively inexpensive, selective for Cu(II) over other transition metals, and well-known in the literature. Formation of the Cu(II)-cyclen complex was confirmed by HRMS and UV-Vis spectroscopy. The Cu(II)-cyclen complex, with a high Log($K_{Cu(II)L}$) (23.3), is stable, resistant to demetallation, and able to outcompete the natural ligands in seawater. Since it

has been reported that the flux of copper ions is necessary for surface toxicity,[114,115] it seemed prudent to determine if such stable complexes could still exert an antimicrobial effect when bound to a surface. In future work, a ligand with a lower Log($K_{Cu(II)L}$) from the series of tetraaza/oxatriaza macrocycles (*e.g.* **6**) could be synthesised, incorporated into a coating, and tested for antimicrobial activity, comparing these results to cyclen to determine if activity increases with decreasing complex-stability. Alternatively, other ligand classes (*e.g.* polyamines, EDTA-type, *etc.*) could be explored.

3 Incorporation of Cu(II)-Ligand Complexes in Coating Binders

3.1 Background

Chapter 2 discussed the selection and synthesis of Cu(II) ligands (*e.g.* DiLevDEG/ADH, cyclen) to function as antifoulants in a coating, and the first explored route for formulation in a paint was incorporating these ligands in coating binders. As shown in **Figure 3.1**, the paint binder is the film-forming resin or polymer that binds together all of the other components, such as the coloured pigments, extenders, and additives. It is either dissolved in the paint or suspended as a colloid, and this binder/liquid mixture is referred to as the vehicle for the pigment. Binders are classified according to their molecular weight: low molecular weight binders require further chemical reactions to solidify in a film, but high molecular weight binders will form solid films without further reactions. Examples of low and high molecular weight film-formers are listed in **Table 3.1**.[29,30]
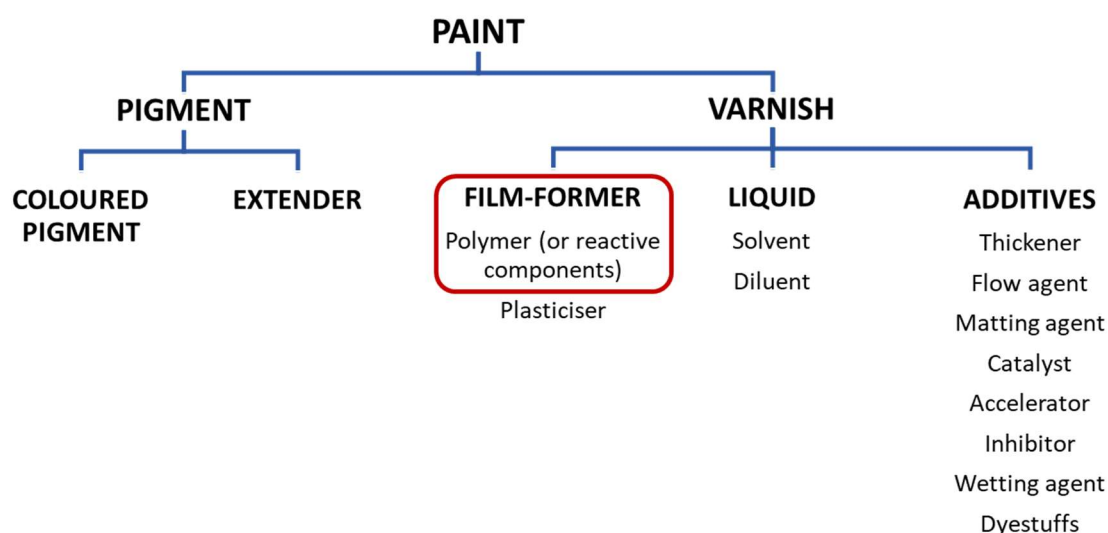
Figure 3.1. Paint components (adapted from *Introduction to Paint Chemistry*).[29]

Table 3.1. Low and high molecular weight binders (adapted from *Paint and Surface Coatings*).[30]

Low Molecular Weight	High Molecular Weight
Oleoresinous binders	Nitrocellulose
Alkyds	Solution vinyls
Polyurethanes	Solution acrylics
Urethane oils	Non-aqueous dispersion polymers
Amino resins	Polyvinyl acetate
Phenolic resins	Acrylic
Epoxide resins	Styrene/butadiene
Unsaturated polyesters	
Chlorinated rubber	

In the work by Daines *et al.*[127] in our research group, the DiLevDEG/ADH polyacylhydrazone was used to substitute a proportion of the crosslinking resin, classified as high molecular weight, in a commercial acrylic paint. Acrylic polymers display exceptional strength, flexibility, gloss, clarity, and weather and chemical resistance, leading to their widespread use.[30,183] In general, the polymers and copolymers (*i.e.* polymer made from more than one type of monomer)[29] of methacrylic and acrylic acid are referred to as acrylic resins (**Figure 3.2**). Copolymers of the corresponding esters with styrene, butadiene, or vinyl acetate are also sometimes called acrylic resins, but the term "acrylic" is usually reserved for resins dominated by the methacrylic or acrylic structures.[183] Acrylic polymers form *via* chain addition polymerisation in which the high molecular weight polymer is generated through initiation by an active species (*e.g.* radical) breaking bonds in the monomer, propagation of the reactive centre at the end of the chain, and, finally, termination of the reactive centre (**Figure 3.3**). This differs from stepwise polymerisation in which monomers, each containing two reactive functional groups, first form dimers, and the molecules continue to link together, resulting in an increase in average molecular weight over time. Stepwise polymerisation is the mechanism by which, for example, polyurethane and epoxy resins are produced.[29,30,184]
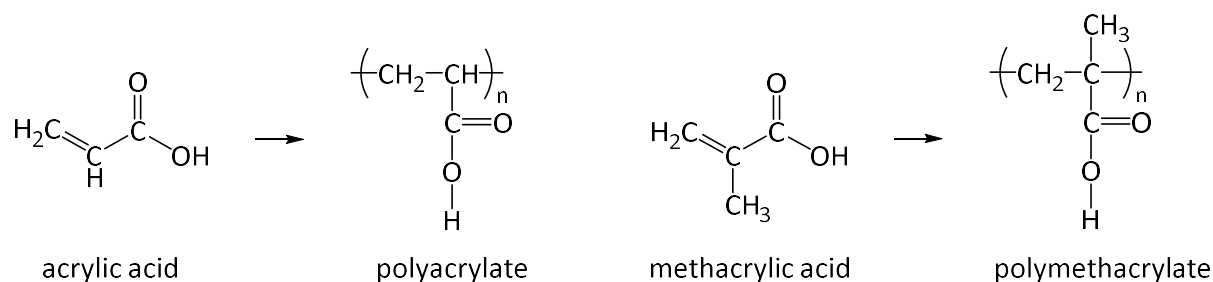
Figure 3.2. Structures of acrylic acid, the monomer of polyacrylate, and methacrylic acid, the monomer of polymethacrylate.
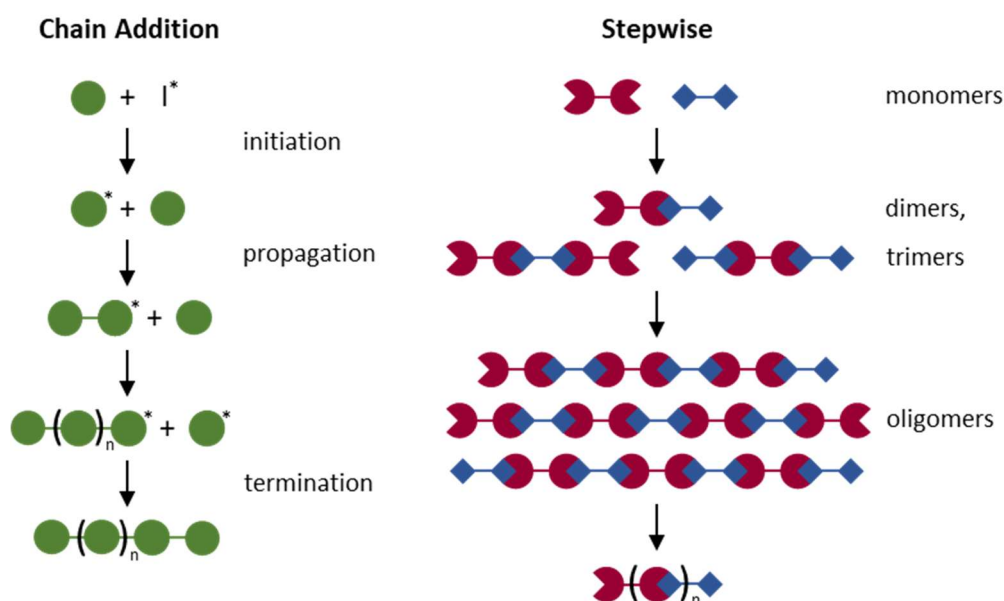
Figure 3.3. Chain addition *vs* stepwise polymerisation (I[*] = initiator, radical; adapted from Bossion *et al.*[184]).

Polyurethane and epoxy resins, both low molecular weight, are common binders in marine paints.[30,185] Polyurethanes are used extensively in the coatings industry, as they are tough, flexible, and exhibit excellent substrate adhesion and resistance to chemicals, abrasion, and corrosion.[29,183] They are characterised by carbamate, also referred to as urethane, linkages (−HN−(C=O)−O−) but may contain other functional groups (*e.g.* esters, ethers, ureas, amides).[183] The urethane linkage is typically formed by the reaction between an isocyanate group (R−N=C=O) and a hydroxyl group. Thus, polyurethanes are produced by the reaction of a polymeric isocyanate or diisocyanate with a polyol (**Scheme 3.1**).[186] Epoxy resins, on the other hand, are popular due to their toughness, corrosion and chemical resistance, thermal stability, and superior substrate adhesion and electrical properties.[30,183] They contain one or more epoxy groups, which react in their preparation or crosslinking; preparation of an epoxy resin usually involves the reaction of bisphenol A with epichlorohydrin (**Scheme 3.2**). The resultant polymer is a reactive intermediate, and, to function as a film-former, this resin requires curing (*i.e.* crosslinking) *via* the reaction of curing agents (*i.e.* hardeners, *e.g.* polyamines) with pendant hydroxyl groups and/or terminal epoxy groups. The result of the curing process is a film with a crosslinked, three-dimensional network.[29,30,183]
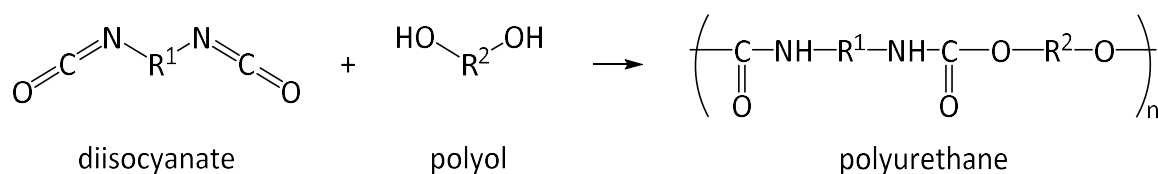
Scheme 3.1. Reaction of a diisocyanate with a polyol to produce a polyurethane.
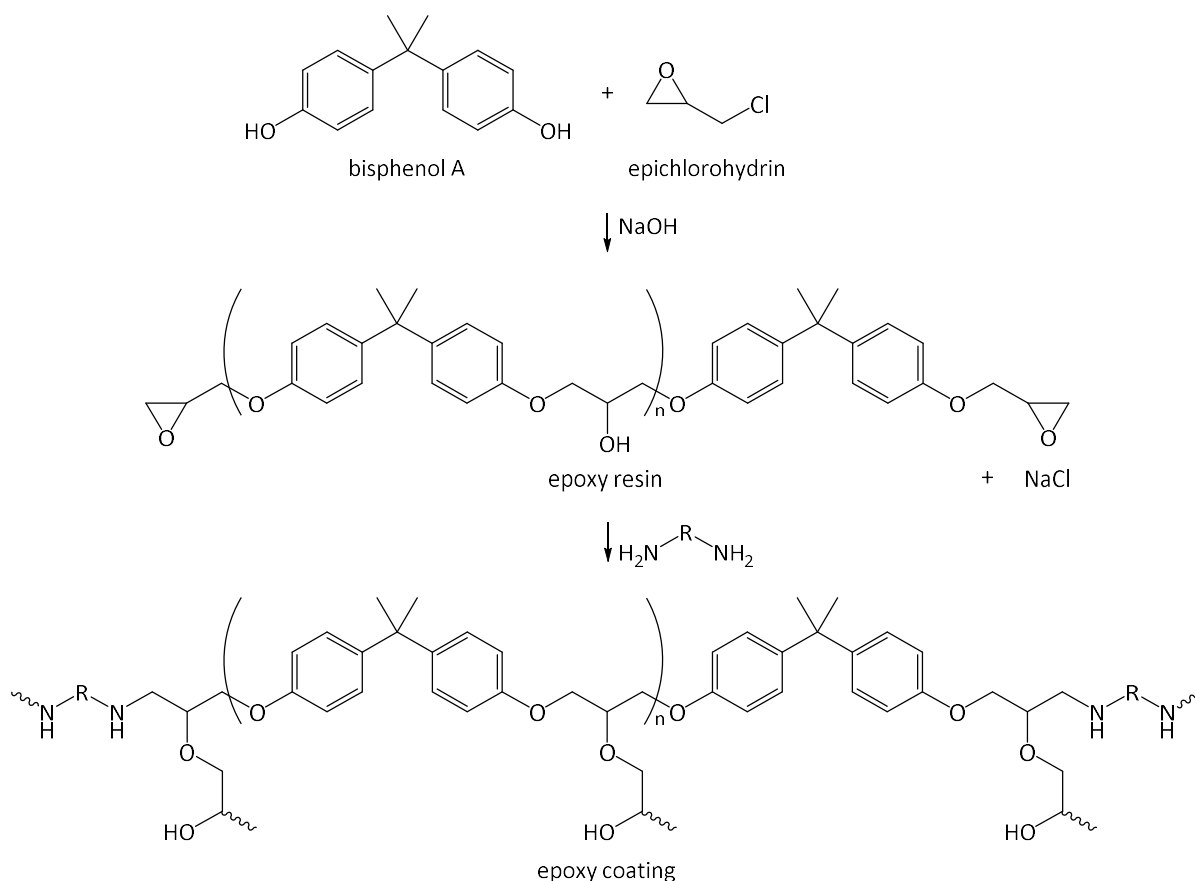
Scheme 3.2. Reaction of bisphenol A with epichlorohydrin to produce an epoxy resin, which then reacts with an amine curing agent and other epoxy groups to form the crosslinked coating (adapted from *Introduction to Paint Chemistry*).[29]

There are multiple examples in the literature of the incorporation of Cu(II) ligands in both polyurethane and epoxy resins.[110,111,187–194] For instance, Hwang and Meyerhoff[110] tethered the Cu(II)-cyclen complex, serving as a nitric oxide (NO)-generating catalyst, to a medical grade polyurethane (Tecophilic, SP-93A-100). Biomedical device coatings capable of releasing NO are desirable, as they improve the biocompatibility of the device, and NO generation was observed when the Cu(II)-cyclen complex-linked polyurethane was in contact with fresh animal whole blood. In a study by Xie *et al.*[188],

marine antifoulant *N*-(2,4,6-trichlorophenyl) maleimide was linked as a pendant group to a polyurethane with poly(dimethylsiloxane) main chains, a polymer used in antifouling, and this surface successfully prevented biofouling by marine organisms (*e.g.* bacterium *Micrococcus luteus*, diatom *Navicula*, barnacle cyprids).

There has been much interest in the incorporation of transition metal complexes in epoxy systems due to the improved physical properties of the coatings, and such complexes have been used as curing agents, catalysts, and cure accelerators.[189] For example, Kurnoskin[111,190–192] synthesised metalliferous epoxy chelate polymers from bisphenol A diglycidyl ether (DGEBA), a constituent of epoxy resins, and transition metals (*e.g.* Cu(II), Co(II), Ni(II), Zn(II), Cd(II), Fe(III), Mn(IV)) coordinated to aliphatic amines (*e.g.* ethylenediamine, diethylenetriamine, triethylenetetramine), which functioned as curing agents. Inclusion of the transition metal complexes resulted in increased strength and, for the Cu(II)-containing polymers in particular, increased water and heat resistance. Given this evidence of the successful formulation of metal-ligand complexes into coating binders, the inclusion of Cu(II) ligands in polyurethanes and epoxy systems, as well DiLevDEG/ADH in the acrylic polymer, was explored.

3.2 Polyacylhydrazone DiLevDEG/ADH-Substituted Resin in a Commercial Acrylic Paint

In the aforementioned, foundational work by Daines *et al.*[127] in our research group (Chapter 2, **Section 2.2**), 30–50% w/w of the crosslinking resin in a commercial acrylic paint was substituted with polyacylhydrazone DiLevDEG/ADH, creating from renewable sources a paint that performed well in standard industry tests. Since DiLevDEG/ADH contains functionality capable of Cu(II)-chelation (Chapter 2, **Figure 2.3**), it was speculated that the paint might serve as the current project's proof-of-concept, being a candidate antifouling coating, and two stages of evaluation were proposed. The first stage involved the synthesis of DiLevDEG/ADH and confirmation of its ability to bind Cu(II), and the successful completion of this stage was discussed in Chapter 2. The second stage involved the formulation of DiLevDEG/ADH into the acrylic paint, the quantification of Cu(II)-loading on the coating surface, and an assessment of the subsequent antimicrobial activity (**Figure 3.4**). The results from the second stage are discussed in the present chapter.
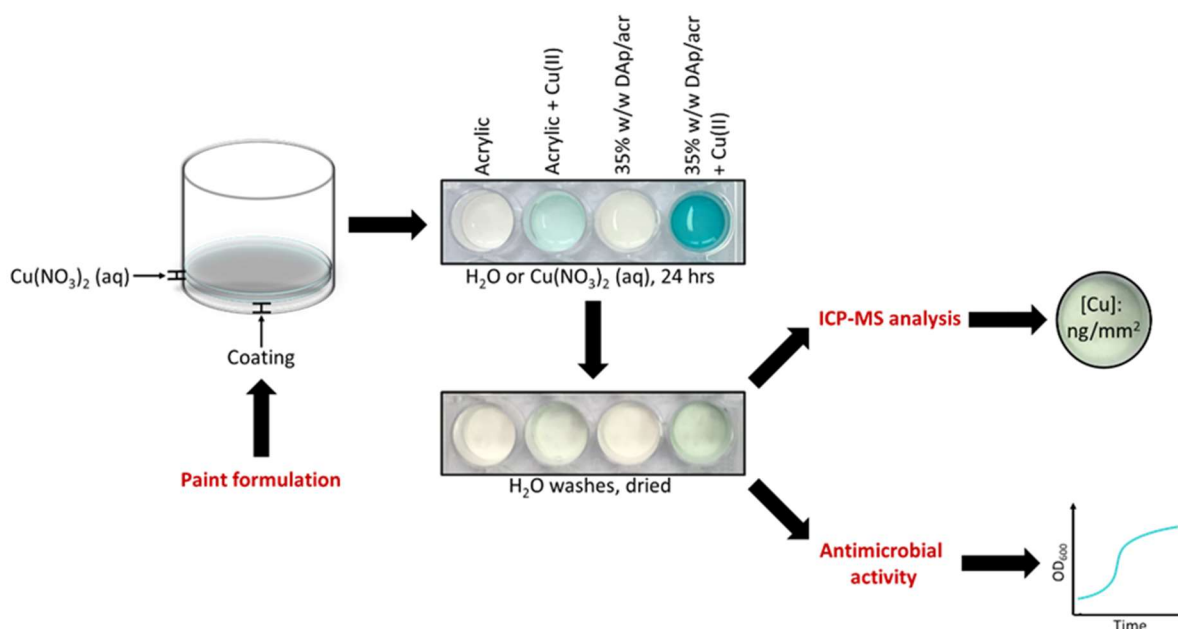
Figure 3.4. Methodology for assessing the Cu(II)-chelating ability of the acrylic and DAp/acr paints and their impact on bacterial growth (± Cu(II); second stage of testing).

The workflow for the second stage of assessments is outlined in **Figure 3.4**. Initially, the commercial acrylic and DiLevDEG/ADH polyacylhydrazone/acrylic (DAp/acr) paints were formulated, and the bottoms of wells or vials were coated with the paints. Once the paints cured, they were exposed to a Cu(II) salt solution for 24 h. After 24 h, the coatings were washed, dried, and assessed for either their ability to retain Cu(II) or their impact on bacterial growth, with and without Cu(II). The amount of Cu(II) sequestered by each coating, as well as the amount of Cu(II) leaching from it into the bacterial growth medium, was quantified *via* inductively coupled plasma mass spectrometry (ICP-MS), a trace metal technique capable of rapid, multi-element determinations. ICP-MS has detection limits in the sub parts *per* trillion (ppt) but can also measure in the high parts *per* million (ppm). For ICP-MS analysis, a sample (diluted as needed) is pumped into a nebulizer and converted into a fine aerosol with argon gas, which is introduced to an argon plasma for ionisation. The positively charged ions then pass into the mass spectrometer to be separated and counted.[195] For the growth assays, the growth of a bacterial culture in contact with the painted surfaces was monitored, and, by pairing the ICP-MS and growth assay results, the effects of the paint surfaces' levels of Cu(II)-loading and Cu(II)-leaching on bacterial growth could be evaluated.

3.2.1 Formulation

The DAp/acr paint was formulated as in Daines *et al.*[127]: 35% w/w of the ADH-crosslinked dispersion polymer in a commercial acrylic paint (LR200) supplied by Resene Paints Ltd. (**Table 3.2**) was substituted with the aqueous solution of ~50% w/v DiLevDEG/ADH prepared in Chapter 2 (**Section 2.2**). For comparison, the acrylic paint was also prepared according to the conventional recipe. The percent substitution of the resin was chosen to be 35% w/w because, although the work by Daines *et al.*[127] showed that substitution up to 50% w/w was possible, a lower level of substitution (*e.g.* 30% w/w) improved properties in the final paint. These properties included gloss, hardness, water resistance, and adherence to standard paint test-cards. Due to the inclusion of titanium dioxide as a pigment, both the acrylic and DAp/acr paints were white and opaque, but the DAp/acr paint was notably less viscous than the acrylic paint. Following formulation, the paints were exposed to Cu(II) and tested for their Cu(II)-retention and impact on bacterial growth.

Table 3.2. Composition of the commercial acrylic paint used in this study.[a]

Ingredient	% w/w
Water	8
Millbase	
Titanium dioxide	26
Water, rheology modifier, dispersant, surfactant, MPG[b], defoamer, biocide, alkali	8
Dispersion mixture	
Dispersion polymer[c]	52
Coalescent, surface wetter, MPG[b], defoamer, biocide, alkali	6

[a] Proprietary composition and specific components confidential to Resene Paints Ltd.
[b] Monopropylene glycol.
[c] Resin = ADH-crosslinked dispersion polymer (45% w/w).

3.2.2 Growth Assay: *E. coli* NZRM 3647

The effects of the acrylic and DAp/acr paints (± Cu(II)) on the growth of *E. coli* NZRM 3647 were determined in an assay developed in our research group. This assay was developed in response to concerns about the industry-accepted protocol used to test surfaces for antimicrobial activity: International Organisation for Standardisation (ISO) 22196 (Japanese Industry Standard (JIS) Z 2801).[196–198] In ISO 22196, standard inocula of *E. coli* or *S. aureus* are delivered in a suspension to test and control surfaces, which are then covered with a plastic film and incubated for 24 ± 1 h at 35 ± 1 °C and > 90% relative humidity. Viable bacteria are recovered and enumerated at 0 and 24 h to calculate antimicrobial activity.[199] This protocol is favoured by manufacturers because it allows ample time for the biocide to diffuse from the coating and exert an effect, confirming antimicrobial activity prior to commercialisation of the product.[196,198] Yet, there are concerns about the reproducibility of the method. For instance, Wiegand *et al*.[197] completed a round robin test that employed the ISO 22196 procedure to elucidate the antimicrobial activity of standard materials. Eight different laboratories participated and reported different results in the first round of testing. Furthermore, in unpublished work in our research team, the reproducibility of results derived from utilisation of the ISO 22196 protocol to determine the antimicrobial activities of different paints was evaluated and found to be poor.[200] Consequently, a more robust method for measuring the antimicrobial activity of a coating was developed.

The new growth assay developed in our research group generated reproducible results and was more high-throughput, requiring less time per sample. For consistency with previous work on ISO 22196, the bacterium used for testing was *E. coli* NZRM 3647 (serotype O157:H7, verocytotoxin negative). In

the assay, the bottoms of wells in a 24-well plate were coated evenly with the paint, which was allowed to cure and then was washed with water and dried. A standard inoculum of *E. coli* NZRM 3647 was delivered to each well, and the plate was incubated at 37 °C. The optical density (OD, 600 nm) of the culture in each well was measured at different time points up until 24 h, generating growth curves of the bacterium. Such growth curves are typically sigmoidal, as bacterial growth proceeds through successive phases (**Figure 3.5**). Immediately following inoculation of a medium, bacteria do not divide, and growth is nil. But, this lag phase is followed by a phase of exponential growth, which eventually plateaus at a maximum population density. In the stationary phase, either growth halts or the growth and death rates of bacterial cells become equal, resulting in no overall growth. As nutrients are depleted, however, bacteria enter a phase of death, and the cells lyse. Although growth curves plot the logarithm (Log_{10}) of bacterial density *vs* time, OD_{600}, a measurement of light scattering, is generally proportional to bacterial density and serves as its proxy in growth experiments, as in the present study.[201,202]
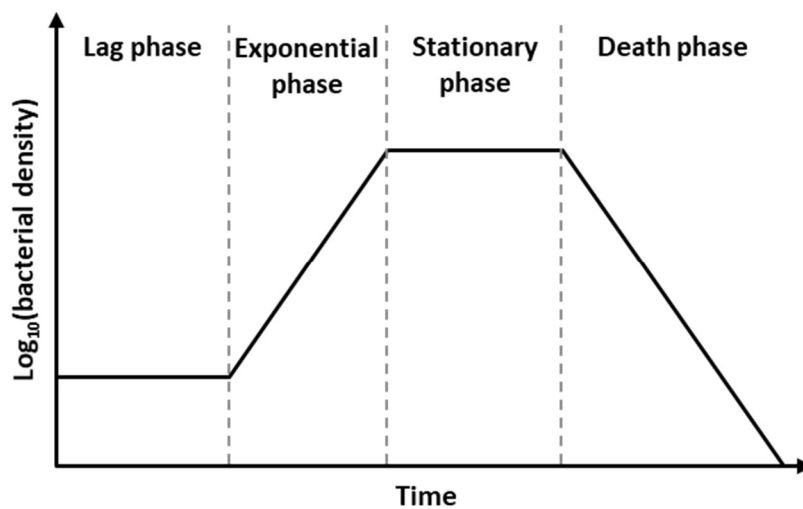
Figure 3.5. Example of a bacterial growth curve.[202]

The developed assay was employed to assess the growth of *E. coli* NZRM 3647 when in contact with the acrylic (± Cu(II)) paint, 35% w/w DAp/acr (± Cu(II)) paint, and a commercial marine paint. The marine paint (Altex Yacht and Boat Paint, Ablative Antifouling No. 5; 40–50% w/w Cu_2O) was included for comparison to a commercial antifouling standard from Resene Paints Ltd., the collaborating paint manufacturer who supplied the acrylic paint. Uncoated wells served as growth controls, and the assay was repeated in triplicate for each coating. In order to determine the effect of Cu(II)-loading on

bacterial growth, the acrylic and DAp/acr paints were prepared for testing with and without exposure to Cu(II) (Appendix, **Figure 8.20**). Cu(II)-loading was achieved *via* exposure to a dilute, aqueous Cu(II) salt solution for 24 h (**Figure 3.6**). These conditions were selected as a starting point because the ultimate application of the coating will require it to bind dilute Cu(II) in seawater. It was observed that, in the DAp/acr-coated wells, the Cu(II) salt solution changed from a light blue to teal colour (**Figure 3.6**, left "35% w/w DAp/acr + Cu(II)"), suggesting that ligands may have leached from the paint into the supernatant to form Cu(II) complexes.[129]
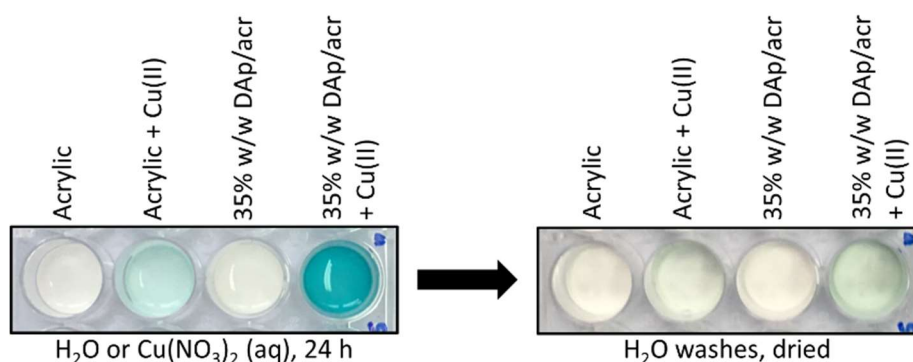
Figure 3.6. Cu(II)-loading process for acrylic and DAp/acr paints.

In the assay, growth inhibition was observed in the wells coated with, in order from least- to most-inhibiting, the acrylic, marine, Cu(II)-loaded 35% w/w DAp/acr ("DAp/acr + Cu(II)"), 35% w/w DAp/acr, and Cu(II)-loaded acrylic ("Acrylic + Cu(II)") paints (**Figure 3.7**). Bacterial growth in the uncoated wells adhered to the classic sigmoidal curve, plateauing at a higher OD_{600} than the other test samples. Growth in the wells coated with the acrylic paint was also sigmoidal but plateaued at a lower OD_{600} than in the uncoated wells, indicating some inhibitory effect by leached components. Yet, growth in these wells was the least-impacted out of all the coated wells. In contrast, the "Acrylic + Cu(II)" paint had the greatest inhibitory effect on bacterial growth; the overall growth was net negative, with alternating stages of death and growth. The DAp/acr paint had the second-greatest inhibitory effect. For the other copper-containing paints (*e.g.* "Marine Paint", "DAp/acr + Cu(II)"), the inhibitory effects were approximately equivalent, being only marginally greater for the Cu(II)-loaded DAp/acr paint, and alternating phases of slowed/negative and positive growth were observed. Such alternating phases were unsurprising, given that the copper coatings were expected to release Cu(II) into the growth medium and, subsequently, cause cell lysis.[115]
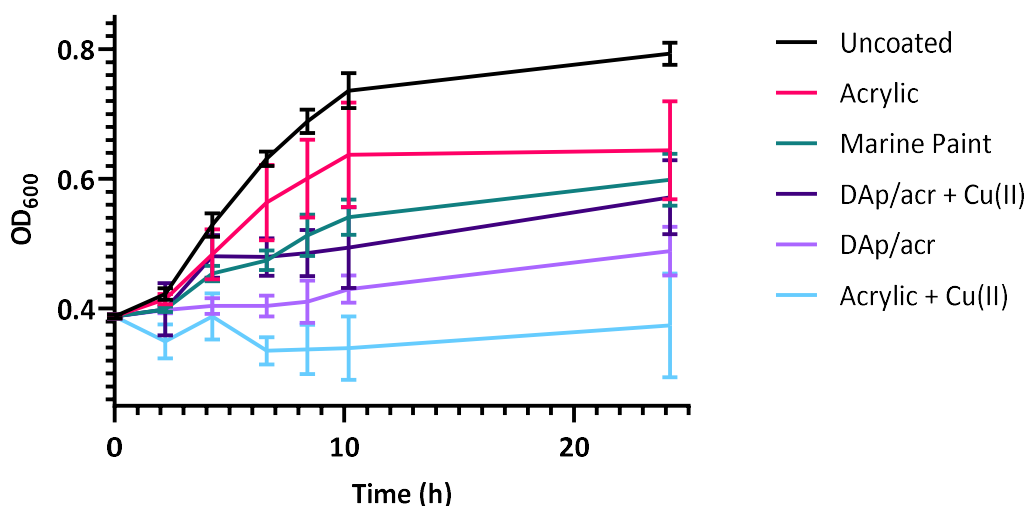
Figure 3.7. Growth curves (OD_{600} *vs* time) of *E. coli* NZRM 3647 in uncoated wells and wells coated with the acrylic ($\pm$ Cu(II)), 35% w/w DAp/acr ($\pm$ Cu(II)), and marine paints. The error bars show the standard deviation (SD) from three biological replicates (br).

Regarding the order of inhibition, the assay results were not as predicted. It had been anticipated that both the marine and Cu(II)-loaded DAp/acr paints would have higher surface concentrations of copper than the Cu(II)-loaded acrylic paint, which is not known to have functionality for stable Cu(II)-complexation, and that they would, therefore, have a more detrimental effect on the growth of *E. coli* NZRM 3647. So, it was unexpected that the "Acrylic + Cu(II)" coating had a greater inhibitory impact than both the marine paint, which is 40–50% w/w cuprous oxide, and the "DAp/acr + Cu(II)" paint, which has 35% w/w of its binder substituted with a polymer capable of binding Cu(II). Due to the presence of Cu(II) ligands in the DAp/acr paint, it was hypothesised that the "DAp/acr + Cu(II)" paint bound significantly more but released less Cu(II) than the "Acrylic + Cu(II)" paint, on which the Cu(II) would be only weakly associated. Since the release of copper ions from a surface is necessary for antimicrobial activity, this could explain the greatest growth inhibition being in the "Acrylic + Cu(II)" wells. Regarding the marine paint, it was hypothesised that, like "DAp/acr + Cu(II)", the surface released less copper than the "Acrylic + Cu(II)" paint. It was also unexpected that *E. coli* NZRM 3647 would exhibit the second-greatest growth defect in the presence of the DAp/acr paint, a paint without copper. But, there was evidence of ligands, perhaps the DiLevDEG/ADH polyacylhydrazone, leaching from the coating, and such leached components may have their own antimicrobial activity. To test these hypotheses, the amounts of copper bound to and released from the surfaces of the

"Acrylic + Cu(II)" and "DAp/acr + Cu(II)" paints, as well as released from the surface of the marine paint, were quantified. Additionally, the DAp/acr paint was tested for the leaching of DiLevDEG/ADH.

3.2.3 Quantification of Cu(II)-Leaching

To quantify the copper leaching from the coatings during the growth assay, the amounts of copper leached from the Cu(II)-loaded commercial acrylic and 35% w/w DAp/acr paints, as well as the marine paint, into the nutrient broth after 24 h were measured. As previously described for the growth assay, this was done by coating the well-bottoms of a 24-well plate with the acrylic, DAp/acr, and marine paints and loading some of the cured acrylic and DAp/acr paints with Cu(II) (Appendix, **Figure 8.20**). Then, nutrient broth was added to uncoated wells and the wells coated with the acrylic (± Cu(II)), DAp/acr (± Cu(II)), and marine paints. The uncoated wells and wells coated with the acrylic and DAp/acr paints but unexposed to Cu(II) served as blanks. After incubating the plate for 24 h at 37 °C, the nutrient broth from each well was removed and diluted for ICP-MS analysis to quantify the amount of copper, likely in the oxidised Cu(II) form, released from the coated surfaces into the growth medium.

The copper results (**Table 3.3**) supported the hypothesis that the extent of growth inhibition of *E. coli* NZRM 3647 in the assay was related to the amount of Cu(II) released by the copper-containing paints. The marine paint leached the least amount of copper (25.2 ± 0.6 μg). This provided an explanation for it having a smaller impact on bacterial growth than the other copper paints but was surprising, given its high copper content. Although, cuprous oxide (Cu_2O), the biocidal agent in the marine paint, is poorly water-soluble, and its dissolution rate depends on the particle size, pH, temperature, and presence of other ligands or ions in solution. When exposed to oxygen in solution, Cu(I) is rapidly oxidised to Cu(II).[203–205] The Cu(II)-loaded acrylic paint had the greatest inhibitory effect on bacterial growth and released the most copper (91 ± 5 μg) out of all of the tested coatings. The Cu(II)-loaded DAp/acr paint, which had a slightly greater inhibitory growth effect than the marine paint, released more copper than the marine paint but less than the "Acrylic + Cu(II)" paint (39 ± 5 μg). Thus, for the copper coatings, increased growth inhibition corresponded to increased Cu(II)-leaching, as hypothesised. This is in agreement with the vital role of surface-released copper ions in the proposed mechanism of contact killing for copper surfaces: in the literature, it is proposed that copper ions released from a surface cause damage to the bacterial membrane and then enter the cell, resulting in oxidative damage, cell death, and DNA degradation.[115] Additionally, Macomber and Imlay[206] found that *E. coli* W3110 exhibited a growth defect at Cu(II) concentrations greater than 8 μM in a minimal

salts medium containing glucose after 10 h at 37 °C. As the Cu(II)-leaching results from the coatings in the present study are an order of magnitude higher (*i.e.* mM *vs* μM), it is reasonable that the "Acrylic + Cu(II)", "DAp/acr + Cu(II)", and marine paints negatively affected the growth of *E. coli* NZRM 3647 in the assay. In light of these Cu(II)-leaching results, measuring the Cu(II)-loading on the surface of the acrylic and DAp/acr paints was of interest, since it was hypothesised that the DAp/acr paint would bind more but release less Cu(II).

Table 3.3. Amounts of copper leached from the Cu(II)-loaded commercial acrylic and 35% w/w DAp/acr paints, as well as the marine paint, into the nutrient broth after 24 h.

Coating	ppm Cu[a]	μg Cu[a]	mM Cu[a]
Acrylic + Cu(II)	180 ± 10	**91 ± 5**	2.9 ± 0.2
DAp/acr + Cu(II)	80 ± 10	**39 ± 5**	1.2 ± 0.2
Marine Paint	50 ± 1	**25.2 ± 0.6**	0.79 ± 0.02

[a] Mean ± SD, n = 3. ppm = μg/mL, μg/g.

3.2.4 Quantification of Cu(II)-Loading

The amounts of Cu(II) retained by the commercial acrylic and 35% w/w DAp/acr paints were quantified (**Figure 3.4**). These paints were used to coat the bottoms of custom-made glass vials that had dimensions matching the wells from the 24-well plate in the growth assay so that the copper results could be directly related to the assay; it was acknowledged that the depth and exposed surface area of the coating would vary in differently sized vials and, thus, affect Cu(II)-loading. The paints were left to cure until they were no longer tacky, and then an aliquot of a dilute, aqueous Cu(II) salt solution was added to each vial. In the DAp/acr-coated vials, again, the supernatant changed from a light blue to teal colour – presumably, from Cu(II) ligands leached from the paint. After 24 h, the vials were washed with water and dried. Following exposure to Cu(II), the surface of the acrylic paint was light green, while the 35% w/w DAp/acr paint surface was a slightly darker shade of green (as in **Figure 3.6**, right). The Cu(II)-loaded coatings were digested in concentrated nitric acid and diluted for copper analysis *via* ICP-MS.

To verify that the digestion procedure was sufficient to release all of the copper into solution, two acrylic paint samples were spiked with a known amount of copper. For the first sample, the copper was homogeneously mixed in the paint before using it to coat the bottom of a vial. For the second sample, the copper was added to the surface of the already-cured paint. The acrylic paint without

added copper served as a blank, and the reported results are blank-subtracted. Post-digestion of these coatings, ICP-MS (Cu) analysis revealed that the percent error between the theoretical and actual amounts of copper were 7% and 4% for the mixed and surface-spiked samples, respectively (**Table 3.4**). The copper-spiked surface was more representative of the Cu(II)-loaded paints, and the percent error calculated from its measured copper content was deemed acceptable. Therefore, the copper results validated the overall efficacy of the digestion procedure.

Table 3.4. ICP-MS (Cu) results of acrylic paint spike study.

Sample	Actual µg Cu in Coating	Theoretical µg Cu in Coating	% Error
Mixed	11.8	11.1	7
Surface	10.8	10.4	4

The Cu(II)-loading results for the acrylic and 35% w/w DAp/acr paints were reported as the amount of copper normalised by the mass of the cured paint in the vial and by the surface area of the paint exposed to the Cu(II) salt solution (**Table 3.5**). This was done to account for variations in the sample preparation (*e.g.* mass, surface area), allowing for comparisons between coatings. Although, such normalisations could be misleading, as the depth of Cu(II)-penetration in the coating is unknown (*e.g.* normalisation by surface area when not all of the copper is necessarily at the surface). Four batches of each paint were prepared and analysed in triplicate on different days to assess the reproducibility of the method for samples both within a batch and between independent batches. Within a batch, the copper results were relatively reproducible, with the percent relative standard deviation (RSD) between the triplicate measurements being, at most, 15%. However, between batches, the results were not consistently reproducible. A one-way ANOVA with Tukey's *post hoc* test revealed no statistically significant differences ($p > 0.05$) between the results for Batch 1 *vs* 2 and Batch 3 *vs* 4, but the results for Batches 1/2 *vs* Batches 3/4 were different. In fact, the percent difference between the mean results for Batches 1/2 *vs* Batches 3/4 was, in some cases, greater than 60%. Furthermore, it was uncertain which paint could retain the most copper, since the mean batch results ranged from 1450–2700 µg Cu/g (730–1400 ng Cu/mm^2) and 1300–2020 µg Cu/g (600–920 ng Cu/mm^2) for the acrylic and DAp/acr paints, respectively.

Table 3.5. Amounts of copper retained by different batches of the commercial acrylic and 35% w/w DAp/acr paints.

Coating	Batch #	μg Cu/g Coating[a]	ng Cu/mm^2 Coating[a,b]
Acrylic + Cu(II)	1	2500 ± 200	1200 ± 100
Acrylic + Cu(II)	2	2700 ± 300	1400 ± 200
Acrylic + Cu(II)	3	1500 ± 100	740 ± 90
Acrylic + Cu(II)	4	1450 ± 80	730 ± 40
35% w/w DAp/acr + Cu(II)	1	1300 ± 200	620 ± 90
35% w/w DAp/acr + Cu(II)	2	1300 ± 100	600 ± 80
35% w/w DAp/acr + Cu(II)	3	1820 ± 10	880 ± 40
35% w/w DAp/acr + Cu(II)	4	2020 ± 40	920 ± 20

[a] Mean ± SD, n = 3.
[b] Surface area (mm^2) exposed to Cu(II) salt solution. Calculated as in the Appendix (**Figure 8.22**).

Because the same procedure was followed to prepare and test the coatings, the source of variability in the copper results between paint batches was unclear. The only difference between batches was that the paint cure-times were inconstant, ranging from 17–66 h. Rather than standardising the length of time the paints were allowed to cure, each batch was left at 50 °C until, at least, all of the samples in the batch were no longer tacky, but sometimes they were left longer. Since triplicate samples within batches were cured for the same time-length, this could explain the absence of such variability between these replicates. Also, Cu(II)-loading experiments for the batches were conducted on different days over the course of two months. Thus, the samples could have been exposed to different atmospheric conditions (*e.g.* humidity) as well, further impacting the curing process. It is probable that the parameters and extent of curing notably affect Cu(II)-loading in a paint. For example, a softer, not yet fully cured paint may allow deeper penetration of the Cu(II) salt solution and, consequently, bind more Cu(II).

Regarding the growth assay, the curing conditions (*e.g.* time, temperature) of the paints in the wells of the 24-well plate were different from the conditions in the Cu(II)-loading experiments. Although, similarly, the paints were allowed to cure until they were no longer tacky. The variability of the copper results between paint batches, possibly due to differences in curing, suggested that the data should only be related semi-quantitatively to the growth assay, meaning that the copper concentrations in the coated vials were not necessarily equivalent to what those had been in the coated wells. Accordingly, it may be concluded that, in the growth assay, similar amounts of Cu(II) were retained by the acrylic and 35% w/w DAp/acr paints post-exposure to the Cu(II) salt solution and that the Cu(II)

concentrations were in the mg/g (μg/mm^2) range. This evidence contradicted the hypothesis that the DAp/acr paint, with the Cu(II) ligand incorporated at 35% w/w, would retain significantly more Cu(II) than the acrylic paint. Since Cu(II)-leaching was measured for samples in triplicate within a single batch, batch variability was also expected to affect the accuracy of these results, but the relative order was not expected to change. Both the leaching and loading of Cu(II) in the DAp/acr paint were likely affected by the additional leaching of a Cu(II) ligand, the identity of which was determined in a separate experiment.

3.2.5 DiLevDEG/ADH Polyacylhydrazone-Leaching

An experiment was conducted to confirm that the Cu(II) ligand leaching from the 35% w/w DAp/acr paint was the DiLevDEG/ADH polyacylhydrazone. This leaching was suspected when, upon the addition of the aqueous Cu(II) salt solution to the DAp/acr-coated well or vial, the supernatant changed colour from light blue to teal, which is consistent with the d-d transitions in Cu(II) complexes.[129] DiLevDEG/ADH is water-soluble and present at a high concentration in the paint, making it a probable candidate for the leachate. The identity of the leachate was confirmed by applying the DAp/acr paint to the bottom of a well in a 24-well plate, allowing it to cure, adding deuterium oxide (D_2O) to the well for 24 h, and then measuring the ^{13}C NMR spectrum of the D_2O supernatant and comparing it to that of DiLevDEG/ADH.

The ^{13}C NMR spectrum of the leachate revealed that the DiLevDEG/ADH polyacylhydrazone binder was indeed leaching out of the DAp/acr paint. As seen in **Figure 3.8**, the signals in the reference spectrum of DiLevDEG/ADH were present in the spectrum of the leachate. For instance, the signals for **C2** (<u>C</u>=N), doubled due to rotamers, were observed at δ_C 163.0 and 159.1 ppm, and the signal for **C5**, the hydrazone carbonyl, was observed at δ_C 173.1 ppm. The signal ratio of end-group **C6** to **C4** was approximately 1:11 in the reference spectrum but 1:4 in the leachate spectrum, indicating that the polyacylhydrazone was releasing small molecules and/or monomers into solution. This was unsurprising, as our research group has observed that the acylhydrazone bond is dynamic, breaking and reforming in aqueous solutions.[128] Because signals unattributed to DiLevDEG/ADH were also present in the leachate's spectrum, it was apparent that other compounds leached from the DAp/acr paint as well, but these compounds were not identified, as the remainder of the paint composition is confidential to Resene Paints Ltd. Undoubtedly, the leaching of this paint's binder impacted the binding and release of Cu(II) and, subsequently, bacterial growth. For example, in the assay with *E. coli* NZRM 3647, the growth defect was greater in the DAp/acr wells without Cu(II) than with. It is possible that the leached polyacylhydrazone had an antimicrobial effect that was mitigated by binding Cu(II),

since the formation of such complexes could even promote DiLevDEG/ADH's retention in the paint. In addition to these effects, the leaching of DiLevDEG/ADH had serious implications regarding the suitability of the DAp/acr paint as the project's proof-of-concept.
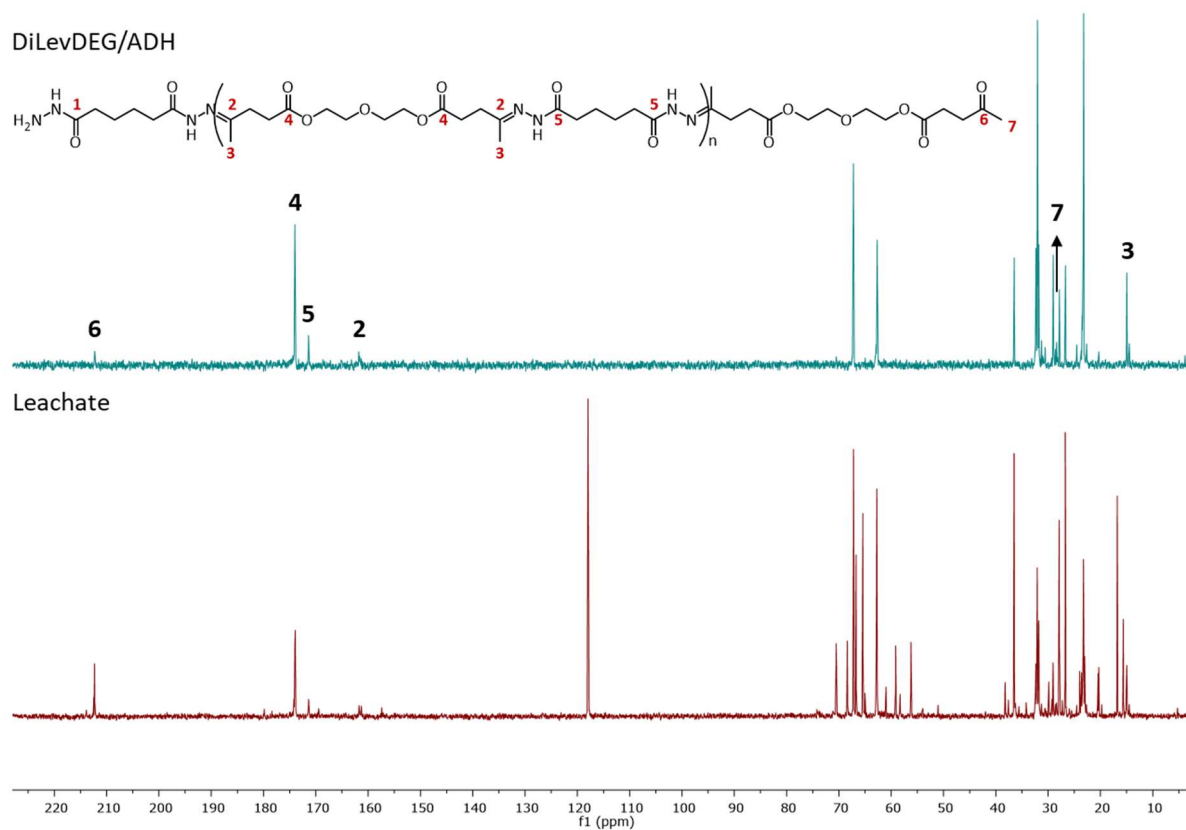
Figure 3.8. ^{13}C NMR spectra (crude; D$_2$O) of the leachate and DiLevDEG/ADH polyacylhydrazone with select carbon assignments (δ_C 118.0 ppm = acetonitrile).

3.2.6 Conclusions

Cumulatively, the Cu(II)-leaching, Cu(II)-loading, polyacylhydrazone-leaching, and growth assay results revealed that the DAp/acr paint was unsuitable as an antifouling coating. As previously stated in Chapter 2 (**Section 2.1**), an ideal ligand to serve as the project's proof-of-concept must be stable and not introduce any new, possibly toxic, components into seawater from the antifouling paint. The DAp/acr paint failed to meet this criterion: it leached small molecules and/or monomers from the DiLevDEG/ADH polyacylhydrazone binder into the aqueous solution (**Figure 3.8**), inhibiting bacterial growth (**Figure 3.7**). This suggested that DiLevDEG/ADH may have some associated toxicity. In fact, the DAp/acr paint had an even more negative impact on the growth of *E. coli* NZRM 3647 than the

Cu(II)-loaded DAp/acr paint, which could be explained by enhanced retention of DiLevDEG/ADH in the paint through Cu(II)-coordination. Furthermore, the Cu(II)-loaded commercial acrylic paint inhibited growth to a greater extent than any of the other tested coatings, including the DAp/acr ($\pm$ Cu(II)) paints and the industry-standard marine paint.

It was discovered that the order of growth inhibition for the copper-containing paints (*i.e*. from most to least: "Acrylic + Cu(II)", "DAp/acr + Cu(II)", "Marine Paint") was due to the relative amounts of copper released by the coatings, rather than the surface concentrations of copper. Both the acrylic and DAp/acr paints bound similar amounts of Cu(II) in the range of 0.1–0.3% w/w (**Table 3.5**), while the marine paint was 40–50% w/w cuprous oxide. Yet, the marine paint had less of an inhibitory effect than either coating. Upon completion of the Cu(II)-leaching experiment, however, it was shown the there was a direct relationship between the degree of growth inhibition and the amount of copper released from the coating into the bacterial culture. For example, the "Acrylic + Cu(II)" paint released the most copper and had the largest inhibitory effect (**Table 3.3**), and the marine paint released the least copper and had the smallest inhibitory effect. When considering these results, it became clear that the results of the growth assay would not be translatable to antifouling in the marine environment.

The growth assay was deemed an inappropriate proxy for testing the antifouling performance of coatings because it determined the antimicrobial activity of leached components, rather than surface activity. The copper concentrations measured in the bacterial cultures would not be achieved in the marine environment; the leached copper would be greatly diluted by seawater, with the concentration of copper ions being highest at the surface and decreasing in a gradient. The flux of copper ions immediately at the surface has a role in antifouling, but this is not what is reflected in the assay. Since the copper ions are not continuously removed from the culture, the copper concentration is allowed to increase until reaching an equilibrium as copper-leaching progresses, exerting a greater inhibitory effect on bacterial growth. This does not provide any understanding of the surface dynamics or proclivity of the paint to be colonised by bacteria. Therefore, it was decided that the growth assay should no longer be used to assess and rank potential antifouling coatings and that an assay testing bacterial adherence to the coatings would be more suitable.

3.3 Cu(II) Ligands in an Epoxy Coating

With the abandonment of the DAp/acr paint and acylhydrazone ligands, efforts were focused on the incorporation of other Cu(II) ligands, particularly tetraaza macrocycle cyclen (**Table 3.6**), into a coating binder. Marine paints commonly use polyurethanes or epoxies as polymeric resins.[185] Therefore, several combinations of amine and/or alcohol components with Desmodur® W (Covestro), a cycloaliphatic diisocyanate, were trialled to produce polyurea or polyurethane coatings, respectively (Experimental, **Scheme 6.6**, **Table 6.4**). However, these combinations resulted in polymers that were unamenable to further manipulation or in no observable polymerisation at all (Appendix, **Table 8.18**), meaning that the reactions were either too fast or too slow/did not occur. This was undesirable, as it precluded spreading of the polymer into a film. Therefore, in consultation with Resene Paints Ltd., an epoxy system was selected to meet our requirements.[207]

The selected, two-pack epoxy system is composed of commercial epoxy resin Epikote™ 235 (Resolution Performance Products) and commercial hardener Ancamine® 2459 (Air Products and Chemicals, Inc.). Epikote™ Resin 235 contains no diluent and is a blend of bisphenol A (BPA) and F (BPF) resins derived from bisphenol A or F and epichlorohydrin (**Table 3.6**). It is generally used in solvent-free, high-solids coatings in the building and civil engineering industries, and its weight *per* epoxide (WPE), which is the weight of resin *per* one gram-equivalent of epoxy groups, is 177–182 g/eq.[208–210]

$$WPE = \frac{molecular\ weight\ of\ epoxy\ resin}{number\ of\ epoxy\ groups} \tag{1}$$

Ancamine® 2459 Curing Agent consists of a ketimine-protected polyamine (**Table 3.6**), and moisture is necessary for its deprotection, freeing each amine to react with an epoxy group (**Scheme 3.3**). Consequently, its cure-time is relatively slow. This is an attractive feature for the purposes of the current project, as it allows time for manipulation of the epoxy system (*e.g.* able to coat a surface with a film). Other attractive features of Ancamine® 2459 include its usage in marine coatings and its high polyamine content (60% w/w)[211]; since polyamines can function as Cu(II) ligands,[130] coatings derived from Ancamine® 2459 may already be capable of Cu(II)-sequestration. Despite its high amine content, Ancamine® 2459 yields low-blush films.[211] Blushing is caused by the sorption of carbon dioxide and moisture by the hygroscopic amine scavengers under conditions of high humidity or cool ambient temperatures and appears as white patches, making a clear coating look hazy or milky.[212] The amine hydrogen equivalent weight (AHEW) of Ancamine® 2459 is 101 g/eq, representing the weight of hardener *per* one gram-equivalent of active hydrogens in the polyamine. The number of active hydrogens is the number of amine hydrogens.[209,211]

$$AHEW \ = \ \frac{molecular\ weight\ of\ amine}{number\ of\ active\ hydrogen\ atoms\ of\ amine} \qquad (2)$$
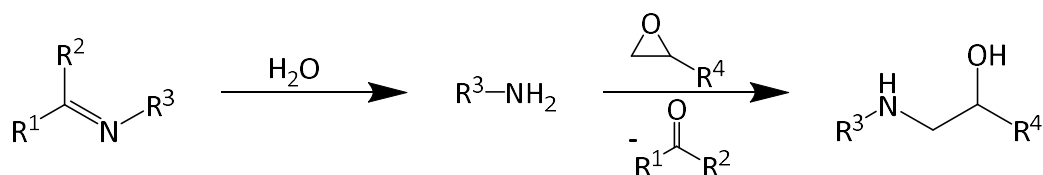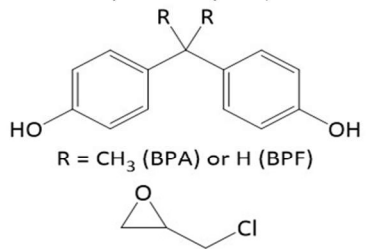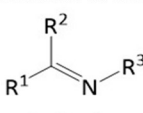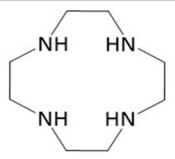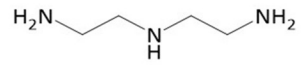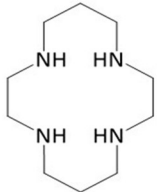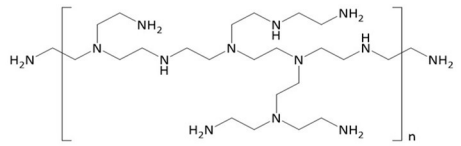
Scheme 3.3. Curing process for Ancamine® 2459: ketimine deprotection of an amine, which then reacts with an epoxide. A side product of the deprotection is a volatile ketone.

In order to obtain the best performance from the two-pack epoxy system, Epikote™ 235 and Ancamine® 2459 should be mixed in stoichiometric proportions so that there is one active amine hydrogen per epoxy group.[209] Both the WPE and AHEW are crucial in this calculation. For example, the WPE of Epikote™ 235 is 177–182 g/eq epoxy group, and the AHEW of Ancamine® 2459 is 101 g/eq amine hydrogen. This means that 177–182 g of Epikote™ 235 are required to react completely with 101 g of Ancamine® 2459. Typically, these stoichiometric proportions are represented by the *per hundred resin* (phr), which is the weight of hardener required to mix stoichiometrically with 100 g of epoxy resin (example calculation in the Appendix, **Scheme 8.1**).

$$phr \ = \ \frac{AHEW}{WPE} \times 100 \qquad (3)$$

Once the phr was known, two types of alterations to the epoxy system were explored: 1) modification of the composition, identity, and/or proportion of hardener, and 2) surface-functionalisation of undercured epoxy coatings. The epoxy resin, hardeners, and surface ligands are described in **Table 3.6**, and all of the tested combinations are displayed in **Table 3.7**. In addition to Ancamine® 2459, the other polyamine hardeners used to prepare coatings with Epikote™ 235 were Cu(II) ligands cyclen, cyclam, and diethylenetriamine (DETA). As previously discussed in Chapter 2 (**Section 2.4**), tetraaza macrocycles, including cyclen and cyclam, selectively bind Cu(II) in highly stable 1:1 complexes.[89,167] DETA is also popular in the literature as a tridentate, nitrogen-donor ligand, forming two five-membered chelate rings with Cu(II).[213–215] Cyclen, cyclam, and DETA, as well as branched PEI, were also used to functionalise the surfaces of undercured Ancamine® 2459/Epikote™ 235 coatings. Branched PEI is a polymer consisting of repeating $-(C_2H_5N)-$ units. Its primary, secondary, and tertiary amines are present in an approximately 1:1:1 ratio, and it has demonstrated a strong preference for Cu(II).[76,77,216]

Table 3.6. Descriptions of epoxy resin, hardeners, and surface ligands used in this study.

Name	Component	Description	WPE[a]	AHEW[b] (phr[c])
Epikote™ Resin 235[d]	epoxy resin	blend of BPA resin (BPA and epichlorohydrin) and BPF resin (BPF and epichlorohydrin) R = CH$_3$ (BPA) or H (BPF) epichlorohydrin	177–182	-
Ancamine® 2459 Curing Agent[e]	hardener	polyamine; ketimine-protected; requires moisture to cure ketimine	-	101 (56.3)
Cyclen	hardener, surface ligand		-	43.1 (24.0)
DETA	hardener, surface ligand		-	20.6 (11.5)
Cyclam	hardener, surface ligand		-	50.1 (27.9)
PEI	surface ligand		-	-

[a] Weight *per* epoxide (WPE) is the grams of resin *per* one gram-equivalent of epoxy groups (g/eq).
[b] Amine hydrogen equivalent weight (AHEW) is the grams of hardener *per* one gram-equivalent of active amine hydrogens (g/eq).
[c] *Per* hundred resin (phr) is the grams of hardener *per* 100 g epoxy resin.
[d] Proprietary composition and specific components confidential to Resolution Performance Products.
[e] Proprietary composition and specific components confidential to Air Products and Chemicals, Inc.

Table 3.7. Epoxy coatings prepared with epoxy resin Epikote™ 235 and the following hardeners: Ancamine® 2459, cyclen, DETA, and cyclam.

Hardener	Surface Functionalisation	% w/w Overcure (+)/Undercure (-)[a]
Ancamine® 2459	-	-50%, -40%, -30%, -20%, -10%, stoichiometric, +10%, +20%, +50%
Ancamine® 2459	cyclam	**-50%, -40%, -30%, -20%, -10%**
Ancamine® 2459	cyclen	**-40%**
Ancamine® 2459	DETA	**-40%, -30%**
Ancamine® 2459	PEI	**-40%**
Ancamine® 2459, cyclen	-	+10%, +20% (cyclen[b])
Ancamine® 2459, DETA	-	+10%, +20% (DETA[c])
Cyclen	-	-20%, -10%, stoichiometric, +10%, +20%
DETA	-	-20%, -10%, stoichiometric, +10%, +20%
DETA (75%), cyclen (25%)[d]	-	stoichiometric
DETA (50%), cyclen (50%)[e]	-	stoichiometric
DETA (25%), cyclen (75%)[f]	-	stoichiometric
DETA (25%), cyclen (100%)[g]	-	+25%
DETA (100%), cyclen (25%)[h]	-	+25%
Cyclam	-	-20%, stoichiometric, +20%

[a] The coatings in **bold** were surface-functionalised, and the coatings in red were determined to be high Cu(II)-loading films based on colour intensity.
[b] Stoichiometric amount of Ancamine® 2459 but overcured with cyclen.
[c] Stoichiometric amount of Ancamine® 2459 but overcured with DETA.
[d] Enough DETA and cyclen added as hardeners to react with 75% and 25% of the epoxy groups, respectively.
[e] Enough DETA and cyclen added as hardeners to each react with half of the epoxy groups.
[f] Enough DETA and cyclen added as hardeners to react with 25% and 75% of the epoxy groups, respectively.
[g] Stoichiometric amount of cyclen but overcured with DETA.
[h] Stoichiometric amount of DETA but overcured with cyclen.

The epoxy coatings prepared from these hardeners and surface-functionalising ligands were evaluated qualitatively and, in some cases, quantitatively for their appearance, mechanical properties, and ability to retain Cu(II) (Appendix, **Table 8.19**). Each coating was applied to a black and white brushout card using the standard draw-down method with a bar film applicator (Experimental, **Figure 6.2**). Then, the coatings were analysed by Fourier-transform mid infrared (FT-MIR) spectroscopy and, in some cases, near infrared (NIR) spectroscopy. Both techniques utilise the interaction of IR radiation with the sample to identify key bonds. However, MIR spectroscopy uses the region from 400–4000 cm^{-1} containing the fundamental molecular vibrations, while NIR absorptions (4000–12500 cm^{-1}) reflect the overtones and combinations of the fundamental vibrations.[217–219] Following analysis by IR spectroscopy, an aliquot of a dilute Cu(II) salt solution was added to each coating surface for 2–6.5 h. The coatings were washed with water, and any colour changes or retention were recorded. An example of this process is seen in **Figure 3.9** in which Cu(II) was added to the surface of a coating of Epikote™ 235 and Ancamine®2459 prepared in stoichiometric proportions and applied to a brushout card *via* the draw-down method. Select coatings were tested for their Cu(II)-loading *via* ICP-MS.
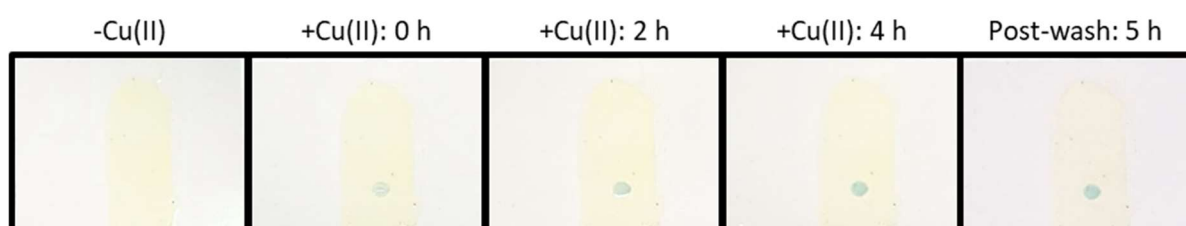
Figure 3.9. Coating composed of Epikote™ 235 and Ancamine® 2459 in stoichiometric proportions applied to a brushout card *via* the draw-down method. Cu(II) was added to the surface ("+Cu(II)", blue spot) and washed off after 5 h.

3.3.1 Modifications of the Hardener Component

3.3.1.1 Epikote™ 235 and Ancamine® 2459

The hardener component of the two-pack epoxy system was modified either by changing the identity/composition of the hardener or altering the proportion of hardener used to react with Epikote™ 235. Initially, a range of super- or sub-stoichiometric amounts of Ancamine® 2459 (±50% w/w) were added to Epikote™ 235 to generate overcured (+) or undercured (-) coatings, respectively. It was thought that overcured coatings would have more free amine groups, a fraction

of which might be presented at the surface, capable of binding Cu(II). Conversely, undercured coatings would have more free epoxy groups at the surface capable of reacting with a prospective Cu(II) ligand, thus functionalising the surface. Curing is commonly monitored by MIR spectroscopy using the band at ~915 cm^{-1} attributed to the C–O stretching vibrations of the epoxy groups in the resin (**Table 3.8**).[218,220] The bands corresponding to the amine groups in the hardener are of little use, as they overlap with other bands: the N–H stretching band (3300–3500 cm^{-1}) overlaps with the O–H stretching band (~3500 cm^{-1}) from the opened epoxy rings, and the N–H deformation band (1490–1650 cm^{-1}) overlaps with the C–C and C=C stretching bands (1509 cm^{-1} and 1609 cm^{-1}, respectively) of the aromatic rings of BPA and BPF.[218,220–222] However, both the primary amine group bands and epoxy group bands are distinct in an NIR spectrum. For the epoxy groups of the resin, the combination band of the second overtone of epoxy ring stretching with the fundamental C–H stretching is observed at 4530 cm^{-1}, while, for the primary amine groups of the hardener, the combination band of N–H bending and stretching is observed at 4900–5000 cm^{-1}. The overtones of the primary and secondary amine groups overlap at 6500 cm^{-1}.[221] Thus, the degree of curing in an epoxy coating can be determined by assessing the relative sizes of the epoxy group band by MIR and NIR spectroscopy and the amine group band by NIR spectroscopy.

In the present work, the undercuring and overcuring (±50% w/w) of the Ancamine® 2459/ Epikote™ 235 coatings were confirmed by MIR and NIR spectroscopy. The epoxy peak area at 914 cm^{-1} in the MIR spectra (**Figure 3.10**) increased with increasingly undercured coatings (*i.e.* +50% < stoichiometric ≈ -10% < -20% < -30% < -40% < -50%). Likewise, this trend was observed in the NIR spectra of the coatings, using the epoxy peak at 4533 cm^{-1}. Yet, the amine group bands at 4900–5000 and 6500 cm^{-1}, which are commonly used to monitor the curing of epoxy resins,[218,221,222] were not present in the NIR spectra. Since both the MIR and NIR spectra contained well-defined, discrete epoxy group peaks and neither contained such peaks for the amine groups in the hardener, there was no clear advantage in analysing the coatings *via* NIR spectroscopy. Furthermore, FT-MIR spectroscopy with attenuated total reflectance (ATR) sampling is more of a surface technique than NIR spectroscopy, which can be considered a bulk measurement, and, in this study, changes to the surface were of interest. Accordingly, it was decided that future analyses of epoxy group content should be conducted by FT-MIR (*i.e.* FT-IR) spectroscopy alone.

Table 3.8. Expected bands in the MIR and NIR spectra of an epoxy coating.[218,220–222]

Epoxy Component	Region	Frequency (cm^{-1})	Assignment
Resin	MIR	915	C–O stretching of epoxy groups
Hardener	MIR	1490–1650; 3300–3500	N–H deformation; N–H stretching
Resin	NIR	4530	combination band of second overtone of epoxy ring stretching with fundamental C–H stretching
Hardener	NIR	4900–5000; 6500	combination band of N–H bending and stretching (1° amine); overlapping overtones of 1° and 2° amines
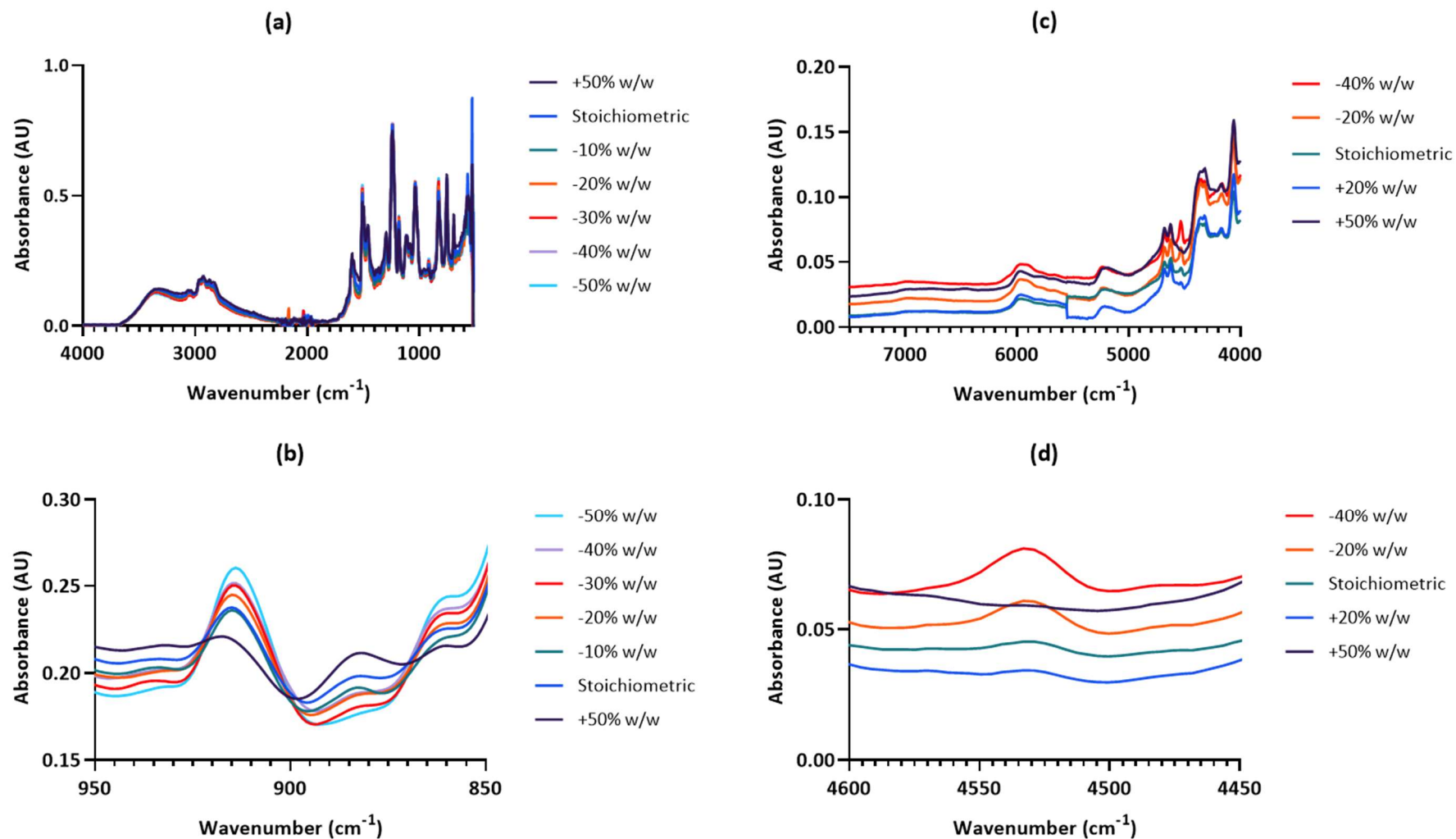
Figure 3.10. FT-MIR (a, b) and NIR (c, d) spectra of overcured (+) and undercured (-) Epikote™ 235/Ancamine® 2459 coatings: (a) and **(c)** are the full spectra, and **(b)** and **(d)** show an expanded view of the bands due to the epoxy group (~915 cm^{-1} for **(b)**, ~4530 cm^{-1} for **(d)**).

In addition to epoxy group content, the Ancamine® 2459/Epikote™ 235 films were evaluated qualitatively for their appearance, hardness, ease of draw-down, and colour following the addition of Cu(II) (**Table 3.9**). Undercuring of the coating by 50% w/w yielded unfavourable mechanical properties: the coating was soft and patchy. The coatings undercured by 30–40% w/w were also patchy but were hard and flexible, and the remaining coatings had no obvious differences compared to the stoichiometrically composed film. An aliquot from a dilute, aqueous Cu(II) salt solution was added to each coating and washed off after 5 h (**Figure 3.11**). The post-wash retention of a blue colour at the site of the Cu(II)-addition was noted for all films, but the blue colour did not appear to change between the initial addition of the aliquot and 5 h later, except, perhaps, increasing in intensity over time. As colour change is often indicative of metal-coordination, the lack thereof was suggestive that the colour retention may be due to adsorption rather than chelation. After these preliminary experiments, the same process was repeated for other hardener compositions with Epikote™ 235.

Table 3.9. Properties of epoxy coatings prepared with epoxy resin Epikote™ 235 and hardener Ancamine® 2459.

Hardener	% Over (+)/ Undercure (-)	Appearance	Softness/ Hardness	Ease of Draw-Down	Colour Change Upon Cu(II)- Addition (Y/N)	Colour Intensity
Ancamine® 2459	-50%	yellow, clear, splotchy	soft	splotchy	-	-
Ancamine® 2459	-40%	yellow, clear	hard, flexible	slightly splotchy	N – retention	weak
Ancamine® 2459	-30%	yellow, clear	hard, flexible	slightly splotchy	N – retention	medium
Ancamine® 2459	-20%	yellow, clear	hard, flexible	easy, uniform	N – retention	medium
Ancamine® 2459	-10%	yellow, clear	hard, flexible	easy, uniform	N – retention	medium
Ancamine® 2459	stoichiometric	yellow, clear	hard, flexible	easy, uniform	N – retention	medium
Ancamine® 2459	+10%	yellow, clear	hard, flexible	easy, uniform	N – retention	medium
Ancamine® 2459	+20%	yellow, clear	hard, flexible	easy, uniform	N – retention	medium
Ancamine® 2459	+50%	yellow, clear	hard, brittle	easy, uniform	N – retention	medium

Figure 3.11. Example of monitoring the Cu(II)-addition to under/overcured (±20% w/w) Ancamine® 2459/Epikote™ 235 coatings.

3.3.1.2 Epikote™ 235 and Cu(II) Ligands

As shown in **Table 3.10**, the other polyamine hardeners or hardener combinations trialled with Epikote™ 235 were Ancamine® 2459/cyclen, Ancamine® 2459/DETA, DETA/cyclen, cyclen, DETA, and cyclam. Regarding the FT-IR spectra of the Ancamine® 2459/Epikote™ 235 coatings overcured with cyclen and DETA (Appendix, **Figures 8.23–24**), no epoxy group peak was observed. However, this peak was present at ~915 cm⁻¹ in the spectra of all of the other coatings (Appendix, **Figures 8.25–28**), regardless of the level of overcuring with hardener. Although the hardener is, in theory, supposed to react completely with the resin in the stoichiometric compositions, the freedom of movement and reaction rate decrease as the polymer crosslinks and builds up molecular weight, which is due to unreacted components becoming separated and unable to react.[223] Therefore, in practice, the reaction does not progress to completion. This explains the presence of the epoxy group band in the stoichiometric and overcured, as well as the undercured, coatings.

The FT-IR spectra of the films prepared from Epikote™ 235/cyclen and Epikote™ 235/cyclam showed a trend of increasing epoxy group peak area with increased undercuring (Appendix, **Figures 8.26**, **28**), but no clear trend was observable in the remaining spectra, which were of coatings using DETA as a hardener. It was unknown whether this was due to the coating preparation (*e.g.* inhomogeneous mixing) or structure of DETA. DETA has two primary amines and one secondary, while cyclen and cyclam both contain only secondary amines. The less sterically hindered primary amines react faster than secondary amines,[224] so the reaction with DETA might be expected to first produce a linear

polymer. Thus, crosslinking *via* the secondary amines could be limited due to steric and diffusional restrictions, leaving unreacted epoxy and amine groups. Indeed, a study by Morgan[223] reported that epoxy coatings prepared from DGEBA (**Figure 3.12**) cured with DETA were not highly crosslinked, and it was suggested that either few epoxy group/secondary amine reactions occurred and/or DGEBA underwent homopolymerisation. In the present work, the epoxy groups in the resin have the same reactivities, and, unlike DETA, the (secondary) amines in cyclen and cyclam have the same reactivities.[224] Therefore, the reactive functional groups in the resin and cyclen/cyclam will react at the same rate.

Table 3.10. Epoxy coatings prepared with Epikote™ 235 and Cu(II) ligands as hardeners.

Hardener	% w/w Overcure (+)/Undercure (-)[a]
Ancamine® 2459, cyclen	+10%, +20% (cyclen[b])
Ancamine® 2459, DETA	+10%, +20% (DETA[c])
Cyclen	-20%, -10%, stoichiometric, +10%, +20%
DETA	-20%, -10%, stoichiometric, +10%, +20%
DETA (75%), cyclen (25%)[d]	stoichiometric
DETA (50%), cyclen (50%)[e]	stoichiometric
DETA (25%), cyclen (75%)[f]	stoichiometric
DETA (25%), cyclen (100%)[g]	+25%
DETA (100%), cyclen (25%)[h]	+25%
Cyclam	-20%, stoichiometric, +20%

[a] The coatings in red were determined to be high Cu(II)-loading films based on colour intensity.
[b] Stoichiometric amount of Ancamine® 2459 but overcured with cyclen.
[c] Stoichiometric amount of Ancamine® 2459 but overcured with DETA.
[d] Enough DETA and cyclen added as hardeners to react with 75% and 25% of the epoxy groups, respectively.
[e] Enough DETA and cyclen added as hardeners to each react with half of the epoxy groups.
[f] Enough DETA and cyclen added as hardeners to react with 25% and 75% of the epoxy groups, respectively.
[g] Stoichiometric amount of cyclen but overcured with DETA.
[h] Stoichiometric amount of DETA but overcured with cyclen.

Figure 3.12. Structure of DGEBA.

The films using DETA and DETA/cyclen as curing agents had undesirable physical and mechanical properties but displayed Cu(II)-binding. The films were milky white, indicative of blushing, and patchy and sticky when DETA made up a greater portion of the hardener (Appendix, **Table 8.19**). At the site of Cu(II)-addition to these coatings, however, a striking surface colour change to cobalt blue occurred, signifying metal-coordination, and the cobalt blue colour was retained after washing the surface with water (**Figure 3.13**; Appendix, **Figure 8.31**). The Ancamine® 2459/Epikote™ 235 films overcured with DETA were hard, brittle, and uniform. Following the addition of Cu(II) though, they also retained their colour change post-wash (Appendix, **Figure 8.30**). This was observed for the cyclen and cyclam coatings as well: the films containing cyclen retained the dark blue colour (Appendix, **Figures 8.29**, **31–32**), and the films containing cyclam retained the light purple colour (Appendix, **Figure 8.33**). The colour changes of these surfaces with ligands incorporated all matched the colours of the corresponding Cu(II)-ligand complexes in solution, providing further qualitative evidence that the surface colour changes may be attributed to metal chelation. Inclusion of tetraaza macrocycles cyclen and cyclam in the films made them hard and brittle, and their degree of uniformity was variable. The brittleness could be explained by the relative inflexibility of the macrocyclic structures, compared to linear, alkyl chains, or, more likely, by a greater degree of crosslinking in the coating, which occurs at multiple, crosslinkable points with limited flexibility (*e.g.* secondary amines in cyclen and cyclam). All of these properties of the Epikote™ 235 films prepared with different hardeners were considered, and the coatings with the most intense colour changes upon Cu(II)-addition and -retention post-wash were noted. Then, functionalisation of the surfaces of undercured films was explored.

Figure 3.13. Monitoring the Cu(II)-addition to coatings prepared from Epikote™ 235 and DETA in stoichiometric proportions or under/overcured (±20% w/w) with DETA.

3.3.2 Surface-Functionalisation

As in **Table 3.11**, the surfaces of Epikote™ 235 films undercured by 10–50% w/w with Ancamine® 2459 were functionalised with cyclam, cyclen, DETA, or PEI. It was proposed that the undercured coatings would have epoxy groups at the surface available for reaction with the amine groups of the Cu(II) ligands. Cyclam and cyclen were dissolved in water/methanol and water, respectively, and the solutions were used to cover defined surface areas of the films. DETA and PEI were added neat. After 16–24 h, the coatings were rinsed with water, analysed by FT-IR spectroscopy, and evaluated for their Cu(II)-coordinating ability. The epoxy group band was still present at ~915 cm^{-1} in the FT-IR spectra of the cyclam- and cyclen-modified surfaces (Appendix, **Figures 8.34–35**), which could be indicative of incomplete surface-functionalisation. This was unsurprising, as secondary amines are less reactive and both cyclen and cyclam were diluted in solution. However, although FT-IR ATR spectroscopy is considered to be a surface-sensitive technique, the ATR samples down to a depth of < 2 μm,[225] so it was difficult to determine if the epoxy peak was the result of sampling below the modified surface layer and/or the result of incomplete reaction at the surface. But, the addition of Cu(II) to the functionalised areas and the subsequent colour changes (*e.g.* light purple for cyclam, dark blue for cyclen; Appendix, **Figures 8.36–37**) demonstrated that some functionalisation had taken place. Generally, the cyclam- and cyclen-modified films were yellow, clear, hard, and flexible, but a few of them were brittle (Appendix, **Table 8.19**). It is possible that the brittleness was due to crosslinking with cyclen/cyclam at the surface.

Table 3.11. Epoxy coatings prepared with Epikote™ 235 and Ancamine® 2459 and surface-functionalised with Cu(II) ligands.

Hardener	Surface Functionalisation	% w/w Overcure (+)/Undercure (-)[a]
Ancamine® 2459	cyclam	-50%, -40%, -30%, -20%, -10%
Ancamine® 2459	cyclen	-40%
Ancamine® 2459	DETA	-40%, -30%
Ancamine® 2459	PEI	-40%

[a] The coatings in red were determined to be high Cu(II)-loading films based on colour intensity.

In contrast, surface-modification of the undercured Ancamine® 2459/Epikote™ 235 coating with DETA and PEI demonstrated Cu(II)-chelation and complete functionalisation by FT-IR spectroscopy, yet the physical properties of the film were undesirable. No epoxy group peak was observed at ~915 cm^{-1} in the FT-IR spectra, meaning that the surface and ATR-sampled underlying layers had no unreacted

epoxy groups (Appendix, **Figure 8.35**). Since DETA and PEI were applied to the surface neat and contain the more reactive primary amines, it seemed reasonable that they would react more extensively with the surface than cyclam and cyclen. Also, it is likely that DETA and PEI penetrated the film more deeply, as it was noted that their application softened the films. Aliquots of the dilute, aqueous Cu(II) salt solution delivered to the modified areas of the film yielded striking colour changes at the surface from light yellow to dark blue (Appendix, **Figure 8.37**). The PEI-functionalised surface retained the colour change particularly well post-wash, but both coating preparations were noted for the intensity of their colour changes. These experiments would have been encouraging, if not for the negative effects of functionalisation on the coating's physical properties: modification with DETA and PEI softened the coating and made it appear matte in the areas of application. Modification with PEI also resulted in significant blushing. Regardless, the DETA- and PEI-functionalised surfaces, as well as the other coatings notable for their post-wash colour retention, were progressed to quantification of the amount of copper bound to the surface.

3.3.3 Quantification of Cu(II)-Loading

Due to the intensity of the colour retained after the addition of Cu(II) and subsequent washes, the coatings in **Table 3.12** were selected for quantification of their Cu(II)-loading abilities. It was thought that colour intensity would increase with increased Cu(II)-binding and, therefore, would be valuable as a preliminary, qualitative assessment of the capacity of each film to chelate Cu(II). The procedure for measuring the surface Cu(II) was similar to the procedure in **Section 3.2.4** used to quantify the Cu(II)-loading for the commercial acrylic and 35% w/w DAp/acr paints. A standard amount of each prepared epoxy coating was delivered to evenly coat the bottom of a glass vial; glass vials of the same size were used in every experiment to keep the depth and exposed surface area of each coating consistent. Then, the coating was allowed to cure, the mass and exposed surface area of the coating were recorded, and an aliquot of a dilute, aqueous Cu(II) salt solution was added. Water was added to the vials serving as blanks. After 24 h, the coatings were washed with water, dried, digested in concentrated nitric acid, and diluted for copper analysis *via* ICP-MS. The reported copper results are blank-subtracted.

Given the poor reproducibility of the Cu(II)-binding results for the acrylic and DAp/acr paints (**Table 3.5**), the first Cu(II)-loading experiment for the epoxies utilised the stoichiometric Ancamine® 2459/Epikote™ 235 coating to validate the method, making the alterations suggested in **Section 3.2.4**. To explain the previous irreproducibility of the method, it was hypothesised that the variability was

due to shifting cure conditions (*i.e.* time, temperature, humidity), and it was suggested that these parameters be kept constant in future experiments. Accordingly, in this experiment, all coatings were cured for 24 h at 50 °C and 50% humidity. The samples were prepared in triplicate, and the experiment was repeated on three different days. Thus, the variability within a set of measurements and between sets could be determined (**Table 3.13**).

Table 3.12. Epoxy coatings prepared with Epikote™ 235 and to be measured for Cu(II)-loading.

Hardener	Surface Functionalisation	% w/w Overcure (+)/Undercure (-)
Ancamine® 2459	DETA	-40%, -30%
Ancamine® 2459	PEI	-40%
Ancamine® 2459, cyclen	-	+10%, +20% (cyclen[a])
Cyclen	-	+20%
DETA	-	+20%
DETA (25%), cyclen (100%)[b]	-	+25%
DETA (100%), cyclen (25%)[c]	-	+25%

[a] Stoichiometric amount of Ancamine® 2459 but overcured with cyclen.
[b] Stoichiometric amount of cyclen but overcured with DETA.
[c] Stoichiometric amount of DETA but overcured with cyclen.

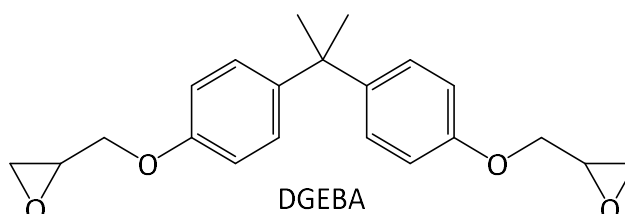**Table 3.13.** Amount of copper retained by the Ancamine® 2459/Epikote™ 235 coating prepared in stoichiometric proportions.

Replicate[a]	Hardener	% w/w Overcure (+)/Undercure(-)	μg Cu/g Coating[b]	ng Cu/mm^2 Coating[b,c]
1	Ancamine® 2459	stoichiometric	5 ± 1	4 ± 1
2	Ancamine® 2459	stoichiometric	3 ± 1	3 ± 1
3	Ancamine® 2459	stoichiometric	7 ± 1	6 ± 1

[a] The experiment was repeated three times (three different days).
[b] Mean ± SD, n = 3.
[c] Surface area (mm^2) exposed to Cu(II) salt solution. Calculated as in the Appendix (**Figure 8.38**).

As seen in **Table 3.13**, the Ancamine® 2459/Epikote™ 235 coatings (stoichiometric) retained very little copper (< 10 μg/g and ng/mm^2). A one-way ANOVA with Tukey's *post hoc* test revealed no statistically significant differences ($p > 0.05$) between the results for replicates 1 and 2 and replicates 1 and 3, but the results for replicates 2 and 3 were different. Due to the extremely low Cu(II)-loading in these coatings, variability in the results was unsurprising, as slight differences in coating preparation would have a larger relative impact on the results. This made it difficult to determine if standardising cure

conditions improved the precision of the results. However, a few tentative conclusions were drawn from the Cu(II)-loading experiments in this chapter (**Table 3.5**, **Table 3.13**):

1) The order of magnitude of each copper result is likely accurate, which, for the most part, is an acceptable degree of accuracy for the purposes of the project,

2) It is probable that differences in curing can significantly impact Cu(II)-loading and -retention, so tight control of the curing conditions in such experiments is advisable, and

3) The percent relative standard deviation within a set of measurements is generally ≤ 20% (with the exception of replicate 2, **Table 3.13**).

Therefore, this method and the results obtained following its implementation are still useful for relative comparisons of Cu(II)-loading in coatings, especially when the coatings are prepared on the same day, but it is important to be aware of the limitations.

The next experiment was to confirm a direct relationship between surface colour intensity and Cu(II)-binding. The epoxy coatings selected for this experiment were Epikote™ 235 cured with cyclen super-stoichiometrically (+20% w/w), sub-stoichiometrically (-20% w/w), and stoichiometrically. As the amount of cyclen in the coatings increased, the intensity of the colour change post Cu(II)-addition increased (**Figure 3.14**).
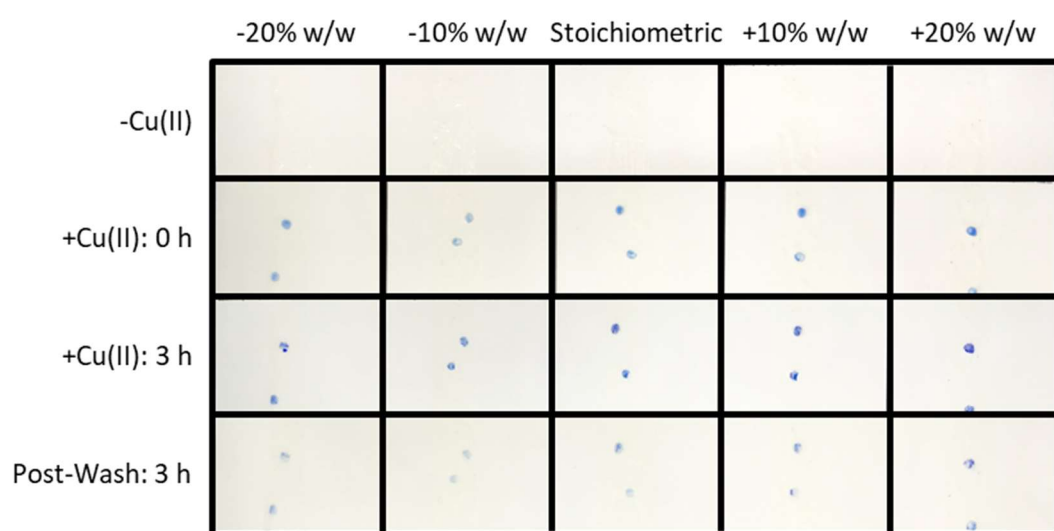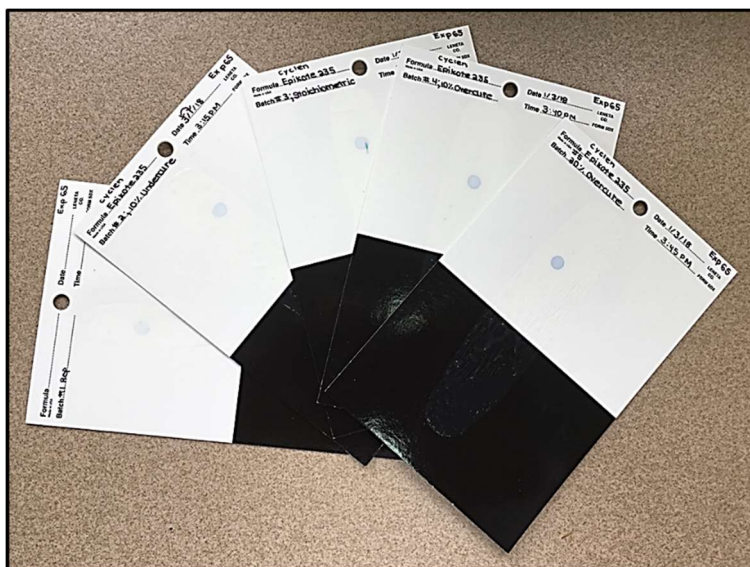

Figure 3.14. Cu(II)-addition to coatings prepared from Epikote™ 235 and cyclen in stoichiometric proportions or under/overcured (±20% w/w) with cyclen (increasing amount of cyclen from left to right).

Measurement of the Cu(II)-loading for these epoxies revealed that the amount of copper retained by the surface increased with increasing amounts of cyclen (**Table 3.14**), confirming the direct relationship between colour intensity and Cu(II)-loading. Furthermore, the increment by which the amount of bound copper increased from the -20% w/w to the stoichiometric coating was nearly equal to the increment by which the amount increased from the stoichiometric to the +20% w/w coating. This was encouraging, as the increment by which the amount of cyclen between these coatings increased was equivalent. Upon substantiation of this relationship, the Cu(II)-binding by the coatings selected based on colour intensity was evaluated.

Table 3.14. Amounts of copper retained by coatings prepared from Epikote™ 235 and cyclen in stoichiometric proportions or under/overcured (±20% w/w) with cyclen.

Number	Hardener	% w/w Overcure (+)/ Undercure (-)	µg Cu/g Coating[a]	ng Cu/mm^2 Coating[a,b]
1	cyclen	-20%	19	20
2	cyclen	stoichiometric	66	75
Δ_{2-1}			**47**	**55**
3	cyclen	+20%	111	127
Δ_{3-2}			**45**	**52**

[a] Estimated variability ±20%, but 2–3 significant figures reported for Δ calculations.
[b] Surface area (mm^2) exposed to Cu(II) salt solution. Calculated as in the Appendix (**Figure 8.38**).

In addition to Epikote™ 235 overcured (+20% w/w) with cyclen (**Table 3.14**), the other coatings determined to be high Cu(II)-loading based on colour intensity and selected for quantification of bound copper were as follows:

1) Epikote™ 235 undercured with Ancamine® 2459 (-30, -40% w/w) and surface-functionalised with PEI and DETA,

2) Epikote™ 235 cured stoichiometrically with Ancamine® 2459 then overcured with cyclen (+10–20% w/w),

3) Epikote™ 235 overcured with DETA (+20% w/w),

4) Epikote™ 235 cured stoichiometrically with cyclen then overcured with DETA (+25% w/w), and

5) Epikote™ 235 cured stoichiometrically with DETA then overcured with cyclen (+25% w/w).

However, attempts to employ the method to measure the copper retained by the PEI- and DETA-functionalised epoxies (1) failed. The addition of PEI and DETA neat to the undercured Ancamine® 2459/Epikote™ 235 surfaces resulted in gel-like coatings that would not harden. This

softening of the coatings had also been observed for the PEI- and DETA-modified surfaces prepared *via* the draw-down method. Consequently, these coatings were not pursued, but the procedure was successfully employed to measure the Cu(II)-loading for the other epoxies (2–5), the results of which are listed in **Table 3.15**. The only standout result was for Epikote™ 235 overcured with DETA (+20% w/w), which bound approximately an order of magnitude more copper (3300 µg/g ≈ 0.3% w/w, 3000 ng/mm^2) than the other coatings. This was about one-third of the available copper. The amount of copper retained by the other epoxies was < 0.05% w/w (*i.e.* < 500 µg/g).

Table 3.15. Amounts of copper retained by coatings determined to be high Cu(II)-loading based on colour intensity. Prepared with epoxy resin Epikote™ 235.

Hardener	% w/w Overcure (+)/ Undercure (-)	µg Cu/g Coating[a]	ng Cu/mm^2 Coating[a,b]
Ancamine® 2459, cyclen	+10% (cyclen)	480	420
Ancamine® 2459, cyclen	+20% (cyclen)	450	410
DETA	**+20%**	**3300**	**3000**
DETA (25%), cyclen (100%)	+25%	240	210
DETA (100%), cyclen (25%)	+25%	330	300

[a] Estimated variability ±20%.
[b] Surface area (mm^2) exposed to Cu(II) salt solution. Calculated as in the Appendix (**Figure 8.38**).

3.3.4 Conclusions

Known Cu(II) ligands cyclen, cyclam, DETA, and PEI were used as curing agents or surface-modifiers of epoxy coatings prepared with resin Epikote™ 235 and, in select cases, hardener Ancamine® 2459 (**Table 3.7**). When serving as hardeners, they were used in super-stoichiometric, sub-stoichiometric, and stoichiometric proportions to over/undercure the films or adhere to the manufacturers' specifications. FT-IR spectroscopy was determined to be useful for monitoring the curing process, and the spectra revealed that the epoxy group band at ~915 cm^{-1} was present for all of the films except those surface-functionalised with DETA or PEI, overcured by 50% w/w with Ancamine® 2459, and cured stoichiometrically with Ancamine® 2459 but overcured with cyclen or DETA by 10–20% w/w. This suggested that, since polymerisation separates reactive components, reaction with every epoxy group is atypical, requiring an excess of hardener. The films using tetraaza macrocycles cyclen and cyclam as curing agents were hard and brittle, which was unsurprising given the relative rigidity of the molecular structures and the expectation of high crosslinking in the film. In contrast, the films using the more flexible, linear polyamine DETA as a hardener were often soft and sticky. To a certain extent,

these trends were also identified in the surface-modifications; functionalisation with the tetraaza macrocycles (*i.e.* cyclen and cyclam) resulted in hard and, occasionally, brittle films, while functionalisation with the linear polyamines (*i.e.* DETA, PEI) often softened the coatings.

Upon delivering an aliquot of a Cu(II) salt solution to the surfaces of the films prepared or surface-functionalised with cyclen, cyclam, DETA, and PEI, a colour change was observed, signalling Cu(II)-coordination. Those with the most intense colour retention were noted (**Table 3.7**), and the amounts of copper retained by these coatings were quantified. The method for quantification of the Cu(II)-loading was evaluated, and the direct relationship between colour intensity and copper content was affirmed. As before, the amount of copper was normalised by the mass of the cured epoxy and the surface area exposed to the Cu(II) salt solution. Although, it was acknowledged that the depth of the Cu(II)-penetration was still unknown. The coatings that were surface-modified with DETA and PEI were not amenable to the method established for determining Cu(II)-loading, as DETA and PEI softened the coatings until they became gel-like. Therefore, these coatings were not pursued. The Epikote™ 235/DETA (+20% w/w) epoxy bound an order of magnitude more copper (~0.3% w/w) than the remaining coatings, which bound < 0.05% w/w copper (**Table 3.15**). Assuming the copper was bound at the surface, the Epikote™ 235/DETA coating bound 4.7×10^{-6} mol Cu/cm^2, while the other coatings bound $< 6.5 \times 10^{-7}$ mol Cu/cm^2. These amounts are very low but substantially higher than the 3.8×10^{-10} mol Cu/cm^2 bound by PEI-functionalised glass with low microbicidal activity for *E. coli* ATCC 10356 in a study by Dacarro *et al.*[216], suggesting that the level of Cu(II) retained by these epoxies might be high enough to exert an antimicrobial effect.

Despite the ability of the highlighted coatings to sequester low levels of copper, the physical properties of these coatings were unfavourable, eliminating them as suitable candidates for this project. The Epikote™ 235/DETA coating, which retained the most Cu(II), was soft and sticky, and, when attempting to spread the epoxy in a uniform film by the draw-down method, the resultant film was patchy and uneven. Thus, the coating would be unsuitable for antifouling applications: covering a surface evenly with such a coating would be infeasible, and a sticky coating would likely result in increased adherence by biofouling organisms. The coatings prepared with combinations of Ancamine® 2459 and cyclen as hardeners were brittle, and those prepared with combinations of DETA and cyclen were brittle, patchy, and sometimes sticky. The DETA/cyclen coatings also exhibited blushing. It became clear that alterations to the paint binders would significantly impact the physical and mechanical properties of the coatings and, therefore, limit the type and amount of hardener that could be added to increase Cu(II)-loading. As a high capacity to bind Cu(II) is essential for this work, alternative routes to include Cu(II) ligands, specifically cyclen, in a paint were pursued.

3.4 SUMMARY AND FUTURE WORK

In continuation of the work in the previous chapter (Chapter 2, **Section 2.2**), the DiLevDEG/ADH polyacylhydrazone was formulated into a commercial acrylic paint, substituting 35% w/w of the binder, and this paint was assessed for its ability to bind Cu(II) and its subsequent effect on bacterial growth. The 35% w/w DAp/acr and commercial acrylic paints sequestered comparable amounts of Cu(II) (**Table 3.5**), but the Cu(II)-loaded acrylic paint had a much more negative impact on the growth of *E. coli* NZRM 3647 (**Figure 3.7**), as it leached over twice the amount of copper into the bacterial culture (**Table 3.3**). A direct relationship between growth inhibition and the amount of copper leached into solution was substantiated, meaning that, instead of surface activity, the growth assay was measuring the antimicrobial activity of leached components. As a result, it was decided that a bacterial adherence assay, rather than the growth assay, would be more useful for initial evaluation of the antifouling performance of coatings, and this is explored in Chapter 5. When exposing the DAp/acr paint to a Cu(II) salt solution, the colour change of the solution indicated that a component had leached from the paint to form a Cu(II) complex. It was assumed that this component was DiLevDEG/ADH, since it is water-soluble and composes a significant percentage of the paint, and the release of small molecules and/or monomers from the polyacylhydrazone was confirmed by ^{13}C NMR spectroscopy (**Figure 3.8**). Consequently, it was decided that a paint which leaches its binder when exposed to water was not useful for the purposes of the project, and further work with the DAp/acr paint was discontinued. Alternative ligands and methods for their incorporation into a paint binder were pursued.

Along with commercial hardener Ancamine® 2459, cyclen, cyclam, DETA, and PEI were used as curing agents and/or surface-modifiers in a two-pack epoxy system with resin Epikote™ 235. Multiple combinations were trialled (**Table 3.7**) by preparing films *via* the draw-down method, recording their physical and mechanical properties, measuring their FT-IR spectra to assess unreacted epoxy group content, and adding Cu(II) to evaluate binding to the incorporated ligands (Appendix, **Table 8.19**). Cu(II)-loading was quantified in the films recorded as having an intense colour change post-addition of Cu(II). The copper data was reported by normalising the amount of copper by the mass of the cured coating or the surface area, but it was recognised that this was misleading, given that the depth of copper penetration in each coating was unknown. In future experiments, depth-profiling *via* laser ablation (LA) ICP-MS could be employed to analyse such surfaces for trace metals, providing a better picture of the copper distribution in the film.[226] Contact angle measurements to determine the wettability of the coatings would also be a useful characterisation technique.[227] Out of the coatings noted for their colour retention, Epikote™ 235 overcured with DETA (+20% w/w) retained the most

copper (**Table 3.15**). Yet, this epoxy, as well as the others, was unsuitable as an antifouling coating because of its undesirable physico-mechanical properties. The realisation that changes to the binder would be restricted due to the negative impact on coating properties led to the consideration of different methods for incorporating Cu(II) ligands in a paint.

4 INCORPORATION OF CU(II)-LIGAND COMPLEXES IN COATING ADDITIVES

4.1 BACKGROUND

Given the limitations of incorporating the Cu(II)-ligand complex into the paint binder, the other option explored was incorporating it as an additive. In general, the simplest paint formulations are usually composed of pigments dispersed in a binder and carried by a solvent. Such simple systems are usually unsatisfactory products, often characterised by defects in the liquid paint and dry film. Some of these defects are as follows: pigment settlement, the formation of a paint skin in the can, bubble retention on application, the appearance of depressions in the film (*i.e.* cissing), the development of a wrinkled surface (*i.e.* shrivelling), excessive, vertical flow of a paint causing an uneven coating (*i.e.* sagging), colour differences in the film from pigment separation post-application (*i.e.* floating), and permanent colour change once an applied paint is subject to shear (*i.e.* flooding). While a number of the defects may be overcome by reformulation of the paint, other defects require the incorporation of small quantities (0.001–5%) of additives as a remedy (**Figure 4.1**).[29,30]
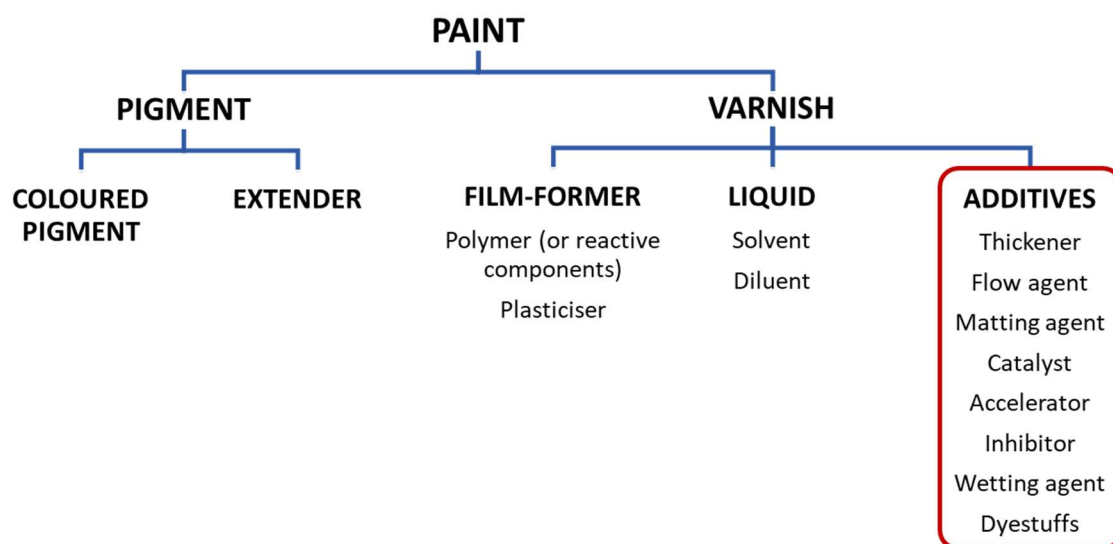
Figure 4.1. Paint components (adapted from *Introduction to Paint Chemistry*).[29]

Silica is a low-cost, common additive and extender that can enhance multiple coating properties. For instance, silica can act as an anti-settling agent. When fine silica particles (15 nm diameter, a few percent loading) are dispersed in a paint, they produce a pseudo-plastic effect due to the surface forces and their relatively large surface area (*e.g.* 190–460 m^2/g). A pseudo-plastic paint is shear-thinning, meaning that the viscosity decreases as the shear-rate increases. This is beneficial because, while the paint is at rest (*e.g.* sitting in a can), its higher viscosity prevents pigment settlement, but, when the paint is applied, the shearing action of, for example, the brush results in a decrease in viscosity for easy application. The viscosity increases again once the shearing action ceases, thus preventing sagging of the coating on the substrate.[29,30] The addition of silica (nano, micro, fumed) to a coating has also been shown to improve its hardness, abrasion and scratch resistance, tensile strength, and weatherability, as well as imparting superhydrophobic properties and acting as a matting agent and rheology modifier.[228–231] Accordingly, silica additives are found in multiple coating types, including antifouling coatings.[232,233]

The properties of silica are tuneable *via* functionalisation, and there is evidence that modified silica particles enhance the antifouling performance of marine paints. For example, in a study by Michailidis *et al.*[234], mesoporous silica nanoparticles (MSNs) were functionalised with quaternary ammonium salts (QASs), which have antimicrobial activity due to the interaction of their positive charge with negatively charged bacterial cell membranes. The QAS-modified MSNs were formulated into a coating, and the coating was tested for its antifouling performance against a control in a field test in the northern Red Sea. Incorporation of the QAS-modified MSNs in the coating reduced the biofouling coverage from 39% to below 10%, suggesting that modified silica particles could serve as functional fillers in antifouling coatings. Therefore, it was decided that the functionalisation of silica with Cu(II)-ligand cyclen (Chapter 2, **Section 2.4**) should be explored for formulation as an additive into an antifouling paint.

The incorporation of cyclen in the coating through the modification of silica, rather than as the free ligand, was preferable for a few reasons. First, given the water-solubility of cyclen, leaching into seawater was probable, but its attachment to a coating filler was considered to be a strategy for more permanent retention in the paint.[234] Second, it was unknown how free cyclen would be presented at the coating surface and if it would be accessible to copper ions for complexation. In contrast, it is known that silica tends to float to the surface of a coating in large aggregates composed of numerous particles, which would result in the exposure of silica-attached cyclen to copper ions in seawater at the coating-liquid interface.[29] Lastly, previous experiments demonstrated the reactivity of cyclen with

other paint components, such as the epoxy resin. Such undesirable interactions are more likely to occur with free cyclen.

The majority of studies involving silica functionalised with macrocycles, such as cyclen and cyclam (**Figure 4.2**), were conducted by Guilard[123,235–241] and Corriu[235,237,239,240,242–245], but a number of others[246–251] have contributed to the literature as well. These materials are mainly used for gas adsorption, catalysis, or chromatography.[252] However, their suitability as adsorbents for the removal of metal ions from wastewater, industrial effluents, and tap water is also recognised; silica is an excellent supporting material for this purpose due to its high surface area, mechanical and chemical stability, low cost, amenability to modification, and commercial availability.[123,236,253] These examples provide further support for the idea that cyclen-functionalised silica can be utilised for the sequestration of copper ions from seawater. Furthermore, work by Díaz-García *et al.*[254] demonstrated that Cu(II)-complexed, ligand-modified silica materials similar to those proposed have moderate antimicrobial activity against *E. coli*, indicating that such materials are capable of both chelating copper ions and, subsequently, exerting an antimicrobial effect.
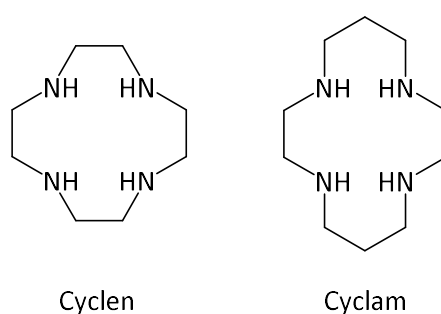
Cyclen   Cyclam

Figure 4.2. Structures of macrocycles cyclen and cyclam.

Although the literature addressing the functionalisation of silica with macrocycles is substantial, the preparation methods and product characterisation techniques are variable. At times, assumptions are made about the product without satisfactory final characterisation, and, in multiple cases, characterisation data of the modified silica are incomplete or absent. For instance, Puranik *et al.*[248] and Bagnoud *et al.*[255] infer the generation of the desired product from its ability to retain Cu(II), rather than from direct measurements and characterisation of the modified silica. For those studies in which data are reported, common characterisation techniques of the silica include FT-IR spectroscopy, CHN elemental analysis, microscopy, solid-state cross-polarisation magic angle spinning nuclear magnetic

resonance spectroscopy (CP-MAS NMR), and Brunauer, Emmett, and Teller (BET) surface area measurements. Frequently used techniques for copper quantification include X-ray fluorescence (XRF) and inductively coupled plasma optical emission spectroscopy (ICP-OES). The literature shows that silica-bound cyclam has typically been prepared either by grafting or sol-gel synthesis. No standard synthetic procedure or characterisation strategy is followed, which makes direct comparisons difficult and reliable data sparse. Consequently, in the present work, methods were investigated, evaluated, and developed for silica modification with cyclen and subsequent characterisation of the products.

4.2 SILICA FUNCTIONALISATION

As in **Scheme 4.1**, two methods were considered for the functionalisation of silica with the cyclen ligand. In Method 1, trialkoxysilane $(RSi(OR^1)_3)$ (3-glycidyloxypropyl)trimethoxysilane (GLYMO) hydrolyses to yield the corresponding silanols. Siloxane linkages form in a condensation reaction between the silanol groups of GLYMO and silica (SiO_2), producing GLYMO-functionalised silica $(GmSiO_2)$.[256] GLYMO is a commercial silane coupling reagent capable of bonding with both organic and inorganic materials and, therefore, acting as an intermediary linker to modify the inorganic matrix of silica with a terminal epoxide functional group (**Figure 4.3**). In turn, the terminal epoxide can react with organic compounds,[257] as in the next step of Method 1 in which the epoxide of $GmSiO_2$ reacts with a secondary amine of cyclen by the S_N2 mechanism to produce cyclen-GLYMO-silica $(CnGmSiO_2)$. This approach was used by Bagnoud *et al.*[255] and Gros *et al.*[241] to bond tetraazacycloalkanes cyclam and cyclen (**Figure 4.2**), respectively, to silica for Cu(II)-retention as the stationary phase in chromatography.
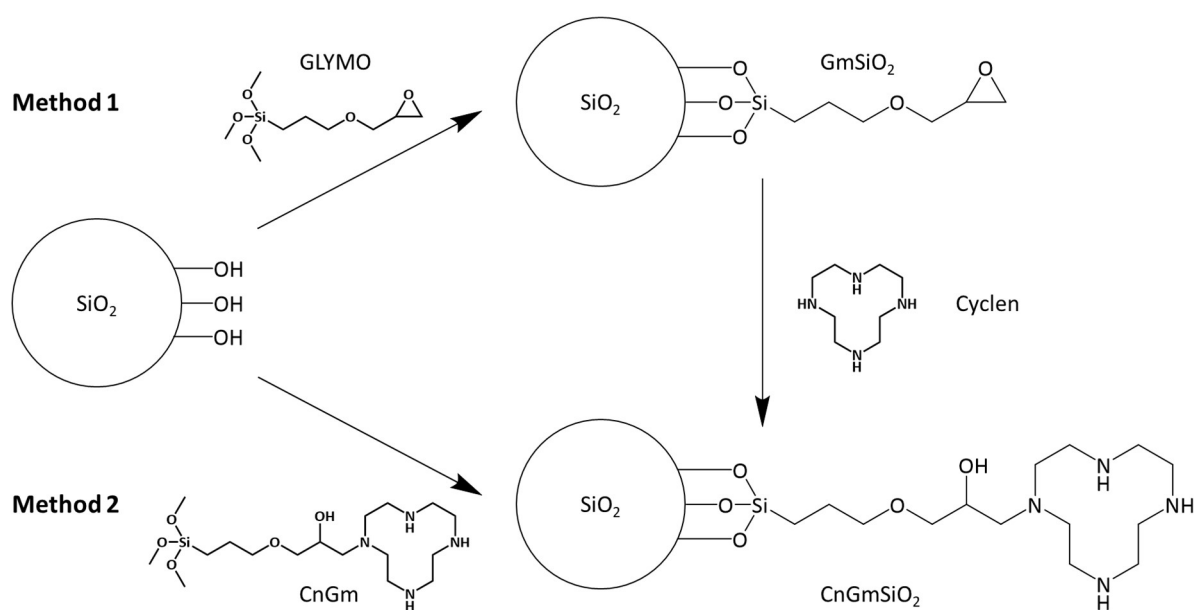
Scheme 4.1. Two silica functionalisation methods. Method 1: Reaction between GLYMO and the silanol groups of silica (SiO_2) produces GLYMO-functionalised silica $(GmSiO_2)$, and then the reaction between $GmSiO_2$ and cyclen produces cyclen-GLYMO-silica $(CnGmSiO_2)$. **Method 2:** GLYMO and cyclen react first to produce cyclen-GLYMO (CnGm), and then CnGm reacts with silica to produce $CnGmSiO_2$.
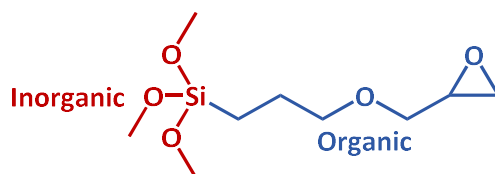
Figure 4.3. The organic and inorganic components of silane coupling agent GLYMO.

In Method 2, the order of reactions differs from Method 1. The first reaction is between cyclen and GLYMO to produce cyclen-GLYMO (CnGm), and then reaction of CnGm with silica produces $CnGmSiO_2$. An advantage of performing the synthesis in this order is that the product of the first reaction, CnGm, may be characterised by NMR spectroscopy. When "pre-loading" CnGm with Cu(II), Cu(II)-chelation by CnGm results in the formation of a dark blue complex (Cu(II)-CnGm), which serves as a visual confirmation of the silica modification with Cu(II)-CnGm (*i.e.* the functionalised silica is blue). Characterisation becomes more difficult once the compounds are bonded to silica, and techniques are limited to, for example, IR spectroscopy, CHN elemental analysis, and gravimetric analyses. Furthermore, since cyclen may become adsorbed to silica, this inverted synthetic approach allows for confidence that the reaction between cyclen and GLYMO has occurred because of the ability to more fully characterise the product. The second step of Method 1 brings a measure of uncertainty as to whether or not changes in mass or the IR spectrum are simply due to cyclen adsorption onto $GmSiO_2$ – *i.e.* non-covalent attachment. Method 2 was employed by Bereczki *et al.*[258] to create reusable catalysts by functionalising mesoporous silica aerogels with Cu(II)-cyclen complexes and by Barreto *et al.*[259] to modify magnetite nanoparticles with cyclen for [64]Cu(II)-labelling, generating superparamagnetic nanoparticles for tumour detection by positron emission tomography (PET) or magnetic resonance imaging (MRI).

The silica used in the experiments in the present study was high-purity grade silica gel with a 60 Å pore size, 220–440 mesh particle size, and 35–75 μm particle size. It was selected to serve as a model compound since the material is less dusty than finer silica, mitigating the safety hazard *via* inhalation. In this work, the silica gel will be referred to simply as silica. The ratio of GLYMO to silica (mmol GLYMO/g silica) for functionalisation was based on the ratio of *n*-octadecyldimethylchlorosilane to silica (0.991 mmol modifier/g silica) used by Ortega *et al.*[260] to synthesise reversed-phase silica gel. Gros *et al.*[241] advised against pre-treatment of the silica with strong acids due to concerns about the introduction of structural changes, and, therefore, such pre-treatment was not conducted in the present study. However, the silica was dried before use, except when stated otherwise.

4.2.1 Method 1

4.2.1.1 Synthesis of GmSiO₂

Following the first step of Method 1, four procedures for the synthesis of $GmSiO_2$ were evaluated (**Scheme 4.2**), and the reaction conditions and outcomes are summarised in **Table 4.1**. Recovery of unreacted GLYMO was used to determine the theoretical amount of GLYMO attached to the silica, which was compared to the corresponding mass increase of the silica post-reaction. The identity of the recovered material was confirmed by ^1H NMR spectroscopy. The maximum loading of GLYMO onto the silica (*i.e.* mmol GLYMO functionalising 1 g SiO_2) was calculated from these data, and the percent functionalisation was calculated by comparing against the supposed maximum level of 0.991 mmol modifier/g SiO_2 from the literature.[260] This maximum level is, presumably, not a robust measure because it would depend on the size of the silica, its porosity, surface area, *etc.*, and, although the specifications of the silica gel used by Ortega *et al.*[260] are similar to those for the silica gel used in the present work, they are not identical. Nevertheless, the maximum level was still used as a crude measure of success. The product from each procedure was characterised by measuring the IR spectrum, and these data, in concert with the gravimetric data, were used to assess the extent of reaction.
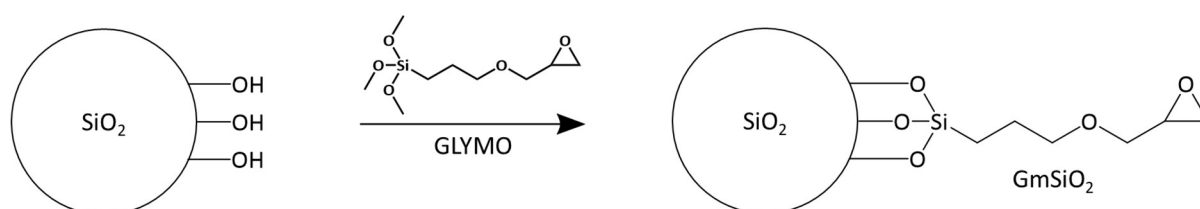
Scheme 4.2. Synthesis of $GmSiO_2$.

Different temperatures, solvent amounts, and reactant stoichiometries were trialled in Procedures 1–4 to determine which conditions were superior for the production of $GmSiO_2$ (**Table 4.1**). In Procedure 1, 1.2 mmol GLYMO/g SiO_2 in anhydrous toluene under argon were reacted for 24 h at room temperature, and the white silica product was filtered, washed, and dried. The clear, colourless filtrate was concentrated *via* rotary evaporation to obtain the mass of unreacted GLYMO, which was 99% of the starting amount. From this amount, the loading was calculated to be 0.01 mmol GLYMO/g SiO_2. This was well below the literature amount (0.991 mmol/g),[260] suggesting a percent functionalisation of, at most, 1%.

Table 4.1. Reaction conditions and outcomes in Procedures 1–4 for GmSiO$_2$ synthesis.

Conditions	Procedure 1	Procedure 2	Procedure 3	Procedure 4
SiO$_2$ (g)	0.91 (dry)	1.02 (dry)	1.00 (wet)	2.50 (dry)
GLYMO (g, mmol)	0.27, 1.1	2.1, 9.1	4.3, 18	3.7, 16
Anhydrous toluene (mL)	5	4	-	35
Triethylamine (µL)	-	-	-	75
Temperature (°C)	20 (RT)	80	100	110.6 (reflux)
Time (h)	24	72	69	42
Outcomes	**Procedure 1**	**Procedure 2**	**Procedure 3**	**Procedure 4**
GLYMO filtrate (g)	0.27	2.0	3.8	2.7
GLYMO - GLYMO filtrate (g)	0.003	0.2	0.5	1.0
% GLYMO recovered	**99**	**92**	**89**	**73**
GmSiO$_2$ (g)	0.97	1.18	1.40	3.17
GmSiO$_2$ - SiO$_2$ (g)	0.06	0.16	0.40	0.67
GmSiO$_2$: mmol GLYMO/g SiO$_2$	0.01	0.65	1.7	1.1
% Functionalisation[a]	**1**	**65**	**170**	**110**

[a] The percent functionalisation was calculated by comparing the mmol GLYMO/g SiO$_2$ to the supposed ideal (0.991 mmol modifier/g SiO$_2$).[260]

The reaction in Procedure 2 was conducted with 8.9 mmol GLYMO/g SiO$_2$ in anhydrous toluene under argon for 3 days at 80 °C, and recovery of 92% of the GLYMO in the filtrate, along with the corresponding mass increase of the silica, revealed a maximum loading of 0.65 mmol GLYMO/g SiO$_2$ or 65% of the literature value. GLYMO and silica (18 mmol GLYMO/g SiO$_2$, silica not dried) were reacted neat for 3 days at 100 °C in Procedure 3. GLYMO recovery was 89%, and the loading was calculated to be 1.7 mmol GLYMO/g SiO$_2$, which was significantly higher than the level noted in the literature (170%). The final procedure, Procedure 4, followed protocols by Bagnoud *et al.*[255] and Gros *et al.*[241], and 6.4 mmol GLYMO/g SiO$_2$ were reacted in anhydrous toluene and triethylamine (0.2% v/v, base catalyst) under argon for 2 days at reflux temperature. The percent recovery of the GLYMO starting material was 73%, and the loading was 1.1 mmol GLYMO/g SiO$_2$ (110%).

To ensure that undesirable starting material transformations did not occur under the reaction conditions, the identity of the material recovered from the filtrate in each procedure was confirmed by comparing its ^{1}H NMR spectrum to the ^{1}H NMR spectrum of GLYMO (**Figure 4.4**). GLYMO may undergo, at least, two major transformations observable by ^{1}H NMR spectroscopy: 1) the epoxide can open, and 2) the methoxy groups can hydrolyse. For the opening of the epoxide, the disappearance of the peak at δ_H 3.14 ppm, attributed to the proton attached to the secondary carbon in the ring (**H2**, **Figure 4.4**), was a simple way to monitor the ring-opening. Hydrolysis of the methoxy groups was

monitored by observing the disappearance of the peak at δ_H 3.57 ppm (methyl protons, **H7**) and the appearance of methanol in the spectrum (δ_H 3.49 ppm for C$\underline{H}_3$OH in chloroform-*d*, CDCl$_3$).[261]
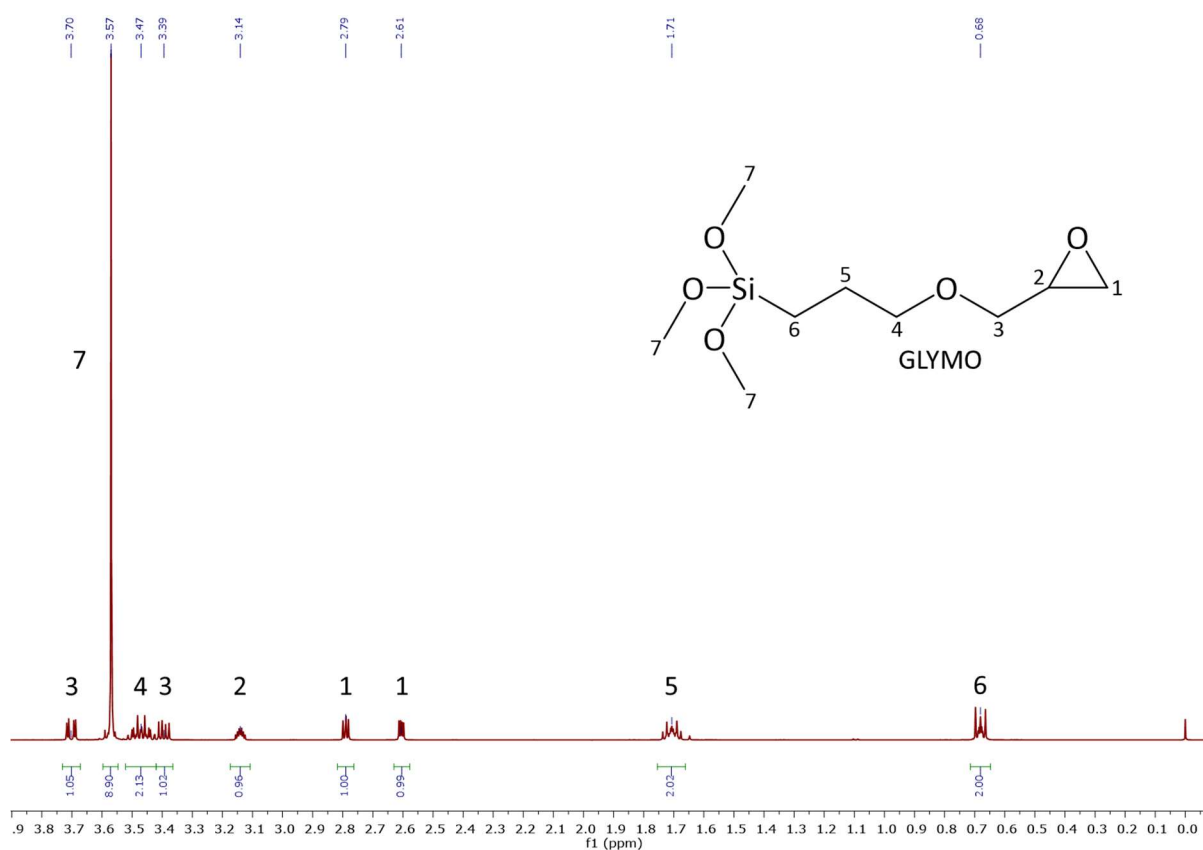
Figure 4.4. ^{1}H NMR spectrum (CDCl$_3$) of GLYMO and peak assignments.

As shown in **Figure 4.5**, the ^{1}H NMR spectra confirmed that the isolated filtrate material in Procedures 1–4 was indeed unreacted GLYMO. In all cases, the peak at δ_H 3.14 ppm was observed, indicating that the epoxide was still present. The only spectrum with differences from the GLYMO starting material was that of the Procedure 3 filtrate, in which it appeared that some of the methoxy groups had hydrolysed: the peak at δ_H 3.57 ppm decreased. Also, rather than being a clear, colourless, viscous liquid, as in the other procedures, the Procedure 3 filtrate material was a yellow colour. Presumably, this relates to the hydrolysis of the Si–OMe groups, which would be consistent with the use of the "wet" silica.
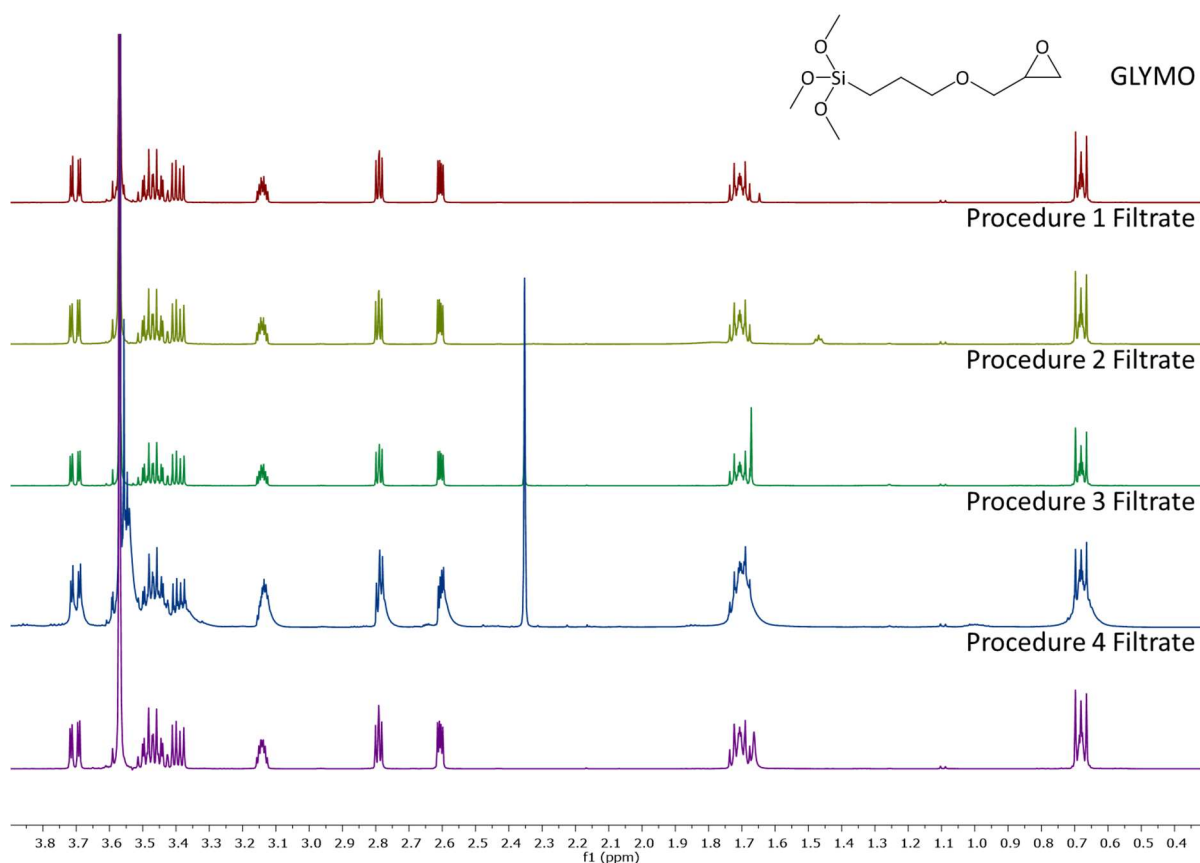
Figure 4.5. ^{1}H NMR spectra (CDCl$_3$) of the filtrates from Procedures 1–4 compared to GLYMO (toluene PhC$\underline{H}_3$ at δ_H 2.35 ppm).

The IR spectra of starting materials GLYMO and silica and the purported GmSiO$_2$ products from Procedures 1–4 were recorded to evaluate the extent of reaction (**Figure 4.6**). The corresponding peak data and assignments are shown in **Table 4.2**. If the GLYMO-functionalisation of silica occurred, the following changes in the IR spectrum would, theoretically, be expected to confirm the production of GmSiO$_2$: 1) the Si–OH stretching peak around 950 cm^{-1} and O–H stretching peak at 3351 cm^{-1} due to the silanol groups of silica would decrease in intensity or disappear, 2) the C–O stretching peak attributed to the GLYMO epoxy ring at 908–920 cm^{-1} would appear, and 3) additional peaks due to GLYMO (2943, 2841, 1467, 1254, 1191, and 1076 cm^{-1}) would appear.[218,221,222,262] In actuality, the O–H stretching peak (3351 cm^{-1}) was much too broad for use as a reaction marker, and the only perceptible evidence of modified silica was the appearance of the epoxy ring C–O peak (908–920 cm^{-1}). For example, the spectra of the GmSiO$_2$ from Procedures 2–4 displayed very weak epoxy ring peaks, and the Si–OH stretching peak was absent in the Procedures 3 and 4 spectra. Otherwise, the spectra of the products from Procedures 2–4 matched the IR spectrum of the silica starting material. The spectrum

of the Procedure 1 product showed no evidence of silica functionalisation, being nearly identical to that of the silica starting material.
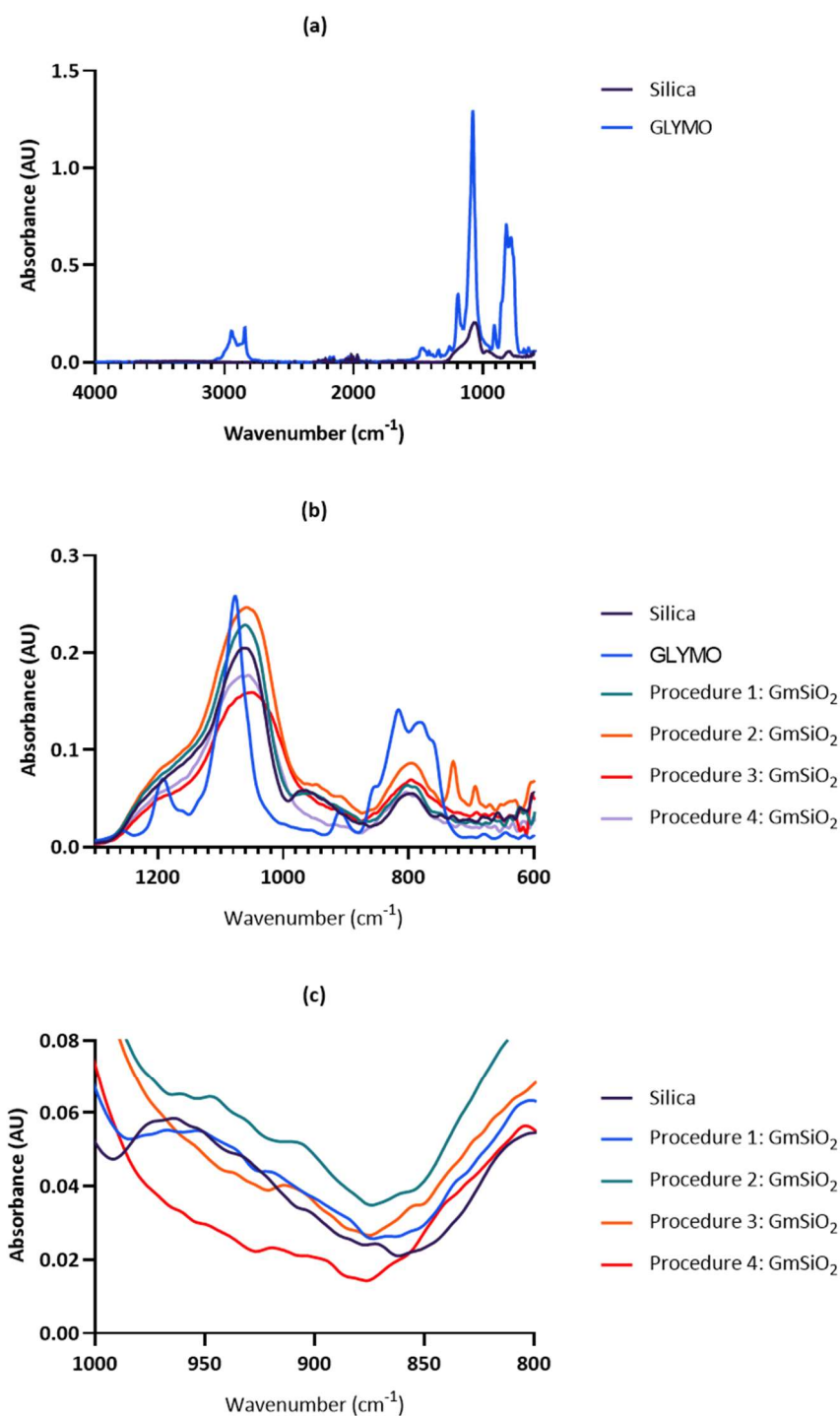
Figure 4.6. IR spectra of (a) silica and GLYMO starting materials, **(b)** silica, GLYMO, and purported GmSiO$_2$ products from Procedures 1–4, and **(c)** silica and purported GmSiO$_2$ products from Procedures 1–4, expanded view of the epoxide C–O region (908–920 cm^{-1}).

Table 4.2. Data and peak assignments from the IR spectra of silica and GLYMO starting materials and purported GmSiO$_2$ products from Procedures 1–4.

GLYMO Frequency (cm^{-1})	Silica Frequency (cm^{-1})	Procedure 1 GmSiO$_2$ Frequency (cm^{-1})	Procedure 2 GmSiO$_2$ Frequency (cm^{-1})	Procedure 3 GmSiO$_2$ Frequency (cm^{-1})	Procedure 4 GmSiO$_2$ Frequency (cm^{-1})	Assignment[218,221,222,262]
	3351 (w, vbr)					O–H stretching
2943 (m)						C–H stretching in Si–O–CH$_3$ and CH$_2$
2841 (m)						C–H stretching in Si–O–CH$_3$ and CH$_2$
1467 (vw)						C–H in-plane rocking in Si–O–CH$_3$ and CH$_2$
1254 (vw)						Si–C bending
1191 (m)						C–O stretching of aliphatic ether
1076 (vs)						Si–O–C stretching
	1063 (s, br)	1060 (s, br)	1058 (s, br)	1049 (s, br)	1066 (s, br)	Si–O–Si asymmetric stretching
	964 (m, br)	953 (m, br)	948 (vw, br)			Si–OH stretching
909 (w)			**908 (vw, br)**	**914 (w, br)**	**920 (vw, br)**	**C–O stretching in epoxy ring**
816 (s)						Si–C stretching
	794 (m, br)	801 (m, br)	797 (m, br)	796 (m, br)	801 (m, br)	Si–O–Si symmetric stretching
			729 (m)			
			694 (w)			

Together, the GLYMO-loading data and the IR spectra of the products from Procedures 1–4 were reviewed to decide which synthetic route and GmSiO$_2$ product should be carried forward for the second step of Method 1, which was the synthesis of CnGmSiO$_2$. Procedure 1 was eliminated from consideration because the IR data yielded no evidence of functionalisation, and the loading was, at most, 0.01 mmol GLYMO/g SiO$_2$ (1%), as 99% of the GLYMO was unreacted. The loading data further narrowed the choices to between Procedures 3 and 4, since both were well above the literature value of 0.991 mmol GLYMO/g SiO$_2$ (1.7 and 1.1 mmol GLYMO/g SiO$_2$, respectively).[260] Procedure 2 had a loading of only 0.65 mmol GLYMO/g SiO$_2$ (65%) and, accordingly, was also eliminated from consideration. In Procedure 3, the ^{1}H NMR spectrum and colour change (*i.e.* yellow instead of colourless) of the GLYMO filtrate indicated that some of the methoxy groups had hydrolysed, and this would be expected to result in self-condensation (**Scheme 4.3**), as well as the desired condensation reaction with the silica silanol groups. For that reason, a large, concentrated excess of GLYMO, as in Procedure 3 (18 mmol GLYMO/g SiO$_2$), is likely problematic because it could lead to polymerisation. Therefore, Procedure 4 was selected, and the protocols reported by Bagnoud *et al.*[255] and Gros *et al.*[241] continued to be followed for the synthesis of CnGmSiO$_2$.
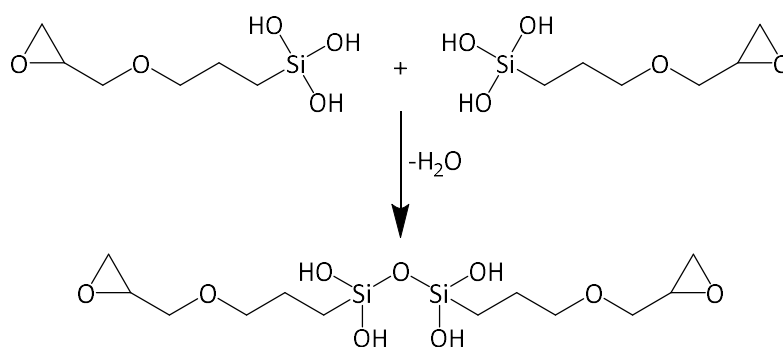
Scheme 4.3. Self-condensation of GLYMO.

4.2.1.2 Synthesis of CnGmSiO$_2$

Continuing with the Procedure 4 product, end-capping of GmSiO$_2$ (**Scheme 4.4**) was undertaken by heating in trimethylchlorosilane (TMCS). This step was recommended by Gros *et al.*[241] because free silanol groups are able to complex metal ions, complicating future measurements of the efficiency of the system to bind Cu(II). However, there was no increase in product mass, suggesting that the end-capping reaction did not occur. In fact, the product mass decreased by 0.6%. The IR spectrum of the putative end-capped GmSiO$_2$ (ec-GmSiO$_2$) was virtually identical to the GmSiO$_2$ starting material, apart from the absence of the epoxide C–O peak at 920 cm^{-1} (**Figure 4.7**, **Table 4.3**). This was contrary to

expectations, since modification with TMCS should yield bands in the IR spectrum at 2977 and 2912 (CH$_3$ stretching), 1415 and 1260 (CH$_3$ deformation), 857 and 767 (CH$_3$ rocking), and 700 and 640 (Si–C stretching) cm^{-1}.[263] None of these bands were observed in the IR spectrum of ec-GmSiO$_2$, and, thus, it was concluded that the reaction did not take place. In fact, the decrease in mass and disappearance of the epoxy ring peak in the IR spectrum were indicative of GLYMO hydrolysis.
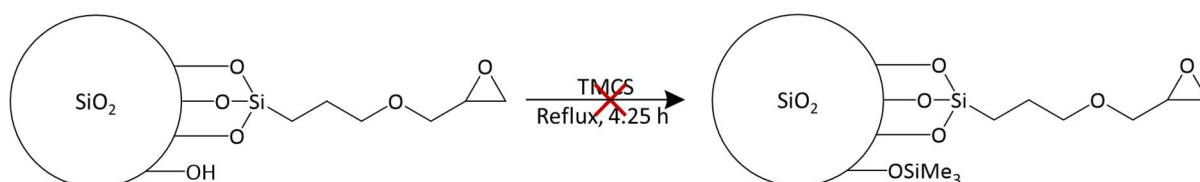
Scheme 4.4. Attempted end-capping of GmSiO$_2$.
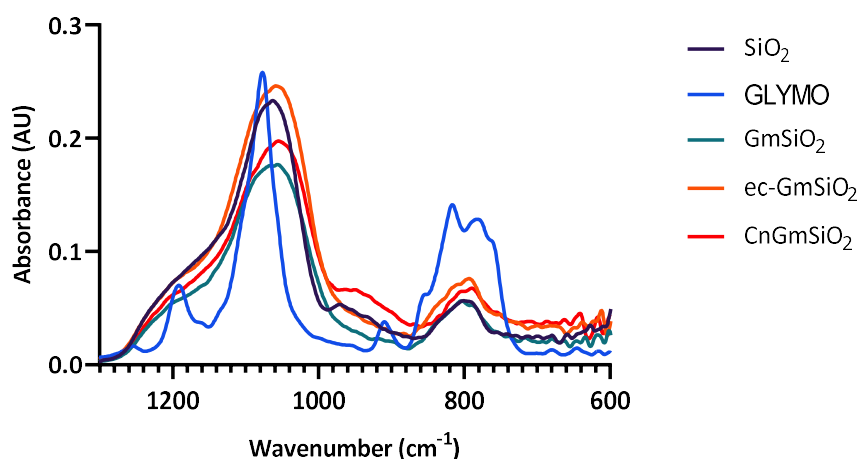
Figure 4.7. IR spectra of GmSiO$_2$ (Procedure 4), ec-GmSiO$_2$, and CnGmSiO$_2$.

Table 4.3. Data and peak assignments from the IR spectra of GmSiO$_2$ (Procedure 4), ec-GmSiO$_2$, and CnGmSiO$_2$.

Silica Frequency (cm^{-1})	Procedure 4 GmSiO$_2$ Frequency (cm^{-1})	Procedure 4 ec-GmSiO$_2$ Frequency (cm^{-1})	Procedure 4 CnGmSiO$_2$ Frequency (cm^{-1})	Assignment
3351 (w, br)				O–H stretching
1063 (s, br)	1066 (s, br)	1059 (s, br)	1055 (s, br)	Si–O–Si asymmetric stretching
964 (m, br)			950 (m, br)	Si–OH stretching
	920 (vw, br)			C–O stretching in epoxy ring
794 (m, br)	801 (m, br)	793 (m, br)	789 (m, br)	Si–O–Si symmetric stretching

The synthesis of CnGmSiO$_2$ (**Scheme 4.5**) proceeded by heating ec-GmSiO$_2$ in an aqueous cyclen solution and then washing the product with dilute hydrochloric acid. Post-reaction, the product mass increased only 0.17%, and, if this mass increase was due to the addition of cyclen to GmSiO$_2$, then the reaction efficiency was only 1%. Like ec-GmSiO$_2$, the epoxy ring peak was absent in the IR spectrum of purported CnGmSiO$_2$ (**Figure 4.7**, **Table 4.3**). Also, a peak at 950 cm^{-1}, attributed to Si–OH stretching, appeared. The N–H stretching band at ~3500 cm^{-1} from the addition of cyclen was absent.[264] So, there was no definitive evidence of the formation of CnGmSiO$_2$, and the practically negligible mass increase of the product suggested that the reaction occurred to a very small extent, if at all.
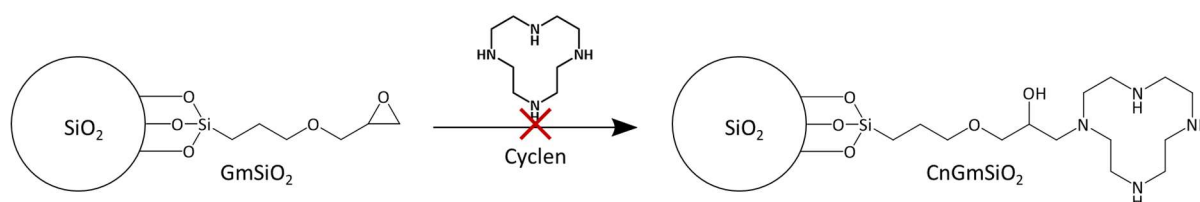
Scheme 4.5. Attempted synthesis of CnGmSiO$_2$.

4.2.1.3 Conclusions

The functionalisation of silica with CnGm *via* Method 1 proceeded, first, with the synthesis of GmSiO$_2$ by Procedure 4, which was selected as the best protocol out of Procedures 1–4. The end-capping of Procedure 4 GmSiO$_2$ and subsequent synthesis of CnGmSiO$_2$ were both unsuccessful, as determined by IR spectroscopy. There are several possible explanations for the differences between the IR spectra of the supposed ec-GmSiO$_2$ and CnGmSiO$_2$ products and the GmSiO$_2$ starting material. For instance, the disappearance of the epoxy ring peak in the IR spectra of ec-GmSiO$_2$ and CnGmSiO$_2$ could be due to hydrolysis of some of the GLYMO from the silica. After all, a decrease in product mass was observed in the end-capping reaction, and the Si–OH stretching peak reappeared for CnGmSiO$_2$. Yet, it is likely that the epoxy ring and Si–OH stretching peaks are both too weak and too broad to be diagnostic, and additional characterisation techniques, such as CHN elemental analysis, are necessary. The characterisation challenges in Method 1 led to its abandonment, in favour of the synthetic route in Method 2.

4.2.2 Method 2

4.2.2.1 Synthesis of Cn(Gm)$_n$

Following the first step of Method 2, six protocols were trialled to synthesise Cn(Gm)$_n$ (**Scheme 4.6**). It was acknowledged that Cn(Gm)$_n$ could be mono- (CnGm), di- (Cn(Gm)$_2$), tri- (Cn(Gm)$_3$), or tetra-substituted (Cn(Gm)$_4$). Under basic conditions, the ring-opening reaction of an epoxide proceeds by the S$_N$2 mechanism, and, in the case of an asymmetric epoxide, the favoured site of nucleophilic attack is the less substituted carbon, since such reactions are governed by steric considerations.[265] Regarding the synthesis of Cn(Gm)$_n$, cyclen has basic nitrogen atoms that serve as nucleophiles to attack GLYMO at **C1**, the less substituted carbon. Purification of the product was expected to be complicated by the tendency of such compounds to self-polymerise, which contraindicates heating and concentration under vacuum, and to functionalise silica, which contraindicates chromatographic purification with silica gel. It was preferable, therefore, to find a procedure in which the reaction went to completion, as evidenced by ^{1}H NMR spectroscopy, and in which any excess starting reactant could be removed by trituration or future washes. The reaction conditions, outcomes, and procedure references are summarised in **Table 4.4**.
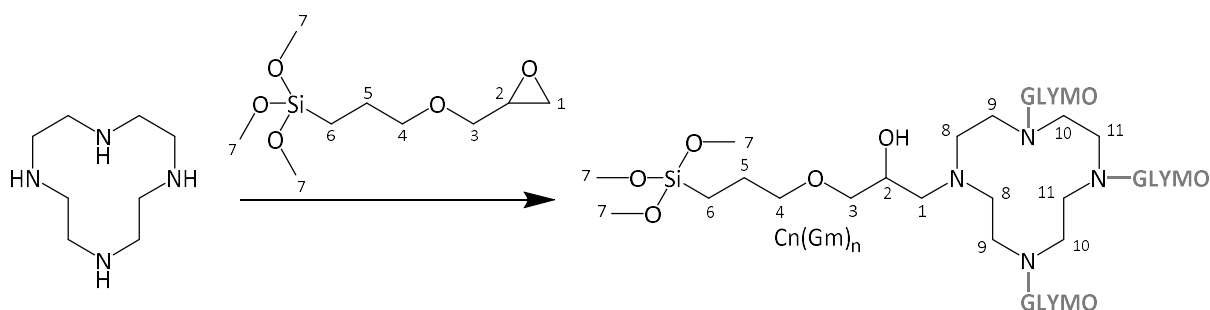
Scheme 4.6. Synthesis of Cn(Gm)$_n$.

The protocol by Bereczki *et al.*[258] was followed in Procedure 1 for Cn(Gm)$_4$ synthesis. GLYMO (3.9 eq) was added to cyclen dissolved in 2:1 methanol:water, and the reaction was stirred for 5 h at room temperature. Concentration of the crude reaction mixture for NMR analysis yielded an intractable polymer. So, test reactions were set up in NMR tubes using deuterated solvents (2:1 methanol-d_4, CD$_3$OD:D$_2$O) to monitor the reaction. ^{1}H NMR spectra of the test reactions revealed that, after 24 h, the majority of GLYMO (62%) remained unreacted. Thus, an alternative method was sought.

Table 4.4. Reaction conditions and outcomes in Procedures 1–6 for Cn(Gm)$_n$ synthesis.

Conditions	Procedure 1	Procedure 2	Procedure 3	Procedure 4	Procedure 5	Procedure 6
GLYMO (mmol)	4.4	1.1	2.3	1.1	1.1	8.9
Cyclen (mmol, eq)	1.1, 0.26	4.8, 4.3	0.56, 0.25	1.2, 1.1	1.2, 1.1	9.7, 1.1
Al(OTf)$_3$ (mmol)	-	-	-	0.1	0.1	-
Solvent	2:1 MeOH:H$_2$O	toluene	toluene	CHCl$_3$	CDCl$_3$	CHCl$_3$
Volume solvent (mL)	23.8	7.5	10	2	2	16
Temperature (°C)	20 (RT)	110.6 (reflux)	110.6 (reflux)	20 (RT)	20 (RT)	20 (RT)
Time	5 h	24 h	97.5 h	90 h	69 h	8–10 days
Outcomes	62% unreacted GLYMO	inconclusive	intractable solid	intractable solid	6% unreacted GLYMO	no unreacted GLYMO
References	Bereczki et al.[258]	Barreto et al.[259]	Barreto et al.[259]	Williams and Cullen[266]	Williams and Cullen[266]	-

Procedures 2 and 3 followed the protocol by Barreto et al.[259] In Procedure 2, GLYMO was added to an excess of cyclen (4.3 eq) in toluene, and the reaction was heated to reflux temperature for 24 h. Cooling of the reaction mixture resulted in the precipitation of much of the excess cyclen, which was removed by filtration. To ensure the removal of any remaining, unreacted cyclen, the filtrate was evaporated to dryness, dissolved in chloroform, and washed with aqueous sodium hydroxide (0.1 M). Drying over magnesium sulfate, filtration, and concentration yielded the presumed CnGm product as a colourless oil. The ^{1}H NMR spectrum of cyclen in chloroform-d showed a singlet at δ_H 2.67 ppm (–C$\underline{H}_2$–), since all of the methylene protons in the molecule are chemically equivalent. Consequently, the appearance of multiple signals from δ_H 2.90–2.40 ppm in the ^{1}H NMR spectrum (CDCl$_3$) of the product suggested coupling of the macrocycle to GLYMO (Experimental, **Section 6.4.1.2.1**). However, neither Cn(Gm)$_n$ nor its possible derivations from the loss of methyl groups were observed in the product's mass spectrum. Rather, there was evidence of GLYMO self-condensation. For example, the peak at m/z 603.3 could be due to the condensation of three GLYMO molecules, protonation, and the loss of a methyl group, as shown in **Figure 4.8**. The conflicting ^{1}H NMR and MS data regarding the formation of Cn(Gm)$_n$ led to another attempt based on the same procedure but, this time, with a small excess of GLYMO.

In Procedure 3, GLYMO (4.0 eq) was added to cyclen in toluene, and the reaction was heated to reflux temperature for 4 days. Concentration of the product under vacuum yielded an intractable polymer, attributed to GLYMO self-polymerisation. Therefore, it was decided that the procedure should always

use an excess of cyclen, instead of GLYMO, and that the reaction mixture should not be heated, since heating drives the condensation reaction. An excess of cyclen was also preferable because it is more easily removed than GLYMO by trituration or washes of the final $CnGmSiO_2$ material. Furthermore, it was better for avoiding the synthesis of $GmSiO_2$, rather than desired product $CnGmSiO_2$, in the following step.
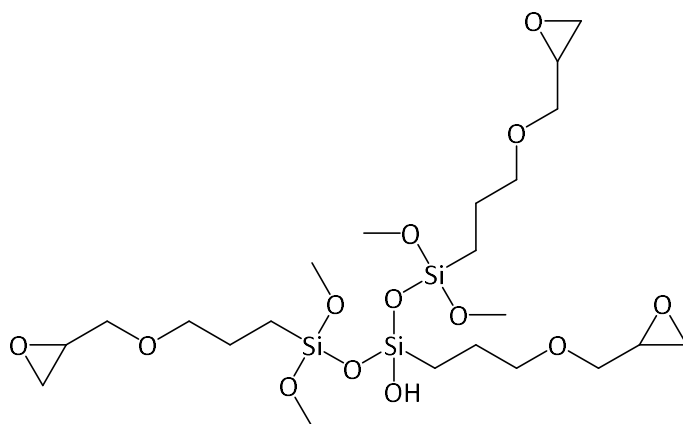
Figure 4.8. Potential structure of self-polymerised GLYMO (m/z 603.2 $[M + H]^+$).

In the study by Williams and Cullen[266] that was referred to for Procedures 4 and 5, aluminium triflate ($Al(OTf)_3$) served as an effective Lewis acid catalyst for the ring-opening reaction of an epoxide with an aliphatic amine, and the reaction was regioselective for nucleophilic attack by the amine at the less hindered carbon of the epoxide, in accordance with the S_N2 reaction mechanism. This mechanism was thought to be favoured due to chelation of the metal by the two oxygen atoms of the glycidyl ether (**Figure 4.9**); chelation diminishes the partial positive charge at the epoxide's more highly substituted carbon and, consequently, decreases reactivity, allowing steric hindrance to play a greater, discriminant role.[266,267]
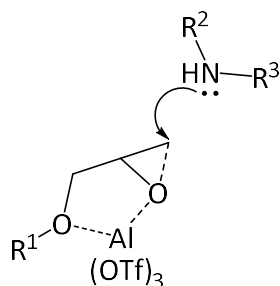
Figure 4.9. Proposed mechanism of nucleophilic attack on the less hindered carbon of the metal-chelating ($Al(OTf)_3$) glycidyl ether.[267]

In Procedure 4, GLYMO was added to cyclen (1.1 eq) and Al(OTf)$_3$ (10 mol%) in anhydrous chloroform under dry conditions and an argon atmosphere. The reaction mixture was stirred at room temperature for 4 days and then was quenched by the addition of aqueous sodium bicarbonate. Extraction with dichloromethane, washing with water, and concentration of the organic layers produced an intractable polymer. As a result, it was decided that concentration of the reaction mixture under vacuum while heating should be avoided, and the protocol was repeated with this modification in Procedure 5.

The reaction in Procedure 5 was monitored *via* ^{1}H NMR spectroscopy by diluting an aliquot of the crude reaction mixture in chloroform-*d* (**Figure 4.10**). As shown in **Figure 4.11**, progress of the ring-opening reaction was determined by observing the disappearance of the peak at δ_H 3.14 ppm, attributed to the proton attached to **C2** in the ring (**H** in the figure; see **Scheme 4.6** for numbering), and the appearance of the peak at δ_H 3.89 ppm, attributed to the downfield shift of that same proton once the epoxide opened. After approximately 3 days, integration of these two peaks revealed that only 6% of GLYMO remained unreacted, and the mass spectrum contained peaks for the tri- (*m/z* 441.4 [Cn(Gm)$_3$ + 2H]$^{+2}$]), di- (*m/z* 645.4 [Cn(Gm)$_2$ + H]$^+$), and mono-functionalised (*m/z* 409.3 [CnGm + H]$^+$) product, as well as for excess cyclen (*m/z* 173.2 [cyclen + H]$^+$). This evidence, therefore, was initially indicative of the formation of Cn(Gm)$_n$. Yet, given that cyclen is capable of metal-chelation, there were concerns about using a Lewis acid catalyst, since the free ligand was desirable. So, the same reaction was performed without Al(OTf)$_3$ in Procedure 6.
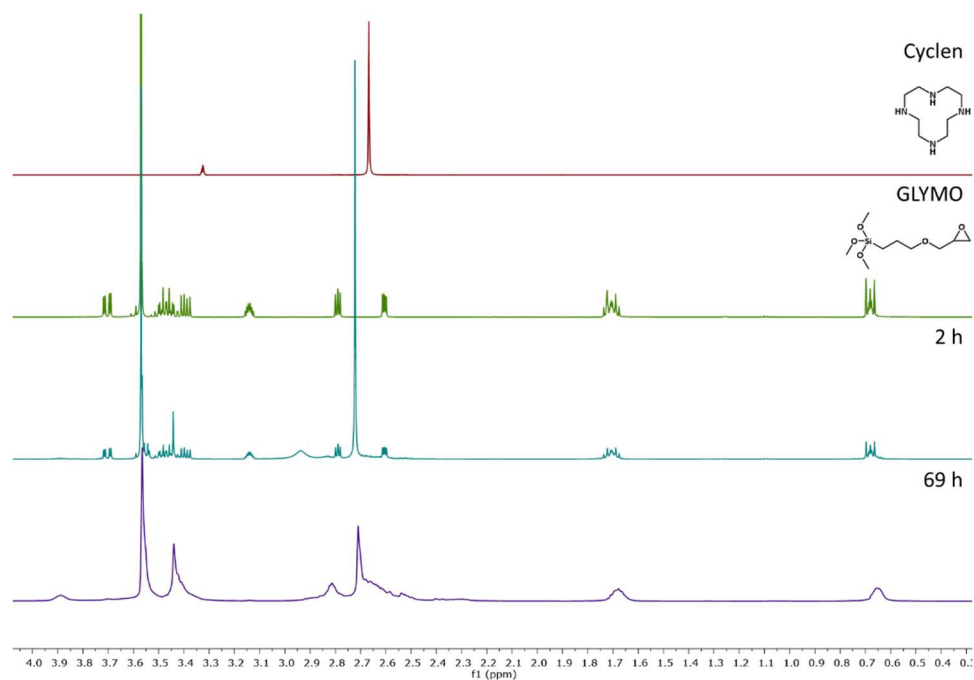
Figure 4.10. ^{1}H NMR spectra (CDCl$_3$) of cyclen, GLYMO, and samples at 2 and 69 h from the Cn(Gm)$_n$ Procedure 5 reaction mixture.
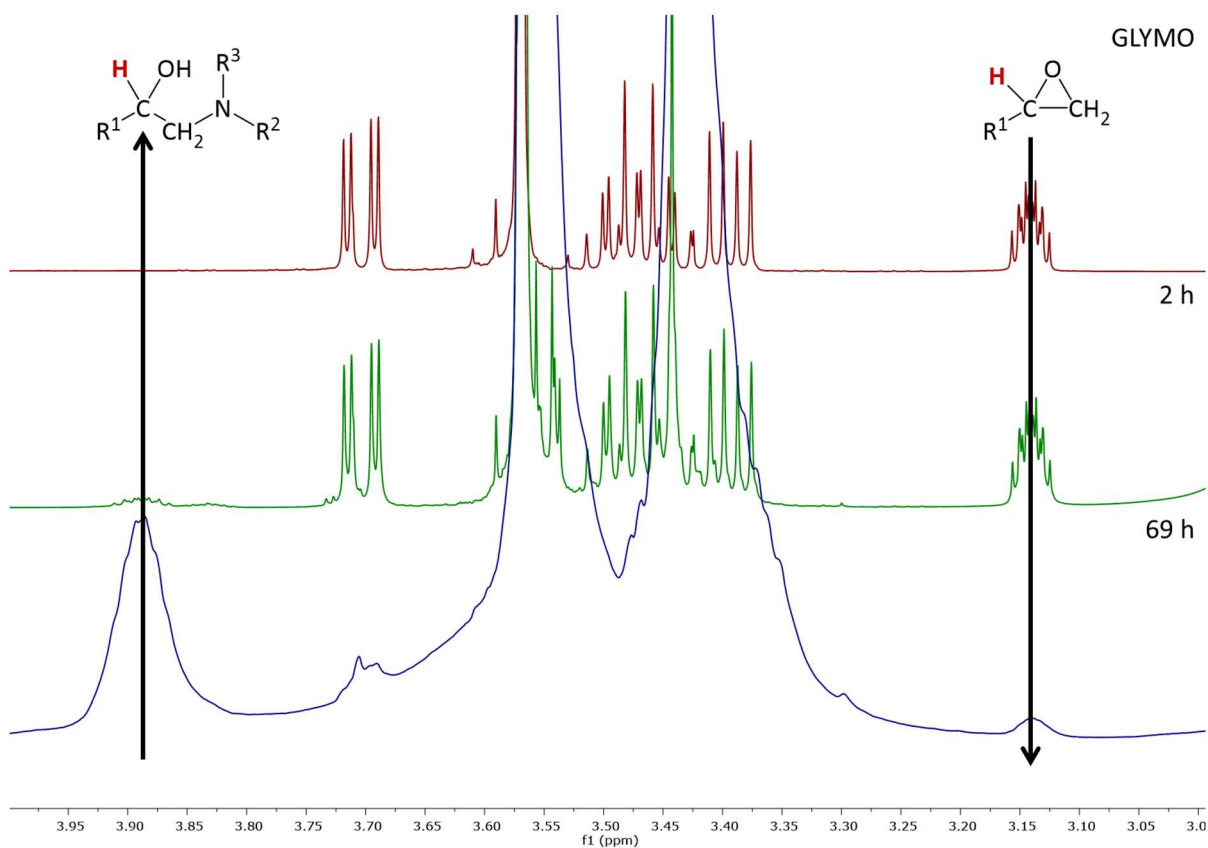
Figure 4.11. ^{1}H NMR spectra (CDCl$_3$, δ_H 4.00–3.00 ppm) of GLYMO and the samples at 2 and 69 h from the Cn(Gm)$_n$ Procedure 5 reaction mixture, showing the change in the spectrum with the progression of the ring-opening reaction. **H** is the proton responsible for the indicated peak.

The reaction in Procedure 6 commenced with the addition of GLYMO to cyclen (1.1 eq) in anhydrous chloroform at room temperature under dry conditions and an argon atmosphere and was monitored by ^{1}H NMR spectroscopy, as in Procedure 5, for 10 days. As shown in **Figure 4.12**, the peak at δ_H 3.14 ppm disappeared in 5–6 days, indicating that the ring-opening reaction of GLYMO was complete. The high-resolution mass spectrometry (HRMS) data confirmed the presence of the CnGm product (calcd for $C_{17}H_{41}N_4O_5Si$ [CnGm + H]$^+$ 409.2846; found 409.2843). Although the ring-opening reaction was monitored by observing the downfield shift of the **H2** peak from δ_H 3.14 ppm to δ_H 3.89 ppm, this did not prove that a bond had formed between a secondary amine of cyclen and the less hindered carbon (**C1**) of the GLYMO epoxy group. Therefore, in order to confirm the identity of the product with complete certainty, full characterisation by NMR spectroscopy was conducted.
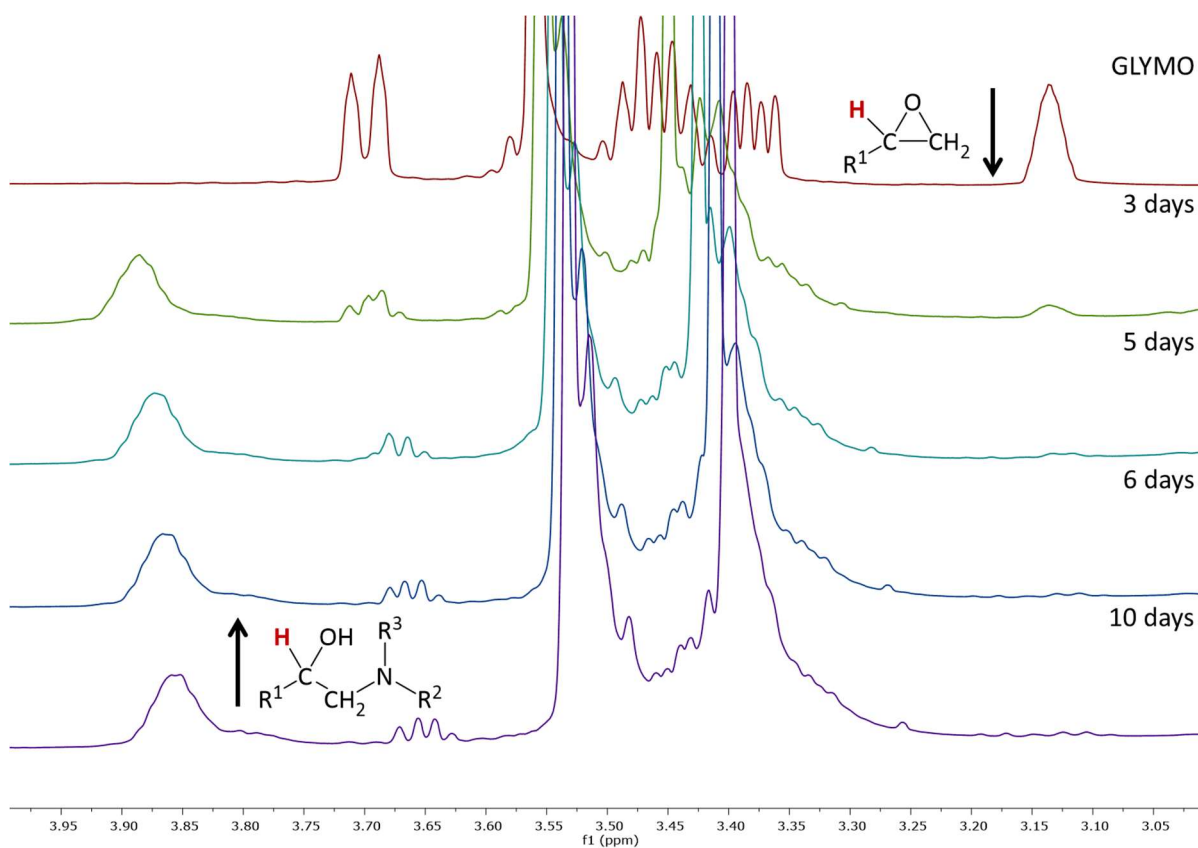
Figure 4.12. ^{1}H NMR spectra (CDCl$_3$, δ_H 4.00–3.00 ppm) of GLYMO and the samples at 3, 5, 6, and 10 days from the Cn(Gm)$_n$ Procedure 6 reaction mixture, showing the change in the spectrum with the progression of the ring-opening reaction. **H** is the proton responsible for the indicated peak.

NMR analyses (HSQC; (^{1}H, ^{13}C)- and (^{1}H, ^{15}N)-HMBC; COSY) of the product from Procedure 6 were completed to confirm the linkage of cyclen and GLYMO. An aliquot from the crude reaction mixture was used for the characterisation, since it had been decided that concentration and purification of Cn(Gm)$_n$ were contraindicated and that the reaction mixture, as is, should be used for subsequent steps to avoid self-polymerisation. The peaks in the ^{1}H and ^{13}C NMR spectra (Appendix, **Figures 8.39–41**, **Table 8.20**) were assigned by approximations from the HSQC correlations in **Figure 4.13**. The (^{1}H, ^{13}C)-HMBC spectrum (**Figure 4.14**) revealed that **H1** of Cn(Gm)$_n$ correlated to **C2** and **C3** of the GLYMO component of the molecule, as well as to the methylene carbons of the macrocycle (**C8** and **C9**, **C10**, or **C11**). This was conclusive evidence for the formation of desired product Cn(Gm)$_n$. Additionally, the (^{1}H, ^{15}N)-HMBC spectrum (Appendix, **Figure 8.42**) contained correlations between the amines and **H1** and **H8–11**, which was further evidence of the coupling of cyclen to GLYMO. The spin-coupling in the (^{1}H, ^{1}H)-COSY spectrum (Appendix, **Figure 8.43**) was consistent with the assignment.
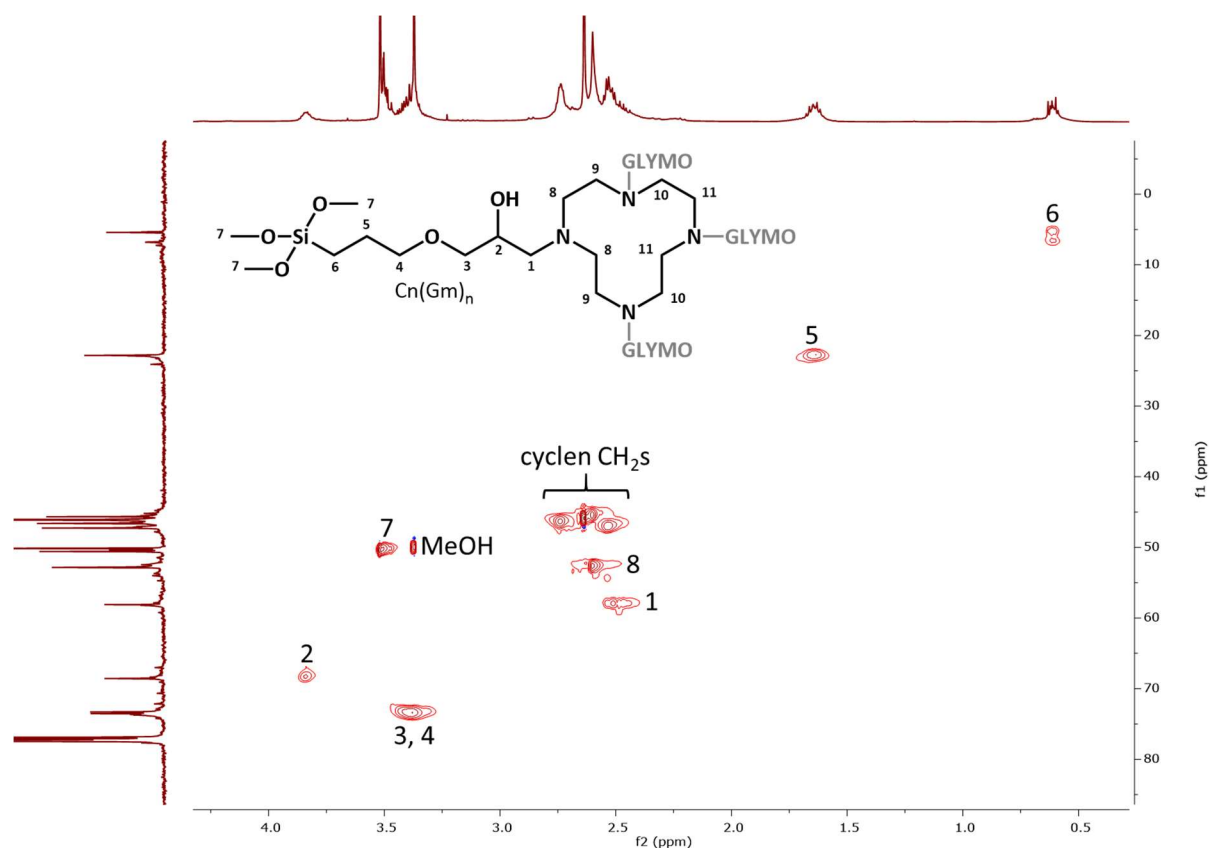
Figure 4.13. 2D HSQC NMR spectrum (CDCl$_3$) of Cn(Gm)$_n$ from Procedure 6 with peak assignments.
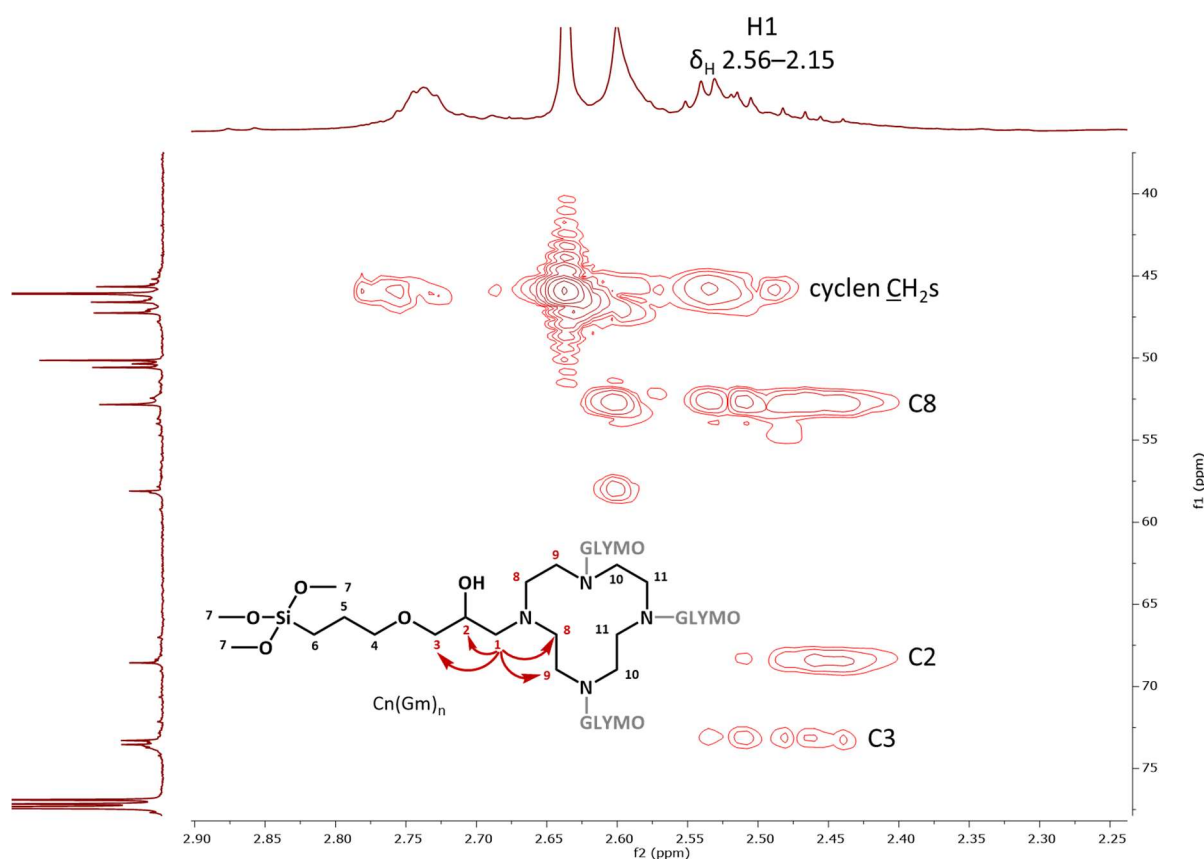
Figure 4.14. 2D (^{1}H, ^{13}C)-HMBC NMR spectrum (CDCl$_3$) of Cn(Gm)$_n$ from Procedure 6 with peak assignments.

The ^{29}Si NMR spectrum (Appendix, **Figure 8.44**) of the product showed two peaks (δ_{Si} -41.8 ppm, -50.2 ppm). This indicated that two products had formed: CnGm and either CnGm with hydrolysed methoxy groups or Cn(Gm)$_2$. The signal at δ_{Si} -41.8 ppm was probably caused by CnGm, since the chemical shift was consistent with previously reported data for GLYMO (δ_{Si} -42.1 ppm).[268] The observation of methanol (**Figure 4.13**) and the reduction in size of the peak at δ_H 3.52 ppm in the ^{1}H NMR spectrum revealed that methoxy group hydrolysis had occurred, to an extent, suggesting that water was still present under the "dry" conditions of the experiment. However, the mass spectrum also revealed the presence of Cn(Gm)$_2$ (*m/z* 645.4 [Cn(Gm)$_2$ + H]$^+$). The presence of these multiple species (*i.e.* CnGm, CnGm with hydrolysed methoxy groups, Cn(Gm)$_2$) in the ^{1}H NMR spectrum was the likely cause of the broad signals observed (Appendix, **Figure 8.39**).

Based on the refinements made to the six procedures for Cn(Gm)$_n$ synthesis, multiple guidelines were established for an optimised protocol. First, to avoid the self-condensation reaction of GLYMO, heating and concentration under vacuum of the reaction mixture should be avoided. Second, an excess of

cyclen, rather than GLYMO, is preferable due to easier removal by trituration or washing, in addition to self-polymerisation concerns. In Procedure 6, CnGm is the dominant product, in opposition to the multi-functionalised cyclen products ($Cn(Gm)_2$, $Cn(Gm)_3$, $Cn(Gm)_4$). This is desirable because mono-functionalised product maximises the amount of ligand attached to the silica; multi-functionalised cyclen would react with more silica silanol groups *per* ligand. It has been reported that increasing the number of arms attached to the macrocycle increases its chemical resistance to degradation, but this also has a dramatic, negative effect on its Cu(II)-binding properties due to rigidity constraints.[252] Third, the ring-opening reaction using a Lewis acid catalyst goes to completion faster than the same reaction without the catalyst: ~3 days *vs* 5–6 days. However, utilisation of a metal catalyst may be inadvisable because of the metal-chelating ability of cyclen. Fourth, the epoxide opening may be monitored by ^{1}H NMR spectroscopy by observing the downfield shift from δ_H 3.14 ppm to δ_H 3.89 ppm of the peak attributed to **H2** (**Scheme 4.6**). Lastly, Procedure 6 should be followed to synthesise CnGm, and the crude reaction mixture should be progressed directly to the next step.

4.2.2.2 Synthesis of ± Cu(II)-CnGmSiO$_2$

As shown in **Scheme 4.7**, silica modification with Procedure 6 CnGm is a multi-step process. First, CnGm may be chelated to Cu(II) to produce, after hydrolysis of the methoxy groups and silica functionalisation, "pre-loaded" Cu(II)-CnGmSiO$_2$. This is useful for comparing the copper content of pre-loaded Cu(II)-CnGmSiO$_2$ to CnGmSiO$_2$ exposed to a Cu(II) solution (*i.e.* "post-loaded", "CnGmSiO$_2$ + Cu(II)"). The methoxy groups of ± Cu(II)-CnGm can be hydrolysed under acidic or basic conditions. However, acidic conditions are less desirable due to concerns about the decomplexation of Cu(II) from the cyclen ligand upon protonation of the amines.[241] The addition of silica to ± Cu(II)-CnGm and heating drives the hydrolytic reaction to completion, and heating and concentration under vacuum promotes the dehydration/condensation reaction between ± Cu(II)-CnGm and the silica silanol groups by removing water. Finally, the ± Cu(II)-CnGmSiO$_2$ product is washed by Soxhlet extraction with water for 24 h to remove unbound impurities, such as excess cyclen. It is generally assumed that anything remaining after this extraction is covalently bound, and hydrolysis of the siloxane linkages is said to be unlikely.[207]
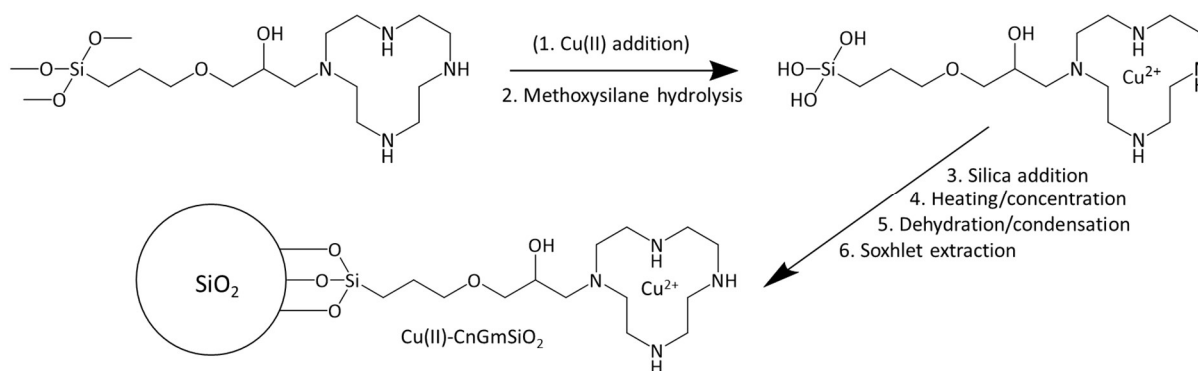
Scheme 4.7. Synthesis of ± Cu(II)-CnGmSiO₂. In order to synthesise Cu(II)-CnGmSiO₂, Cu(II) may be added first to produce the Cu(II)-CnGm complex **(1)**. Then, hydrolysis of the methoxysilane groups **(2)** is followed by the addition of silica **(3)** and heating and concentration **(4)** to drive the dehydration/condensation reaction **(5)**. Finally, the ± Cu(II)-CnGmSiO₂ product is washed *via* Soxhlet extraction **(6)**.

As listed in **Table 4.5**, four batches of ± Cu(II)-CnGmSiO₂ were prepared: Batches 1 and 2 were pre-loaded with Cu(II) (Cu(II)-CnGmSiO₂), and Batches 3 and 4 were the free, uncoordinated ligand (CnGmSiO₂). Also, Batches 2–4 were synthesised following the same procedure. Batch 1 was synthesised following a different procedure (A *vs* B).

Table 4.5. Batches of ± Cu(II)-CnGmSiO₂ prepared.

Batch #	± Cu(II)	Product	Procedure
1	+	Cu(II)-CnGmSiO₂	A
2	+	Cu(II)-CnGmSiO₂	B
3	-	CnGmSiO₂	B
4	-	CnGmSiO₂	B

For Batch 1, an excess of copper(II) nitrate (aq, light blue solution) was added to the CnGm reaction mixture in chloroform from Procedure 6, and complexation was evidenced by the colour change of the reaction mixture from colourless to dark blue. The Cu(II)-CnGm complex was extracted into the aqueous layer by washing the organic layer with water until the chloroform was no longer blue, and analysis of the organic layer by ^{1}H NMR spectroscopy (1:1 v/v CDCl₃:CD₃OD) confirmed that very little CnGm remained in the organic phase. To hydrolyse the CnGm methoxy groups under basic conditions, ammonium hydroxide was added to the isolated, dark blue aqueous layer to give a final concentration

of 0.05% v/v ammonium hydroxide in water, and the mass spectrum of a sample of this solution revealed the presence of Cu(II)-CnGm, less the three methoxy groups (m/z 428.1 [Cu(II)-CnGm - 3CH$_3$ + 2H]$^+$, 214.6 [Cu(II)-CnGm - 3CH$_3$ + 3H]$^{2+}$). The addition of silica, concentration of the reaction mixture under vacuum while heating, and Soxhlet extraction yielded the royal blue Cu(II)-CnGmSiO$_2$ product (**Figure 4.15**). In contrast, the exposure of unmodified silica to an aqueous Cu(II) solution did not result in any colour change: the silica remained white.
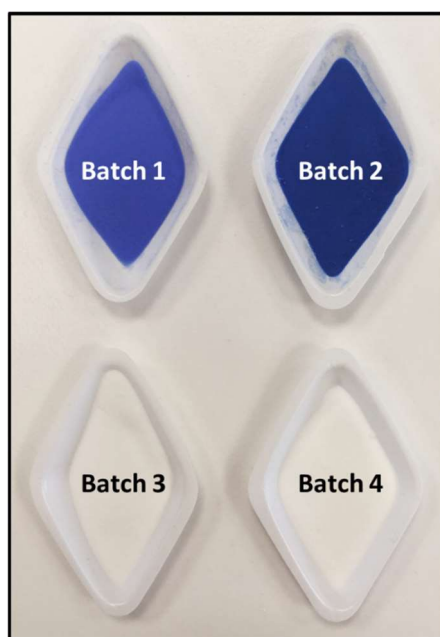
Figure 4.15. ± Cu(II)-CnGmSiO$_2$ products from Batches 1–4.

Batch 1 Cu(II)-CnGmSiO$_2$ was submitted for CHN elemental analysis and copper quantification by ICP-MS. CHN analysis of the product revealed a percent functionalisation of 32% (**Table 4.6**), which was calculated based on the measured %N value compared to the theoretical maximum (*i.e.* if all of the Procedure 6 CnGm functionalised the silica). To determine if the ratio of C to N was as expected for Cu(II)-CnGmSiO$_2$, the expected %N (0.60%) was calculated from the measured %C and compared to the measured %N (0.47%), yielding a -22% error. The difference between the measured and theoretical %N was unsurprising, given that some Cn(Gm)$_2$ was also produced in the Procedure 6 reaction, as evidenced by MS data, and that calculations were based on the mono-functionalised product (CnGm). The ICP-MS results (**Table 4.7**) revealed that the sample was 0.48% w/w Cu, which was 91% of the theoretical value (0.53% w/w Cu). This theoretical value was calculated from the theoretical maximum adjusted for the percent functionalisation. Again, the theoretical maximum was based on the modification of silica with all of the Cu(II)-CnGm.

Table 4.6. CHN elemental analysis and percent functionalisation results for Batch 1 Cu(II)-CnGmSiO$_2$, as well as the percent error between the expected and measured %N.

CHN Results[a]	Batch 1 Cu(II)-CnGmSiO$_2$
Measured %C	1.80
Measured %H	0.77
Measured %N	0.47
Expected %N[b]	0.60
% Error	**-22**
% Functionalisation[c]	**32**

[a] Reported as the mean of duplicate measurements within ≤ 0.30% of each other.
[b] Calculated from the measured %C data.
[c] Calculated based on the measured %N value compared to the theoretical maximum.

Table 4.7. ICP-MS (Cu) results for Batch 1 Cu(II)-CnGmSiO$_2$ compared to the calculated theoretical % w/w Cu.

ICP-MS Results	Batch 1 Cu(II)-CnGmSiO$_2$
Measured % w/w Cu[a]	**0.48**
Theoretical % w/w Cu[b]	**0.53**

[a] Measured in triplicate. The percent error of the measurement is ±5%.
[b] Calculated based on the percent functionalisation data (**Table 4.6**) and theoretical maximum.

Given the low percent functionalisation for Batch 1 (32%), experiments were conducted to gauge the extent of hydrolysis of the GLYMO methoxy groups (**Scheme 4.8**) under the conditions in the procedure and to explore alternative conditions. Failure of the methoxy groups to hydrolyse would preclude subsequent silica modification. Thus, incomplete hydrolysis would result in a lower percent functionalisation, and it was hypothesised that the conditions employed might be insufficient for complete hydrolysis. As shown in **Figure 4.16**, hydrolysis was tracked *via* ^{1}H NMR spectroscopy by observing the decrease over time in the intensity of the peak attributed to the methoxy protons (δ$_H$ 3.57 ppm, –Si(OC$\underline{H}_3$)$_3$) and, inversely, by observing an increase in the methanol peak (δ$_H$ 3.47 ppm in CDCl$_3$, C$\underline{H}_3$OH).[261] The hydrolytic stability of GLYMO was initially tested in chloroform at room temperature and in methanol at 60 °C. GLYMO was stable in chloroform for the 6 days during which it was monitored, but the methoxy groups hydrolysed completely after heating in methanol for 40 h. It was useful to know that the CnGm product would be stable in chloroform for, at least, 6 days. Then, the hydrolysis conditions (**Table 4.8**) used for Batch 1 (0.05% v/v ammonium hydroxide, water, RT)

were tested, and it was found that, under these conditions, 78% of the methoxy groups were hydrolysed within 0.2 h (**Figure 4.17**). However, hydrolysis was still incomplete after 4.7 h, which may account, in part, for the low percent functionalisation. Therefore, it was decided that other hydrolysis conditions should be tested to optimise the method.
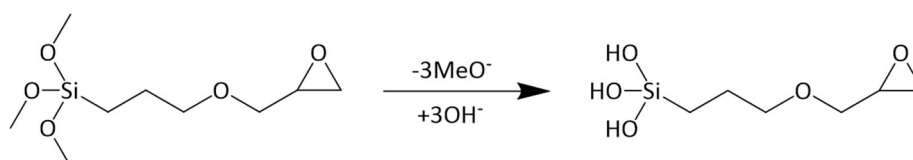
Scheme 4.8. Hydrolysis of GLYMO methoxysilane groups.
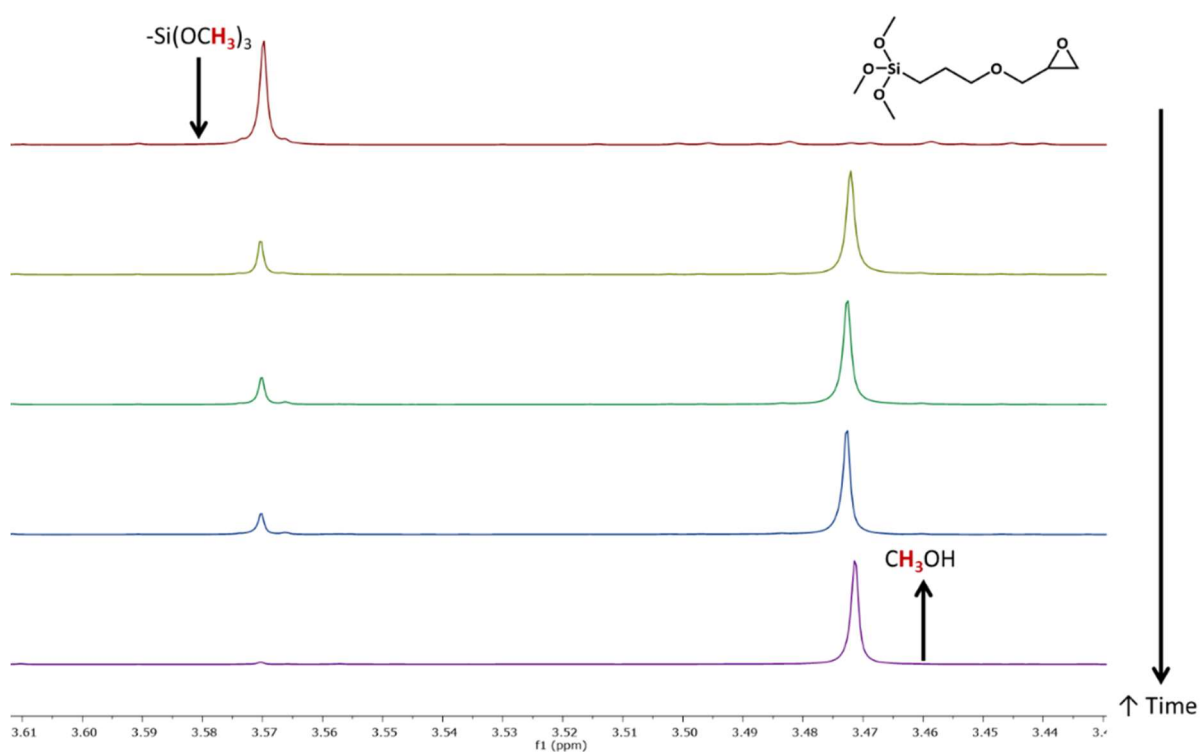
Figure 4.16. ^{1}H NMR spectra (CDCl$_3$) of GLYMO (δ_H 3.61–3.43 ppm), following methoxy group hydrolysis over time.

Table 4.8. Conditions for GLYMO hydrolysis experiments. The concentration of GLYMO was approximately 63 mM.

Conditions	% v/v NH₄OH	Solvent	Temperature (°C)
Batch 1	0.05	D_2O	20 (RT)
Lu, 0.4%	0.04	CD_3OD, 1.6% v/v H_2O	60
Lu, 1%	1	CD_3OD, 3.6% v/v H_2O	60
Batches 2–4	1	CD_3OD, 3.7% v/v H_2O, 11% v/v $CHCl_3$	60
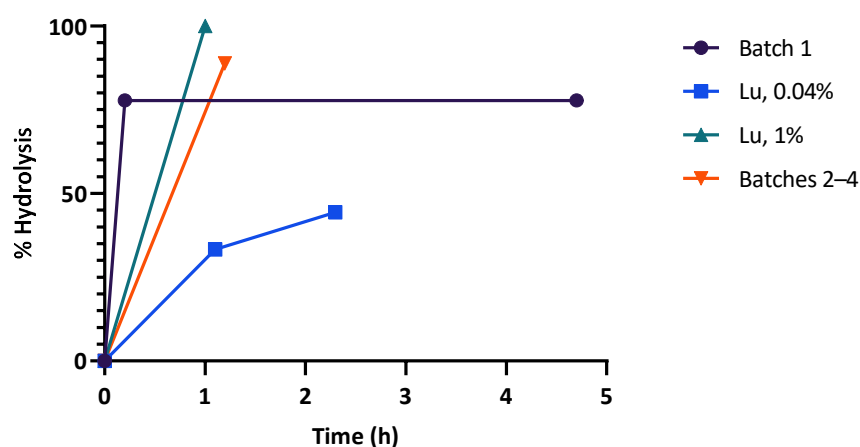
Figure 4.17. GLYMO hydrolysis over time under the sets of conditions reported in **Table 4.8**.

Aspects of the procedure by Lu[269] were utilised for the next three sets of hydrolysis conditions tested, as shown in **Table 4.8**. First, GLYMO (~63 mM) in 0.04% v/v ammonium hydroxide in methanol and water (1.6% v/v) only partly hydrolysed (44%, **Figure 4.17**) after 2.3 h heating at 60 °C. Consequently, the percentage (v/v) of ammonium hydroxide was increased from 0.04% to 1%. This resulted in complete hydrolysis after 1 h, and, therefore, this set of conditions was chosen for subsequent silica modification experiments. Since the CnGm reaction mixture would be introduced as a solution in chloroform to the basic mixture containing silica, the same set of conditions was tested again with the appropriate amount of chloroform (11% v/v), and almost complete hydrolysis of the methoxy groups was observed after 1.2 h. Self-polymerisation of GLYMO was not observed. It was decided that this set of hydrolysis conditions was acceptable for the synthesis of ± Cu(II)-CnGmSiO₂, in the hope of improving the percent functionalisation relative to Batch 1.

Following the outcomes from the GLYMO hydrolysis experiments, Batch 2 of Cu(II)-CnGmSiO$_2$ was prepared. An excess of copper(II) nitrate in methanol was added to the Procedure 6 CnGm reaction mixture in chloroform. The colour change of the reaction mixture from colourless to dark blue indicated the formation of the Cu(II)-CnGm complex, which was confirmed by HRMS (calcd for C$_{17}$H$_{39}$CuN$_4$O$_5$Si [Cu(II)-CnGm - H]$^+$ 470.1986; found 470.1978). Then, the Cu(II)-CnGm reaction mixture was added to silica in a basic water/methanol solution, resulting in a final concentration of 1% v/v ammonium hydroxide in methanol and water (3.6% v/v). The mixture was heated at 60 °C for 1 h while stirring to hydrolyse the methoxysilane groups. Subsequent heating and concentration under vacuum of the mixture promoted the dehydration/condensation reactions, and Soxhlet extraction of the product yielded dark blue Cu(II)-CnGmSiO$_2$. Batches 3 and 4 were prepared in the same manner, but without the addition of Cu(II), to produce CnGmSiO$_2$ (**Figure 4.15**) as a white solid. The Cu(II)-chelating ability of the CnGmSiO$_2$ from Batches 3 and 4 was tested by immersing the ligand-functionalised silica in an aqueous copper(II) nitrate solution for 24 h and then washing the now-blue product. This "post-loaded" Batches 3 and 4 CnGmSiO$_2$ with Cu(II), rather than pre-loading the modified silica, as for Batches 1 and 2.

In order to determine if a comparable amount of cyclen ligand could be retained by the silica without the GLYMO linker, the adsorption of Cu(II)-cyclen to the silica was tested. An excess of copper(II) nitrate was added to a basic, aqueous solution of cyclen. Silica was added to the dark blue Cu(II)-cyclen complex, and the mixture was concentrated under vacuum while heating and washed by Soxhlet extraction with water for 1 day. The light blue product was compared to Batches 1–4 to determine if covalent attachment of the cyclen ligand to silica *via* the GLYMO linker was necessary, since polyamine compounds are already well-retained by silica through acid/base interactions.

Batches 1–4 and the silica with adsorbed Cu(II)-cyclen were submitted for CHN elemental analysis, and the results are tabulated (**Table 4.9**). Unmodified silica was submitted as a blank, and its %C and %N results were below the detection limit. Batch 1 had a much lower percent functionalisation than Batches 2–4: 32% *vs* 73%, 75%, and 88%, respectively. Therefore, it was concluded that the procedure employed for Batch 1 was significantly less effective than the new procedure followed for Batches 2–4. Furthermore, these results suggested that the new procedure was fairly reproducible: the percent relative standard deviation (RSD) between the %N results for Batches 2–4 was approximately 11%. The CHN results for the Cu(II)-cyclen-adsorbed silica indicated that < 17% of the Cu(II)-cyclen was retained by the silica, suggesting that covalent attachment of the ligand through the GLYMO linker was necessary for retention.

Table 4.9. CHN elemental analysis and percent functionalisation/adsorption results for silica, Batches 1–4 ± Cu(II)-CnGmSiO$_2$, and adsorbed Cu(II)-cyclen.

Product	%C[a]	%H[a]	%N[a]	% Functionalisation/ Adsorption[b]
Silica	< 0.30	0.96	< 0.30	-
Batch 1 Cu(II)-CnGmSiO$_2$	1.80	0.77	0.47	**32**
Batch 2 Cu(II)-CnGmSiO$_2$	4.17	0.92	1.18	**73**
Batch 3 CnGmSiO$_2$	4.52	1.22	1.24	**75**
Batch 4 CnGmSiO$_2$	4.81	0.94	1.46	**88**
Adsorbed Cu(II)-cyclen	0.53	0.87	< 0.30	**< 17**

[a] Reported as the mean of duplicate measurements within ≤ 0.30% of each other.
[b] Calculated based on the measured %N value compared to the theoretical maximum.

The percent error between the expected and measured %N from the CHN results was also calculated (**Table 4.10**). As before, the expected %N was calculated from the measured %C. Out of Batches 1–4, at -22%, Batch 1 had the largest error, and, at -9%, Batch 4 had the smallest. All of the ± Cu(II)-CnGmSiO$_2$ samples had a lower measured %N than expected, and, as before, this was unsurprising due to the presence of multi-functionalised, as well as mono-functionalised, Cn(Gm)$_n$ in the reaction mixture. The percent error could not be calculated for the Cu(II)-cyclen-adsorbed silica, as the measured %N was below the detection limit.

Table 4.10. Percent error between the expected and measured %N from CHN results.

Product	Measured %N	Expected %N[a]	% Error
Batch 1 Cu(II)-CnGmSiO$_2$	0.47	0.60	**-22**
Batch 2 Cu(II)-CnGmSiO$_2$	1.18	1.39	**-15**
Batch 3 CnGmSiO$_2$	1.24	1.51	**-18**
Batch 4 CnGmSiO$_2$	1.46	1.60	**-9**
Adsorbed Cu(II)-cyclen	< 0.3	0.17	**-**

[a] Calculated from the measured %C data (**Table 4.9**).

To characterise the materials further, the copper content of pre-loaded and post-loaded CnGm-modified silica from Batches 1–4, as well as the Cu(II)-cyclen-adsorbed silica, was measured by ICP-MS and compared to the calculated theoretical % w/w Cu (**Table 4.11**). As it has been reported that free silanol groups are capable of metal ion-complexation,[241] the ability of unfunctionalised silica to retain

Cu(II) was also determined. The samples were prepared for ICP-MS analysis by digestion in concentrated hydrofluoric acid and then nitric acid (9M) and dilution in nitric acid (3% v/v) to bring the samples into the range of the standards. Batches 1 and 2 Cu(II)-CnGmSiO$_2$ were both pre-loaded with Cu(II) in the first step of the functionalisation procedures. However, the measured copper content of Batch 1 (0.48% w/w) was much lower than that of Batch 2 (2.60% w/w). This served as further evidence that the new procedure for Batches 2–4 was superior to the Batch 1 procedure. The measured amount of copper in Batch 2 was almost twice the calculated theoretical amount (1.33% w/w), but the cause for this disparity remains unclear. The copper content in Batches 3 and 4 CnGmSiO$_2$ was measured before post-loading with Cu(II). Thus, they served as blanks, and copper was only detected at the level of parts *per* million. After exposure to an aqueous copper(II) nitrate solution for 24 h (*i.e.* post-loading with Cu(II): "CnGmSiO$_2$ + Cu(II)"), the measured copper contents of Batches 3 and 4 were 0.96% w/w and 1.02% w/w, respectively. These values agreed well, but both were lower than the calculated theoretical % w/w Cu and lower than pre-loaded Batch 2. It is possible that the Cu(II) complexes formed more easily in solution, as in for the pre-loading, than in the aqueous silica mixture, as in for the post-loading. In fact, previous studies in the literature found that harsh conditions (2–3 h refluxing in ethanol with an excess of Cu(II)) were necessary for complete metalation of cyclam-modified silica.[240,243,252]

Table 4.11. ICP-MS (Cu) results for silica ± Cu(II), Batches 1–4 ± Cu(II)-CnGmSiO$_2$, and adsorbed Cu(II)-cyclen compared to the calculated theoretical % w/w Cu.

Product	Measured % w/w Cu	% RSD	Theoretical % w/w Cu[a]
Silica (unexposed to Cu(II))[b]	< 0.0001	-	0
Silica (exposed to Cu(II))	**0.06**	1.0	-
Batch 1 Cu(II)-CnGmSiO$_2$[c]	**0.48**	d	**0.53**
Batch 2 Cu(II)-CnGmSiO$_2$	**2.60**	0.3	**1.33**
Batch 3 CnGmSiO$_2$	0.00	0.4	0
Batch 3 CnGmSiO$_2$ + Cu(II)	**0.96**	0.3	**1.41**
Batch 4 CnGmSiO$_2$	0.00	1.6	0
Batch 4 CnGmSiO$_2$ + Cu(II)	**1.02**	0.3	**1.65**
Adsorbed Cu(II)-cyclen[b]	**0.28**	d	**0.35**

[a] Calculated based on the percent functionalisation/adsorption data (**Table 4.9**) and theoretical maximum.
[b] Measured in duplicate.
[c] Measured in triplicate.
[d] The percent error of the measurement is ±5%.

In the present work, the copper content for the Cu(II)-cyclen-adsorbed silica was 0.28% w/w, which was 80% of the theoretical amount and even lower than Batch 1. This further reinforced the necessity of covalent attachment. The copper content of unfunctionalised silica before and after exposure to an aqueous copper(II) nitrate solution was < 0.0001% w/w and 0.06% w/w, respectively. Thus, it was demonstrated that, even without modification, silica is able to retain a relatively significant amount of Cu(II).

4.2.2.3 Conclusions

A successful method was developed for the functionalisation of silica with $\pm$ Cu(II)-CnGm, and a simple process was established for characterisation of the product. Two methods with differing approaches were trialled (**Scheme 4.1**): in Method 1, silica was modified with GLYMO and then reacted with cyclen, but, in Method 2, cyclen and GLYMO were reacted first, followed by silica modification with CnGm. Method 2 was found to be superior to Method 1 for the synthesis of $\pm$ Cu(II)-CnGmSiO$_2$. The main advantage of Method 2 was that the product of the first reaction, CnGm, could be characterised by NMR spectroscopy. In Method 1, characterisation of the products was complicated by their attachment to the inorganic silica matrix, and it was difficult to prove that, first, the GLYMO linker was covalently bound to the silica and, second, that the cyclen ligand was covalently bound to GLYMO. Following Method 2, the six procedures for Cn(Gm)$_n$ synthesis (**Table 4.4**) established guidelines in order to avoid GLYMO self-condensation and to generate free-ligand CnGm as the major product. It was decided that the crude CnGm (Procedure 6) reaction mixture in chloroform should be used for subsequent silica functionalisation. Multiple sets of conditions for hydrolysis of the methoxysilane groups were tested (**Table 4.8**), and the results led to the establishment of a fairly reproducible silica modification procedure with a percent functionalisation consistently greater than 70% (Batches 2–4). Pre-loading the CnGmSiO$_2$ with Cu(II) yielded a % w/w Cu more than twice that achieved by post-loading (Batch 2: 2.60% *vs* Batch 3: 0.96% and Batch 4: 1.02%). Finally, the poor retention of Cu(II)-cyclen adsorbed onto silica demonstrated the necessity of covalent attachment of the ligand to silica through a linker.

The loading of the macrocycle and copper on the silica from Batches 2–4 was comparable to previous studies (**Table 4.12**). Prior works achieved macrocycle concentrations ranging from 0.20–0.93 mmol/g silica. In comparison, the macrocycle-loading for Batches 2–4 was 0.21–0.26 mmol/g silica, which, albeit at the lower end, was within the range reported in the literature. Similarly, the copper content (0.15–0.41 mmol/g silica) was within the reported range (0.03–0.78 mmol/g silica). This indicated that

the new, optimised method for ± Cu(II)-CnGmSiO$_2$ synthesis could generate products with similar ligand- and copper-loading to those in the literature.

Table 4.12. Loading of the macrocycle and copper on silica.

Samples in This Work	Loading (mmol macrocycle/g silica)[a]	Loading (mmol Cu/g silica)[b]
Batch 1 Cu(II)-CnGmSiO$_2$	**0.08**	**0.08**
Batch 2 Cu(II)-CnGmSiO$_2$	**0.21**	**0.41**
Batch 3 CnGmSiO$_2$ + Cu(II)	**0.22**	**0.15**
Batch 4 CnGmSiO$_2$ + Cu(II)	**0.26**	**0.16**
Adsorbed Cu(II)-cyclen	**0.05**	**0.04**
References	**Loading (mmol macrocycle/g silica)**	**Loading (mmol Cu/g silica)**
Bagnoud *et al.*[255]	-	0.20
Gros *et al.*[241]	0.33–0.44	0.054–0.31
Bereczki *et al.*[258]	-	0.21–0.33
Barreto *et al.*[259]	0.20–0.24	-
Goubert-Renaudin *et al.*[252]	0.25–0.63	0.03–0.35
Corriu *et al.*[243]	0.48–0.93	0.45–0.78
Dubois *et al.*[238]	0.38–0.81	0.35–0.75
Cuenot *et al.*[123]	0.30–0.61	-

[a] Calculated from the measured %N values in **Table 4.9**.
[b] Calculated from the measured % w/w Cu values in **Table 4.11**.

4.3 INCORPORATION OF SILICA IN A COATING

To incorporate the functionalised silica products into a coating, it was suggested that the silica be applied to an uncured resin, which would then be allowed to cure with silica adhered to the surface. In other words, the resin would glue the silica to the substratum. A similar procedure is implemented in industry for textured paints.[207] The intention was to evaluate bacterial adherence to the coatings with the biocidal ingredient at the surface, which was desirable for a couple of reasons. First, part of the motivation for modifying silica with the ligand was because it is known that silica tends to float to the surface of a coating,[29] meaning that the bacteria would, ideally, be exposed to the biocide at the coating/water interface anyway. Second, it was assumed that the maximum effect of the biocide on bacterial adherence would be achieved when the surface is purely the biocide, rather than diluted throughout a coating. Therefore, if bacterial adherence to a surface composed of the putative biocide was uninhibited, then it could be concluded that the modified silica would likely be unsuccessful as an antifouling agent. This method, however, is complicated by the propensity of bacteria to colonise rough surfaces, such as the proposed silica surfaces.

The positive relationship between surface roughness and bacterial colonisation has a few explanations. The initial adhesion of bacteria is facilitated on rough surfaces because they provide shelter from shear forces that would, otherwise, remove the bacteria, thus allowing time for the attachment to become irreversible. Rough surfaces also have a greater surface area for bacterial adhesion and are difficult to clean.[270] Consequently, increased bacterial adherence to the rough silica coatings might be hypothesised. But, the increase in colonisation by bacteria with the roughening of a surface does not always hold true; if the biocide at the surface is at the appropriate concentration, even if the surface is rough, bacterial adhesion will be deterred. For example, in a study by Kozlovsky *et al.*[271], chlorhexidine (CHX), a chemical antiplaque agent, was adsorbed to both sand-blasted, acid-etched rough and machined-smooth titanium disks, and the antibacterial activity of the disks was assessed against *Streptococcus mutans*, a human odontopathogen.[272] It was found that the greater surface area of the rough disk provided more adsorption sites for CHX, and, as a result, the rough titanium surface demonstrated improved antimicrobial performance compared to the smooth surface. Therefore, in this work, the aim of the functionalised silica coatings was to achieve a high enough copper concentration at the silica surface *via* the Cu(II)-ligand to be antimicrobial, despite the roughness of the surface.

A two-pack epoxy, composed of a commercial hardener and epoxy resin, was chosen as the resin on which to apply the $\pm$ Cu(II)-CnGmSiO$_2$ products. It was chosen due to familiarity with its use, curing process, and properties (Chapter 3, **Section 3.3**). The hardener (Ancamine® 2459 Curing Agent) and

epoxy resin (Epikote™ 235) were mixed manually, according to the manufacturers' specifications, and the viscous, dark yellow mixture was applied by the standard draw-down technique with a bar film applicator (Experimental, **Figure 6.2**) to one side of a black, plastic sheet (vinyl chloride/acetate copolymer, Leneta). The silica was applied to a defined surface area of the still-uncured epoxy resin with an inverted funnel so that, at least, one layer of silica covered the resin, and the coating was left to cure at room temperature overnight. The following day, the same procedure was repeated for the second side of the substratum. Once the second side had cured, the silica/epoxy (SiO_2/epx)-type coatings were brushed, washed with water, and dried to remove non-adhered particles, and squares (23 mm × 23 mm) coated on both sides were cut from the material for immediate bacterial adherence testing. The four silica samples incorporated into coatings for testing were as follows: 1) Batch 4 $CnGmSiO_2$ (free ligand), 2) Batch 4 $CnGmSiO_2$ + Cu(II) (post-loaded), 3) Batch 2 Cu(II)-$CnGmSiO_2$ (pre-loaded), and 4) unmodified, commercial silica (SiO_2). Batch 4 $CnGmSiO_2$ was arbitrarily chosen over Batch 3 $CnGmSiO_2$, but, in retrospect, Batch 3 would have been more appropriate due to its elemental composition being closer to Batch 2 Cu(II)-$CnGmSiO_2$ (**Table 4.9**). To post-load $CnGmSiO_2$ with Cu(II), the cut-out squares coated on both sides with $CnGmSiO_2$ were submerged for 24 h in an aqueous solution containing an excess of copper(II) nitrate, washed with water, dried, and immediately tested for bacterial adherence. The prepared squares are shown in **Figure 4.18** (top left corner), and the bacterial adherence results are discussed in Chapter 5 (**Sections 5.3–4**).

Although the silica application on each square sample was, unsurprisingly, inhomogeneous, the goal of the application was to simply cover the underlying epoxy resin with silica so that the bacteria were only exposed to the silica. Magnified images of the SiO_2/epx-type coatings were obtained by scanning electron microscopy (SEM; Appendix, **Figures 8.45–47**), and SEM images of the squares at 200× magnification (**Figure 4.18**) revealed the desired surface coverage. Homogeneous application of the silica would require more specialised equipment. Differences in the numbers of layers of silica adhered to the coatings would likely affect bacterial adhesion results if the total surface area of the square was variable and the biocide (*i.e.* Cu(II)) was ineffective. But, it was thought that, if the biocide was effective, relative differences between the coatings with and without Cu(II) would still be observable, since the differences would need to be orders of magnitude to be meaningful.

In tandem with imaging the squares, the elemental compositions of the coatings were obtained *via* scanning electron microscopy/energy dispersive X-ray spectroscopy (SEM-EDS; **Table 4.13**). The EDS spectra are in the Appendix (**Figures 8.48–51**). EDS is an elemental analysis technique based on the ionisation of atoms in a sample by an incident electron beam, resulting in the emission of characteristic X-rays as the atoms return to their ground state. The X-ray photons are detected, and a proportional output signal is generated to create an X-ray spectrum of counts or intensity *vs* X-ray energy

(**Figure 4.19**). The information contained in the spectrum is both qualitative and semi-quantitative: the peak position in the spectrum (*i.e.* the X-ray energy) identifies the element, while the peak area is proportional to the atomic percent of the particular element in the irradiated area.[273,274] The data are considered semi-quantitative because physical standards are not measured. Rather, the standardless analysis refers to libraries of standard spectra for the calculations.[275]
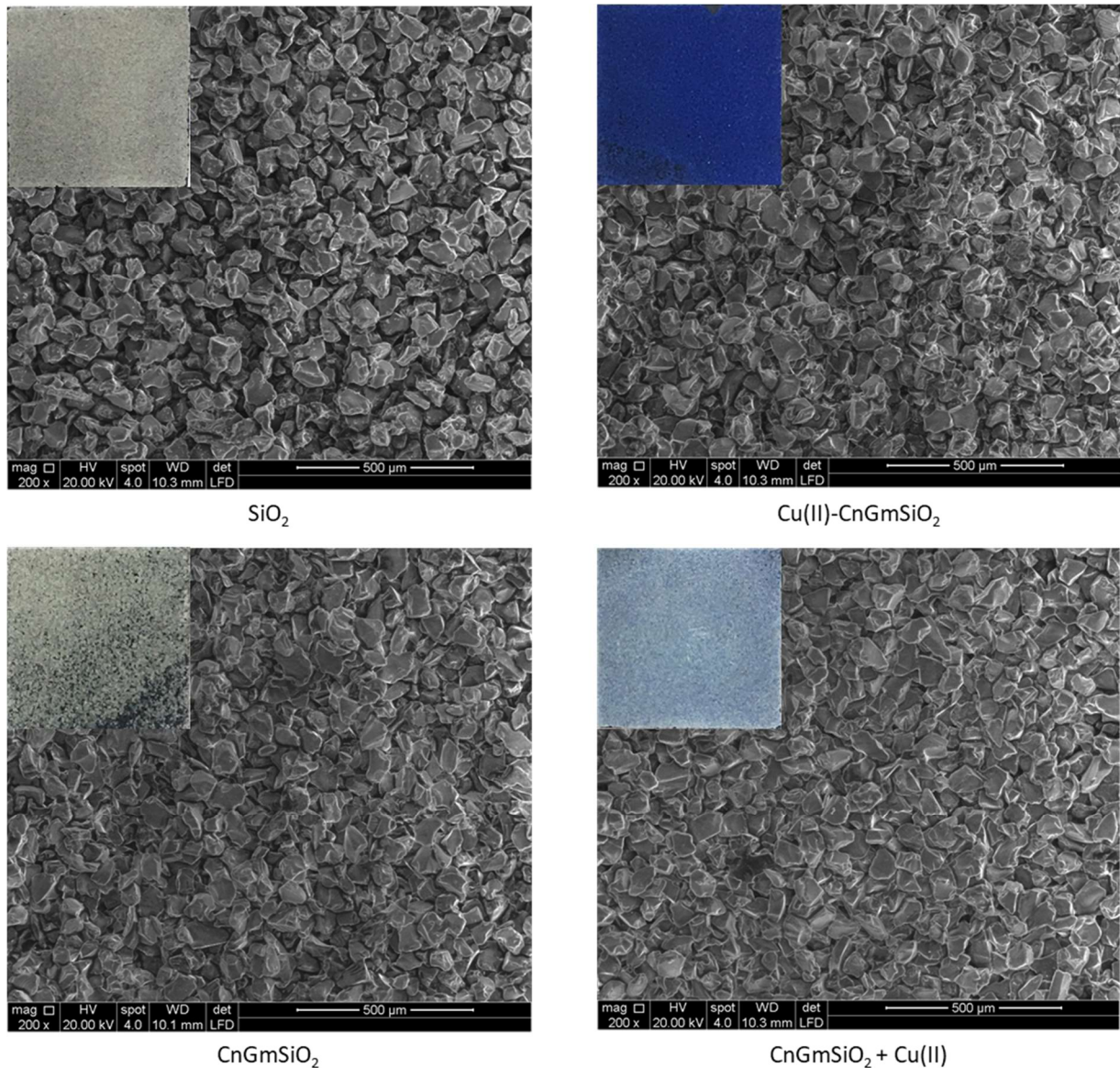
Figure 4.18. SEM secondary electron images at 200× magnification of the SiO₂/epx-type squares to be tested for bacterial adherence (HV 20 kV, spot size 4, WD 10 mm, LFD). The coatings include SiO₂/epx, Batch 2 Cu(II)-CnGmSiO₂/epx, Batch 4 CnGmSiO₂/epx, and Batch 4 CnGmSiO₂ + Cu(II)/epx, and pictures of these coatings are in the top left corner of each SEM image.

Table 4.13. EDS results for Batch 2 Cu(II)-CnGmSiO$_2$/epx, Batch 4 CnGmSiO$_2$/epx, Batch 4 CnGmSiO$_2$ + Cu(II)/epx, and SiO$_2$/epx.

Batch 2 Cu(II)-CnGmSiO$_2$/epx		
Element	*Weight %*	*Atomic %*
C K	45 ± 4	55 ± 5
N K	4.0 ± 0.7	4.2 ± 0.8
O K	36 ± 4	33 ± 3
Si K	13.9 ± 0.6	7.3 ± 0.4
Cu K	**1.4 ± 0.2**	**0.32 ± 0.06**
Batch 4 CnGmSiO$_2$/epx		
Element	*Weight %*	*Atomic %*
C K	43 ± 4	53 ± 5
N K	3.9 ± 0.7	4.2 ± 0.8
O K	38 ± 4	35 ± 4
Si K	15.7 ± 0.6	8.3 ± 0.4
Batch 4 CnGmSiO$_2$ + Cu(II)/epx		
Element	*Weight %*	*Atomic %*
C K	40 ± 4	50 ± 5
N K	4.7 ± 0.8	5.0 ± 0.9
O K	39 ± 4	37 ± 4
Si K	16.1 ± 0.8	8.6 ± 0.5
Cu K	**1.0 ± 0.2**	**0.23 ± 0.06**
SiO$_2$/epx		
Element	*Weight %*	*Atomic %*
C K	42 ± 4	53 ± 5
O K	40 ± 4	38 ± 4
Si K	17.3 ± 0.5	9.3 ± 0.3
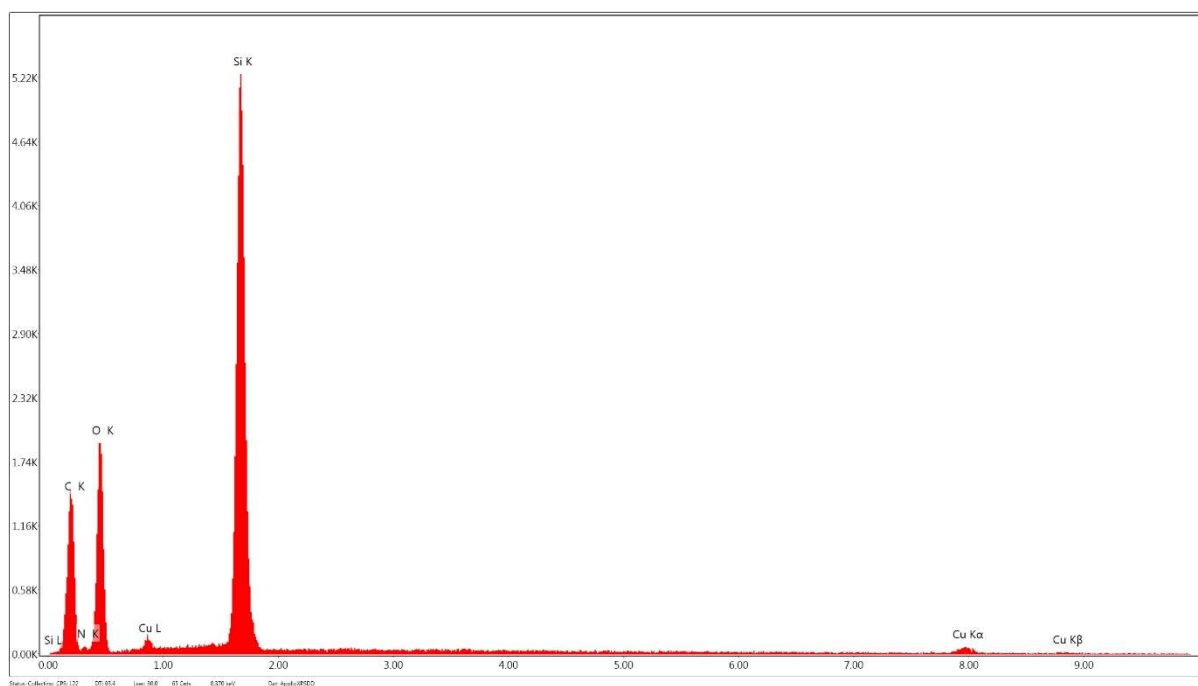
Figure 4.19. Example EDS spectrum (counts *vs* keV).

As predicted, all of the modified-silica coatings were found to be composed of C, O, N, and Si, with the Cu(II)-CnGmSiO$_2$/epx and CnGmSiO$_2$ + Cu(II)/epx coatings also containing Cu (**Table 4.13**). Hydrogen could not be detected by this technique because it has no core electrons – only a valence electron that participates in chemical bonding, meaning that it will not produce X-rays.[275,276] The major constituents were C, O, and Si, and the minor constituents were N and Cu. A larger percentage of the elemental composition than expected was carbon, with a weight percent between 40% and 50%. However, the accumulation of carbon as a contaminant on the sample surface in an electron microscope is common, making carbon measurements unreliable.[277] For Batch 4 CnGmSiO$_2$ + Cu(II)/epx, the copper results were comparable to those obtained by ICP-MS (**Table 4.11**), but, in the case of Batch 2 Cu(II)-CnGmSiO$_2$/epx, the results were not as comparable: 1.02% w/w (ICP-MS) *vs* 1.0% (SEM-EDS) for CnGmSiO$_2$ + Cu(II)/epx and 2.60% w/w (ICP-MS) *vs* 1.4% w/w (SEM-EDS) for Cu(II)-CnGmSiO$_2$/epx. Any consistency was actually somewhat surprising, given the inhomogeneity of the samples and the different sampling methods of the two techniques. The samples were prepared for ICP-MS by total digestion of the material, and, consequently, the results are presented as % w/w Cu in the bulk material. In contrast, the onion-shaped interaction volume sampled by SEM-EDS (**Figure 4.20**) had a width and depth of up to a few micrometres. Since the functionalised silica was heterogeneous, with the ligand and copper on the surface and an interior of silicon dioxide, it was thought that the elemental composition results by EDS would be skewed by the sampling method.
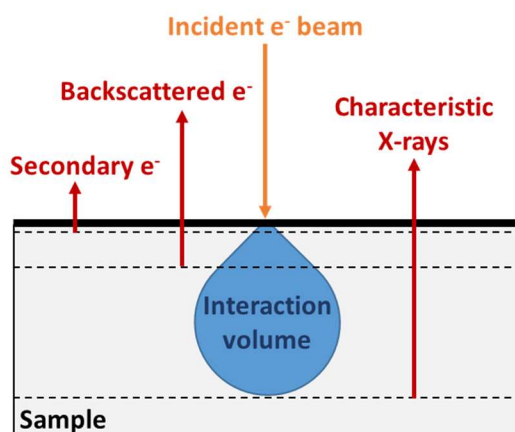
Figure 4.20. Interactions between the sample and the incident electron (e⁻) beam.[278,279]

The quantitative results were even more questionable due to specimen geometry effects, which are variations in the topography of the sample. These variations in shape and inclination of the surface relative to the incident electron beam modify the measured X-ray intensities. For accurate quantitative analyses by EDS, it is assumed that the only factor affecting X-ray intensity is the composition, and sample surfaces are polished to a surface roughness below 50 nm. If this condition is violated, the error associated with each measurement can be so large that it renders the compositional results unusable.[280,281] The topography of the SiO_2/epx-type coatings was rough and likely impacted the quantitative results. Considering all of the complications, it was decided that SEM-EDS was not an appropriate technique for determining the elemental compositions of the silica coatings with accuracy, but the qualitative results still had value. It was not visibly apparent that these complications in the analyses of the silica coatings were applicable to the commercial marine paint (Altex Yacht and Boat Paint, Aurora Red, Ablative Antifouling No. 5; 40–50% Cu_2O) used as a benchmark comparison throughout this study, and, so, the marine paint was analysed by SEM-EDS.

SEM-EDS analysis was completed to better-understand the topography and copper distribution at the surface of the marine paint. The marine paint served as the commercial standard against which the silica coatings were compared – particularly in the microbiological assays. Therefore, as with the silica coatings, it was reasonable to examine the physical and chemical features of the coating's surface, since these properties are responsible for the outcome of the bacteria-surface interaction. A sample was prepared for analysis by applying one coat of the marine paint *via* the standard draw-down technique with a bar film applicator (Experimental, **Figure 6.2**) to the substratum. SEM images of the cured paint (**Figure 4.21**) revealed a heterogeneous surface containing areas of high and low copper content. Different areas of the surface were sampled for EDS measurements, and it was found that a

couple of these areas had a % w/w Cu (1.3–1.5%, Areas 1 and 2, **Table 4.14**) comparable to the Cu(II)-containing silica coatings. However, there was also an area that was 37.4% w/w Cu (Area 3), and this high-copper area, as well as others, appeared as a white spot in the SEM image. These results were unsurprising, as the marine paint is a dispersion of cuprous oxide in solvent, zinc oxide, rosin-colophony, and thiram. Given the commercial success of the paint, the inhomogeneity of the copper distribution does not appear to significantly impact its efficacy, and fouling organisms do not colonise the low-copper areas. The marine paint was tested with the silica coatings in a bacterial adherence assay, and the results are reported in Chapter 5 (**Sections 5.3–4**).
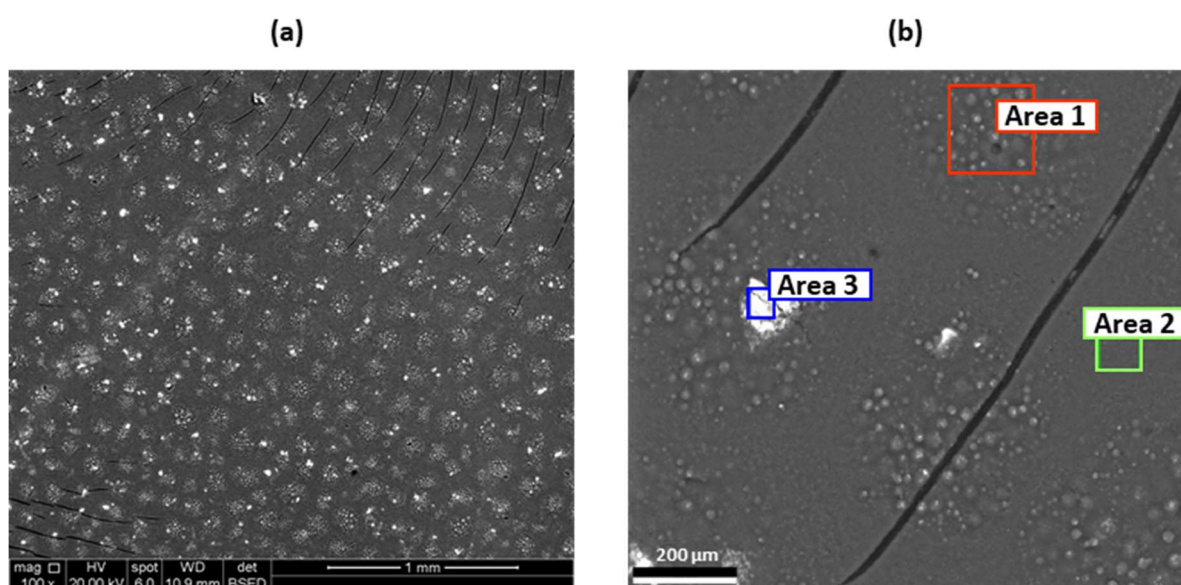
Figure 4.21. SEM backscatter electron images of the marine paint at (a) 100× magnification (HV 20 kV, spot size 6, WD 11 mm, BSED) and **(b)** sampling three areas for elemental analysis by EDS (white in the images = areas of high copper content).

Table 4.14. EDS results for the marine paint at the sampled areas in **Figure 4.21**.

Area	Element	Weight %	Atomic %
1	Cu K	**1.5 ± 0.2**	0.31 ± 0.04
2	Cu K	**1.3 ± 0.2**	0.27 ± 0.04
3	Cu K	**37.4 ± 0.9**	11.2 ± 0.3

4.4 SUMMARY AND FUTURE WORK

In this work, a simple, optimised, reproducible method, with a similar macrocycle-loading and copper-capacity to macrocycle-functionalised silica from other studies, was developed for the synthesis of $\pm$ Cu(II)-CnGmSiO$_2$. Despite the numerous examples in the literature, this chemistry was non-trivial: the challenges included characterisation and avoiding GLYMO self-condensation. In the literature, characterisation of the modified silica was, at times, incomplete or based solely on product performance. The characterisation process developed in this work (*e.g.* NMR spectroscopy for CnGm, CHN elemental analysis and ICP-MS for $\pm$ Cu(II)-CnGmSiO$_2$) was straightforward and allowed for confidence in the identities of the products. The literature procedures referenced also failed to mention the difficulties of working with silane coupling agents like GLYMO. For example, Barreto *et al.*[259] recommended heating cyclen and GLYMO in toluene at reflux temperature to synthesise CnGm. However, implementation of this protocol resulted in an intractable solid from the polymerisation of GLYMO. The developed procedure circumvented or overcame these challenges, but there are still areas for improvement.

Although the macrocycle- and copper-loadings of the $\pm$ Cu(II)-CnGmSiO$_2$ synthesised *via* this method were within reported ranges, both were at the lower end (**Table 4.12**). So, future work could explore a few alterations to improve the method. First, the amount of modifier *per* gram silica could be increased. Second, Soxhlet extraction could be conducted in a non-aqueous solvent. Despite reassurances that hydrolysis of the modifier from the silica was unlikely during water extraction,[207] it would be worthwhile to verify the claim by, instead, using a solvent like acetonitrile for the extraction. Finally, different types of silica (*e.g.* MSNs) could be modified with cyclen for formulation into a paint. All of these alterations may increase the macrocycle-loading and, subsequently, the copper-loading of the material, which might be essential for preventing bacterial adherence.

To test its effect on bacterial adherence, the modified silica was incorporated in a coating by application to the surface of an uncured epoxy resin on a plastic substrate. Squares coated on both sides in this manner were appraised in a bacterial adherence assay described in the following chapter. The goal was to achieve a high enough copper concentration at the surface to discourage colonisation by bacteria, which is one of the first steps of biofouling. Squares coated with the following silica materials were prepared for evaluation: Batch 4 CnGmSiO$_2$, Batch 4 CnGmSiO$_2$ + Cu(II), Batch 2 Cu(II)-CnGmSiO$_2$, and unmodified, commercial silica. Bacterial adherence to these coatings was tested, and the results are reported in the following chapter (Chapter 5, **Sections 5.3–4**).

5 BACTERIAL ADHERENCE TO COATINGS

5.1 BACKGROUND

In Chapter 3 (**Section 3.2.6**), it was concluded that the method employed for determining the antimicrobial activity of coatings was inappropriate for the purposes of this project; the assay measured the effect of leachates on bacterial growth, which, although of interest, is not a measurement of surface activity. Rather, the propensity of bacteria to adhere to a coating is more directly relevant to antifouling technology.[282] In the microfouling stage of biofouling, unicellular microorganisms, including bacteria, adhere to surfaces immersed in seawater and form complex biofilms.[15] The control of biofilm formation is a main goal for biofouling mitigation because these biofilms produce vital cues for the settlement of larvae of sessile marine organisms.[9] For an antifouling coating to be effective, colonisation of the surface by fouling organisms must be deterred. Therefore, measurements of this deterrence at the microfouling stage better-model the desired effect of antifouling coatings, and it was decided that an assay to test bacterial adherence to coatings should be developed and used for the SiO$_2$/epx-type coatings. However, assay development first necessitated a review of the attachment process and factors influencing adherence.

Despite extensive study, the process and mechanisms of bacterial attachment are not yet well-understood, but mechanistic models based on physico-chemical interactions between the bacterium and the substrate have been developed. The Derjaguin-Landau-Verwey-Overbeek (DLVO) model is a commonly used mechanistic model that describes adhesion as a two-step process: a reversible physical step followed by an irreversible molecular/cellular step. When planktonic (*i.e.* free-living) bacteria are transported to a conditioned surface, the DLVO model describes the reversible adsorption of cells as a balance between attractive Van der Waals forces and repulsive electrostatic interactions of the negatively charged cells and substrate. For the bacteria to remain attached, the attractive forces must be greater than the repulsive. Once the cells overcome the electrostatic repulsion and are in close contact (< 1–2 nm) with the substrate, hydrogen bonding and dipole, ionic, and hydrophobic interactions further promote adhesion. Molecular reactions between the substrate and bacterial surface structures (*e.g.* flagella, fimbriae, pili) occur, making the attachment irreversible.[283–286]

Factors influencing attachment are the substrate, conditioning film, hydrodynamics, the medium, and the cell surface (**Figure 5.1**). Regarding the substrate, microbial colonisation usually increases with increasing surface roughness due to a larger surface area and protection from shear forces. Studies provide conflicting reports about the effect of surface hydrophobicity, but many conclude that the

attachment of bacteria to hydrophobic materials proceeds more rapidly than to hydrophilic, since hydrophobic interactions between the cell surface and substrate promote adherence.[284,287] The electrostatic charge, microtopography, surface free energy, vulnerability to wear, and wettability are additional properties of the substrate that impact colonisation.[12] Once the substrate is submerged in an aqueous medium, it becomes coated in polymers, and the rate and extent of bacterial attachment, as well as the species of bacteria present at the surface, depend on the chemical nature of this conditioning film.[12,287]
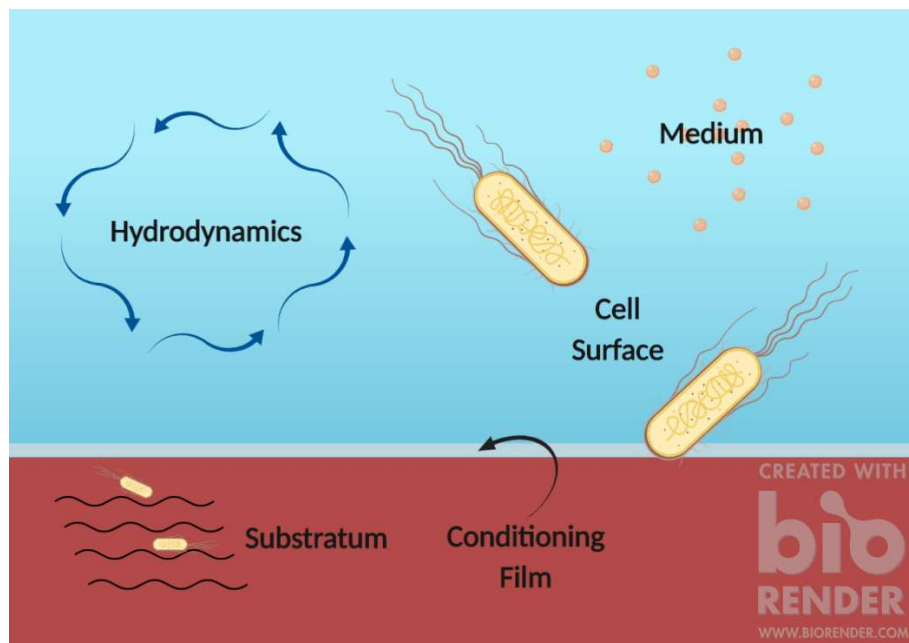
Figure 5.1. Factors that affect bacterial surface attachment (created with Biorender.com).

Transport of bacteria from the medium to the conditioned surface depends on hydrodynamics, including the velocity characteristics of the medium. An increase in velocity results in greater turbulence and mixing, and, consequently, bacteria associate with the surface rapidly until shear forces are sufficient for removal.[287,288] When the velocity of the medium is low, the surface-association of bacteria is largely dependent on the size of the microorganism and its motility (*i.e.* presence of fimbriae and flagella). Additional characteristics of the medium that affect adherence are nutrient concentration, temperature, ionic strength, and pH, and other important properties of the bacteria are cell surface hydrophobicity and the production of adhesins, including EPS. Although most bacteria are negatively charged, they still contain hydrophobic components on their surface (*e.g.* fimbriae) that promote adhesion.[287]

All of these attachment conditions may be summarised as follows: 1) surfaces are more prone to colonisation if they are rough, hydrophobic, and coated by a conditioning film; 2) the medium promotes surface adhesion with increasing velocity, temperature, and nutrient concentration, provided they do not exceed a certain threshold; and 3) fimbriae, flagella, EPS, and other adhesins are surface components of bacteria that play a significant role in attachment.[287] Since the adhesion mechanisms are poorly understood and testing methodologies suffer from a lack of standardisation, it should be noted that conflicting reports do exist about the effects of many of these factors on attachment.[284] For example, a study by Dewanti and Wong[289] reported the promotion of biofilm formation by *E. coli* (serotype O157:H7) under nutrient-limiting conditions. However, it is generally acknowledged that all of the factors addressed do play a role, so they were considered during assay development and implementation.

In order to quantify bacterial attachment to the coatings in this work, establishment of the testing framework was necessary. It was decided that *E. coli* NZRM 3647 (O157:H7, verocytotoxin negative) would be used in the method development of this assay due to the ease with which it can be cultured and for the sake of continuity with previous experiments (Chapter 3, **Section 3.2.2**). *E. coli* often serves as a representative Gram-negative bacterium for testing antimicrobial activity because it is easy to culture; it has a fast growth rate and simple nutritional requirements. Marine bacteria typically grow more slowly than *E. coli*,[290] and, thus, the use of *E. coli* for the timely completion of method development seemed logical. However, this was done with the intent of also testing the coatings with marine bacteria once the protocol was established and validated, and marine bacterium *Vibrio harveyi* NZRM 2698 (ATCC 14126, NCIMB 1280, type strain) was selected. *V. harveyi* is a Gram-negative, bioluminescent, coastal marine bacterium that has been isolated from fouled surfaces in the marine environment and used in antifouling assays.[290–294]

Many antifouling assays incubate the coated substrate in a culture of bacteria under static conditions and then examine the samples for bacterial colonisation, often by enumeration of the adhered microbes.[14,282,295–298] Although, under a threshold, agitation can promote adhesion, the shear forces present in a dynamic marine environment are sufficient to remove biofouling from marine objects (*e.g.* boats), and, to a greater extent, biofouling occurs when these objects are stationary.[299] Therefore, the assay in the present work was designed so that plastic squares coated on both sides with the potential antifouling coating would be submerged in the liquid bacterial culture without agitation, allowing cells time to adhere before enumeration. This was modelled after the work by Mendonça *et al.*[300] in which the adhesion of *E. coli* O157:H7 to stainless steel and poly(vinyl chloride) covered by thick or thin cloths was tested by their incubation in diluted cultures of *E. coli*, removal,

washing, transfer to a fresh solution, vortexing to detach cells, and enumeration of viable, adherent cells *via* the drop plate method.

Once the framework for the assay was established, procedural details, such as the medium, length of incubation, and processes of detachment and enumeration, were chosen based on bacterial adherence protocols in the literature. These preliminary conditions and processes were assessed during method development of the assay with *E. coli* NZRM 3647, but it was recognised that some of the conditions (*e.g.* medium) would need to be altered for testing the adherence of *V. harveyi* NZRM 2698 to coated samples. Similar *E. coli* attachment assays by Danese *et al.*[301] and O'Toole *et al.*[302] utilised M63 minimal medium as the diluent for an overnight culture of *E. coli* because adherence was promoted under the nutrient-poor conditions.[303] Then, the test substrate was submerged in the diluted culture. In contrast, assays with marine bacterium *V. harveyi* required a high-salt (1–2% w/w) medium, such as Luria marine broth (LMB) or artificial seawater.[291,293–295,304] Regarding the length of incubation in the diluted culture of *E. coli*, multiple studies required incubation of the substrate for 24 h before rinsing it and detaching the bacteria.[301,302,305] Detachment was achieved by vortexing 1–2 min and/or sonication,[300,305–307] and agar plating, specifically by the drop plate method, was performed to determine the colony forming units (CFU) *per* cm^2 of the substrate.[300,305] For the drop plate method (**Figure 5.2**), aliquots (10 µL) of each dilution were dispensed in small, separate drops on agar plates and then were allowed to absorb into the agar, followed by incubation of the plate and colony-counting within the drops. The countable dilution yielded 3–30 colonies *per* 10 µL drop.[308] All of these details were incorporated for establishment of the initial testing protocol, which then required experimental development and validation.
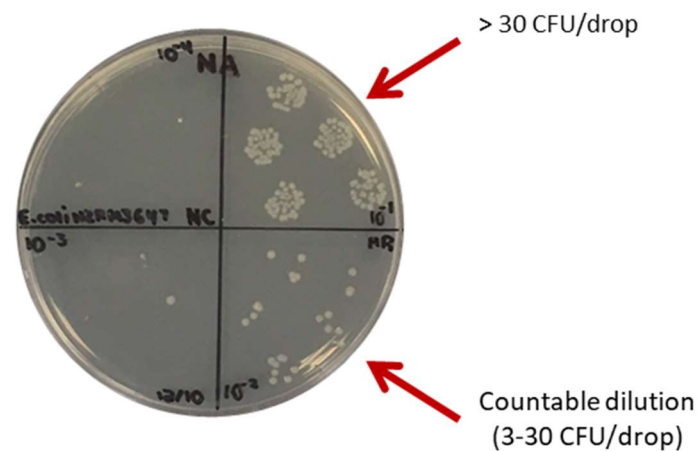
Figure 5.2. Enumeration of *E. coli* NZRM 3647 cells *via* the drop plate method.

5.2 Method Development with *E. coli* NZRM 3647

In summary, the proposed bacterial adherence assay (**Figure 5.3**), which is a composite of the processes and conditions in multiple literature procedures,[300–302,305–308] would begin with dilution to OD_{600} 0.05 of an overnight (16 h) culture of *E. coli* NZRM 3647 in M63 minimal medium. As in Chapter 4 (**Section 4.3**), the coated, plastic test square (23 mm × 23 mm or 25 mm × 25 mm) would be prepared by applying a single layer of the test coating *via* the draw-down technique to both sides of a vinyl chloride/acetate copolymer, allowing each side to cure overnight, and cutting out a square to the desired dimensions. This would be followed by submersion of the prepared square in the diluted culture and static incubation for 24 h at 37 °C to allow the bacteria time to adhere. Then, the square would be taken from the culture, washed with saline (*i.e.* 0.85% w/w aq NaCl) to remove the planktonic cells, and transferred to a saline solution containing 0.05% v/v Tween 20. Tween 20 is a nonionic surfactant that is included to prevent bacterial agglomeration.[309] The solution would be vortexed and sonicated to detach the bacteria adhered to the square, and serial dilutions of the detachment solution, followed by the drop plate method, would be completed to determine the CFU/cm^2 on the test square. For a coating to be deemed bactericidal (*i.e.* kills bacteria), a ≥ 3 Log_{10} reduction in the CFU/cm^2 is required.[310]
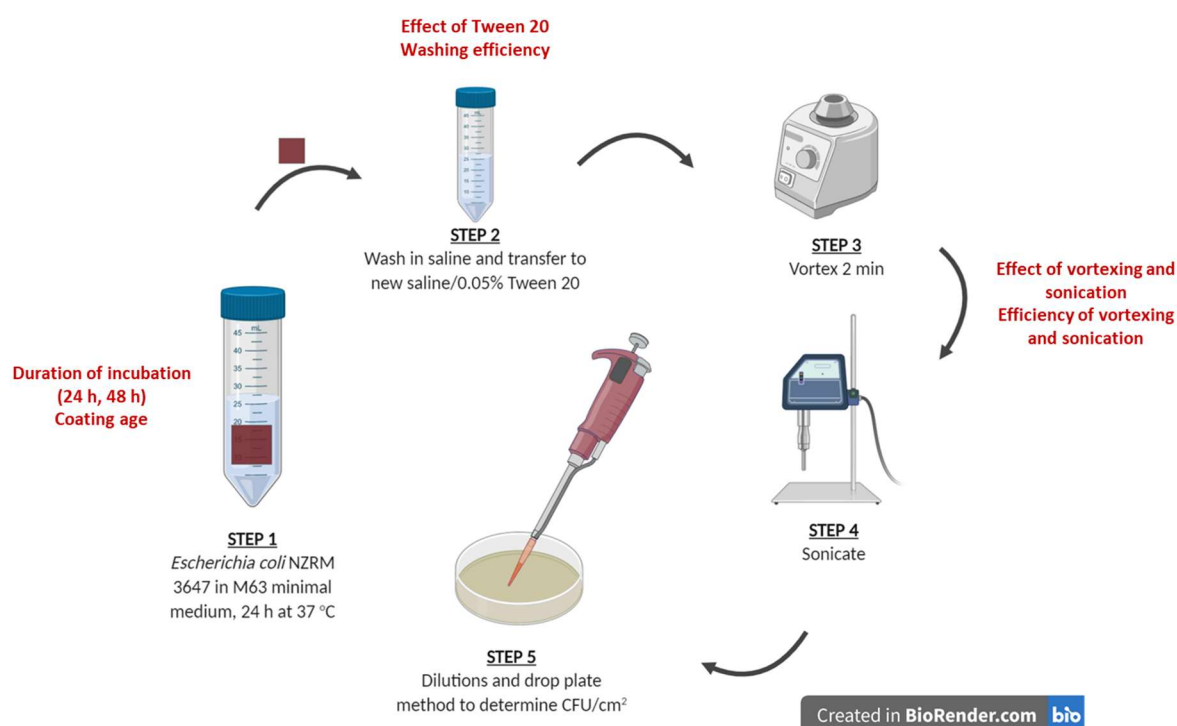
Figure 5.3. Steps of the bacterial adherence assay and, in red, areas to be addressed for method development (created with Biorender.com).

The goal of method development was to optimise conditions for the attachment and recovery of viable, adherent cells so that bactericidal effects would be detectable. In order to develop and validate this method, the following aspects of the protocol, shown in red in **Figure 5.3**, were evaluated:

1) The duration of incubation of the test square in the bacterial culture (24 h *vs* 48 h),
2) The effect of coating age on bacterial adherence,
3) The effect of Tween 20 on bacteria,
4) The efficiency of the saline wash in removing planktonic bacteria,
5) The combined effect of vortexing and sonication on bacteria, and
6) The combined efficiency of vortexing and sonication (± Tween 20) for the detachment of bacteria.

5.2.1 Duration of Incubation

Although multiple studies set the incubation period of the test sample in the diluted *E. coli* culture at 24 h, most of those studies also allowed for the extension of this time period to ≥ 48 h.[301,302,305] Therefore, in order to assess the difference in the numbers of viable, adherent cells after 24 h *vs* 48 h, an experiment was conducted in which one uncoated square was incubated for 24 h and the other for 48 h (**Figure 5.4a**). Uncoated squares were used because they had the least variability between prepared samples. Following incubation, both squares were rinsed, and the adherent cells were enumerated.
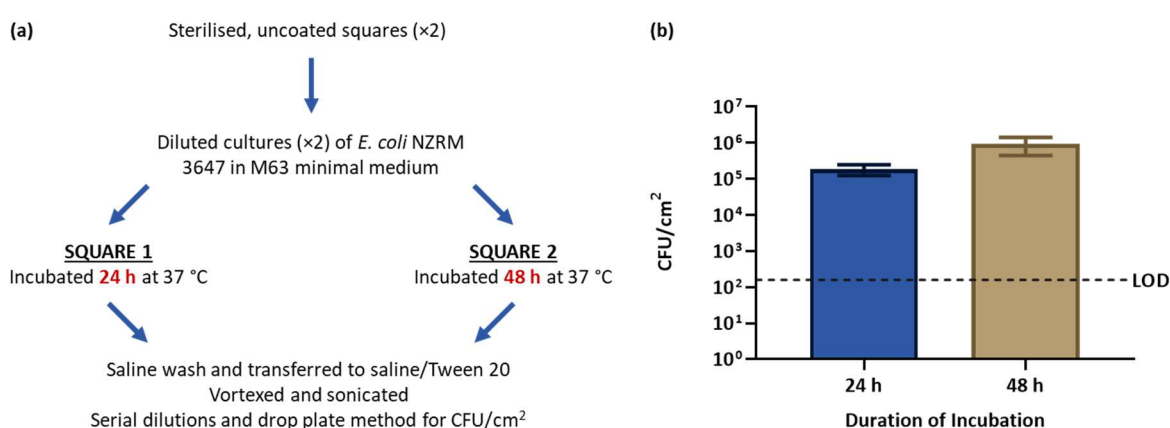
Figure 5.4. Testing the effect of the duration of incubation on bacterial adherence (24 h *vs* 48 h): **(a)** procedure and **(b)** results of CFU/cm^2 on uncoated squares obtained after incubation for 24 h and 48 h. The bars represent the mean of five technical replicates (tr), and the error bars show the SD. The limit of detection (LOD) is 160 CFU/cm^2.

As shown in **Figure 5.4b**, incubation of the uncoated square for 48 h yielded an approximately fivefold increase in the number of adherent cells, compared to incubation for 24 h. Because the increase was < 1 Log_{10} over an additional 24 h, it was decided that the total incubation time should remain at 24 h. The shorter assay was more practical, since the turnaround time was quicker, and lengthening the incubation time did not seem to drastically increase the number of attached cells. Growth curves of *E. coli* NZRM 3647 in nutrient broth and M63 minimal medium revealed that the bacteria were in the stationary phase after 14 h and 20 h, respectively (Appendix, **Figure 8.52**).

5.2.2 Coating Age

It was acknowledged that variability in the coating age could confound the assay results, given that fresh coatings are likely to be more antimicrobial than older coatings. Fresh coatings contain potential antimicrobial ingredients that wash out, evaporate, or wear away over time.[207] To determine if the coating age was a parameter in the adherence assay that should be kept constant, fresh and two-week-old coatings were tested and the results compared. The coatings assessed were the same ones from Chapter 3: the marine paint (**Section 3.2.2**; Altex Yacht and Boat Paint, Aurora Red, Ablative Antifouling No. 5; 40–50% Cu_2O), the commercial, two-pot epoxy resin (**Section 3.3**; Epikote™ 235 and Ancamine® 2459), and the commercial acrylic paint (**Section 3.2.1**; LR200, Resene Paints Ltd.). Uncoated squares served as controls. The epoxy resin was included because it was used to prepare the SiO_2/epx-type coatings in Chapter 4 (**Section 4.3**), and the marine paint was included because it was the commercial antifouling standard to which the coatings produced in this work were compared. Following the usual procedure (**Figure 5.5a**), the experiment was repeated three times, and the viable, adherent cells on the fresh and two-week-old test squares were enumerated.

The results revealed no statistically significant differences between the average numbers of viable, adherent bacteria *per* cm^2 on the fresh versus the two-week-old coatings (**Figure 5.5b**), even when the data were normalised by the results for the uncoated squares (**Figure 5.5c**). However, for all samples, a trend was observable in which the numbers of CFUs on the two-week-old coatings were 1 Log_{10} higher than on the fresh coatings. This was consistent with the expectation that the fresh coatings would be more antimicrobial and affirmed that the coating age could be a confounding factor if not controlled. Therefore, it was decided that bacterial adherence to the coatings should be measured immediately after overnight curing, since the shorter coating preparation time was preferable. However, it should be kept in mind that the antifouling activity of such coatings may decrease over time.
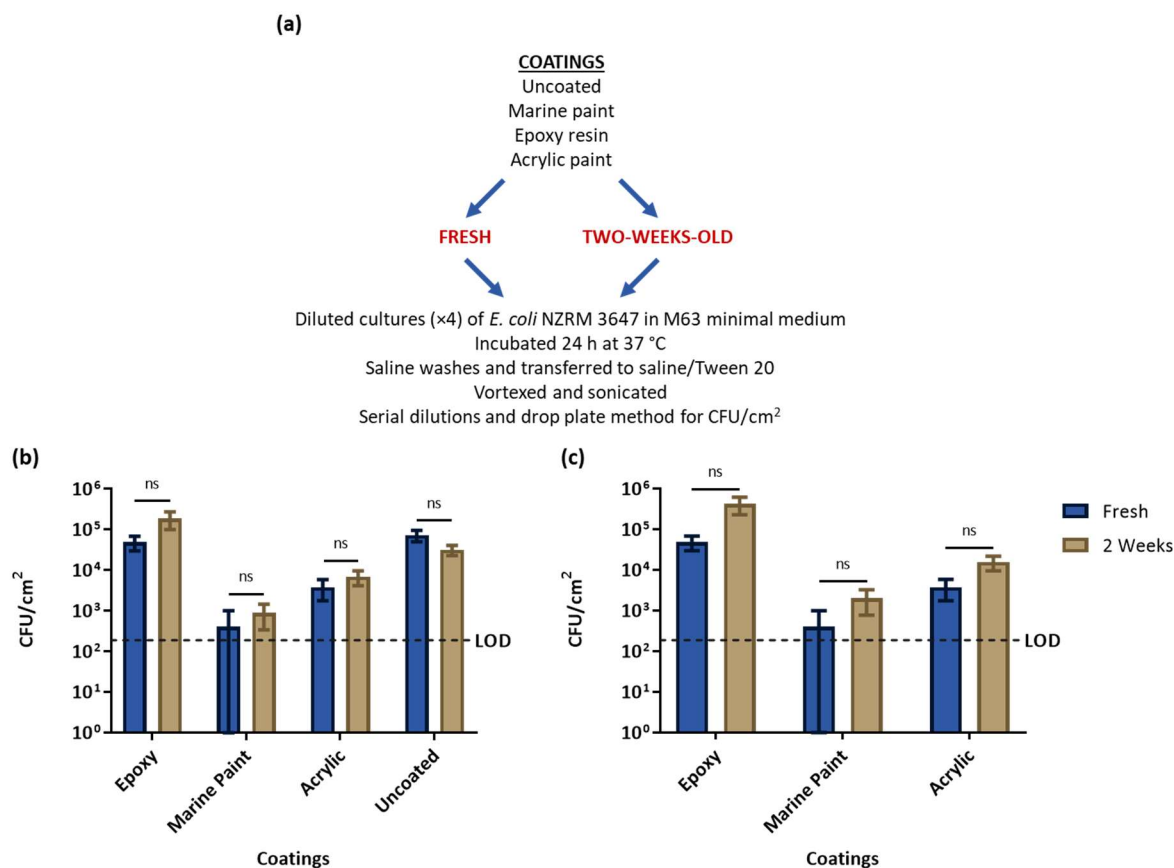
Figure 5.5. Testing the effect of coating age on bacterial adherence: (a) procedure and **(b)/(c)** results of CFU/cm^2 on fresh and two-week-old test squares coated with the epoxy resin, marine paint, and acrylic paint. Uncoated squares served as controls. **(b)** Un-normalised data and **(c)** data normalised by the "Uncoated" results. The bars represent the mean of three biological replicates (br), and the error bars show the SD. To determine if the means from the "Fresh" and "2 Weeks" data sets were significantly different from each other, a two-sample, two-tail Student's t-test was conducted, and the difference was considered to be significant when the p-value was < 0.05 (ns = not significant; LOD = 189 CFU/cm^2).

5.2.3 Effect of Tween 20

The addition of nonionic detergent Tween 20 (T20) to the detachment solution was recommended as standard practice to disaggregate the bacteria prior to agar plating,[311] thus ensuring that each bacterial colony represented one CFU. So, the inclusion of Tween 20 was assessed to confirm that it would not negatively affect the assay results. The concern was that bacteria already stressed by Tween 20 would be killed by subsequent detachment methods, since the use of Tween 20 at or above a concentration of 0.1% v/v has been shown to impair bacterial growth.[309] Consequently, it was

recommended that Tween 20 be included at 0.05% v/v,[311] and an experiment was performed to determine the effect of Tween 20 in the detachment solution on the assay results. This was done by incubating two uncoated squares in diluted cultures of *E. coli*, rinsing, and transferring them to detachment solutions with or without 0.05% v/v Tween 20, followed by vortexing and agar plating (**Figure 5.6a**). The results showed no difference in the number of viable bacteria attached to the squares, whether or not Tween 20 was used in the detachment solution (**Figure 5.6b**). Therefore, the inclusion of 0.05% v/v Tween 20 did not negatively impact the assay results, and its addition to the detachment solutions continued. Although, it acknowledged that, when testing antimicrobial surfaces, it would be important to confirm that Tween 20 did not amplify the antibacterial effect, as the cells exposed to the coating would likely be more fragile and vulnerable to lysis.
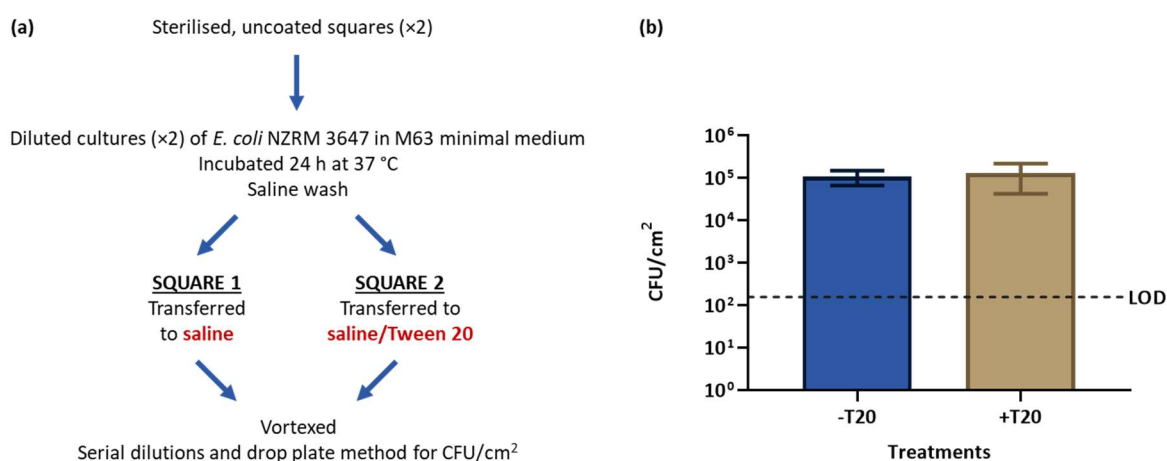
Figure 5.6. Testing the effect of Tween 20 in the bacterial adherence assay: (a) procedure and **(b)** results of CFU/cm^2 on uncoated squares obtained after detachment in solutions with and without 0.05% v/v Tween 20. The bars represent the mean (tr = 5) ± SD (LOD = 160 CFU/cm^2).

5.2.4 Washing Efficiency

In the assay's proposed protocol, the test squares are washed with saline to remove planktonic *E. coli*, leaving only the adherent cells. Thus, an experiment was performed to assess the washing efficiency *via* the enumeration of cells in successive saline washes of an uncoated sample, comparing the counts to those obtained after vortexing and sonicating the sample for the detachment of adherent cells. It was thought that the counts from the washes would be from planktonic cells carried over from the 24 h culture in M63 minimal medium and from some cells detaching from the surface due to the shear forces experienced by the sample upon delivery and removal from each saline solution. It was also thought that, if the samples were subjected to multiple rinses before bacterial detachment, higher

CFUs in the detachment solution than in the previous wash would confirm that bacteria were remaining attached to the substrate throughout the short washes. The uncoated sample was incubated in a diluted culture of *E. coli* in M63 minimal medium and, after 24 h, transferred to the first saline wash (**Figure 5.7a**). It was transferred to a second saline wash and then to the saline/Tween 20 solution for the detachment of cells *via* vortexing and sonication.
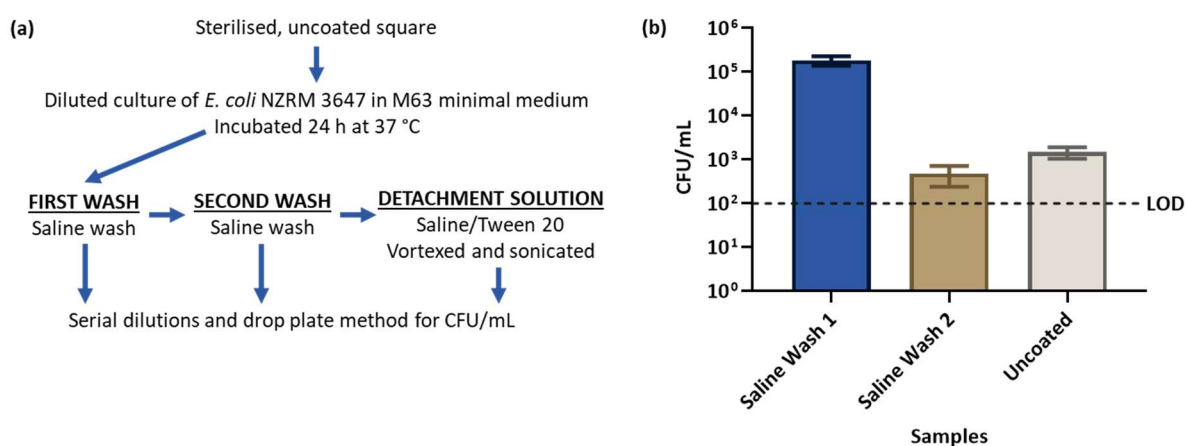
Figure 5.7. Enumeration of bacterial counts in the saline washes: (a) procedure and **(b)** results of CFU/mL in saline washes and the detachment solution containing an uncoated square. The bars represent the mean (tr = 5) ± SD (LOD = 100 CFU/mL).

The cell counts in the detachment solution containing the uncoated sample were an order of magnitude higher than the counts in the second wash (**Figure 5.7b**). "Saline Wash 2" contained only ~500 CFU/mL, which was 2–3 Log_{10} fewer cells than "Saline Wash 1". This meant that few cells were carried over from the first wash or detached from the sample in the second wash, and it was decided that one wash in the assay was sufficient. Cells remained adhered to the substrate through multiple, short saline rinses until detachment by vortexing and sonication, which confirmed that the assay was working as intended. Repetition of the experiment with an SiO_2/epx-type coating, which has very different physico-chemical properties, yielded similar results (Appendix, **Figure 8.53**). A certain background count of CFUs from the carryover of planktonic cells was expected, leading to some variability in the results. However, to look for a bactericidal effect, the coating containing the biocide (*i.e.* Cu(II)) was to be compared to the control (*i.e.* coating without Cu(II)) and the industry-standard marine paint. A successful coating would need a ≥ 3 Log_{10} reduction in the CFU/cm^2, compared to the control, or perform similarly to the marine paint. Therefore, it was reasoned that such large differences would still be apparent, despite the variability of the assay.

5.2.5 Effect of Vortexing and Sonication

Since vortexing (V) plus sonication (S) was proposed as a detachment method in the adherence assay, an experiment was completed to test its effect on planktonic *E. coli*. This was done to confirm that the combined technique of vortexing for 2 min and sonicating for 8 s did not negatively affect cell viability and, thus, skew bacterial counts. The sonication conditions were derived from a study by Merritt *et al.*[306] (8 s, 40% amplitude). In the present experiment, a diluted culture of *E. coli* was incubated 24 h, an aliquot was removed, and then the culture was vortexed and sonicated (**Figure 5.8a**). The culture and the aliquot taken before vortexing and sonication were serially diluted and plated. The means (CFU/mL) from the two data sets were within one standard deviation of each other (**Figure 5.8b**), and it was concluded that the combined effect of vortexing and sonication on the viability of planktonic cells in the 24 h culture was likely neutral. Like Tween 20, however, it was recognised that exposure to an antimicrobial surface could predispose the bacterial cells to injury from vortexing and sonication.
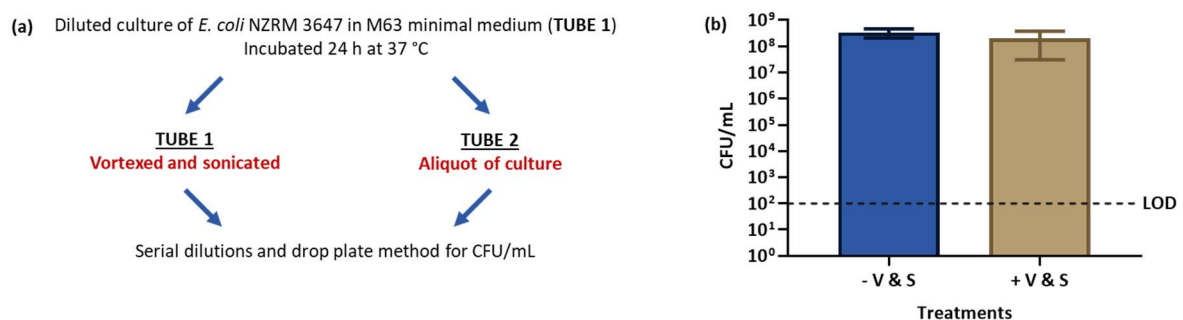
Figure 5.8. **Testing the combined effect of vortexing and sonication on planktonic bacteria: (a)** procedure and **(b)** results of CFU/mL in a vortexed and sonicated culture ("+V & S") and a culture that was neither vortexed nor sonicated ("-V & S"). The bars represent the mean (tr = 10) ± SD (LOD = 100 CFU/mL).

5.2.6 Efficiency of Vortexing and Sonication (± Tween 20)

In addition to the effect of vortexing plus sonication on planktonic bacteria, the efficiency of the technique as a detachment method was considered. The detachment methods were evaluated by comparing the numbers of viable, adherent bacteria recovered after vortexing and vortexing plus sonication to the control, which was neither vortexed nor sonicated. Three uncoated squares were incubated in dilute cultures of *E. coli*, washed, and transferred to solutions of saline/Tween 20

(**Figure 5.9a**). The first square received no further treatment ("Control": "-V & S"), but the second square was vortexed ("Vortex 1×": "+V 1×"), removed, transferred to a fresh saline/Tween 20 solution, and vortexed again ("Vortex 2×": "+V 2×"). The second round of vortexing was done to ascertain if vortexing once was sufficient to remove the vast majority of adherent cells. The third square was both vortexed and sonicated ("Vortex & Sonicate": "+V & S"). The "Control", "Vortex 1×", "Vortex 2×", and "Vortex & Sonicate" solutions were serially diluted and plated to count colonies.
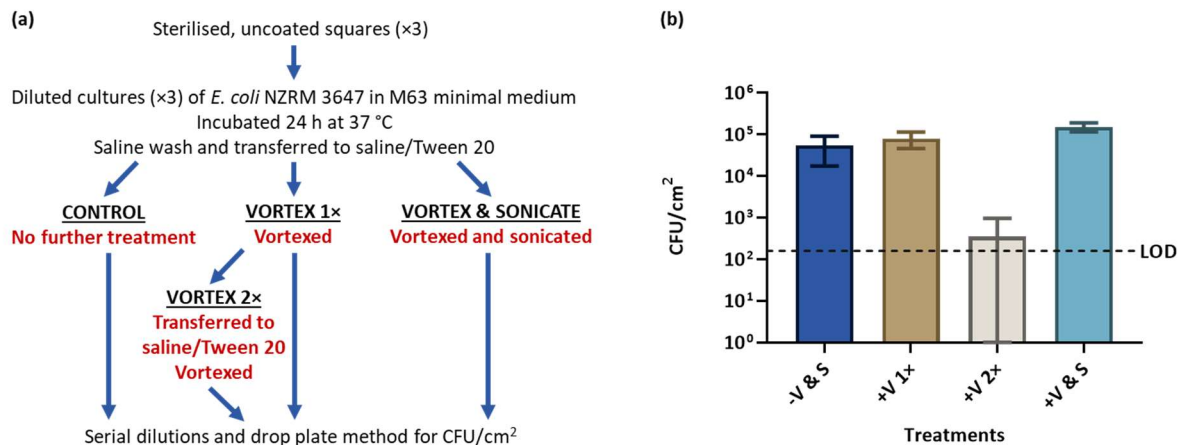
Figure 5.9. Testing the efficiency of vortexing and sonication with Tween 20 in the removal of adherent bacteria from uncoated squares: (a) procedure and **(b)** results of CFU/cm^2 on uncoated squares obtained after vortexing (once, "+V 1×"; twice, "+V 2×"), vortexing and sonicating ("+V & S"), and neither vortexing nor sonicating ("-V & S"). The bars represent the mean (tr = 5) ± SD (LOD = 160 CFU/cm^2).

The number of CFUs in the "Vortex 2×" solution was at the assay's limit of detection, meaning that the second round of vortexing yielded relatively few additional counts. Vortexing once plus sonication yielded higher average counts than vortexing alone, which yielded higher average counts than the control (**Figure 5.9b**). However, the experiment needed to be repeated with biological replicates to identify any truly significant differences. Regarding the control, a considerable number of bacteria were detached just upon transference of the square to saline/Tween 20. Consequently, a role for Tween 20 in detachment was postulated, and an experiment was conducted to elucidate the true effects of vortexing plus sonication and Tween 20.

An experiment was completed to determine if differences in bacterial counts after vortexing plus sonication with or without Tween 20 were statistically significant. This was done by incubating three uncoated squares in diluted cultures of *E. coli* in M63 minimal medium, and, after incubation, washing

them with saline (**Figure 5.10a**). Then, the first and second squares were transferred to saline/Tween 20 solutions, and the first square was vortexed and sonicated. The third square was delivered to a fresh saline solution. All square-containing solutions were serially diluted, and the dilutions were plated.
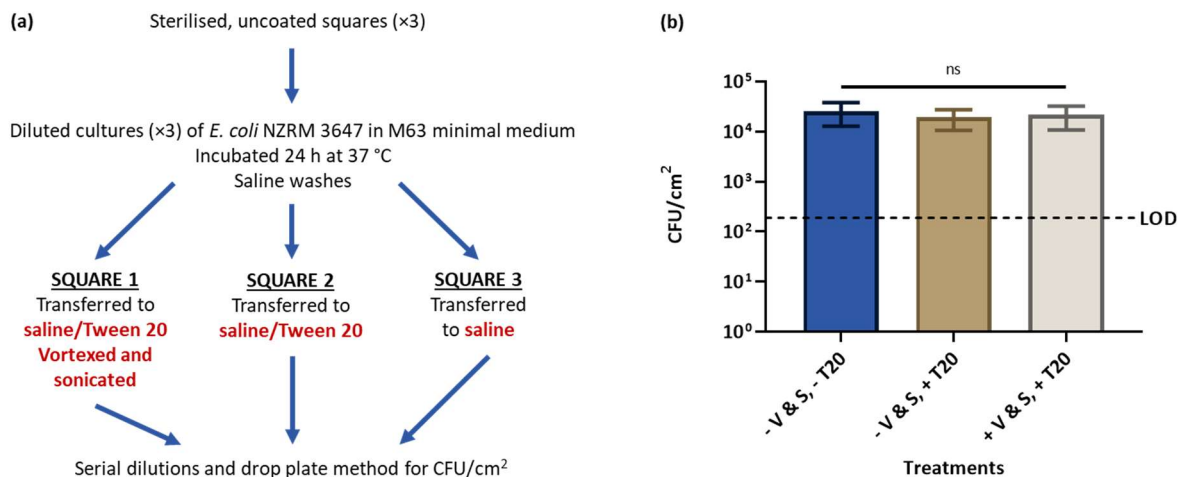
Figure 5.10. Testing the efficiency of vortexing and sonication with or without Tween 20 in the removal of adherent bacteria from uncoated squares: (a) procedure and **(b)** results of CFU/cm^2 on uncoated squares obtained under the conditions of ± vortexing and sonication ("V & S") and ± Tween 20 ("T20"). The bars represent the mean (br = 6 for "-V & S, +T20", br = 3 for all others) ± SD. To determine if the means from the data sets were significantly different from each other, a one-way analysis of variance (ANOVA) with Tukey's *post hoc* test was conducted, and the difference was considered to be significant when the *p*-value was < 0.05 (ns = not significant; LOD = 189 CFU/cm^2).

The differences in the viable counts between the three solutions were not statistically significant (**Figure 5.10b**). This meant that vortexing and sonicating an uncoated square in saline/Tween 20 yielded the same counts as from simply transferring the square to saline or saline/Tween 20, which was surprising. The experimental design was based on the premise that *E. coli* would attach to the squares within 24 h and require removal *via* vortexing and, possibly, sonication, and, as seen in a previous experiment (**Figure 5.7b**), cells remained attached to an uncoated sample through multiple washes until their removal by vortexing and sonication. It was hypothesised that *E. coli* does not strongly adhere to the vinyl chloride/acetate copolymer and that the cells easily detach from the surface. The cells could have detached upon delivery of the uncoated sample to the detachment solution, during the prolonged time period between delivery and dilutions (0.5–1 h), or from gentle inversion of the tube for the homogeneous distribution of cells before serial dilutions. This experiment

was repeated, in part, with a coated sample to determine if a substrate with different physico-chemical properties would require vortexing and sonication for cellular detachment.

To test if vortexing plus sonication and Tween 20 aid the detachment of cells from a coated substrate, the same experiment (**Figure 5.10**) was repeated for samples coated with SiO_2/epx (Experimental, **Section 6.4.2**). The rough SiO_2/epx coating was chosen because of its vastly different physico-chemical properties, compared to the smooth, uncoated vinyl chloride/acetate copolymer. Two SiO_2/epx-coated squares were incubated in diluted *E. coli* cultures in M63 minimal medium, and, after 24 h, the squares were rinsed with saline (**Figure 5.11a**). The first square was transferred to a saline/Tween 20 solution, vortexed, and sonicated, and the second square was delivered to fresh saline and gently inverted for the homogeneous distribution of cells. The cell counts in both solutions were enumerated.
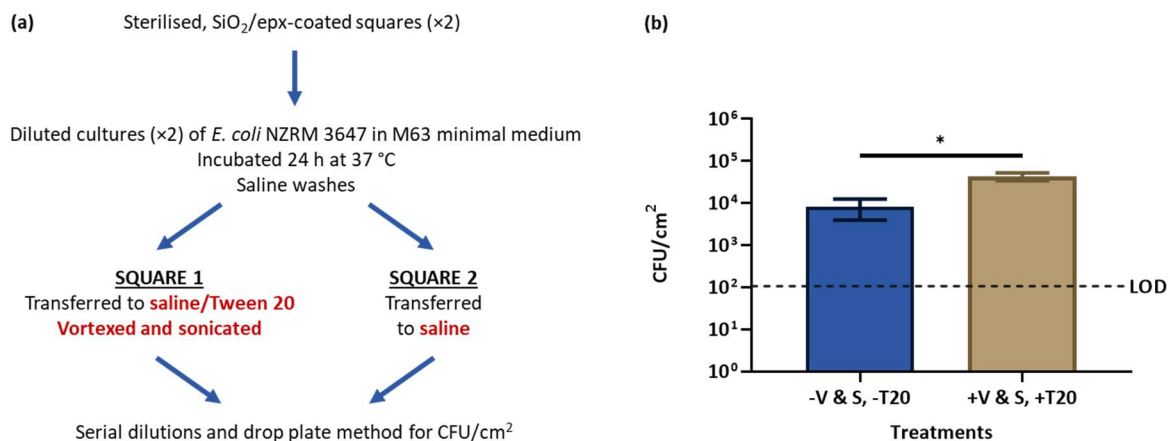
Figure 5.11. Testing the efficiency of vortexing and sonication with or without Tween 20 in the removal of adherent bacteria from SiO_2/epx-coated squares: (a) procedure and **(b)** results of CFU/cm^2 on SiO_2/epx-coated squares obtained under the conditions of ± vortexing and sonication ("V & S") and ± Tween 20 ("T20"). The bars represent the mean (br = 3) ± SD. To determine if the means from the data sets were significantly different from each other, a two-sample, two-tail Student's *t*-test was conducted, and the difference was considered to be significant when the *p*-value was < 0.05 (* *p* < 0.05; LOD = 106 CFU/cm^2).

As shown in **Figure 5.11b**, the average CFUs in the solution containing the first square ("+V & S, +T20") were an order of magnitude higher than the average CFUs in the solution containing the second square ("-V & S, -T20"), and the difference in counts between the two was statistically significant ($p < 0.05$). This indicated that, unlike the uncoated sample, vortexing and sonicating the saline/Tween 20 solution

aided the detachment of cells from the SiO$_2$/epx-coated samples. It is unknown if this was due to more and/or stronger interactions at the molecular level between the surface and bacteria or if the rough surface topography simply protected cells from removal by shear forces. In either case, it was decided that the use of vortexing plus sonication as a detachment method and Tween 20 in the detachment solution should be continued.

5.2.7 Conclusions

Multiple aspects of the designed procedure were probed for development and validation (**Figure 5.3**). It was decided that 24 h was an adequate incubation period and that the coatings should be tested directly after application to the substrate. Yet, further testing would be necessary to determine the antifouling efficacy of each coating over time, as it is likely to decrease. Assessment of washing efficiency revealed that one sample wash was adequate but that a certain background count from planktonic cells was expected. However, it was thought that they would make a relatively insignificant contribution to the total, depending on the order of magnitude of the result. In this experiment, it was also demonstrated that cells adhered to the substrate and remained attached during multiple rinses, verifying that, to a certain extent, the assay was working as anticipated. When used in the assay, the effect of Tween 20 was neutral, and the combination of vortexing and sonication did not seem to affect the viability of planktonic cells in the 24 h culture.

It appeared that vortexing and sonication were unnecessary for bacterial detachment from uncoated samples: there was not a statistically significant difference in counts between the uncoated sample that was vortexed and sonicated in saline/Tween 20 and the uncoated sample that was simply transferred to the detachment solution, with or without Tween 20. In order to evaluate adherence to a substrate with different physico-chemical properties, the experiment was repeated with an SiO$_2$/epx-coated sample, comparing samples with and without vortexing plus sonication and Tween 20. The significantly higher counts recovered from the vortexed and sonicated sample in Tween 20 suggested that, unlike for the uncoated substrate, the detachment methods were necessary for the removal of adherent cells from the rough SiO$_2$/epx-coated substrate. With the completion of the method development, the refined assay protocol was used to test bacterial attachment to the SiO$_2$/epx-type coatings prepared in Chapter 4 (**Section 4.3**).

5.3 ADHERENCE OF *E. COLI* NZRM 3647 TO SiO$_2$/EPX-TYPE COATINGS

5.3.1 Adherence Assay

The SiO$_2$/epx-coated squares (**Figure 5.12**, pictured right) were prepared for the bacterial adherence assay as described in Chapter 4 (**Section 4.3**) and tested immediately after preparation. These coatings included Batch 4 CnGmSiO$_2$/epx (free ligand), Batch 4 CnGmSiO$_2$ + Cu(II)/epx (post-loaded), Batch 2 Cu(II)-CnGmSiO$_2$/epx (pre-loaded), and unfunctionalised SiO$_2$/epx. The adherence results were compared to the industry-standard marine paint (Altex Yacht and Boat Paint, Aurora Red, Ablative Antifouling No. 5; 40–50% Cu$_2$O) because such paints are the current standard in antifouling technology. For the functionalised silica coatings to be viable alternatives and worthy of pursuit, they would need to have similar activity to or better activity than the marine paint, or they would need a ≥ 3 Log$_{10}$ reduction in the CFU/cm^2 on the biocide-containing coatings (*i.e.* CnGmSiO$_2$ + Cu(II)/epx, Cu(II)-CnGmSiO$_2$/epx), compared to the controls (*i.e.* epoxy, SiO$_2$/epx, CnGmSiO$_2$/epx). The attachment of bacteria to the uncoated substrate (vinyl chloride/acetate copolymer) and epoxy resin used to glue the silica to the plastic (Epikote™ 235 and Ancamine® 2459; Chapter 3, **Section 3.3**) was also tested. Each test square was incubated for 24 h at 37 °C in an overnight culture (16 h) of *E. coli* diluted with M63 minimal medium to OD$_{600}$ 0.05. After 24 h, the squares were rinsed with saline and then transferred to saline/Tween 20 solutions in which they were vortexed and sonicated. The detachment solutions were serially diluted, and the dilutions were plated to count colonies. The experiment was independently repeated three times for each coating.

Interestingly, Cu(II)-CnGmSiO$_2$/epx had the greatest number of viable, adherent bacteria, and this result was statistically different from the adherence results for all of the other coatings but SiO$_2$/epx (**Figure 5.12**). The number of bacteria attached to Cu(II)-CnGmSiO$_2$/epx was approximately six-fold higher than the number for CnGmSiO$_2$/epx and CnGmSiO$_2$ + Cu(II)/epx and approximately twice the number for SiO$_2$/epx. This was unexpected, given that Cu(II)-CnGmSiO$_2$ had the highest % w/w copper (2.6 ± 0.3; **Table 5.1**) out of all of the SiO$_2$/epx-type coatings. The counts were not significantly different between the following samples: CnGmSiO$_2$/epx, CnGmSiO$_2$ + Cu(II)/epx, SiO$_2$/epx, epoxy resin, and uncoated. These results showed that there was no deterrence of bacterial adhesion on any of the functionalised silica coatings, including the Cu(II) biocide-containing CnGmSiO$_2$ + Cu(II)/epx and Cu(II)-CnGmSiO$_2$/epx coatings. For the marine paint, the CFU/cm^2 (± SD) was at the LOD of the assay, and none of the other coatings had comparable activity.
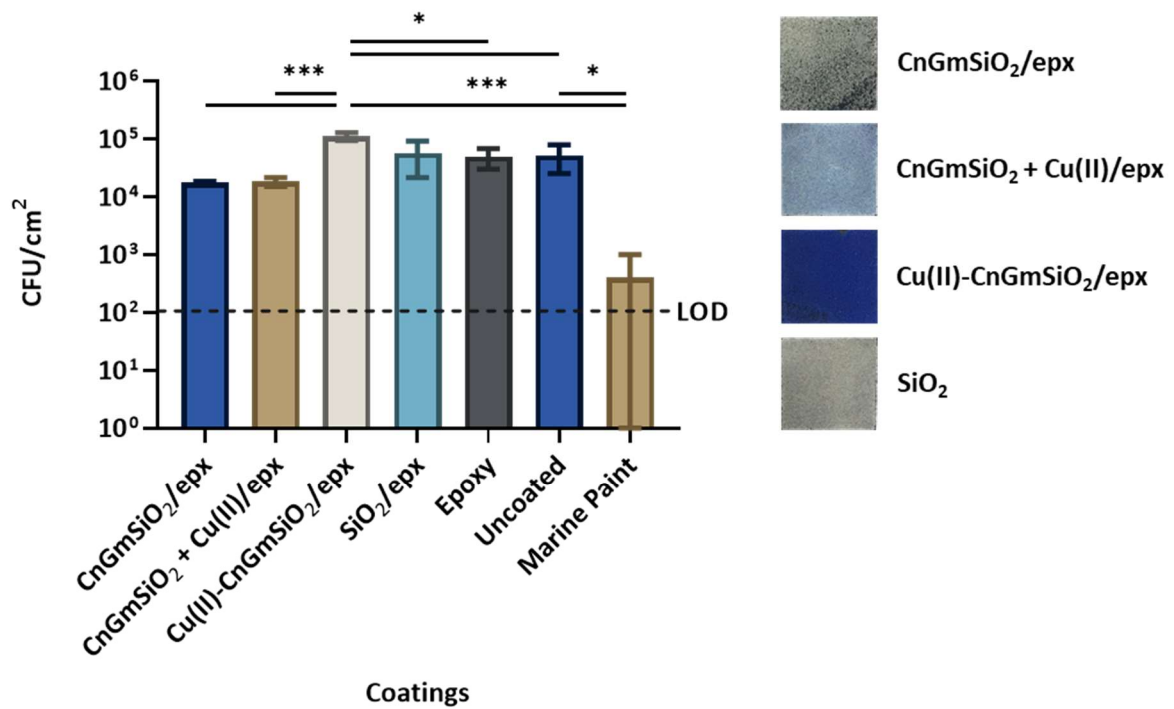
Figure 5.12. Results of _E. coli_ NZRM 3647 CFU/cm^2 on the SiO$_2$/epx-type coatings (pictured right), as well as on uncoated squares, the epoxy resin, and the marine paint. The bars represent the mean (br = 6 for "Uncoated", br = 3 for all others) ± SD. To determine if the means from the data sets were significantly different from each other, a one-way ANOVA with Tukey's _post hoc_ test was conducted, and the difference was considered to be significant when the _p_-value was < 0.05 (*_p_ < 0.05, ** _p_ < 0.01, *** _p_ < 0.001; LOD = 106 CFU/cm^2).

Table 5.1. The OD$_{600}$ of the *E. coli* cultures after 24 h incubation and the copper content of the test squares, as well as the copper-leachate concentrations after 24 h.

Coating	OD$_{600}$ (24 h, M63)[a]	% w/w Cu[b]	ppm (µM) Leached Cu[a]
CnGmSiO$_2$/epx	0.119 ± 0.007	0	-
CnGmSiO$_2$ + Cu(II)/epx	**0.057 ± 0.003**	**1.0 ± 0.3[a]**	**2.3 ± 0.1 (36 ± 2)[c], 12 ± 2 (190 ± 30)[d]**
Cu(II)-CnGmSiO$_2$/epx	**0.072 ± 0.003**	**2.6 ± 0.3[a]**	**3.6 ± 0.3 (57 ± 5)[c], 6.0 ± 0.4 (94 ± 6)[d]**
SiO$_2$/epx	0.116 ± 0.004	0	-
Epoxy	0.151 ± 0.008	-	-
Uncoated	0.148 ± 0.009	-	-
Marine Paint	**0.101 ± 0.006**	**40–50**	**3.3 ± 0.5 (52 ± 8)[c], 7.3 ± 0.4 (115 ± 6)[d]**

[a] Mean ± SD. Experiment repeated 3×.
[b] % w/w Cu in the (un)functionalised silica component or in the marine paint.
[c] M63 minimal medium without *E. coli* NZRM 3647.
[d] M63 minimal medium with *E. coli* NZRM 3647.

In order to investigate possible factors impacting the adherence results, the amount of copper leaching from each copper-containing coating into the medium during the 24 h incubation was measured – both in the presence and absence of *E. coli* (**Table 5.1**). The mechanisms of the contact killing of bacteria on a copper surface are not fully understood, but there is a consensus in the literature that copper ions released from the surface play a role.[115,117,121,312] It is proposed that, following damage to the bacterial cell membrane, the influx of copper ions into the cell causes oxidative damage by ROS and enzyme inhibition, leading to cell death and DNA degradation.[115,117] In culture, copper toxicity is due to the displacement of iron by copper in iron-sulfur cluster dehydratases, which are essential for the branched-chain biosynthesis of amino acids.[206]

Given the direct relationship between bactericidal effects and copper ion concentration, the concentrations of copper leachate from CnGmSiO$_2$ + Cu(II)/epx, Cu(II)-CnGmSiO$_2$/epx, and the marine paint were determined by incubating the test squares in M63 minimal medium statically for 24 h at 37 °C. This experiment was conducted with and without *E. coli* in order to determine if the presence of bacteria affected copper-leaching. After 24 h incubation of the samples with *E. coli*, each culture was filter-sterilised and centrifuged, and the supernatant was isolated for analysis. All solutions were diluted, as needed, with dilute nitric acid for copper quantification by ICP-MS. Although the copper concentrations in the marine paint (40–50% w/w) and Cu(II)-CnGmSiO$_2$ (2.6 ± 0.3% w/w) were vastly different, the concentrations of copper leachate in the absence of *E. coli* were statistically equivalent: 3.3 ± 0.5 ppm (52 ± 8 µM) and 3.6 ± 0.3 ppm (57 ± 5 µM), respectively (**Table 5.1**). The concentration of copper leached from CnGmSiO$_2$ + Cu(II)/epx was slightly lower (2.3 ± 0.1 ppm, 36 ± 2 µM) than the other coatings when bacteria were absent. However, the presence of bacteria resulted in increased

copper-leaching for all samples, and CnGmSiO$_2$ + Cu(II)/epx leached the most copper (12 ± 2 ppm, 190 ± 30 µM), while the marine paint (7.3 ± 0.4 ppm, 115 ± 6 µM) and Cu(II)-CnGmSiO$_2$/epx (6.0 ± 0.4 ppm, 94 ± 6 µM) leached similar, lower amounts.

This increase in copper-leaching in the presence of *E. coli* could be due to the uptake of Cu(II) from the surface by bacteria, since cations are attracted to the negatively charged lipopolysaccharide (LPS) in *E. coli*'s outer membrane.[313,314] Some of the Cu(II) at the surface of CnGmSiO$_2$ + Cu(II)/epx is likely adsorbed, rather than chelated, and, thus, is more easily sequestered from the surface, leading to a higher copper-leachate concentration. Tetraaza macrocycles (*e.g.* cyclen) form incredibly stable Cu(II) complexes with enhanced inertness to demetallation,[76] but it is possible that bacteria have a role in competition with the cyclen-functionalised surfaces (*e.g.* Cu(II)-CnGmSiO$_2$/epx) and the subsequent release of Cu(II). Although, studies have reported the protective effects of copper-chelators, such as EDTA, in the context of the contact killing of bacteria.[115,314] Furthermore, even if the bacteria sequestered Cu(II), those bacteria were removed from solution prior to copper analysis by ICP-MS, and it is unknown if the copper would have been released back into solution before the removal of bacteria. Therefore, the cause of the increased leaching was not easily determined.

Comparison of the copper leachate data to copper toxicity data in the literature revealed that the copper concentrations in this work were high enough to cause injury to *E. coli* cells in culture (**Table 5.2**). For instance, Macomber and Imlay[206] found that *E. coli* W3110 exhibited a growth defect when incubated for 10 h at 37 °C in M9 minimal medium containing glucose as the sole carbon source and Cu(II) concentrations greater than 8 µM (*e.g.* 16 µM, 32 µM). After three days in inorganic carbon buffer (pH 7) at 4 °C, Singh *et al.*[315] observed that Cu(II) concentrations ranging from 9 to 16 µM in culture were sufficient to cause > 84% injury and 63–83% lethality for all *E. coli* strains tested (TX432, E7, H10407, E6). All of the copper leachate concentrations in this study exceeded these thresholds (36–190 µM, **Table 5.1**), and the growth of *E. coli* was inhibited in the presence of copper coatings, as evidenced by the optical densities of the sample-containing cultures after incubation for 24 h at 37 °C in M63 minimal medium. Compared to the CnGmSiO$_2$/epx control, the OD$_{600}$ of the 24 h cultures decreased 52% and 39% when CnGmSiO$_2$ + Cu(II)/epx and Cu(II)-CnGmSiO$_2$/epx, respectively, were present during incubation. And, compared to the uncoated control, the OD$_{600}$ of the 24 h culture decreased 32% when the marine paint was present. The largest decrease in OD$_{600}$ (52% for CnGmSiO$_2$ + Cu(II)/epx) did not correspond to the coating that contained (40–50% w/w for the marine paint) the most copper, but it did correspond to the coating that leached (190 ± 30 µM for CnGmSiO$_2$ + Cu(II)/epx) the most copper in the presence of *E. coli*. This result is in agreement with previous results (Chapter 3, **Section 3.2.3**) in which there was a direct relationship between the degree of growth inhibition and the amount of copper leached from the coated surface.

Table 5.2. Literature data of Cu(II) toxicity in cultures of *E. coli*.

Reference	[Cu(II)] Necessary for Toxicity in Culture	Effect	*E. coli* Strain	Conditions
Macomber and Imlay[206]	> 8 μM	growth defect	W3110	M9 minimal medium (glucose); 37 °C; 10 h
Grey and Steck[316]	100–500 μM	removal of all culturable cells (90% lethality at 500 μM)	ES80	saline; 25 °C; 10 days
Singh *et al.*[315]	9–16 μM	> 84% injury (63–83% lethality)	TX432, E7, H10407, E6	inorganic carbon buffer (pH 7); 4 °C; 3 days
Santo *et al.*[312]	600 mM	complete killing	W3110	$CuCl_2$ solutions (aq); 23 °C; 1 min

Regardless of the sample, the optical densities of all the cultures measured after 24 h incubation were unusually low, being at most 0.151 for the culture containing the epoxy-coated substrate (**Table 5.1**). The growth curve of *E. coli* NZRM 3647 in M63 minimal medium plateaued in the stationary phase by 20 h at OD_{600} ~1.5 (Appendix, **Figure 8.52**) – nearly ten-times the highest OD_{600} in the assay. The two differences between the incubation conditions for the assay and growth curve were that, for the assay, the cultures were incubated under static conditions with test squares, while, for the growth curve, the cultures were incubated with periodic shaking but without test squares. Therefore, an experiment was completed in which cultures of *E. coli* NZRM 3647 in M63 minimal medium were incubated for 24 h at 37 °C, with and without shaking and with and without an uncoated test square (Experimental, **Figure 6.13**). The results clearly showed that the low optical densities in the assay were the consequence of incubation under static conditions (**Table 5.3**). This was likely due to poor aeration and/or the inhomogeneous distribution of nutrients in the culture, and it was also likely that the cells were not remaining suspended in culture, impacting the adherence results. Therefore, it was decided that, in future experiments, the cultures should be incubated with shaking, despite the multiple examples in the literature of antifouling assays performed under static conditions.[14,282,295–298]

Table 5.3. OD_{600} of cultures of *E. coli* NZRM 3647 in M63 minimal medium after incubation for 24 h at 37 °C, ± uncoated test squares and ± shaking.

Square (±)	Shaking (±)	OD_{600}
−	+	0.958
+	+	0.962
−	−	0.131
+	−	0.139

The copper leachate data for the marine paint were compared to a similar paint with a lower copper content in a study by Lindgren *et al.*[317] The reference paint used in the present study is a commercial marine antifouling paint composed of 40–50% w/w cuprous oxide in a rosin-based coating. After 24 h in M63 minimal medium, the amount of copper that leached from the marine paint in the presence of *E. coli* was 11 µg/cm^2 (**Table 5.4**). Lindgren *et al.*[317] prepared and tested the antifouling ability of a similar rosin-based paint, which was 8.5% w/w cuprous oxide and leached 3.04 µg/cm^2 copper into the sea after 24 h. Although the copper content in this paint was much lower than the commercial marine paint, they found that biofouling was still deterred, suggesting that antifouling performance could still be maintained with less copper and lower copper leachate concentrations. In the present work, Cu(II)-CnGmSiO$_2$ and CnGmSiO$_2$ + Cu(II) contained < 3% w/w copper and leached

2–10 µg Cu(II)/cm^2 when incorporated in a coating, but the adherence of *E. coli* was not deterred on these substrates as it was on the marine paint.

In the literature, surfaces functionalised with Cu(II)-ligand complexes still had antimicrobial activity with surface and leached copper concentrations even lower than or equal to Cu(II)-CnGmSiO$_2$/epx and CnGmSiO$_2$ + Cu(II)/epx (**Table 5.4**). For example, He *et al.*[318] prepared a surface containing ~2.75% w/w copper by grafting a Cu(II)-polydopamine (PDA) complex onto titanium, and, after 24 h immersed in phosphate-buffered saline, the concentration of Cu(II) released from the coating was 0.15–0.2 ppm. Antimicrobial activity was assessed by the enumeration of CFUs after incubation of the sample for 24 h in a culture of *E. coli*, and incubation with the modified titanium surface was lethal for ~82.5% of the bacteria in the culture. In the present work, the % w/w copper in Cu(II)-CnGmSiO$_2$ (2.6%) was almost equal to the PDA-modified titanium surface, which leached less Cu(II) (0.15–0.2 *vs* 3.6–6.0 ppm for Cu(II)-CnGmSiO$_2$/epx). The % w/w copper in CnGmSiO$_2$ + Cu(II) (1.0%) was relatively lower, but CnGmSiO$_2$ + Cu(II)/epx also leached more Cu(II) (2.3–12 ppm) than the PDA-modified surface. Although the Cu(II) released by the silica coatings negatively affected bacterial growth in liquid culture, *E. coli* surface adherence was enhanced on Cu(II)-CnGmSiO$_2$/epx and unaffected on CnGmSiO$_2$ + Cu(II)/epx. Therefore, bactericidal activity against planktonic bacteria in liquid culture due to the leaching of copper ions from a surface does not necessarily correspond to the deterrence of cellular attachment to that surface.

Copper leachate concentrations were measured because they were thought to be relevant to the bacterial adherence results, but there was not a straightforward relationship between the two. The marine paint and Cu(II)-CnGmSiO$_2$/epx leached the same amount of copper (94–115 µM, **Table 5.1**), but there was an almost 3 Log$_{10}$ reduction in the number of viable, adherent bacteria when the test square was coated with the marine paint instead of Cu(II)-CnGmSiO$_2$/epx (**Figure 5.12**). The copper leachate concentration was high enough to cause injury to *E. coli* cells in culture but too low for complete killing (> 500 µM, **Table 5.2**). There is evidence in the literature of metal ions in solution effecting change in planktonic bacteria: Perrin *et al.*[319] reported that a sub-inhibitory concentration of Ni(II) (100 µM) encouraged biofilm formation in *E. coli* K-12. Therefore, it was hypothesised that, in the present work, the sub-lethal copper concentrations in liquid culture encouraged stressed bacteria to form biofilms on the coatings, but, in the case of the marine paint, the copper content at the surface (40–50% w/w) was sufficiently high to trigger the viable but nonculturable condition (*i.e.* viable bacteria that do not grow or divide) or to be bactericidal. In contrast, increased adherence to Cu(II)-CnGmSiO$_2$/epx was observed because either the surface copper content (2.6% w/w) was not above the threshold for lethality or the Cu(II) was not bioavailable, since it was complexed by a strong ligand. Therefore, this is a possible explanation for the enhanced adherence to Cu(II)-CnGmSiO$_2$/epx.

Table 5.4. Literature data from copper ion-containing coatings compared to data from this study.

Reference	Surface	Cu in Coating	Cu Leachate	Leaching Conditions	Outcome
Lindgren *et al.*[317]	Cu_2O in generic paint (hard, rosin-based)	8.5% w/w	3.04 μg/cm^2	sea, 24 h	fouling deterred
Pallavicini *et al.*[313]	glass (11.5 cm^2) functionalised with Cu(II)-cyclam complex	~1.6 x 10^{-9} mol/cm^2 (1.2 μg total)	< 8% Cu (8.1 ng/cm^2)	H_2O, 48 h	low microbicidal activity for *E. coli* ATCC 10356
Dacarro *et al.*[216]	glass (11.5 cm^2) functionalised with polyethyleneimine	3.8 x 10^{-10} mol/cm^2 (0.28 μg total)	< 5% Cu (1.2 ng/cm^2)	H_2O, 24 h	low microbicidal activity for *E. coli* ATCC 10356
He *et al.*[318]	Cu(II)-polydopamine grafted onto titanium	~2.75% w/w	0.15–0.2 ppm	phosphate-buffered saline, 24 h	~17.5% survival rate for *E. coli*
This study	**CnGmSiO$_2$ + Cu(II)/epx (18.9 cm^2)**	**1.0% w/w (1.1 mg total)**	**2.3 ppm (3% Cu, 2.0 μg/cm^2)[a], 12 ppm (17% Cu, 10 μg/cm^2)[b]**	M63 minimal medium, 24 h	adherence of *E. coli* NZRM 3647 unchanged
This study	**Cu(II)-CnGmSiO$_2$/epx (18.9 cm^2)**	**2.6% w/w (2.0 mg total)**	**3.6 ppm (3% Cu, 3.1 μg/cm^2)[a], 6.0 ppm (7%, 5.2 μg/cm^2)[b]**	M63 minimal medium, 24 h	increased adherence of *E. coli* NZRM 3647
This study	**Marine Paint (10.6 cm^2)**	**40–50% w/w (25–31 mg total)**	**3.3 ppm (0.2% Cu, 5.1 μg/cm^2)[a], 7.3 ppm (0.6% Cu, 11 μg/cm^2)[b]**	M63 minimal medium, 24 h	decreased adherence of *E. coli* NZRM 3647

[a] M63 minimal medium without *E. coli* NZRM 3647.
[b] M63 minimal medium with *E. coli* NZRM 3647.

The aforementioned enhanced attachment was not observed for $CnGmSiO_2 + Cu(II)/epx$, which had a lower copper content but higher copper leachate concentration in the presence of *E. coli* than $Cu(II)-CnGmSiO_2/epx$. Instead of enhanced bacterial adherence, the viable counts from $CnGmSiO_2 + Cu(II)/epx$ were equivalent to the control, $CnGmSiO_2/epx$. Two possible explanations were considered: first, the higher copper leachate concentration in the culture (190 μM) likely resulted in increased killing or growth inhibition, as evidenced by the 24 h culture having the lowest OD_{600} (**Table 5.1**), and, second, it is possible that some of the Cu(II) in $CnGmSiO_2 + Cu(II)/epx$ was adsorbed onto the silica surface during post-loading, rather than chelated, meaning that it was more weakly associated with the surface and, consequently, more bioavailable. The increased bioavailability of Cu(II) at the surface and in solution could have had a marginal antimicrobial effect, counteracting any inducement of biofilm formation.

The surface topography was also considered in regard to the results of the assay, but bacterial adherence appeared to be unaffected by different topographies. The surfaces of the SiO_2/epx-type coatings were rough, and, as previously discussed, increased surface roughness generally results in increased colonisation by bacteria.[287] Nevertheless, the only coating of this type with increased bacterial attachment was $Cu(II)-CnGmSiO_2/epx$. There was no observable difference in surface topography between the silica coatings, as evidenced by SEM (Chapter 4, **Figure 4.18**). So, increased adherence to $Cu(II)-CnGmSiO_2/epx$ was not because it was the roughest out of all the tested coatings. The counts from SiO_2/epx, $CnGmSiO_2$/epx, and $CnGmSiO_2 + Cu(II)$/epx were statistically equivalent to each other and to the epoxy resin and uncoated sample (**Figure 5.12**), both of which were much smoother than the silica coatings.

5.3.2 Conclusions

Bacterial adherence to the SiO_2/epx-type coatings, epoxy coating, marine paint, and uncoated substrate was tested (**Figure 5.12**). All of the results were statistically equivalent, except for the marine paint and $Cu(II)-CnGmSiO_2/epx$. There were approximately 2 Log_{10} fewer cells recovered from the marine paint, compared to the other coatings, and this result was at the LOD of the assay. In contrast, the number of adherent cells *per* cm^2 was highest on $Cu(II)-CnGmSiO_2/epx$, which could be due to low levels of copper in the culture precipitating biofilm formation by stressed cells. It has been reported that 10^5–10^7 adherent cells *per* cm^2 are required for biofilm formation to occur,[300] and $Cu(II)-CnGmSiO_2/epx$ is the only coating approaching this value. It is possible that *E. coli* NZRM 3647 does not readily form biofilms or requires more than 48 h for biofilm formation, and future adherence

assays should be carried out with a different bacterial species (*e.g.* marine). Measurement of the amounts of copper leached from $CnGmSiO_2 + Cu(II)/epx$, $Cu(II)-CnGmSiO_2/epx$, and the marine paint in the presence and absence of *E. coli* revealed enhanced leaching in the presence of bacteria, and comparisons to copper toxicity data in the literature showed that the copper concentrations were high enough to cause injury to *E. coli* cells in culture (**Table 5.2**). The highest concentration of leached copper corresponded to the culture with the lowest OD_{600} ($CnGmSiO_2 + Cu(II)/epx$: 12 ppm Cu, OD_{600} 0.057). However, all of the optical densities of the *E. coli* cultures in M63 minimal medium measured after 24 h incubation were unusually low, and it was discovered that this was due to incubating the cultures under static conditions. Therefore, for future testing, it was decided that the cultures should be shaken during incubation. Further investigations of the literature yielded examples of Cu(II) ligand-functionalised surfaces with antimicrobial activity – even at equivalent or lower surface and leached copper concentrations than $Cu(II)-CnGmSiO_2/epx$ and $CnGmSiO_2 + Cu(II)/epx$ (**Table 5.4**). Unfortunately, none of the SiO_2/epx-type coatings had comparable activity to the marine paint, but it should be noted that the marine paint also contains other antimicrobial ingredients (*e.g.* thiram) capable of leaching into the culture or exerting a bactericidal surface effect.[320]

There are several limitations and aspects of the assay that could seriously impact or skew the results. First, the assay is not high-throughput, being that it is quite lengthy and labour-intensive, and its precision is too low to identify anything less than Log_{10}-differences between coatings as statistically significant. Second, because the counts are reported as CFUs *per* unit surface area of the coatings (*e.g.* cm^2), the estimated surface area notably influences the results. For the relatively flat and smooth samples, such as the uncoated substrate, epoxy coating, and marine paint, the surface area was calculated as a square (10.6 cm^2 for 23 mm × 23 mm, two-sided), but this was not valid for the rougher silica coatings. The surface area of the silica coatings (18.9 cm^2 for 23 mm × 23 mm, two-sided) was estimated by treating the silica particles like spheres confined in a square (Appendix**, Scheme 8.2**), since the particle diameter is known to be 35–75 μm. However, as seen by SEM (Chapter 4, **Figure 4.18**), the particles are not spherical, and the estimated surface area may be quite different from the true value, meaning that the CFU/cm^2 may be quite different as well. BET surface area analysis of Batch 4 $CnGmSiO_2$, Batch 2 $Cu(II)-CnGmSiO_2$, and the unfunctionalised silica was conducted (Appendix, **Table 8.21**), but the results were not particularly useful, as the technique includes the surface area of the pores. *E. coli* (1–3 μm length, 0.4–0.7 μm diameter) is too big to fit in the pores (60 Å diameter),[321] so the surface area measured by BET analysis is not reflective of the surface area available for bacterial colonisation.

A third critique of the assay's design is that it only measures the number of viable bacteria that are attached to the coating; it does not reveal if bacteria have adhered and then died, but, in the context

of biofouling, the remaining biomass can still be problematic. Unfortunately, staining is contraindicated because most stains would also be retained by the coating or substrate, which is supported by the result of staining adherent biomass with crystal violet (Appendix, **Figure 8.54**). Fourth, there were concerns that Tween 20 could have a synergistic effect with the antimicrobial coatings by making cells more vulnerable to lysis. To determine if a detergent is even necessary, Gram-staining should be performed to check for cellular aggregation. Also, the experiment testing the effect of Tween 20 (**Section 5.2.3**, **Figure 5.6**) could be repeated with a standard amount of Cu(II) (comparable to the leached Cu(II) concentrations) added to the 24 h cultures. Finally, there are concerns that the assay will not accurately predict coating performance in field experiments. For example, the copper leachate concentration may impact the assay's results, but it is unlikely to have an extensive effect in the ocean in which the copper will be greatly diluted. Despite these concerns, establishment of such an assay is vital for the project.

Even though it is acknowledged that the data from laboratory-based antifouling bioassays do not always correlate with the data from field experiments, these bioassays are still essential for the selection of a lead product. Field experiments in which the coatings are immersed in the ocean are expensive because they require large quantities of the test products and long immersion times. Consequently, proceeding directly from coating formulation to field experiments for each antifouling candidate is unfeasible, and numerous laboratory antifouling assays have been developed to serve as the first gate for narrowing down the candidates to a manageable number for field experiments.[282] The adherence assay in this work is practical and relevant, and the assay, with the recommended adjustments, was progressed to test the adherence of marine bacterium *V. harveyi* NZRM 2698 to the SiO$_2$/epx-type coatings.

5.4 ADHERENCE ASSAY: *V. HARVEYI* NZRM 2698

5.4.1 Optimisation

Prior to testing bacterial adherence to the SiO_2/epx-type coatings, the assay was optimised for marine bacterium *V. harveyi* NZRM 2698. Optimisation involved adjusting the growth conditions, such as the temperature to 30 °C and medium to Luria marine broth, and performing many of the same experiments conducted during the method development with *E. coli* NZRM 3647 (**Figure 5.3**). First, the effects of vortexing, sonication, and Tween 20 (0.05% v/v) on planktonic *V. harveyi* were assessed (Experimental, **Figure 6.14**), and it was found that the addition of Tween 20 to the culture before diluting for enumeration *via* the drop plate method resulted in a 3.5–4.5 Log_{10} reduction in the CFU/mL, compared to the control (**Figure 5.13a**). Therefore, Tween 20 had a bactericidal effect on *V. harveyi*. Vortexing and/or sonication yielded similar counts to the control, meaning that the cells were unaffected by the vortexing and sonication conditions in the assay. For the samples without Tween 20, however, similar counts were recorded in multiple dilutions (*e.g.* 10^{-10} and 10^{-11}), which is indicative of the transfer of agglomerated cells.
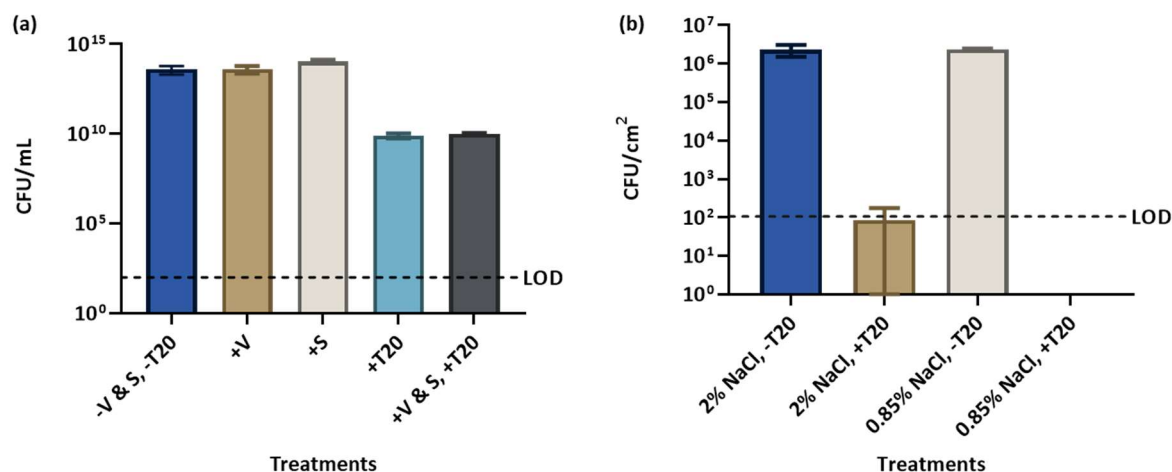
Figure 5.13. Optimisation of the bacterial adherence assay for *V. harveyi* NZRM 2698: (a) results of CFU/mL in an untreated planktonic culture ("-V & S, -T20") and planktonic cultures treated with vortexing ("+V"), sonication ("+S"), Tween 20 ("+T20"), and vortexing plus sonication and Tween 20 ("+V & S, +T20"; LOD = 100 CFU/mL) and **(b)** results of CFU/cm^2 on $CnGmSiO_2$/epx-coated samples obtained using ± 0.05% v/v Tween 20 for deagglomeration and 0.85% *vs* 2% w/w NaCl for washes and dilutions (LOD = 106 CFU/cm^2). The bars represent the mean (tr = 5) ± SD.

Gram-staining revealed that cells of *V. harveyi* were indeed clumping. The aggregation of cells was observed after staining an overnight culture of *V. harveyi* (**Figure 5.14a**). Nonionic detergent Tween 20 (0.05% v/v) was added, and the culture was checked once more for clumping cells *via* Gram-staining. The clumps dispersed in the presence of Tween 20 (**Figure 5.14b**). Agglomerated cells could affect the results of the assay by making it difficult to deliver a standard inoculum for the 24 h culture and by propagation of the clumps through serial dilutions and plating, resulting in multiple cells being counted as a single colony. However, the use of Tween 20 (0.05% v/v) to mitigate clumping was contraindicated by its bactericidal effect on planktonic *V. harveyi*.

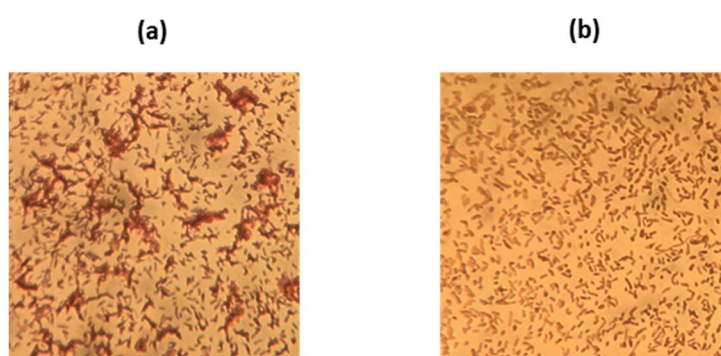**Figure 5.14. Gram-staining of a culture of *V. harveyi* NZRM 2698 in Luria marine broth: (a)** before and **(b)** after the addition of Tween 20.

An experiment was conducted to determine the impact of Tween 20 (0.05% v/v) in the adherence assay when used to break up clumps 1) prior to inoculation for 24 h incubation of the CnGmSiO$_2$/epx-coated sample, 2) in the vortexed detachment solution, and 3) in the serial dilutions to be plated for counting (Experimental, **Figure 6.15**). CnGmSiO$_2$/epx, rather than the uncoated substrate, was used because testing the attachment of *V. harveyi* to the SiO$_2$/epx-type coatings was the ultimate goal, so optimising conditions with coatings of this type was reasonable. Also, in previous experiments (**Figure 5.10**), strong interactions did not seem to be promoted between *E. coli* and the uncoated substrate, and it was unknown if *V. harveyi* would behave similarly. Since both CnGmSiO$_2$/epx and SiO$_2$/epx were negative controls for the Cu(II)-containing SiO$_2$/epx-type coatings, they were used in the optimisation experiments. Treatment of the samples with Tween 20 resulted in a 4–5 Log$_{10}$ reduction in the number of adherent cells (**Figure 5.13b**), and, for this reason, Tween 20 was not used in the adherence assay, despite concerns about cells aggregating. Time constraints did not allow for further optimisations regarding the use of alternative detergents or lower concentrations of Tween 20. In the same experiment, different concentrations of salt (0.85% *vs* 2% w/w NaCl) in the

aqueous rinses and diluent yielded equivalent bacterial counts (**Figure 5.13b**); this was checked because saline (*i.e.* 0.85% w/w NaCl) was normally used in the assay, but marine bacterium *V. harveyi* is cultured in high-salt media (*e.g.* 2% w/w in Luria marine broth).

The duration of incubation of a sample with *V. harveyi* and the efficiency of vortexing and sonication in the subsequent detachment of the cells were also evaluated (Experimental, **Figure 6.16**). SiO_2/epx-coated samples were incubated 24 h or 48 h in diluted cultures of *V. harveyi* with shaking (Appendix, **Figure 8.55**, stationary phase by 16 h). To detach the adherent cells, the samples were treated with and without vortexing and/or sonication, and the efficacy of one round of vortexing *vs* two was assessed. Incubation for 48 h yielded 1–2 Log_{10} fewer adherent cells than incubation for 24 h (**Figure 5.15a**), so 24 h remained the incubation time-length. The combination of vortexing and sonication as a detachment method resulted in approximately the same number of CFUs recovered from the substrate as vortexing alone, and one round of vortexing appeared to be sufficient for the removal of the majority of adherent cells. Therefore, it was decided that one round of vortexing alone was an adequate detachment method. The substrate not subjected to any detachment methods revealed that a percentage of the CFUs were attributable to the carryover of planktonic cells from washes or the detachment of weakly adhered cells.
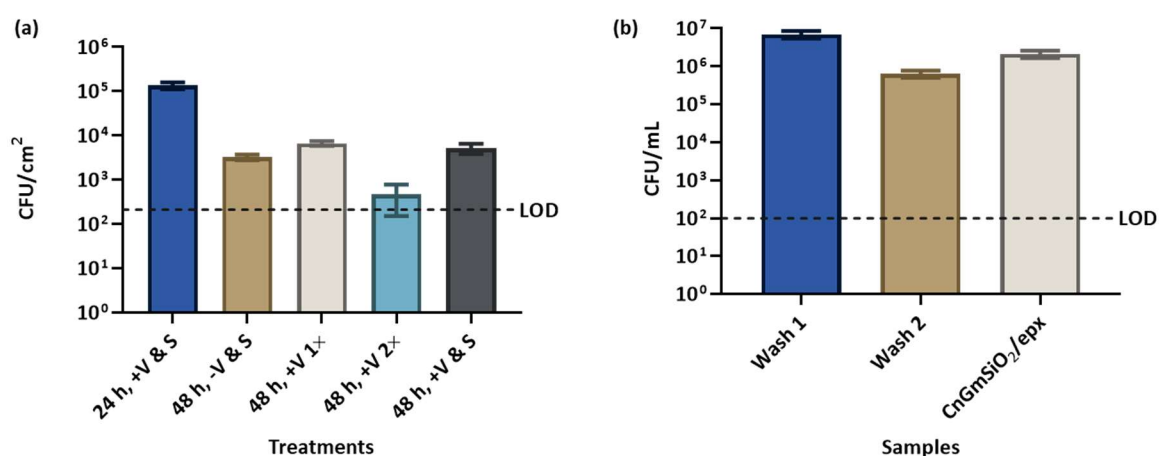
Figure 5.15. Optimisation of the bacterial adherence assay for *V. harveyi* NZRM 2698 (continued): **(a)** results of CFU/cm^2 on the SiO_2/epx-coated substrate after incubating 24 h *vs* 48 h and obtained under the conditions of ± vortexing and sonication, vortexing once ("1×"), and vortexing the same sample a second time ("2×"; LOD = 212 CFU/cm^2) and **(b)** results of CFU/mL in 2% w/w NaCl washes and in the detachment solution containing a CnGmSiO$_2$/epx-coated square (LOD = 100 CFU/mL). The bars represent the mean (tr = 5) ± SD.

An experiment was conducted, as in **Figure 5.7**, to enumerate the cells in successive washes of a CnGmSiO$_2$/epx-coated sample (Experimental, **Figure 6.17**). The cells were then detached from the sample *via* vortexing and enumerated. More bacteria were recovered from the detachment solution containing the sample than from the second wash, demonstrating that cells remained attached through multiple washes (**Figure 5.15b**). The number of cells in the second wash was ~4 Log$_{10}$ higher than the LOD of the assay. This would be problematic if the counts were indeed from the carryover of planktonic cells from the 24 h culture, rather than cells detaching from the surface, since the large number of carryover cells could mask effects of deterred adherence to the test samples. Thus, it would be possible to determine if the coatings were not bactericidal, but the reverse would be difficult, if not impossible. Unfortunately, this line of inquiry could not be pursued further due to time constraints. With the aforementioned limitations in mind, as well as the optimisations to the protocol, the adherence of *V. harveyi* to the SiO$_2$/epx-type coatings was tested.

5.4.2 Adherence to SiO$_2$/epx-Type Coatings

The attachment of marine bacterium *V. harveyi* NZRM 2698 to the SiO$_2$/epx-type coatings, epoxy coating, commercial marine paint, and uncoated substrate was assessed, following the optimised protocol. The samples were incubated with *V. harveyi* in a liquid culture while shaking for 24 h at 30 °C. After incubation, the samples were rinsed with an aqueous salt solution (2% w/w NaCl) and transferred to a fresh solution for detachment *via* vortexing. The detached cells were enumerated, yielding the number of adherent cells *per* cm^2 for each sample. As shown in **Figure 5.16**, all of the differences in the CFU/cm^2 between samples were statistically significant ($p < 0.01$), with the following exceptions: the differences between the marine paint and the epoxy and SiO$_2$/epx were not significant, and the difference between the uncoated substrate and Cu(II)-CnGmSiO$_2$/epx was not significant.

Unexpectedly, the fewest cells adhered to SiO$_2$/epx. The addition of unfunctionalised silica to the epoxy surface resulted in a 1 Log$_{10}$ reduction in the number of adherent cells, compared to the epoxy. Functionalisation of the silica with CnGm yielded a 2 Log$_{10}$ increase in the number of adherent cells, which was the largest number out of the tested coatings. Measurement of the optical densities in each 24 h culture revealed that the lowest OD$_{600}$ was measured in the culture containing SiO$_2$/epx (OD$_{600}$ 0.71, **Table 5.5**), demonstrating that the presence of silica had a growth-inhibitory or killing effect. It is possible that cation sequestration by the weakly acidic (pK_a 4) silanol groups at the silica gel surface could have negatively impacted planktonic *V. harveyi* and cellular attachment.[322,323]

However, this antimicrobial effect was not observed by Sarkheil *et al.*[324] in a study in which silver nanoparticles were immobilised on silica sand beads to create an antibacterial material against *Vibrio* sp. Persian1. Although the modified silica sand beads killed 100% of bacteria after 2 h contact, the unmodified silica sand beads had no such bactericidal activity.
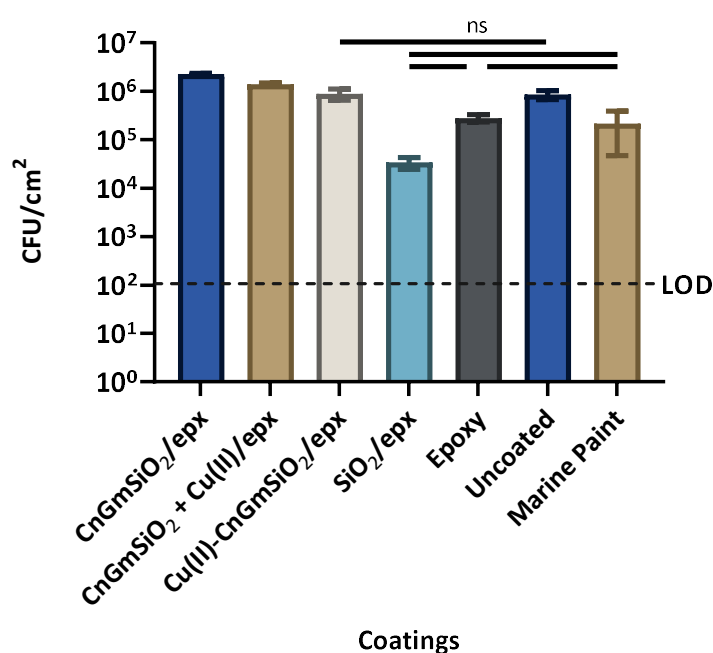
Figure 5.16. Results of *V. harveyi* NZRM 2698 CFU/cm^2 on the SiO$_2$/epx-type coatings, as well as on uncoated squares, the epoxy resin, and the marine paint. The bars represent the mean (br = 6 for "SiO$_2$/epx" and "Marine Paint", br = 3 for all others) ± SD (LOD = 106 CFU/cm^2). To determine if the means from the data sets were significantly different from each other, a one-way ANOVA with Tukey's *post hoc* test was conducted, and the difference was considered to be significant when the *p*-value was < 0.05. Unless annotated as not significant (ns), the results were significantly different ($p < 0.01$).

Table 5.5. The OD_{600} of the *V. harveyi* cultures after 24 h incubation and the copper content of the test squares.

Coating	OD_{600} (24 h, LMB)[a]	% w/w Cu[b]
CnGmSiO$_2$/epx	1.22 ± 0.05	0
CnGmSiO$_2$ + Cu(II)/epx	0.95 ± 0.03	1.0 ± 0.3[a]
Cu(II)-CnGmSiO$_2$/epx	1.04 ± 0.01	2.6 ± 0.3[a]
SiO$_2$/epx	**0.71 ± 0.04**	**0**
Epoxy	1.34 ± 0.02	-
Uncoated	1.46 ± 0.05	-
Marine Paint	1.23 ± 0.12	40–50

[a] Mean ± SD. Experiment repeated 3×.
[b] % w/w Cu in the (un)functionalised silica component or in the marine paint.

In the present experiment, another unexpected result was for the marine paint, on which > 10^5 CFU/cm^2 were recovered. The result is somewhat suspicious, as the marine paint is known to be antifouling. It is uncertain if this result is truly reflective of the propensity of bacteria to colonise the surface or, rather, if the coating's activity is being masked by counts from planktonic cells carried over from washes; the antifouling ability of the marine paint or SiO$_2$/epx might actually be greater than what is reflected in the assay. Yet, the results for coatings with significantly higher counts than the marine paint (*e.g.* uncoated, CnGmSiO$_2$/epx, CnGmSiO$_2$ + Cu(II)/epx, Cu(II)-CnGmSiO$_2$/epx) are likely accurate, in as much as they show that bacterial adherence is undeterred on these coatings. Further method development is required to ensure that the washes in future testing are efficient in removing planktonic cells.

5.4.3 Conclusions

The adherence assay was optimised for marine bacterium *V. harveyi* NZRM 2698. First, the effects of vortexing, sonication, and Tween 20 (0.05% v/v) on planktonic *V. harveyi* were evaluated, and it was found that cells were unaffected by vortexing and sonication. Gram-staining of a culture of *V. harveyi* revealed that the cells were aggregating, and, although Tween 20 dispersed the clumps, it was found to be bactericidal and was not used. In another experiment, more cells were recovered after an incubation time of 24 h, compared to 48 h, and one round of vortexing alone was found to be sufficient for the removal of surface-adherent cells. Enumeration of the cells in successive washes of CnGmSiO$_2$/epx and its detachment solution demonstrated that cells remained adhered through

multiple rinses, but the large numbers of bacteria in the sample washes called into the question the washing efficiency. Had time permitted, further experimentation would have examined increasing the number of washes.

The optimised protocol was followed to test the adherence of *V. harveyi* to the SiO_2/epx-type coatings, epoxy coating, marine paint, and uncoated substrate. Attachment was undeterred on the functionalised silica coatings, both with and without copper, and the highest average counts out of all the tested coatings were recovered from $CnGmSiO_2$/epx. Interestingly, the CFU/cm^2 were lowest on SiO_2/epx, rather than the marine paint. It was unknown if these results were a true reflection of the number of adherent cells or if bactericidal effects were being masked by planktonic cells carried over from the wash step. It is probable that carryover is more of a problem with *V. harveyi* than with *E. coli* due to cellular agglomeration. Therefore, future work should explore the use of a different detergent or a lower concentration of Tween 20 to disperse clumps, as well as exploring the benefit of additional wash steps. The Cu(II)-leaching from the coatings into the shaken 24 h cultures of *V. harveyi* in Luria marine broth should also be measured.

5.5 SUMMARY AND FUTURE WORK

To rank antifouling products and select a lead coating, a bacterial adherence assay was developed using representative, Gram-negative bacterium *E. coli* NZRM 3647. In this assay, freshly coated squares were incubated with the bacteria in M63 minimal medium, and, after 24 h, they were removed, rinsed, delivered to a saline/Tween 20 solution, vortexed, and sonicated. The CFUs in the detachment solutions were enumerated *via* the drop plate method to reveal the number of viable cells attached *per* cm^2 of each coating. This procedure was employed to test the adherence of *E. coli* to the SiO_2/epx-type coatings prepared in Chapter 4 (**Section 4.3**). Surprisingly, Cu(II)-CnGmSiO$_2$/epx had the greatest number of viable, adherent bacteria, despite it having the highest % w/w copper out of the prepared coatings. The counts from CnGmSiO$_2$/epx, CnGmSiO$_2$ + Cu(II)/epx, SiO$_2$/epx, the epoxy resin, and the uncoated sample were statistically equivalent, and the counts for the marine paint were at the LOD of the assay. The amount of copper released from each copper-containing coating (*i.e.* Cu(II)-CnGmSiO$_2$/epx, CnGmSiO$_2$ + Cu(II)/epx, and the marine paint) over the 24 h incubation period was measured. Interestingly, the amount of leached copper increased when bacteria were present in the culture, and the highest amount of leached copper corresponded to the 24 h culture with the lowest OD_{600} (*i.e.* CnGmSiO$_2$ + Cu(II)/epx). With the validation of the assay, the samples were progressed to testing the propensity of a marine bacterium to colonise their surfaces.

The assay protocol was optimised to examine the attachment of marine bacterium *V. harveyi* NZRM 2698 to these coatings. The procedure for *V. harveyi* differed from the one for *E. coli* in the following ways: the bacteria were cultured in Luria marine broth at 30 °C, the samples were rinsed and detached in an aqueous salt solution (2% w/w NaCl) without Tween 20, and vortexing alone was used as a detachment method. For the assay with *V. harveyi*, however, planktonic cells carried over from the rinses may have contributed more significantly to the total CFUs than in the assay with *E. coli*, possibly due to the tendency of *V. harveyi* cells to aggregate. Tween 20 dispersed clumps of cells but had a bactericidal effect and, therefore, was not used. Testing the adherence of *V. harveyi* to the SiO_2/epx-type coatings revealed that cellular attachment was deterred on SiO_2/epx but undeterred on CnGmSiO$_2$/epx, CnGmSiO$_2$ + Cu(II)/epx, and Cu(II)-CnGmSiO$_2$/epx. The possible contribution of agglomerated planktonic cells to the total cell count made it difficult to determine the actual magnitude of any attachment-deterrent effects.

The goals of future work should be to improve and expand the bacterial adherence assay and answer questions raised by this study. Since both *E. coli* and *V. harveyi* are Gram-negative bacteria, the colonisation of the surfaces by other, especially Gram-positive (*e.g. Micrococcus luteus*), marine bacteria should also be assessed, preferably using seawater as the growth medium. The enumeration

of the viable, adherent cells is an indirect, laborious method for evaluating bacterial colonisation by a surface, and, without visual confirmation, it is difficult to have confidence that the assay is working as designed. The assay would greatly benefit from a different detection method, such as staining (*e.g.* live/dead) and microscopy (*e.g.* fluorescence, SEM), with which the surface colonisation could be observed directly. Although, the opacity and dye-retention of the samples complicates the implementation of these techniques. Instead of using dyes, the bioluminescence of *V. harveyi* could be exploited to determine the percent coverage of a surface, or fluorescent bacteria could be used. These adjustments would shorten the assay, making it more high-throughput. Another improvement to the assay would be to find an antifouling coating with a high copper content that does not contain other antimicrobial components, and this coating would be tested alongside the marine paint. Furthermore, it would be beneficial to determine the wettability of each surface *via* contact angle measurements.

Testing the adherence of both *E. coli* and *V. harveyi* to the SiO_2/epx-type coatings revealed that the functionalised silica coatings, with and without Cu(II), did not deter cellular attachment. Thus, stage four of the current project in which the antifouling ability of the lead product would be tested in the marine environment (Chapter 1, **Table 1.5**) is not achievable, and other antifouling candidates should be pursued in the future. Following the present line of inquiry, the functionalisation of different kinds of silica with different ligands (*e.g.* other ligands in the tetraaza/oxatriaza series; Chapter 2, **Figure 2.18**) could be pursued to create products with a range of Cu(II)-loading and -leaching abilities, establishing the parameters of the Cu(II) flux required to make a surface antifouling.

6 Experimental

6.1 General

6.1.1 Materials and Procedures

Anhydrous solvents were obtained commercially, and Milli-Q water was used throughout. The model ligand in this work, cyclen, was purchased from Chem-Impex International, Inc., and key precursor molecule ADH was supplied by Nuplex Industries. For silica functionalisation reactions, silica gel (high-purity grade, pore size 60 Å, 220–440 mesh particle size, 35–75 μm particle size; Sigma-Aldrich), unless otherwise stated, was dried for 24 h at 180 °C under vacuum before use. The ratio of GLYMO to silica (mmol GLYMO/g silica) used in functionalisation reactions was based on the ratio of *n*-octadecyldimethylchlorosilane to silica (0.991 mmol modifier/g silica) used by Ortega *et al.*[260] to synthesise reversed-phase silica gel. All acids used for ICP-MS analysis were double-distilled at sub-boiling temperatures in a Teflon system in-house (School of Geography, Environment and Earth Sciences), starting from reagent grade acids to generate quality-controlled products equal to or better than Optima (Thermo Fisher) grade acids. The acids were distilled at the azeotropic concentration (*i.e.* concentrated for HNO_3 and 6.02 M for HCl) and then diluted, as needed, using Milli-Q water (resistivity > 18.6 MΩ), which was also regularly checked as a blank. Air-sensitive reactions were performed under an atmosphere of argon, and rotary evaporation was completed at 10 mmHg and a suitable temperature. Reaction progress was monitored by NMR spectroscopy or normal-phase thin-layer chromatography (TLC) on aluminium sheets coated with silica gel 60 F_{254} (Merck) and visualised by staining or UV light. Flash chromatography was performed on a Reveleris® X2 flash chromatography system (BUCHI) using FlashPure Cartridges (BUCHI), silica (50 μm), and a gradient of petroleum ether and ethyl acetate.

6.1.2 Instrumentation, Equipment, and Analysis

NMR spectra were recorded on a 500 MHz Bruker NMR Spectrometer or 500 MHz Jeol Resonance NMR Spectrometer in the indicated deuterated solvents. The ^1H NMR spectra were referenced to tetramethylsilane (TMS) or the solvent peak, and the ^{13}C NMR spectra were referenced to the solvent peak. The major solvent was referenced in mixed systems. NMR spectral data will be reported for key and novel compounds. Mass spectrometry was conducted on a Waters Q-TOF Premier™ Electrospray

Mass Spectrometer with a MassLynx 4.1 operating system in positive mode. Samples were prepared for analysis by mixing in aqueous methanol containing trace formic acid. IR spectra were measured on a PerkinElmer Spectrum One FT-IR Spectrometer with a Universal ATR sampling accessory or on a Bruker Tensor II FT-IR Spectrometer with a Platinum ATR sampling accessory, and NIR spectra were measured on a PerkinElmer LAMBDA 1050 UV/Vis/NIR Spectrophotometer with a 3D WB Det. Module. A SpectraMax M4 Multi-Mode Microplate Reader (Molecular Devices) and Cary 50 Bio UV-Visible Spectrophotomer (Agilent) were used to obtain UV-Vis spectra, measure absorbance, or measure OD_{600}. The functionalised silica products were submitted to The Campbell Microanalytical Laboratory (University of Otago; Dunedin, NZ) for CHN elemental and, in the cases of Batch 1 Cu(II)-CnGmSiO$_2$ and the Cu(II)-cyclen adsorbed onto silica, for ICP-MS analyses. CHN results were reported as duplicates within 0.30% of one another. All other metal analyses *via* ICP-MS were conducted in-house (School of Geography, Environment and Earth Sciences) on a Thermo Scientific Element 2 sector field ICP-MS. Images and the atomic compositions of coatings were obtained with an FEI Quanta 450 scanning electron microscope (tungsten filament) positioned at a 10 mm working distance and an Apollo X Silicon Drift Detector (EDAX) for SEM-EDS. Images were taken at 200× and 800× magnification with an electron beam spot size set at 4 and an accelerating voltage of 20 kV. EDS measurements were conducted at 200× magnification with the following parameters: spot size 6 (> 1000 cps), 20 kV accelerating voltage, 30 s live time, 1.6 μs amplitude time, 35–36° take-off angle, and 129 eV resolution. BET surface area analyses were conducted on a Flowsorb II 2300 Surface Area Analyser (Micromeritics) at 21.6 °C and 1027 hPa. In bacterial adherence testing, sonication was carried out with a Bandelin Sonopuls Ultrasonic Homogeniser mini20 (2.0 sonotrode, 2.5 tip). Samples were centrifuged at 3000 relative centrifugal force (RCF) in a Rotina 380 centrifuge (Hettich).

6.1.3 Bacterial Strains and Culture Conditions

The strains of bacteria used in this work were *Escherichia coli* NZRM 3647 and *Vibrio harveyi* NZRM 2698 (**Table 6.1**), which were handled using aseptic technique and maintained by re-streaking from the seed stock every month for single colonies on agar plates. The plates were stored at 4 °C, and the strains were stored at -80 °C in 25% v/v glycerol in liquid medium. *E. coli* was grown at 37 °C in nutrient broth, on nutrient agar plates, or in M63 minimal medium. *V. harveyi* was grown at 30 °C in Luria marine broth or on Luria marine agar plates.

Table 6.1. Bacterial strains used in this study.[325,326]

NZRM Strain #	Name	Description	Source
3647	*Escherichia coli*	Biotech Australia - BTA 2850. O157 verocytotoxin negative. Originally from The Royal Children's Hospital, Melbourne 01/12/1995.	Callaghan Innovation, Wellington, NZ
2698	*Vibrio harveyi*	ATCC 14126 (NCIMB 1280). Type strain.	NZCC[a]

[a] The New Zealand Reference Culture Collection: Medical Section, Environmental Science and Research.

6.1.4 Bacterial Media Preparation

All media were stored at 2–8 °C and handled using aseptic technique, which was implemented whenever a sterile environment was required. Sterilisation of media *via* autoclaving was conducted at 121 °C for 20 min.

6.1.4.1 Nutrient Broth

Nutrient broth was prepared as in ISO 22196.[199] Beef Extract (3 g; Lab M), BBL™ Trypticase™ Peptone (10 g; BD Biosciences), and sodium chloride (5 g) were dissolved in double-distilled water (ddH$_2$O; 1 L). The broth was adjusted to pH 7.0 ± 0.2 and autoclaved. Alternatively, dehydrated nutrient broth (13 g; Oxoid) was dissolved in ddH$_2$O (1 L), and the broth was adjusted to pH 7.4 ± 0.2 and autoclaved.

6.1.4.2 Nutrient Agar

Nutrient agar was prepared as in ISO 22196.[199] Beef Extract (5 g; Lab M), BBL™ Trypticase™ Peptone (10 g; BD Biosciences), sodium chloride (5 g), and Bacto™ Agar (15 g; BD Biosciences) were dissolved in ddH$_2$O (1 L). The solution was adjusted to pH 7.1 ± 0.1 and autoclaved. Alternatively, dehydrated nutrient agar (28 g; Oxoid) was dissolved in ddH$_2$O (1 L), and the solution was adjusted to pH 7.4 ± 0.2 and autoclaved. Molten agar was delivered aseptically to 90 mm Petri dishes (25 mL *per* plate), and the agar plates were allowed to solidify at room temperature (~15 min). Before use, the plates were dried at 37 °C or at room temperature in a laminar flow hood.

6.1.4.3 M63 Minimal Medium

To prepare M63 minimal medium, ammonium sulfate (2 g), monobasic potassium phosphate (13.6 g), and ferrous sulfate heptahydrate (0.5 mg) were dissolved in ddH$_2$O (1 L). The solution was adjusted to pH 7.0 and autoclaved. After the solution cooled to below 50 °C, filter-sterilised 20% v/v glycerol (aq; 10 mL) and filter-sterilised 1 M magnesium sulfate (aq; 1 mL) were added.[327]

6.1.4.4 Luria Marine Broth

Luria marine broth was prepared as in Mire *et al.*[304]: tryptone (10 g; Oxoid), yeast extract (5 g; Oxoid), and sodium chloride (20 g) were dissolved in ddH$_2$O (1 L), and the solution was autoclaved.

6.1.4.5 Luria Marine Agar

Luria marine agar was prepared as in Mire *et al.*[304]: tryptone (10 g; Oxoid), yeast extract (5 g; Oxoid), sodium chloride (20 g), and bacteriological agar (15 g; Oxoid) were dissolved in ddH$_2$O (1 L), and the solution was autoclaved. Molten agar was delivered aseptically to 90 mm Petri dishes (25 mL *per* plate), and the agar plates were allowed to solidify at room temperature (~15 min). Before use, the plates were dried at 37 °C or at room temperature in a laminar flow hood.

6.1.5 Optical Density Measurements

The optical densities of bacterial cultures were measured at 600 nm with a Unicam Helios UV-Vis spectrophotometer (Biolab Scientific Ltd.) in 1 mL cuvettes (1 cm path length). The appropriate growth medium was used as a blank and to dilute the sample, as needed.

6.1.6 Growth Curves

An overnight culture was prepared by inoculating the appropriate liquid medium (3 mL) with a colony of the bacterium from an agar plate and incubating the culture for 16 h at the appropriate temperature with shaking. In a well of a 96-well plate (Thermo Scientific), fresh liquid medium was inoculated with overnight culture to OD$_{600}$ 0.05. Uninoculated medium served as a blank. The plate was incubated for 20.8 h at the appropriate temperature, and, every 5 min, the OD$_{600}$ of each well was recorded by a

SPECTROstar[Nano] plate reader (BMG LABTECH) after the plate was shaken 10 s (orbital) to generate a growth curve for the bacterium.

6.1.7 Enumeration of Cells by the Drop Plate Method

Ten-fold serial dilutions of the samples in sterile 0.85% w/w aq sodium chloride (*i.e.* saline; *E. coli*) or 2% w/w aq sodium chloride (*V. harveyi*) were performed to quantify the number of CFUs in a given volume or area by the drop plate method in which five aliquots (10 µL; technical replicates) of each dilution were delivered to and allowed to absorb into an agar plate. The plates were incubated overnight at the appropriate temperature until the colonies were countable, and the countable dilution contained 3–30 colonies *per* 10 µL drop. The results from the technical replicates were averaged.

6.1.8 Gram Staining

Following the protocol published by the American Society for Microbiology,[328] a loopful of fresh liquid culture was smeared on a microscope slide and allowed to air dry. Once the inoculum was dry, the cells were heat-fixed to the slide by passing it, cell side up, 3× through the top of a flame, warming the glass. The heat-fixed cells were dyed with crystal violet staining reagent for 1 min and then briefly (< 5 s) washed with ddH$_2$O. They were covered with Gram's iodine solution, a mordant to fix the dye, for 1 min and then briefly (< 5 s) washed with ddH$_2$O. The slide was rinsed with 95% v/v ethanol (aq) for < 10 s to decolourise the cells and then rinsed with ddH$_2$O (< 5 s) to stop the decolourisation. The cells were counterstained with safranin for < 30 s and then briefly (< 5 s) rinsed with ddH$_2$O. The slide was gently blotted dry, and the cells were examined under a light microscope.

6.1.9 Graphing and Statistical Analyses

Graphs were created and statistical analyses were performed using GraphPad Prism 8 (GraphPad Software, Inc.) or Microsoft® Excel® for Office 365. The bacterial enumeration data were presented as the mean value ± the standard deviation (SD), and statistical analyses were conducted when there were three or more biological replicates for each sample in the experiment. To determine if the means from two data sets were significantly different from each other, a two-sample, two-tail Student's *t*-test (unequal variance) was conducted, and the difference was considered to be significant when the

p-value was < 0.05. For the graphs, statistical significance was denoted as follows: * p < 0.05, ** p < 0.01, and *** p < 0.001. One-way analyses of variance (ANOVAs) were completed to determine if the differences between the means of two or more independent data sets were statistically significant, and Tukey's *post hoc* test was used to identify which groups were statistically different.

6.2 CHAPTER 2

6.2.1 Polyacylhydrazone: DiLevDEG/ADH

Procedures by Daines *et al.*[127] (**Scheme 6.1**) were followed for the synthesis of the DiLevDEG/ADH polyacylhydrazone.
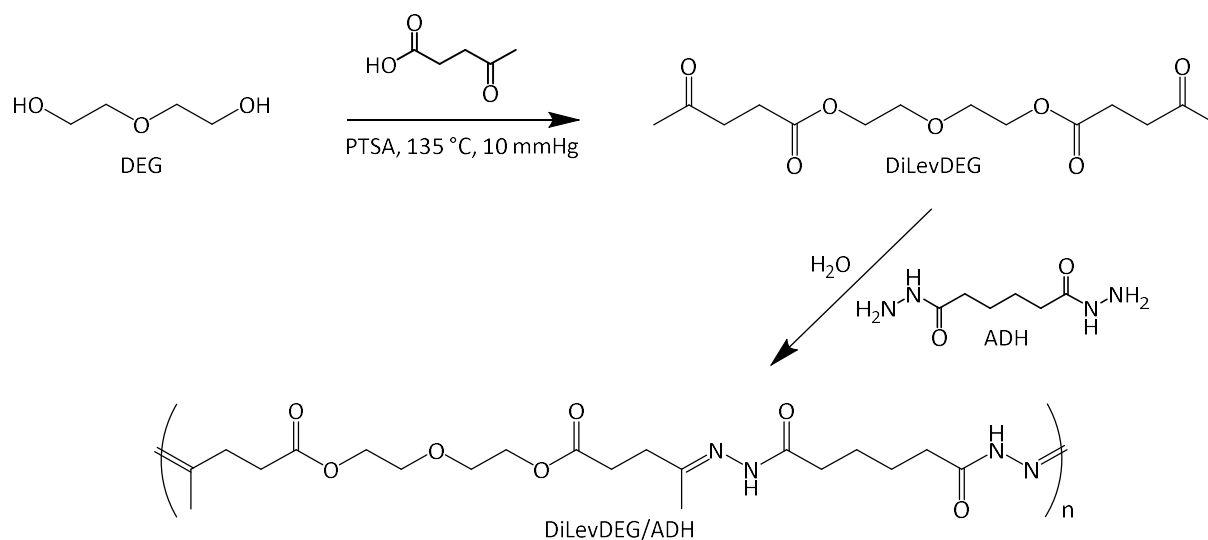
Scheme 6.1. Synthesis of DiLevDEG/ADH polyacylhydrazone.

6.2.1.1 Synthesis of DiLevDEG

Levulinic acid (61.91 g, 0.5225 mol, 1.4 eq), DEG (40 g, 0.37 mol), and PTSA monohydrate (0.208 g, 1.18 mmol, 0.003 eq) were heated at 135 °C under reduced pressure (10 mmHg). The water produced by the reaction was collected by distillation, and the reaction was determined to be complete when water production ceased (approximately 8 h). The reaction mixture was cooled to room temperature, washed with water (3 × 100 mL) and sodium chloride (saturated, aq; 100 mL), dried over magnesium sulfate, and concentrated to give the product as an orange, viscous oil (56.81 g, 50% yield). NMR spectral data were consistent with those in the literature.[127]

^{1}H NMR (500 MHz, CDCl$_3$): δ 4.23 (t, *J* = 4.7 Hz, 4H), 3.69 (t, *J* = 4.7 Hz, 4H), 2.76 (t, *J* = 6.5 Hz, 4H), 2.61 (t, *J* = 6.5 Hz, 4H), 2.19 (s, 6H); **^{13}C NMR** (126 MHz, CDCl$_3$): δ 206.6, 172.8, 69.2, 63.8, 38.0, 30.0, 28.1.

## 6.2.1.2 Synthesis of DiLevDEG/ADH

ADH (1.298 g, 7.302 mmol, 0.9 eq) was added to a solution of DiLevDEG (2.453 g, 8.114 mmol) in water (5 mL) to give a clear, viscous solution of ~50% w/v solids. To obtain NMR spectra, a test reaction was set up in an NMR tube by adding ADH (13 mg, 73 µmol, 0.9 eq) to a solution of DiLevDEG (25 mg, 83 µmol) in deuterium oxide (1 mL). NMR spectral data were consistent with previously recorded laboratory data.

^{1}H NMR (500 MHz, D$_2$O): δ 4.58–4.18 (m, 2H), 3.93–3.66 (m, 2H), 3.02–2.92 (m, 1H), 2.84–2.52 (m, 4H), 2.49–2.36 (m, 1H), 2.35–2.21 (m, 3H), 2.12–1.92 (m, 2H), 1.80–1.55 (m, 4H); **^{13}C NMR** (126 MHz, D$_2$O): δ 213.5, 175.3, 172.7, 163.1, 68.5, 64.0, 37.8, 33.7, 33.6, 33.4, 33.3, 33.1, 32.5, 31.8, 30.3, 29.9, 29.7, 29.1, 28.0, 25.8, 24.8, 24.7, 24.6, 24.5, 23.9, 21.6, 16.2, 15.8.

6.2.2 Simple Acylhydrazones

## 6.2.2.1 Synthesis of Precursor Compounds

6.2.2.1.1 Synthesis of Acethydrazide
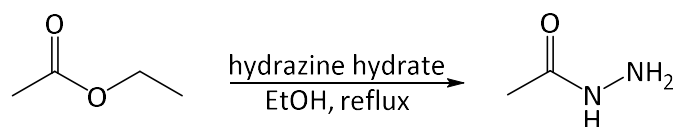
Scheme 6.2. Synthesis of acethydrazide.

Acethydrazide was synthesised following the procedure by Sadek *et al.*[329] (**Scheme 6.2**). Hydrazine hydrate (80% w/w; 8.0 mL, 0.13 mol) was added dropwise to ethanol (5 mL), and the solution was heated (< 50 °C). Then, ethyl acetate (20 mL, 0.20 mol) was added dropwise to the solution, which was heated under reflux for 96 h. The white, crystalline product was isolated *via* rotary evaporation and cooling to 0 °C (8.131 g, 108% yield, presence of contaminants in NMR spectra). Aside from the contaminants, NMR spectral data were consistent with those in the literature.[329]

6.2.2.1.2 Synthesis of Methyl and Ethyl Levulinate
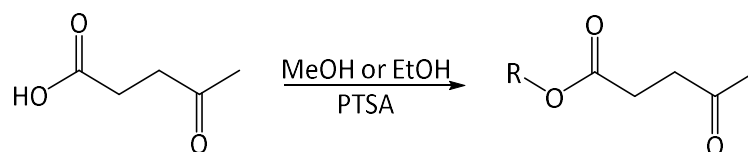
Scheme 6.3. Synthesis of methyl/ethyl levulinate (R = -Me, -Et).

Methyl and ethyl levulinate were synthesised by following established procedures in the laboratory (**Scheme 6.3**), and the characterisation data were compared to previous records. Methyl levulinate was produced by adding methanol (31 mL) to levulinic acid (3.034 g, 25.35 mmol), PTSA monohydrate (0.317 g, 1.79 mmol), and 3 Å molecular sieves. The reaction mixture was heated under reflux for 44.5 h. Upon reaction completion, the mixture was filtered and concentrated by rotary evaporation. Ethyl acetate (10 mL) was added to the concentrated reaction mixture, and the organic layer was washed with sodium chloride (saturated, aq; 1 × 10 mL) and dried over magnesium sulfate. The solvent was removed by rotary evaporation to yield the product as a clear, colourless liquid (1.230 g, 37% yield). Following the same procedure, ethyl levulinate was generated by adding ethanol (31 mL) to levulinic acid (3.069 g, 25.64 mmol), PTSA monohydrate (0.322 g, 1.82 mmol), and 3 Å molecular sieves (2.745 g, 74% yield; clear, colourless liquid). NMR spectral data were consistent with previously recorded laboratory data.

6.2.2.1.3 Derivatisation of Vanillin: Acylation with Acetic, Trimethylacetic, and Butyric Anhydride
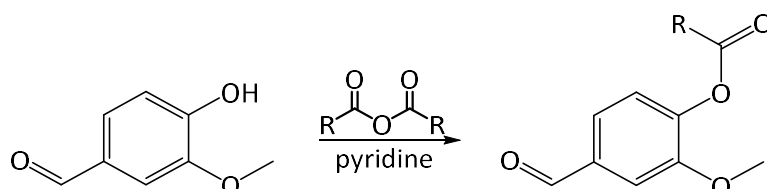

Scheme 6.4. Synthesis of acylated vanillin (R = -Me, -*t*Bu, -Pr).

Acylated vanillin was synthesised following the procedure by Yang *et al.*[330] (**Scheme 6.4**). Acetic, trimethylacetic, and butyric anhydride (3 eq) were each added to separate solutions of vanillin (1.0 g, 6.4 mmol) in pyridine (5 mL). The reactions with acetic and butyric anhydride were stirred for 3 h at room temperature until they were determined to be complete *via* TLC. After 30 h stirring at room temperature, the reaction with trimethylacetic anhydride was still incomplete, as determined by TLC, so 4-dimethylaminopyridine (10 mg, 81 μmol) was added. The reaction was stirred at room temperature for an additional 23 h until completion. All reaction mixtures were diluted with diethyl ether (50 mL) and washed with hydrochloric acid (10% v/v, aq; 5 × 10 mL) and sodium chloride (saturated, aq; 1 × 10 mL), and the organic layers were dried over magnesium sulfate for 30 min. The organic layers were then filtered and concentrated under vacuum to yield the crude products, which were purified by flash chromatography. Vanillin acetate was isolated as a cream-coloured solid (0.935 g, 74% yield), vanillin pivalate was isolated as a white solid (0.769 g, 51% yield), and vanillin butyrate was isolated as a brown liquid (> 0.350 g, > 23% yield). NMR spectral data were consistent with those in the literature.[330–332]

6.2.2.2 General Procedure for Synthesis of Acylhydrazones

The acylhydrazones in **Scheme 6.5** were synthesised following the general procedure by Zha and You.[133] The hydrazide (**1–5**) was added to a solution of the aldehyde or ketone (~1 eq for monoacylhydrazones, ~2 eq for acyldihydrazones) in methanol or ethanol. Glacial acetic acid (AcOH) was then added dropwise to adjust to pH 4–5, and the reaction mixture was heated under reflux to yield a white or yellow precipitate, which was isolated by vacuum filtration and washed with methanol or ethanol (2 × 5 mL). The acylhydrazones were generally soluble in dimethylformamide and dimethylsulfoxide. However, **1a** and **3h** were also soluble in chloroform containing 10% v/v methanol, and ligands **1i** and **1j** were soluble in chloroform. Ligand **5h** was only poorly soluble in chloroform/methanol (10% v/v). Refer to the Appendix (**Figures 8.3–19**, **Table 8.1–17**) for the NMR spectra and peak assignments. In describing the ^{1}H NMR data for molecules that display rotamers in solution, the convention followed is to list the two signals demonstrating the rotameric forms, then their multiplicity and the *total* value for which they integrate (*e.g.* δ 11.60 & 11.21 (s, 1H)).
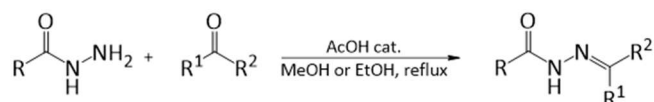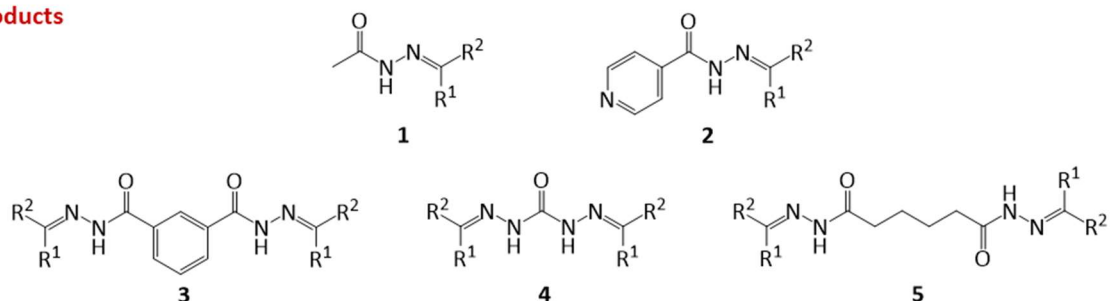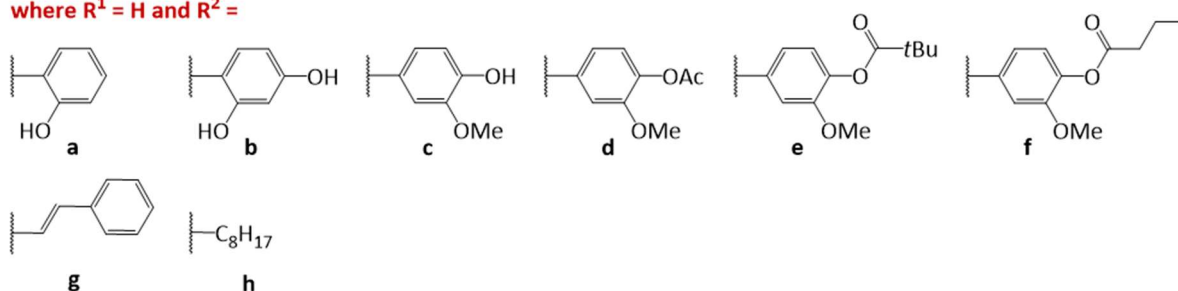
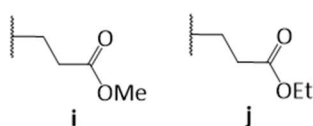**Scheme 6.5. General scheme for the synthesis of acylhydrazones** (top; R, R^1, R^2: same or different). The synthesised acylhydrazones are as follows: **1a–b**, **1i–j**, **2a–b**, **3c–f**, **3h**, **4c**, **4g**, **5c**, and **5h–j**.

6.2.2.2.1 Monoacylhydrazones

Compound **1a** was prepared by reacting acethydrazide (0.490 g, 5.95 mmol) and salicylaldehyde (0.753 g, 6.10 mmol) for 18 h in 5 mL methanol (0.717 g, 64% yield). **^{1}H NMR** (500 MHz, DMSO-d_6): δ 11.60 & 11.21 (s, 1H), 10.13 (s, 1H), 8.34 & 8.27 (s, 1H), 7.62 & 7.49 (dd, J = 7.8, 1.7 Hz, J = 7.5, 1.7 Hz, 1H), 7.28 & 7.24 (td, J = 7.6, 1.6 Hz, J = 7.5, 1.6 Hz, 1H), 6.94–6.83 (m, 2H), 2.18 & 1.98 (s, 3H); **^{13}C NMR** (126 MHz, DMSO-d_6): δ 171.4, 165.4, 157.3, 156.3, 146.3, 140.9, 131.1, 130.8, 129.4, 126.8, 119.9, 119.4, 119.2, 118.5, 116.3, 116.1, 21.3, 20.3. **ESI-HRMS:** calcd for $C_9H_{10}N_2O_2Na$ [M + Na]$^+$ 201.0640; found 201.0641.

Compound **1b** was prepared by reacting acethydrazide (0.481 g, 5.84 mmol) and 2,4-dihydroxybenzaldehye (0.861 g, 6.11 mmol) for 16 h in 10 mL ethanol (0.812 g, 68% yield). **^{1}H NMR** (500 MHz, DMSO-d_6): δ 11.39 & 11.02 (s, 1H), 9.89 (s, 1H), 8.20 & 8.13 (s, 1H), 7.38 & 7.25 (d, J = 9.1 Hz, J = 8.4 Hz, 1H), 6.37–6.27 (m, 2H), 2.13 & 1.94 (s, 3H); **^{13}C NMR** (126 MHz, DMSO-d_6): δ 171.0, 165.0, 160.5, 160.2, 159.3, 158.1, 147.3, 142.3, 131.2, 128.8, 111.4, 110.4, 107.8, 107.6, 102.6, 102.4, 21.3, 20.3. **ESI-HRMS:** calcd for $C_{13}H_{11}N_3O_3$ [M + H]$^+$ 258.0879; found 258.0878.

Compound **1i** was prepared by reacting acethydrazide (0.152 g, 1.85 mmol) and methyl levulinate (0.274 g, 2.08 mmol) for 46 h in 6 mL methanol (0.159 g, 46% yield). **^{1}H NMR** (500 MHz, CDCl$_3$): δ 8.84 (s, 1H), 3.68 (s, 3H), 2.63–2.57 (m, 4H), 2.20 (s, 3H), 1.87 (s, 3H); **^{13}C NMR** (126 MHz, CDCl$_3$): δ 173.8, 173.5, 149.6, 51.7, 33.3, 29.9, 20.4, 15.9. **ESI-HRMS:** calcd for $C_8H_{14}N_2O_3$ [M + H]$^+$ 187.1083; found 187.1087.

Compound **1j** was prepared by reacting acethydrazide (0.149 g, 1.81 mmol) and ethyl levulinate (0.305 g, 2.09 mmol) for 46 h in 6 mL ethanol (0.412 g, 39% yield). **^{1}H NMR** (500 MHz, CDCl$_3$): δ 8.79 (s, 1H), 4.13 (q, J = 7.1 Hz, 2H), 2.62–2.58 (m, 4H), 2.21 (s, 3H), 1.86 (s, 3H), 1.25 (t, J = 7.1 Hz, 3H); **^{13}C NMR** (126 MHz, CDCl$_3$): δ 173.7, 173.0, 149.7, 60.5, 33.3, 30.2, 20.5, 15.9, 14.4. **ESI-HRMS:** calcd for $C_9H_{16}N_2O_3$ [M + H]$^+$ 201.1239; found 201.1245.

Compound **2a** was prepared by reacting isonicotinic hydrazide (0.397 g, 2.87 mmol) and salicylaldehyde (0.310 mL, 2.85 mmol) for 16 h in 10 mL ethanol (0.600 g, 85% yield). **^{1}H NMR** (500 MHz, DMSO-d_6): δ 12.28 & 12.01 (s, 1H), 11.09 & 9.97 (s, 1H), 8.81 & 8.74 (dd, J = 4.5, 1.6 Hz, d, J = 4.3 Hz, 2H), 8.69 & 8.38 (s, 1H), 7.85 & 7.64 (dd, J = 4.4, 1.7 Hz, d, J = 4.6 Hz, 2H), 7.61 & 7.41 (dd, J = 7.7, 1.8 Hz, d, J = 7.5 Hz, 1H), 7.33 & 7.22 (td, J = 7.4, 1.6 Hz, t, J = 7.3, 1H), 6.98–6.90 & 6.88–6.79 (m, 2H); **^{13}C NMR** (126 MHz, DMSO-d_6): δ 161.3, 157.5, 156.5, 150.4, 149.6, 149.0, 143.2, 140.0, 131.7, 131.1, 129.2, 127.1, 122.6, 121.5, 119.4, 118.7, 116.4, 116.1. **ESI-HRMS:** calcd for $C_{13}H_{11}N_3O_2$ [M + H]$^+$ 242.0930; found 242.0932.

Compound **2b** was prepared by reacting isonicotinic hydrazide (0.398 g, 2.87 mmol) and 2,4-dihydroxybenzaldehyde (0.404 g, 2.87 mmol) for 16 h in 10 mL ethanol (0.691 g, 89% yield). **^{1}H NMR** (500 MHz, DMSO-d_6): δ 12.11 & 11.82 (s, 1H), 11.28 (s, 1H), 10.00 (s, 1H), 8.79 & 8.72 (dd, J = 4.4, 1.6 Hz, d, J = 5.3 Hz, 2H), 8.55 & 8.24 (s, 1H), 7.84 & 7.61 (dd, J = 4.5, 1.5 Hz, d, J = 5.1 Hz, 2H), 7.37 & 7.22 (d, J = 8.4 Hz, J = 8.3 Hz, 1H), 6.39 & 6.30–6.25 (dd, J = 8.4, 2.3 Hz, m, 1H), 6.35 & 6.30–6.25 (d, J = 2.4 Hz, m, 1H); **^{13}C NMR** (126 MHz, DMSO-d_6): δ 161.0, 160.9, 159.5, 158.2, 150.3, 150.0, 149.7, 144.4, 140.1, 131.2, 129.2, 122.5, 121.4, 110.4, 107.9, 102.7, 102.4. **ESI-HRMS:** calcd for $C_{13}H_{11}N_3O_3$ [M + H]$^+$ 258.0879; found 258.0878.

6.2.2.2.2 Acyldihydrazones

Compound **3c** was prepared by reacting isophthalic dihydrazide (0.396 g, 1.98 mmol) and vanillin (0.622 g, 3.97 mmol) for 18 h in 140 mL methanol (0.591 g, 64% yield). **^{1}H NMR** (500 MHz, DMSO-d_6): δ 11.82 (s, 2H), 9.54 (s, 2H), 8.42 (s, 1H), 8.37 (s, 2H), 8.09 (d, J = 7.7 Hz, 2H), 7.67 (t, J = 7.7 Hz, 1H), 7.34 (s, 2H), 7.11 (d, J = 8.0 Hz, 2H), 6.86 (d, J = 8.1 Hz, 2H), 3.85 (s, 6H); **^{13}C NMR** (126 MHz, DMSO-d_6): δ 162.4, 149.1, 148.8, 148.1, 133.9, 130.5, 128.7, 126.8, 125.6, 122.2, 115.5, 109.1, 55.6. **ESI-HRMS:** calcd for $C_{24}H_{22}N_4O_6$ [M + Na]$^+$ 485.1437; found 485.1430.

Compound **3d** was prepared by reacting isophthalic dihydrazide (0.138 g, 0.689 mmol) and 4-formyl-2-methoxyphenyl acetate (0.270 g, 1.36 mmol) for 3 h in 50 mL methanol (0.312 g, 42% yield). **^{1}H NMR** (500 MHz, DMSO-d_6): δ 12.05 (s, 2H), 8.49 (s, 2H), 8.47 (s, 1H), 8.13 (d, J = 7.5 Hz, 2H), 7.71 (t, J = 7.6 Hz, 1H), 7.49 (s, 2H), 7.32 (d, J = 7.9 Hz, 2H), 7.20 (d, J = 8.1 Hz, 2H), 3.86 (s, 6H), 2.28 (s, 6H); **^{13}C NMR** (126 MHz, DMSO-d_6): δ 168.4, 162.6, 151.2, 147.6, 140.9, 133.7, 133.1, 130.8, 128.8, 126.9, 123.3, 120.6, 109.9, 55.9, 20.4. **ESI-HRMS:** calcd for $C_{28}H_{26}N_4O_8$ [M + Na]$^+$ 569.1648; found 569.1655.

Compound **3e** was prepared by reacting isophthalic dihydrazide (0.096 g, 0.48 mmol) and (4-formyl-2-methoxy-phenyl) 2,2-dimethylpropanoate (0.221 g, 0.935 mmol) for 5.5 h in 35 mL methanol (0.231 g, 39% yield). **^{1}H NMR** (500 MHz, DMSO-d_6): δ 12.05 (s, 2H), 8.48 (s, 2H), 8.46 (s, 1H), 8.13 (d, J = 7.5 Hz, 2H), 7.71 (t, J = 7.6 Hz, 1H), 7.48 (s, 2H), 7.32 (d, J = 7.9 Hz, 2H), 7.17 (d, J = 8.1 Hz, 2H), 3.85 (s, 6H), 1.32 (s, 18H); **^{13}C NMR** (126 MHz, DMSO-d_6): δ 175.6, 162.6, 151.3, 147.6, 141.3, 133.7, 133.0, 130.8, 128.8, 126.9, 123.2, 120.6, 110.0, 56.0, 38.6, 26.8. **ESI-HRMS:** calcd for $C_{34}H_{38}N_4O_8$ [M + Na]$^+$ 653.2587; found 653.2593.

Compound **3f** was prepared by reacting isophthalic dihydrazide (0.053 g, 0.26 mmol) and 4-formyl-2-methoxyphenyl butanoate (0.131 g, 0.560 mmol) for 16 h in 20 mL methanol (0.089 g, 56% yield). **^{1}H NMR** (500 MHz, DMSO-d_6): δ 12.04 (s, 2H), 8.49 (s, 2H), 8.46 (s, 1H), 8.13 (d, J = 7.3 Hz, 2H), 7.71 (t, J = 7.4 Hz, 1H), 7.48 (s, 2H), 7.32 (d, J = 7.7 Hz, 2H), 7.19 (d, J = 8.0 Hz, 2H), 3.85 (s, 6H), 2.56 (t, J = 7.1 Hz, 4H), 1.68 (sxt, J = 7.1 Hz, 4H), 1.00 (t, J = 7.3 Hz, 6H); **^{13}C NMR** (126 MHz, DMSO-d_6): δ 170.9, 162.6, 151.2, 147.6, 141.0, 133.7, 133.1, 130.8, 128.8, 126.9, 123.3, 120.6, 110.0, 55.9, 35.0, 18.0, 13.3. **ESI-HRMS:** calcd for $C_{32}H_{34}N_4O_8$ [M + H]$^+$ 603.2455; found 603.2464.

Compound **3h** was prepared by reacting isophthalic dihydrazide (0.395 g, 1.97 mmol) and nonanal (0.750 mL, 4.14 mmol) for 17 h in 12 mL ethanol (0.577 g, 66% yield). **^{1}H NMR** (500 MHz, CDCl$_3$/10% v/v CD$_3$OD): δ 11.10 (s, 2H), 8.03 (s, 1H), 7.91 (d, J = 7.7 Hz, 2H), 7.66 (t, J = 5.7 Hz, 2H), 7.44 (t, J = 7.7 Hz, 1H), 2.37–2.24 (m, 4H), 1.51 (p, J = 7.6 Hz, 4H), 1.38–1.21 (m, 20H), 0.88 (t, J = 6.9 Hz, 6H); **^{13}C NMR**

(126 MHz, CDCl$_3$/10% v/v CD$_3$OD): δ 164.5, 154.5, 133.4, 131.0, 128.9, 125.8, 32.6, 31.8, 29.3, 29.3, 29.2, 26.6, 22.6, 14.0. **ESI-HRMS:** calcd for C$_{26}$H$_{42}$N$_4$O$_2$ [M + H]$^+$ 443.3386; found 443.3390.

Compound **4c** was prepared by reacting carbohydrazide (0.395 g, 4.30 mmol) and vanillin (2.050 g, 13.07 mmol) for 23 h in 140 mL methanol (1.101 g, 72% yield). **^{1}H NMR** (500 MHz, DMSO-d_6): δ 10.43 (s, 2H), 9.38 (s, 2H), 8.06 (s, 2H), 7.36 (s, 2H), 7.08 (d, J = 8.0 Hz, 2H), 6.82 (d, J = 8.1 Hz, 2H), 3.84 (s, 6H); **^{13}C NMR** (126 MHz, DMSO-d_6): δ 152.2, 148.3, 148.0, 143.4, 126.1, 121.3, 115.4, 109.4, 55.7. **ESI-HRMS:** calcd for C$_{17}$H$_{18}$N$_4$O$_5$ [M + Na]$^+$ 381.1175; found 381.1170.

Compound **4g** was prepared by reacting carbohydrazide (0.397 g, 4.32 mmol) and *trans*-cinnamaldehyde (1.170 g, 8.764 mmol) for 18 h in 140 mL methanol (0.999 g, 73% yield). **^{1}H NMR** (500 MHz, DMSO-d_6): δ 10.57 (s, 2H), 7.97 (d, J = 6.4 Hz, 2H), 7.57 (d, J = 7.3 Hz, 4H), 7.39 (t, J = 7.5 Hz, 4H), 7.31 (t, J = 7.3 Hz, 2H), 7.02–6.89 (m, 4H); **^{13}C NMR** (126 MHz, DMSO-d_6): δ 151.7, 145.0, 137.0, 136.1, 128.8, 128.5, 126.7, 125.7. **ESI-HRMS:** calcd for C$_{19}$H$_{18}$N$_4$O [M + Na]$^+$ 341.1378; found 341.1376.

Compound **5c** was prepared by reacting ADH (0.406 g, 2.26 mmol) and vanillin (0.714 g, 4.55 mmol) for 40 h in 140 mL methanol (0.809 g, 82% yield). **^{1}H NMR** (500 MHz, DMSO-d_6): δ 11.14 & 11.02 (d, J = 5.3 Hz, J = 5.0 Hz, 2H), 9.45 (s, 2H), 8.05 & 7.86 (s, 2H), 7.25 & 7.22 (s, 2H), 7.08–7.00 (m, 2H), 6.84–6.76 (m, 2H), 3.81 & 3.77 (s, 6H), 2.69–2.60 & 2.26–2.17 (m, 4H), 1.70–1.57 (m, 4H); **^{13}C NMR** (126 MHz, DMSO-d_6): δ 173.9, 173.9, 168.2, 168.1, 148.8, 148.5, 148.5, 148.0, 147.9, 146.4, 146.3, 142.9, 142.8, 125.8, 125.8, 121.8, 120.8, 115.5, 115.4, 109.5, 109.3, 109.0, 55.5, 55.5, 34.1, 34.1, 31.8, 31.7, 25.0, 24.9, 24.2, 24.0. **ESI-HRMS:** calcd for C$_{22}$H$_{26}$N$_4$O$_6$ [M + Na]$^+$ 465.1750; found 465.1752.

Compound **5h** was prepared by reacting ADH (0.395 mmol, 2.20 mmol) and nonanal (0.810 mL, 4.47 mmol) for 18 h in 12 mL ethanol (0.894 g, 95% yield). **^{1}H NMR** (500 MHz, CDCl$_3$/5% v/v CD$_3$OD): δ 10.16, 9.84, 8.97, & 8.94 (s, 2H, exchangeable), 7.46–7.39 & 7.16–7.07 (m, 2H), 2.70–2.60 & 2.28–2.20 (m, expected 4H, overlapping HDO peak), 2.36–2.28 & 2.28–2.20 (m, expected 4H, overlapping HDO peak), 1.79–1.64 (m, 4H), 1.57–1.43 (m, 4H), 1.38–1.19 (m, 20H), 0.93–0.81 (m, 6H); **^{13}C NMR** (126 MHz, CDCl$_3$/5% v/v CD$_3$OD): δ 175.5, 170.1, 169.6, 152.6, 152.1, 148.5, 147.7, 34.8, 34.3, 32.5, 32.4, 32.2, 32.0, 31.9, 29.7, 29.4, 29.4, 29.3, 29.2, 26.7, 26.4, 26.1, 25.2, 24.9, 24.4, 23.8, 22.7, 14.1. **ESI-HRMS:** calcd for C$_{24}$H$_{46}$N$_4$O$_2$ [M + Na]$^+$ 445.3518; found 445.3519.

Compound **5i** was prepared by reacting ADH (0.201 g, 1.10 mmol) and methyl levulinate (0.328 g, 2.50 mmol) for 46 h in 6 mL methanol (0.378 g, 87% yield). **^{1}H NMR** (500 MHz, DMSO-d_6): δ 9.96 & 9.90 (s, 2H), 3.58 (s, 6H), 2.57–2.46 (m, expected 8H, overlapping DMSO-d_6 peak), 2.46–2.37 & 2.24–2.17 (m, 4H), 1.84 & 1.82 (s, 6H), 1.60–1.45 (m, 4H); **^{13}C NMR** (126 MHz, DMSO-d_6): δ 174.5,

172.8, 168.3, 155.4, 149.9, 51.2, 51.1, 33.8, 33.0, 32.7, 32.0, 29.7, 29.4, 25.1, 24.1, 16.7, 16.3. **ESI-HRMS:** calcd for $C_{18}H_{30}N_4O_6$ [M + H]$^+$ 399.2238; found 399.2230.

Compound **5j** was prepared by reacting ADH (0.201 g, 1.10 mmol) and ethyl levulinate (0.372 g, 2.55 mmol) for 46 h in 6 mL methanol (0.242 g, 52% yield). **^{1}H NMR** (500 MHz, DMSO-d_6): δ 9.96 & 9.90 (s, 2H), 4.09–3.99 (m, 4H), 2.55–2.47 (m, expected 8H, overlapping DMSO-d_6 peak), 2.47–2.40 & 2.22–2.18 (m, 4H), 1.84 & 1.82 (s, 6H), 1.59–1.46 (m, 4H), 1.22–1.13 (m, 6H); **^{13}C NMR** (126 MHz, DMSO-d_6): δ 174.4, 172.3, 168.2, 155.3, 149.9, 59.7, 59.6, 33.8, 33.1, 32.7, 32.0, 30.0, 29.6, 25.1, 24.1, 16.6, 16.3, 14.0. **ESI-HRMS:** calcd for $C_{20}H_{34}N_4O_6$ [M + H]$^+$ 427.2557; found 427.2547.

6.2.3 Preparation of Cu(II)-Ligand Complexes

6.2.3.1 DiLevDEG/ADH

The teal-coloured Cu(II)-DiLevDEG/ADH complex was prepared by adding an aliquot of the DiLevDEG/ADH solution (~50% w/v; 56 μL) to copper(II) nitrate trihydrate (32 mg, 0.13 mmol) dissolved in water (1 mL).

6.2.3.2 1a

The Cu(II)-**1a** complex was prepared by stirring copper(II) chloride dihydrate (0.043 g, 0.25 mmol) and ligand **1a** (0.045 g, 0.25 mmol) in methanol (10 mL). The green, precipitated Cu(II) complex was isolated and analysed by ESI-HRMS.

ESI-HRMS: calcd for $C_9H_9CuN_2O_2$ [M - H]$^+$ 239.9960; found 239.9963.

6.2.3.3 Cyclen

The Cu(II)-cyclen complex was prepared by adding cyclen (0.044 g, 0.25 mmol) and copper(II) chloride dihydrate (0.091 g, 0.53 mmol, 2.2 eq) to methanol (10 mL) and stirring for 2 h. The dark blue, precipitated Cu(II)-cyclen complex was isolated and analysed by ESI-HRMS.

ESI-HRMS: calcd for $C_8H_{19}CuN_4$ [M - H]$^+$ 234.0906; found 234.0916.

6.2.4 UV-Vis Spectrophotometry

6.2.4.1 DiLevDEG/ADH

The UV-Vis spectra of DiLevDEG/ADH, the Cu(II)-DiLevDEG/ADH complex, and copper(II) nitrate (50 mM, aq) were recorded. The samples were diluted, as needed, with water for measurement.

6.2.4.2 1a

6.2.4.2.1 Job Plot

Aliquots of 100 µM solutions of copper(II) nitrate and ligand **1a** in 9:1 chloroform:methanol containing 0.1 M tetrabutylammonium nitrate were added as shown in **Table 6.2**, and the absorption spectra from 240–1000 nm were measured. The absorbance at 388 nm, corresponding to the Cu(II)-**1a** complex, was used in subsequent calculations to determine the metal:ligand stoichiometry.

Table 6.2. Aliquots (mL) of 100 µM solutions of $Cu(NO_3)_2$ and ligand **1a**.

Solution	mL 100 µM $Cu(NO_3)_2$	mL 100 µM 1a
1	0.00	2.00
2	0.25	1.75
3	0.50	1.50
4	0.75	1.25
5	1.00	1.00
6	1.25	0.75
7	1.50	0.50
8	1.75	0.25
9	2.00	0.00

6.2.4.2.2 Formation Constant (K_f)

The UV-Vis spectra from 265–450 nm of solutions containing 0.100 mM ligand **1a** and 0, 0.013, 0.025, 0.038, 0.050, 0.063, 0.075, 0.088, 0.100, 0.113, 0.125, 0.138, 0.150, 0.175, 0.200, 0.250, 0.300, 0.350, 0.400, 0.450, and 0.500 mM copper(II) nitrate in 9:1 v/v chloroform:methanol (100 mL total) were measured, as well as a baseline spectrum of 9:1 v/v chloroform:methanol. The λ_{max} of the Cu(II)-**1a** complex to be used for subsequent calculations of the K_f was determined to be 388 nm.

6.2.4.3 Cyclen

An aqueous solution of the dark blue Cu(II)-cyclen complex was prepared by adding copper(II) nitrate and cyclen to give final concentrations of 50.5 mM each. The solution was diluted 100×, and its UV-Vis spectrum was recorded. The UV-Vis spectrum of copper(II) nitrate (50 mM, aq) was also measured.

6.3 CHAPTER 3

6.3.1 DiLevDEG/ADH-Substituted Resin in a Commercial Acrylic Paint

As shown in **Figure 6.1**, a commercial acrylic paint with 35% w/w of its resin substituted with the DiLevDEG/ADH polyacylhydrazone (DAp/acr) was prepared and evaluated, along with the acrylic paint, for its ability to retain Cu(II) and the subsequent impact on bacterial growth.
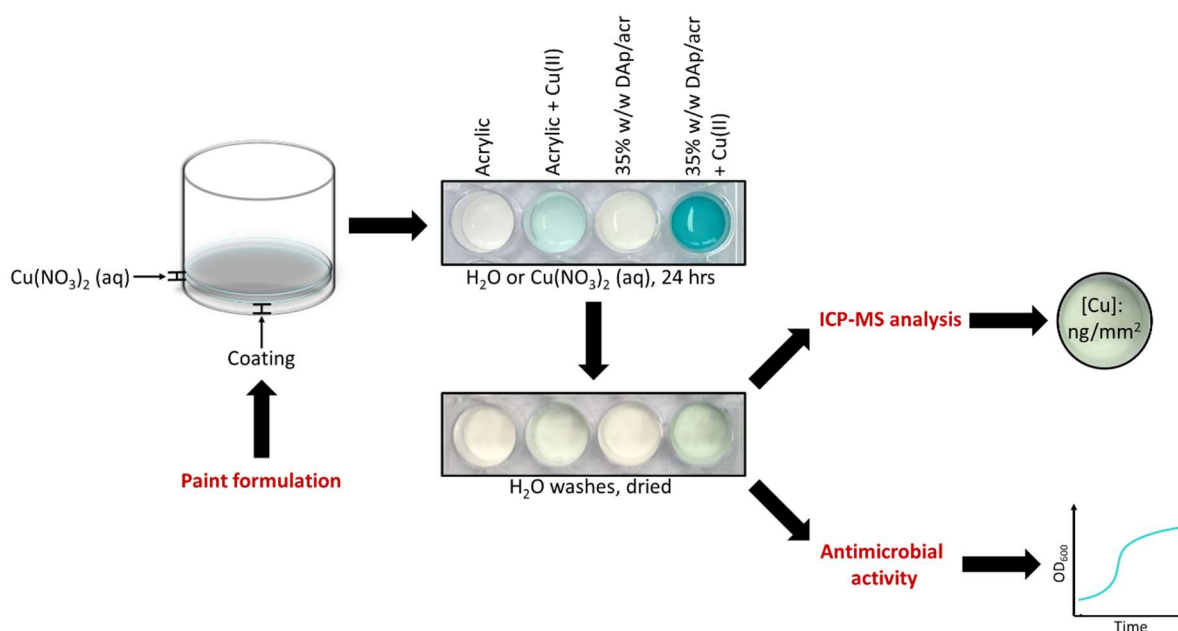
Figure 6.1. Methodology for assessing the Cu(II)-chelating ability of the acrylic and DAp/acr paints and their impact on bacterial growth (± Cu(II)).

6.3.1.1 Formulation

The aqueous solution of ~50% w/v DiLevDEG/ADH from **Section 6.2.1.2** was used to substitute 35% w/w of the resin component in a commercial acrylic paint, the composition of which is tabulated (**Table 6.3**). The resin was an ADH crosslinked dispersion polymer.

Table 6.3. Composition of the commercial acrylic paint used in this study.[a]

Ingredient	% w/w
Water	8
Millbase	
Titanium dioxide	26
Water, rheology modifier, dispersant, surfactant, MPG[b], defoamer, biocide, alkali	8
Dispersion mixture	
Dispersion polymer[c]	52
Coalescent, surface wetter, MPG[b], defoamer, biocide, alkali	6

[a] Proprietary composition and specific components confidential to Resene Paints Ltd.
[b] Monopropylene glycol.
[c] Resin = ADH crosslinked dispersion polymer (45% w/w).

6.3.1.2 Growth Assay: E. coli NZRM 3647

Refer to **Figure 6.1** and the Appendix (**Figures 8.20** & **8.21**) for the plate setup. To wells in a 24-well plate (JET BIOFIL®), 250 µL of the commercial acrylic paint, 35% w/w DAp/acr paint, or the commercial marine paint (Altex Yacht and Boat Paint, Ablative Antifouling No. 5; 40–50% w/w Cu_2O) were delivered, and the plate was agitated to coat the well bottoms evenly. The marine paint was included to compare to an industry standard, and uncoated wells served as growth controls. The paints were cured at 25 °C while shaking gently for 72 h, at which point they were no longer tacky. Then, they were washed with water (3 × 500 µL) and air-dried. An aqueous solution of copper(II) nitrate (50 mM; 500 µL/well) was added to a row of wells coated with the acrylic paint ("Acrylic + Cu(II)") and a row of wells coated with the DAp/acr paint ("DAp/acr + Cu(II)"; **Figure 8.20**). Water (500 µL/well) was added to a row of uncoated wells and to rows of wells coated with the acrylic, DAp/acr, and marine paints. After 24 h, all wells were washed with water (3 × 500 µL), air-dried, and sterilised with UV light for 20 min. The approximate surface area of the paint in each well was recorded. The prepared plates were used to determine the effects of the coatings on the growth of *E. coli* NZRM 3647, following the previously established laboratory procedure (unpublished data)[200]: an overnight culture was prepared by inoculating nutrient broth (3 mL) with a colony of *E. coli* NZRM 3647 from a nutrient agar plate and incubating for 16 h at 37 °C with shaking. This overnight culture was diluted 1:1 v/v with nutrient broth, and an aliquot of the diluted culture (500 µL; 1.3 x 10^8 CFU/mL) was added to each well. The plate was incubated at 37 °C, and the OD_{600} of the culture in each well was measure at t = 0, 2, 4, 6, 8, 10, and 24 h to generate growth curves (**Figure 8.21**). The experiment was independently repeated three times.

6.3.1.3 Quantification of Cu(II)-Leaching

As in **Section 6.3.1.2**, a coated, 24-well plate (JET BIOFIL®) was prepared (Appendix, **Figure 8.20**): aliquots (250 ± 10 mg) of the commercial acrylic paint, 35% w/w DAp/acr paint, and the commercial marine paint were delivered to wells in the 24-well plate, which was agitated to coat the well bottoms evenly. The paints were cured at 50 °C for 20 h, at which point they were no longer tacky. Then, they were washed with water (4×) and air-dried. An aqueous solution of copper(II) nitrate (50 mM; 500 µL/well) was added to three of the wells coated with the acrylic paint ("Acrylic + Cu(II)") and three of the wells coated with the DAp/acr paint ("DAp/acr + Cu(II)"). Water (500 µL) was added to three uncoated wells and wells coated with the acrylic, DAp/acr, and marine paints (three wells *per* coating). The uncoated wells and water-exposed acrylic- and DAp/acr-coated wells served as blanks. After 24 h, all wells were washed with water (4×) and air-dried, and nutrient broth (500 µL) was added to each well. The plate was incubated at 37 °C for 24 h. Then, the supernatant was removed from each well, diluted 10,000× with 3% v/v aq nitric acid, and analysed by ICP-MS to quantify the copper that had leached into the nutrient broth after 24 h.

6.3.1.4 Acrylic Paint Spike Study

In order to validate the Cu(II)-loading and quantification method, two samples were prepared with the commercial acrylic paint and a known amount of copper from an ICP-MS stock copper standard (Inorganic Ventures, 1001 µg/mL Cu). For the first sample, the copper was homogeneously mixed in a paint: the acrylic paint (200 ± 10 mg) was spiked with the copper standard (10 µL, 10.01 µg), mixed, and delivered to uniformly cover the bottom of a 7 mL glass vial that had been washed with water (3×) and air-dried. Then, the paint was cured at 50 °C overnight (19 h), at which point it was no longer tacky. For the second sample, the copper was added to the top of an already-cured paint: the acrylic paint (200 ± 10 mg) was delivered to uniformly cover the bottom of a 7 mL glass vial that had been washed with water (3×) and air-dried. The paint was cured at 50 °C overnight (19 h), at which point it was no longer tacky. Then, an aliquot of the copper standard (10 µL, 10.01 µg) was added to the surface of the cured paint and left for 24 h at 50 °C. For both samples, the acrylic paint without copper served as a blank. To prepare all samples for ICP-MS (Cu) analysis, the samples were digested in concentrated nitric acid (70% v/v, aq; 500 µL) for 3 h at 80 °C, and the digested solutions were diluted 2,500× with 1% v/v aq nitric acid to bring them into the range of the ICP-MS copper standards.

6.3.1.5 Quantification of Cu(II)-Loading

Special-made glass vials with dimensions matching the wells of the 24-well plates in **Section 6.3.1.2** (7.3 ± 0.1 mm radius) were washed with water (3×) and air-dried. An aliquot (250 ± 10 mg) of the acrylic paint or 35% w/w DAp/acr paint was delivered to the bottom of each vial, which was agitated for an even coating. Six vials coated with the acrylic paint and six vials coated with the DAp/acr paint were prepared. The paints were cured at 50 °C until, at least, they were no longer tacky, and then they were washed with water (3×) and air-dried. Aqueous copper(II) nitrate (50 mM; 500 µL/vial) was added to three of the vials coated with acrylic paint and three of the vials coated with the DAp/acr paint. Water (500 µL/vial) was added to the remaining vials, which served as blanks. The vials sat at room temperature for 24 h and then were washed with water (4×) and air-dried. The surface area exposed to liquid (Appendix, **Figure 8.22**) and the mass of each coating were recorded. To prepare the samples for ICP-MS (Cu) analysis, concentrated nitric acid (70% v/v, aq; 1 mL) was added to each vial, and the vials were heated at 80 °C for 3 h to digest the paint and release the copper into solution. The digested solutions were diluted 10,000× with 1% v/v aq nitric acid, bringing them into the range of the ICP-MS standards. If any particles were observed in a dilution, the sample was centrifuged for 10 min at 1788 RCF. The copper adsorbed onto or coordinated by each coating was quantified *via* ICP-MS analysis. The experiment was independently repeated four times. The cure-time was consistent within a batch of three replicates *per* coating but inconsistent between batches, varying from 16–67 h.

6.3.1.6 DiLevDEG/ADH Polyacylhydrazone-Leaching

The bottom of a well in a 24-well plate (JET BIOFIL®) was coated evenly *via* agitation with 260 mg of the 35% w/w DAp/acr paint, which was cured at 50 °C for 24 h, at which point it was no longer tacky. Then, the cured paint was washed with water (3×) and air-dried, and deuterium oxide (500 µL) was added to the well and left for 24 h. The ^{13}C NMR spectrum of the deuterium oxide supernatant was measured to assess whether or not the DiLevDEG/ADH polyacylhydrazone was leaching out of the coating. The key signals below are in **bold**.

^{13}**C NMR** (126 MHz, D$_2$O): δ **214.2**, **214.0**, **175.9**, **175.7**, **175.6**, **173.1**, **163.4**, **163.0**, **159.1**, 119.7, 72.2, 72.1, 70.1, 68.9, 68.9, 68.4, 67.1, 67.0, 66.7, 64.6, 64.5, 62.7, 60.9, 60.0, 57.9, 55.7, 52.8, 39.9, 39.3, 38.2, 37.3, 35.9, 34.1, 33.8, 33.8, 33.5, 33.0, 31.6, 31.0, **30.8**, **30.3**, **30.1**, 29.7, 29.6, 29.0, 28.4, 26.2, 25.7, 25.3, 25.1, 25.0, 25.0, 24.7, 24.4, 22.2, 22.0, 21.5, 18.5, 17.3, **16.8**, **16.7**, **16.2**, 7.0.

6.3.2 Polyurethane and Polyurea Coatings

Diisocyanate Desmodur® W (Covestro) was added to the following amine or alcohol components to form polyurea or polyurethane coatings, respectively: DETA, triethylene glycol (TEG), and 1,2-dianilinoethane (**Scheme 6.6**). Reactant amounts, reaction conditions, and treatments are summarised in **Table 6.4**. Refer to the Appendix (**Table 8.18**) for the result of each combination.
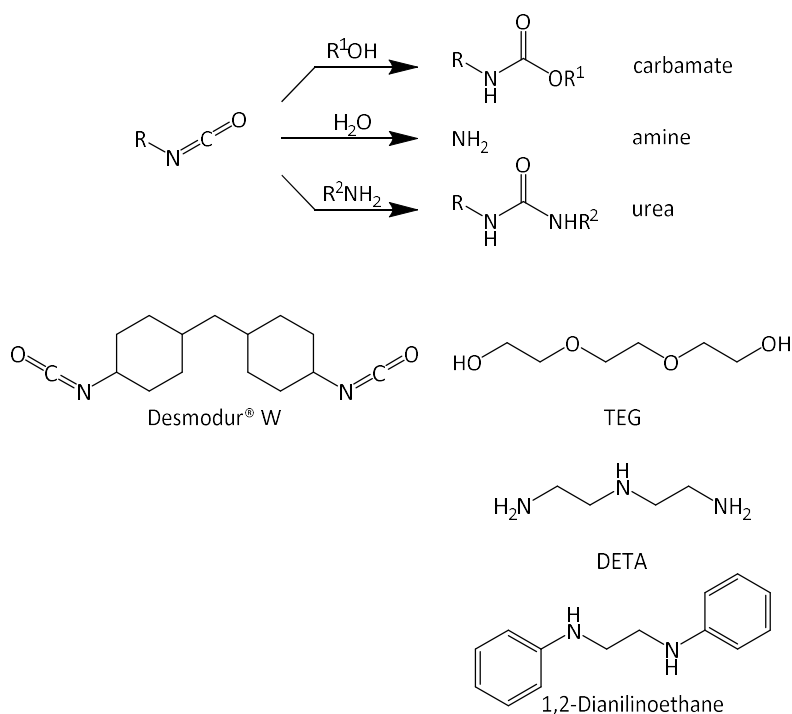
Scheme 6.6. Isocyanate reactions and structures of Desmodur® W, TEG, DETA, and 1,2-dianilinoethane.

Table 6.4. Amounts of amine and/or alcohol component reacted with Desmodur® W under the tabulated conditions.

Amine/Alcohol Component	mol Amine and/or Alcohol Component *per* 1 mol Desmodur® W	Amounts of Amine and/or Alcohol Component (mmol)	Conditions/Treatment
DETA	0.67	4.58	20 °C (RT)
DETA	0.67	4.58	0 °C
TEG	0.99	3.8	draw-down; cured at 70 °C for 19 h
TEG, DETA	0.90 (TEG); 0.071 (DTA)	3.5 (TEG); 0.3 (DTA)	20 °C (RT)
1,2-Dianilinoethane	0.99	3.85	20 °C (RT), 1 h; 1.5 mL CHCl$_3$

6.3.2.1 DETA

Desmodur® W (1.77 mL, 6.86 mmol) was added to DETA (0.500 mL, 4.58 mmol) and mixed manually at room temperature or 0 °C. The reaction mixture solidified immediately.

6.3.2.2 TEG

Desmodur® W (1.00 mL, 3.87 mmol) was added to TEG (0.52 mL, 3.8 mmol) and mixed manually at room temperature. The reaction mixture was applied to a Leneta Form 5DX Brushout card using the standard draw-down method with a bar film applicator (1120/25/100, S232228, Sheen; **Figure 6.2**), and the film was cured at 70 °C for 19 h.

6.3.2.3 TEG/DETA

Desmodur® W (1.00 mL, 3.87 mmol) was added to TEG (0.47 mL, 3.5 mmol) and DETA (0.03 mL, 0.3 mmol) and mixed manually at room temperature. The application of the reaction mixture to a Leneta Form 5DX Brushout card using the standard draw-down method with a bar film applicator (1120/25/100, S232228, Sheen; **Figure 6.2**) was attempted.

6.3.2.4 1,2-Dianilinoethane

Desmodur® W (1.00 mL, 3.87 mmol) was added to 1,2-dianilinoethane (0.834 g, 3.85 mmol) in chloroform (1.5 mL) and stirred for 1 h at room temperature.
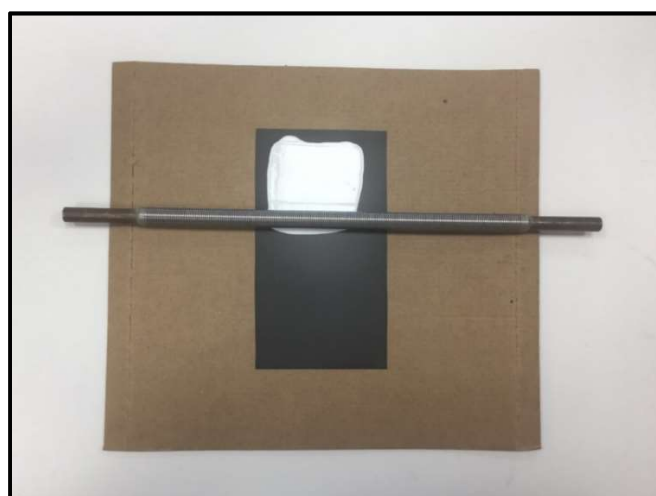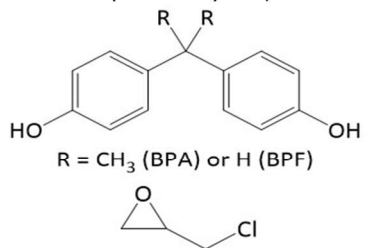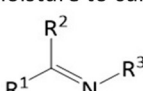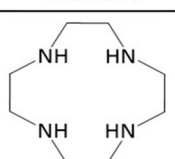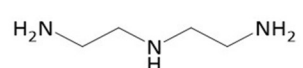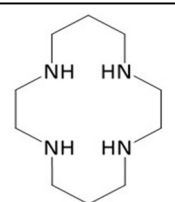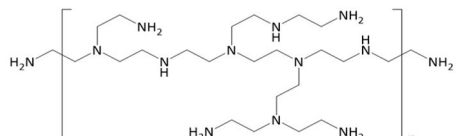

Figure 6.2. Demonstration of the standard draw-down technique with a bar film applicator.

6.3.3 Cu(II) Ligands in an Epoxy Coating

The epoxy resin, hardeners, and surface ligands used in this study are described in **Table 6.5**, and the prepared epoxy coatings are listed in **Table 6.6**.

Table 6.5. Descriptions of epoxy resin, hardeners, and surface ligands used in this study.

Name	Component	Description	WPE[a]	AHEW[b] (phr[c])
Epikote™ Resin 235[d]	epoxy resin	blend of BPA resin (BPA and epichlorohydrin) and BPF resin (BPF and epichlorohydrin) R = CH$_3$ (BPA) or H (BPF) epichlorohydrin	177–182	-
Ancamine® 2459 Curing Agent[e]	hardener	polyamine; ketimine-protected; requires moisture to cure ketimine	-	101 (56.3)
Cyclen	hardener, surface ligand		-	43.1 (24.0)
DETA	hardener, surface ligand		-	20.6 (11.5)
Cyclam	hardener, surface ligand		-	50.1 (27.9)
PEI	surface ligand		-	-

[a] Weight *per* epoxide (WPE) is the grams of resin *per* one gram-equivalent of epoxy groups (g/eq).
[b] Amine hydrogen equivalent weight (AHEW) is the grams of hardener *per* one gram-equivalent of active amine hydrogens (g/eq).
[c] *Per* hundred resin (phr) is the grams of hardener *per* 100 g epoxy resin.
[d] Proprietary composition and specific components confidential to Resolution Performance Products.
[e] Proprietary composition and specific components confidential to Air Products and Chemicals, Inc.

Table 6.6. Epoxy coatings prepared with epoxy resin Epikote™ 235 and the following hardeners: Ancamine® 2459, cyclen, DETA, and cyclam.

Hardener	Surface Functionalisation	% w/w Overcure (+)/Undercure (-)[a]
Ancamine® 2459	-	-50%, -40%, -30%, -20%, -10%, stoichiometric, +10%, +20%, +50%
Ancamine® 2459	cyclam	**-50%**, **-40%**, **-30%**, **-20%**, -10%
Ancamine® 2459	cyclen	**-40%**
Ancamine® 2459	DETA	**-40%**, **-30%**
Ancamine® 2459	PEI	**-40%**
Ancamine® 2459, cyclen	-	+10%, +20% (cyclen[b])
Ancamine® 2459, DETA	-	+10%, +20% (DETA[c])
Cyclen	-	-20%, -10%, stoichiometric, +10%, +20%
DETA	-	-20%, -10%, stoichiometric, +10%, +20%
DETA (75%), cyclen (25%)[d]	-	stoichiometric
DETA (50%), cyclen (50%)[e]	-	stoichiometric
DETA (25%), cyclen (75%)[f]	-	stoichiometric
DETA (25%), cyclen (100%)[g]	-	+25%
DETA (100%), cyclen (25%)[h]	-	+25%
Cyclam	-	-20%, stoichiometric, +20%

[a] The coatings in **bold** were surface-functionalised, and the coatings in red were determined to be strongly Cu(II)-chelating films based on colour intensity.
[b] Stoichiometric amount of Ancamine® 2459 but overcured with cyclen.
[c] Stoichiometric amount of Ancamine® 2459 but overcured with DETA.
[d] Enough DETA and cyclen added as hardeners to react with 75% and 25% of the epoxy groups, respectively.
[e] Enough DETA and cyclen added as hardeners to each react with half of the epoxy groups.
[f] Enough DETA and cyclen added as hardeners to react with 25% and 75% of the epoxy groups, respectively.
[g] Stoichiometric amount of cyclen but overcured with DETA.
[h] Stoichiometric amount of DETA but overcured with cyclen.

6.3.3.1 Preparation of Epoxy Coatings

A two-pack epoxy was prepared by manually mixing a commercial hardener (Ancamine® 2459 Curing Agent; Air Products and Chemicals, Inc.) and a commercial epoxy resin (Epikote™ 235; Resolution Performance Products) stoichiometrically, in accordance with the manufacturers' specifications: *per* hundred resin (phr) = 56.3 g Ancamine® 2459 *per* 100 g Epikote™ 235 (example calculation in the Appendix, **Scheme 8.1**). Ancamine® 2459 is slow-curing, requiring moisture for deprotection of the ketimine-protected amine group before reacting with an epoxy group (**Scheme 6.7**). Alternative and/or additional polyamine hardeners that could also serve as Cu(II) ligands (*e.g.* cyclen, DETA, and cyclam) were mixed manually with Epikote™ 235. These hardeners and combinations are displayed in **Table 6.6**, and the phr values are listed in **Table 6.5**, showing the amount of each hardener required to mix stoichiometrically with 100 g of Epikote™ 235. For the coatings using cyclen as a hardener, cyclen was dissolved in the minimum amount of methanol (0.8–2.2 mg/µL) before mixing with Epikote™ 235, and, for the coatings using cyclam as a hardener, cyclam was dissolved in the minimum amount of 2:1 v/v chloroform:methanol (~0.3 mg/ µL) before mixing with Epikote™ 235. DETA was used neat. In the particular cases tabulated, the amounts of hardener were varied up to ±50% w/w and mixed manually with Epikote™ 235. All of the coatings were applied to a Leneta Form 5DX Brushout card using the standard draw-down method with a bar film applicator (1120/25/100, S232228, Sheen), demonstrated in **Figure 6.2**, and they were cured overnight at room temperature.
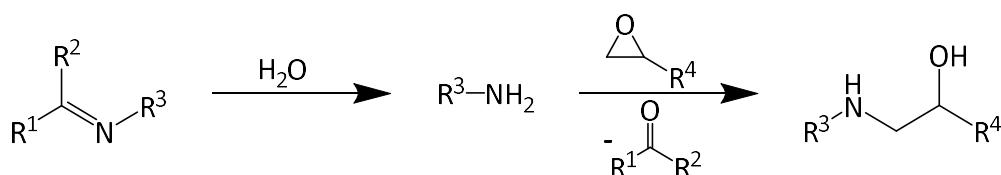
Scheme 6.7. Curing process for Ancamine® 2459: ketimine deprotection of an amine, which then reacts with an epoxide. A side product of the deprotection is a volatile ketone.

6.3.3.2 Surface-Functionalisation of Epoxy Coatings

As in **Table 6.6**, the surfaces of the epoxy coatings undercured with Ancamine® 2459 were functionalised with cyclam, cyclen, DETA, and PEI:

Cyclam (51 mg, 0.25 mmol) was dissolved in 2:1 v/v water:methanol (750 µL), and then an aliquot (125 µL) of the solution was added to a defined surface area of each of the following

coatings: -50%, -40%, -30%, and -20% w/w epoxy coatings (Ancamine® 2459 and Epikote™ 235). The aliquots were left on the coatings overnight (~16 h), and then the coatings were washed with water.

Cyclen (60 mg, 0.35 mmol) was dissolved in water (300 µL) and added to cover a defined surface area of the -40% w/w epoxy coating (Ancamine® 2459 and Epikote™ 235). After 24 h, the aliquot was removed *via* pipetting, and the coating was washed with water.

DETA was added neat to the -40% and -30% w/w epoxy coatings (Ancamine® 2459 and Epikote™ 235), covering a defined surface area for 24 h before removal *via* pipetting. Then, the coatings were washed with water.

PEI (branched, average M_w ~800, average M_n ~600; Sigma-Aldrich) was added neat to the -40% w/w epoxy coating (Ancamine® 2459 and Epikote™ 235), covering a defined surface area for 24 h before removal *via* pipetting. Then, the coating was washed with water.

6.3.3.3 Application of Cu(II) to Epoxy Coatings

To each prepared epoxy coating, including the surface-functionalised areas, a drop of aqueous copper(II) nitrate (50 mM; 20 µL) was added with an Eppendorf pipette for 2–6.5 h. Then, the coatings were washed with water.

6.3.3.4 Quantification of Cu(II)-Loading

The epoxy coatings assessed for Cu(II)-loading were prepared as in **Section 6.3.3.1** and were as follows: Ancamine® 2459 and Epikote™ 235 (stoichiometric), cyclen and Epikote™ 235 (±20% w/w, +10% w/w, stoichiometric), Ancamine® 2459/cyclen and Epikote™ 235 (+20% w/w, +10% w/w), DETA (25%)/cyclen (100%) and Epikote™ 235 (+25% w/w), and DETA (100%)/cyclen (25%) and Epikote™ 235 (+25% w/w). With the exception of stoichiometric Ancamine® 2459/Epikote™ 235, these are the supposed strongly Cu(II)-chelating films highlighted in red in **Table 6.6**. Glass vials were washed with water (3×) and air-dried. Each prepared epoxy coating (150 ± 10 mg) was delivered to the bottom of a vial and cured uncapped at 50 °C and 50% humidity for 24 h. Once cured, the coatings were washed with water (3×) and air-dried, and the mass and exposed surface area (Appendix, **Figure 8.38**) of each coating were recorded. Aqueous copper(II) nitrate (50 mM; 500 µL/vial) was added to the vials, which sat capped at room temperature. Water (500 µL/vial) was added to the vials serving as blanks. After 24 h, the coatings were washed with water (3×) and air-dried. In preparation for ICP-MS (Cu) analysis,

concentrated nitric acid (70% v/v, aq; 500 μL) was added to each vial, and the vials were heated at 70 °C for 2 h to digest the resin and release the copper into solution. The digested solutions were diluted 1,000–10,000× with 3% v/v aq nitric acid, bringing them into the range of the ICP-MS standards. If any particles were observed in a dilution, the sample was centrifuged for 10 min at 1788 RCF. The copper retained by each coating was quantified *via* ICP-MS analysis.

6.4 Chapter 4

6.4.1 Silica Functionalisation
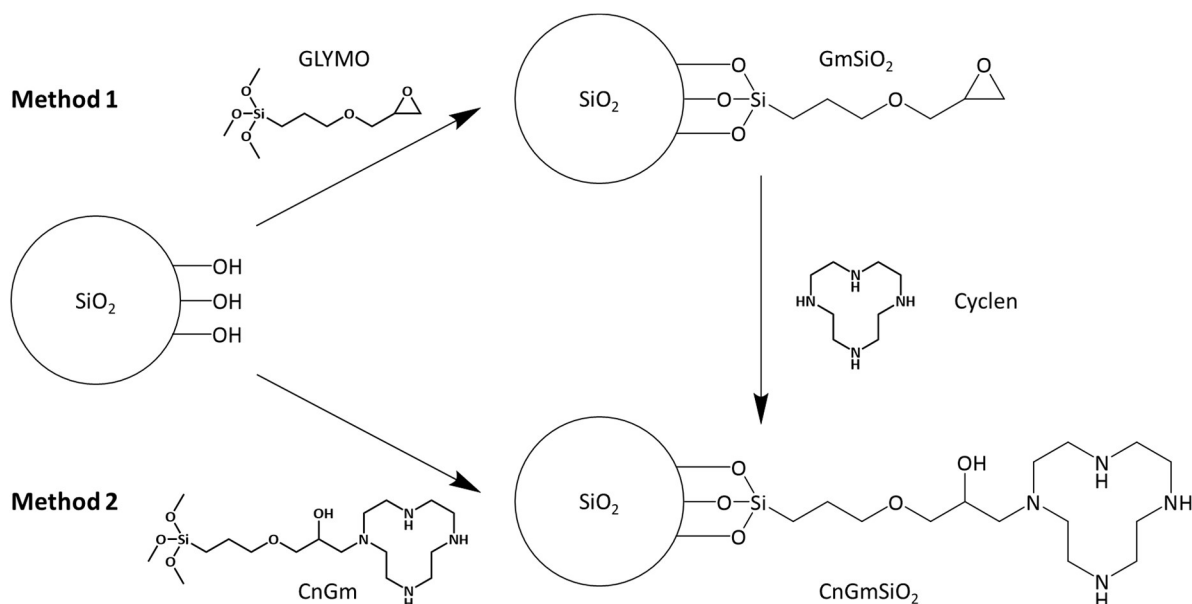
Scheme 6.8. Two silica functionalisation methods. Method 1: Reaction between GLYMO and the silanol groups of silica (SiO$_2$) produces GLYMO-functionalised silica (GmSiO$_2$), and then the reaction between GmSiO$_2$ and cyclen produces cyclen-GLYMO-silica (CnGmSiO$_2$). **Method 2:** GLYMO and cyclen react first to produce cyclen-GLYMO (CnGm), and then CnGm reacts with silica to produce CnGmSiO$_2$.

6.4.1.1 Method 1

6.4.1.1.1 Synthesis of GmSiO$_2$

Reaction conditions in the procedures for silica-functionalisation with GLYMO (**Scheme 6.9**) are summarised in **Table 6.7**.
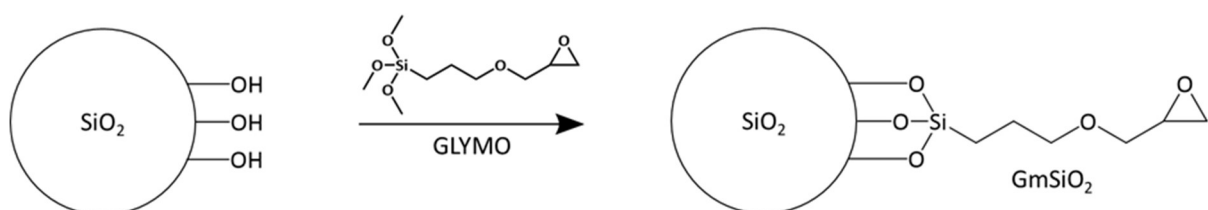
Scheme 6.9. Synthesis of GmSiO$_2$.

Table 6.7. Reaction conditions in Procedures 1–4 for $GmSiO_2$ synthesis.

Conditions	Procedure 1	Procedure 2	Procedure 3	Procedure 4
SiO_2 (g)	0.91 (dry)	1.02 (dry)	1.00 (wet)	2.50 (dry)
GLYMO (g, mmol)	0.27, 1.1	2.1, 9.1	4.3, 18	3.7, 16
Anhydrous toluene (mL)	5	4	-	35
Triethylamine (µL)	-	-	-	75
Temperature (°C)	20 (RT)	80	100	110.6 (reflux)
Time (h)	24	72	69	42

Procedure 1

GLYMO (0.25 mL, 1.1 mmol) was added to silica (0.91 g) in anhydrous toluene (5 mL) under argon, and the reaction mixture was stirred 24 h at room temperature. The white silica product (0.97 g) was filtered, washed with anhydrous toluene (6 × 10 mL), and dried by rotary evaporation for 30 min.

IR: *Silica* – v_{max}/cm^{-1} 3351w (br, O–H stretching), 1063s (br, Si–O–Si asymmetric stretching), 964m (br, Si–OH stretching), 794m (br, Si–O–Si symmetric stretching);[262,333,334] *GLYMO* – v_{max}/cm^{-1} 2943m and 2841m (C–H stretching in Si–O–CH$_3$ and CH$_2$), 1467vw (C–H in-plane rocking in Si–O–CH$_3$ and CH$_2$), 1254vw (Si–C bending), 1191m (C–O stretching of aliphatic ether), 1076vs (Si–O–C stretching), 909w (epoxy ring C–O stretching), 816s (Si–C stretching);[335] *Procedure 1 GmSiO$_2$* – v_{max}/cm^{-1} 1060s (br, Si–O–Si asymmetric stretching), 953m (br, Si–OH stretching), 801m (br, Si–O–Si symmetric stretching).[262,333,334]

Procedure 2

GLYMO (2.0 mL, 9.1 mmol) was added to silica (1.02 g) in anhydrous toluene (4 mL) under argon, and the reaction mixture was stirred 72 h at 80 °C. The white silica product (1.18 g) was filtered, washed with anhydrous toluene (6 × 10 mL), and dried *via* rotary evaporation.

IR: v_{max}/cm^{-1} 1058s (br, Si–O–Si asymmetric stretching), 948vw (br, Si–OH stretching), 908vw (br, epoxy ring C–O stretching), 797m (br, Si–O–Si symmetric stretching), 729m, 694w.

Procedure 3

In this procedure, the silica was used without drying. GLYMO (4.0 mL, 18 mmol) was added to silica (1.00 g), and the reaction mixture was stirred 69 h at 100 °C. The white silica product (1.40 g) was filtered, washed with toluene (80 mL), and dried by rotary evaporation.

IR: v_{max}/cm^{-1} 1049s (br, Si–O–Si asymmetric stretching), 914w (br, epoxy ring C–O stretching), 796m (br, Si–O–Si symmetric stretching).

Procedure 4

Protocols by Bagnoud *et al.*[255] and Gros *et al.*[241] were followed. GLYMO (3.5 mL, 16 mmol) and triethylamine (75 μL, 0.54 mmol) were added to silica (2.50 g) in anhydrous toluene (35 mL) under argon, and the reaction mixture was stirred and heated to reflux temperature for 42 h. The pale-yellow silica product (3.17 g) was filtered, washed (70 mL anhydrous toluene, 100 mL acetone, 100 mL ether), and dried *via* rotary evaporation.

IR: v_{max}/cm^{-1} 1066s (br, Si–O–Si asymmetric stretching), 920vw (br, epoxy ring C–O stretching), 801m (br, Si–O–Si symmetric stretching).

6.4.1.1.2 End-Capping GmSiO$_2$
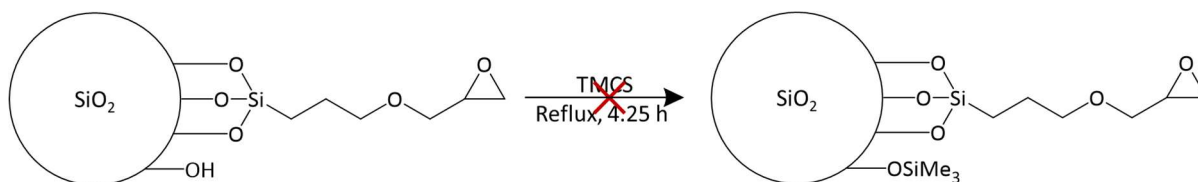
Scheme 6.10. Attempted end-capping of GmSiO$_2$.

Following the protocol by Gros *et al.*[241] (**Scheme 6.10**), GmSiO$_2$ from Procedure 4 (2.95 g) suspended in trimethylchlorosilane (TMCS; 12 mL, 92 mmol) was heated to reflux temperature for 4.25 h under argon. The silica product (2.93 g) was vacuum-filtered to remove excess TMCS, washed with water to neutral pH, and dried for 18 h under high vacuum (0.2–1.5 mmHg).

IR: v_{max}/cm^{-1} 1059s (br, Si–O–Si asymmetric stretching), 793m (br, Si–O–Si symmetric stretching).

6.4.1.1.3 Synthesis of CnGmSiO$_2$
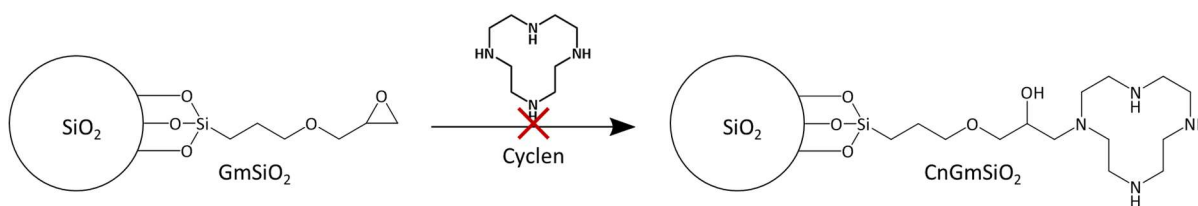
Scheme 6.11. Attempted synthesis of CnGmSiO$_2$.

CnGmSiO$_2$ was synthesised following the procedure by Gros *et al.*[241] (**Scheme 6.11**). A solution of cyclen (0.59 g, 3.3 mmol) in water (59 mL) was added to the end-capped GmSiO$_2$ (2.93 g) from Procedure 4. The suspension was heated at 80 °C for 48 h without stirring but was occasionally mixed by gentle swirling, thus preventing damage to the particles. After 48 h, the product (2.95 g) was filtered to remove excess cyclen and was washed with dilute hydrochloric acid (0.1 M, aq; 2 × 10 mL), water (until the filtrate no longer turned a dark blue colour upon the addition of 50 mM aq copper(II) sulfate), and hot methanol.

IR: v_{max}/cm^{-1} 1055s (br, Si–O–Si asymmetric stretching), 950m (br, Si–OH stretching), 789m (br, Si–O–Si symmetric stretching).

6.4.1.2 Method 2

6.4.1.2.1 Synthesis of Cn(Gm)$_n$

Reaction conditions in the procedures for Cn(Gm)$_n$ synthesis (**Scheme 6.12**) are summarised in **Table 6.8**.

Table 6.8. Reaction conditions in Procedures 1–6 for Cn(Gm)$_n$ synthesis.

Conditions	Procedure 1	Procedure 2	Procedure 3	Procedure 4	Procedure 5	Procedure 6
GLYMO (mmol)	4.4	1.1	2.3	1.1	1.1	8.9
Cyclen (mmol, eq)	1.1, 0.26	4.8, 4.3	0.56, 0.25	1.2, 1.1	1.2, 1.1	9.7, 1.1
Al(OTf)$_3$ (mmol)	-	-	-	0.1	0.1	-
Solvent	2:1 MeOH:H$_2$O	toluene	toluene	CHCl$_3$	CDCl$_3$	CHCl$_3$
Volume solvent (mL)	23.8	7.5	10	2	2	16
Temperature (°C)	20 (RT)	110.6 (reflux)	110.6 (reflux)	20 (RT)	20 (RT)	20 (RT)
Time	5 h	24 h	97.5 h	90 h	69 h	8–10 days
References	Bereczki *et al.*[258]	Barreto *et al.*[259]	Barreto *et al.*[259]	Williams and Cullen[266]	Williams and Cullen[266]	-
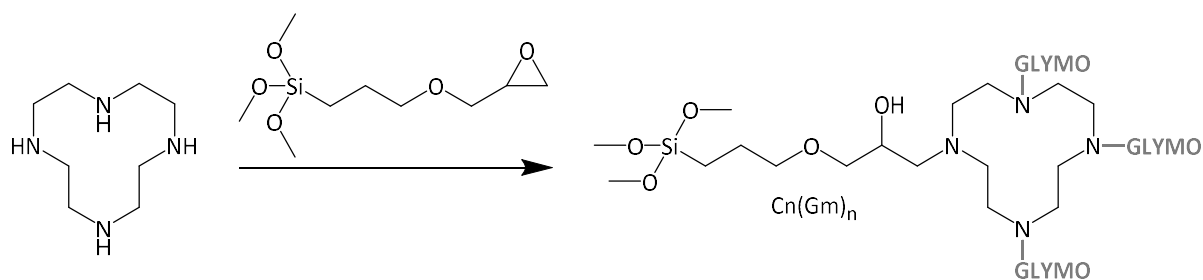
Scheme 6.12. Synthesis of Cn(Gm)$_n$.

Procedure 1

Following the procedure by Bereczki *et al.*[258], GLYMO (1.0 mL, 4.4 mmol, 3.9 eq) was added to cyclen (0.20 g, 1.1 mmol) dissolved in a solution of water (8 mL) and methanol (15.8 mL) under argon, and the reaction mixture was stirred at room temperature for 5 h. In order to monitor the reaction by ^{1}H NMR spectroscopy, an aliquot (1 mL) of the crude reaction was dried by rotary evaporation and dissolved in a deuterated solvent. However, the residue was insoluble in a range of solvents (2:1 v/v CD$_3$OD:D$_2$O, CHCl$_3$, H$_2$O, DMSO, 1:1 v/v DCM:MeOH). Therefore, test reactions in NMR tubes were set up to monitor the reaction. An aliquot (5 mL) of an aqueous solution of copper(II) acetate (0.24 M; teal solution) was added to the reaction mixture, and immediate complexation was evidenced by a colour change from teal to dark blue.

Test Reaction 1

GLYMO (0.040 mL, 0.18 mmol, 3.9 eq) was added to cyclen (0.008 g, 0.05 mmol) dissolved in a solution of deuterium oxide (0.322 mL) and methanol-d_4 (0.635 mL), and the reaction was monitored by ^{1}H NMR spectroscopy for 2 h. The ^{1}H NMR spectra revealed that the majority of GLYMO remained unreacted in this time period.

Test Reaction 2

GLYMO (0.030 mL, 0.13 mmol, 4.6 eq) was added to cyclen (0.005 g, 0.03 mmol) dissolved in a solution of deuterium oxide (0.242 mL) and methanol-d_4 (0.476 mL), and the reaction was monitored by ^{1}H NMR spectroscopy for 24 h. The ^{1}H NMR spectra revealed that the majority of GLYMO remained unreacted in this time period.

Procedure 2

Following the procedure by Barreto *et al.* [259], GLYMO (0.26 mL, 1.1 mmol) in toluene (5 mL) was added dropwise to a solution of cyclen (0.84 g, 4.8 mmol, 4.3 eq) in hot toluene (7.5 mL). The reaction mixture

was heated to reflux temperature for 24 h and then cooled to room temperature to precipitate the excess cyclen, which was removed by filtration and washed with cold toluene (25 mL). The toluene filtrate was evaporated to dryness *via* rotary evaporation, and the residual solid was dissolved in chloroform (10 mL), washed with sodium hydroxide (0.1 M, aq; 2 × 5 mL), dried over magnesium sulfate, filtered, and concentrated to yield the product as a colourless oil (0.32 g, 44% if Cn(Gm)$_2$–70% if CnGm). The reaction was monitored for the disappearance of GLYMO by TLC and ^{1}H NMR spectroscopy.

^{1}H NMR (500 MHz, CDCl$_3$): δ 4.31–4.11 (m, 1H), 3.86 (dd, *J* = 10.8, 2.9 Hz, 1H), 3.66–3.59 (m, 1H), 3.57 (s, 2H), 3.56–3.33 (m, 5H), 3.21 (t, *J* = 10.4 Hz, 1H), 2.88–2.72 (m, 5H), 2.69 (s, 4H), 2.68–2.39 (m, 14H), 2.14–1.88 (m, 1H), 1.86–1.75 (m, 1H), 1.75–1.58 (m, 1H), 1.19–0.93 (m, 1H), 0.91–0.51 (m, 2H). **ESI-MS m/z (rel intensity):** 605.3 (34), 604.3 (66), 603.3 (82, [3GLYMO - CH$_3$ + 2H]$^+$), 589.3 (21, [3GLYMO - 2CH$_3$ + 3H]$^+$), 583.3 (59), 582.3 (95), 581.3 (100), 567.3 (21), 558.3 (29), 557.2 (61), 535.3 (45), 424.2 (17), 399.2 (18, [2GLYMO - 2CH$_3$ + 3H]$^+$), 378.3 (21), 377.3 (74), 291.3 (82), 284.3 (21), 275.2 (45), 268.2 (39), 212.7 (32), 189.2 (59), 173.2 (20, [cyclen + H]$^+$).

Procedure 3

Following the procedure by Barreto *et al.*[259] with modification, GLYMO (0.51 mL, 2.3 mmol, 4.0 eq) in toluene (5 mL) was added dropwise to a solution of cyclen (0.10 g, 0.56 mmol) in hot toluene (5 mL). The reaction mixture was heated to reflux temperature for 97.5 h and then cooled to room temperature. The product was concentrated by rotary evaporation, dried further with a high vacuum pump (0.2–1.5 mmHg) at room temperature, and, subsequently, formed a highly insoluble, intractable solid.

Procedure 4

Based on the procedure by Williams and Cullen[266], GLYMO (0.25 mL, 1.1 mmol) was added dropwise to a mixture of cyclen (0.22 g, 1.2 mmol, 1.1 eq) and Al(OTf)$_3$ (0.05 g, 0.1 mmol) in anhydrous chloroform (2 mL) at room temperature under dry conditions and argon. An aliquot of the reaction mixture (150 µL) was sampled 67 h later and prepared for ^{1}H NMR analysis by the addition of sodium bicarbonate (saturated, aq; 1 mL), extraction with dichloromethane (2 mL), washing of the organic layers with water (2 mL), drying over magnesium sulfate, filtration, concentration, and dissolution in chloroform-*d*. The reaction mixture was stirred for 90 h total and then was quenched by the addition of sodium bicarbonate (saturated, aq; 5 mL) and extracted with dichloromethane (3 × 5 mL). Washing the combined organic layers with water (2 × 10 mL) resulted in the precipitation of a white solid. The organic layers were concentrated, yielding a clear, intractable, plastic-like film.

Procedure 5

Based on the procedure by Williams and Cullen[266], GLYMO (0.25 mL, 1.1 mmol) was added dropwise to a mixture of cyclen (0.22 g, 1.2 mmol, 1.1 eq) and Al(OTf)$_3$ (0.06 g, 0.1 mmol) in anhydrous chloroform-*d* (2 mL) at room temperature under dry conditions and argon. The reaction was monitored by ^{1}H NMR spectroscopy by diluting an aliquot of the crude reaction mixture (40 µL) with chloroform-*d* (650 µL). The reaction mixture was stirred for 69 h until the reaction was complete, as determined by ^{1}H NMR spectroscopy. An aliquot of the completed reaction mixture (100 µL) was prepared for ^{1}H NMR analysis by the addition of chloroform-*d* (700 µL) and sodium carbonate (10% w/w, aq; 5 mL), drying of the organic layer over magnesium sulfate, and filtration. Attempts to concentrate the reaction mixture produced a clear, intractable, plastic-like film.

^{1}H NMR (500 MHz, CDCl$_3$): δ 3.89 (s, 1H), 3.56 (s, 6H), 3.43 (s, 6H), 3.00–2.71 (m, 3H), 2.71–2.61 (m, 4H), 2.61–2.10 (m, 5H), 1.88–1.47 (m, 2H), 0.84–0.39 (m, 2H). **ESI-MS *m/z* (rel intensity):** 904.5 (26), 903.5 (48), 889.5 (19), 858.4 (22), 857.4 (41), 843.4 (28), 688.4 (46), 687.4 (93), 645.4 (100, [Cn(Gm)$_2$ + H]$^+$), 631.4 (57), 621.3 (63), 599.3 (74), 585.3 (46), 571.3 (22), 441.4 (19, [Cn(Gm)$_3$ + 2H]$^{+2}$]), 409.3 (56, [CnGm + H]$^+$), 395.3 (81), 381.2 (67, [CnGm - 2CH$_3$ + 3H]$^+$), 367.2 (70, [CnGm - 3CH$_3$ + 4H]$^+$), 323.3 (65, [Cn(Gm)$_2$ + 2H]$^{+2}$]), 316.3 (43), 284.3 (24), 173.2 (19, [cyclen + H]$^+$), 166.2 (15).

Procedure 6

GLYMO (2.0 mL, 8.9 mmol) was added dropwise to a solution of cyclen (1.73 g, 9.74 mmol, 1.12 eq) in anhydrous chloroform (16 mL) at room temperature under dry conditions and an argon atmosphere. The reaction was monitored by ^{1}H NMR spectroscopy by diluting an aliquot of the crude reaction mixture (40 µL) with chloroform-*d* (650 µL), and the reaction mixture, which was clear with a faint yellow tinge, was stirred for 8–10 days until the closed epoxide of GLYMO was undetectable by ^{1}H NMR spectroscopy. The crude material was used without purification.

^{1}H NMR (500 MHz, CDCl$_3$): δ 3.91–3.72 (m, 1H), 3.58–3.51 (m, 3H), 3.51–3.46 (m, 2H), 3.46–3.24 (m, 7H), 2.91–2.66 (m, 4H), 2.64 (s, 5H), 2.60 (s, 4H), 2.56–2.15 (m, 6H), 1.82–1.42 (m, 2H), 0.78–0.42 (m, 2H); **^{13}C NMR** (126 MHz, CDCl$_3$): δ 73.5, 73.3, 68.6, 58.1, 52.8, 50.6, 50.4, 47.3, 46.6, 46.1, 45.7, 24.1, 22.9, 22.8, 7.3, 6.8, 5.4, 5.3. **ESI-HRMS:** calcd for C$_{17}$H$_{41}$N$_4$O$_5$Si [M + H]$^+$ 409.2846; found 409.2843; **ESI-MS *m/z* (rel intensity):** 645.4 (4, [Cn(Gm)$_2$ + H]$^+$), 613.4 (9), 599.4 (18), 585.3 (5), 488.3 (3), 411.3 (3), 410.3 (16), 409.3 (100, [CnGm + H]$^+$), 377.3 (51), 367.2 (6, [CnGm - 3CH$_3$ + 4H]$^+$), 279.1 (12), 252.1 (3), 225.8 (6), 173.2 (51, [cyclen + H]$^+$), 142.0 (31).

6.4.1.2.2 Synthesis of ± Cu(II)-CnGmSiO$_2$
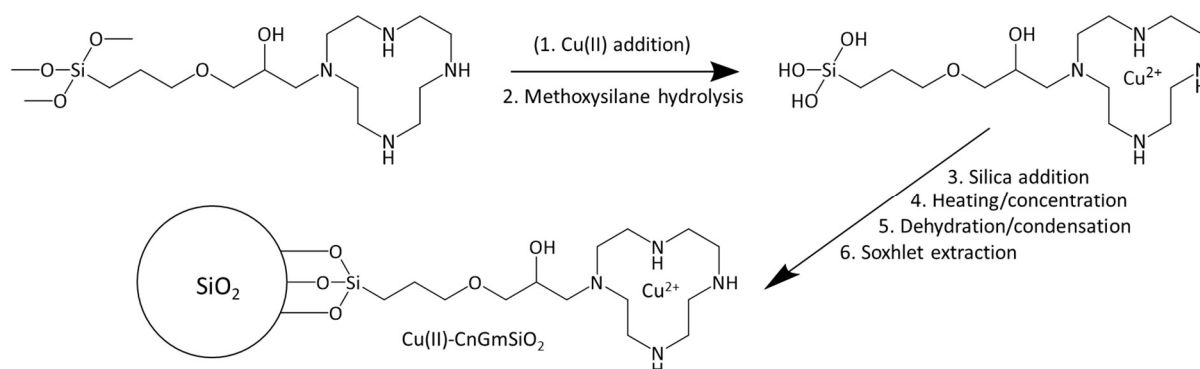
Scheme 6.13. Synthesis of ± Cu(II)-CnGmSiO$_2$.

In order to synthesise Cu(II)-CnGmSiO$_2$ (**Scheme 6.13**), Cu(II) may be added first to produce the Cu(II)-CnGm complex **(1)**. Then, hydrolysis of the methoxysilane groups **(2)** is followed by the addition of silica **(3)** and heating and concentration **(4)** to drive the dehydration/condensation reaction **(5)**. Finally, the ± Cu(II)-CnGmSiO$_2$ product is washed *via* Soxhlet extraction **(6)**.

Batch 1: Cu(II)-CnGmSiO$_2$

Aqueous copper(II) nitrate (0.3 M; 20 mL) was added to the reaction mixture (approximately 1.8 g or 4.3 mmol CnGm in 7.8 mL CHCl$_3$) from implementation of scaled-down Procedure 6 for CnGm synthesis. The organic layer was extracted further with aqueous copper(II) nitrate (0.3 M; 2 × 10 mL) and washed with water until it was no longer a blue colour (5 × 5 mL). The organic layer was analysed by ^{1}H NMR spectroscopy (1:1 v/v CDCl$_3$:CD$_3$OD). Aqueous ammonium hydroxide (1% v/v; 3.55 mL) was added to the isolated, dark blue aqueous layer and vortexed, and a sample was analysed by MS. Then, silica (14.60 g) was added, and the mixture was vortexed and concentrated under vacuum at 70 °C for 1 h. The royal blue Cu(II)-CnGmSiO$_2$ product (16.687 g) was washed *via* Soxhlet extraction with water for 24 h, dried at 120 °C for 2 h, and submitted for CHN elemental and IPC-MS (Cu) analyses.

ESI-HRMS: calcd for C$_{14}$H$_{31}$CuN$_4$O$_4$Si [M - H$_2$O]$^+$ 410.1411; found 410.1364; **ESI-MS *m/z* (rel intensity):** 607.2 (3), 606.2 (8), 604.2 (14), 431.2 (4), 430.1 (16), 428.1 (30, [Cu(II)-CnGm - 3CH$_3$ + 2H]$^+$), 410.1 (24, [Cu(II)-CnGm - 3CH$_3$ - H$_2$O + 3H]$^+$), 311.6 (3), 304.1 (6), 303.6 (18), 302.6 (30), 293.6 (5), 233.1 (2), 216.1 (10), 215.6 (54), 214.6 (100, [Cu(II)-CnGm - 3CH$_3$ + 3H]$^{2+}$), 205.6 (38), 190.0 (27), 117.5 (16, [Cu(II)-cyclen]$^{2+}$). **CHN:** *Silica* – found C, < 0.30%; H, 0.96%; N, < 0.30%; *Batch 1 Cu(II)-CnGmSiO$_2$* – found C,

1.80%; H, 0.77%; N, 0.47%. **ICP-MS:** *Silica* – < 0.0001% w/w Cu; *Batch 1 Cu(II)-CnGmSiO₂* – 0.48% w/w Cu.

Batch 2: Cu(II)-CnGmSiO₂

Copper(II) nitrate in methanol (0.25 M; 50 mL) was added to the reaction mixture (approximately 3.6 g or 8.8 mmol CnGm in 15.8 mL CHCl₃) from Procedure 6 for CnGm synthesis. A sample of the dark blue solution of Cu(II)-CnGm was analysed by MS. Methoxysilane hydrolysis followed the procedure by Lu[269]. Methanol (67.57 mL), aqueous ammonium hydroxide (28% v/v; 5 mL), and silica (26.68 g) were added to the reaction mixture, which was stirred and heated for 1 h at 60 °C. The mixture was concentrated under vacuum at 70 °C for 1 h, and the royal blue Cu(II)-CnGmSiO₂ product (28.57 g) was washed by Soxhlet extraction with water for 24 h, dried, and submitted for CHN elemental and ICP-MS (Cu) analyses.

The samples were prepared for ICP-MS analysis as follows: the mass of the silica sample (~50 mg) in a pre-cleaned Teflon beaker was recorded to five decimal-points, as were all other masses, and a few drops of concentrated nitric acid (67–69% v/v) were added to wet the sample. Concentrated hydrofluoric acid (48% v/v; 2 mL) was added, and the sample was capped and heated at reflux temperature for 3 days. Then, the sample was evaporated to dryness, nitric acid (9M; 2 mL) was added, and the sample was capped and heated at reflux temperature overnight. Again, the sample was evaporated to dryness, nitric acid (9M; 2 mL) was added, and the sample was capped and heated at reflux temperature until complete dissolution. The solution was transferred to a pre-cleaned polypropylene bottle, and water was added to the bottle until the recorded mass was approximately 50 g. If required, the sample was diluted further for analysis by diluting an aliquot (~100 mg) of the solution in a centrifuge tube with nitric acid (3% v/v; ~10 mL final volume).

ESI-HRMS: calcd for $C_{17}H_{39}CuN_4O_5Si$ $[M - H]^+$ 470.1986; found 470.1978; **ESI-MS *m/z* (rel intensity):** 927.3 (2), 895.3 (3), 835.4 (6), 833.4 (8), 819.4 (2), 709.2 (1), 662.3 (3), 648.2 (7), 646.2 (8), 618.2 (4), 529.2 (2), 473.2 (3), 471.2 (6), 470.2 (3, $[Cu(II)\text{-}CnGm - H]^+$), 458.2 (9), 456.2 (16, $[Cu(II)\text{-}CnGm - CH_3]^+$), 442.2 (9, $[Cu(II)\text{-}CnGm - 2CH_3 + H]^+$), 428.2 (6, $[Cu(II)\text{-}CnGm - 3CH_3 + 2H]^+$), 424.2 (10), 330.6 (4), 324.6 (7), 316.6 (11), 307.6 (7), 234.1 (9), 214.6 (12), 212.6 (15), 192.0 (25), 190.0 (55), 145.0 (100). **CHN:** found C, 4.17%; H, 0.92%; N, 1.18%. **ICP-MS:** 2.60% w/w Cu.

Batch 3: CnGmSiO₂

The Batch 2 procedure was followed without the addition of copper(II) nitrate, and methoxysilane hydrolysis followed the procedure by Lu[269]. Methanol (57.30 mL), aqueous ammonium hydroxide (28% v/v; 2.5 mL), and silica (13.00 g) were added to the reaction mixture (approximately 1.7 g or

4.3 mmol CnGm in 7.7 mL CHCl₃) from implementation of scaled-down Procedure 6 for CnGm synthesis. The mixture was heated while stirring for 1 h at 60 °C and then dried *via* rotary evaporation for 1 h. The white CnGmSiO$_2$ product (16.03 g) was washed by Soxhlet extraction with water for 24 h, dried, and submitted for CHN elemental analysis.

CHN: found C, 4.52%; H, 1.22%; N, 1.24%.

Batch 4: CnGmSiO$_2$

The procedure from Batch 3 was repeated exactly, and the white CnGmSiO$_2$ product (16.28 g) was submitted for CHN elemental analysis.

CHN: found C, 4.81%; H, 0.94%; N, 1.46%.

6.4.1.2.3 Study of GLYMO Hydrolysis

The hydrolytic stability of GLYMO (**Scheme 6.14**) was tested under basic conditions, with and without heating, and in various solvents and solvent combinations.
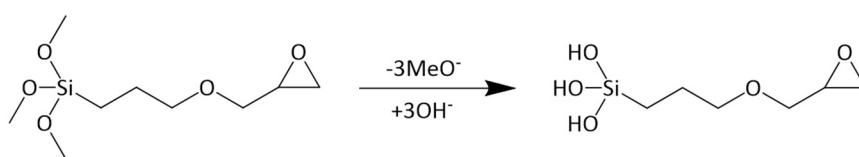
Scheme 6.14. Hydrolysis of GLYMO methoxysilane groups.

CDCl$_3$, RT

GLYMO (20 mg, 0.085 mmol) was added to chloroform-*d* (700 μL), and the ¹H NMR spectrum was acquired immediately, as well as after 6 days sitting at room temperature.

CD$_3$OD, 60 °C

GLYMO (27 mg, 0.11 mmol) was added to methanol-*d$_4$* (800 μL), and the solution was heated for 2 days at 60 °C. The ¹H NMR spectrum was acquired at 19 h and 40 h.

Batch 1 Conditions: 0.05% v/v NH$_4$OH, D$_2$O, RT

GLYMO (11 mg, 0.045 mmol) was added to a solution of ammonium hydroxide (0.05% v/v) in deuterium oxide (total solution volume 685.5 μL), and the ¹H NMR spectrum was acquired at 0.2 h and 4.7 h.

Lu^{269} Conditions: 0.04% v/v NH₄OH, CD₃OD, 1.6% v/v H₂O, 60 °C

GLYMO (10 mg, 0.044 mmol) was added to a solution of ammonium hydroxide (0.04% v/v) in water (1.6% v/v) and methanol-d_4 (total solution volume 691 µL), and the solution was heated at 60 °C. The ^{1}H NMR spectrum was acquired at 1.1 h and 2.3 h.

Lu^{269} Conditions: 1% v/v NH₄OH, CD₃OD, 3.6% v/v H₂O, 60 °C

GLYMO (10 mg, 0.044 mmol) was added to a solution of ammonium hydroxide (1% v/v) in water (3.6% v/v) and methanol-d_4 (total solution volume 691 µL), and the solution was heated for 1 h at 60 °C. Then, the ^{1}H NMR spectrum was acquired.

Batches 2–4 Conditions: 1% v/v NH₄OH, CD₃OD, 3.7% v/v H₂O, 11% v/v CHCl₃, 60 °C

GLYMO (10 mg, 0.044 mmol) was added to a solution of ammonium hydroxide (1% v/v) in water (3.7% v/v), chloroform (11% v/v), and methanol-d_4 (total solution volume 675.2 µL), and the solution was heated for 1 h at 60 °C. Then, the ^{1}H NMR spectrum was acquired.

6.4.1.2.4 Cu(II)-Loading by CnGmSiO₂ (Batches 3 and 4)

CnGmSiO₂ (0.10 g) from Batches 3 and 4 was added to an aqueous solution of copper(II) nitrate (50 mM; 3 mL), and the mixture was stirred for 24 h and filtered. The now-blue silica was washed with water (5 × 5 mL) and acetone (1 × 3 mL), dried, and submitted for ICP-MS (Cu) analysis, following the sample preparation outlined for Batch 2 Cu(II)-CnGmSiO₂ in **Section 6.4.1.2.2**.

ICP-MS: *Batch 3* – 0.96% w/w Cu; *Batch 4* – 1.02% w/w Cu.

6.4.1.2.5 Adsorption of Cu(II)-Cyclen on Silica

Copper(II) nitrate trihydrate (91 mg, 0.38 mmol) and aqueous ammonium hydroxide (1% v/v; 0.24 mL) were added to cyclen (59 mg, 0.34 mmol) in water (7.58 mL). Then, silica (1.00 g) was added, and the mixture was concentrated *via* rotary evaporation for 1 h at 70 °C. The resulting light blue silica was washed by Soxhlet extraction with water for 25.3 h, dried, and submitted for CHN elemental and ICP-MS (Cu) analyses.

CHN: found C, 0.53%; H, 0.87%; N, < 0.30%. **ICP-MS:** 0.28% w/w Cu.

6.4.1.2.6 Cu(II)-Retention by Unfunctionalised Silica

Silica (0.10 g) was added to an aqueous solution of copper(II) nitrate (50 mM; 3 mL), and the mixture was stirred for 24 h and filtered. The silica was washed with water (5 × 5 mL) and acetone (1 × 3 mL), dried, and submitted for ICP-MS (Cu) analysis, following the sample preparation outlined for Batch 2 Cu(II)-CnGmSiO$_2$ in **Section 6.4.1.2.2**. A blank was prepared by repeating the procedure with silica in water.

ICP-MS: 0.06% w/w Cu.

6.4.2 Incorporation of Silica in a Coating

A two-pack epoxy was prepared by mixing a commercial hardener (Ancamine® 2459 Curing Agent; Air Products and Chemicals, Inc.) and a commercial epoxy resin (Epikote™ 235; Resolution Performance Products) in accordance with the manufacturers' specifications: 0.563 g Ancamine® 2459/g Epikote™ 235. Immediately following manual mixing of the two components, one coat of the viscous, dark yellow epoxy resin was applied using the standard draw-down method (bar film applicator: 1120/25/100, S232228, Sheen; **Figure 6.2**) to a single side of a black vinyl chloride/acetate copolymer (black scrub test panel, Leneta). An inverted funnel was then used to add silica to a defined surface area of the still-uncured resin so that, at minimum, one layer of silica covered the resin. The coating was allowed to cure at room temperature overnight, and, the following day, the procedure was repeated for the second side. After allowing the second side to cure at room temperature overnight, the silica/epoxy (SiO$_2$/epx)-type samples were brushed, washed with water, and dried with compressed air, and squares (23 mm × 23 mm) coated on both sides were cut from the material. These squares were tested immediately for bacterial adherence. The four silica samples prepared for testing were as follows: 1) Batch 4 CnGmSiO$_2$ (free ligand), 2) Batch 4 CnGmSiO$_2$ + Cu(II) (post-loaded), 3) Batch 2 Cu(II)-CnGmSiO$_2$ (pre-loaded), and 4) unfunctionalised SiO$_2$. To post-load the Batch 4 CnGmSiO$_2$, the squares coated on both sides with CnGmSiO$_2$ were submerged in an aqueous solution of an excess of copper(II) nitrate (50 mM; 16.5 mL) for 24 h, washed with water, dried with compressed air, and tested immediately for bacterial adherence. Images and the elemental composition of the SiO$_2$/epx-type coatings were obtained by SEM-EDS (Appendix, **Figures 8.45–51**).

6.5 Chapter 5

6.5.1 Method Development with *E. coli* NZRM 3647

In **Figure 6.3**, the bacterial adherence assay is illustrated and the areas to be addressed for method development are highlighted in red.
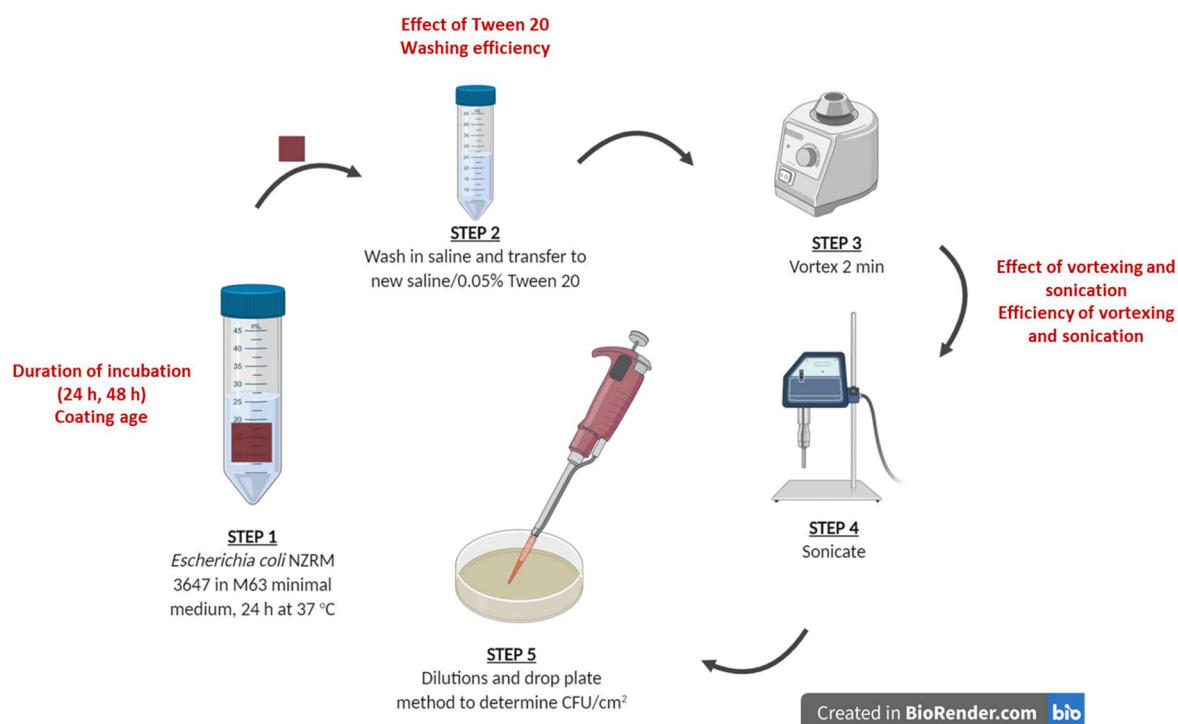
Figure 6.3. Steps of the bacterial adherence assay and, in red, areas to be addressed for method development (created with Biorender.com).

6.5.1.1 Duration of Incubation

An overnight culture was prepared by inoculating nutrient broth (3 mL) with a colony of *E. coli* NZRM 3647 from a nutrient agar plate and incubating for 16 h at 37 °C with shaking. Two squares (25 mm × 25 mm) cut from a vinyl chloride/acetate copolymer (black scrub test panel, Leneta) and sterilised with 70% v/v aq ethanol were submerged in overnight culture diluted 50× with M63 minimal medium (final volume 16.5 mL) in two tubes (one square/tube; **Figure 6.4**). At 37 °C without shaking, one tube was incubated 24 h, and the other tube was incubated 48 h. Following incubation, the OD_{600} of each culture was measured, and each square was transferred to sterile saline (20 mL) for 5 min to

remove planktonic bacteria. After the saline wash, the squares were transferred to tubes containing sterile solutions of 0.05% v/v Tween 20 in saline (final volume 20.040 mL), and then the solutions were vortexed 2 min at maximum speed and sonicated 8 s at 40% amplitude to detach bacteria from the squares. Serial dilutions (10×) of these solutions were performed to count colonies by the drop plate method.
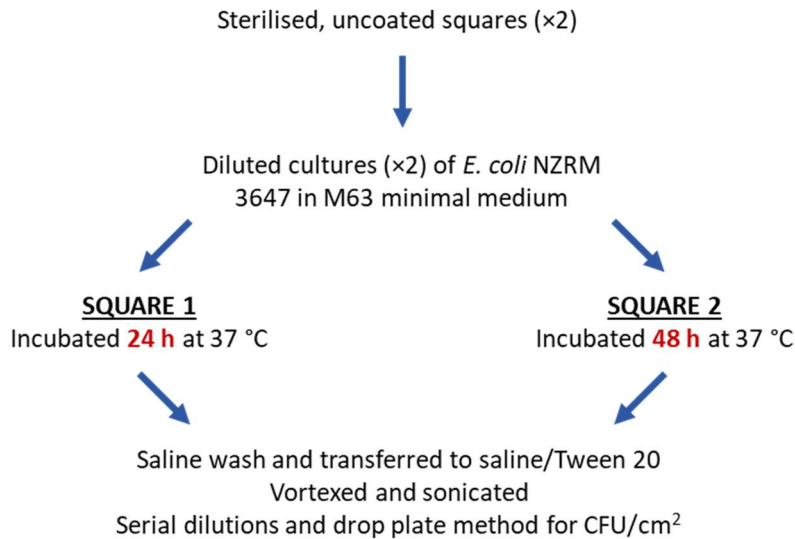

Figure 6.4. Testing the effect of the duration of incubation on bacterial adherence (24 h *vs* 48 h).

6.5.1.2 Coating Age

A single coat of paint or resin was applied to one side of a black plastic sheet (vinyl chloride/acetate copolymer, black scrub test panel, Leneta) by the standard draw-down method (**Figure 6.2**, bar film applicator: 1120/25/100, S232228, Sheen) and was cured at room temperature overnight. The following day, the procedure was repeated for the other side of the plastic sheet. After overnight curing of the second side, squares (23 mm × 23 mm) were cut from the coated sheets for immediate testing of bacterial adherence to "fresh" coatings, or the coated sheets were allowed to sit for two weeks at room temperature before cutting out the squares for bacterial adherence testing. Four sample square types were prepared: 1) uncoated plastic squares, 2) plastic squares coated with marine paint (Altex Yacht and Boat Paint, Aurora Red, Ablative Antifouling No. 5) containing high amounts of copper (40–50% Cu_2O), 3) plastic squares coated with a commercial, two-pot epoxy resin (Epikote™ 235 and Ancamine® 2459; prepared as in **Section 6.4.2**), and 4) plastic squares coated with a commercial acrylic paint (LR200, Resene Paints Ltd.). The samples were sterilised with UV light for 20 min *per* side in a laminar flow hood.

An overnight culture was prepared by inoculating nutrient broth (3 mL) with a colony of *E. coli* NZRM 3647 from a nutrient agar plate and incubating for 16 h at 37 °C with shaking. Each of the sterilised sample squares were submerged in overnight culture diluted with M63 minimal medium to OD_{600} 0.05 (final volume 16.5 mL; 5 ± 2 ($\times 10^7$) CFU/mL), and the diluted cultures were incubated 24 h at 37 °C without shaking (**Figure 6.5**). Then, the OD_{600} of each culture was measured. The squares were transferred to sterile saline (20 mL) for 5 min to remove planktonic bacteria, and a pipet was used to rinse both sides of the squares with sterile saline (500 µL/side). The squares were transferred to tubes containing sterile solutions of 0.05% v/v Tween 20 in saline (final volume 20.040 mL), and the solutions were vortexed 2 min at maximum speed and sonicated 8 s at 40% amplitude to detach bacteria from the squares. Serial dilutions (10×) of these solutions were performed to count colonies by the drop plate method. The experiment was independently repeated three times.

COATINGS
Uncoated
Marine paint
Epoxy resin
Acrylic paint

FRESH   TWO-WEEKS-OLD

Diluted cultures (×4) of *E. coli* NZRM 3647 in M63 minimal medium
Incubated 24 h at 37 °C
Saline washes and transferred to saline/Tween 20
Vortexed and sonicated
Serial dilutions and drop plate method for CFU/cm^2
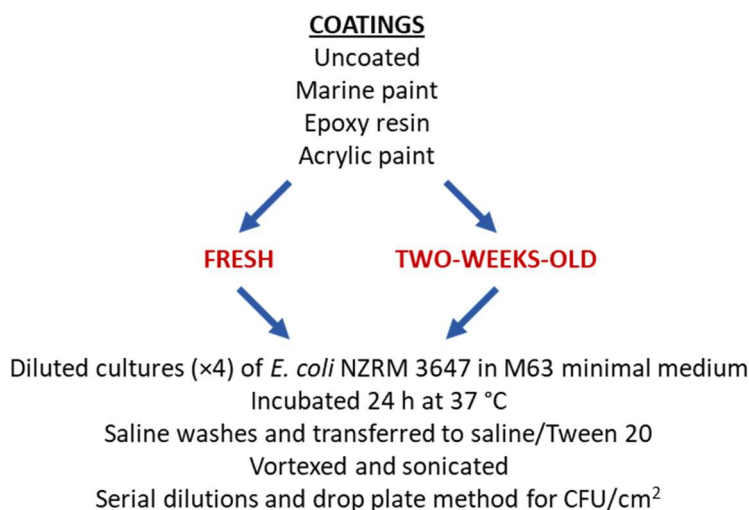
Figure 6.5. Testing the effect of coating age on bacterial adherence.

6.5.1.3 Effect of Tween 20

An overnight culture was prepared by inoculating nutrient broth (3 mL) with a colony of *E. coli* NZRM 3647 from a nutrient agar plate and incubating for 16 h at 37 °C with shaking. Two squares (25 mm × 25 mm) cut from a vinyl chloride/acetate copolymer (black scrub test panel, Leneta) and sterilised with 70% v/v aq ethanol were submerged in overnight culture diluted 50× with M63 minimal medium (final volume 20 mL) in two tubes (one square/tube), and the diluted cultures were incubated 24 h at 37 °C without shaking (**Figure 6.6**). Following incubation, the OD_{600} of each culture was measured, and each square was transferred to sterile saline (20 mL) for 5 min to remove planktonic

bacteria. Then, one square was transferred to another tube of sterile saline (20 mL), and the other square was transferred to a tube containing a sterile solution of 0.05% v/v Tween 20 in saline (final volume 20.0401 mL). Both tubes were vortexed 2 min at maximum speed to detach bacteria from the squares. Serial dilutions (10×) of the vortexed solutions were performed to count colonies by the drop plate method.
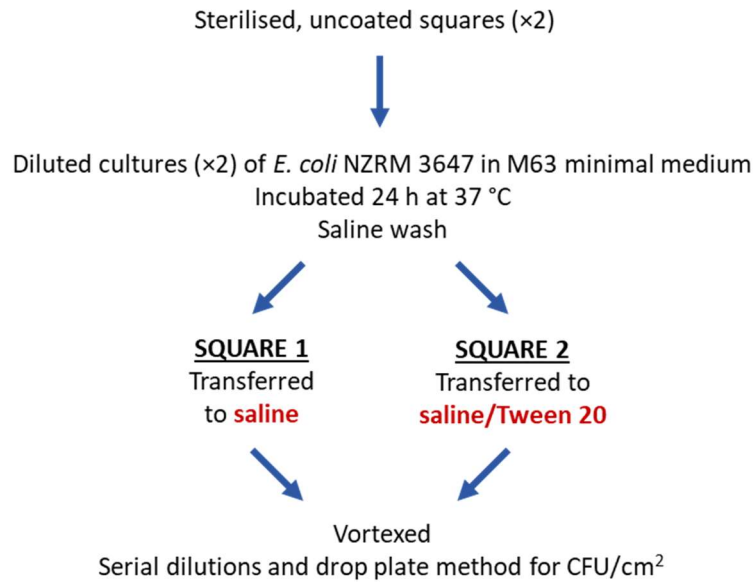
Figure 6.6. Testing the effect of Tween 20 in the bacterial adherence assay.

6.5.1.4 Washing Efficiency

An overnight culture was prepared by inoculating nutrient broth (3 mL) with a colony of *E. coli* NZRM 3647 from a nutrient agar plate and incubating for 16 h at 37 °C with shaking. One square (23 mm × 23 mm squares) was cut from a vinyl chloride/acetate copolymer (black scrub test panel, Leneta) and sterilised with UV light for 20 min *per* side in a laminar flow hood (**Figure 6.7**). The sterilised square was submerged in overnight culture diluted with M63 minimal medium to OD_{600} 0.05 (final volume 16.5 mL; 5 ± 2 ($\times 10^7$) CFU/mL), and the diluted culture was incubated 24 h at 37 °C without shaking. Following incubation, the OD_{600} of each culture was measured. For the first wash, the square was transferred to sterile saline (20 mL) for 5 min to remove planktonic bacteria, and a pipet was used to rinse both sides of the square with sterile saline (500 µL/side). For the second wash, the square was transferred to sterile saline (20 mL) for 5 min. Then, the square was transferred to a tube containing sterile saline/0.05% v/v Tween 20 (final volume 20.0401 mL), vortexed 2 min at maximum speed, and sonicated 8 s at 40% amplitude. Tween 20 (25% v/v, aq; 40.1 µL) was added to both wash solutions to bring the final concentration of Tween 20 to 0.05% v/v. Serial dilutions (10×) of the first

and second wash solutions and the detachment solution containing the square were performed to count colonies by the drop plate method. This experiment was repeated for a Cu(II)-CnGmSiO$_2$/epx-coated square (**Section 6.4.2**).

Sterilised, uncoated or Cu(II)-CnGmSiO$_2$/epx-coated square

Diluted culture of *E. coli* NZRM 3647 in M63 minimal medium
Incubated 24 h at 37 °C

FIRST WASH
Saline wash

SECOND WASH
Saline wash

DETACHMENT SOLUTION
Saline/Tween 20
Vortexed and sonicated

Serial dilutions and drop plate method for CFU/mL
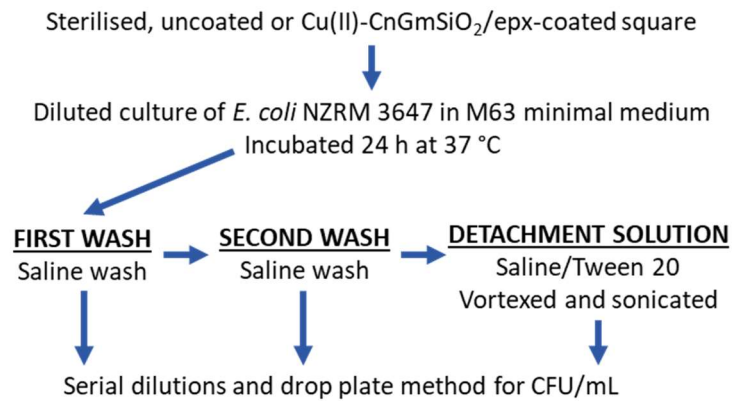
Figure 6.7. Enumeration of bacterial counts (*E. coli*) in washes.

6.5.1.5 Effect of Vortexing and Sonication

An overnight culture was prepared by inoculating nutrient broth (3 mL) with a colony of *E. coli* NZRM 3647 from a nutrient agar plate and incubating for 16 h at 37 °C with shaking. A tube containing overnight culture diluted 50× with M63 minimal medium (final volume 25 mL) was incubated 24 h at 37 °C without shaking (**Figure 6.8**). Then, the OD$_{600}$ of the culture was measured, and an aliquot of the culture (5 mL) was transferred to another tube. The first tube (now containing 20 mL) was vortexed for 2 min at maximum speed and sonicated 8 s at 40% amplitude. Serial dilutions (10×) of the cultures in both tubes were performed to count colonies by the drop plate method.

Diluted culture of *E. coli* NZRM 3647 in M63 minimal medium (**TUBE 1**)
Incubated 24 h at 37 °C

TUBE 1
Vortexed and sonicated

TUBE 2
Aliquot of culture

Serial dilutions and drop plate method for CFU/mL
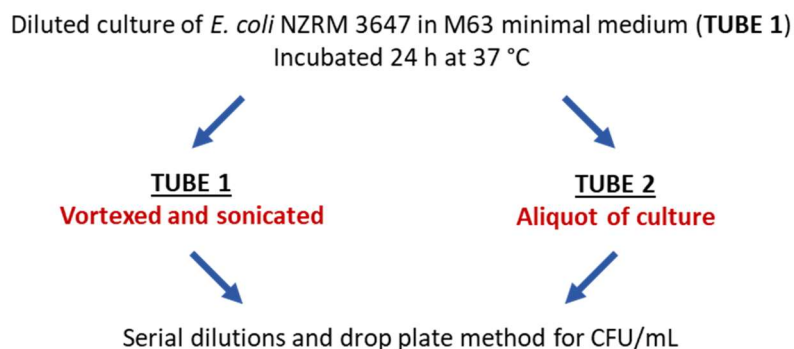
Figure 6.8. Testing the combined effect of vortexing and sonication on planktonic bacteria.

6.5.1.6 Efficiency of Vortexing and Sonication (± Tween 20)

6.5.1.6.1 Uncoated Squares: Tween 20 (+)

An overnight culture was prepared by inoculating nutrient broth (3 mL) with a colony of *E. coli* NZRM 3647 from a nutrient agar plate and incubating for 16 h at 37 °C with shaking. Three squares (25 mm × 25 mm) cut from a vinyl chloride/acetate copolymer (black scrub test panel, Leneta) and sterilised with 70% v/v aq ethanol were submerged in overnight culture diluted 50× with M63 minimal medium (final volume 16.5 mL) in three tubes (one square/tube), and the diluted cultures were incubated 24 h at 37 °C without shaking (**Figure 6.9**). Following incubation, the OD_{600} of each culture was measured, and each square was transferred to sterile saline (20 mL) for 5 min to remove planktonic bacteria. After the saline wash, the squares were transferred to tubes containing sterile saline/0.05% v/v Tween 20 (final volume 20.040 mL). The three tubes received different treatments: 1) the first tube was gently inverted 3× for the homogeneous distribution of cells ("Control"), 2) the second tube ("Vortex 1×") was vortexed 2 min at maximum speed, the square was transferred to another tube containing sterile saline/0.05% v/v Tween 20 (final volume 20.040 mL), and then that tube ("Vortex 2×") was vortexed 2 min at maximum speed, and 3) the third tube ("Vortex & Sonicate") was vortexed 2 min at maximum speed and sonicated 8 s at 40% amplitude. Serial dilutions (10×) of the "Control", "Vortex 1×", "Vortex 2×", and "Vortex & Sonicate" solutions were performed to count colonies by the drop plate method.
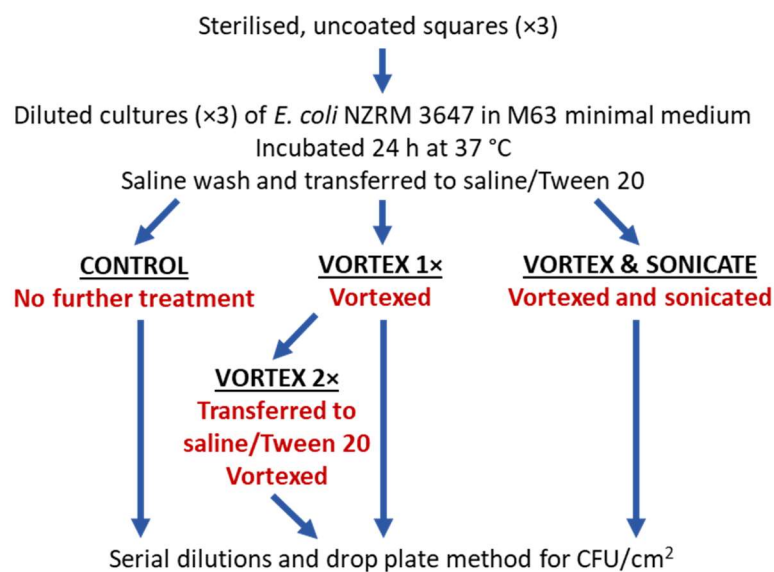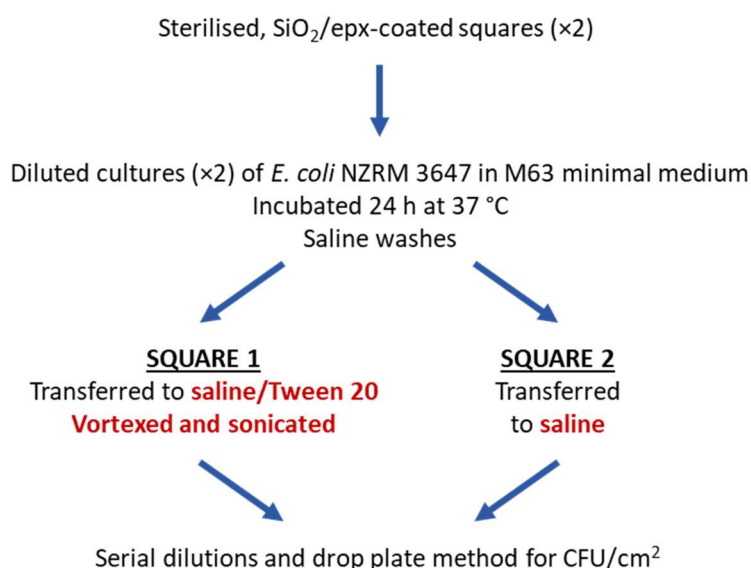

Figure 6.9. Testing the efficiency of vortexing and sonication with Tween 20 in the removal of adherent bacteria from uncoated squares.

6.5.1.6.2 Uncoated Squares: Tween 20 (±)

An overnight culture was prepared by inoculating nutrient broth (3 mL) with a colony of *E. coli* NZRM 3647 from a nutrient agar plate and incubating for 16 h at 37 °C with shaking. Three squares (23 mm × 23 mm) were cut from a vinyl chloride/acetate copolymer (black scrub test panel, Leneta) and sterilised with UV light for 20 min *per* side in a laminar flow hood (**Figure 6.10**). Then, each sterilised square was submerged in overnight culture diluted with M63 minimal medium to OD_{600} 0.05 (final volume 16.5 mL; 5 ± 2 ($\times 10^7$) CFU/mL), and the diluted cultures were incubated 24 h at 37 °C without shaking. Following incubation, the OD_{600} of each culture was measured. The squares were transferred to sterile saline (20 mL) for 5 min to remove planktonic bacteria, and a pipet was used to rinse both sides of the squares with sterile saline (500 µL/side). Two of the squares were transferred to tubes (one square/tube) containing sterile saline/0.05% v/v Tween 20 (final volume 20.0401 mL), and the last square was transferred to a tube containing sterile saline (20 mL). One of the Tween 20 solutions was vortexed 2 min at maximum speed and sonicated 8 s at 40% amplitude. The other two detachment solutions were gently inverted 3× for the homogeneous distribution of cells in each solution. Serial dilutions (10×) of all square-containing solutions were performed to count colonies by the drop plate method. The experiment was independently repeated three times.
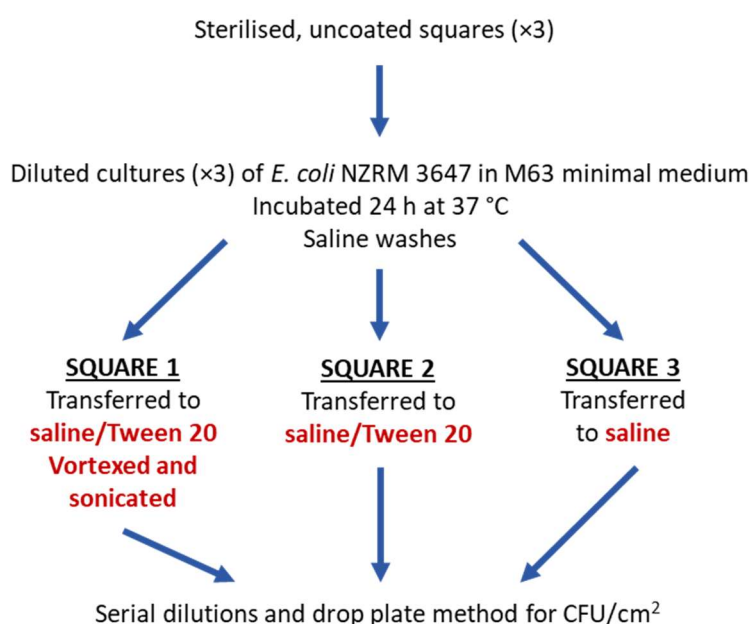
Figure 6.10. Testing the efficiency of vortexing and sonication with or without Tween 20 in the removal of adherent bacteria from uncoated squares.

6.5.1.6.3 SiO₂/epx-Coated Squares

Overnight cultures (×2) were prepared by inoculating nutrient broth (3 mL) with a colony of *E. coli* NZRM 3647 from a nutrient agar plate and incubating for 16 h at 37 °C with shaking. Two SiO$_2$/epx-coated squares (23 mm × 23 mm) were prepared (**Section 6.4.2**) and sterilised with UV light for 20 min *per* side in a laminar flow hood (**Figure 6.11**). Then, each sterilised square was submerged in overnight culture diluted with M63 minimal medium to OD$_{600}$ 0.05 (final volume 16.5 mL; 5 ± 2 (× 10^7) CFU/mL), and the diluted cultures were incubated 24 h at 37 °C without shaking. Following incubation, the OD$_{600}$ of each culture was measured. The squares were transferred to sterile saline (20 mL) for 5 min to remove planktonic bacteria, and a pipet was used to rinse both sides of the squares with sterile saline (500 µL/side). One square was transferred to a tube containing sterile saline/0.05% v/v Tween 20 (final volume 20.0401 mL), vortexed 2 min at maximum speed, and sonicated 8 s at 40% amplitude. The other square was transferred to a tube containing sterile saline (20 mL) and gently inverted 3× for the homogeneous distribution of cells in solution. Serial dilutions (10×) of all square-containing solutions were performed to count colonies by the drop plate method. The experiment was independently repeated three times.

Figure 6.11. Testing the efficiency of vortexing and sonication with or without Tween 20 in the removal of adherent bacteria from SiO₂/epx-coated squares.

6.5.1.6.4 Crystal Violet Staining

The procedure by O'Toole *et al.*[302] was utilised for this experiment. An overnight culture was prepared by inoculating nutrient broth (3 mL) with a colony of *E. coli* NZRM 3647 from a nutrient agar plate and incubating for 16 h at 37 °C with shaking. Two squares (25 mm × 25 mm) cut from a vinyl chloride/acetate copolymer (black scrub test panel, Leneta) and sterilised with 70% v/v aq ethanol were submerged in overnight culture diluted 50× with M63 minimal medium (final volume 16.5 mL) in two tubes (one square/tube), and the diluted cultures were incubated 24 h at 37 °C without shaking (**Figure 6.12**). Following incubation, the OD_{600} of each culture was measured, and each square was transferred to sterile saline (20 mL) for 5 min to remove planktonic bacteria. Then, the squares were transferred to tubes containing sterile saline/0.05% v/v Tween 20 (final volume 20.0401 mL). One tube was vortexed 2 min at maximum speed to detach bacteria from the square. Then, both squares were transferred to 0.005% v/v aq crystal violet (20 mL) for 15 min, rinsed in sterile water, and transferred to 4:1 v/v ethanol:acetone (20 mL) for 10 min to de-stain the squares. As a blank, following previous staining procedures, a plastic square unexposed to bacteria was dyed, rinsed, and de-stained. The absorbance of the dye in each de-staining solution was measured at 570 nm.
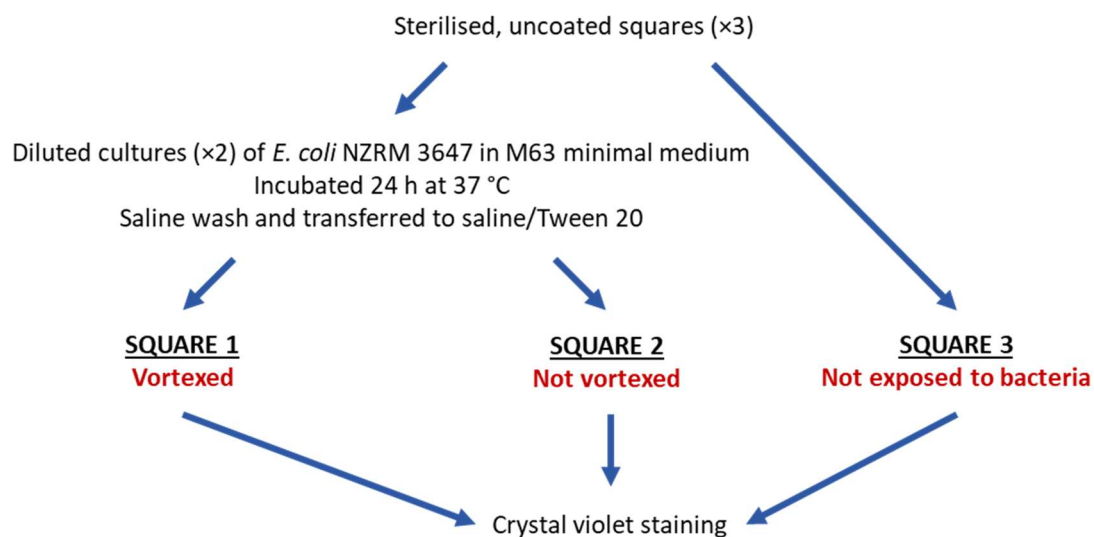
Figure 6.12. Testing the efficiency of vortexing in the removal of adherent bacteria *via* crystal violet staining.

6.5.2 Adherence of *E. coli* NZRM 3647 to SiO$_2$/epx-Type Coatings

6.5.2.1 *Adherence Assay*

Refer to **Figure 6.3**. The adherence of *E. coli* NZRM 3647 to the SiO$_2$/epx-type samples from **Section 6.4.2** was tested. An uncoated sample square and sample squares coated with the commercial epoxy resin and marine paint, as in **Section 6.5.1.2**, were also tested. An overnight culture was prepared by inoculating nutrient broth (3 mL) with a colony of *E. coli* NZRM 3647 from a nutrient agar plate and incubating for 16 h at 37 °C with shaking. The squares were sterilised with UV light for 20 min *per* side in a laminar flow hood, and then each of the sterilised squares were submerged in overnight culture diluted with M63 minimal medium to OD$_{600}$ 0.05 (final volume 16.5 mL; 5 ± 2 ($\times$ 10^7) CFU/mL). The diluted cultures were incubated 24 h at 37 °C without shaking. Following incubation, the OD$_{600}$ of each culture was measured, and the squares were transferred to sterile saline (20 mL) for 5 min to remove planktonic bacteria. A pipet was used to rinse both sides of the squares with sterile saline (500 µL/side) before transferring the squares to tubes containing sterile solutions of 0.05% v/v Tween 20 in saline (final volume 20.0401 mL). These solutions were vortexed 2 min at maximum speed and sonicated 8 s at 40% amplitude to detach bacteria from the squares. Serial dilutions (10$\times$) of the solutions were performed to count colonies by the drop plate method. The experiment was independently repeated three times.

6.5.2.2 *Copper-Leaching Experiments*

The amount of copper leaching out of the copper coatings into the liquid medium during the 24 h incubation period was measured both in the absence and presence of *E. coli* NZRM 3647. Squares were coated with the commercial marine paint (Altex Yacht and Boat Paint, Aurora Red, Ablative Antifouling No. 5), as in **Section 6.5.1.2**, and with Batch 2 Cu(II)-CnGmSiO$_2$/epx and Batch 4 CnGmSiO$_2$ + Cu(II)/epx, as in **Section 6.4.2**.

6.5.2.2.1 *E. coli* Absent

Coated squares (23 mm $\times$ 23 mm) were sterilised by exposure of each side to UV light for 20 min in a laminar flow hood and were submerged in M63 minimal medium (16.5 mL) at 37 °C without shaking. After 24 h, the squares were removed. In order to quantify the copper in the liquid medium *via* ICP-MS,

the solutions were diluted 10,000–25,000× with 3% v/v nitric acid (aq) to bring the copper concentration within the range of the standards. M63 minimal medium served as a blank. The experiment was independently repeated three times.

ICP-MS: *Marine Paint* – 3.3 ± 0.5 ppm Cu; *Batch 2 Cu(II)-CnGmSiO$_2$/epx* – 3.6 ± 0.3 ppm Cu; *Batch 4 CnGmSiO$_2$ + Cu(II)/epx* – 2.3 ± 0.1 ppm Cu.

6.5.2.2.2 *E. coli* Present

An overnight culture was prepared by inoculating nutrient broth (3 mL) with a colony of *E. coli* NZRM 3647 from a nutrient agar plate and incubating for 16 h at 37 °C with shaking. Coated squares (23 mm × 23 mm) were submerged in overnight culture diluted with M63 minimal medium to OD$_{600}$ 0.05 (final volume 16.5 mL; 5 ± 2 (× 10^7) CFU/mL) for 24 h at 37 °C without shaking. Following incubation, the cultures were filter-sterilised (0.2 μm pore size, Sartorius Minisart®) and centrifuged (10 min, 3000 RCF). The supernatant was submitted for copper analysis *via* ICP-MS and diluted 1,000–50,000× with 3% v/v nitric acid (aq) to bring the copper concentration within the range of the standards. M63 minimal medium served as a blank. The experiment was independently repeated three times.

ICP-MS: *Marine Paint* – 7.3 ± 0.4 ppm Cu; *Batch 2 Cu(II)-CnGmSiO$_2$/epx* – 6.0 ± 0.4 ppm Cu; *Batch 4 CnGmSiO$_2$ + Cu(II)/epx* – 12 ± 2 ppm Cu.

6.5.2.3 Growth of E. coli ± Shaking

An overnight culture was prepared by inoculating nutrient broth (3 mL) with a colony of *E. coli* NZRM 3647 from a nutrient agar plate and incubating for 16 h at 37 °C with shaking. Two squares (23 mm × 23 mm) were cut from a vinyl chloride/acetate copolymer (black scrub test panel, Leneta) and sterilised with UV light for 20 min *per* side in a laminar flow hood (**Figure 6.13**). Then, each sterilised square was submerged in overnight culture diluted with M63 minimal medium to OD$_{600}$ 0.05 (final volume 16.5 mL; 5 ± 2 (× 10^7) CFU/mL), and the diluted cultures were incubated 24 h at 37 °C – one without shaking and the other with shaking. To prepare two other cultures without squares, the overnight culture was diluted with M63 minimal medium to OD$_{600}$ 0.05 (final volume 16.5 mL; 5 ± 2 (× 10^7) CFU/mL), and the diluted cultures were incubated 24 h at 37 °C – one without shaking and the other with shaking. Following incubation, the OD$_{600}$ of each culture was measured.
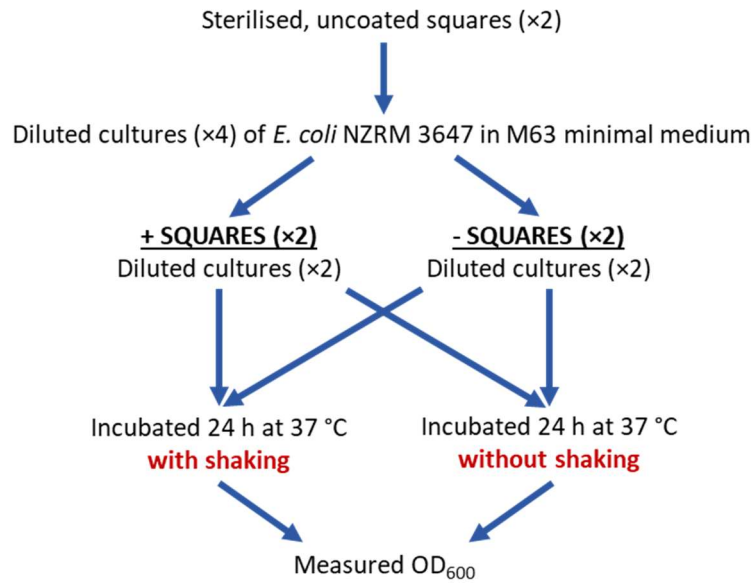
Figure 6.13. Testing the growth of *E. coli* NZRM 3647 with and without shaking and in the presence or absence of an uncoated square.

6.5.3 Adherence Assay: *V. harveyi* NZRM 2698

6.5.3.1 Effects of Vortexing, Sonication, and Tween 20 on Planktonic Bacteria

An overnight culture was prepared by inoculating Luria marine broth (10 mL) with a colony of *V. harveyi* NZRM 2698 from a Luria marine agar plate and incubating for 16 h at 30 °C with shaking. Then, in a sterile flask, the overnight culture was diluted to OD_{600} 0.05 with Luria marine broth (final volume 100 mL; 1.4 ± 0.3 ($\times 10^8$) CFU/mL) and incubated 24 h at 30 °C with shaking (**Figure 6.14**). After 24 h, the OD_{600} of the culture was measured, and five aliquots (20 mL) were transferred to five different tubes:

1) The first tube was vortexed for 2 min at maximum speed.
2) The second tube was sonicated for 8 s at 40% amplitude (~0.2 kJ).
3) Tween 20 (25% v/v, aq; 40.1 uL) was added to the third tube and gently mixed by inversion, yielding a final concentration of 0.05% v/v Tween 20.
4) Tween 20 (25% v/v, aq; 40.1 uL) was added to the fourth tube, yielding a final concentration of 0.05% v/v Tween 20. This tube was then vortexed for 2 min at maximum speed and sonicated for 8 s at 40% amplitude (~0.2 kJ).

5) The fifth tube served as a control and was only gently mixed by inversion prior to serial dilutions.

Serial dilutions (10×) of the cultures in all five tubes were performed to count colonies by the drop plate method.
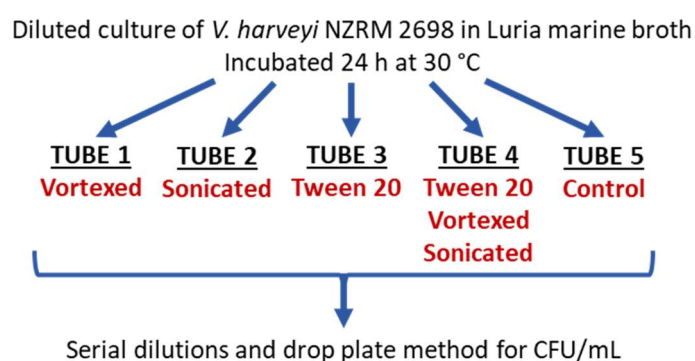
Figure 6.14. Testing the effects of vortexing, sonication, and Tween 20 on planktonic bacteria.

6.5.3.2 Checking for Cells Clumping

An overnight culture was prepared by inoculating Luria marine broth (3 mL) with a colony of *V. harveyi* NZRM 2698 from a Luria marine agar plate and incubating for 16 h at 30 °C with shaking. The overnight culture was checked for clumping cells *via* Gram staining, as in **Section 6.1.8**. Then, Tween 20 (25% v/v, aq) was added to the culture and mixed, yielding a final concentration of 0.05% v/v Tween 20, and this culture was also checked for clumping cells *via* Gram staining.

6.5.3.3 Effect of Tween 20 in Adherence Assay (2% vs 0.85% w/w NaCl)

An overnight culture was prepared by inoculating Luria marine broth (3 mL) with a colony of *V. harveyi* NZRM 2698 from a Luria marine agar plate and incubating for 16 h at 30 °C with shaking. Four CnGmSiO$_2$/epx-coated squares (23 mm × 23 mm) were prepared, as in **Section 6.4.2**, and sterilised with UV light for 20 min *per* side in a laminar flow hood (**Figure 6.15**). Two of the sterilised squares ("-Tween 20") were submerged in overnight culture diluted with Luria marine broth to OD$_{600}$ 0.05 (final volume 16.5 mL; 1.4 ± 0.3 (× 10^8) CFU/mL). Tween 20 (25% v/v, aq) was added to the remaining overnight culture and mixed, yielding a final concentration of 0.05% v/v Tween 20. The other two sterilised squares ("+Tween 20") were submerged in 0.05% v/v Tween 20/overnight culture diluted

with Luria marine broth to OD_{600} 0.05 (final volume 16.5 mL). All of the diluted cultures were incubated 24 h at 30 °C with shaking. Following incubation, the OD_{600} of each culture was measured. Two squares ("0.85% NaCl") – one "+Tween 20" and one "-Tween 20" – were transferred to sterile saline (0.85% w/w NaCl, aq; 20 mL) for 5 min to remove planktonic bacteria, and a pipet was used to rinse both sides of the squares with sterile saline (500 µL/side). The other two squares ("2% NaCl") were transferred to sterile 2% w/w aq sodium chloride (20 mL) for 5 min to remove planktonic bacteria, and a pipet was used to rinse both sides of the squares with sterile 2% w/w aq sodium chloride (500 µL/side). Then, the four squares were transferred to the following solutions for the detachment of adherent bacteria:

1) "0.85% NaCl, +Tween 20": sterile saline/0.05% Tween 20 (20 mL),
2) "0.85% NaCl, -Tween 20": sterile saline (20 mL),
3) "2% NaCl, +Tween 20": sterile 2% w/w aq sodium chloride/0.05% v/v Tween 20 (20 mL), and
4) "2% NaCl, -Tween 20": sterile 2% w/w aq sodium chloride (20 mL).

The detachment solutions were vortexed 2 min at maximum speed. Serial dilutions (10×) of the detachment solutions were performed using the appropriate diluent (as above) to count colonies by the drop plate method.
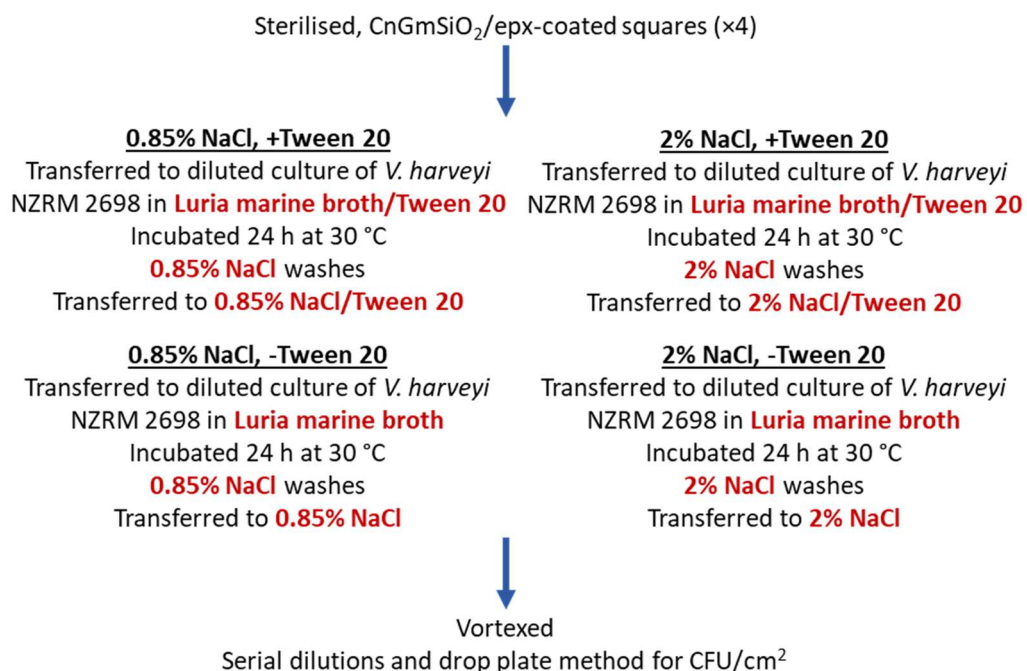
Figure 6.15. Testing the effect of Tween 20 in the adherence assay and comparing the use of saline *vs* 2% w/w aq NaCl for the washes, detachment solution, and the diluent.

6.5.3.4 Duration of Incubation and Efficiency of Vortexing and Sonication

An overnight culture was prepared by inoculating Luria marine broth (3 mL) with a colony of *V. harveyi* NZRM 2698 from a Luria marine agar plate and incubating for 16 h at 30 °C with shaking. Four SiO$_2$/epx-coated samples (11.5 mm × 23 mm) were prepared, as in **Section 6.4.2**, and sterilised with UV light for 20 min *per* side in a laminar flow hood (**Figure 6.16**). The sterilised samples were submerged in overnight culture diluted to OD$_{600}$ 0.05 with Luria marine broth (final volume 16.5 mL; 1.4 ± 0.3 ($\times 10^8$) CFU/mL) in four tubes (one square/tube), and the diluted cultures were incubated at 30 °C with shaking. The different samples were treated as follows:

1) **Sample 1** was incubated for 24 h at 30 °C with shaking. After incubation, the OD$_{600}$ of the culture was measured, and the sample was transferred to 2% w/w aq sodium chloride (20 mL) for 5 min to remove planktonic bacteria. A pipet was used to rinse both sides of the sample with sterile 2% w/w aq sodium chloride before transferring it to a tube containing sterile 2% w/w sodium chloride (20 mL). This tube was vortexed 2 min at maximum speed and sonicated 8 s at 40% amplitude (~0.2 kJ) to detach bacteria from the sample.

2) **Sample 2** was incubated for 48 h at 30 °C with shaking. After incubation, the OD$_{600}$ of the culture was measured, and the sample was transferred to sterile 2% w/w aq sodium chloride (20 mL) for 5 min to remove planktonic bacteria. A pipet was used to rinse both sides of the sample with sterile 2% w/w aq sodium chloride before transferring it to a tube containing sterile 2% w/w aq sodium chloride (20 mL). This tube was vortexed 2 min at maximum speed and sonicated 8 s at 40% amplitude (~0.2 kJ) to detach bacteria from the sample.

3) **Sample 3** was incubated for 48 h at 30 °C with shaking. After incubation, the OD$_{600}$ of the culture was measured, and the sample was transferred to sterile 2% w/w aq sodium chloride (20 mL) for 5 min to remove planktonic bacteria. A pipet was used to rinse both sides of the sample with sterile 2% w/w aq sodium chloride before transferring it to a tube containing sterile 2% w/w aq sodium chloride (20 mL). The contents of the tube were gently mixed by inversion prior to serial dilutions.

4) **Sample 4** was incubated for 48 h at 30 °C with shaking. After incubation, the OD$_{600}$ of the culture was measured, and the sample was transferred to sterile 2% w/w aq sodium chloride (20 mL) for 5 min to remove planktonic bacteria. A pipet was used to rinse both sides of the sample with sterile 2% w/w aq sodium chloride before transferring it to a tube containing sterile 2% w/w aq sodium chloride (20 mL). This tube was vortexed 2 min at maximum speed ("Sample 4, ×1"). Then, the sample was transferred to another tube containing sterile 2% w/w

aq sodium chloride (20 mL), and this tube was also vortexed 2 min at maximum speed ("Sample 4, ×2").

Serial dilutions (10×) of the "Sample 1", "Sample 2", "Sample 3", "Sample 4, ×1", and "Sample 4, ×2" detachment solutions were performed to count colonies by the drop plate method.
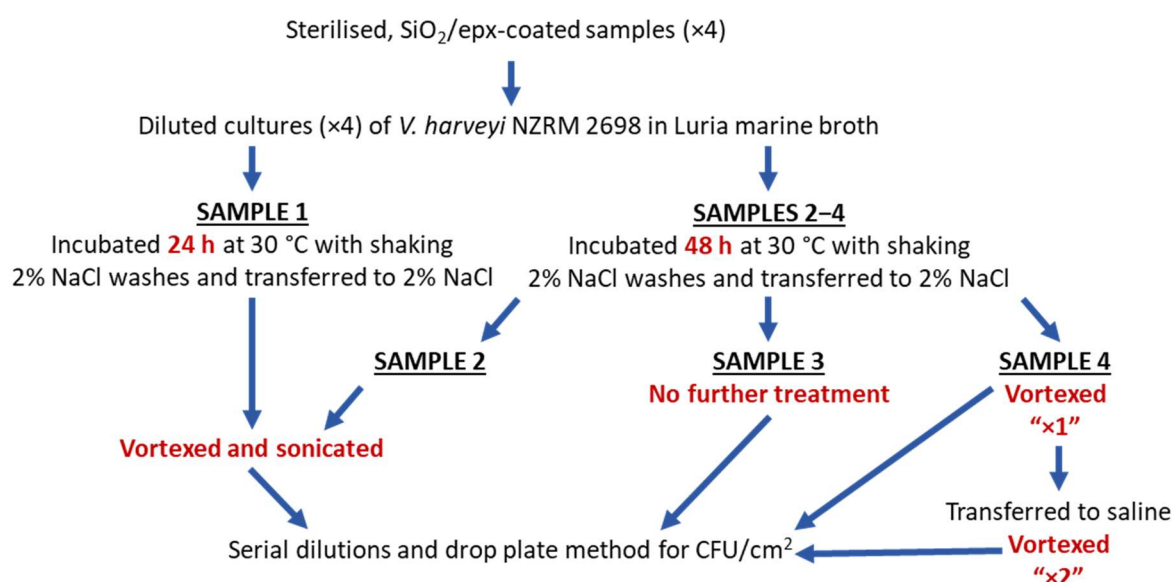
Figure 6.16. Testing the duration of incubation and the efficiency of vortexing and sonication in the removal of adherent bacteria.

6.5.3.5 Enumeration of Cells in Washes

An overnight culture was prepared by inoculating Luria marine broth (3 mL) with a colony of *V. harveyi* NZRM 2698 from a Luria marine agar plate and incubating for 16 h at 30 °C with shaking. One CnGmSiO$_2$/epx-coated square (23 mm × 23 mm) was prepared, as in **Section 6.4.2**, and sterilised with UV light for 20 min *per* side in a laminar flow hood (**Figure 6.17**). The sterilised square was submerged in overnight culture diluted with Luria marine broth to OD$_{600}$ 0.05 (final volume 16.5 mL; 1.4 ± 0.3 (× 10^8) CFU/mL), and the diluted culture was incubated 24 h at 30 °C with shaking. Following incubation, the OD$_{600}$ of the culture was measured. For the first wash, the square was transferred to sterile 2% w/w aq sodium chloride (20 mL) for 5 min to remove planktonic bacteria, and a pipet was used to rinse both sides of the square with sterile 2% w/w aq sodium chloride (500 µL/side). For the second wash, the square was transferred to sterile 2% w/w aq sodium chloride (20 mL) for 5 min. Then, the square was transferred to another tube containing sterile 2% w/w aq sodium chloride

(20 mL) and vortexed 2 min at maximum speed. Both wash solutions were vortexed, and serial dilutions (10×) of the first and second wash solutions and the detachment solution containing the square were performed to count colonies by the drop plate method.
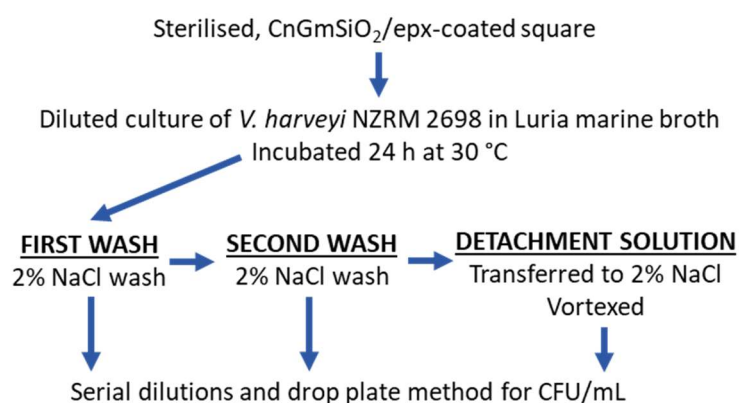
Figure 6.17. Enumeration of bacterial counts (*V. harveyi*) in washes.

6.5.3.6 Adherence of V. harveyi NZRM 2698 to SiO₂/epx-Type Coatings

The adherence of *V. harveyi* NZRM 2698 to the SiO$_2$/epx-type coatings from **Section 6.4.2** was tested. An uncoated sample square and sample squares coated with the commercial epoxy resin and marine paint, as in **Section 6.5.1.2**, were also tested. An overnight culture was prepared by inoculating Luria marine broth (3 mL) with a colony of *V. harveyi* NZRM 2698 from a Luria marine agar plate and incubating for 16 h at 30 °C with shaking. The squares were sterilised with UV light for 20 min *per* side in a laminar flow hood, and then each of the sterilised squares were submerged in overnight culture diluted with Luria marine broth to OD$_{600}$ 0.05 (final volume 16.5 mL; 1.4 ± 0.3 (× 10^8) CFU/mL). The diluted cultures were incubated 24 h at 30 °C with shaking. Following incubation, the OD$_{600}$ of each culture was measured, and the squares were transferred to sterile 2% w/w aq sodium chloride (20 mL) for 5 min to remove planktonic bacteria. A pipet was used to rinse both sides of the squares with sterile 2% w/w aq sodium chloride (500 µL/side) before transferring the squares to new tubes containing sterile 2% w/w aq sodium chloride (20 mL). These solutions were vortexed 2 min at maximum speed and serially-diluted (10×) to count colonies by the drop plate method. The experiment was independently repeated three times.

7 REFERENCES

1. Bighiu, M. A., Eriksson-Wiklund, A.-K. & Eklund, B. Biofouling of leisure boats as a source of metal pollution. *Environ. Sci. Pollut. Res.* **24**, 997–1006 (2017).

2. Gittens, J. E., Smith, T. J., Suleiman, R. & Akid, R. Current and emerging environmentally-friendly systems for fouling control in the marine environment. *Biotechnol. Adv.* **31**, 1738–1753 (2013).

3. Almeida, E., Diamantino, T. C. & de Sousa, O. Marine paints: the particular case of antifouling paints. *Prog. Org. Coatings* **59**, 2–20 (2007).

4. Callow, M. E. & Callow, J. A. Marine biofouling: a sticky problem. *Biologist* **49**, 1–5 (2002).

5. Davidson, I. *et al.* Mini-review: assessing the drivers of ship biofouling management – aligning industry and biosecurity goals. *Biofouling* **32**, 411–428 (2016).

6. Townsin, R. L. The ship hull fouling penalty. *Biofouling* **19**, 9–15 (2003).

7. Martín-Rodríguez, A. J. *et al.* From broad-spectrum biocides to quorum sensing disruptors and mussel repellents: antifouling profile of alkyl triphenylphosphonium salts. *PLoS One* **10**, 1–30 (2015).

8. Amara, I., Miled, W., Slama, R. B. & Ladhari, N. Antifouling processes and toxicity effects of antifouling paints on marine environment. A review. *Environ. Toxicol. Pharmacol.* **57**, 115–130 (2018).

9. Qian, P. Y., Lau, S. C. K., Dahms, H. U., Dobretsov, S. & Harder, T. Marine biofilms as mediators of colonization by marine macroorganisms: implications for antifouling and aquaculture. *Mar. Biotechnol.* **9**, 399–410 (2007).

10. Flemming, H.-C. Why microorganisms live in biofilms and the problem of biofouling. in *Marine and Industrial Biofouling* (eds. Flemming, H.-C., Sriyutha Murthy, P., Venkatesan, R. & Cooksey, K. E.) 3–12 (Spring-Verlag Berlin Heidelberg, 2009). doi:10.1007/978-3-540-69796-1

11. Flemming, H.-C. Biofouling and me: my Stockholm syndrome with biofilms. *Water Res.* **173**, 1–15 (2020).

12. Dang, H. & Lovell, C. R. Microbial surface colonization and biofilm development in marine environments. *Microbiol. Mol. Biol. Rev.* **80**, 91–138 (2016).

13. Fusetani, N. Biofouling and antifouling. *Nat. Prod. Rep.* **21**, 94–104 (2004).

14. Burgess, J. G. *et al.* The development of a marine natural product-based antifouling paint. *Biofouling* **19 Suppl**, 197–205 (2003).

15. Callow, J. A. & Callow, M. E. Trends in the development of environmentally friendly fouling-resistant marine coatings. *Nat. Commun.* **2**, 244 (2011).

16. Lindholdt, A., Dam-Johansen, K., Olsen, S. M., Yebra, D. M. & Kiil, S. Effects of biofouling development on drag forces of hull coatings for ocean-going ships: a review. *J. Coatings Technol. Res.* **12**, 415–444 (2015).

17. Al-Naamani, L., Dobretsov, S., Dutta, J. & Burgess, J. G. Chitosan-zinc oxide nanocomposite coatings for the prevention of marine biofouling. *Chemosphere* **168**, 408–417 (2017).

18. Schultz, M. P. Effects of coating roughness and biofouling on ship resistance and powering. *Biofouling* **23**, 331–41 (2007).

19. Schultz, M. P., Bendick, J. A., Holm, E. R. & Hertel, W. M. Economic impact of biofouling on a naval surface ship. *Biofouling* **27**, 87–98 (2011).

20. Carve, M., Scardino, A. & Shimeta, J. Effects of surface texture and interrelated properties on marine biofouling: a systematic review. *Biofouling* **35**, 597–617 (2019).

21. Boren, T. *Eco-efficiency: a new tool to support better decisions on hull coating investments*. (2010).

22. Buskens, P., Wouters, M., Rentrop, C. & Vroon, Z. A brief review of environmentally benign antifouling and foul-release coatings for marine applications. *J. Coat. Technol. Res.* **10**, 29–36 (2013).

23. Dafforn, K. A., Lewis, J. A. & Johnston, E. L. Antifouling strategies: history and regulation, ecological impacts and mitigation. *Mar. Pollut. Bull.* **62**, 453–465 (2011).

24. Hopkins, G. A. & Forrest, B. M. A preliminary assessment of biofouling and non-indigenous marine species associated with commercial slow-moving vessels arriving in New Zealand. *Biofouling* **26**, 613–621 (2010).

25. Coutts, A. D. M. & Taylor, M. D. A preliminary investigation of biosecurity risks associated with biofouling on merchant vessels in New Zealand. *New Zeal. J. Mar. Freshw. Res.* **38**, 215–229 (2004).

26. Coutts, A. D. M. & Forrest, B. M. Development and application of tools for incursion response: lessons learned from the management of the fouling pest *Didemnum vexillum. J. Exp. Mar. Bio. Ecol.* **342**, 154–162 (2007).

27. Hole, W. *Marine Fouling and Its Prevention, Contribution No. 580 from the Woods Hole Oceanographic Institution*. (United States Naval Institute, 1952). doi:10.1575/1912/191

28. Yebra, D. M., Kiil, S. & Dam-Johansen, K. Antifouling technology – past, present and future steps towards efficient and environmentally friendly antifouling coatings. *Prog. Org. Coatings* **50**, 75–104 (2004).

29. Bentley, J. & Turner, G. P. A. *Introduction to Paint Chemistry and Principles of Paint Technology*. (Chapman & Hall, 1998).

30. *Paint and Surface Coatings: Theory and Practice*. (Woodhead Publishing Limited, 1999).

31. Yang, W. J., Neoh, K.-G., Kang, E.-T., Teo, S. L.-M. & Rittschof, D. Polymer brush coatings for combating marine biofouling. *Prog. Polym. Sci.* **39**, 1017–1042 (2014).

32. Evans, S. M., Leksono, T. & McKinnell, P. D. Tributyltin pollution: a diminishing problem following legislation limiting the use of TBT-based anti-fouling paints. *Mar. Pollut. Bull.* **30**, 14–21 (1995).

33. Tribou, M. & Swain, G. The effects of grooming on a copper ablative coating: a six year study. *Biofouling* **33**, 494–504 (2017).

34. Schiff, K., Diehl, D. & Valkirs, A. Copper emissions from antifouling paint on recreational vessels. *Mar. Pollut. Bull.* **48**, 371–377 (2004).

35. Voulvoulis, N., Scrimshaw, M. D. & Lester, J. N. Comparative environmental assessment of biocides used in antifouling paints. *Chemosphere* **47**, 789–795 (2002).

36. Lagerström, M., Norling, M. & Eklund, B. Metal contamination at recreational boatyards linked to the use of antifouling paints – investigation of soil and sediment with a field portable XRF. *Environ. Sci. Pollut. Res.* **23**, 10146–10157 (2016).

37. Karlsson, J., Ytreberg, E. & Eklund, B. Toxicity of anti-fouling paints for use on ships and leisure boats to non-target organisms representing three trophic levels. *Environ. Pollut.* **158**, 681–687 (2010).

38. Andersson, S. & Kautsky, L. Copper effects on reproductive stages of Baltic Sea *Fucus vesiculosus*. *Mar. Biol.* **125**, 171–176 (1996).

39. Debourg, C., Johnson, A., Lye, C., Törnqvist, L. & Unger, C. *Antifouling Products: Pleasure Boats, Commercial Vessels, Nets, Fish Cages and Other Underwater Equipment*. (The Swedish National Chemicals Inspectorate, 1993).

40. Ytreberg, E., Karlsson, J. & Eklund, B. Comparison of toxicity and release rates of Cu and Zn from anti-fouling paints leached in natural and artificial brackish seawater. *Sci. Total Environ.* **408**, 2459–2466 (2010).

41. Lindén, J. B., Larsson, M., Coad, B. R., Skinner, W. M. & Nydén, M. Polyethyleneimine for copper absorption: kinetics, selectivity and efficiency in artificial seawater. *RSC Adv.* **4**, 25063 (2014).

42. Kennish, M. J. *Practical Handbook of Marine Science*. (CRC Press LLC, 2001).

43. Banerjee, I., Pangule, R. C. & Kane, R. S. Antifouling coatings: recent developments in the design of surfaces that prevent fouling by proteins, bacteria, and marine organisms. *Adv. Mater.* **23**, 690–718 (2011).

44. Francolini, I., Vuotto, C., Piozzi, A. & Donelli, G. Antifouling and antimicrobial biomaterials: an overview. *Apmis* **125**, 392–417 (2017).

45. Roosjen, A., van der Mei, H. C., Busscher, H. J. & Norde, W. Microbial adhesion to poly(ethylene oxide) brushes: influence of polymer chain length and temperature. *Langmuir* **20**, 10949–10955 (2004).

46. Brady, R. F. & Singer, I. L. Mechanical factors favoring release from fouling release coatings. *Biofouling* **15**, 73–81 (2000).

47. Jones, D. R. H. & Ashby, M. F. *Engineering Materials 1: An Introduction to Properties, Applications and Design*. (Elsevier Ltd., 2019).

48. Brady, R. F. Properties which influence marine fouling resistance in polymers containing silicon and fluorine. *Prog. Org. Coatings* **35**, 31–35 (1999).

49. Damodaran, V. B. & Murthy, N. S. Bio-inspired strategies for designing antifouling biomaterials. *Biomater. Res.* **20**, 1–11 (2016).

50. Curtis, A. S. G. & Varde, M. Control of cell behavior: topological factors. *J. Natl. Cancer Inst.* **33**, 15–26 (1964).

51. Recum, A. F. *et al.* Surface roughness, porosity, and texture as modifiers of cellular adhesion. *Tissue Eng* **2**, 241–253 (1996).

52. Curtis, A. & Wilkinson, C. Topographical control of cells. *Biomaterials* **18**, 1573–1583 (1997).

53. Bettinger, C. J., Langer, R. & Borenstein, J. T. Engineering substrate topography at the micro- and nanoscale to control cell function. *Angew. Chemie - Int. Ed.* **48**, 5406–5415 (2009).

54. Schumacher, J. F. *et al.* Engineered antifouling microtopographies – effect of feature size, geometry, and roughness on settlement of zoospores of the green alga *Ulva*. *Biofouling* **23**, 55–62 (2007).

55. Carman, M. L. *et al.* Engineered antifouling microtopographies – correlating wettability with cell attachment. *Biofouling* **22**, 11–21 (2006).

56. Cao, X. *et al.* Interaction of zoospores of the green alga *Ulva* with bioinspired micro- and nanostructured surfaces prepared by polyelectrolyte layer-by-layer self-assembly. *Adv. Funct. Mater.* **20**, 1984–1993 (2010).

57. Fu, J. *et al.* Combat biofouling with microscopic ridge-like surface morphology: a bioinspired study. *J. R. Soc. Interface* **15**, 1–8 (2018).

58. Zhang, P., Lin, L., Zang, D., Guo, X. & Liu, M. Designing bioinspired anti-biofouling surfaces based on a superwettability strategy. *Small* **13**, 1–9 (2017).

59. Zorba, V. *et al.* Biomimetic artificial surfaces quantitatively reproduce the water repellency of a lotus leaf. *Adv. Mater.* **20**, 4049–4054 (2008).

60. Sanchez-Cano, C. & Carril, M. Recent developments in the design of non-biofouling coatings for nanoparticles and surfaces. *Int. J. Mol. Sci.* **21**, 1–24 (2020).

61. Xie, Q., Pan, J., Ma, C. & Zhang, G. Dynamic surface antifouling: mechanism and systems. *Soft Matter* **15**, 1087–1107 (2019).

62. Zhang, Z. *et al.* Polysulfobetaine-grafted surfaces as environmentally benign ultralow fouling marine coatings. *Langmuir* **25**, 13516–13521 (2009).

63. Gudipati, C. S., Greenlief, C. M., Johnson, J. A., Prayongpan, P. & Wooley, K. L. Hyperbranched fluoropolymer and linear poly(ethylene glycol) based amphiphilic crosslinked networks as efficient antifouling coatings: an insight into the surface compositions, topographies, and morphologies. *J. Polym. Sci. Part A Polym. Chem.* **42**, 6193–6208 (2004).

64. Gudipati, C. S., Finlay, J. A., Callow, J. A., Callow, M. E. & Wooley, K. L. The antifouling and fouling-release performance of hyperbranched fluoropolymer (HBFP)-poly(ethylene glycol) (PEG) composite coatings evaluated by adsorption of biomacromolecules and the green fouling alga *Ulva*. *Langmuir* **21**, 3044–3053 (2005).

65. Olsen, S. M., Pedersen, L. T., Laursen, M. H., Kiil, S. & Dam-Johansen, K. Enzyme-based antifouling coatings: a review. *Biofouling* **23**, 369–383 (2007).

66. de Souza Santos, M., Salomon, D., Li, P., Krachler, A.-M. & Orth, K. *Vibrio parahaemolyticus* virulence determinants. in *The Comprehensive Sourcebook of Bacterial Protein Toxins* (eds. Alouf, J., Ladant, D. & Popoff, M. R.) 230–260 (Elsevier Ltd., 2015).

67. Aykin, E., Omuzbuken, B. & Kacar, A. Microfouling bacteria and the use of enzymes in eco-friendly antifouling technology. *J. Coatings Technol. Res.* **16**, 847–856 (2019).

68. Tasso, M. *et al.* Antifouling potential of Subtilisin A immobilized onto maleic anhydride copolymer thin films. *Biofouling* **25**, 505–516 (2009).

69. Dobretsov, S. *et al.* Inhibition of marine biofouling by bacterial quorum sensing inhibitors. *Biofouling* **27**, 893–905 (2011).

70. Dobretsov, S., Teplitski, M. & Paul, V. Mini-review: quorum sensing in the marine environment and its relationship to biofouling. *Biofouling* **25**, 413–427 (2009).

71. Maximilien, R. *et al.* Chemical mediation of bacterial surface colonisation by secondary metabolites from the red alga *Delisea pulchra*. *Aquat. Microb. Ecol.* **15**, 233–246 (1998).

72. Manefield, M. *et al.* Evidence that halogenated furanones from *Delisea pulchra* inhibit acylated homoserine lactone (AHL)-mediated gene expression by displacing the AHL signal from its receptor protein. *Microbiology* **145**, 283–291 (1999).

73. Ozcelik, B. *et al.* Poly(ethylene glycol)-based coatings combining low-biofouling and quorum-sensing inhibiting properties to reduce bacterial colonization. *ACS Biomater. Sci. Eng.* **3**, 78–87 (2017).

74. Egan, S., James, S., Holmström, C. & Kjelleberg, S. Inhibition of algal spore germination by the

marine bacterium *Pseudoalteromonas tunicata*. *FEMS Microbiol. Ecol.* **35**, 67–73 (2001).

75.   Satheesh, S., Ba-akdah, M. A. & Al-Sofyani, A. A. Natural antifouling compound production by microbes associated with marine macroorganisms – a review. *Electron. J. Biotechnol.* **21**, 26–35 (2016).

76.   Pallavicini, P., Dacarro, G., Diaz-Fernandez, Y. A. & Taglietti, A. Coordination chemistry of surface-grafted ligands for antibacterial materials. *Coord. Chem. Rev.* **275**, 37–53 (2014).

77.   Lindén, J. B. *et al.* Polyethyleneimine for copper absorption II: kinetics, selectivity and efficiency from seawater. *RSC Adv.* **5**, 51883–51890 (2015).

78.   Kaur, S., Kempon, I. M., Lindén, J. B., Larsson, M. & Nydén, M. Unhindered copper uptake by glutaraldehyde-polyethyleneimine coatings in an artificial seawater model system with adsorbed swollen polysaccharides and competing ligand EDTA. *Biofouling* **33**, 184–194 (2017).

79.   Movahedi, A., Lundin, A., Kann, N., Nydén, M. & Moth-Poulsen, K. Cu(I) stabilizing crosslinked polyethyleneimine. *Phys. Chem. Chem. Phys.* **17**, 18327–18336 (2015).

80.   Hirose, K. Conditional stability constants of metal complexes of organic ligands in sea water: past and present, and a simple coordination chemistry model. *Anal. Chim. Acta* **284**, 621–634 (1994).

81.   Nydén, B. M. *et al.* Metal ion binding polymers and uses thereof. (2014).

82.   Elmas, S. *et al.* Porous PEI coating for copper ion storage and its controlled electrochemical release. *Adv. Sustain. Syst.* **1900123**, 1–9 (2020).

83.   *Ligand Design in Medicinal Inorganic Chemistry.* (John Wiley & Sons, Ltd, 2014). doi:10.1002/9781118697191.ch2

84.   Lawrance, G. A. *Introduction to Coordination Chemistry*. (John Wiley & Sons, Inc., 2009).

85.   Hancock, R. D. & Martell, A. E. Ligand design for selective complexation of metal ions in aqueous solution. *Chem. Rev.* **89**, 1875–1914 (1989).

86.   Delangle, P. & Mintz, E. Chelation therapy in Wilson's disease: from D-penicillamine to the design of selective bioinspired intracellular Cu(I) chelators. *Dalt. Trans.* **41**, 6359–6370 (2012).

87.   Andersson Trojer, M., Movahedi, A., Blanck, H. & Nydén, M. Imidazole and triazole coordination chemistry for antifouling coatings. *J. Chem.* **2013**, 1–23 (2013).

88.   Lu, J. *et al.* Copper(II)-selective chelation improves function and antioxidant defences in cardiovascular tissues of rats as a model of diabetes: comparisons between triethylenetetramine and three less copper-selective transition-metal-targeted treatments. *Diabetologia* **53**, 1217–1226 (2010).

89.   Amorim, M. T. S., Chaves, S., Delgado, R. & Frausto da Silva, J. J. R. Oxatriaza macrocyclic ligands: studies of protonation and metal complexation. *J. Chem. Soc. Dalt. Trans.* 3065–3072

(1991).

90.   Cooper, G. J. S. Therapeutic potential of copper chelation with triethylenetetramine in managing diabetes mellitus and Alzheimer's disease. *Drugs* **71**, 1281–1320 (2011).

91.   Roberts, E. A. & Schilsky, M. L. Diagnosis and treatment of Wilson disease: an update. *Hepatology* **47**, 2089–2111 (2008).

92.   Granholm, K., Harju, L. & Ivaska, A. Desorption of metal ions from kraft pulps. Part 1. Chelation of hardwood and softwood kraft pulp with EDTA. *BioResources* **5**, 206–226 (2010).

93.   Jones, C. J. Bonding in transition metal complexes. in *d- and f-Block Chemistry* (ed. Abel, E. W.) 97–129 (Royal Society of Chemistry, 2001). doi:10.1021/ic50006a055

94.   Hosmane, N. S. Review of bonding theories for d-block metal complexes. in *Advanced Inorganic Chemistry* 89–114 (Elsevier Inc., 2017). doi:10.1016/b978-0-12-801982-5.00006-0

95.   Persson, I., Persson, P., Sandström, M. & Ullström, A.-S. Structure of Jahn-Teller distorted solvated copper(II) ions in solution, and in solids with apparently regular octahedral coordination geometry. *J. Chem. Soc. Dalt. Trans.* 1256–1265 (2002). doi:10.1039/b200698g

96.   Halcrow, M. A. Jahn-Teller distortions in transition metal compounds, and their importance in functional molecular and inorganic materials. *Chem. Soc. Rev.* **42**, 1784–1795 (2013).

97.   Jones, C. J. The thermodynamics of complex formation. in *d- and f- Block Chemistry* (ed. Abel, E. W.) 71–96 (John Wiley & Sons, Ltd, 2001). doi:10.1039/9781847550682-00071

98.   Fraústo da Silva, J. J. R. The chelate effect redefined. *J. Chem. Educ.* **60**, 390–392 (1983).

99.   Jones, C. J. Coordination compounds. in *d- and f-Block Chemistry* (ed. Abel, E. W.) 54–70 (Royal Society of Chemistry, 2001). doi:https://doi.org/10.1039/9781847550682

100.   Hutton, A. T. & Linder, P. W. Stability constants & their determination. in *Encyclopedia of Inorganic Chemistry* 1–9 (John Wiley & Sons, Ltd., 2006). doi:10.1002/0470862106.ia227

101.   Gans, P., Sabatini, A. & Vacca, A. Investigation of equilibria in solution. Determination of equilibrium constants with the HYPERQUAD suite of programs. *Talanta* **43**, 1739–1753 (1996).

102.   Hill, Z. D. & MacCarthy, P. Novel approach to Job's method: an undergraduate experiment. *J. Chem. Educ.* **63**, 162–167 (1986).

103.   Bruneau, E., Lavabre, D., Levy, G. & Micheau, J. C. Quantitative analysis of continuous-variation plots with a comparison of several methods: spectrophotometric study of organic and inorganic 1:1 stoichiometry complexes. *J. Chem. Educ.* **69**, 833–837 (1992).

104.   de Araújo, E. L., Barbosa, H. F. G., Dockal, E. R. & Cavalheiro, É. T. G. Synthesis, characterization and biological activity of Cu(II), Ni(II) and Zn(II) complexes of biopolymeric Schiff bases of salicylaldehydes and chitosan. *Int. J. Biol. Macromol.* **95**, 168–176 (2017).

105.   Kumar, S., Pandey, P. K., Sinha, N., Chaudhari, S. & Sharma, S. Spectroscopic characterisation

of metal complexes with tetradentate ligand. *J. Phys. Sci.* **29**, 1–11 (2018).

106. Alkaya, Z. A. *et al.* Synthesis and characterization of Cu(II) complexes of 2-amino-6-sulfamoylbenzothiazole and their inhibition studies on carbonic anhydrase isoenzymes. *Polyhedron* **151**, 199–205 (2018).

107. Okagu, O. D. *et al.* Synthesis and characterization of Cu(II), Co(II) and Ni(II) complexes of a benzohydrazone derivative: spectroscopic, DFT, antipathogenic and DNA binding studies. *J. Mol. Struct.* **1183**, 107–117 (2019).

108. Ramadan, S., Hambley, T. W., Kennedy, B. J. & Lay, P. A. NMR spectroscopic characterization of copper(II) and zinc(II) complexes of indomethacin. *Inorg. Chem.* **43**, 2943–2946 (2004).

109. Parodi, F. Physics and chemistry of microwave processing. in *Comprehensive Polymer Science and Supplements* (eds. Allen, G. & Bevington, J. C.) 669–728 (Elsevier Ltd., 1989).

110. Hwang, S. & Meyerhoff, M. E. Polyurethane with tethered copper(II)-cyclen complex: preparation, characterization and catalytic generation of nitric oxide from S-nitrosothiols. *Biomaterials* **29**, 2443–2452 (2008).

111. Kurnoskin, A. V. Metalliferous epoxy chelate polymers: 1. synthesis and properties. *Polymer (Guildf).* **34**, 1060–1067 (1993).

112. Abd El-Wahab, H., Abd El-Fattah, M., Ahmed, A. H., Elhenawy, A. A. & Alian, N. A. Synthesis and characterization of some arylhydrazone ligand and its metal complexes and their potential application as flame retardant and antimicrobial additives in polyurethane for surface coating. *J. Organomet. Chem.* **791**, 99–106 (2015).

113. González-Rodríguez, V. *et al.* Improving titanium dioxide dispersion in water through surface functionalization by a dicarboxylic acid. *J. Dispers. Sci. Technol.* **40**, 1039–1045 (2019).

114. Vincent, M., Duval, R. E., Hartemann, P. & Engels-Deutsch, M. Contact killing and antimicrobial properties of copper. *J. Appl. Microbiol.* **124**, 1032–1046 (2018).

115. Grass, G., Rensing, C. & Solioz, M. Metallic copper as an antimicrobial surface. *Appl. Environ. Microbiol.* **77**, 1541–1547 (2011).

116. Solioz, M. Copper disposition in bacteria. in *Clinical and Translational Perspectives on WILSON DISEASE* (eds. Kerkar, N. & Roberts, E. A.) 101–113 (Elsevier Inc., 2019). doi:10.1016/b978-0-12-810532-0.00011-2

117. Hans, M., Mathews, S., Mücklich, F. & Solioz, M. Physicochemical properties of copper important for its antibacterial activity and development of a unified model. *Biointerphases* **11**, 1–8 (2016).

118. Sato, T. *et al.* Assessment of the anti-biofouling potentials of a copper iodide-doped nylon mesh. *Appl. Microbiol. Biotechnol.* **95**, 1043–1050 (2012).

119. Luo, J., Hein, C., Mücklich, F. & Solioz, M. Killing of bacteria by copper, cadmium, and silver surfaces reveals relevant physicochemical parameters. *Biointerphases* **12**, 1–6 (2017).

120. Dupont, C. L., Grass, G. & Rensing, C. Copper toxicity and the origin of bacterial resistance – new insights and applications. *Metallomics* **3**, 1109–1118 (2011).

121. Stevenson, J., Barwinska-Sendra, A., Tarrant, E. & Waldron, K. J. Mechanism of action and applications of the antimicrobial properties of copper. in *Microbial Pathogens and Strategies for Combating Them: Science, Technology and Education* 468–479 (2013).

122. McElroy, D. J. *et al.* Effect of copper on multiple successional stages of a marine fouling assemblage. *Biofouling* **33**, 904–916 (2017).

123. Cuenot, F., Meyer, M., Bucaille, A. & Guilard, R. A molecular approach to remove lead from drinking water. *J. Mol. Liq.* **118**, 89–99 (2005).

124. Chester, R. & Jickells, T. *Marine Geochemistry*. (John Wiley & Sons, Ltd, 2012). doi:10.1007/978-94-010-9488-7

125. Gattuso, J.-P. & Hansson, L. *Ocean Acidification*. (Oxford University Press, Inc., 2011).

126. Chouyyok, W. *et al.* Selective removal of copper(II) from natural waters by nanoporous sorbents functionalized with chelating diamines. *Environ. Sci. Technol.* **44**, 6390–6395 (2010).

127. Daines, A. M., Robinson, H., Glenny, M., Williams, D. B. G. & Hinkley, S. F. R. Linear and macrocyclic water soluble polyacylhydrazones and their utilisation in coatings. *Prog. Org. Coatings* **121**, 38–44 (2018).

128. Daines, A. Personal communication.

129. Harris, D. C. & Bertolucci, M. D. *Symmetry and Spectroscopy: An Introduction to Vibrational and Electronical Spectroscopy*. (Dover Publications, Inc., 1978).

130. Conry, R. R. Copper: inorganic & coordination chemistry. in *Encyclopedia of Inorganic Chemistry* 1–19 (John Wiley & Sons, Ltd., 2006). doi:10.1002/0470862106.ia052

131. El-Wahab, H. A. The synthesis and characterization of the hydrazone ligand and its metal complexes and their performance in epoxy formulation surface coatings. *Prog. Org. Coatings* **89**, 106–113 (2015).

132. Rodríguez-Argüelles, M. C. *et al.* Antibacterial and antifungal activity of metal(II) complexes of acylhydrazones of 3-isatin and 3-(N-methyl)isatin. *Polyhedron* **28**, 2187–2195 (2009).

133. Zha, D. & You, L. Multiresponsive dynamic covalent assemblies for the selective sensing of both Cu^{2+} and CN^- in water. *ACS Appl. Mater. Interfaces* (2016). doi:10.1021/acsami.5b11552

134. Sayer, J. M., Pinsky, B., Schonbrunn, A. & Washtien, W. Mechanism of carbinolamine formation. *J. Am. Chem. Soc.* **96**, 7998–8009 (1974).

135. Brokaite, K., Mickevicius, V. & Mikulskiene, G. Synthesis and structural investigation of some

1,4-disubstituted-2-pyrrolidinones. *ARKIVOC* 61–67 (2006).

136. Ershov, A. Y. *et al.* Tautomerism and conformational isomerism of mercaptoacetylhydrazones of aliphatic and aromatic aldehydes. *Russ. J. Org. Chem.* **45**, 660–666 (2009).

137. Gu, W. *et al.* Synthesis and antibacterial evaluation of new *N*-acylhydrazone derivatives from dehydroabietic acid. *Molecules* **17**, 4634–4650 (2012).

138. Wyrzykiewicz, E. & Prukała, D. New isomeric *N*-substituted hydrazones of 2-, 3- and 4-pyridinecarboxaldehydes. *J. Heterocycl. Chem.* **35**, 381–387 (1998).

139. Palla, G., Predieri, G., Domiano, P., Vignali, C. & Turner, W. Conformational behaviour and *E/Z* isomerization of *N*-acyl and *N*-aroylhydrazones. *Tetrahedron* **42**, 3649–3654 (1986).

140. Ferraresi-Curotto, V., Echeverría, G. A., Piro, O. E., Pis-Diez, R. & González-Baró, A. C. Synthesis and characterization of a series of isoniazid hydrazones. Spectroscopic and theoretical study. *J. Mol. Struct.* **1133**, 436–447 (2017).

141. Cordier, C. *et al.* Salicylaldehyde benzoyl hydrazone: isomerization due to water. A structural analysis using a combination of NMR, IR, and theoretical investigations. *Struct. Chem.* **15**, 295–307 (2004).

142. Koh, L. L. *et al.* Complexes of salicylaldehyde acylhydrazones: cytotoxicity, QSAR and crystal structure of the sterically hindered *t*-butyl dimer. *J. Inorg. Biochem.* **72**, 155–162 (1998).

143. Friestad, G. K. Chiral *N*-acylhydrazones: versatile imino acceptors for asymmetric amine synthesis. *European J. Org. Chem.* **2005**, 3157–3172 (2005).

144. Van Dijken, D. J., Kovaříček, P., Ihrig, S. P. & Hecht, S. Acylhydrazones as widely tunable photoswitches. *J. Am. Chem. Soc.* **137**, 14982–14991 (2015).

145. Chaur, M. N., Collado, D. & Lehn, J.-M. Configurational and constitutional information storage: multiple dynamics in systems based on pyridyl and acyl hydrazones. *Chem. - A Eur. J.* **17**, 248–258 (2011).

146. Popov, L. D., Askalepova, O. I., Levchenkov, S. I. & Kogan, V. A. Protolitic complexing properties of acylhydrazones of substituted salicylaldehydes and stability constants of their copper(II) complexes. *Russ. J. Inorg. Chem.* **52**, 626–629 (2007).

147. Renuka, M. & Hussain Reddy, K. Non-extractive spectrophotometric determination of copper(II) in leafy vegetable samples using salicylaldehyde acetoylhydrazone (SAAH). *Int. J. Curr. Multidiscip. Stud.* **1**, 32–36 (2013).

148. Yousef Ebrahimipour, S., Sheikhshoaie, I., Crochet, A., Khaleghi, M. & Fromm, K. M. A new mixed-ligand copper(II) complex of (*E*)-*N'*-(2-hydroxybenzylidene) acetohydrazide: synthesis, characterization, NLO behavior, DFT calculation and biological activities. *J. Mol. Struct.* **1072**, 267–276 (2014).

149. Abd El Wahed, M. G., Bayoumi, H. A. & Mohammed, M. I. Physical properties of some acetylbenzaldehydehydrazone metal complexes. *Bull. Korean Chem. Soc.* **24**, 1313–1318 (2003).

150. Sanjeev, R., Jagannadham, V. & Vrath, R. V. Implications of a novel interpretation of the isosbestic point. *Chem. New Zeal.* **76**, 133–135 (2012).

151. Nowicka-Jankowska, T. Some properties of isosbestic points. *J. Inorg. Nucl. Chem.* **33**, 2043–2050 (1971).

152. Gans, P. Personal communication.

153. Hinkley, S. F. R. Personal communication.

154. Lehn, J.-M. Dynamers: dynamic molecular and supramolecular polymers. *Prog. Polym. Sci.* **30**, 814–831 (2005).

155. Roy, N., Bruchmann, B. & Lehn, J.-M. DYNAMERS: dynamic polymers as self-healing materials. *Chem. Soc. Rev.* **44**, 3786–3807 (2015).

156. Zhang, Y. & Barboiu, M. Constitutional dynamic materials – toward natural selection of function. *Chem. Rev.* **116**, 809–834 (2016).

157. Buchs, B. *et al.* Release of bioactive volatiles from supramolecular hydrogels: influence of reversible acylhydrazone formation on gel stability and volatile compound evaporation. *Org. Biomol. Chem.* **9**, 2906–2919 (2011).

158. Butler, A. Acquisition and utilization of transition metal ions by marine organisms. *Science* **281**, 207–210 (1998).

159. Singh, V. P. & Gupta, P. Synthesis, physico-chemical characterization and antimicrobial activity of cobalt(II), nickel(II), copper(II), zinc(II) and cadmium(II) complexes with some acyldihydrazones. *J. Enzyme Inhib. Med. Chem.* **23**, 797–805 (2008).

160. Ozay, H., Baran, Y. & Miyamaez, H. The stabilities and formation kinetics of some macrocycles with copper(II): crystal structures of some pendant arm macrocycles. *J. Coord. Chem.* **64**, 1469–1480 (2011).

161. Lee, S. C. *et al.* Highly selective copper(II) ion receptors: tetraazacrown ethers bearing two 8-hydroxyquinoline side arms. *Inorganica Chim. Acta* **317**, 174–180 (2001).

162. Esteves, C. V. *et al.* Remarkable inertness of copper(II) chelates of cyclen-based macrobicycles with two *trans-N*-acetate arms. *Inorg. Chem.* **52**, 5138–5153 (2013).

163. Füzerová, S. *et al.* Cyclam (1,4,8,11-tetraazacyclotetradecane) with one methylphosphonate pendant arm: a new ligand for selective copper(II) binding. *Dalt. Trans.* 2908–2915 (2005). doi:10.1039/b507062g

164. Lima, L. M. P., Esteban-Gómez, D., Delgado, R., Platas-Iglesias, C. & Tripier, R. Monopicolinate

cyclen and cyclam derivatives for stable copper(II) complexation. *Inorg. Chem.* **51**, 6916–6927 (2012).

165. Thom, V. J., Hosken, G. D. & Hancock, R. D. Anomalous metal ion size selectivity of tetraaza macrocycles. *Inorg. Chem.* **24**, 3378–3381 (1985).

166. Kodama, M. & Kimura, E. A thermodynamic and kinetic interpretation of the macrocyclic effect. Polarographic studies on copper(II) 1,4,7,10-tetraazacyclododecane complexation. *J. Chem. Soc., Chem. Commun.* 326–327 (1975).

167. Martell, A. E. & Hancock, R. D. The chelate, macrocyclic, and cryptate effects. in *Coordination Chemistry* (ed. Kauffman, G. B.) 240–254 (American Chemical Society, 1994). doi:10.1021/bk-1994-0565.ch020

168. Hancock, R. D. & McDougall, G. J. The macrocyclic effect in tetraaza-macrocyclic ligands. *Adv. Mol. Relax. Interact. Process.* **18**, 99–108 (1980).

169. Firdaus, F., Fatma, K., Azam, M. & Shakir, M. Synthesis, spectroscopic, thermal, and antimicrobial studies of tetradentate 12 and 14 member Schiff bases and their complexes with Fe(III), Co(II), and Cu(II). *J. Coord. Chem.* **63**, 3956–3968 (2010).

170. Li, S. *et al.* The synthesis and activities of novel mononuclear or dinuclear cyclen complexes bearing azole pendants as antibacterial and antifungal agents. *Eur. J. Med. Chem.* **84**, 677–686 (2014).

171. Shakir, M., Azim, Y., Chishti, H. T. N. & Parveen, S. Synthesis, characterization of complexes of Co(II), Ni(II), Cu(II) and Zn(II) with 12-membered Schiff base tetraazamacrocyclic ligand and the study of their antimicrobial and reducing power. *Spectrochim. Acta - Part A Mol. Biomol. Spectrosc.* **65**, 490–496 (2006).

172. Hirose, K., Dokiya, Y. & Sugimura, Y. Determination of conditional stability constants of organic copper and zinc complexes dissolved in seawater using ligand exchange method with EDTA. *Mar. Chem.* **11**, 343–354 (1982).

173. Hirose, K. Metal-organic matter interaction: ecological roles of ligands in oceanic DOM. *Appl. Geochemistry* **22**, 1636–1645 (2007).

174. Felix, V. *et al.* Electron spin resonance studies and crystal structures of copper(II) complexes of some 12-, 13- and 14-membered oxatriaza macrocycles. *J. Chem. Soc. Dalt. Trans.* 3099–3106 (1994).

175. Kodama, M. & Kimura, E. Reaction of cobalt(II) macrocyclic tetra-amine complexes with dioxygen. *J. Chem. Soc. Dalt. Trans.* 327–333 (1980).

176. Thom, V. J. & Hancock, R. D. The stability of nickel(II) complexes of tetra-aza macrocycles. *J. Chem. Soc. Dalt. Trans.* 1877–1880 (1985). doi:10.1039/DT9850001877

177. Kodama, B. M. & Kimura, E. Equilibria and kinetics of complex formation between zinc(II), lead(II), and cadmium(II), and 12-, 13-, 14-, and 15-membered macrocyclic tetra-amines. *J. Chem. Soc. Dalt. Trans.* 2269–2276 (1977).

178. Hancock, R. D., Wade, P. W., Ngwenya, M. P., de Sousa, A. S. & Damu, K. V. Ligand design for complexation in aqueous solution. 2. Chelate ring size as a basis for control of size-based selectivity for metal ions. *Inorg. Chem.* **29**, 1968–1974 (1990).

179. Hinz, F. P. & Margerum, D. W. Ligand solvation and the macrocyclic effect. Nickel(II)-tetramine complexes. *Inorg. Chem.* **13**, 2941–2949 (1974).

180. Nakani, B. S. & Hancock, R. D. The chelate, cryptate and macroyclic effects. *S. Afr. J. Chem.* **36**, 117 (1983).

181. Wadas, T. J., Wong, E. H., Weisman, G. R. & Anderson, C. J. Coordinating radiometals of copper, gallium, indium, yttrium and zirconium for PET and SPECT imaging of disease. *Chem Rev.* **110**, 2858–2902 (2010).

182. Hancock, R. D. Macrocycles and their selectivity for metal ions on the basis of size. *Pure Appl. Chem.* **58**, 1445–1452 (1986).

183. Paul, S. Crosslinking: chemistry of surface coatings. in *Comprehensive Polymer Science and Supplements* (eds. Allen, G. & Bevington, J. C.) 149–192 (Elsevier Ltd., 1996). doi:10.1016/b978-0-08-096701-1.00186-5

184. Bossion, A. *et al.* Opportunities for organocatalysis in polymer synthesis via step-growth methods. *Prog. Polym. Sci.* **90**, 164–210 (2019).

185. Armelin, E. *et al.* Marine paint fomulations: conducting polymers as anticorrosive additives. *Prog. Org. Coatings* **59**, 46–52 (2007).

186. Prisacariu, C. *Polyurethane Elastomers: From Morphology to Mechanical Aspects*. (Springer-Verlag/Wien, 2011). doi:10.1007/978-3-7091-0514-6

187. Puiu, S. C. *et al.* Metal ion-mediated nitric oxide generation from polyurethanes via covalently linked copper(II)-cyclen moieties. *J. Biomed. Mater. Res. - Part B Appl. Biomater.* **91B**, 203–212 (2009).

188. Xie, Q., Ma, C., Liu, C., Ma, J. & Zhang, G. Poly(dimethylsiloxane)-based polyurethane with chemically attached antifoulants for durable marine antibiofouling. *ACS Appl. Mater. Interfaces* **7**, 21030–21037 (2015).

189. Hamerton, I., Howlin, B. J. & Jepson, P. Metals and coordination compounds as modifiers for epoxy resins. *Coord. Chem. Rev.* **224**, 67–85 (2002).

190. Kurnoskin, A. V. Metalliferous epoxy chelate polymers: 2. influence of structural fragments on properties. *Polymer (Guildf).* **34**, 1068–1076 (1993).

191. Kurnoskin, A. V. Metalliferous epoxy chelate polymers: 3. influence of structural fragments on the properties of similar matrices. *Polymer (Guildf).* **34**, 1077–1088 (1993).

192. Kurnoskin, A. V. Water resistance of metalliferous epoxy chelate polymers. *J. Appl. Polym. Sci.* **45**, 1557–1567 (1992).

193. Döring, M. & Arnold, U. Polymerization of epoxy resins initiated by metal complexes. *Polym. Int.* **58**, 976–988 (2009).

194. Lakshmi, B., Shivananda, K. N., Prakash, G. A., Rama, K. R. K. & Mahendra, K. N. Synthesis of Co(II), Ni(II) and Cu(II) complexes from Schiff base ligand and reactivity studies with thermosetting epoxy resin. *Bull. Korean Chem. Soc.* **32**, 1613–1619 (2011).

195. Thomas, R. *Practical Guide to ICP-MS: A Tutorial for Beginners*. (CRC Press LLC, 2013).

196. Ojeil, M., Jermann, C., Holah, J., Denyer, S. P. & Maillard, J. Y. Evaluation of new *in vitro* efficacy test for antimicrobial surface activity reflecting UK hospital conditions. *J. Hosp. Infect.* **85**, 274–281 (2013).

197. Wiegand, C. *et al.* Critical physiological factors influencing the outcome of antimicrobial testing according to ISO 22196 / JIS Z 2801. *PLoS One* **13**, 1–15 (2018).

198. Campos, M. D., Zucchi, P. C., Phung, A., Leonard, S. N. & Hirsch, E. B. The activity of antimicrobial surfaces varies by testing protocol utilized. *PLoS One* **11**, 1–11 (2016).

199. Standard, I. *ISO 22196:2007 – Plastics – Measurement of antibacterial activity on plastics surfaces*. **2007**, (2007).

200. Burr, D. Personal communication.

201. Mytilinaios, I., Salih, M., Schofield, H. K. & Lambert, R. J. W. Growth curve prediction from optical density data. *Int. J. Food Microbiol.* **154**, 169–176 (2012).

202. Monod, J. The growth of bacterial cultures. *Annu. Rev. Microbiol.* **3**, 371–394 (1949).

203. Ferry, J. D. & Carritt, D. E. Action of antifouling paints. *Ind. Eng. Chem.* **38**, 612–617 (1946).

204. Rascio, V. J. D. Antifouling coatings: where do we go from here. *Corros. Rev.* **18**, 133–154 (2000).

205. Woods Hole Oceanographic Institute. The physical chemistry of compounds of copper and mercury and their interactions with sea water. in *Marine Fouling and Its Prevention* 264–276 (George Banta Publishing Co., 1952).

206. Macomber, L. & Imlay, J. A. The iron-sulfur clusters of dehydratases are primary intracellular targets of copper toxicity. *Proc. Natl. Acad. Sci. U. S. A.* **106**, 8344–8349 (2009).

207. Glenny, M. Personal communication.

208. Dorsey, J. G., Dorsey, G. F., Rutenberg, A. C. & Green, L. A. Determination of the epoxide equivalent weight of glycidyl ethers by proton magnetic resonance spectrometry. *Anal. Chem.*

49, 1144–1145 (1977).

209.   González Garcia, F., Montedo da Silva, P., Guenther Soares, B. & Rieumont Briones, J. Combined analytical techniques for the determination of the amine hydrogen equivalent weight in aliphatic amine epoxide hardeners. *Polym. Test.* **26**, 95–101 (2007).

210.   Product data sheet Epikote™ Resin 235. (2004).

211.   Epoxy curing agents and modifiers: Ancamine® 2459 Curing Agent.

212.   Burton, B. L. Amine-blushing problems? No sweat! in *Epoxy Resin Formulators' Meeting of the Society of the Plastics Industry* 1–17 (2001).

213.   Patel, R. N. *et al.* Characterization and biological activities of two copper(II) complexes with diethylenetriamine and 2,2'-bipyridine or 1,10-phenanthroline as ligands. *Spectrochim. Acta Part A Mol. Biomol. Spectrosc.* **62**, 261–268 (2005).

214.   Villis, P. C. M. *et al.* Diethylenetriamine ion-imprinted silica gel for copper determination in tap water. *J. Appl. Electrochem.* **48**, 867–883 (2018).

215.   Fang, Z., Yan, J., Yu, W., Zhang, N. & Zhang, S. Three Schiff base complexes based on diethylenetriamine: synthesis, structure, DNA binding and cleavage, and *in vitro* cytotoxicity. *Transit. Met. Chem.* **44**, 463–474 (2019).

216.   Dacarro, G. *et al.* Monolayers of polyethilenimine on flat glass: a versatile platform for cations coordination and nanoparticles grafting in the preparation of antibacterial surfaces. *Dalt. Trans.* **41**, 2456–2463 (2012).

217.   Shaw, R. A. & Mantsch, H. H. Near-IR spectrometers. in *Encyclopedia of Spectroscopy and Spectrometry* (ed. Lindon, J. C.) 1451–1461 (Elsevier Ltd., 2000).

218.   Cholake, S. T. *et al.* Quantitative analysis of curing mechanisms of epoxy resin by mid- and near-Fourier transform infrared spectroscopy. *Def. Sci. J.* **64**, 341–321 (2014).

219.   Beć, K. B. & Huck, C. W. Breakthrough potential in near-infrared spectroscopy: spectra simulation. A review of recent developments. *Front. Chem.* **7**, 1–22 (2019).

220.   Cañavate, J., Colom, X., Pagès, P. & Carrasco, F. Study of the curing process of an epoxy resin by FTIR spectroscopy. *Polym. Plast. Technol. Eng.* **39**, 937–943 (2000).

221.   González González, M., Cabanelas, J. C. & Baselga, J. Applications of FTIR on epoxy resins – identification, monitoring the curing process, phase separation and water uptake. in *Infrared Spectroscopy – Materials Science, Engineering and Technology* (ed. Theophile, T.) 261–284 (IntechOpen, 2012).

222.   Poisson, N., Lachenal, G. & Sautereau, H. Near- and mid-infrared spectroscopy studies of an epoxy reactive system. *Vib. Spectrosc.* **12**, 237–247 (1996).

223.   Morgan, R. J. The effect of thermal history and strain rate on the mechanical properties of

diethylenetriamine-cured bisphenol-A-diglycidyl ether epoxies. *J. Appl. Polym. Sci.* **23**, 2711–2717 (1979).

224.   Matějka, L. Amine cured epoxide networks: formation, structure, and properties. *Macromolecules* **33**, 3611–3619 (2000).

225.   Saucy, D. A., Simko, S. J. & Linton, R. W. Comparison of photoacoustic and attentuated total reflectance sampling depths in the infrared region. *Anal. Chem.* **57**, 871–875 (1985).

226.   Hobbs, A. L. & Almirall, J. R. Trace elemental analysis of automotive paints by laser ablation-inductively coupled plasma-mass spectrometry (LA-ICP-MS). *Anal. Bioanal. Chem.* **376**, 1265–1271 (2003).

227.   Hebbar, R. S., Isloor, A. M. & Ismail, A. F. Contact angle measurements. in *Membrane Characterization* 219–255 (Elsevier B.V, 2017).

228.   Al-Kattan, A. *et al.* Characterization of materials released into water from paint containing nano-SiO$_2$. *Chemosphere* **119**, 1314–1321 (2015).

229.   Zhou, S., Wu, L., Sun, J. & Shen, W. The change of the properties of acrylic-based polyurethane *via* addition of nano-silica. *Prog. Org. Coatings* **45**, 33–42 (2002).

230.   Manoudis, P. N., Tsakalof, A., Karapanagiotis, I., Zuburtikudis, I. & Panayiotou, C. Fabrication of super-hydrophobic surfaces for enhanced stone protection. *Surf. Coatings Technol.* **203**, 1322–1328 (2009).

231.   Wallström, E., Jespersen, H. T. & Schaumburg, K. A new concept for anti-fouling paint for yachts. *Prog. Org. Coatings* **72**, 109–114 (2011).

232.   Masato Kishihara, O., Akira Saito, F., Hiroshi Yamashita, H., Toshimitsu Muramatsu, Y. & Yoichi Yonehara, C. Antifouling coating composition. (1999).

233.   Simendinger, W. H. Antifouling coating composition. (2003).

234.   Michailidis, M. *et al.* Modified mesoporous silica nanoparticles with a dual synergetic antibacterial effect. *ACS Appl. Mater. Interfaces* **9**, 38364–38372 (2017).

235.   Brandès, S., David, G., Suspène, C., Corriu, R. J. P. & Guilard, R. Exceptional affinity of nanostructured organic-inorganic hybrid materials towards dioxygen: confinement effect of copper complexes. *Chem. - A Eur. J.* **13**, 3480–3490 (2007).

236.   Barbette, F. *et al.* Extraction of uranyl ions from aqueous solutions using silica-gel-bound macrocycles for alpha contaminated waste water treatment. *Anal. Chim. Acta* **502**, 179–187 (2004).

237.   Dubois, G. *et al.* Coordination chemistry in the solid: study of the incorporation of Cu(II) into cyclam-containing hybrid materials. *Angew. Chemie - Int. Ed.* **40**, 1087–1090 (2001).

238.   Dubois, G., Tripier, R., Brandès, S., Denat, F. & Guilard, R. Cyclam complexes containing silica

gels for dioxygen adsorption. *J. Mater. Chem.* **12**, 2255–2261 (2002).

239. Dubois, G. *et al.* First organic-inorganic hybrid materials with controlled porosity incorporating cyclam units. *Chem. Commun.* 2283–2284 (1999). doi:10.1039/a907217i

240. Corriu, R. J. P., Embert, F., Guari, Y., Reyé, C. & Guilard, R. Coordination chemistry in the solid: evidence for coordination modes within hybrid materials different from those in solution. *Chem. - A Eur. J.* **8**, 5732–5741 (2002).

241. Gros, C. *et al.* New silica-gel-bound polyazacycloalkanes and characterization of their copper(II) complexes using electron spin resonance spectroscopy. *J. Chem. Soc. - Dalt. Trans.* 1209–1214 (1996). doi:10.1039/DT9960001209

242. Corriu, R. J. P. *et al.* Preparation of ordered SBA-15 mesoporous silica containing chelating groups. Study of the complexation of Eu(II) inside the pore channels of the materials. *New J. Chem.* **28**, 156–160 (2004).

243. Corriu, R. J. P., Mehdi, A., Reyé, C. & Thieuleux, C. Direct synthesis of functionalized mesoporous silica by non-ionic assembly routes. Quantitative chemical transformations within the materials leading to strongly chelated transition metal ions. *Chem. Mater.* **16**, 159–166 (2004).

244. Kassiba, A. *et al.* EPR investigations of mesoporous silica doped with metal transitions ions. *J. Phys. Chem. Solids* **67**, 875–881 (2006).

245. Corriu, R. J. P., Mehdi, A., Reyé, C. & Thieuleux, C. Control of coordination chemistry in both the framework and the pore channels of mesoporous hybrid materials. *New J. Chem.* **27**, 905–908 (2003).

246. Gong, Y. & Lee, H. K. Application of cyclam-capped β-cyclodextrin-bonded silica particles as a chiral stationary phase in capillary electrochromatography for enantiomeric separations. *Anal. Chem.* **75**, 1348–1354 (2003).

247. Sujandi, Han, S.-C., Han, D.-S., Jin, M.-J. & Park, S.-E. Catalytic oxidation of cycloolefins over Co(cyclam)-functionalized SBA-15 material with H_2O_2. *J. Catal.* **243**, 410–419 (2006).

248. Puranik, D. B. *et al.* Copper removal from fuel by solid-supported polyamine chelating agents. *Energy and Fuels* **12**, 792–797 (1998).

249. Veuthey, J. L., Bagnoud, M. A. & Haerdi, W. Enrichment of amino and carboxylic acids using copper-loaded silica pre-columns coupled on-line with HPLC. *Int. J. Environ. Anal. Chem.* **26**, 157–166 (1986).

250. Bagnoud, M. A. & Haerdi, W. Metal-loaded silicas for on-line coupling of enrichment pre-column and analytical columns. *Int. J. Environ. Anal. Chem.* **38**, 97–104 (1990).

251. Bradshaw, J. S. *et al.* New nitrogen-containing macrocyclic ligands covalently attached to silica

gel and their use in separating metal cations. *Solvent Extr. Ion Exch.* **7**, 855–864 (1989).

252. Goubert-Renaudin, S. *et al.* Factors affecting copper(II) binding to multiarmed cyclam-grafted mesoporous silica in aqueous solution. *Langmuir* **25**, 9804–9813 (2009).

253. Da'na, E. Adsorption of heavy metals on functionalized-mesoporous silica: a review. *Microporous Mesoporous Mater.* **247**, 145–157 (2017).

254. Díaz-García, D. *et al.* Preparation and study of the antibacterial applications and oxidative stress induction of copper maleamate-functionalized mesoporous silica nanoparticles. *Pharmaceutics* **11**, 1–18 (2019).

255. Bagnoud, M. A., Haerdi, W. & Veuthey, J. L. Outer-sphere ligand-exchange chromatography with copper-loaded macrocyclic-bonded silica column. *Chromatographia* **29**, 495–499 (1990).

256. Plueddemann, E. P. *Silane Coupling Agents*. (Springer Science + Business Media, LLC, 1982).

257. Jal, P. K., Patel, S. & Mishra, B. K. Chemical modification of silica surface by immobilization of functional groups for extractive concentration of metal ions. *Talanta* **62**, 1005–1028 (2004).

258. Bereczki, H. F., Daróczi, L., Fábián, I. & Lázár, I. Sol-gel synthesis, characterization and catalytic activity of silica aerogels functionalized with copper(II) complexes of cyclen and cyclam. *Microporous Mesoporous Mater.* **234**, 392–400 (2016).

259. Barreto, J. A., Matterna, M., Graham, B., Stephan, H. & Spiccia, L. Synthesis, colloidal stability and ^{64}Cu labeling of iron oxide nanoparticles bearing different macrocyclic ligands. *New J. Chem.* **35**, 2705–2712 (2011).

260. Ortega, F., Velez, E. & Somanathan, R. Synthesis and use of reverse-phase silica gel for HPLC in undergraduate chemistry. *J. Chem. Educ.* **73**, A26 (1996).

261. Fulmer, G. R. *et al.* NMR chemical shifts of trace impurities: common laboratory solvents, organics, and gases in deuterated solvents relevant to the organometallic chemist. *Organometallics* **29**, 2176–2179 (2010).

262. Capeletti, L. B. & Zimnoch, J. H. Fourier Transform Infrared and Raman characterization of silica-based materials. in *Applications of Molecular Spectroscopy to Current Research in the Chemical and Biological Sciences* (ed. Stauffer, M. T.) 3–22 (IntechOpen, 2016). doi:10.5772/64477

263. Tripp, C. P. & Hair, M. L. Reaction of chloromethylsilanes with silica: a low-frequency infrared study. *Langmuir* **7**, 923–927 (1991).

264. Wan, F., Li, C., Jiang, L. & Li, Y. Synthesis and characterization of binuclear Zn(II)-cyclen complexes bridged by α,ω-bis(4-methylphenoxy) alkanes. *Res. Chem. Intermed.* **38**, 2085–2096 (2012).

265. Parker, R. E. & Isaacs, N. S. Mechanisms of epoxide reactions. *Chem. Rev.* **59**, 737–799 (1959).

266. Williams, D. B. G. & Cullen, A. Al(OTf)₃-mediated epoxide ring-opening reactions: toward

piperazine-derived physiologically active products. *J. Org. Chem.* **74**, 9509–9512 (2009).

267. Williams, D. B. G. & Lawton, M. Aluminium triflate: a remarkable Lewis acid catalyst for the ring opening of epoxides by alcohols. *Org. Biomol. Chem.* **3**, 3269–3272 (2005).

268. Sepeur, S. *Nanotechnology: Technical Basics and Applications*. (Vincentz Network, 2008).

269. Lu, H.-T. Synthesis and characterization of amino-functionalized silica nanoparticles. *Colloid J.* **75**, 311–318 (2013).

270. Teughels, W., Van Assche, N., Sliepen, I. & Quirynen, M. Effect of material characteristics and/or surface topography on biofilm development. *Clin. Oral Implants Res.* **17**, 68–81 (2006).

271. Kozlovsky, A., Artzi, Z., Moses, O., Kamin-Belsky, N. & Greenstein, R. B.-N. Interaction of chlorhexidine with smooth and rough types of titanium surfaces. *J. Periodontol.* **77**, 1194–1200 (2006).

272. Loesche, W. J. Role of *Streptococcus mutans* in human dental decay. *Microbiol. Rev.* **50**, 353–380 (1986).

273. Miyoshi, K. *Surface Characterization Techniques: An Overview*. (Glenn Research Center, 2002).

274. Scimeca, M., Bischetti, S., Lamsira, H. K., Bonfiglio, R. & Bonanno, E. Energy dispersive X-ray (EDX) microanalysis: a powerful tool in biomedical research and diagnosis. *Eur. J. Histochem.* **62**, 1–10 (2018).

275. Goldstein, J. I. *et al. Scanning Electron Microscopy and X-ray Microanalysis*. (Springer-Verlag New York, 2018). doi:10.1007/978-1-4939-6676-9

276. Stojilovic, N. Why can't we see hydrogen in X-ray photoelectron spectroscopy? *J. Chem. Educ.* **89**, 1331–1332 (2012).

277. Konopka, J. *Options for quantitative analysis of light elements by SEM/EDS*. (Thermo Fisher Scientific Inc., 2013).

278. Inkson, B. J. 2 - Scanning electron microscopy (SEM) and transmission electron microscopy (TEM) for materials characterization. in *Materials Characterization Using Nondestructive Evaluation (NDE) Methods* (eds. Hübschen, G., Altpeter, I., Tschuncky, R. & Herrmann, H.-G.) 17–43 (Woodhead Publishing, 2016).

279. Ni, C. Scanning electron microscopy (SEM). in *Encyclopedia of Tribology* (eds. Wang, Q. J. & Chung, Y.-W.) **150**, 2977–2982 (Springer US, 2013).

280. Newbury, D. E. & Ritchie, N. W. M. Is scanning electron microscopy/energy dispersive X-ray spectrometry (SEM/EDS) quantitative? *Scanning* **35**, 141–168 (2013).

281. Newbury, D. E. & Ritchie, N. W. M. Performing elemental microanalysis with high accuracy and high precision by scanning electron microscopy/silicon drift detector energy-dispersive X-ray spectrometry (SEM/SDD-EDS). *J. Mater. Sci.* **50**, 493–518 (2015).

282. Briand, J. F. Marine antifouling laboratory bioassays: an overview of their diversity. *Biofouling* **25**, 297–311 (2009).

283. Garrett, T. R., Bhakoo, M. & Zhang, Z. Bacterial adhesion and biofilms on surfaces. *Prog. Nat. Sci.* **18**, 1049–1056 (2008).

284. Wang, Y., Lee, S. M. & Dykes, G. The physicochemical process of bacterial attachment to abiotic surfaces: challenges for mechanistic studies, predictability and the development of control strategies. *Crit. Rev. Microbiol.* **41**, 452–464 (2015).

285. Hermansson, M. The DLVO theory in microbial adhesion. *Colloids Surfaces B Biointerfaces* **14**, 105–119 (1999).

286. Harder, T. & Yee, L. H. Bacterial adhesion and marine fouling. in *Advances in Marine Antifouling Coatings and Technologies* (eds. Hellio, C. & Yebra, D.) 113–131 (Elsevier Science & Technology, 2009). doi:10.1533/9781845696313.1.113

287. Donlan, R. M. Biofilms: microbial life on surfaces. *Emerg. Infect. Dis.* **8**, 881–890 (2002).

288. Rijnaarts, H. H. M., Norde, W., Bouwer, E. J., Lyklema, J. & Zehnder, A. J. B. Bacterial adhesion under static and dynamic conditions. *Appl. Environ. Microbiol.* **59**, 3255–3265 (1993).

289. Dewanti, R. & Wong, A. C. L. Influence of culture conditions on biofilm formation by *Escherichia coli* O157:H7. *Int. J. Food Microbiol.* **26**, 147–164 (1995).

290. Moodie, L. W. K. *et al.* Probing the structure-activity relationship of the natural antifouling agent polygodial against both micro- and macrofoulers by semisynthetic modification. *J. Nat. Prod.* **80**, 515–525 (2017).

291. Cuadrado-Silva, C. T., Castellanos, L., Arévalo-Ferro, C. & Osorno, O. E. Detection of quorum sensing systems of bacteria isolated from fouled marine organisms. *Biochem. Syst. Ecol.* **46**, 101–107 (2013).

292. Nandhini, S. & Revathi, K. Study on biofouling organisms present on the surface of boats in Royapuram, Chennai. *Nat. Environ. Pollut. Technol.* **15**, 257–261 (2016).

293. Mittelman, M. W. *et al.* Test systems for determining antifouling coating efficacy using on-line detection of bioluminescence and fluorescence in a laminar-flow environment. *J. Microbiol. Methods* **18**, 51–60 (1993).

294. Angell, P., Arrage, A. A., Mittelman, M. W. & White, D. C. On line, non-destructive biomass determination of bacterial biofilms by fluorometry. *J. Microbiol. Methods* **18**, 317–327 (1993).

295. Karunasagar, I., Otta, S. K. & Karunasagar, I. Biofilm formation by *Vibrio harveyi* on surfaces. *Aquaculture* **140**, 241–245 (1996).

296. Armstrong, E., Boyd, K. G., Pisacane, A., Peppiatt, C. J. & Burgess, J. G. Marine microbial natural products in antifouling coatings. *Biofouling* **16**, 215–224 (2000).

297. Xu, Q., Barrios, C. A., Cutright, T. & Newby, B. M. Z. Assessment of antifouling effectiveness of two natural product antifoulants by attachment study with freshwater bacteria. *Environ. Sci. Pollut. Res.* **12**, 278–284 (2005).

298. Barrios, C. A., Xu, Q., Cutright, T. & Newby, B. M. Z. Incorporating zosteric acid into silicone coatings to achieve its slow release while reducing fresh water bacterial attachment. *Colloids Surfaces B Biointerfaces* **41**, 83–93 (2005).

299. Cassé, F. & Swain, G. W. The development of microfouling on four commercial antifouling coatings under static and dynamic immersion. *Int. Biodeterior. Biodegrad.* **57**, 179–185 (2006).

300. Santos Mendonça, R. C., Morelli, A. M. F., Pereira, J. A. M., de Carvalho, M. M. & de Souza, N. L. Prediction of *Escherichia coli* O157:H7 adhesion and potential to form biofilm under experimental conditions. *Food Control* **23**, 389–396 (2012).

301. Danese, P. N., Pratt, L. A., Dove, S. L. & Kolter, R. The outer membrane protein, Antigen 43, mediates cell-to-cell interactions within *Escherichia coli* biofilms. *Mol. Microbiol.* **37**, 424–432 (2000).

302. O'Toole, G. A. *et al.* Genetic approaches to study of biofilms. *Methods Enzymol.* **310**, 91–109 (1999).

303. Naves, P. *et al.* Measurement of biofilm formation by clinical isolates of *Escherichia coli* is method-dependent. *J. Appl. Microbiol.* **105**, 585–590 (2008).

304. Mire, C. E., Tourjee, J. A., O'Brien, W. F., Ramanujachary, K. V. & Hecht, G. B. Lead precipitation by *Vibrio harveyi*: evidence for novel quorum-sensing interactions. *Appl. Environ. Microbiol.* **70**, 855–864 (2004).

305. Muazu, A. *et al.* Differential biofilm formation and chemical disinfection resistance of *Escherichia coli* on stainless steel and polystyrene tissue culture plate. *Int. J. Res. Med. Sci.* **3**, 3300–3307 (2015).

306. Merritt, J. H., Kadouri, D. E. & O'Toole, G. A. Growing and analyzing static biofilms. *Curr. Protoc. Microbiol.* **Chapter 1**, 1–29 (2005).

307. Epstein, A. K., Hochbaum, A. I., Kim, P. & Aizenberg, J. Control of bacterial biofilm growth on surfaces by nanostructural mechanics and geometry. *Nanotechnology* **22**, 1–18 (2011).

308. Herigstad, B., Hamilton, M. & Heersink, J. How to optimize the drop plate method for enumerating bacteria. *J. Microbiol. Methods* **44**, 121–129 (2001).

309. Wu, C., Lim, J. Y., Fuller, G. G. & Cegelski, L. Disruption of *E. coli* amyloid-integrated biofilm formation at the air-liquid interface by a polysorbate surfactant. *Langmuir* **29**, 920–926 (2013).

310. Pankey, G. A. & Sabath, L. D. Clinical relevance of bacteriostatic *versus* bactericidal mechanisms of action in the treatment of Gram-positive bacterial infections. *Clin. Infect. Dis.* **38**, 864–870

(2004).

311.	Day, D. Personal communication.

312.	Santo, C. E., Taudte, N., Nies, D. H. & Grass, G. Contribution of copper ion resistance to survival of *Escherichia coli* on metallic copper surfaces. *Appl. Environ. Microbiol.* **74**, 977–986 (2008).

313.	Pallavicini, P. *et al.* A monolayer of a Cu^{2+}-tetraazamacrocyclic complex on glass as the adhesive layer for silver nanoparticles grafting, in the preparation of surface-active antibacterial materials. *New J. Chem.* **35**, 1198–1201 (2011).

314.	Warnes, S. L., Caves, V. & Keevil, C. W. Mechanism of copper surface toxicity in *Escherichia coli* O157:H7 and *Salmonella* involves immediate membrane depolarization followed by slower rate of DNA destruction which differs from that observed for Gram-positive bacteria. *Environ. Microbiol.* **14**, 1730–1743 (2012).

315.	Singh, A., Yeager, R. & McFeters, G. A. Assessment of *in vivo* revival, growth, and pathogenicity of *Escherichia coli* strains after copper- and chlorine-induced injury. *Appl. Environ. Microbiol.* **52**, 832–837 (1986).

316.	Grey, B. & Steck, T. R. Concentrations of copper thought to be toxic to *Escherichia coli* can induce the viable but nonculturable condition. *Appl. Environ. Microbiol.* **67**, 5325–5327 (2001).

317.	Lindgren, J. F. *et al.* Copper release rate needed to inhibit fouling on the west coast of Sweden and control of copper release using zinc oxide. *Biofouling* **34**, 453–463 (2018).

318.	He, T. *et al.* Polydopamine assisted immobilisation of copper(II) on titanium for antibacterial applications. *Mater. Technol.* **30**, B68–B72 (2015).

319.	Perrin, C. *et al.* Nickel promotes biofilm formation by *Escherichia coli* K-12 strains that produce curli. *Appl. Environ. Microbiol.* **75**, 1723–1733 (2009).

320.	Long, T. E. Repurposing thiram and disulfiram as antibacterial agents for multidrug-resistant *Staphylococcus aureus* infections. *Antimicrob. Agents Chemother.* **61**, 1–8 (2017).

321.	Trueba, F. J. & Woldringh, C. L. Changes in cell diameter during the division cycle of *Escherichia coli*. *J. Bacteriol.* **142**, 869–878 (1980).

322.	Law, B. Pharmaceuticals/basic drugs: liquid chromatography. in *Encyclopedia of Separation Science* (ed. Wilson, I. D.) 3701–3708 (Elsevier Science Ltd., 2000).

323.	Arrage, A. A. *et al.* On-line monitoring of antifouling and fouling-release surfaces using bioluminescence and fluorescence measurements during laminar flow. *J. Ind. Microbiol.* **15**, 277–282 (1995).

324.	Sarkheil, M., Sourinejad, I., Mirbakhsh, M., Kordestani, D. & Johari, S. A. Antibacterial activity of immobilized silver nanoparticles on TEPA-Den-SiO_2 against shrimp pathogen, *Vibrio* sp. Persian1. *Aquac. Res.* **48**, 2120–2132 (2017).

325. Brandt, S. & Podivinsky, E. Resuscitation of putative viable but non-culturable (VNC) foodborne bacteria of significance to New Zealand. 1–44 (2008).

326. Wang, L. *et al.* Use of bacteriophages to control *Escherichia coli* O157:H7 in domestic ruminants, meat products, and fruits and vegetables. *Foodborne Pathog. Dis.* **14**, 483–493 (2017).

327. M63 Medium Broth. 1–3 (2015).

328. Smith, A. C. & Hussey, M. A. Gram stain protocols. 1–9 (2005).

329. Sadek, B. *et al.* Non-imidazole histamine H3 receptor ligands incorporating antiepileptic moieties. *Eur. J. Med. Chem.* **77**, 269–279 (2014).

330. Yang, Z. D., Song, Z. W., Ren, J., Yang, M. J. & Li, S. Improved thin-layer chromatography bioautographic assay for the detection of actylcholinesterase inhibitors in plants. *Phytochem. Anal.* **22**, 509–515 (2011).

331. Gao, W., Li, Q., Chen, J., Wang, Z. & Hua, C. Total synthesis of six 3,4-unsubstituted coumarins. *Molecules* **18**, 15613–15623 (2013).

332. Kozlov, N. G. & Basalaeva, L. I. Vanillin esters in reactions with indan-1,3-dione. *Chem. Heterocycl. Compd.* **42**, 1223–1228 (2006).

333. Bois, L. *et al.* Functionalized silica for heavy metal ions adsorption. *Colloids Surfaces A Physicochem. Eng. Asp.* **221**, 221–230 (2003).

334. Cui, Y. *et al.* A dual solvent evaporation route for preserving carbon nanoparticle fluorescence in silica gel and producing white light-emitting diodes. *Mater. Chem. Front.* **1**, 387–393 (2017).

335. Li, J. *et al.* Liquid oxygen compatibility and cryogenic mechanical properties of a novel phosphorous/silicon containing epoxy-based hybrid. *RSC Adv.* **6**, 91012–91023 (2016).

8 APPENDIX

8.1 CHAPTER 2
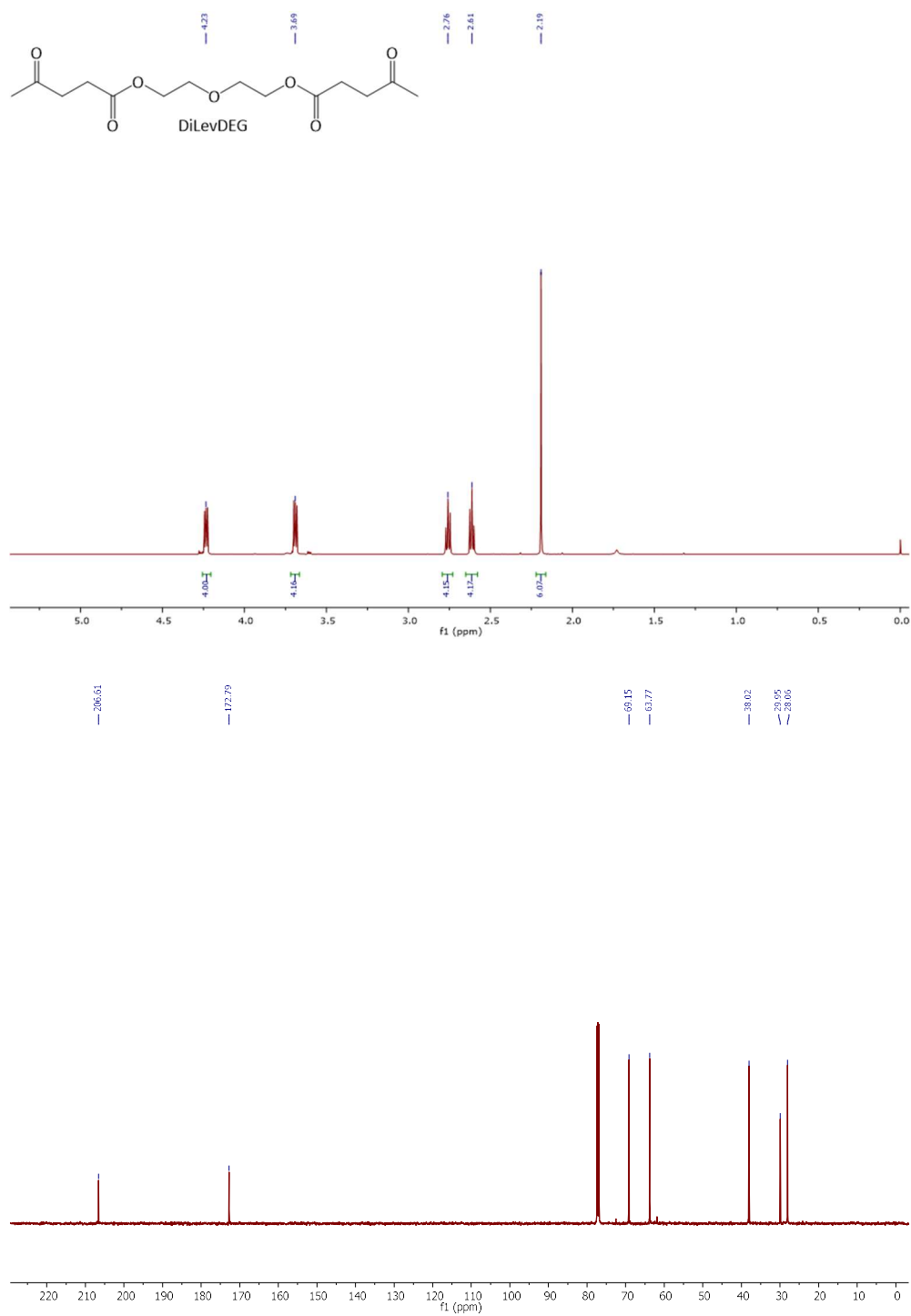
Figure 8.1. ^{1}H and ^{13}C NMR spectra (CDCl$_3$) of DiLevDEG (δ_H 1.73 ppm = water; δ_H 4.26 & 3.60 ppm = DEG).
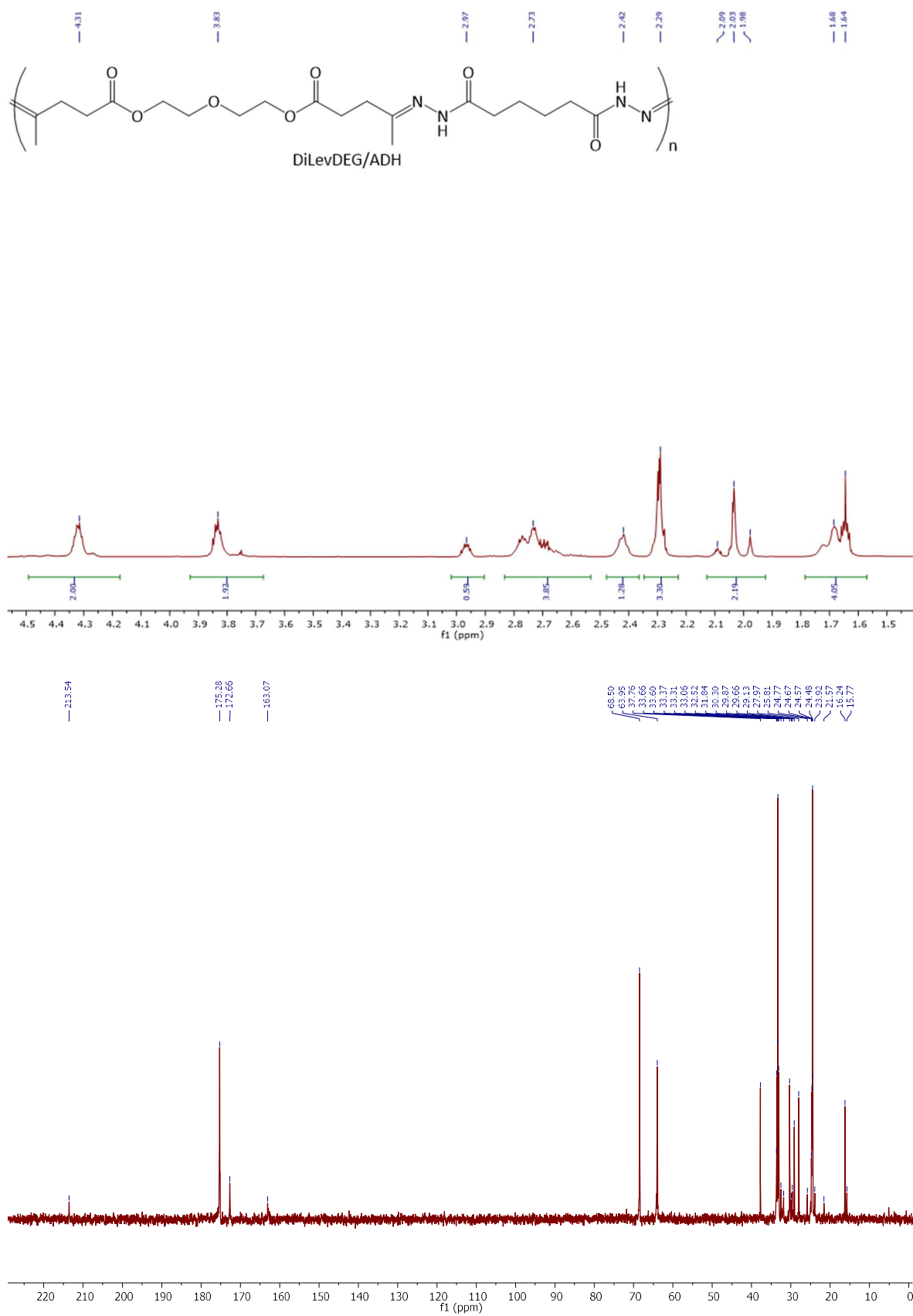
Figure 8.2. ^{1}H and ^{13}C NMR spectra (crude; D_2O) of DiLevDEG/ADH polyacylhydrazone.
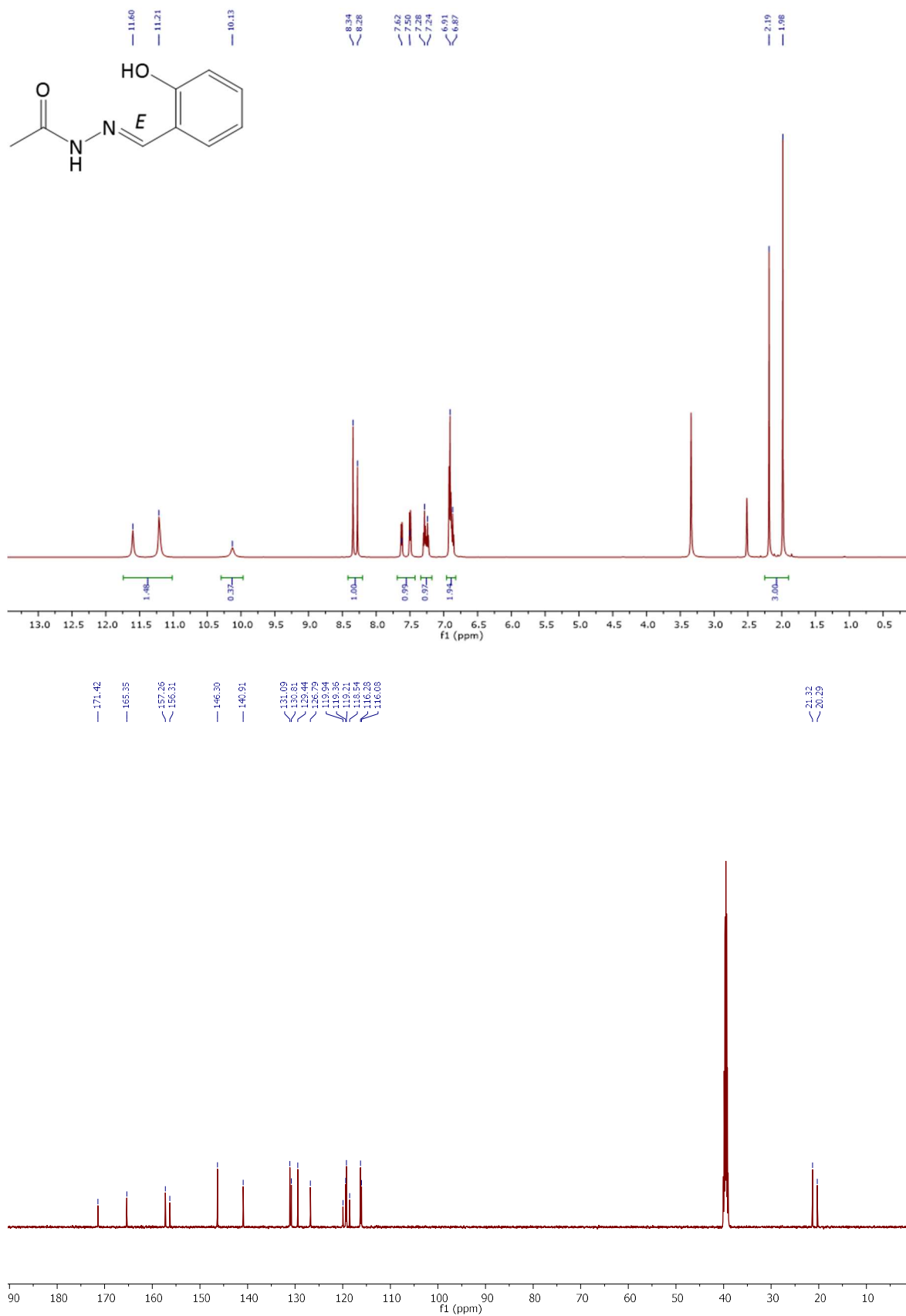
Figure 8.3. ^{1}H and ^{13}C NMR spectra (DMSO-d_6) of **1a** (δ_H 3.33 ppm = water).
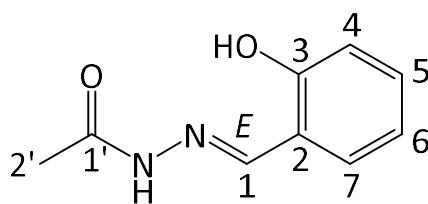
Table 8.1. Peak assignments in ^{1}H and ^{13}C NMR spectra of **1a**.

Position	$\delta_C{}^{a,b}$, Type	$\delta_H{}^{a,c}$ (*J* in Hz)
1	146.3, 140.9, CH	8.34, s; 8.27, s
2	119.9, 118.5, C	-
3	157.3, 156.3, C	-
4	116.3, 116.1, CH	6.94–6.83, m
5	131.1, 130.8, CH	7.28, td (7.6, 1.6); 7.24, td (7.5, 1.6)
6	119.4, 119.2, CH	6.94–6.83, m
7	129.4, 126.8, CH	7.62, dd (7.8, 1.7); 7.49, dd (7.5, 1.7)
1'	171.4, 165.4, C	-
2'	21.3, 20.3, CH$_3$	2.18, s; 1.98, s
OH	-	10.13, s
NH	-	11.60, s; 11.21, s

^{a} Where multiple values are provided, rotamers were observed in solution.
^{b} 126 MHz, Referenced to DMSO-d_6 (δ_C 39.52 ppm).[261] Elucidated/confirmed by DEPT, HSQC, and HMBC.
^{c} 500 MHz, Referenced to TMS (δ_H 0.00 ppm). Elucidated/confirmed by HSQC, HMBC, and COSY.
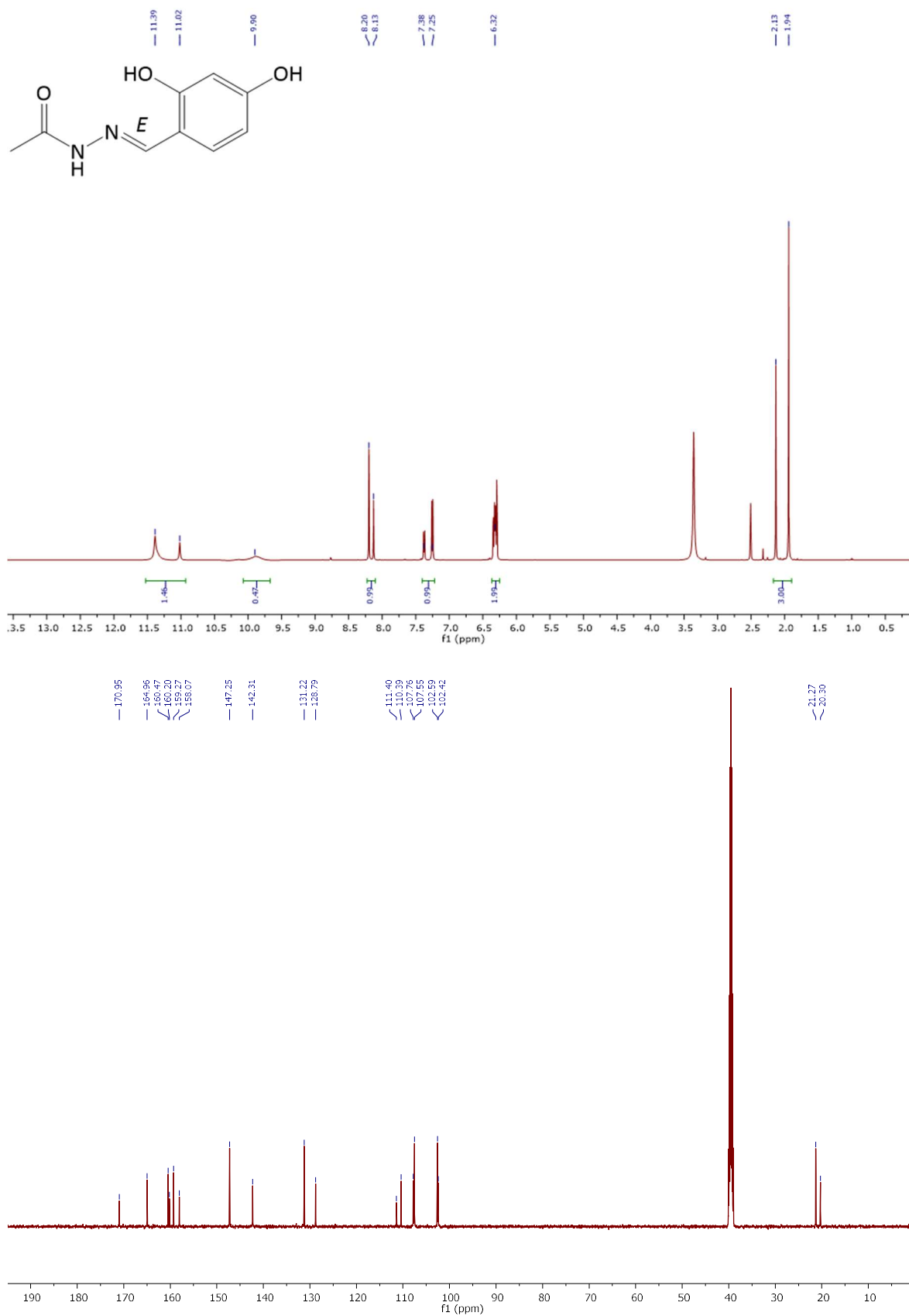
Figure 8.4. ^{1}H and ^{13}C NMR spectra (DMSO-d_6) of **1b** (δ_H 3.36 ppm = water; δ_H 2.32 ppm = contaminant).
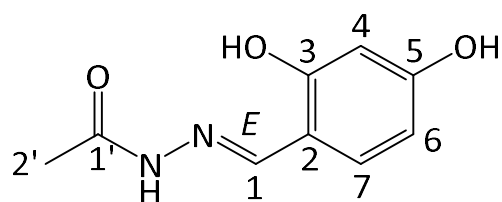
Table 8.2. Peak assignments in ^{1}H and ^{13}C NMR spectra of **1b**.

Position	$\delta_C{}^{a,b}$, Type	$\delta_H{}^{a,c}$ (*J* in Hz)
1	147.3, 142.3, CH	8.20, s; 8.13, s
2	111.4, 110.4, C	-
3 or 5	160.5, 160.2, C	-
4	102.6, 102.4, CH	6.37–6.27, m
5 or 3	159.3, 158.1, C	-
6	131.2, 128.8, CH	7.38, d (9.1); 7.25, d (8.4)
7	107.8, 107.6, CH	6.37–6.27, m
1'	171.0, 165.0, C	-
2'	21.3, 20.3, CH$_3$	2.13, s; 1.94, s
3 or 5 OH	-	9.89, s
NH	-	11.39, s; 11.02, s

[a] Where multiple values are provided, rotamers were observed in solution.
[b] 126 MHz, Referenced to DMSO-d_6 (δ 39.52 ppm).[261] Elucidated/confirmed by DEPT, HSQC, and HMBC.
[c] 500 MHz, Referenced to TMS (δ 0.00 ppm). Elucidated/confirmed by HSQC, HMBC, and COSY.
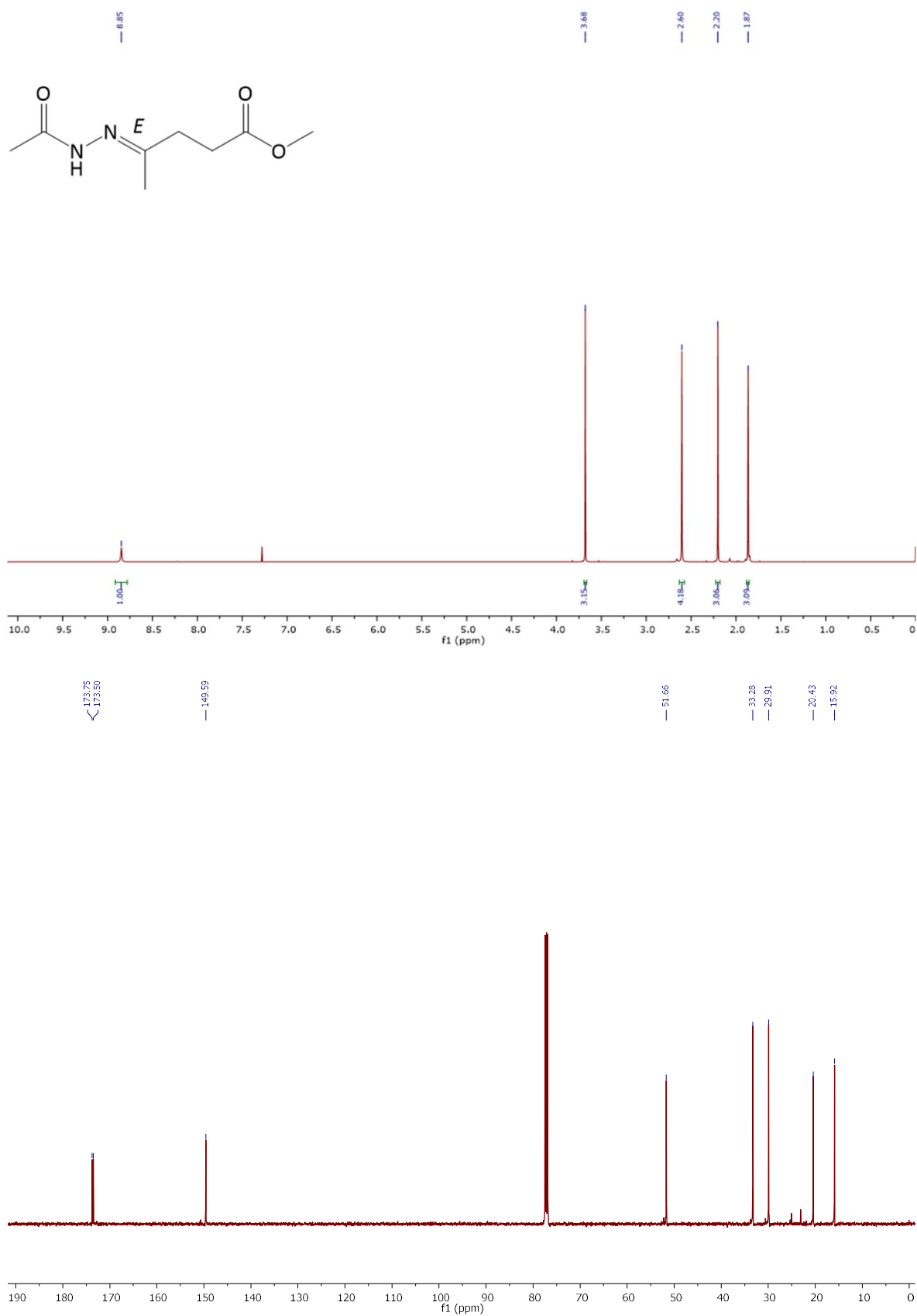
Figure 8.5. ^{1}H and ^{13}C NMR spectra (CDCl$_3$) of **1i**.
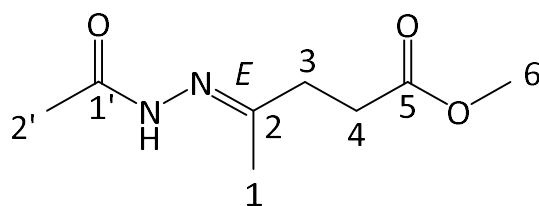
Table 8.3. Peak assignments in ^{1}H and ^{13}C NMR spectra of **1i**.

Position	$\delta_C{}^a$, Type	$\delta_H{}^b$ (*J* in Hz)
1	15.9, CH$_3$	1.87, s
2	149.6, C	-
3	33.3, CH$_2$	2.63–2.57, m
4	29.9, CH$_2$	2.63–2.57, m
5	173.5, C	-
6	51.7, CH$_3$	3.68, s
1'	173.8, C	-
2'	20.4, CH$_3$	2.20, s
NH	-	8.84, s

^{a} 126 MHz, Referenced to CDCl$_3$ (δ 77.16 ppm).[261] Elucidated/confirmed by DEPT, HSQC, and HMBC.
^{b} 500 MHz, Referenced to TMS (δ 0.00). Elucidated/confirmed by HSQC, HMBC, and COSY.
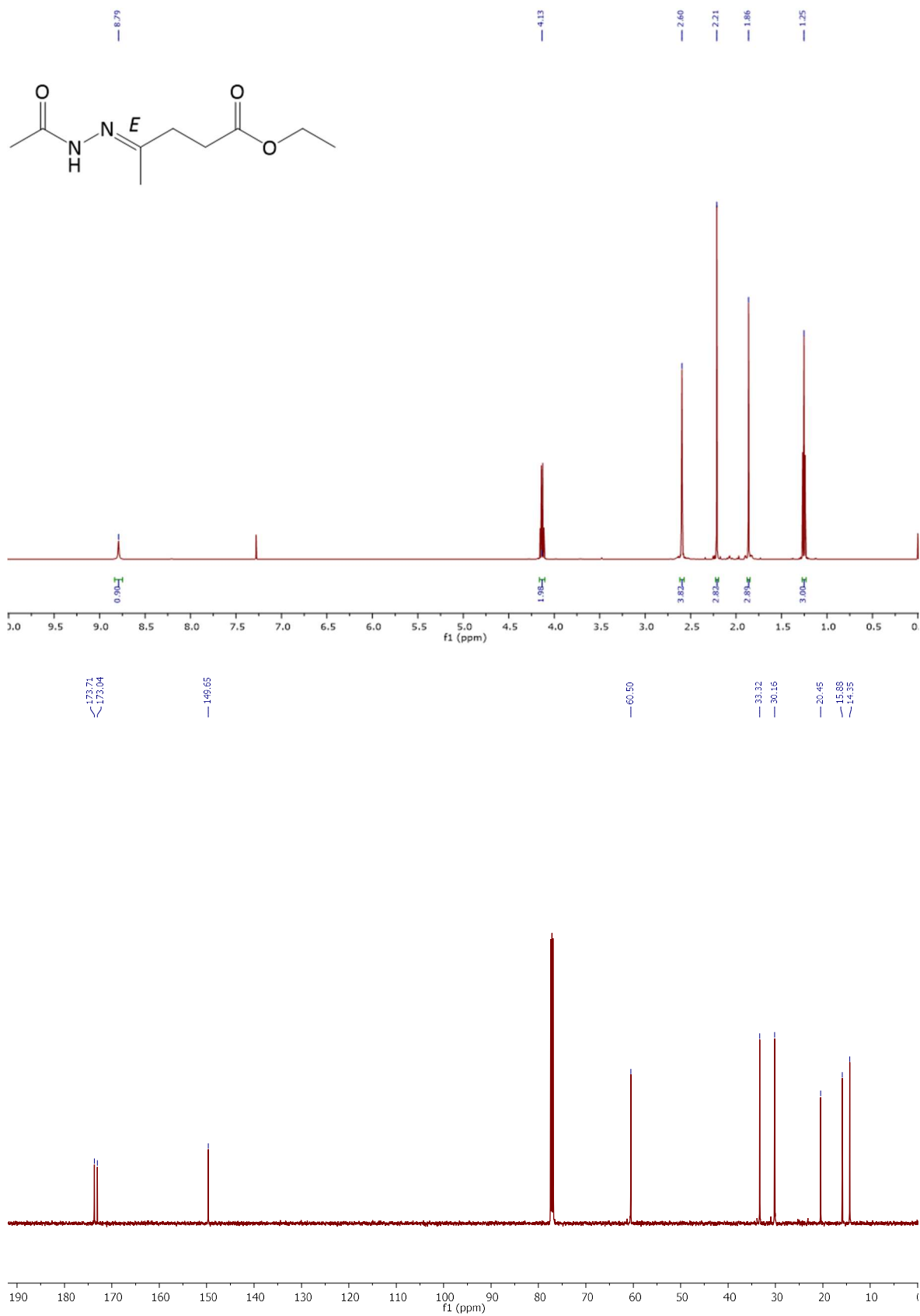
Figure 8.6. ^{1}H and ^{13}C NMR spectra (CDCl₃) of **1j**.
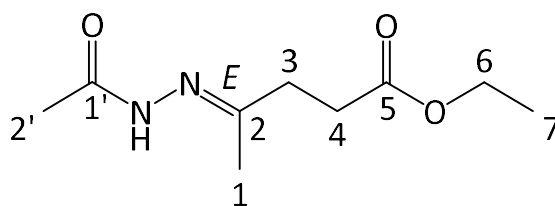
Table 8.4. Peak assignments in ^{1}H and ^{13}C NMR spectra of **1j**.

Position	$\delta_C{}^a$, Type	$\delta_H{}^b$ (*J* in Hz)
1	15.9, CH$_3$	1.86, s
2	149.7, C	-
3	33.3, CH$_2$	2.62–2.58, m
4	30.2, CH$_2$	2.62–2.58, m
5	173.0, C	-
6	60.5, CH$_2$	4.13, q (7.1)
7	14.4, CH$_3$	1.25, t (7.1)
1'	173.7, C	-
2'	20.5, CH$_3$	2.21, s
NH	-	8.79, s

^{a} 126 MHz, Referenced to CDCl$_3$ (δ 77.16 ppm).[261] Elucidated/confirmed by DEPT, HSQC, and HMBC.
^{b} 500 MHz, Referenced to TMS (δ 0.00 ppm). Elucidated/confirmed by HSQC, HMBC, and COSY.
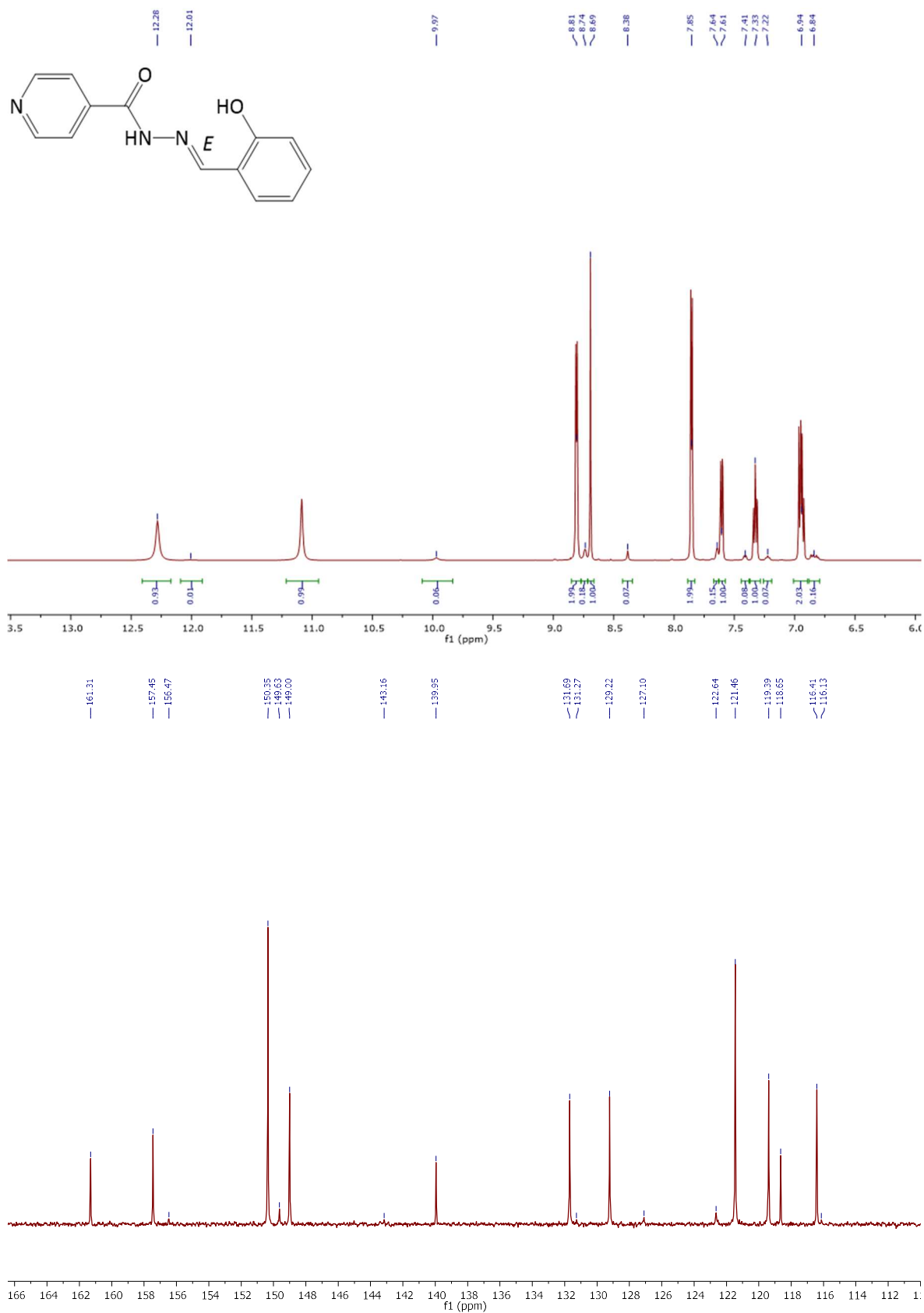
Figure 8.7. ^{1}H and ^{13}C NMR spectra (DMSO-d_6) of **2a**.
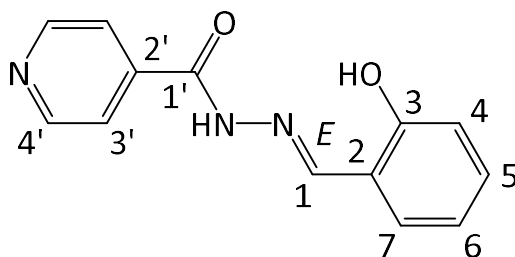
Table 8.5. Peak assignments in ^{1}H and ^{13}C NMR spectra of **2a**.

Position	$\delta_C^{a,b}$, Type	$\delta_H^{a,c}$ (*J* in Hz)
1	149.0, 143.2, CH	8.69, s; 8.38, s
2	118.7, C	-
3	157.5, 156.5, C	-
4	116.4, 116.1, CH	6.98–6.90, m; 6.88–6.79, m
5	131.7, 131.1, CH	7.33, td (7.4, 1.6); 7.22, t (7.3)
6	119.4, CH	6.98–6.90, m; 6.88–6.79, m
7	129.2, 127.1, CH	7.61, dd (7.7, 1.8); 7.41, d (7.5)
1'	161.3, C	-
2'	140.0, C	-
3'	122.6, 121.5, CH	7.85, dd (4.4, 1.7); 7.64, d (4.6)
4'	150.4, 149.6, CH	8.81, dd (4.5, 1.6); 8.74, d (4.3)
OH	-	11.09, s; 9.97, s
NH	-	12.28, s; 12.01, s

^{a} Where multiple values are provided, rotamers were observed in solution.
^{b} 126 MHz, Referenced to DMSO-d_6 (δ 39.52 ppm).[261] Elucidated/confirmed by HSQC.
^{c} 500 MHz, Referenced to TMS (δ 0.00 ppm). Elucidated/confirmed by HSQC and COSY.
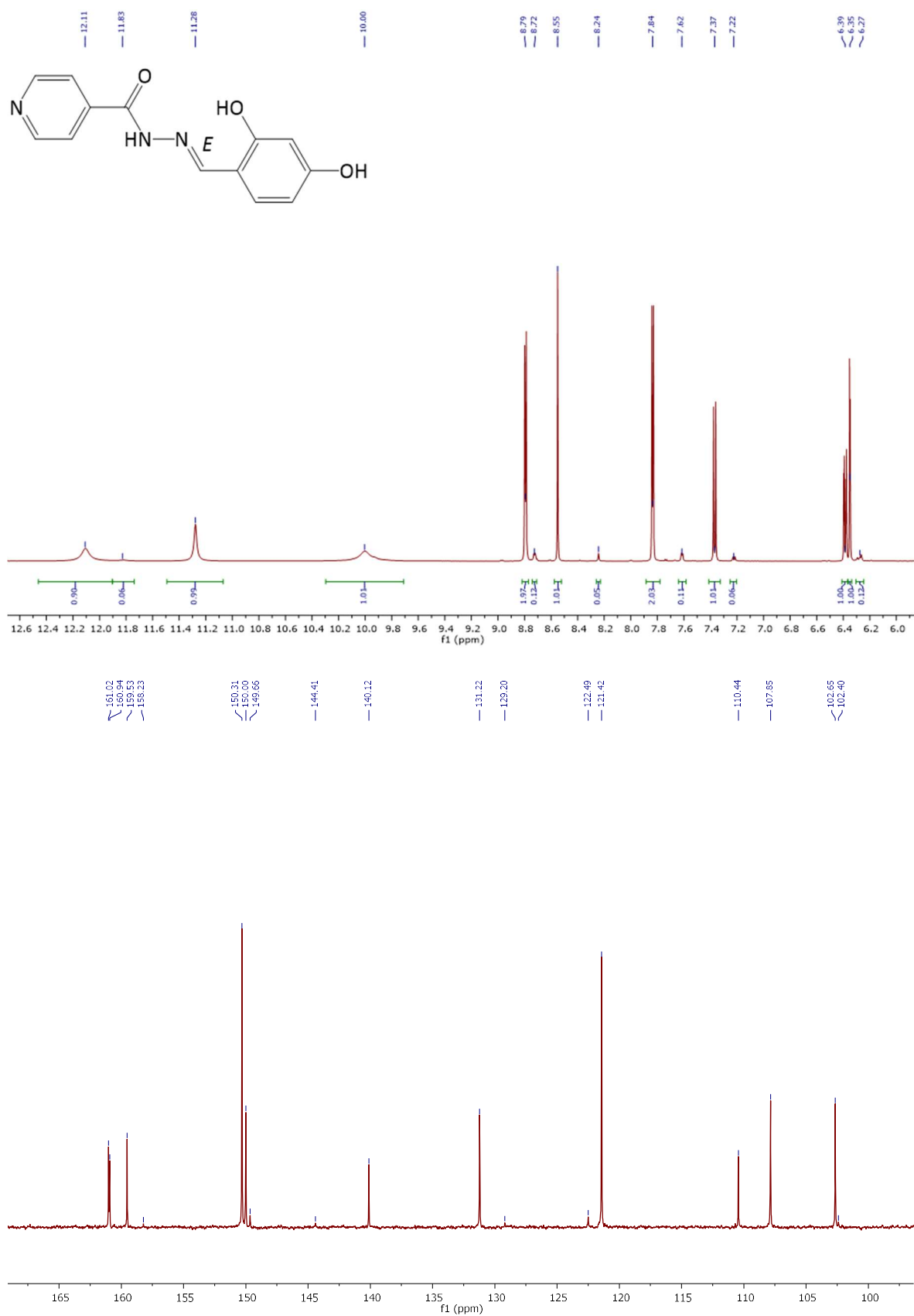
Figure 8.8. ^{1}H and ^{13}C NMR spectra (DMSO-d_6) of **2b**.
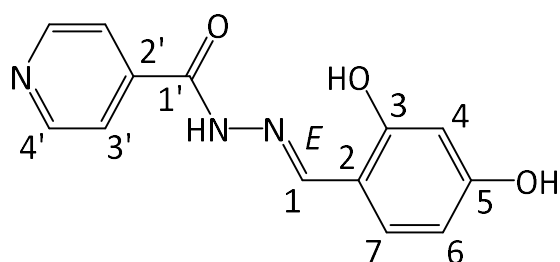
Table 8.6. Peak assignments in ^{1}H and ^{13}C NMR spectra of **2b**.

Position	δ_C[a,b], Type	δ_H[a,c] (*J* in Hz)
1	150.0, 144.4, CH	8.55, s; 8.24, s
2	110.4, C	-
3	161.0, 160.9, 159.5, or 158.2, C	-
4	102.7, 102.4, CH	6.35, d (2.4); 6.30–6.25, m
5	161.0, 160.9, 159.5, or 158.2, C	-
6	107.9, CH	6.39, dd (8.4, 2.3); 6.30–6.25, m
7	131.2, 129.2, CH	7.37, d (8.4); 7.22, d (8.3)
1'	161.0, 160.9, 159.5, or 158.2, C	-
2'	140.1, C	-
3'	122.5, 121.4, CH	7.84, dd (4.5, 1.5); 7.61, d (5.1)
4'	150.3, 149.7, CH	8.79, dd (4.4, 1.6); 8.72, d (5.3)
3 OH	-	12.11, s; 11.82, s
5 OH	-	10.00, s
NH	-	11.28, s

[a] Where multiple values are provided, rotamers were observed in solution.
[b] 126 MHz, Referenced to DMSO-*d6* (δ 39.52 ppm).[261] Elucidated/confirmed by HSQC.
[c] 500 MHz, Referenced to TMS (δ 0.00 ppm). Elucidated/confirmed by HSQC and COSY.
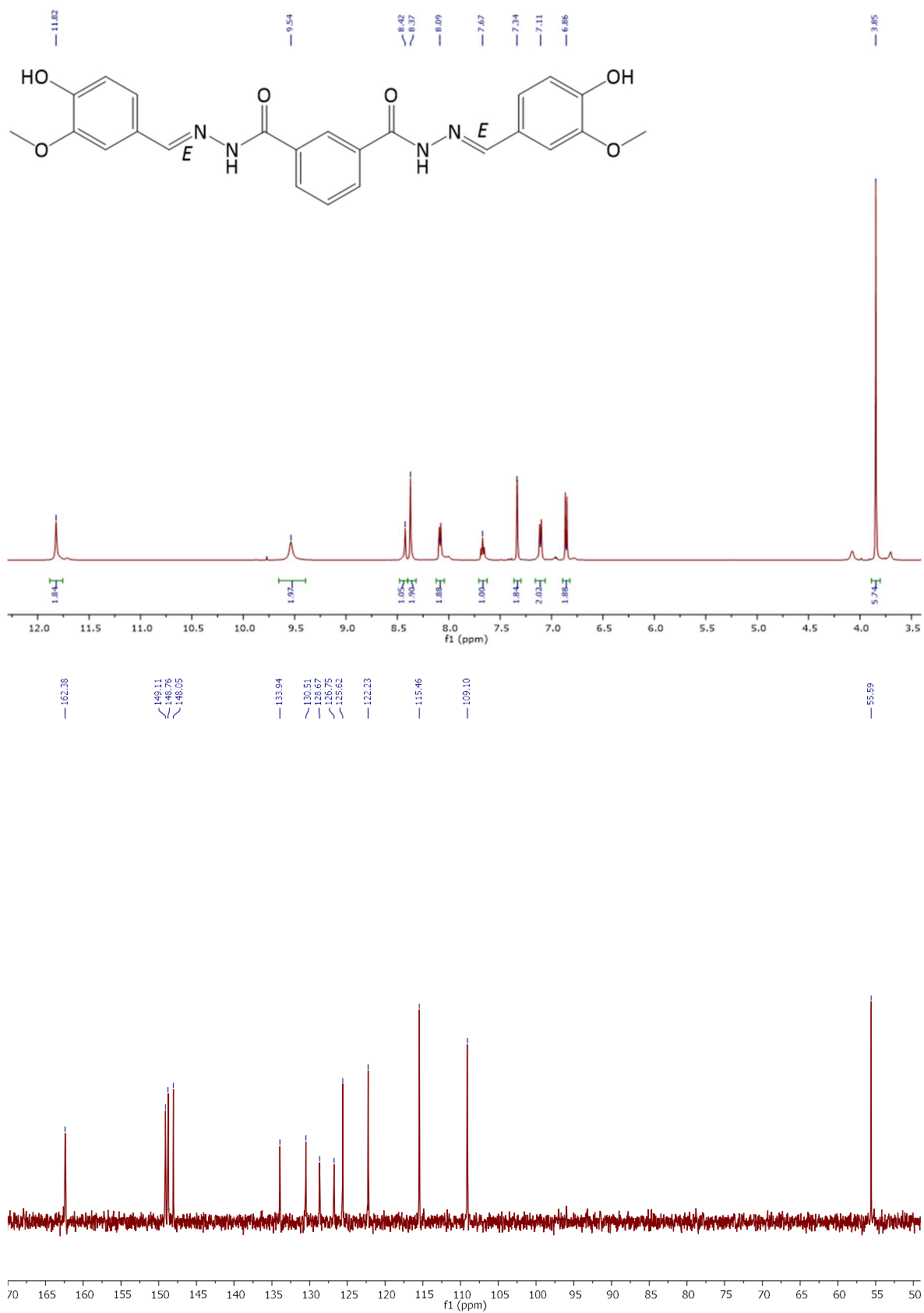
Figure 8.9. ^{1}H and ^{13}C NMR spectra (DMSO-d_6) of **3c**.
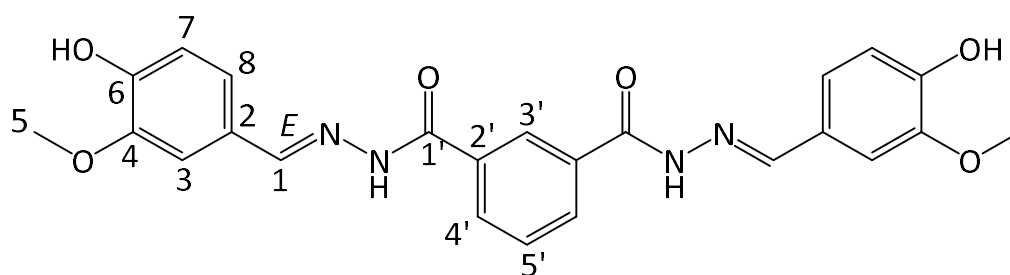
Table 8.7. Peak assignments in ^{1}H and ^{13}C NMR spectra of **3c**.

Position	$\delta_C{}^a$, Type	$\delta_H{}^b$ (*J* in Hz)
1	148.8, CH	8.37, s
2	125.6, C	-
3	109.1, CH	7.34, s
4	148.1, C	-
5	55.6, CH$_3$	3.85, s
6	149.1, C	-
7	115.5, CH	6.86, d (8.1)
8	122.2, CH	7.11, d (8.0)
1'	162.4, C	-
2'	133.9, C	-
3'	126.8, CH	8.42, s
4'	130.5, CH	8.09, d (7.7)
5'	128.7, CH	7.67, t (7.7)
OH	-	9.54, s
NH	-	11.82, s

^{a} 126 MHz, Referenced to DMSO-d_6 (δ 39.52 ppm).[261] Elucidated/confirmed by DEPT.
^{b} 500 MHz, Referenced to TMS (δ 0.00 ppm). Elucidated/confirmed by HSQC.
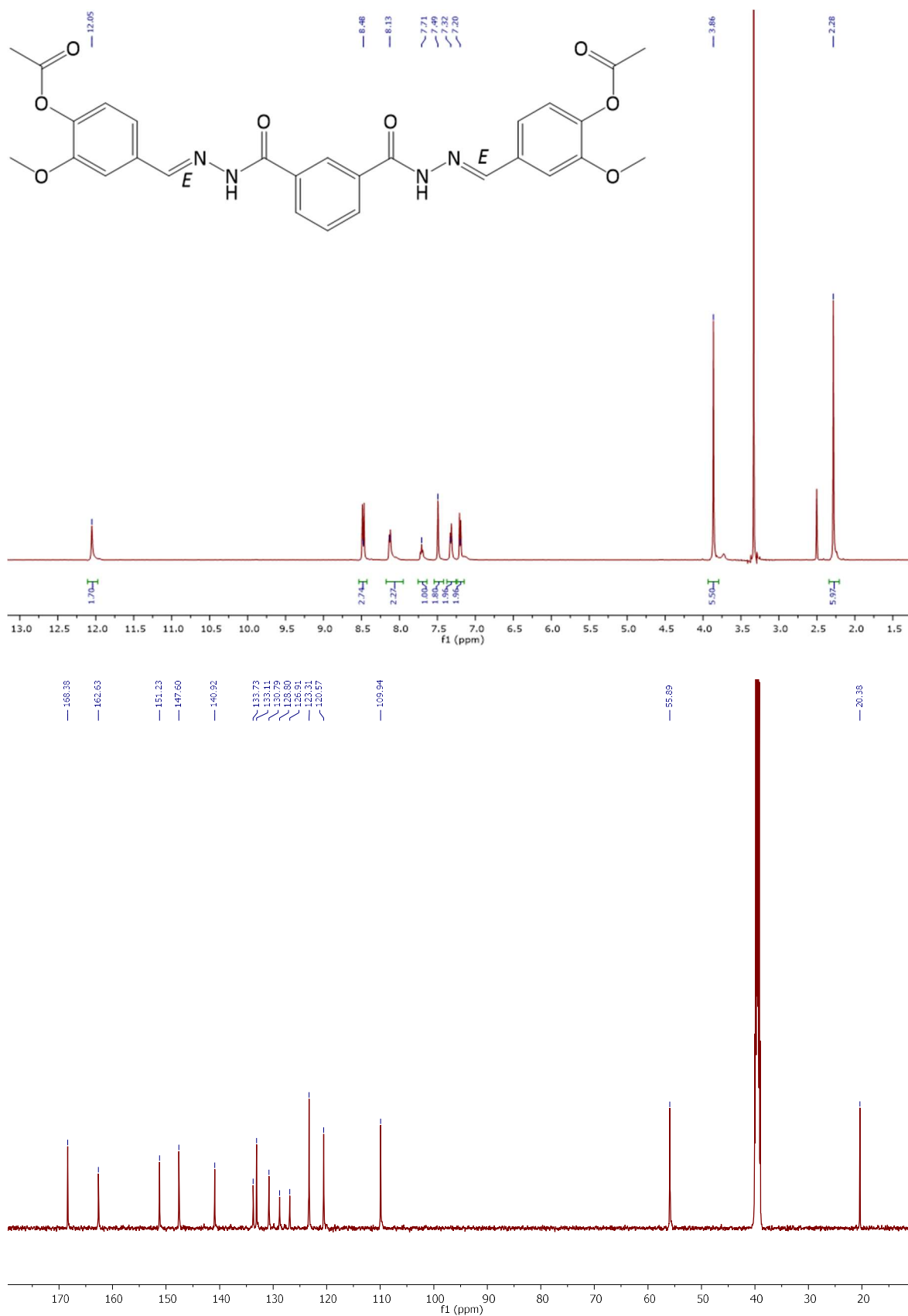
Figure 8.10. ^{1}H and ^{13}C NMR spectra (DMSO-d_6) of **3d** (δ_H 3.33 ppm = water).
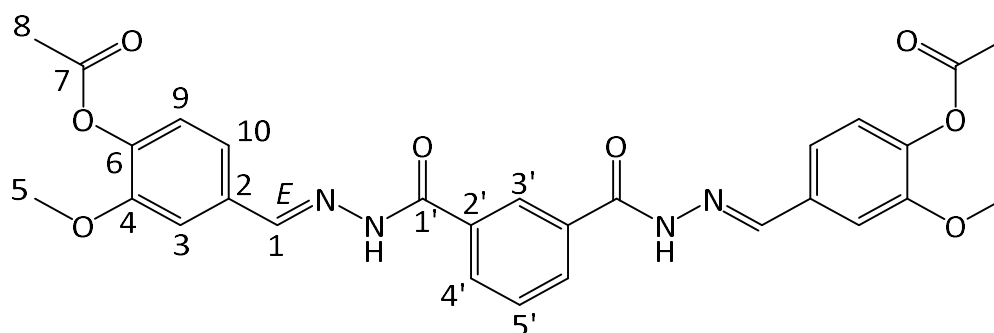
Table 8.8. Peak assignments in ^{1}H and ^{13}C NMR spectra of **3d**.

Position	$\delta_C{}^a$, Type	$\delta_H{}^b$ (*J* in Hz)
1	147.6, CH	8.49, s
2	133.7, C	-
3	109.9, CH	7.49, s
4	151.2, C	-
5	55.9, CH_3	3.86, s
6	140.9, C	-
7	168.4, C	-
8	20.4, CH_3	2.28, s
9	123.3, CH	7.20, d (8.1)
10	120.6, CH	7.32, d (7.9)
1'	162.6, C	-
2'	133.1, C	-
3'	126.9, CH	8.47, s
4'	130.8, CH	8.13, d (7.5)
5'	128.8, CH	7.71, t (7.6)
NH	-	12.05, s

[a] 126 MHz, Referenced to DMSO-*d₆* (δ 39.52 ppm).[261] Elucidated/confirmed by DEPT.
[b] 500 MHz, Referenced to TMS (δ 0.00 ppm). Elucidated/confirmed by HSQC.
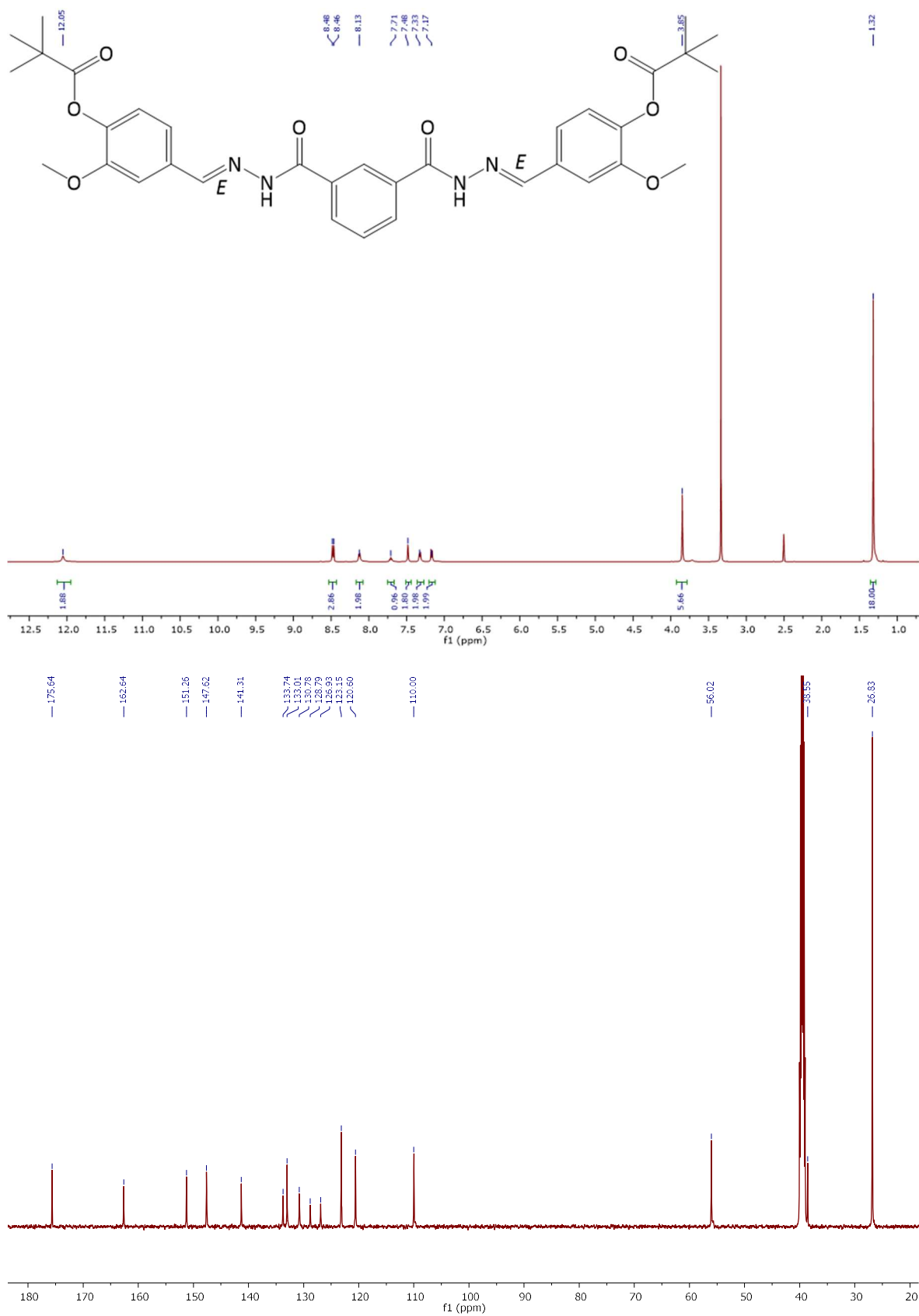
Figure 8.11. ^{1}H and ^{13}C NMR spectra (DMSO-d_6) of **3e** (δ_H 3.34 ppm = water).
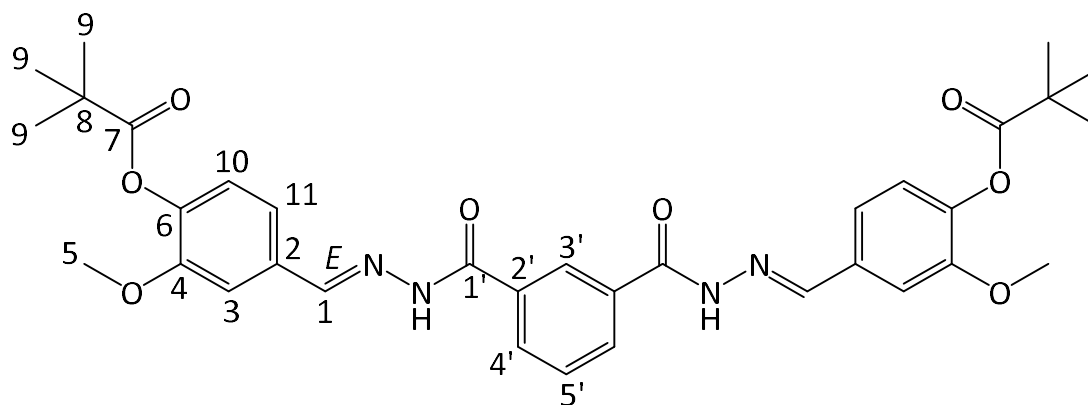
Table 8.9. Peak assignments in ^{1}H and ^{13}C NMR spectra of **3e**.

Position	$\delta_C{}^a$, Type	$\delta_H{}^b$ (*J* in Hz)
1	147.6, CH	8.48, s
2	133.7, C	-
3	110.0, CH	7.48, s
4	151.3, C	-
5	56.0, CH$_3$	3.85, s
6	141.3, C	-
7	175.6, C	-
8	38.6, C	-
9	26.8, CH$_3$	1.32, s
10	123.2, CH	7.17, d (8.1)
11	120.6, CH	7.32, d (7.9)
1'	162.6, C	-
2'	133.0, C	-
3'	126.9, CH	8.46, s
4'	130.8, CH	8.13, d (7.5)
5'	128.8, CH	7.71, t (7.6)
NH	-	12.05, s

^{a} 126 MHz, Referenced to DMSO-d_6 (δ 39.52 ppm).[261] Elucidated/confirmed by DEPT.
^{b} 500 MHz, Referenced to TMS (δ 0.00 ppm). Elucidated/confirmed by HSQC.
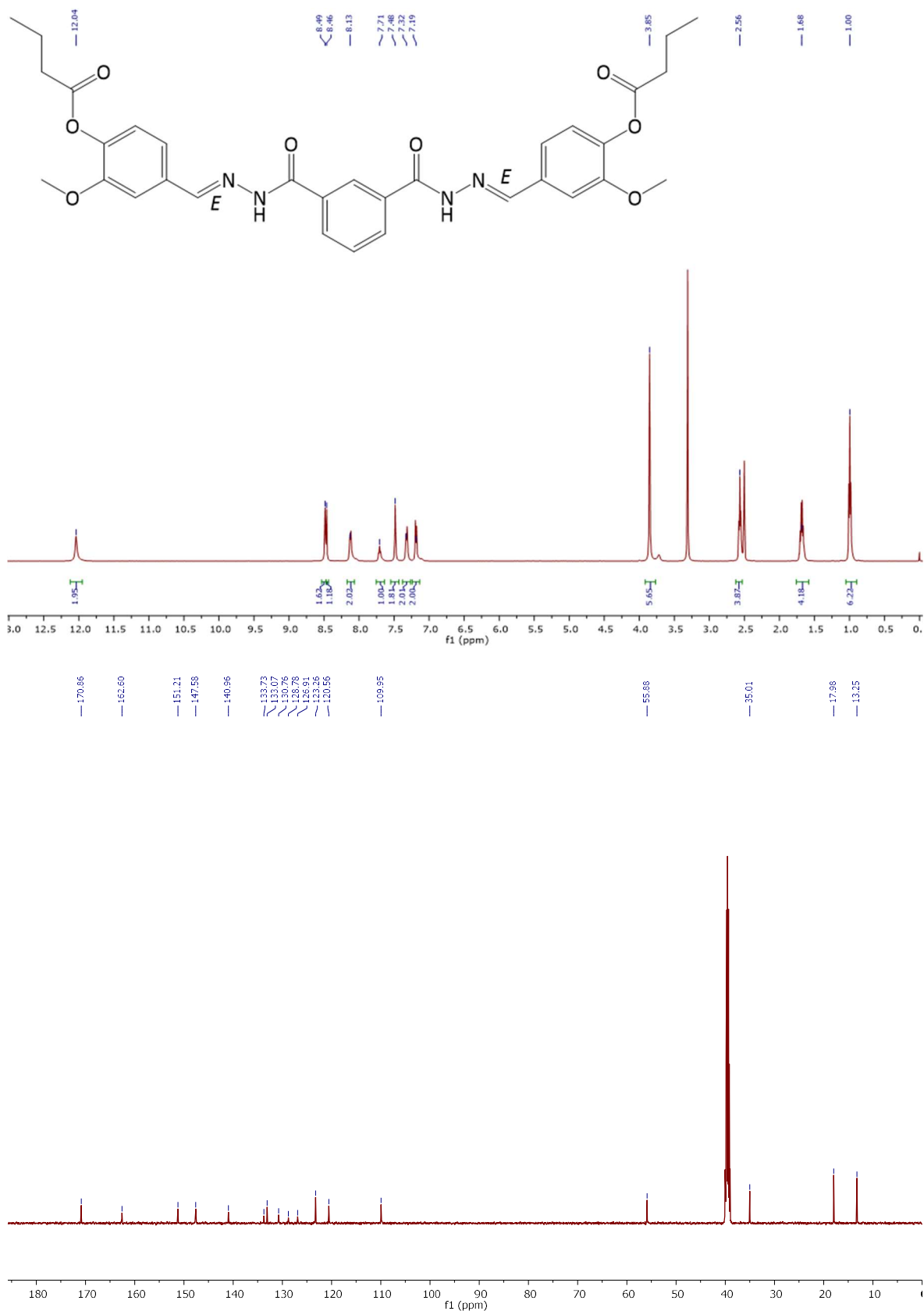
Figure 8.12. ^{1}H and ^{13}C NMR spectra (DMSO-d_6) of **3f** (δ_H 3.31 ppm = HDO).
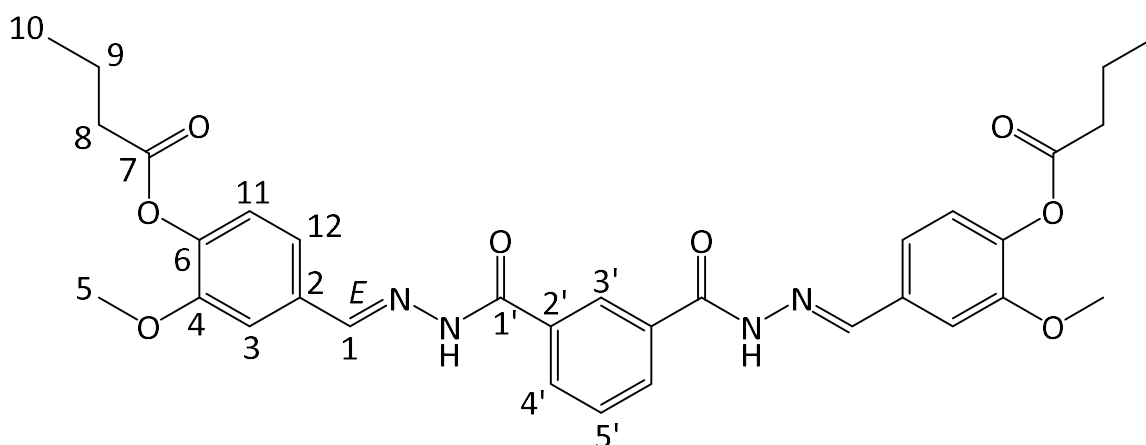
Table 8.10. Peak assignments in ^{1}H and ^{13}C NMR spectra of **3f**.

Position	$\delta_C{}^a$, Type	$\delta_H{}^b$ (*J* in Hz)
1	147.6, CH	8.49, s
2	133.7, C	-
3	110.0, CH	7.48, s
4	151.2, C	-
5	55.9, CH$_3$	3.85, s
6	141.0, C	-
7	170.9, C	-
8	35.0, CH$_2$	2.56, t (7.1)
9	18.0, CH$_2$	1.68, sxt (7.1)
10	13.3, CH$_3$	1.00, t (7.3)
11	123.3, CH	7.19, d (8.0)
12	120.6, CH	7.32, d (7.7)
1'	162.6, C	-
2'	133.1, C	-
3'	126.9, CH	8.46, s
4'	130.8, CH	8.13, d (7.3)
5'	128.8, CH	7.71, t (7.4)
NH	-	12.04, s

[a] 126 MHz, Referenced to DMSO-*d$_6$* (δ 39.52 ppm).[261] Elucidated/confirmed by DEPT.
[b] 500 MHz, Referenced to TMS (δ 0.00 ppm). Elucidated/confirmed by HSQC.
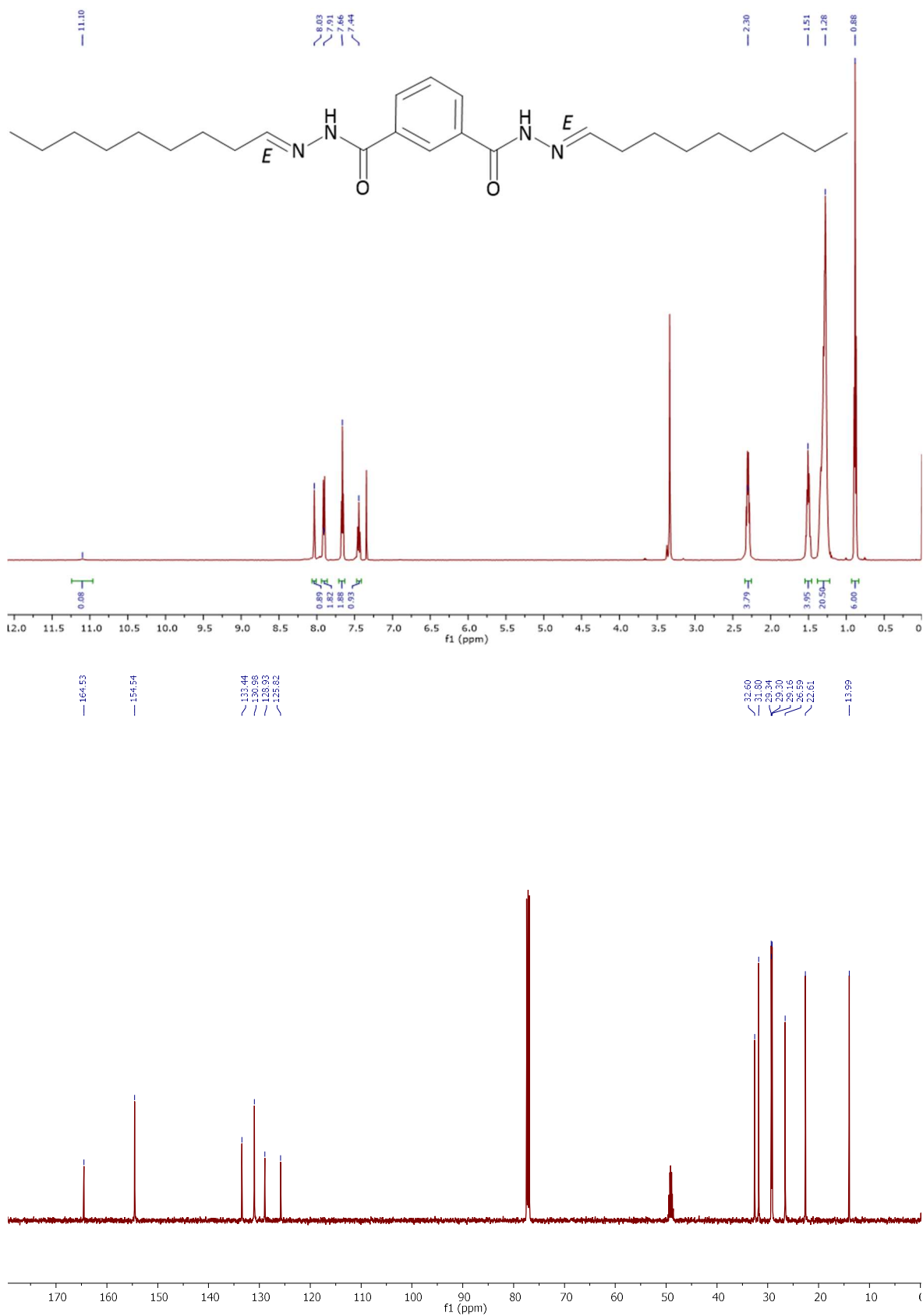
Figure 8.13. ^{1}H and ^{13}C NMR spectra (CDCl$_3$/10% v/v CD$_3$OD) of **3h** (δ_H 3.35 & δ_c 49.1 ppm = methanol).

276
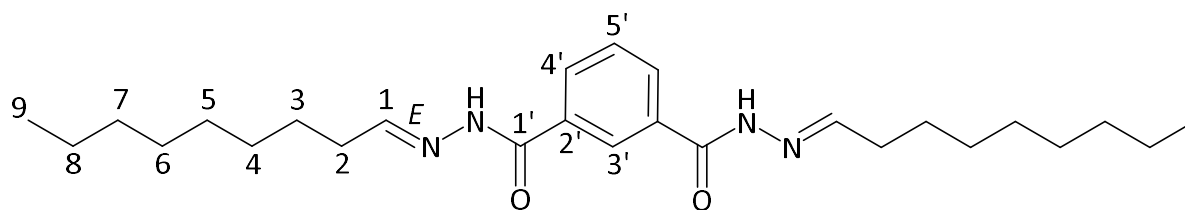
Table 8.11. Peak assignments in ^{1}H and ^{13}C NMR spectra of **3h**.

Position	$\delta_C{}^a$, Type	$\delta_H{}^b$ (*J* in Hz)
1	154.5, CH	7.66, t (5.7)
2	32.6, CH$_2$	2.37–2.24, m
3	26.6, CH$_2$	1.51, p (7.6)
4	29.3 or 29.2, CH$_2$	1.38–1.21, br m
5	29.3 or 29.2, CH$_2$	1.38–1.21, br m
6	29.3 or 29.2, CH$_2$	1.38–1.21, br m
7	31.8, CH$_2$	1.38–1.21, br m
8	22.6, CH$_2$	1.38–1.21, br m
9	14.0, CH$_3$	0.88, t (6.9)
1'	164.5, C	-
2'	133.4, C	-
3'	125.8, CH	8.03, s
4'	131.0, CH	7.91, d (7.7)
5'	128.9, CH	7.44, t (7.7)
NH	-	11.10, s

^{a} 126 MHz, Referenced to CDCl$_3$ (δ 77.16 ppm).[261] Elucidated/confirmed by DEPT.
^{b} 500 MHz, Referenced to TMS (δ 0.00 ppm). Elucidated/confirmed by HSQC and COSY.

277
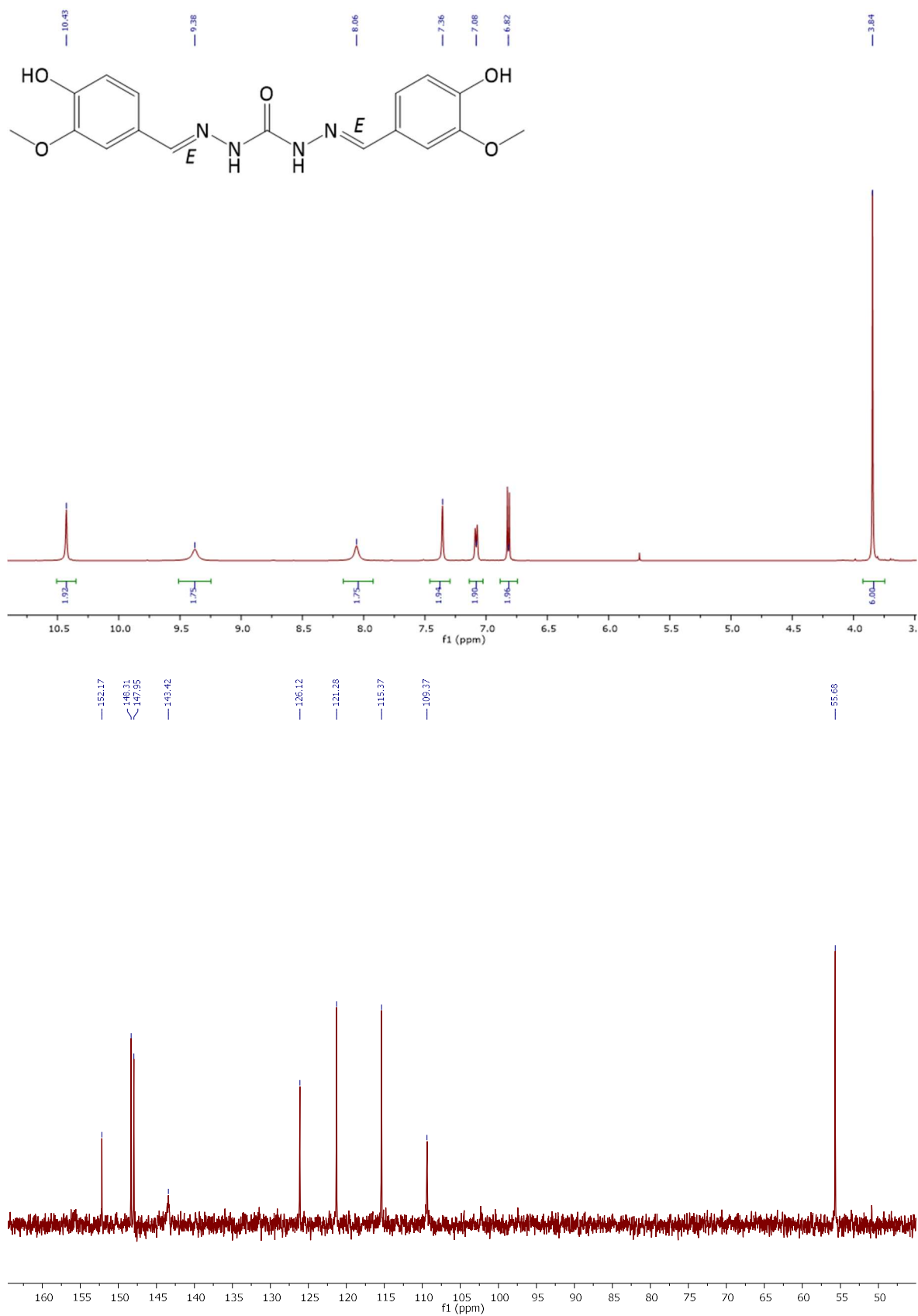
Figure 8.14. ^{1}H and ^{13}C NMR spectra (DMSO-d_6) of **4c** (δ_H 5.75 ppm = DCM).
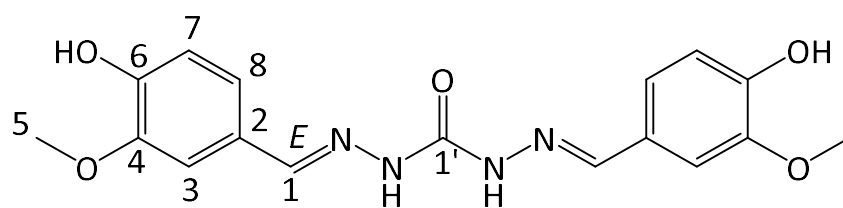
Table 8.12. Peak assignments in ^{1}H and ^{13}C NMR spectra of **4c**.

Position	δ_C[a], Type	δ_H[b] (J in Hz)
1	143.4, CH	8.06, s
2	126.1, C	-
3	109.4, CH	7.36, s
4	148.0, C	-
5	55.7, CH$_3$	3.84, s
6	148.3, C	-
7	115.4, CH	6.82, d (8.1)
8	121.3, CH	7.08, d (8.0)
1'	152.2, C	-
OH	-	9.38, s
NH	-	10.43, s

[a] 126 MHz, Referenced to DMSO-d_6 (δ 39.52 ppm).[261] Elucidated/confirmed by DEPT.
[b] 500 MHz, Referenced to TMS (δ 0.00 ppm). Elucidated/confirmed by HSQC.
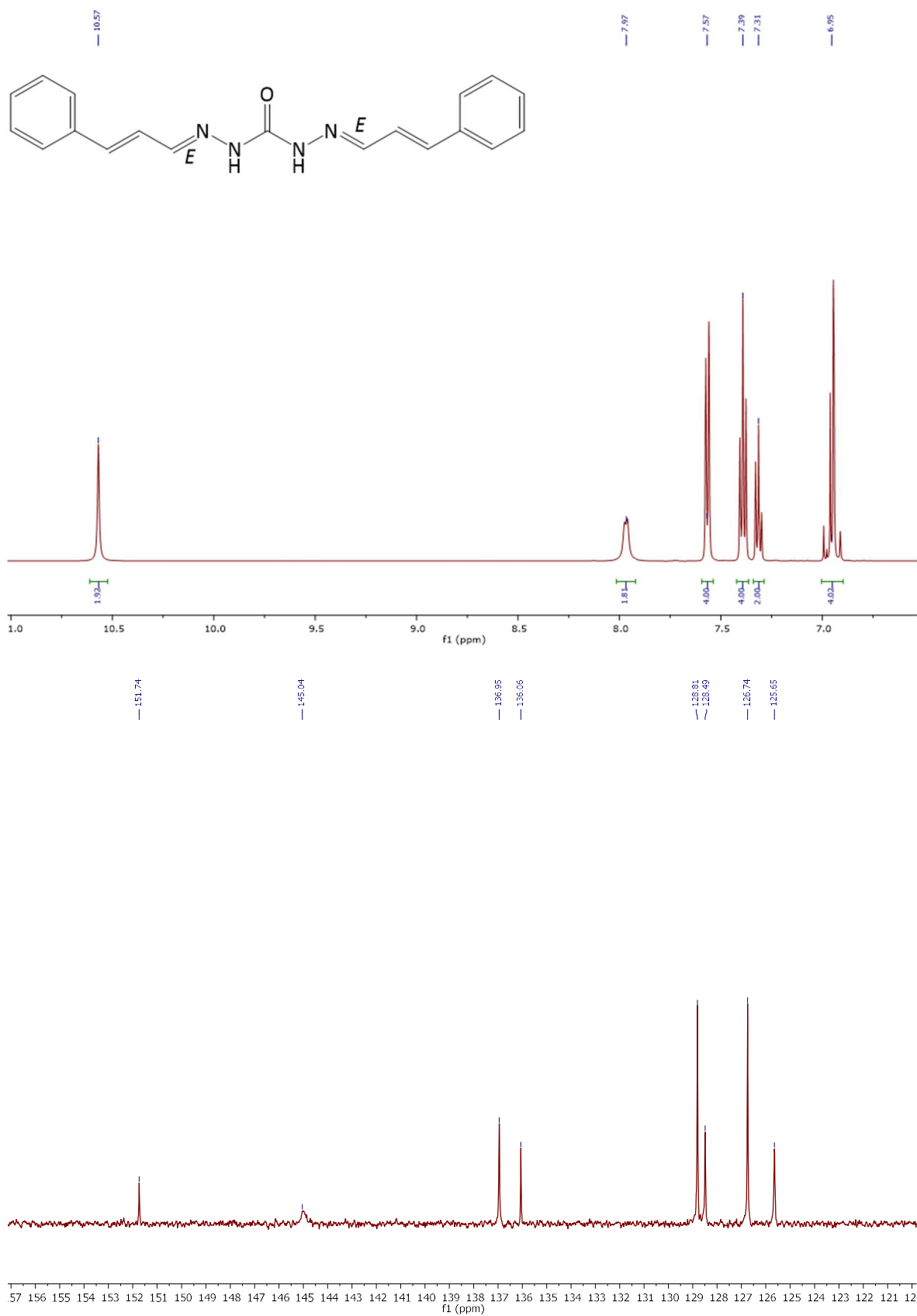
Figure 8.15. ^{1}H and ^{13}C NMR spectra (DMSO-d_6) of **4g**.
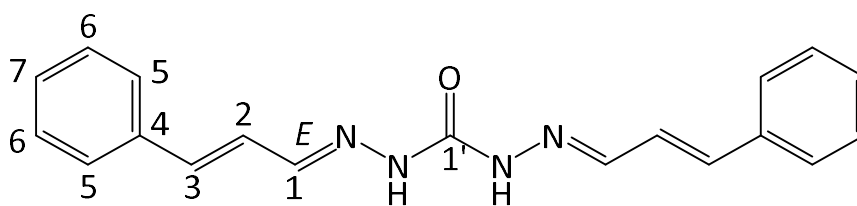
Table 8.13. Peak assignments in ^{1}H and ^{13}C NMR spectra of **4g**.

Position	$\delta_C{}^a$, Type	$\delta_H{}^b$ (*J* in Hz)
1	145.0, CH	7.97, d (6.4)
2	137.0, CH	7.02–6.89, m
3	125.7, CH	7.02–6.89, m
4	136.1, C	-
5	126.7, CH	7.57, d (7.3)
6	128.8, CH	7.39, t (7.5)
7	128.5, CH	7.31, t (7.3)
1'	151.7, C	-
NH	-	10.57, s

^{a} 126 MHz, Referenced to DMSO-d_6 (δ 39.52 ppm).[261] Elucidated/confirmed by DEPT.
^{b} 500 MHz, Referenced to TMS (δ 0.00 ppm). Elucidated/confirmed by HSQC.
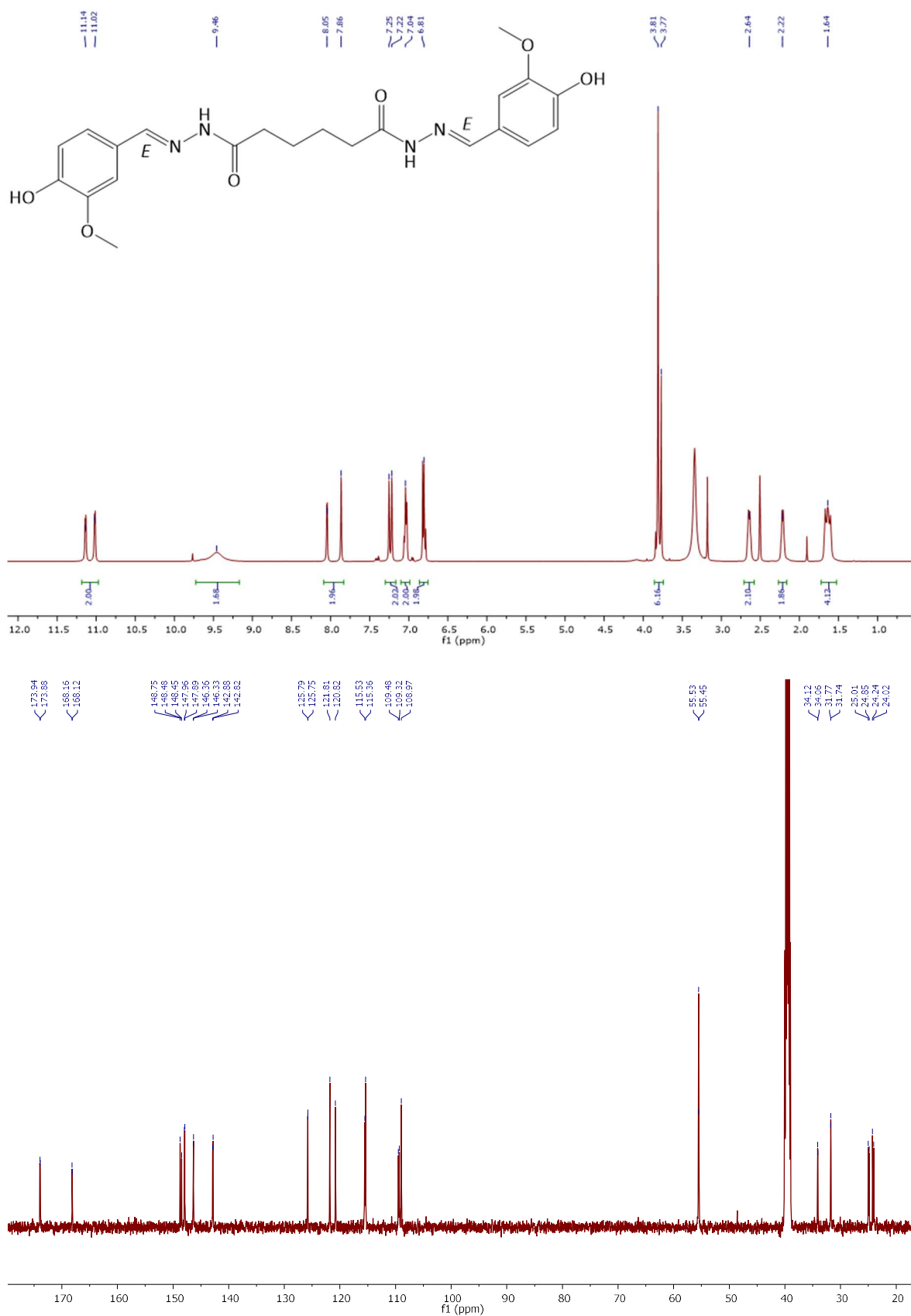
Figure 8.16. ^{1}H and ^{13}C NMR spectra (crude; DMSO-d_6) of **5c** (δ_H 9.77 ppm = contaminant, δ_H 3.34 ppm = water, δ_H 3.18 ppm = methanol, δ_H 1.90 ppm = acetic acid).
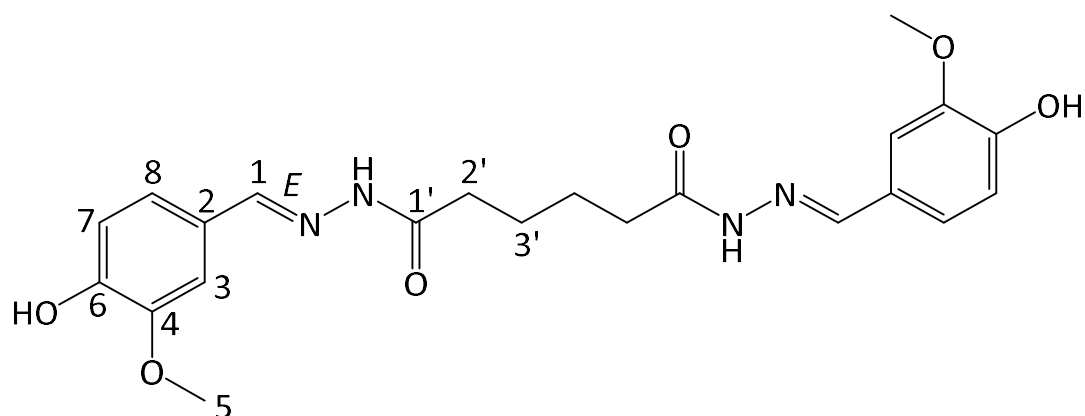
Table 8.14. Peak assignments in ^1H and ^{13}C NMR spectra of **5c**.

Position	$\delta_C{}^{a,b}$, Type	$\delta_H{}^{a,c}$ (*J* in Hz)
1	146.4, 146.3, 142.9, 142.8, CH	8.05, s; 7.86, s
2	125.8, 125.8, C	-
3	109.5, 109.3, 109.0, CH	7.25, s; 7.22, s
4	148.0, 147.9, C	-
5	55.5, 55.5, CH$_3$	3.81, s; 3.77, s
6	148.8, 148.5, 148.5, C	-
7	115.5, 115.4, CH	6.84–6.76, m
8	121.8, 120.8, CH	7.08–7.00, m
1'	173.9, 173.9, 168.2, 168.1, C	-
2'	34.1, 34.1, 31.8, 31.7, CH$_2$	2.69–2.60, m; 2.26–2.17, m
3'	25.0, 24.9, 24.2, 24.0, CH$_2$	1.70–1.57, m
OH	-	9.45, s
NH	-	11.14, d (5.3); 11.02, d (5.0)

^{a} Where multiple values are provided, rotamers were observed in solution.
^{b} 126 MHz, Referenced to DMSO-d_6 (δ 39.52 ppm).[261] Elucidated/confirmed by DEPT.
^{c} 500 MHz, Referenced to TMS (δ 0.00 ppm). Elucidated/confirmed by HSQC.

283
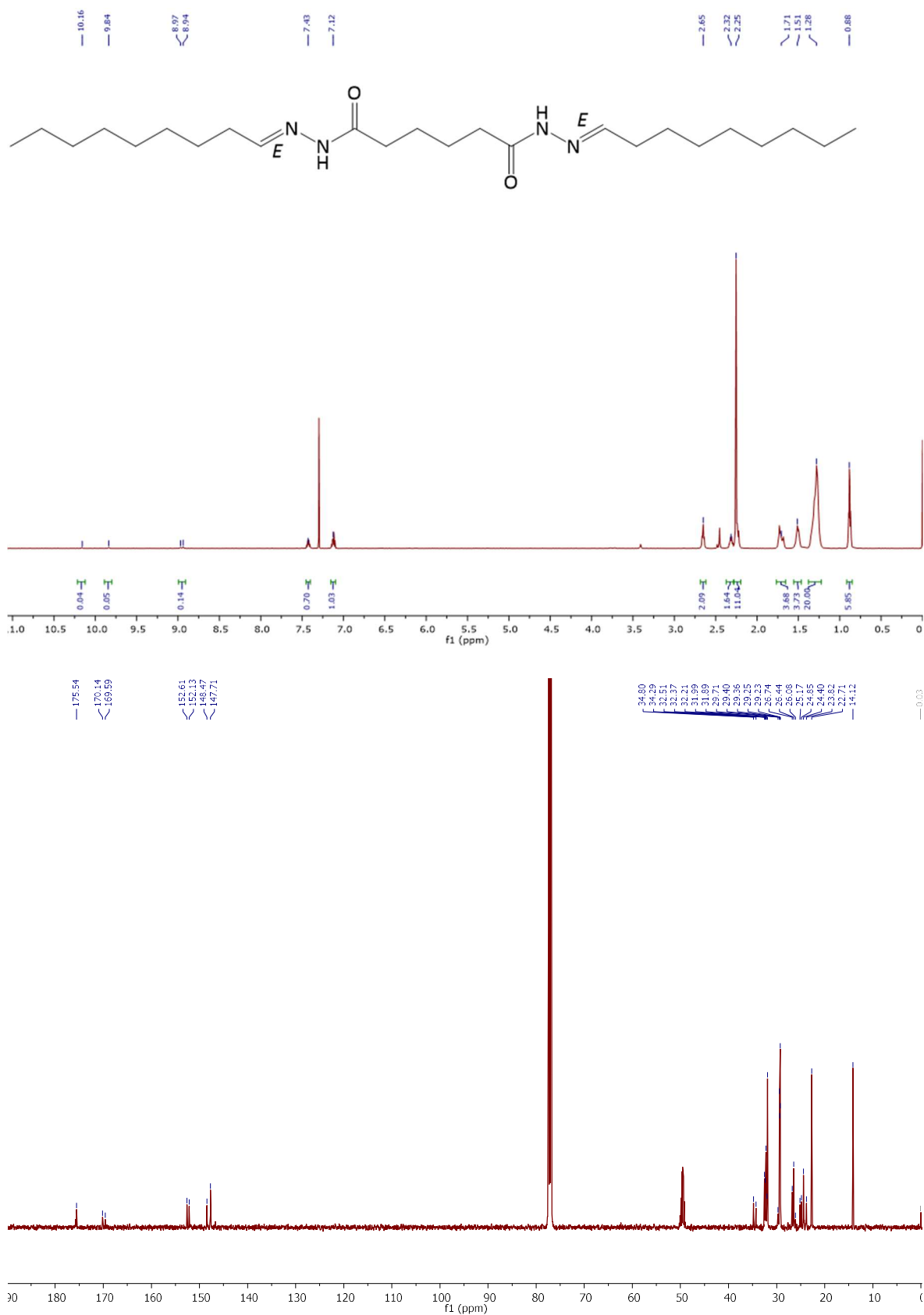
Figure 8.17. ¹H and ¹³C NMR spectra (crude; CDCl₃/5% v/v CD₃OD) of **5h** (δ$_H$ 2.45 & 2.42 ppm = contaminant, δ$_H$ 3.37 & δc 49.5 ppm = methanol).
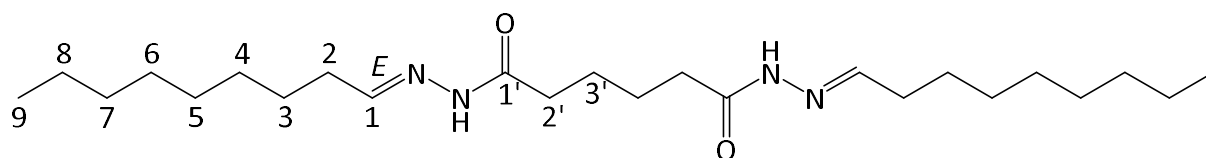
Table 8.15. Peak assignments in ^{1}H NMR spectra of **5h**.

Position	δ_C[a,b], Type	δ_H[a,c] (*J* in Hz)
1	152.6, 152.1, 148.5, 147.7, CH	7.46–7.39, m; 7.16–7.07, m
2	32.5 (possibly 34.8 or 34.3), CH$_2$	2.36–2.28, m; 2.28–2.20[d], m
3	26.7, 26.4, 26.1, CH$_2$	1.57–1.43, m
4–8	32.0, 31.9, 29.7, 29.4, 29.4, 29.3, 29.2, 22.7, CH$_2$	1.38–1.19, m
9	14.1, CH$_3$	0.93–0.81, m
1'	175.5, 170.1, 169.6, C	-
2'	32.4, 32.2 (possibly 34.8 or 34.3), CH$_2$	2.70–2.60, m; 2.28–2.20[d], m
3'	25.2, 24.9, 24.4, 23.8, CH$_2$	1.79–1.64, m
NH[e]	-	10.16, s; 9.84, s; 8.97, s; 8.94, s

[a] Where multiple values are provided, rotamers were observed in solution.
[b] 126 MHz, Referenced to CDCl$_3$ (δ 77.16 ppm).[261] Elucidated/confirmed by DEPT and HSQC.
[c] 500 MHz, Referenced to TMS (δ 0.00 ppm). Elucidated/confirmed by COSY and HSQC.
[d] Overlapping HDO peak.
[e] Exchangeable.
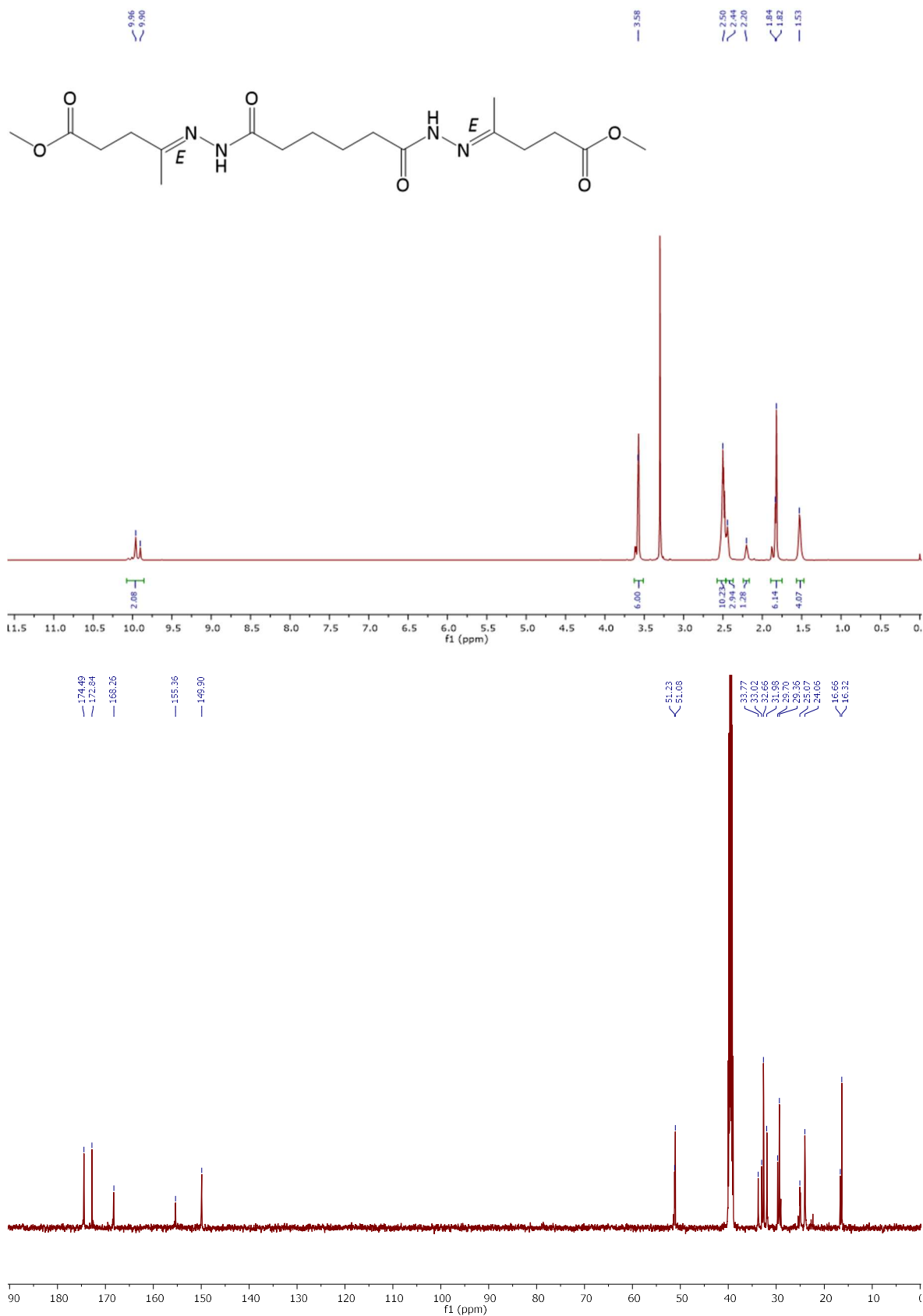
Figure 8.18. ^1H and ^{13}C NMR spectra (DMSO-d_6) of **5i** (δ_H 3.30 ppm = HDO).
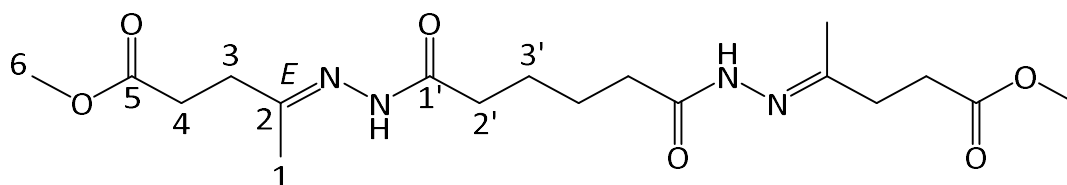
Table 8.16. Peak assignments in ^{1}H and ^{13}C NMR spectra of **5i**.

Position	$\delta_C{}^{a,b}$, Type	$\delta_H{}^{a,c}$ (J in Hz)
1	16.7, 16.3, CH$_3$	1.84, s; 1.82, s
2	155.4, 149.9, C	-
3	33.0, 32.7, CH$_2$	2.57–2.46^d, m
4	29.7, 29.4, CH$_2$	2.57–2.46^d, m
5	172.8, C	-
6	51.2, 51.1, CH$_3$	3.58, s
1'	174.5, 168.3, C	-
2'	33.8, 32.0, CH$_2$	2.46–2.37, m; 2.24–2.17, m
3'	25.1, 24.1, CH$_2$	1.60–1.45, m
NH	-	9.96, s; 9.90, s

^{a} Where multiple values are provided, rotamers were observed in solution.
^{b} 126 MHz, Referenced to DMSO-d_6 (δ 39.52 ppm).[261] Elucidated/confirmed by DEPT, HSQC, and HMBC.
^{c} 500 MHz, Referenced to TMS (δ 0.00 ppm). Elucidated/confirmed by HSQC, HMBC, and COSY.
^{d} Overlapping DMSO-d_6 peak.

287
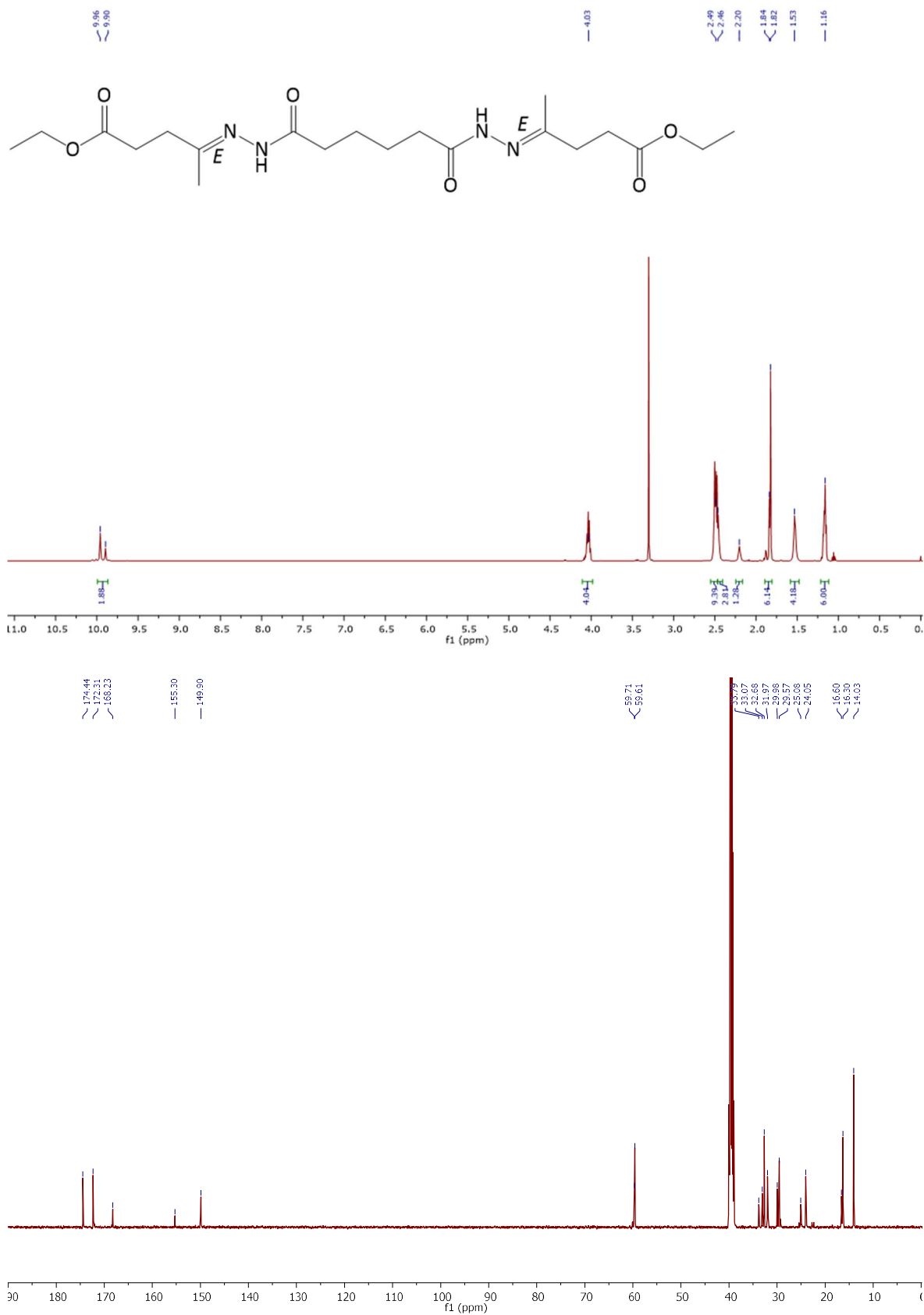
Figure 8.19. ^{1}H and ^{13}C NMR spectra (DMSO-d_6) of **5j** (δ_H 3.30 ppm = HDO, δ_H 1.06 ppm = ethanol).
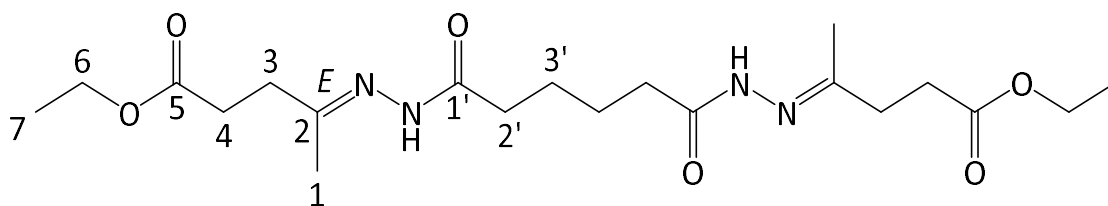
Table 8.17. Peak assignments in ^{1}H and ^{13}C NMR spectra of **5j**.

Position	δ$_C$^{a,b}, Type	δ$_H$^{a,c} (*J* in Hz)
1	16.6, 16.3, CH$_3$	1.84, s; 1.82, s
2	155.3, 149.9, C	-
3	33.1, 32.7, CH$_2$	2.55–2.47^d, m
4	30.0, 29.6, CH$_2$	2.55–2.47^d, m
5	172.3, C	-
6	59.7, 59.6, CH$_2$	4.09–3.99, m
7	14.0, CH$_3$	1.22–1.13, m
1'	174.4, 168.2, C	-
2'	33.8, 32.0, CH$_2$	2.47–2.40, m, 2.22–2.18, m
3'	25.1, 24.1, CH$_2$	1.59–1.46, m
NH	-	9.96, s; 9.90, s

^{a} Where multiple values are provided, rotamers were observed in solution.
^{b} 126 MHz, Referenced to DMSO-d_6 (δ 39.52 ppm).[261] Elucidated/confirmed by DEPT, HSQC, and HMBC.
^{c} 500 MHz, Referenced to TMS (δ 0.00 ppm). Elucidated/confirmed by HSQC, HMBC, and COSY.
^{d} Overlapping DMSO-d_6 peak.

8.2 CHAPTER 3
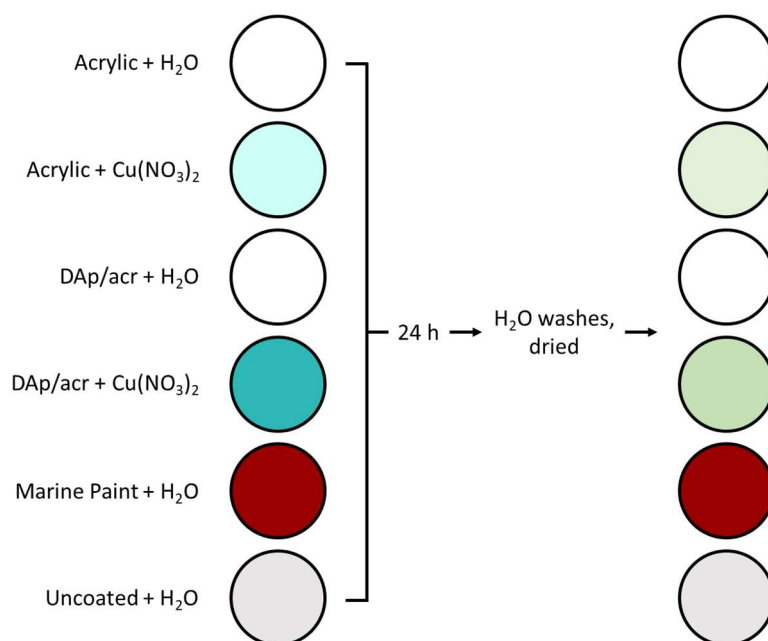
Figure 8.20. Preparation of the coated, 24-well plate(s) in Chapters 3 (**Sections 3.2.2** and **3.2.3**) and 6 (**Sections 6.3.1.2** and **6.3.1.3**).
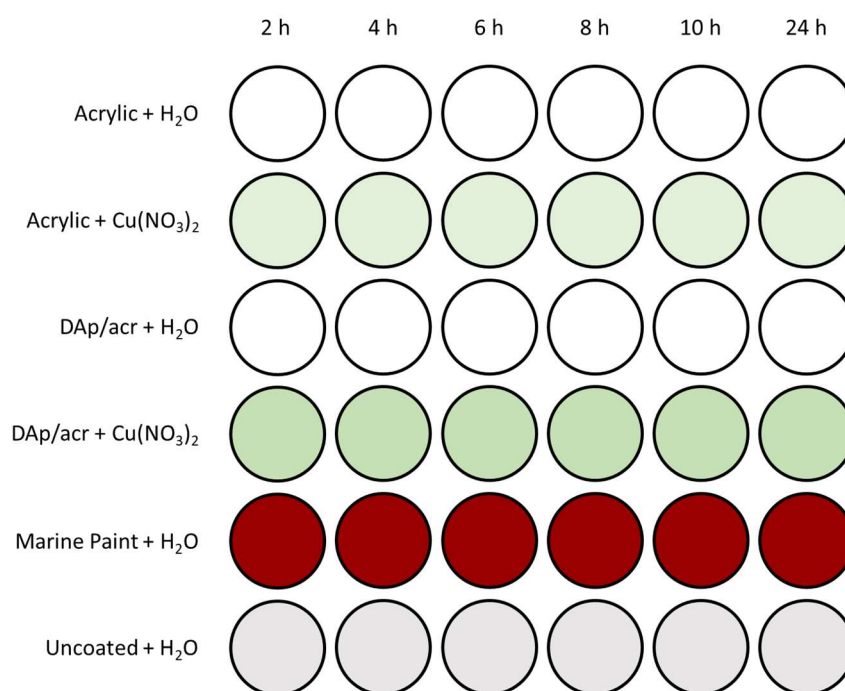
Figure 8.21. Plate setup for growth assay (Chapters 3 and 6, **Sections 3.2.2** and **6.3.1.2**).
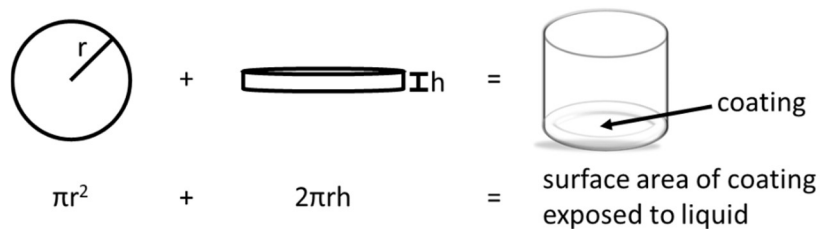
Figure 8.22. Formula for calculating the coating's surface area (cylindrical shape) exposed to liquid (Chapters 3 and 6, **Sections 3.2.4** and **6.3.1.5**).

Table 8.18. Results of combinations of amine and/or alcohol components with Desmodur® W.

Amine/Alcohol Component	mol Amine and/or Alcohol Component *per* 1 mol Desmodur® W	Results
DETA (20 °C, RT)	0.67	exothermic; immediate solidification; soft polyurea
DETA (0 °C)	0.67	exothermic; immediate solidification; soft polyurea
TEG	0.99	clear, patchy polyurethane coating
TEG, DETA	0.90 (TEG); 0.071 (DTA)	polyurethane/polyurea gel
1,2-Dianilinoethane	0.99	no observable reaction with the hindered amine

Epikote™ 235: Epoxy Resin

WPE = 177–182 g/eq epoxy group (mean = 179.5 g/eq epoxy group)

Ancamine® 2459: Hardener

AHEW = 101 g/eq amine hydrogen

$$phr = \frac{AHEW}{WPE} \times 100 = \frac{101\frac{g}{eq}}{179.5\frac{g}{eq}} \times 100 = 56.3 \text{ g hardener } per \text{ 100 g resin}$$

Scheme 8.1. Example calculation of the weight of hardener required *per* 100 g resin (phr).

Table 8.19. Properties of epoxy coatings prepared with epoxy resin Epikote™ 235 and hardeners Ancamine® 2459, cyclen, DETA, and cyclam, as well as surface-functionalised with cyclam, cyclen, DETA, and PEI (**bold red** = strongly Cu(II)-chelating films, based on colour intensity).

Hardener	Surface Functionalisation	% Over (+)/ Undercure (-)	Appearance	Softness/ Hardness	Ease of Draw-Down	Colour Change Upon Cu(II)-Addition (Y/N)	Colour Intensity	Free Epoxy by IR (Y/N)
Ancamine® 2459	-	-50%	yellow, clear, splotchy	soft	splotchy	-	-	Y
Ancamine® 2459	cyclam	-50%	yellow, clear, uneven surface	hard, flexible	-	Y – purple	medium	Y
Ancamine® 2459	-	-40%	yellow, clear	hard, flexible	slightly splotchy	N – retention but no obvious change	weak	Y
Ancamine® 2459	cyclen	-40%	yellow, blushing, matte	hard, flexible	easy, uniform	Y – dark blue	medium	Y
Ancamine® 2459	cyclam	-40%	yellow, clear	hard, flexible	-	N – retention but no obvious change	weak	Y
Ancamine® 2459	**DETA**	**-40%**	**yellow, matte**	**soft**	**easy, uniform**	**Y – dark blue**	**v. strong**	**N**
Ancamine® 2459	**PEI**	**-40%**	**yellow, opaque, blushing, matte**	**flexible**	**easy, uniform**	**Y – dark blue**	**strong**	**N**
Ancamine® 2459	-	-30%	yellow, clear	hard, flexible	slightly splotchy	N – retention but no obvious change	medium	Y
Ancamine® 2459	cyclam	-30%	yellow, clear	hard, flexible	-	N – retention but no obvious change	weak	Y
Ancamine® 2459	**DETA**	**-30%**	**yellow, matte**	**soft**	**-**	**Y – dark blue**	**v. strong**	**N**
Ancamine® 2459	-	-20%	yellow, clear	hard, flexible	easy, uniform	N – retention but no obvious change	medium	Y
Ancamine® 2459	cyclam	-20%	yellow, clear	hard, brittle	-	N – retention but no obvious change	weak	Y
Ancamine® 2459	-	-10%	yellow, clear	hard, flexible	easy, uniform	N – retention but no obvious change	medium	Y
Ancamine® 2459	cyclam	-10%	yellow, clear	hard, brittle	-	N – retention but no obvious change	weak	Y

Ancamine® 2459	-	stoichiometric	yellow, clear	hard, flexible	easy, uniform	N – retention but no obvious change	medium	Y
Ancamine® 2459	-	+10%	yellow, clear	hard, flexible	easy, uniform	N – retention but no obvious change	medium	Y
Ancamine® 2459	-	+20%	yellow, clear	hard, flexible	easy, uniform	N – retention but no obvious change	medium	Y
Ancamine® 2459	-	+50%	yellow, clear	hard, brittle	easy, uniform	N – retention but no obvious change	medium	N
Ancamine® 2459, cyclen[a]	**-**	**+10% (cyclen)**	**yellow, clear**	**hard, brittle**	**easy, uniform**	**Y – dark blue**	**strong**	**N**
Ancamine® 2459, cyclen[a]	**-**	**+20% (cyclen)**	**yellow, clear**	**hard, brittle**	**easy, uniform**	**Y – dark blue**	**strong**	**N**
Ancamine® 2459, DETA[b]	-	+10% (DETA)	yellow, clear	hard, brittle	easy, uniform	Y – dark blue	medium	N
Ancamine® 2459, DETA[b]	-	+20% (DETA)	yellow, clear	hard, brittle	easy, uniform	Y – dark blue	medium	N
Cyclen	-	-20%	milky, clear	hard, brittle	poor, uneven	Y – dark blue	medium	Y
Cyclen	-	-10%	milky, clear	hard, brittle	poor, uneven	Y – dark blue	medium	Y
Cyclen	-	stoichiometric	milky, clear	hard, brittle	slightly uneven	Y – dark blue	medium	Y
Cyclen	-	+10%	milky, clear	hard, brittle	slightly uneven	Y – dark blue	medium–strong	Y
Cyclen	**-**	**+20%**	**milky, clear**	**hard, brittle**	**poor, uneven**	**Y – dark blue**	**v. strong**	**Y**
DETA	-	-20%	splotchy, white blushing	soft, sticky	v. poor, uneven, splotchy	Y – dark blue	medium, uneven	Y
DETA	-	-10%	splotchy, white blushing	soft, sticky	v. poor, uneven, splotchy	Y – dark blue	medium, uneven	Y
DETA	-	stoichiometric	splotchy, white blushing	soft, sticky	v. poor, uneven, splotchy	Y – dark blue	medium, uneven	Y
DETA	-	+10%	splotchy, white blushing	soft, sticky	v. poor, uneven, splotchy	Y – dark blue	medium, uneven	Y

DETA	**-**	**+20%**	**splotchy, white blushing**	**soft, sticky**	**v. poor, uneven, splotchy**	**Y – dark blue**	**strong, uneven**	**Y**
DETA (75%), cyclen (25%)[c]	-	stoichiometric	splotchy, milky white blushing	sticky, brittle	v. poor, uneven, splotchy	Y – dark blue	medium	Y
DETA (50%), cyclen (50%)[d]	-	stoichiometric	milky white blushing	hard, brittle	slightly splotchy	Y – dark blue	medium	Y
DETA (25%), cyclen (75%)[e]	-	stoichiometric	milky white blushing	hard, brittle	slightly splotchy/uneven	Y – dark blue	medium	Y
DETA (25%), cyclen (100%)[f]	**-**	**+25%**	**milky white blushing**	**hard, brittle**	**slightly splotchy, mostly uniform**	**Y – dark blue**	**strong**	**Y**
DETA (100%), cyclen (25%)[g]	**-**	**+25%**	**splotchy, milky white blushing**	**sticky, brittle**	**v. poor, uneven, splotchy**	**Y – dark blue**	**strong**	**Y**
Cyclam	-	-20%	clear, colourless	hard, brittle	easy, uniform	Y – purple	v. weak (aq), medium (MeOH)	Y
Cyclam	-	stoichiometric	clear, colourless	hard, brittle	easy, uniform	Y – purple	v. weak (aq), medium (MeOH)	Y
Cyclam	-	+20%	clear, colourless	hard, slight flexibility	easy, uniform	Y – purple	v. weak (aq), medium (MeOH)	Y

[a] Stoichiometric amount of Ancamine® 2459 but overcured with cyclen.

[b] Stoichiometric amount of Ancamine® 2459 but overcured with DETA.

[c] Enough DETA and cyclen added as hardeners to react with 75% and 25% of the epoxy groups, respectively.

[d] Enough DETA and cyclen added as hardeners to each react with half of the epoxy groups.

[e] Enough DETA and cyclen added as hardeners to react with 25% and 75% of the epoxy groups, respectively.

[f] Stoichiometric amount of cyclen but overcured with DETA.

[g] Stoichiometric amount of DETA but overcured with cyclen.
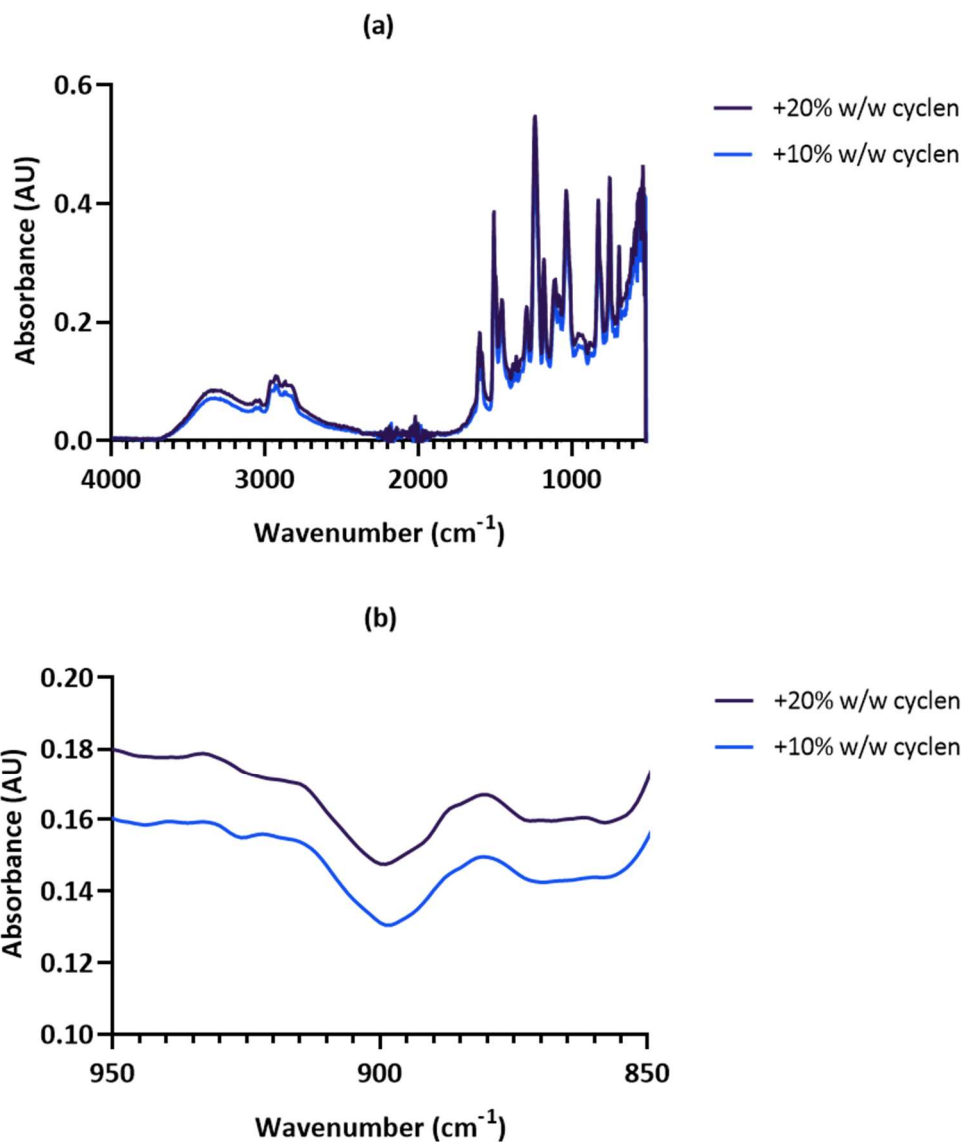
Figure 8.23. **FT-IR spectra of coatings prepared from Epikote™ 235 and Ancamine® 2459 in stoichiometric proportions and overcured (+10% w/w, +20% w/w) with cyclen: (a)** is the full spectrum, and **(b)** shows an expanded view of the bands due to the epoxy group (~915 cm^{-1}).
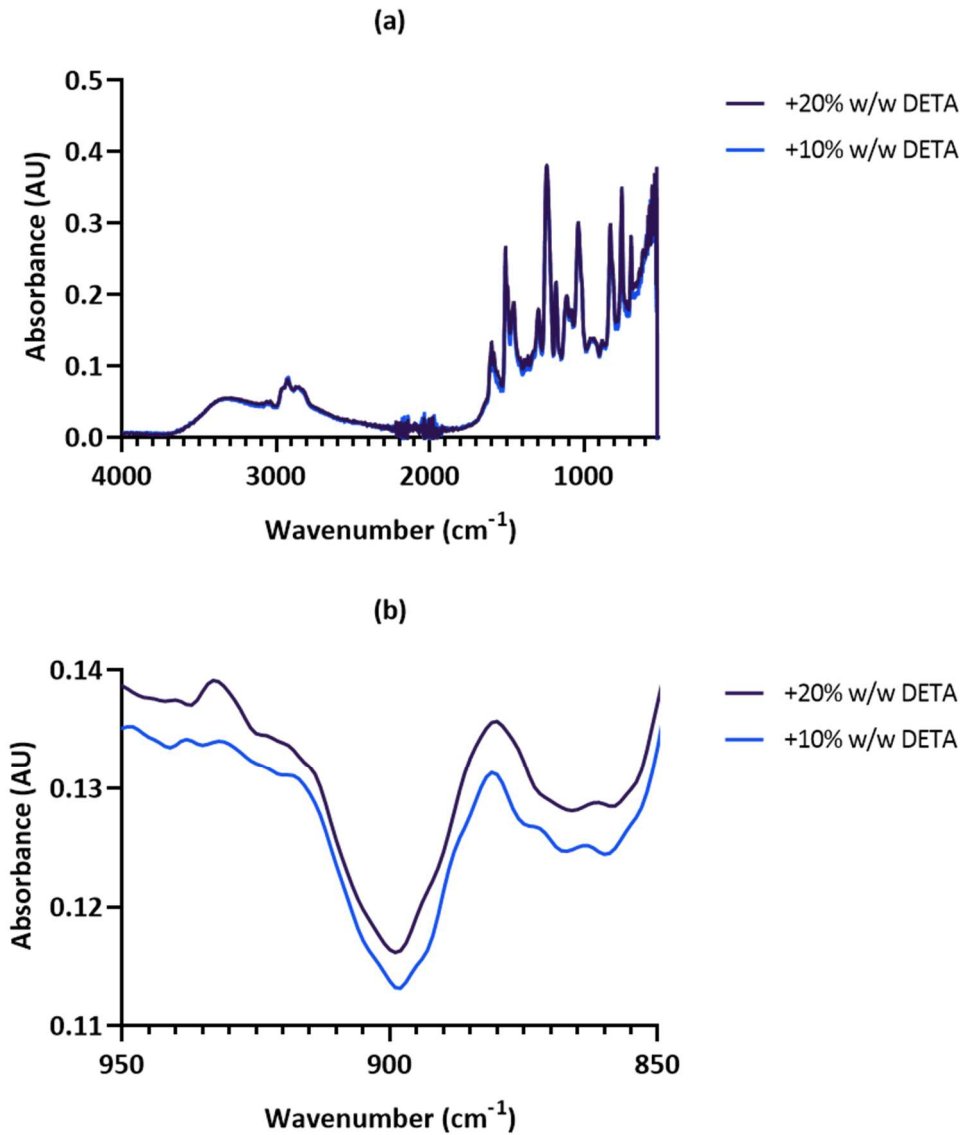
Figure 8.24. FT-IR spectra of coatings prepared from Epikote™ 235 and Ancamine® 2459 in stoichiometric proportions and overcured (+10% w/w, +20% w/w) with DETA: (a) is the full spectrum, and **(b)** shows an expanded view of the bands due to the epoxy group (~915 cm^{-1}).
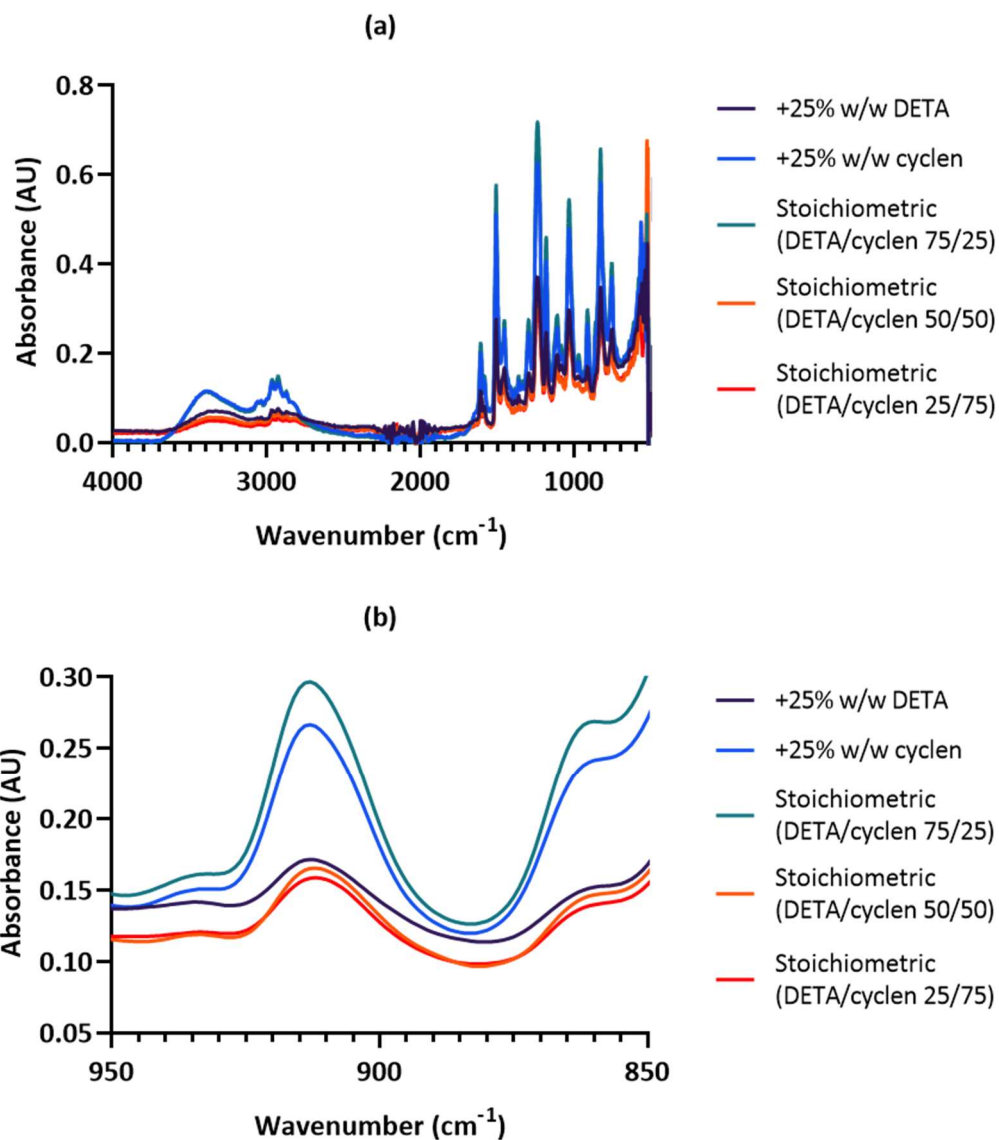
Figure 8.25. FT-IR spectra of coatings prepared from Epikote™ 235 and DETA and/or cyclen in stoichiometric proportions or overcured (+25% w/w) with DETA or cyclen: (a) is the full spectrum, and **(b)** shows an expanded view of the bands due to the epoxy group (~915 cm^{-1}; adjusted baseline).
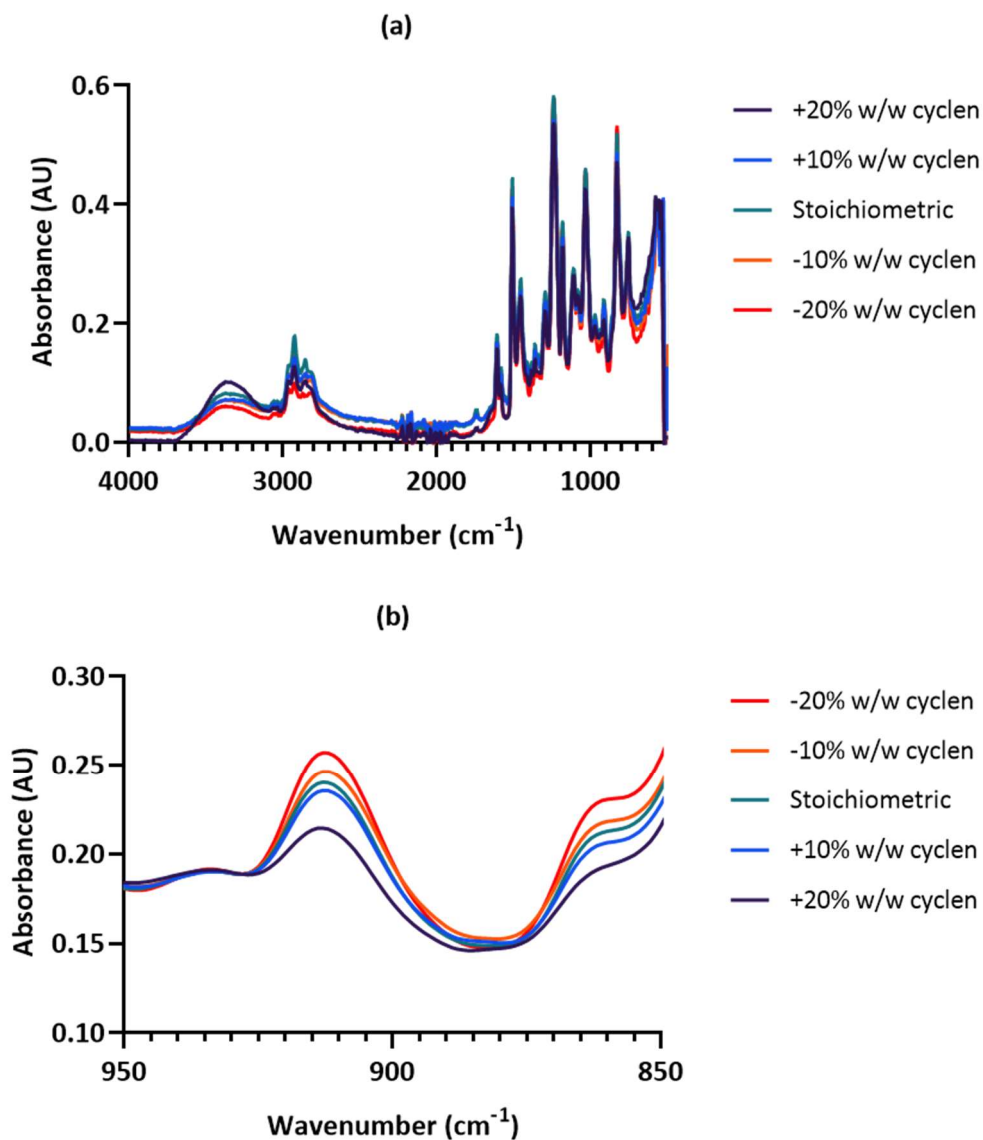
Figure 8.26. FT-IR spectra of coatings prepared from Epikote™ 235 and cyclen in stoichiometric proportions or under/overcured (±20% w/w) with cyclen: (a) is the full spectrum, and **(b)** shows an expanded view of the bands due to the epoxy group (~915 cm^{-1}; adjusted baseline).
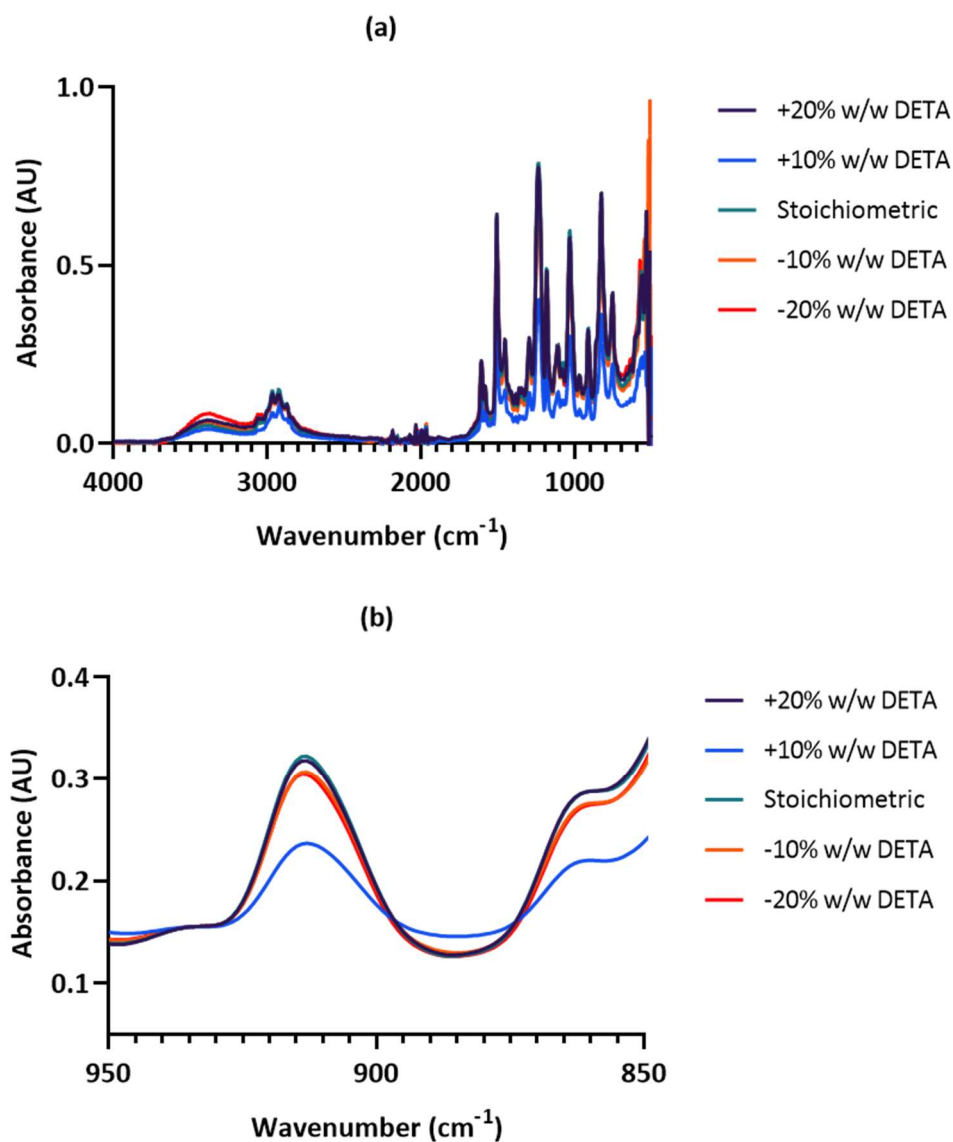
Figure 8.27. FT-IR spectra of coatings prepared from Epikote™ 235 and DETA in stoichiometric proportions or under/overcured (±20% w/w) with DETA: (a) is the full spectrum, and **(b)** shows an expanded view of the bands due to the epoxy group (~915 cm^{-1}; adjusted baseline).
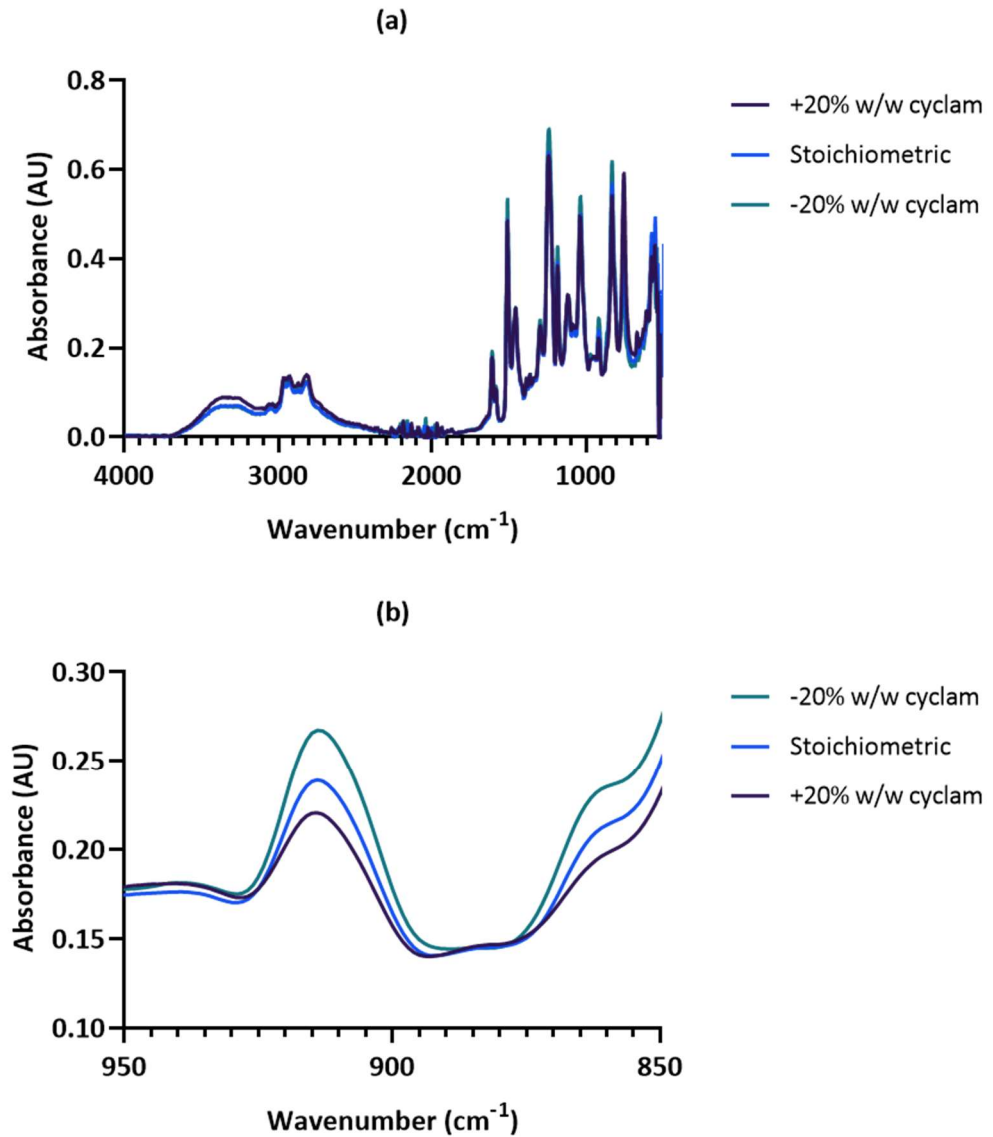
Figure 8.28. FT-IR spectra of coatings prepared from Epikote™ 235 and cyclam in stoichiometric proportions or under/overcured (±20% w/w) with cyclam: **(a)** is the full spectrum, and **(b)** shows an expanded view of the bands due to the epoxy group (~915 cm^{-1}).
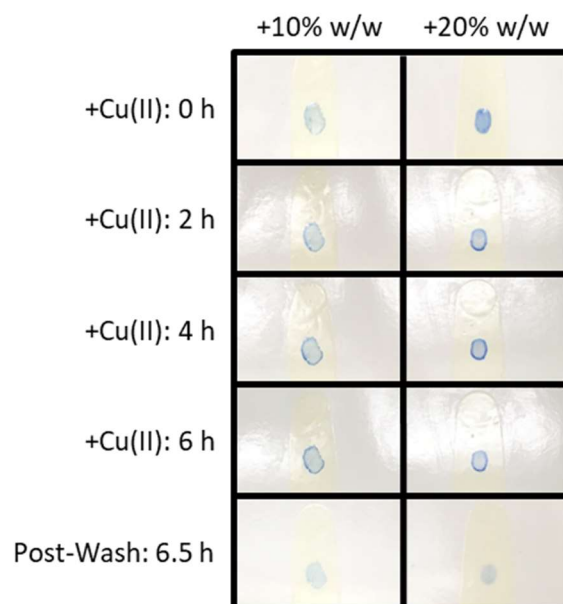
Figure 8.29. Monitoring the Cu(II)-addition to coatings prepared from Epikote™ 235 and Ancamine® 2459 in stoichiometric proportions and overcured (+10% w/w, +20% w/w) with cyclen.
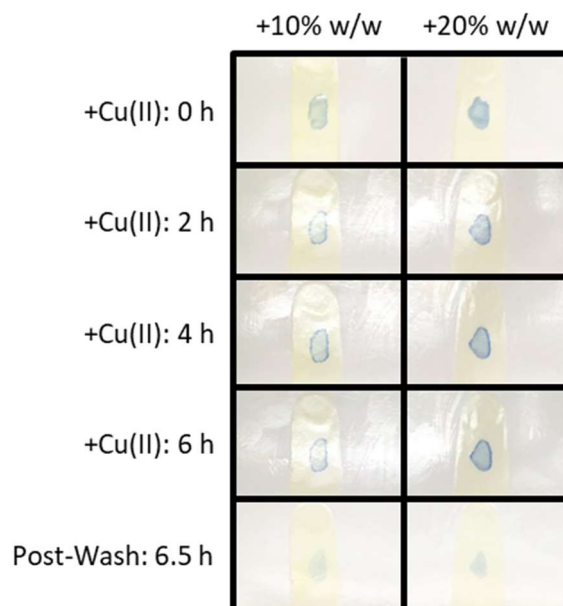
Figure 8.30. Monitoring the Cu(II)-addition to coatings prepared from Epikote™ 235 and Ancamine® 2459 in stoichiometric proportions and overcured (+10% w/w, +20% w/w) with DETA.

Figure 8.31. Monitoring the Cu(II)-addition to coatings prepared from Epikote™ 235 and DETA and/or cyclen in stoichiometric proportions or overcured (+25% w/w) with DETA or cyclen.

Figure 8.32. Monitoring the Cu(II)-addition to coatings prepared from Epikote™ 235 and cyclen in stoichiometric proportions or under/overcured (±20% w/w) with cyclen.

Figure 8.33. Monitoring the Cu(II)-addition to coatings prepared from Epikote™ 235 and cyclam in stoichiometric proportions or under/overcured (±20% w/w) with cyclam.

(a)

(b)
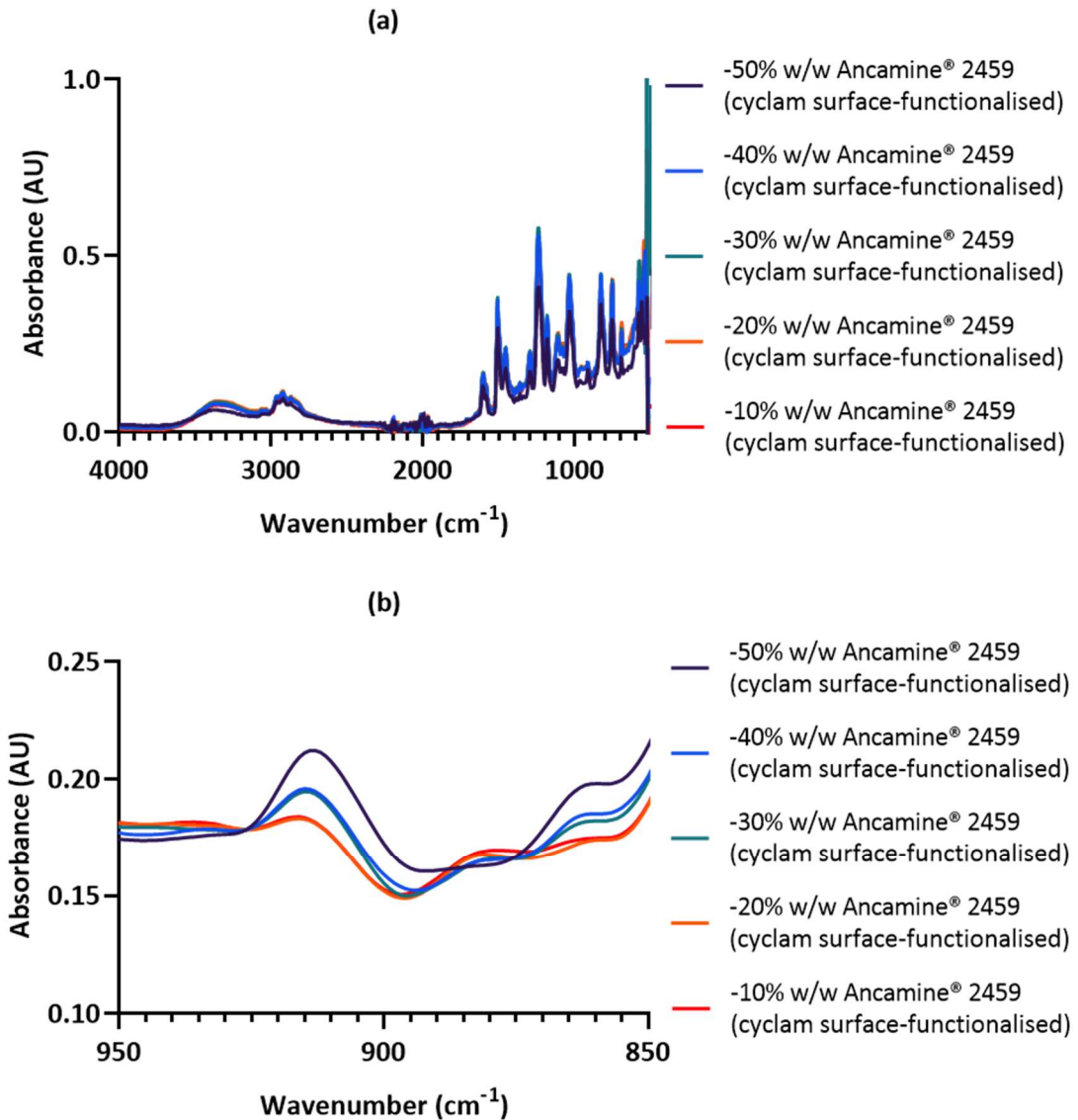
Figure 8.34. FT-IR spectra of coatings prepared from Epikote™ 235 undercured (10–50% w/w) with Ancamine® 2459 and surface-functionalised with cyclam: (a) is the full spectrum, and **(b)** shows an expanded view of the bands due to the epoxy group (~915 cm^{-1}; adjusted baseline).

(a)

(b)
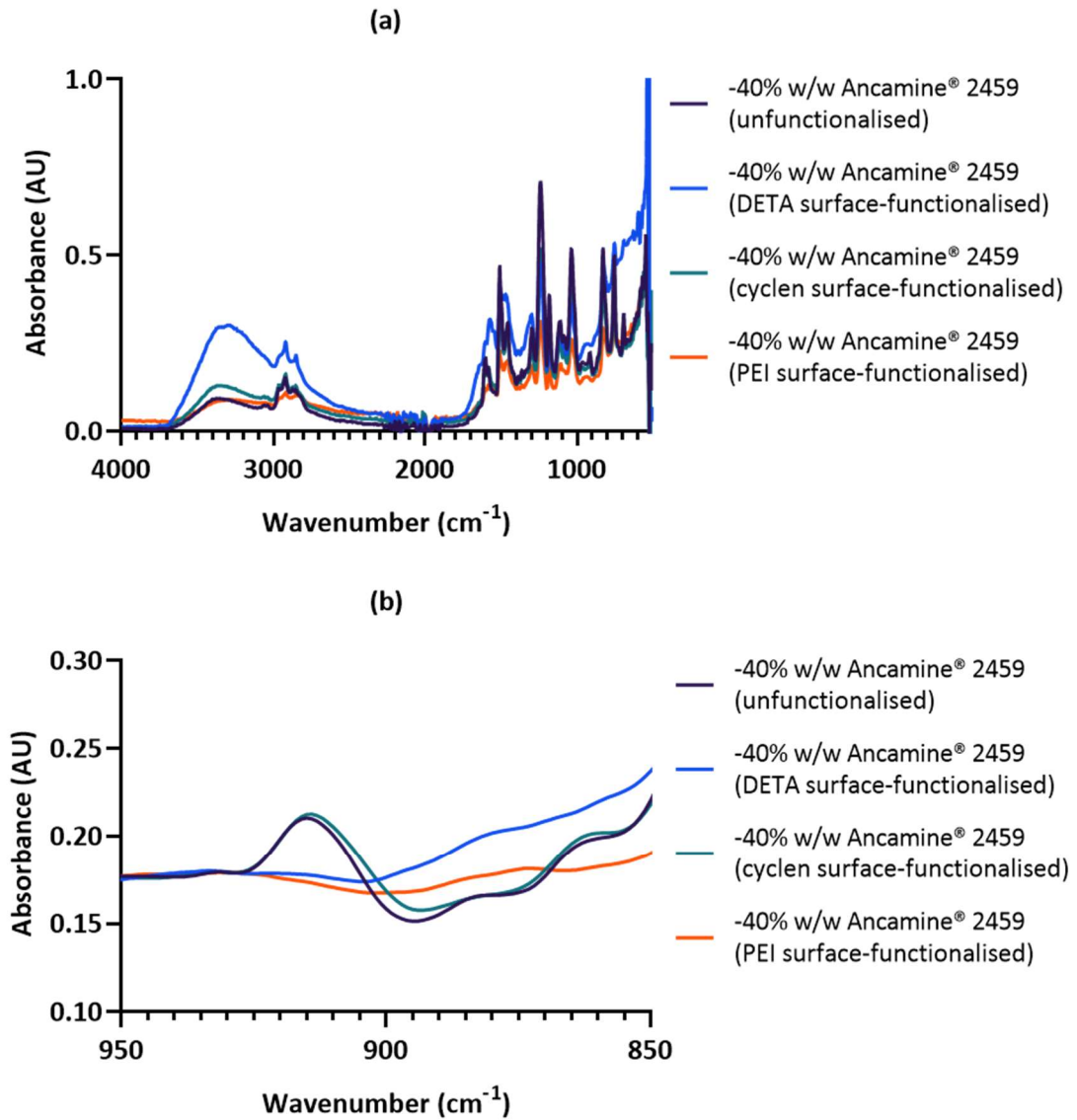
Figure 8.35. FT-IR spectra of coatings prepared from Epikote™ 235 undercured (40% w/w) with Ancamine® 2459 and surface-functionalised with DETA, cyclen, and PEI: (a) is the full spectrum, and **(b)** shows an expanded view of the bands due to the epoxy group (~915 cm^{-1}; adjusted baseline).
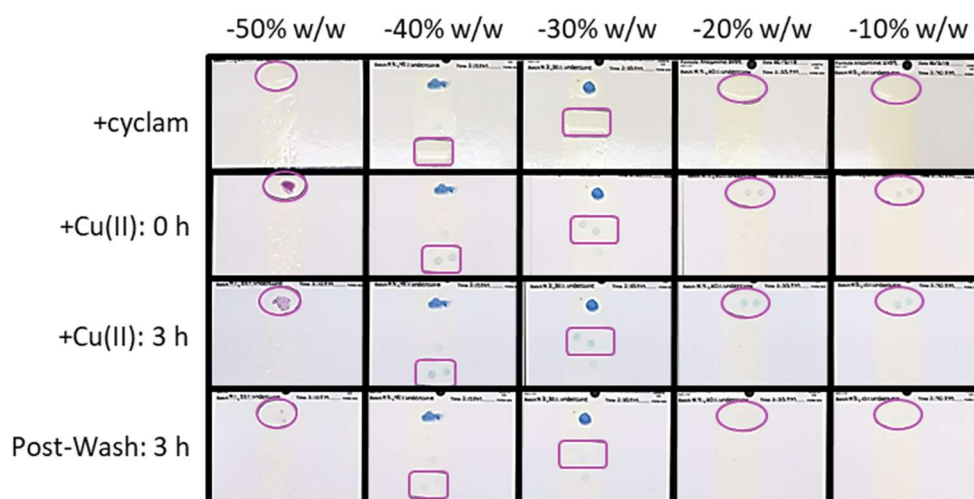
Figure 8.36. Monitoring the Cu(II)-addition to coatings prepared from Epikote™ 235 undercured (10–50% w/w) with Ancamine® 2459 and surface-functionalised with cyclam in the purple-outlined area.
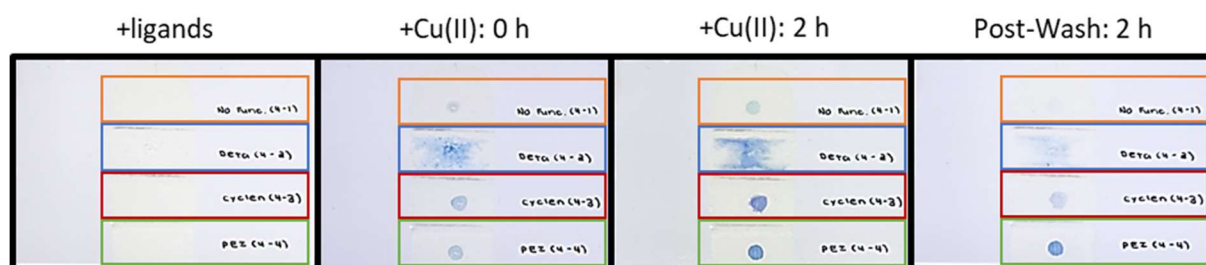
Figure 8.37. Monitoring the Cu(II)-addition to coatings prepared from Epikote™ 235 undercured (40% w/w) with Ancamine® 2459 and surface-functionalised with DETA (blue), cyclen (red), and PEI (green). The area outlined in orange was unfunctionalised.
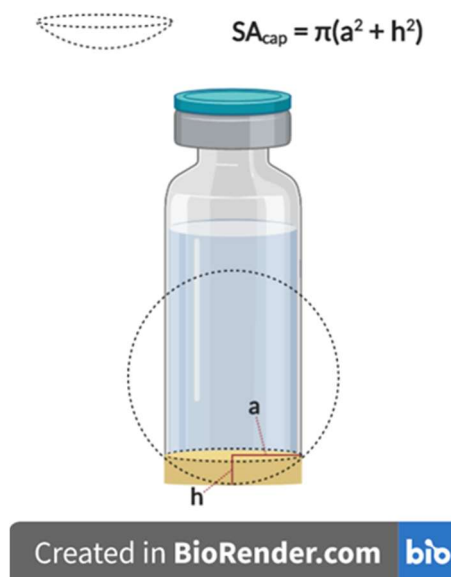
Figure 8.38. Formula for calculating the coating's surface area (spherical shape) exposed to liquid (created with Biorender.com; Chapters 3 and 6, **Sections 3.3.3** and **6.3.3.4**).

8.3 Chapter 4
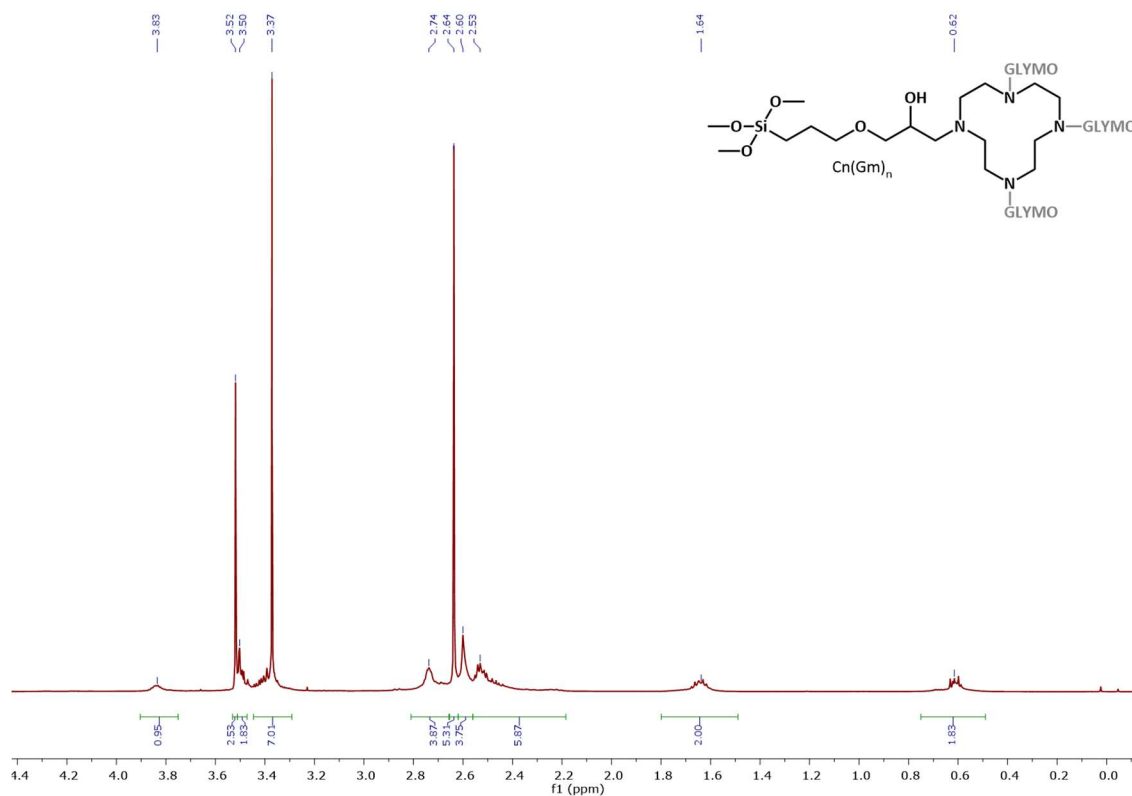
Figure 8.39. ^{1}H NMR spectrum (crude; CDCl$_3$) of Cn(Gm)$_n$ from Procedure 6.
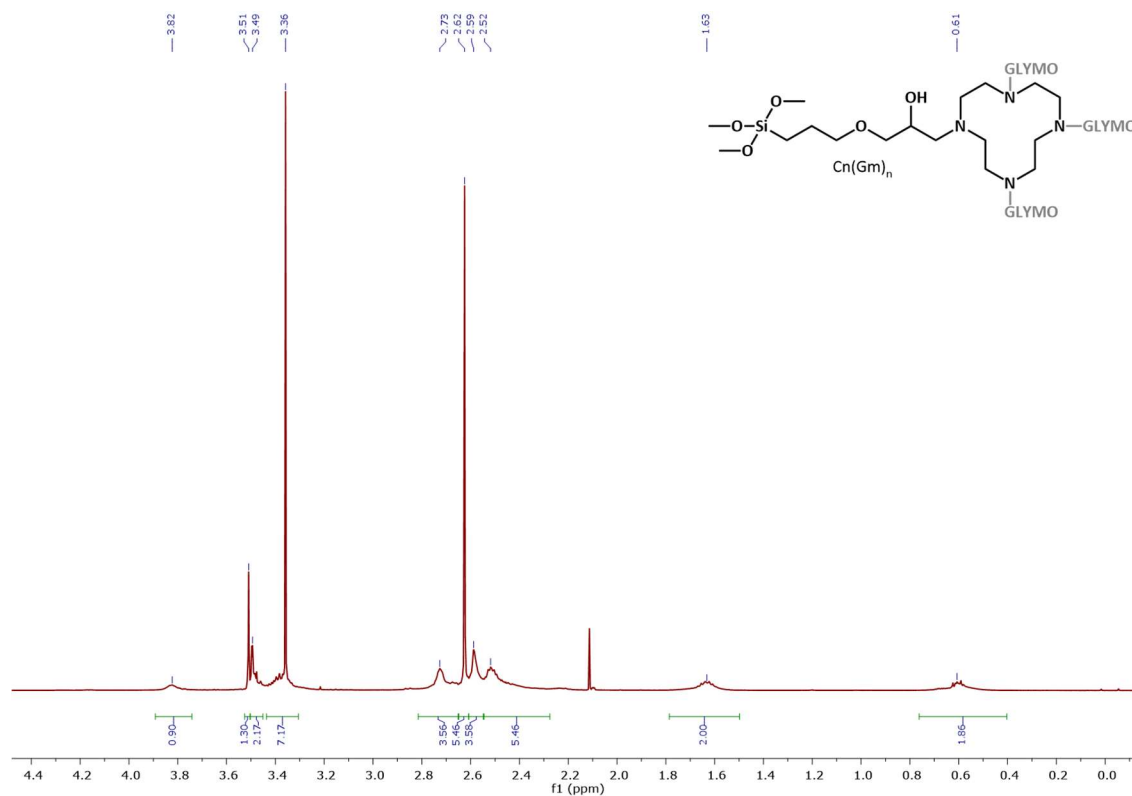
Figure 8.40. ^{1}H NMR spectrum (crude; CDCl$_3$) of Cn(Gm)$_n$ from Procedure 6 + pyridine-d_5.
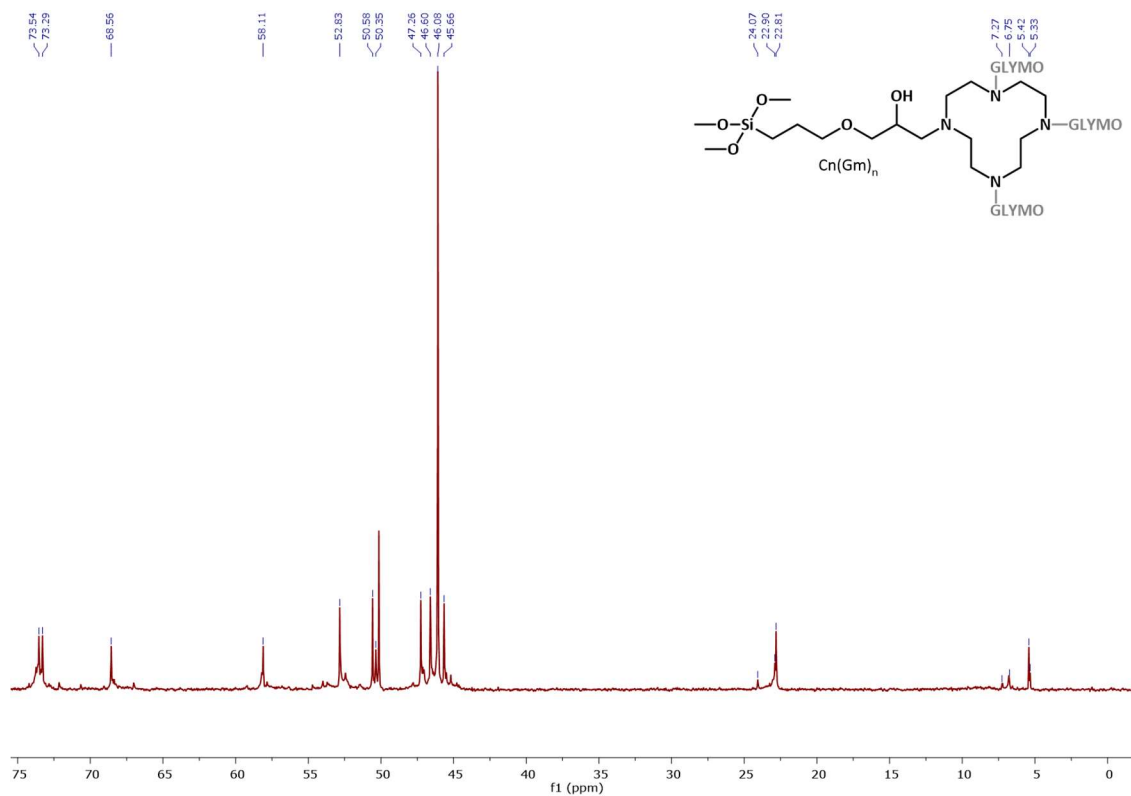
Figure 8.41. ^{13}C NMR spectrum (crude; CDCl$_3$) of Cn(Gm)$_n$ from Procedure 6.
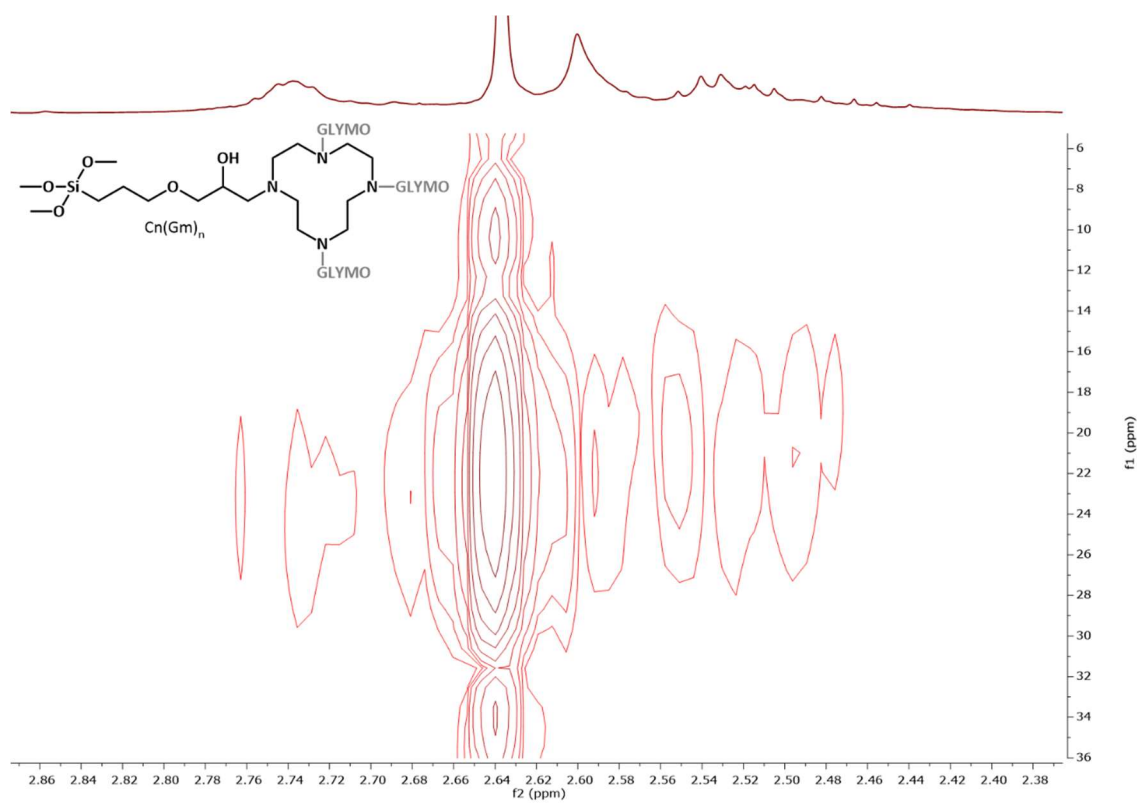
Figure 8.42. 2D (^{1}H, ^{15}N)-HMBC NMR spectrum (crude; CDCl$_3$) of Cn(Gm)$_n$ from Procedure 6.
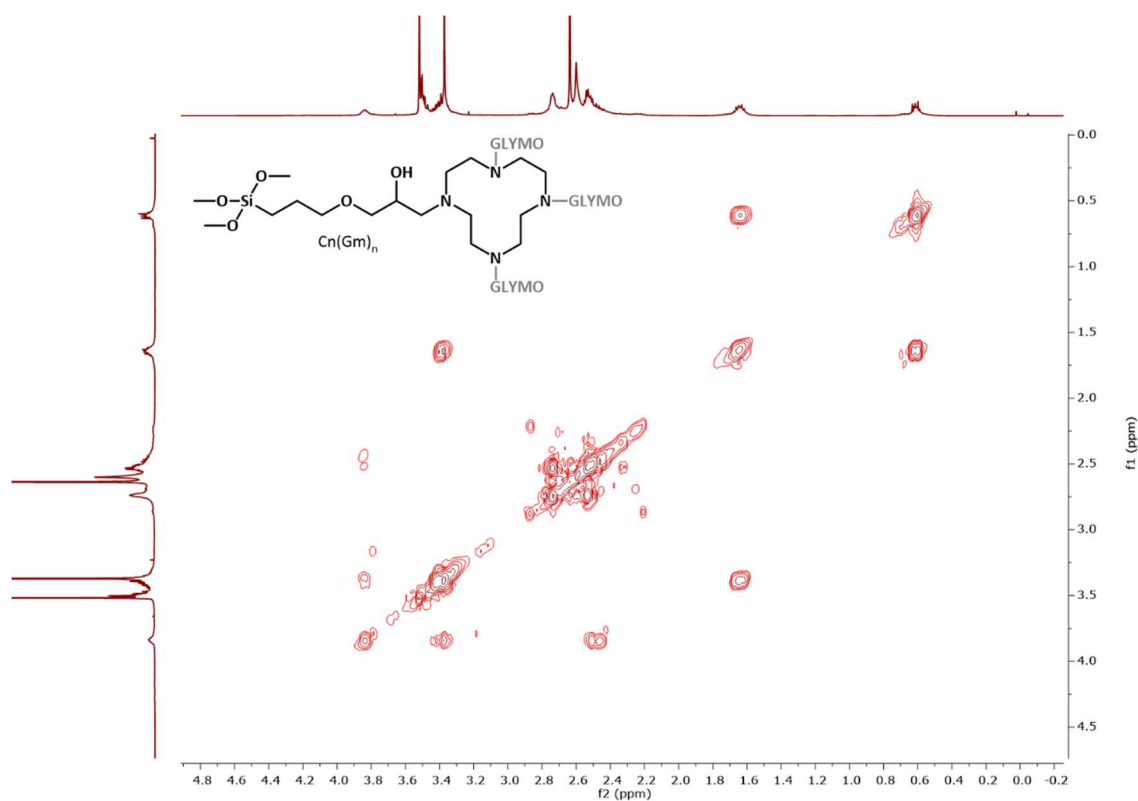
Figure 8.43. 2D (^{1}H, ^{1}H)-COSY NMR spectrum (crude; CDCl$_3$) of Cn(Gm)$_n$ from Procedure 6.
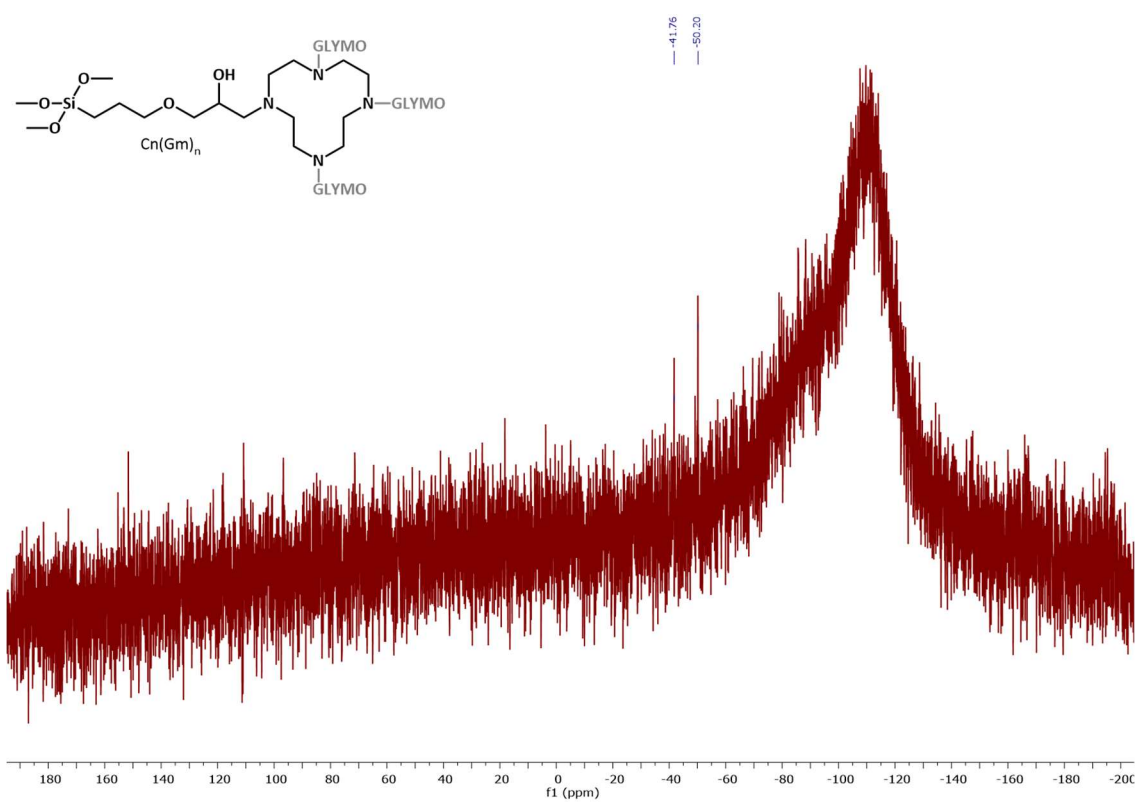
Figure 8.44. ^{29}Si NMR spectrum (crude; CDCl$_3$) of Cn(Gm)$_n$ from Procedure 6 (δ_{Si} -109.7 ppm = NMR tube).
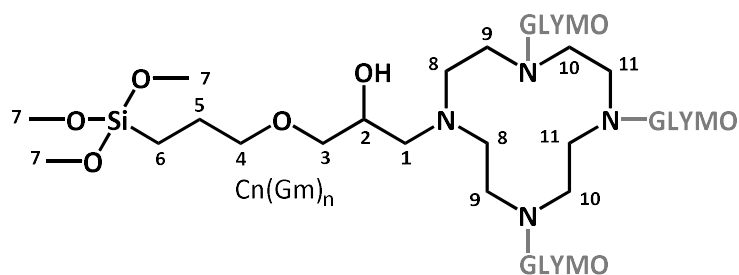
Table 8.20. Peak assignments in ^{1}H and ^{13}C NMR spectra of Procedure 6 Cn(Gm)$_n$.

Position	δ_C, Type[a,c]	δ_H (#H)[b,c]
1	58.1, CH$_2$	2.56–2.15, m (6H)
2	68.6, CH	3.91–3.72, m (1H)
3	73.3, CH$_2$	3.46–3.24, m (7H)
4	73.5, CH$_2$	3.46–3.24, m (7H)
5	24.1, 22.9, 22.8, CH$_2$	1.82–1.42, m (2H)
6	7.3, 6.8, 5.4, 5.3, CH$_2$	0.78–0.42, m (2H)
7	50.6, 50.4, CH$_3$	3.58–3.51, m (3H); 3.51–3.46, m (2H)
8	52.8, CH$_2$	2.60, s (4H)
Cyclen CH$_2$s	47.3, 46.6, 46.1, 45.7, CH$_2$	2.91–2.66, m (4H); 2.64, s (5H); 2.60, s (4H); 2.56–2.15, m (6H)

[a] 126 MHz, Referenced to CDCl$_3$ (δ 77.16 ppm).[261] Elucidated/confirmed by DEPT, HSQC, and HMBC.
[b] 500 MHz, Referenced to CDCl$_3$ (δ 7.26 ppm).[261] Elucidated/confirmed by HSQC, HMBC, and COSY.
[c] Multiple signals exist from multiple species in the reaction mixture.
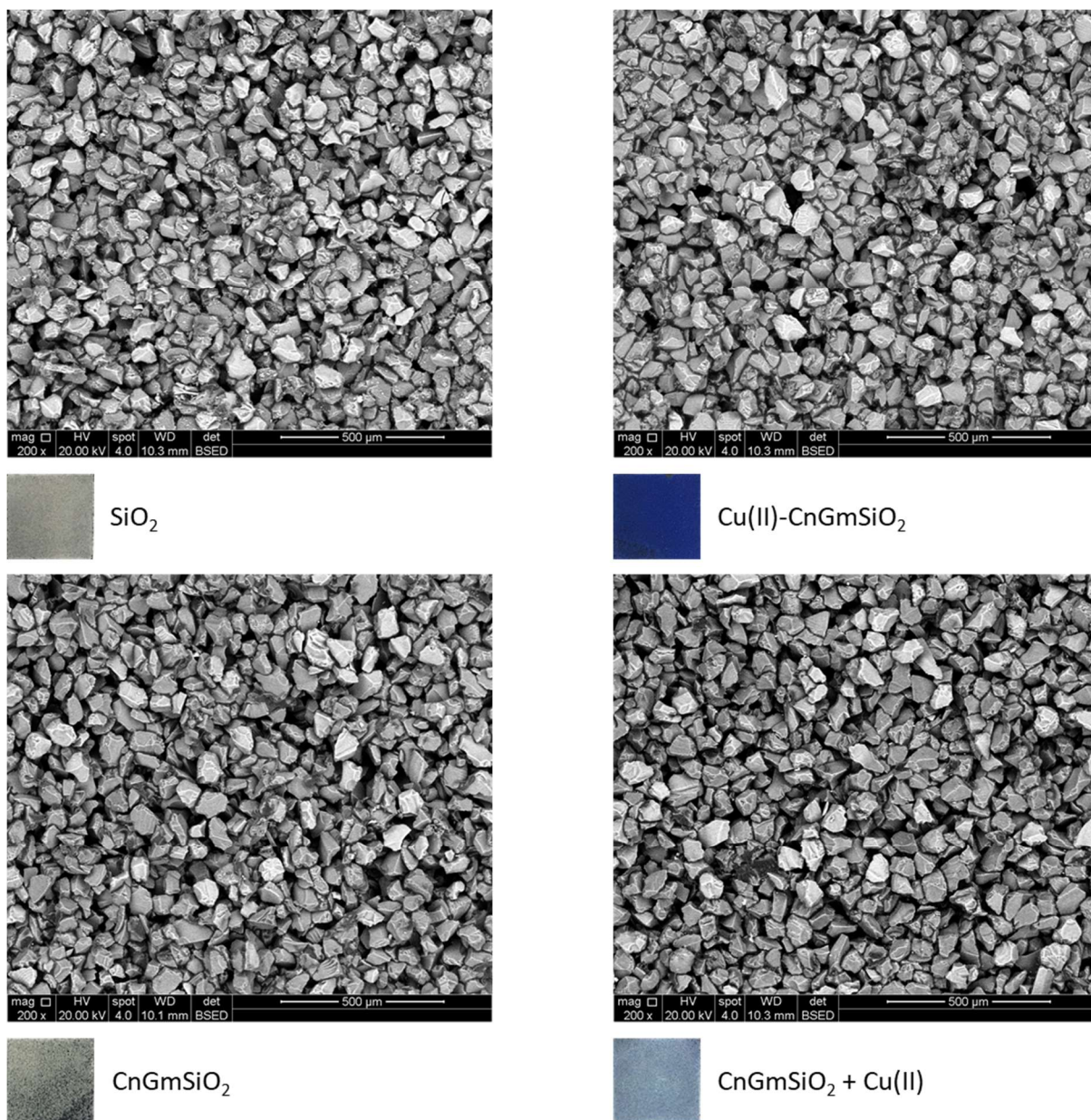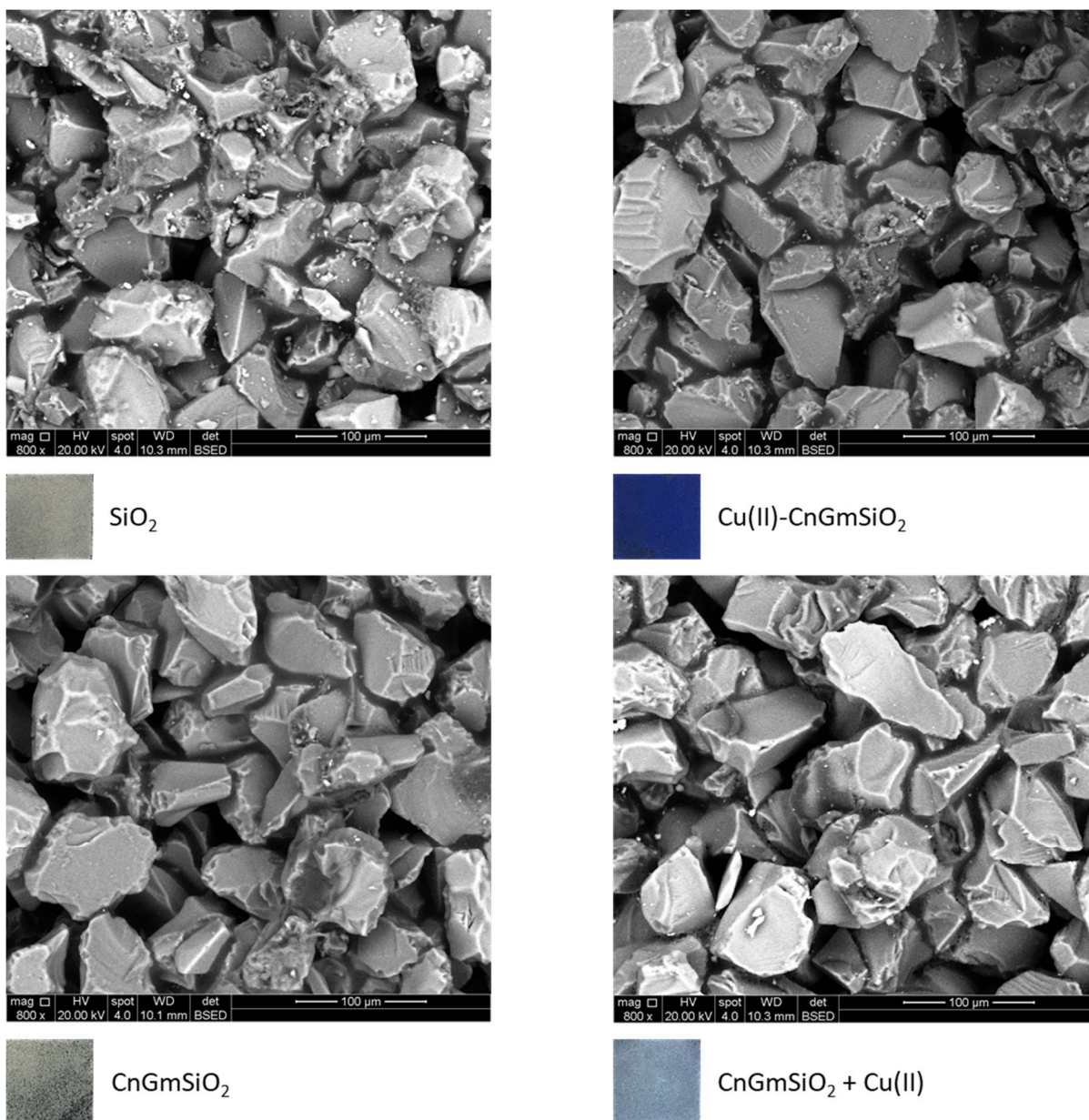
Figure 8.45. SEM backscatter images at 200× magnification of the SiO$_2$/epx-type squares to be tested for bacterial adherence (HV 20 kV, spot size 4, WD 10 mm, BSED). The coatings include unfunctionalised SiO$_2$/epx, Batch 2 Cu(II)-CnGmSiO$_2$/epx (pre-loaded), Batch 4 CnGmSiO$_2$/epx (free ligand), and Batch 4 CnGmSiO$_2$ + Cu(II)/epx (post-loaded).

Figure 8.46. SEM secondary electron images at 800× magnification of the SiO$_2$/epx-type squares to be tested for bacterial adherence (HV 20 kV, spot size 4, WD 10 mm, LFD). The coatings include unfunctionalised SiO$_2$/epx, Batch 2 Cu(II)-CnGmSiO$_2$/epx (pre-loaded), Batch 4 CnGmSiO$_2$/epx (free ligand), and Batch 4 CnGmSiO$_2$ + Cu(II)/epx (post-loaded).
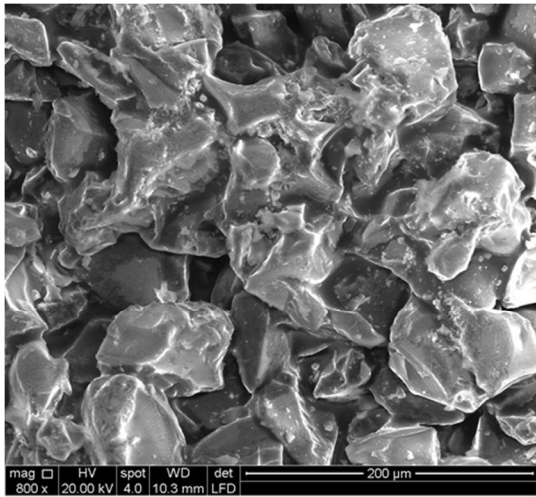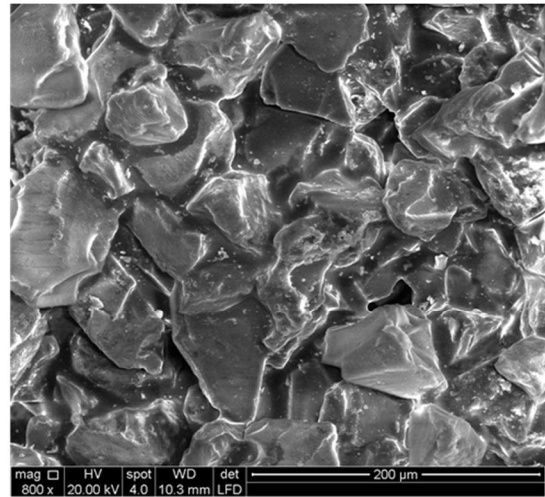
SiO$_2$

Cu(II)-CnGmSiO$_2$
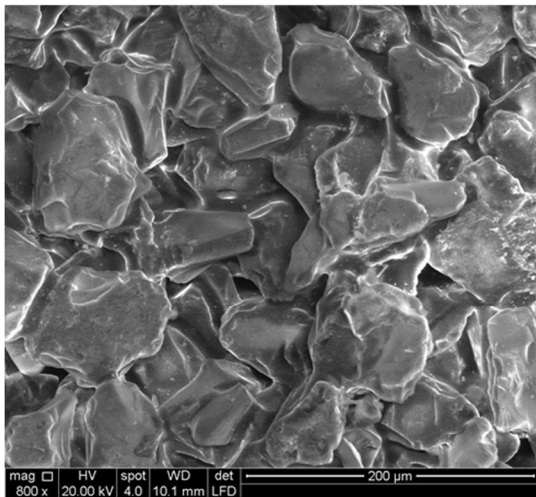
CnGmSiO$_2$

CnGmSiO$_2$ + Cu(II)

Figure 8.47. SEM backscatter images at 800× magnification of the SiO$_2$/epx-type squares to be tested for bacterial adherence (HV 20 kV, spot size 4, WD 10 mm, BSED). The coatings include unfunctionalised SiO$_2$/epx, Batch 2 Cu(II)-CnGmSiO$_2$/epx (pre-loaded), Batch 4 CnGmSiO$_2$/epx (free ligand), and Batch 4 CnGmSiO$_2$ + Cu(II)/epx (post-loaded).
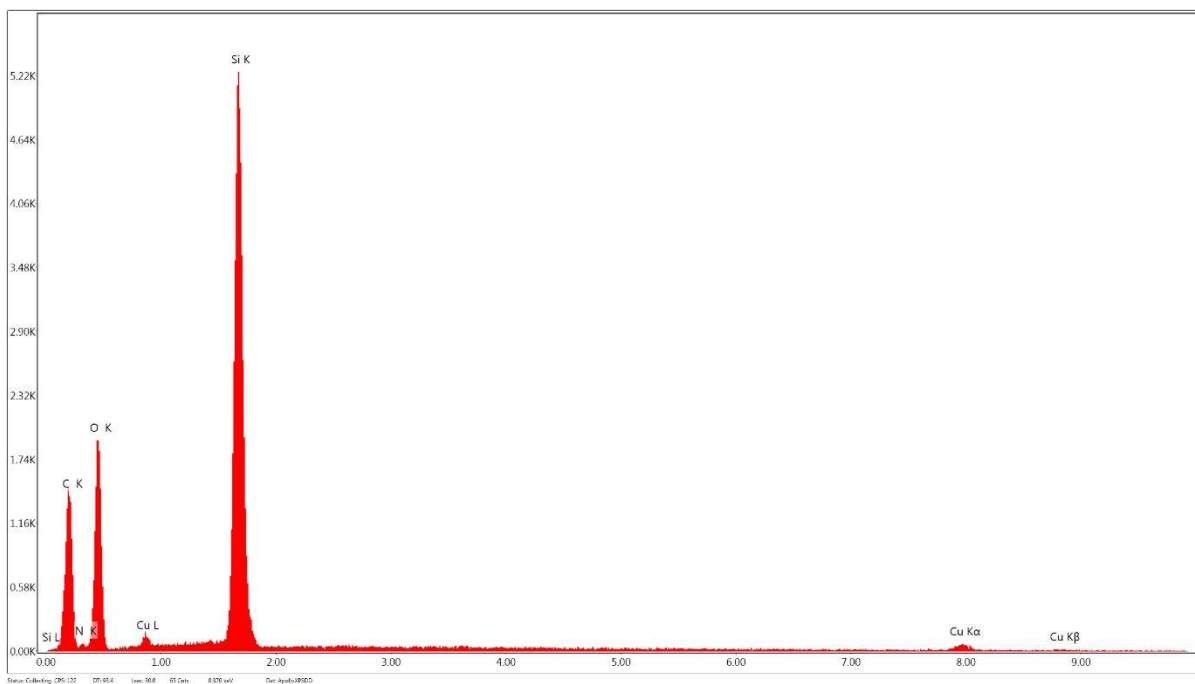
Figure 8.48. EDS spectrum (counts *vs* keV) of Batch 2 Cu(II)-CnGmSiO$_2$/epx (pre-loaded) coating (200× magnification, HV 20 kV, spot size 6, WD 10 mm, 30 s live time, 1.6 µs amplitude time, 35.3° take-off angle, 129 eV resolution).
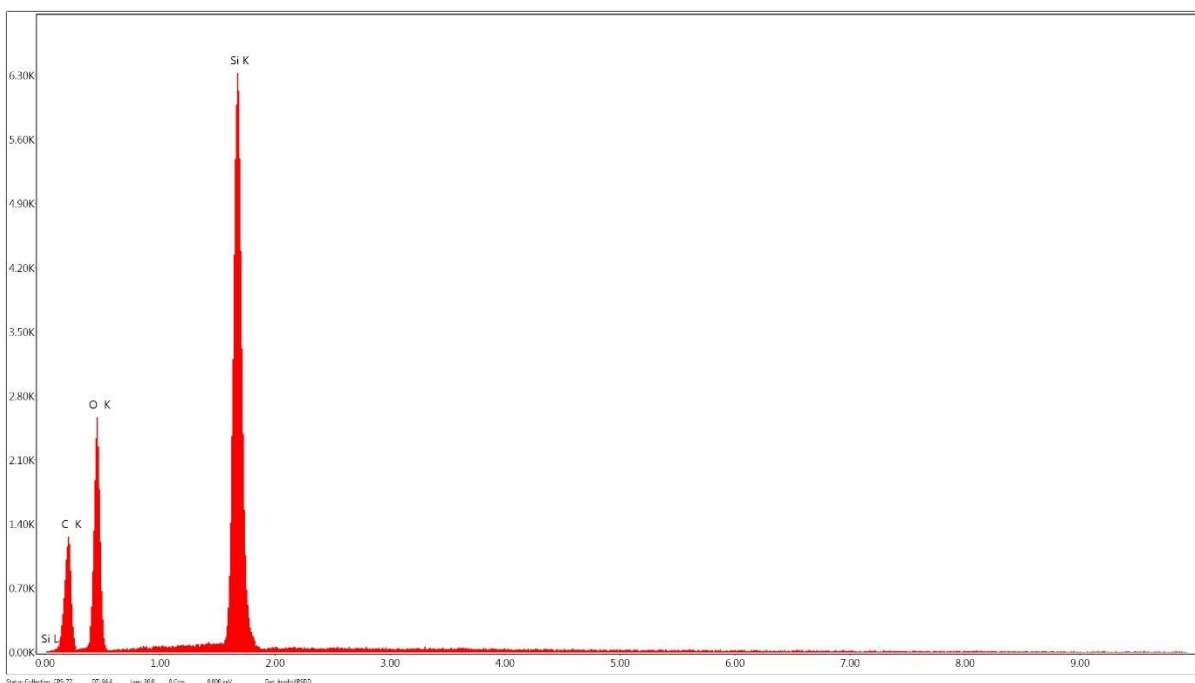

Figure 8.49. EDS spectrum (counts *vs* keV) of Batch 4 CnGmSiO$_2$/epx (free ligand) coating (200× magnification, HV 20 kV, spot size 6, WD 10 mm, 30 s live time, 1.6 µs amplitude time, 35.1° take-off angle, 129 eV resolution).
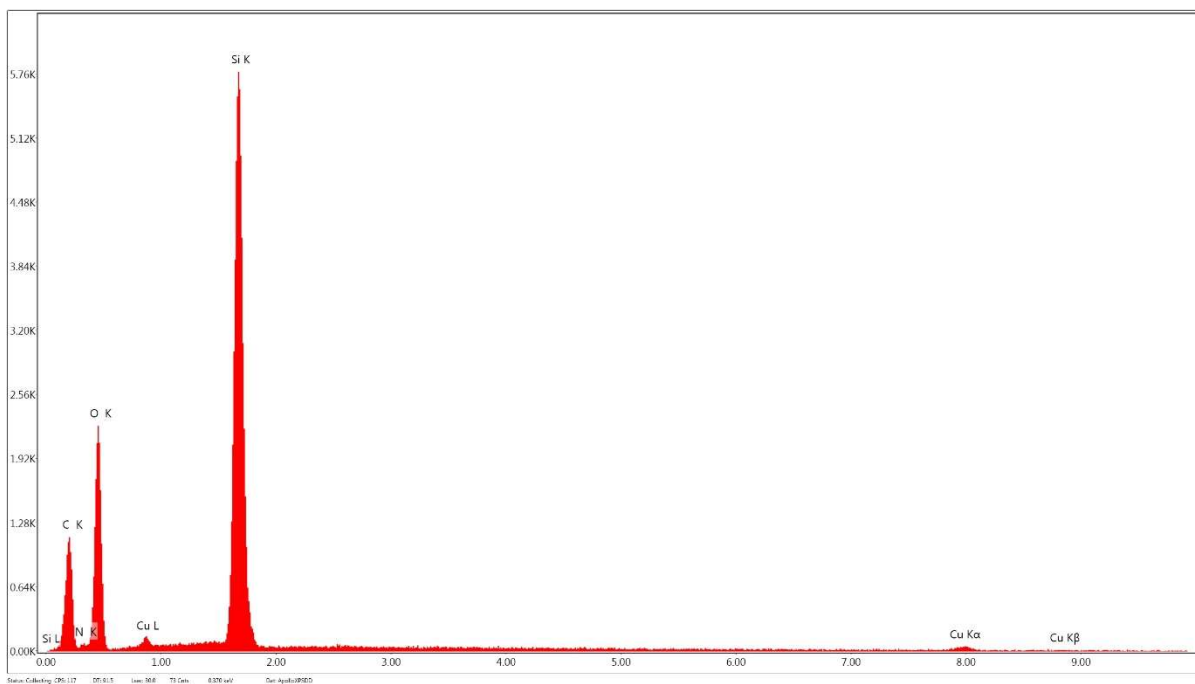
Figure 8.50. EDS spectrum (counts *vs* keV) of Batch 4 CnGmSiO$_2$ + Cu(II)/epx (post-loaded) coating (200× magnification, HV 20 kV, spot size 6, WD 10 mm, 30 s live time, 1.6 µs amplitude time, 35.3° take-off angle, 129 eV resolution).

Figure 8.51. EDS spectrum (counts *vs* keV) of unfunctionalised SiO$_2$/epx coating (200× magnification, HV 20 kV, spot size 6, WD 10 mm, 30 s live time, 1.6 µs amplitude time, 35.3° take-off angle, 129 eV resolution).

8.4 CHAPTER 5
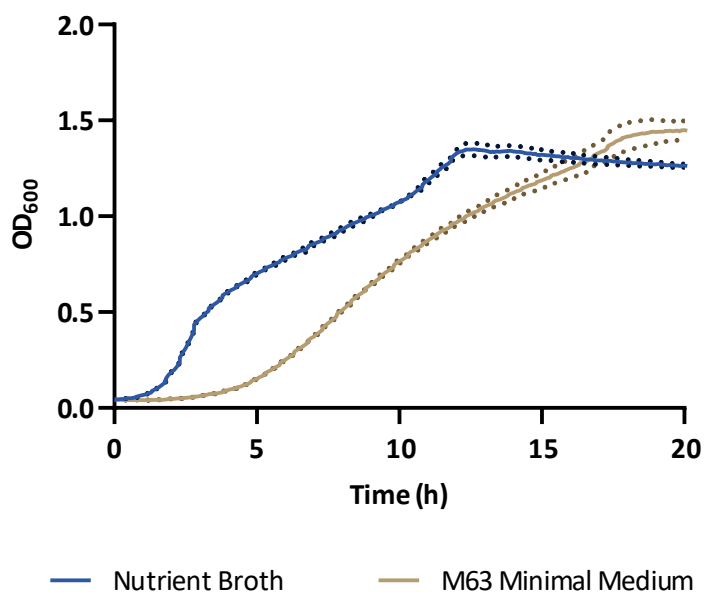
Figure 8.52. Growth curves of *E. coli* NZRM 3647 cultured in nutrient broth or M63 minimal medium.
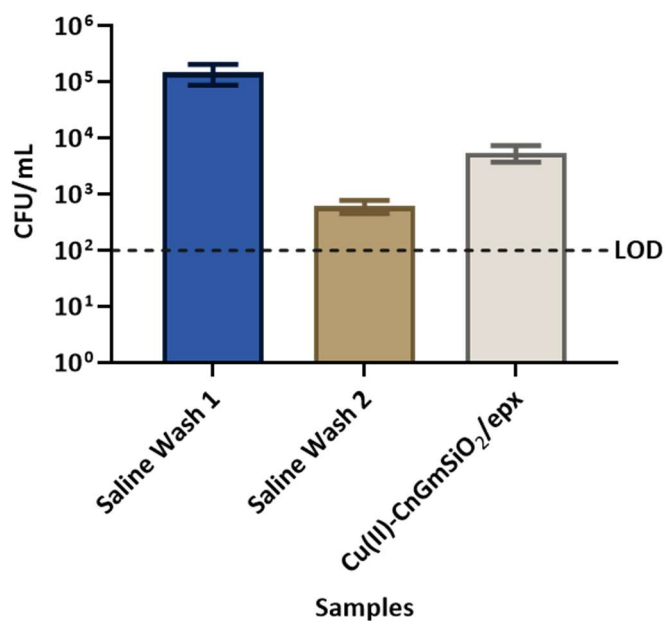The solid line represents the mean (br = 3), and the dotted line represents the SD.

Figure 8.53. Enumeration of bacterial counts in the saline washes: results of CFU/mL in saline washes and the detachment solution containing a Cu(II)-CnGmSiO$_2$/epx-coated square. The bars represent the mean (tr = 5) ± SD (LOD = 100 CFU/mL).

Diameter SiO₂ particles: 35–75 μm (treat particles as spheres)

Dimensions of sample square: 23 mm × 23 mm
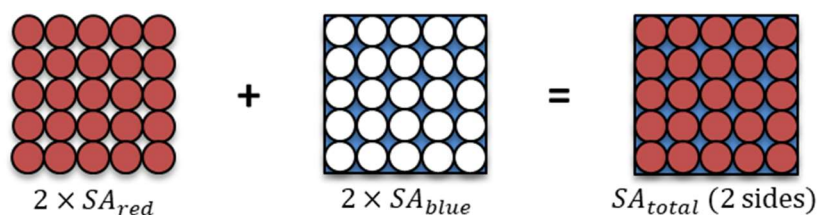
$$SA_{red} = \frac{1}{2} \times 4\pi r^2 \times (\#spheres\ in\ row) \times (\#spheres\ in\ column)$$

$$SA_{red} = 2\pi r^2 \times \left(\frac{23}{d}\right)^2 = 264.5\pi = 831\ \text{mm}^2 = 8.31\ \text{cm}^2$$

$$SA_{blue} = (23 \times 23) - (\pi r^2 \times total\ \#circles)$$

$$SA_{blue} = 529 - \left(\pi r^2 \times \left(\frac{23}{d}\right)^2\right) = 529 - \frac{529\pi}{4} = 114\ \text{mm}^2 = 1.14\ \text{cm}^2$$

$$SA_{total} = (2 \times 8.31) + (2 \times 1.14) = 18.9\ \text{cm}^2$$

Scheme 8.2. Surface area calculation for SiO₂/epx-type coatings.

Table 8.21. Results of BET surface area analysis of SiO₂, Batch 4 CnGmSiO₂, and Batch 2 Cu(II)-CnGmSiO₂.

Sample	Specific Surface Area (m²/g)[a]
SiO₂ (Sigma-Aldrich)[b]	500
SiO₂ (measured)[c]	411
Batch 4 CnGmSiO₂	271
Batch 2 Cu(II)-CnGmSiO₂	255

[a] 2–5% error.
[b] Value reported by Sigma-Aldrich.
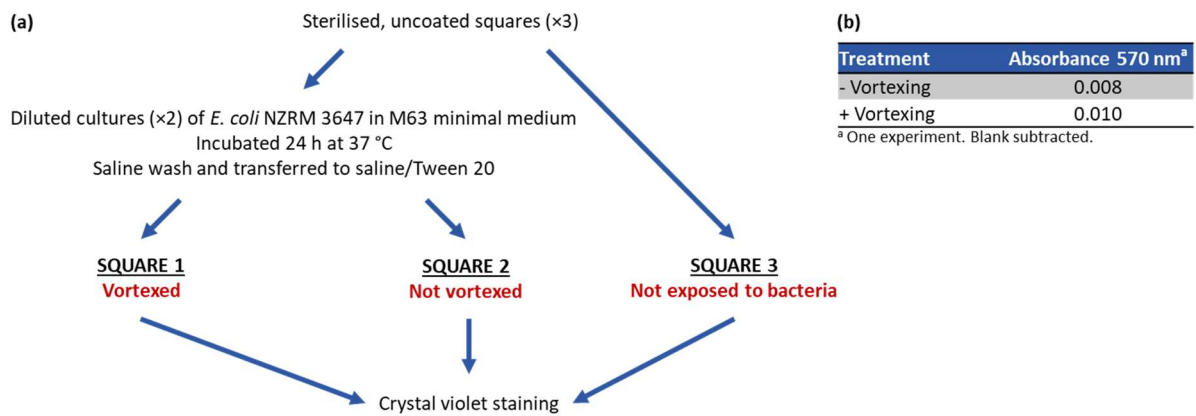[c] Value measured in this work.

Figure 8.54. Testing the efficiency of vortexing in the removal of adherent bacteria *via* crystal violet staining: (a) procedure and **(b)** tabulated results of crystal violet staining of vortexed (+) and not vortexed (−) samples.
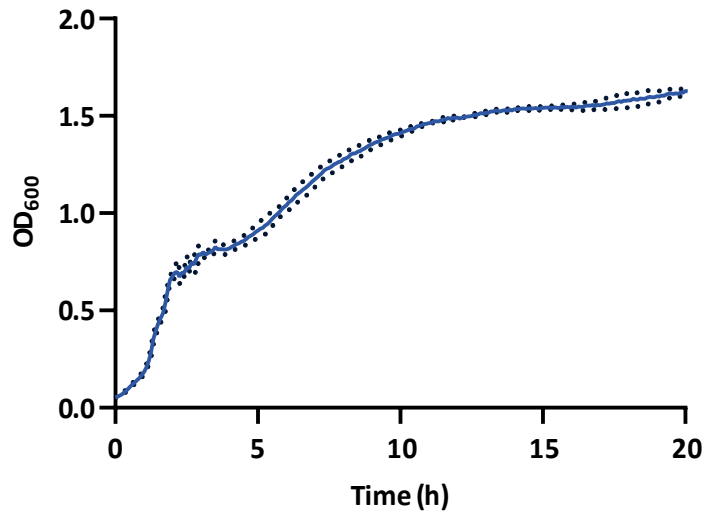

Figure 8.55. Growth curve of *V. harveyi* NZRM 2698 cultured in Luria marine broth. The solid line represents the mean (br = 3), and the dotted line represents the SD.